Issues 1-4 2014 | Volume 10

The Journal on Advanced Studies in Theoretical and Experimental Physics, including Related Themes from Mathematics

PROGRESS IN PHYSICS

"All scientists shall have the right to present their scientific research results, in whole or in part, at relevant scientific conferences, and to publish the same in printed scientific journals, electronic archives, and any other media." — Declaration of Academic Freedom, Article 8

ISSN 1555-5534

The Journal on Advanced Studies in Theoretical and Experimental Physics, including Related Themes from Mathematics

PROGRESS IN PHYSICS

A quarterly issue scientific journal, registered with the Library of Congress (DC, USA). This journal is peer reviewed and included in the abstracting and indexing coverage of: Mathematical Reviews and MathSciNet (AMS, USA), DOAJ of Lund University (Sweden), Zentralblatt MATH (Germany), Scientific Commons of the University of St. Gallen (Switzerland), Open-J-Gate (India), Referativnyi Zhurnal VINITI (Russia), etc.

Electronic version of this journal:
http://www.ptep-online.com

ISSN: 1555-5534 (print)
ISSN: 1555-5615 (online)

Standard Address Number: 297-5092
Printed in the United States of America

January 2014 **Vol. 10, Issue 1**

CONTENTS

Information for Authors and Subscribers

Progress in Physics has been created for publications on advanced studies in theoretical and experimental physics, including related themes from mathematics and astronomy. All submitted papers should be professional, in good English, containing a brief review of a problem and obtained results.

All submissions should be designed in LaTeX format using *Progress in Physics* template. This template can be downloaded from *Progress in Physics* home page http://www.ptep-online.com. Abstract and the necessary information about author(s) should be included into the papers. To submit a paper, mail the file(s) to the Editor-in-Chief.

All submitted papers should be as brief as possible. We accept brief papers, no larger than 8 typeset journal pages. Short articles are preferable. Large papers can be considered in exceptional cases to the section *Special Reports* intended for such publications in the journal. Letters related to the publications in the journal or to the events among the science community can be applied to the section *Letters to Progress in Physics*.

All that has been accepted for the online issue of *Progress in Physics* is printed in the paper version of the journal. To order printed issues, contact the Editors.

This journal is non-commercial, academic edition. It is printed from private donations. (Look for the current author fee in the online version of the journal.)

LETTERS TO PROGRESS IN PHYSICS

Book Review: "Inside Stars. A Theory of the Internal Constitution of Stars, and the Sources of Stellar Energy According to General Relativity"

Pierre A. Millette

Astrophysics research on stellar atmospheres at Department of Physics, University of Ottawa (alumnus), Ottawa, Canada. E-mail: PierreAMillette@alumni.uottawa.ca

This book provides a general relativistic theory of the internal constitution of liquid stars. It is a solid contribution to our understanding of stellar structure from a general relativistic perspective. It raises new ideas on the constitution of stars and planetary systems, and proposes a new approach to stellar structure and stellar energy generation which is bound to help us better understand stellar astrophysics.

The book "Inside Stars. A Theory of the Internal Constitution of Stars, and the Sources of Stellar Energy According to General Relativity" by Larissa Borissova and Dmitri Rabounski [1] provides a general relativistic theory of the internal constitution of liquid stars.

The generally accepted model of stellar constitution considers stars to be high-temperature gaseous plasmas obeying the ideal gas equation of state. However, in the late nineteenth and early twentieth centuries, the question of whether stars are gaseous or liquid was the subject of much debate. P.-M. Robitaille provides a detailed discussion of this debate in his work [2, 3]. Recent evidence for liquid stars, in particular the extensive research performed by P.-M. Robitaille on the liquid metallic hydrogen model of the Sun, and his proposed liquid plasma model of the Sun [4], have re-opened the question.

In this book, the authors provide a novel general relativistic theory of the internal constitution of liquid stars, using a mathematical formalism first introduced by Abraham Zelmanov for calculating physically observable quantities in a four-dimensional pseudo-Riemannian space, known as the theory of chronometric invariants. This mathematical formalism allows to calculate physically observable chronometric-invariant tensors of any rank, based on operators of projection onto the time line and the spatial section of the observer. The basic idea is that physically observable quantities obtained by an observer should be the result of a projection of four-dimensional quantities onto the time line and onto the spatial section of the observer.

In the book, a star is modelled as a sphere of incompressible liquid described by Schwarzschild's metric. However, unlike Schwarzschild's solution which requires that the metric be free of singularities, space-time singularities are considered in this model. The conditions for a spatial singularity, known as a space break, are derived.

For our Sun, a space break is found to be within the Asteroid belt. The theory thus also provides a model of the internal constitution of our solar system. It provides an explanation for the presence of the Asteroid belt, the general structure of the planets inside and outside that orbit, and the net emission of energy by the planet Jupiter.

There is another space break located within a star's field. As a result of their analysis, the authors propose a new classification of stars based on the location of the space breaking of a star's field with respect to its surface. This classification of stars results in three main types: regular stars (covering white dwarfs to super-giants) covered in Chapter 2, of which Wolf-Rayet stars are a subtype, neutron stars and pulsars, covered in Chapter 4 and collapsars (i.e. black holes), covered in Chapter 5. Chapter 3 examines the properties of the stellar wind within their liquid star model.

The stellar mass-luminosity relation, which is the main empirical relation of observational astrophysics, is compared by the authors to that derived in the framework of the liquid model. From this they obtain the physical characteristics of the mechanism that produces energy inside the stars. Using the liquid model, the pressure inside stars can be calculated as a function of radius, including the central pressure. As pointed out by the authors, the temperature of the incompressible liquid star does not depend on pressure, only on the source of stellar energy. The authors match the calculated energy production of the suggested mechanism of thermonuclear fusion of the light atomic nuclei in the Hilbert core (the "inner sun") of the stars to the empirical mass-luminosity relation of observational astrophysics, to determine the density of the liquid stellar substance in the Hilbert core.

In the general relativistic model of liquid stars, the inside of the star is homogeneous, with a small core (about a few kilometres in radius) in its centre. The core is separated from the main mass of the star by the model's collapse surface with the radius depending on the star's mass. Despite almost all the mass of the star being located outside the core (the core is not a black hole), the force of gravity approaches to infinity on the surface of the core due to the inner space breaking of the star's field within it. The super-strong force of gravity is sufficient for the transfer of the necessary kinetic energy to the

lightweight atomic nuclei of the stellar substance, to sustain the process of thermonuclear fusion. Thus, thermonuclear fusion of the light atomic nuclei is possible in the Hilbert core of each star. The energy produced by the thermonuclear fusion is the energy emitted by the stars: the small core of each star is its luminous "inner sun", while the generated stellar energy is transferred to the physical surface of the star by thermal conductivity. Due to the fact that the star's substance is liquid, more and more "nuclear fuel" is delivered from other regions of the star to its luminous Hilbert core, thus supporting the combustion inside the "nuclear boiler", until the time when all the nuclear fuel of the star is spent.

Pulsars and neutron stars are found to be stars whose physical radius is close to the radius of their Hilbert core. They are modelled by introducing an electromagnetic field in the theory to account for their rotation and gravitation. Electromagnetic radiation is found to be emitted only from the poles of those stars, along the axis of rotation of the stars.

Finally, the properties of black holes as derived from the model are considered. The authors find that regular stars cannot collapse. They derive the conditions for pulsars and neutron stars to become collapsars. Interestingly, the authors apply their model to the Universe and, based on their results, suggest that the Universe can be considered as a sphere of perfect liquid which is in a state of gravitational collapse (the liquid model of the Universe). Hence they deduce that the observable Universe is a collapsar, a huge black hole.

This book represents a solid contribution to our understanding of stellar structure from a general relativistic perspective. It provides a general relativistic underpinning to the theory of liquid stars. It raises new ideas on the constitution of stars and planetary systems, and proposes a new approach to stellar structure and stellar energy generation which is bound to generate much new research, and help us better understand stellar astrophysics.

Submitted on October 24, 2013 / Accepted on October 25, 2013

References

1. Borissova L. and Rabounski D. Inside Stars. American Research Press, Rehoboth (NM, USA), 2013 (available from Progress in Physics website).
2. Robitaille P.-M. A Thermodynamic History of the Solar Constitution — I: The Journey to a Gaseous Sun, *Progress in Physics*, 2011, v. 7(3), pp. 3–25.
3. Robitaille P.-M. A Thermodynamic History of the Solar Constitution — II: The Theory of a Gaseous Sun and Jeans' Failed Liquid Alternative, *Progress in Physics*, 2011, v. 7(3), pp. 41–59.
4. Robitaille P.-M. A High Temperature Liquid PLasma Model of the Sun, *Progress in Physics*, 2007, v. 3(1), pp. 70–81.

Mass-Radius Relations of Z and Higgs-Like Bosons

Bo Lehnert

Alfvén Laboratory, Royal Institute of Technology, SE-10044 Stockholm, Sweden. E-mail: Bo.Lehnert@ee.kth.se

Relations between the rest mass and the effective radius are deduced for the Z boson and the experimentally discovered Higgs-like boson, in terms of a revised quantum electrodynamic (RQED) theory. The latter forms an alternative to the Standard Model of elementary particles. This results in an effective radius of the order of 10^{-18} m for the Z boson, in agreement with accepted data. A composite model for the Higgs-like boson is further deduced from the superposition of solutions represented by two Z bosons. This model satisfies the basic properties of the observed Higgs-like particle, such as a vanishing charge and spin, a purely electrostatic and strongly unstable state, and an effective radius of about 10^{-18} m for a rest mass of 125 GeV.

1 Introduction

Recently an elementary particle has been discovered at the projects ATLAS [1] and CMS [2] of CERN, being unstable, having vanishing net electric charge and spin, and a rest mass of 125 GeV. This discovery was made in connection with a search for the Higgs boson and its theoretical base given by the Standard Model of an empty vacuum state.

Being distinguished from the latter model, a revised quantum electrodynamic (RQED) theory has been elaborated [3], as founded on the principle of a non-empty vacuum state. It is supported by the quantum mechanical Zero Point Energy [4] and the experimentally verified Casimir force [5]. This relativistic and gauge invariant theory of broken symmetry is based on a nonzero electric field divergence in the vacuum, in combination with a vanishing magnetic field divergence due to the non-existence of observed magnetic monopoles.

Among the subjects being treated by RQED theory, this report is devoted to the mass-radius relation obtained for the Z boson, and to that associated with a model of the Higgs-like boson. This provides an extension of an earlier analysis on a Higgs-like particle [6].

2 Particle with vanishing net electric charge

Due to the RQED theory of axisymmetric particle-shaped steady states with rest mass, a separable generating function

$$F(r,\theta) = CA - \phi = G_0 G(\rho,\theta)\,, \quad G = R(\rho)\cdot T(\theta) \tag{1}$$

can be introduced in a spherical frame (r,θ,φ) of reference [3]. There is an electrostatic potential ϕ and an electric charge density $\bar{\rho} = \varepsilon_0 \operatorname{div}\mathbf{E}$, a current density $\mathbf{j} = (0,0,C\bar{\rho})$ with $\mathbf{C}^2 = c^2$ and $C = \pm c$ representing the two spin directions along φ, and a magnetic vector potential $\mathbf{A} = (0,0,A)$. A dimensionless radial coordinate $\rho = r/r_0$ is introduced with a characteristic radius r_0, and a dimensionless generating function G with the characteristic amplitude G_0.

As based on the function (1), the general forms of the potentials and the charge density become

$$CA = -(\sin\theta)^2\, DF\,, \tag{2}$$

$$\phi = -\left[1 + (\sin\theta)^2\, D\right] F\,, \tag{3}$$

$$\bar{\rho} = -\frac{\varepsilon_0}{r_0^2\rho^2}\, D\left[1 + (\sin\theta)^2\, D\right] F\,, \tag{4}$$

where the operators are

$$D = D_\rho + D_\theta$$
$$D_\rho = -\frac{\partial}{\partial\rho}\left(\rho^2\frac{\partial}{\partial\rho}\right) \qquad D_\theta = -\frac{\partial^2}{\partial\theta^2} - \frac{\cos\theta}{\sin\theta}\frac{\partial}{\partial\theta}\,. \tag{5}$$

Since the analysis will be applied to the special class of particles with vanishing net electric charge, such as the Z and Higgs-like bosons, the radial part R of the function (1) has to be convergent at the origin $\rho = 0$, and a polar part T is chosen having top-bottom symmetry with respect to the equatorial plane $\theta = \pi/2$. This is due to earlier performed basic deductions [3].

Due to the non-zero electric field divergence, there are local intrinsic charges even when the net integrated charge vanishes. For a convergent generating function the total integrated energy W can either be expressed in terms of the field energy density

$$w_f = \frac{1}{2}\,\varepsilon_0\left(\mathbf{E}^2 + c^2\mathbf{B}^2\right) \tag{6}$$

or of the source energy density

$$w_s = \frac{1}{2}\,\bar{\rho}\,(\phi + CA) \tag{7}$$

from which

$$W = \int w_f\, dV = \int w_s\, dV. \tag{8}$$

We shall use the option (7) for which the local contribution to the particle mass becomes

$$dm_0 = \frac{w_s}{c^2}\, dV \tag{9}$$

and that related to the angular momentum (spin) becomes

$$ds_0 = Cr(\sin\theta)\; dm_0 \tag{10}$$

for a volume element $dV = 2\pi r^2 (\sin\theta)\, d\theta dr$ in a spherical frame.

A generating function being convergent both at $\rho = 0$ and at large ρ, and having top-bottom symmetry, is finally chosen through the form

$$R = \rho^{\gamma} \cdot e^{-\rho}, \qquad T = (\sin\theta)^{\alpha}, \tag{11}$$

where $\gamma \geqslant 1$ and $\alpha \geqslant 1$. The part R then increases to a maximum at the effective radius $\hat{r} = \gamma r_0$ after which it drops steeply towards zero at large ρ.

3 Model of a Z boson

A Z boson is first considered, having zero net electric charge, spin $h/2\pi$, a rest mass of 91 GeV, and an effective radius of about 10^{-18} m according to given data [7].

From (1)–(5), (8), (9) and (11) the product of the mass m_{0Z} and the effective radius $\hat{r}_Z = \gamma r_{0Z}$ becomes

$$\hat{r}_Z m_{0Z} = \pi \left(\varepsilon_0 / c^2\right) r_{0Z}^2 G_0^2 \gamma J_{mZ}, \tag{12}$$

where

$$J_{mZ} = \int_0^{\infty} \int_0^{\pi} f\, g_Z\, d\rho\, d\theta \tag{13}$$

and

$$f = -(\sin\theta)\, D \left[1 + (\sin\theta)^2\, D\right] G, \tag{14}$$

$$g_Z = -\left[1 + 2\,(\sin\theta)^2\, D\right] G. \tag{15}$$

The spin is further given by

$$s_{0Z} = \pi \varepsilon_0 \left(C/c^2\right) r_{0Z}^2 G_0^2 J_{sZ} = \pm h/2\pi \tag{16}$$

where

$$J_{sZ} = \int_0^{\infty} \int_0^{\pi} \rho\, (\sin\theta)\, f\, g_Z\, d\rho\, d\theta. \tag{17}$$

Combination of (12)–(17) yields

$$\hat{r}_Z m_{0Z} = \frac{h}{2\pi c} \frac{\gamma J_{mZ}}{J_{sZ}}. \tag{18}$$

This relates the mass to the effective radius, in a way being dependent on the profile shape of the generating function:

- A numerical analysis of the $1 \leqslant \gamma \leqslant 10$ and $1 \leqslant \alpha \leqslant 10$ cases, results in the large ranges $17.7 \leqslant J_{mZ} \leqslant 9.01 \times 10^{15}$ and $39.8 \leqslant J_{sZ} \leqslant 1.83 \times 10^{16}$ of the amplitudes J_{mZ} and J_{sZ}. The last factor of the right-hand member in (18) stays however within the limited range of $0.445 \leqslant (\gamma J_{mZ}/J_{sZ}) \leqslant 0.904$.
- In the asymptotic cases $\gamma \gg \alpha \gg 1$ and $\alpha \gg \gamma \gg 1$ the values of $(\gamma J_{mZ}/J_{sZ})$ become $15/38$ and 1, respectively. This is verified in an earlier analysis [8].
- In spite of the large variations of J_{mZ} and J_{sZ} with the profile shape, the factor $\gamma J_{mZ}/J_{sZ}$ thus has a limited variation within a range of about 0.4 to 1.

For the present deduced model, the rest mass of 91 GeV then results in an effective radius in the range of 0.87×10^{-18} to 2.2×10^{-18} m. This is consistent with the given value of $\hat{r}_Z$.

For the expressions (2) and (3) combined with the form (11) can finally be seen that there is a moderately large deviation from a state $\mathbf{E}^2 = c^2 \mathbf{B}^2$ of equipartition between the electrostatic and magnetostatic particle energies.

4 Model of a Higgs-like boson

One of the important reactions being considered in the experiments at CERN is the decay of the observed Higgs-like boson into two Z bosons, and further into four leptons. Since the Higgs-like boson was found to have a mass of 125 GeV, and the Z bosons have masses of 91 GeV each, an extra contribution of 57 GeV is required for the decay into the Z bosons. It can then be conceived that this extra energy is "borrowed" from the Heisenberg uncertainty relation when the entire decay process takes place in a very short time. At least one of the involved Z bosons then behaves as a virtual particle. In this connection is also observed that the magnitude of the Higgs-like boson mass has not been predicted through the theory by Higgs [9].

With the decay process in mind, a relation will now be elaborated between the mass and the effective radius of the Higgs-like boson. Then it has first to be observed that a relation similar to equation (18) cannot be straightforwardly deduced. This is because the Higgs-like boson has no spin, and its related effective radius can on account of the required extra energy not become identical with that of a single Z boson.

Solutions for models of massive individual bosons and leptons are available from RQED theory. The field equations are linear, and these solutions can be superimposed to form a model of a Higgs-like particle having vanishing charge and spin. It can be done in terms of four leptons or two Z bosons. Choosing the latter option [6], superposition of the potentials (2) and (3) for two modes with opposite spin directions results in a composite Higgs-like mode with zero charge and spin but nonzero rest mass. This mode has no magnetic field, is purely electrostatic, and is thus expected to be highly unstable. In analogy with the deductions (1)–(11), the corresponding integrated mass m_{0H} becomes

$$\hat{r}_H m_{0H} = \pi \left(\varepsilon_0 / c^2\right) r_{0H}^2 G_0^2 \gamma J_{mH} \tag{19}$$

with the effective radius $\hat{r}_H \neq \hat{r}_Z$ and

$$J_{mH} = \int_0^{\infty} \int_0^{\pi} f\, g_H\, d\rho\, d\theta. \tag{20}$$

Here f is still obtained from (14) and

$$g_H = -2\left[1 + (\sin\theta)^2\, D\right] G = g_Z - G \tag{21}$$

with g_Z given by (15). Combination of (19) and (12) yields

$$\frac{\hat{r}_H}{\hat{r}_Z} = \frac{r_{0H}}{r_{0Z}} = \frac{m_{0H}}{m_{0Z}} \frac{J_{mZ}}{J_{mH}} . \qquad (22)$$

The dependence on the profile shape of the generating function is as follows:

- Numerical analysis in the ranges $1 \leqslant \gamma \leqslant 10$ and $1 \leqslant \alpha \leqslant 10$ results in the amplitude variations $138 \leqslant J_{mZ} \leqslant 9.8 \times 10^{15}$ and $287 \leqslant J_{mH} \leqslant 1.8 \times 10^{16}$, but their ratio is strongly limited to $2.03 \leqslant J_{mH}/J_{mZ} \leqslant 2.20$.
- From expression (21) at large γ and α can further be seen that J_{mH}/J_{mZ} approaches the asymptotic value 2.

With these evaluations, and the experimentally determined masses $m_{0Z} = 91$ GeV and $m_{0H} = 125$ GeV, the effective radius $\hat{r}_H$ of the Higgs-like boson comes from (22) out to be in the range 0.54×10^{-18} to 1.5×10^{-18} m.

5 Summary

The present model of the Z boson leads to an effective radius of the order of 10^{-18} m, in agreement with given data. This can be taken as support of the present theory.

Concerning the present model of a Higgs-like boson, the following results should be observed:

- An imagined "reversal" of the decay of a Higgs-like boson into two Z bosons initiates the idea of superimposing two Z boson modes to form a model of such a particle. The resulting composite particle solution is consistent with the point made by Quigg [7] that the Higgs is perhaps not a truly fundamental particle but is built out of as yet unobserved constituents.
- The present model of a Higgs-like boson satisfies the basic properties of the particle observed at CERN. It has a vanishing electric charge and spin, a nonzero rest mass, and is unstable due to its purely electrostatic nature.
- The present theory finally results in an effective radius of the order of 10^{-18} m for the experimentally detected Higgs-like particle having a rest mass of 125 GeV, and vice versa.

Acknowledgement

The author is indebted to Dr. Ahmed Mirza for valuable help with the numerical evaluations of this report.

Submitted on November 4, 2013 / Accepted on November 10, 2013

References

1. Aad G. et al., ATLAS Collaboration. Observation of a new particle in the search for the Standard Model Higgs boson with the ATLAS detector at the LHC. *Phys.Lett.*, 2012, v. B716, 1–29.
2. Chatrchyan S. et al., CMS Collaboration. Observation of a new boson at a mass of 125 GeV with the CMS experiment at the LHC. *Phys.Lett.*, 2012, v. B716, 30–61.
3. Lehnert B. Revised Quantum Electrodynamics. In Dvoeglazov V. V. (ed). Contemporary Fundamental Physics. Nova Science Publishers Inc., New York, 2013.
4. Schiff L. I. Quantum Mechanics. McGraw-Hill Book Comp. Inc., New York-Toronto-London, 1949, Ch.IV, Sec.13.
5. Casimir H. B. G. On the attraction between two perfectly conducting plates. *Proc.K.Ned.Akad.Wet.*,1948, v. 51, 793–795.
6. Lehnert B. Higgs-like particle due to revised quantum electrodynamics. *Progress in Physics*, 2013, v. 3, 31–32.
7. Quigg C. The coming revolutions in particle physics. *Scientific American*, February 2008, 38–45.
8. Lehnert B. and Roy S. Extended electromagnetic theory. World Scientific Publishers, Co. Pte. Ltd, Singapore, 1998, Ch.5.2.
9. Higgs P. W. Spontaneous symmetry breakdown without massless bosons. *Physical Review*, 1966, v. 145, 1156–1168.

Reexamination of Nuclear Shape Transitions in Gadolinium and Dysprosium Isotopes Chains by Using the Geometric Collective Model

Khalaf A.M.[1], Aly H.F.[2], Zaki A.A.[2] and Ismail A.M.[2]

[1]Physics Department, Faculty of Science, Al-Azhar University, Cairo, Egypt. E-mail: ali_khalaf43@hotmail.com
[2]Hot Laboratories Center, Atomic Energy Authority, P.No. 13759, Cairo, Egypt. E-mail: dr_ahmedph@yahoo.com

The geometric collective model proposed in a previous paper in examined to describe the nuclear shape transitions for Gd and Dy isotopes chains. The optimized model parameters for each nucleus have been adjusted by fitting procedure using a computer simulated search program in order to reproduce the excitation energies ($2_1^+, 4_1^+, 6_1^+, 8_1^+, 0_2^+, 2_3^+, 4_3^+, 2_2^+, 3_1^+$ and 4_2^+) and the two neutron separation energies in all nuclei in each isotopic chain. Calculated potential energy surface (PES'S) describing all deformation effects of each nucleus have been extracted. Our systematic studies on Gd / Dy chains have revealed a shape transition from spherical vibrator to axially deformed rotor when moving from the lighter to heavier isotopes.

1 Introduction

Recent developments in nuclear structure have brought considerable focusing on the problems of shape phase transition and shape coexistence phenomena [1]. For instance, several isotopes have been found to undergo shape phase evolution of first order from spherical vibrator to deformed axially symmetric rotor [2–6] and phase transition of second order from spherical vibrator to deformed γ - soft [7–9]. The study of shape phase transitions in nuclei was best done by using the interacting boson model (IBM) [10]. The original version of IBM (IBM-1) includes s and d bosons, it defines six-dimensional space and this leads to a description in terms of a unitary group U(6). Three dynamical symmetries in the IBM-1 were shown [11]: the U(5) symmetry corresponding to spherical oscillator, the SU(3) symmetry corresponding to deformed axially rotor and the O(6) symmetry corresponding to the γ - soft asymmetric rotor shapes. These three symmetry limits from a triangle known as a Casten triangle that represents the nuclear phase diagram [12]. The X(5) critical point symmetry [13] has been found to correspond to the first order transition between U(5) and SU(3), while the E(5) critical point symmetry [14] has been found to correspond to the second order transition between U(5) and O(6).

In the previous paper [3], we used the flexible and powerful geometric collective model (GCM) [3, 15–18] to describe the quantum phase transition between spherical and deformed shapes for doubly even nuclei in lanthanide and actinide isotopes chains. The potential energy surfaces (PES'S) describing all deformed effects of each nucleus were extracted in terms of the intrinsic shape parameters β and γ. The parameter β is related to the axial deformation of the nucleus, while γ measure the deviation from axial symmetry. In the present work, it is of interest to examine the GCM in investigating the shape transition from spherical vibrator to axially deformed rotor for Gd and Dy isotopic chains by analyzing the PES'S. In section 2, we construct the GCM Hamiltonian and its eigenfunction. In section 3, we generated the PES'S to classify shape phase transitions and to decide if a nucleus is close to criticality. In section 4, we applied our model to the rare earth Gd / Dy isotopic chains which evolve a rapid structural charges from spherical to well-deformed nuclei when moving from lighter to the heavier isotopes.

2 The GCM Hamiltonian and eigenstates

In GCM, the Hamiltonian of the nucleus, in appropriate units, can be expressed as a series expansion in terms of the surface deformation coordinates α and the conjugate momenta π as [3]:

$$\begin{aligned} H = & \frac{1}{2B_2}[\pi\times\pi]^{(0)} + C_2[\alpha\times\alpha]^{(2)} \\ & + C_3[[\alpha\times\alpha]^{(2)}\times\alpha]^{(0)} \\ & + C_4[\alpha\times\alpha]^{(0)}[\alpha\times\alpha]^{(0)} \end{aligned} \tag{1}$$

The eigenstates of the the Hamiltonian 1 associated with the number ν of quanta and definite seniority λ, angular momentum L and projection M can be denoted by the Ket

$$|\nu\lambda\mu LM\rangle = F_\ell^\lambda(\beta)\sum_k \varphi_k^{\lambda\mu L}(\gamma)D_{Mk}^{L_*}(\omega_i) \tag{2}$$

where

$$\ell = \frac{1}{2}(\nu-\lambda) \tag{3}$$

and μ indicates the remaining quantum numbers required to fully characterize the states of the Hamiltonian 1. ω_i are the Euler angles, β and γ are the intrinsic coordinates. $D_{Mk}^{L_*}(\omega_i)$ are the Wigner functions that are the irreducible representation of the O(3) group.

In equation 2 $F_\ell^\lambda(\beta)$ are functions of β associated with the radial part of a five-dimensional oscillator

$$\begin{aligned} F_\ell^\lambda(\beta) = & \left[\frac{2(n_i)}{\Gamma(n+\lambda+\frac{5}{2})}\right]^{1/2}\left(\frac{C_2}{\hbar\omega}\right)^{\frac{5}{4}+\frac{\lambda}{2}}\beta^\lambda \\ & \cdot L_n^{\lambda+\frac{3}{2}}\cdot\left(\left(\frac{C_2}{\hbar\omega}\right)\beta^2\right)e^{-\frac{1}{2}\frac{C_2}{\hbar\omega}\beta^2} \end{aligned} \tag{4}$$

where $L_n^{\lambda+\frac{3}{2}}$ are the well-known Laguerre polynomials and the function is normalized for the volume element $\beta 4 d\beta$. The γ-dependent functions $\varphi_k^{\lambda\mu L}$ satisfy the differential equation

$$\Lambda^2 \varphi_k^{\lambda\mu L} = \lambda(\lambda+3)\varphi_k^{\lambda\mu L} \tag{5}$$

where Λ^2 is the seniority operator (Casimir operator of O(5)) which has the form

$$\Lambda^2 = -\frac{1}{\sin 3\gamma}\frac{\partial}{\partial\gamma} + \sum_{k=1}^{3} I_k^{-1}\grave{L}_k^2(\omega_i) \tag{6}$$

with

$$I_k = 4B_2 \sin^2\left(\gamma - \frac{2\pi}{3}k\right) \tag{7}$$

I_k are the moments of inertia with respect to the principle axes. For arbitrary angular momentum L and λ , $\varphi(\gamma)$ reads

$$\varphi_{\grave{k}}^{\lambda+2,\mu,L+2}(\gamma) = \sum_k \varphi_{k,\bar{k}}^{\lambda LL+2}\left(\gamma, \frac{\partial}{\partial\gamma}\right)\varphi_k^{\lambda\mu L}(\gamma) \tag{8}$$

$$\varphi_{\bar{k}}^{\lambda+2,\mu,L+2}(\gamma) =$$

$$= \sum_{\bar{L}\bar{k}k}\left(\sqrt{35(2\bar{L}+1)}W(L,L+2,2,2,2\bar{L}) \times \right. \tag{9}$$

$$\left. Q_{\bar{k},\grave{k}}^{\lambda+1,\bar{L},L+2}\left(\gamma, \frac{\partial}{\partial\gamma}\right) Q_{k,\bar{k}}^{\lambda,L,\bar{L}}\left(\gamma, \frac{\partial}{\partial\gamma}\right)\varphi_k^{\lambda\mu L}(\gamma)\right)$$

where W is a Racah coefficient and $Q_{k,\bar{k}}^{\lambda,L,\bar{L}}(\gamma, \frac{d}{d\gamma})$ is an operator function of γ and $\frac{d}{d\gamma}$.

3 Potential energy surfaces (PES'S) and critical point symmetries

The PES depends only upon the shape of the nucleus not it orientation in space, and can thus be expressed purely in terms of the shape coordinates β and γ as [3]:

$$V(\beta,\gamma) = C_2\frac{1}{\sqrt{5}}\beta^2 - C_3\sqrt{\frac{2}{35}}\beta^3\cos 3\gamma + C_4\frac{1}{5}\beta^4 \tag{10}$$

where $\beta \in [0,\infty]$ and $\gamma \in [0, 2\pi/3]$

The equilibrium shape associated to the GCM Hamiltonian can be obtained by determining the minimum of energy surface with respect to the geometric variables β and γ, i.e the first derivative vanish. Since the parameter C_2 controls the steepness of the potential, and therefore, the dynamical fluctuations in γ, it strongly affects the energies of excited intrinsic states. The parameter $C_3 = 0$ gives a γ-flat potential and an increase of C_3 introduces a γ-dependence the potential with a minimum at $\gamma = 0$. Changing C_3 will indeed induce a γ-unstable to symmetric rotor transition, it is best to simultaneously vary C_2 and C_4 as well. The shape transition from vibrator to rotor is achieved by starting from the vibrator limit, lowering C_2 from positive to negative value, increasing C_4 to large positive value, which gradually increasing C_3 (lowering C_2 from positive to negative value, introducing a large positive C_4 and a positive C_3).

4 Numerical results applied to Gd and Dy isotopes chains

The N = 90 isotones ^{154}Gd [15, 16] and ^{156}Dy [17, 18] were seen to provide good example to transition from spherical to axially deformed. In our calculation we will examine and systematically study the lanthanide $^{148-162}$Gd and $^{150-164}$Dy isotopes because of the richness of available experimental data indicating a transition of nuclear shapes from spherical to deformed form. The ground band levels are shown in Figure (1). We can see that the energy values for each spin states in lanthanide change almost linearly for $N \leq 88$ and become quite flat for N ≥ 90. This is consistent with the onset of the Z = 64 sub-shell effect. For actinide the energy levels become flat for N ≥ 144. The optimized model parameters for each nucleus was adjusted by fitting procedure using a computer simulated search program in order to describe the gradual change in the structure as neutron number varied and to reproduce the properties of the selected reliable state of positive parity excitation ($2_1^+, 4_1^+, 6_1^+, 8_1^+, 0_2^+, 2_3^+, 4_3^+, 2_2^+, 3_1^+$ and 4_2^+) and the two neutron separation energies of all isotopes in each isotopic chain. The resulting parameters are listed explicitly in Tables (1).

For the isotopic chains investigated here, the collective properties are illustrated by represented the calculated potential energy surface (PES) describing all deformation effects of the nucleus. We investigated the change of nuclear structure

Table 1: The GCM parameters as derived in fitting procedure used in the calculation of the Gd and Dy isotopes.

Nucleus	C_2	C_3	C_4
^{148}Gd	16.53067	1.48970	-34.76151
^{150}Gd	9.79566	11.28331	-5.21603
^{152}Gd	-26.55250	53.24420	138.12500
^{154}Gd	-71.41529	104.21630	313.83380
^{156}Gd	-91.19133	127.81150	392.95380
^{158}Gd	-101.97220	141.63350	437.50440
^{160}Gd	-111.19320	153.76500	476.06680
^{162}Gd	-120.17800	165.64110	513.72330
^{150}Dy	18.56558	1.70251	-38.99710
^{152}Dy	10.69898	12.69373	-5.14990
^{154}Dy	-29.90650	59.16022	154.37500
^{156}Dy	-79.02660	114.63790	346.26770
^{158}Dy	-99.93424	139.43080	429.68950
^{160}Dy	-110.88850	153.43620	474.89930
^{162}Dy	-120.13350	165.59310	513.55260
^{164}Dy	-129.12150	177.47260	551.221306

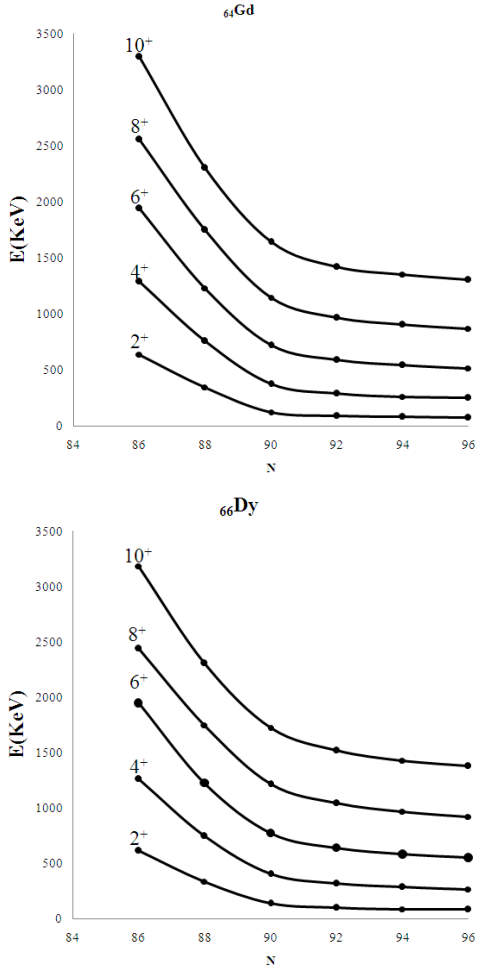

Fig. 1: Systematics of low-lying yrast level energies in even-even lanthanides Gd/Dy isotopes. The $2^+, 4^+, ...10^+$ level energies are plotted. The states are labeled by I^π.

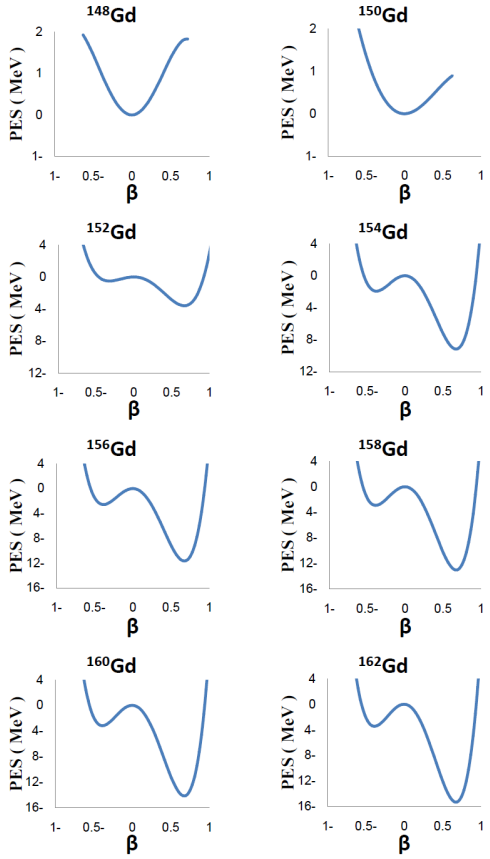

Fig. 2: Potential energy surface (PES) calculated with GCM as a function of the shape parameter β for shape phase transition from spherical to prolate deformed for Gadolinium isotope chain $^{148-162}_{64}$Gd.

within these chains as illustrated in Figures (2, 3). The PES's versus the deformation parameter β for lanthanide isotopic chains of nuclei evolving from spherical to axially symmetric well deformed nuclei. We remark that for all mentioned nuclei, the PES is not flat, exhibiting a deeper minimum in the prolate ($\beta > 0$) region and a shallower minimum in the oblate ($\beta < 0$) region. Relatively flat PES occur for the N = 86 nuclei ^{150}Gd and ^{152}Dy. A first order shape phase transition with change in number of neutrons when moving from the lighter to heavier isotopes, i.e U(5) - SU(3) transitional region are observed.

The present result for ^{154}Gd is in good agreement with Nilsson-Strutinsky BCS calculations [18]. However, the existence of a bump in the PES is related to the success of the confined γ-soft (BCS) rotor model [19], employing an infinite square well potential displaced from zero, as well as to the relevance of Davidson potentials [20–22]. It also be related to the significant five-dimensional centrifugal effect [22–25].

5 Conclusion

In the present paper exact numerical results of GCM Hamiltonian along the shape phase transition line from harmonic spherical vibrator shape to axially deformed rotor shape are obtained. A systematic study of even-even $^{148-162}$Gd and $^{150-164}$Dy isotopes chains in the lanthanide region is presented. For each nucleus the GCM parameters C_2, C_3, C_4 were optimized to fit the energy ratios between selected low-lying states. The geometric character of the nuclei has been visualized by plotting the PES'S obtained from the GCM Hamiltonian. In these chains, nuclei evolve from spherical to prolate axially deformed rotor when moving from the lighter to the heavier isotopes. Also we have analyzed the critical points of the shape phase transition in the space of the GCM parameters C_2, C_3 and C_4.

Submitted on: July 25, 2013 / Accepted on: August 02, 2013

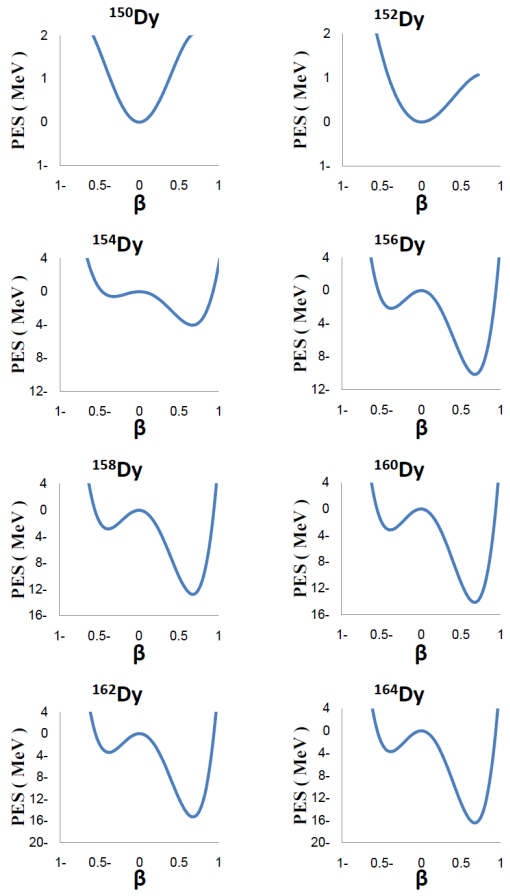

Fig. 3: Potential energy surface (PES) calculated with GCM as a function of the shape parameter β for shape phase transition from spherical to prolate deformed for Dysprosium isotope chain $^{150-164}_{66}$Dy.

References

1. Iachello F. and Zamfir N.V. Quantum Phase Transitions in Mesoscopic Systems. *Physical Review Letters*, 2004, v. 92(3), 212501–212505.
2. Khalaf A.M. and Awwad T.M. A Theoretical Description of U(5)-SU(3) Nuclear Shape Transitions in the Interacting Boson Model. *Progress in Physics*,2013, v. 1, 7–11.
3. Khalaf A.M. and Ismail A.M. The Nuclear Shape Phase Transitions Studied Within the Geometric Collective Model. *Progress in Physics*, 2013, v. 2, 51–55.
4. Khalaf A.M. and Ismail A.M. Structure Shape Evolution in Lanthanide and Actinide Nuclei. *Progress in Physics*, 2013, v. 2, 98-104.
5. Rosensteel G and Rowe D.J. Phase Transitions and Quasidynamical Symmetry in Nuclear Collective Models, III: The U(5) to SU(3) Phase Transition in the IBM. *Nuclear Physics*, 2005, v. A759, 92–128.
6. Liu Y.X., Mu L.Z. and Wei H. Approach to The Rotation Driven Vibrational to Axially Rotational Shape Phase Transition Along The Yrast Line of a Nucleus. *Physics Letters*, 2006, v. B633, 49–53.
7. Heinze S. et al. Evolution of spectral properties along the O(6)-U(5) transition in the interacting boson model. I. Level dynamics. *Physical Review*, 2006, v. C76, 014306–014316.
8. Zhang Y., Hau Z. and Liu Y.X. Distinguishing a First Order From a Second Order Nuclear Shape Phase Transition in The Interacting Boson Model. *Physical Review*, 2007, v. C76, 011305R–011308R.
9. Casten R.F. and Zamfir N.V. Evidence for a Possible E(5) Symmetry in 134Ba. *Physical Review Letters*, 2000, v. 85, 3584–3586, Casten R.F. and Zamfir N.V. Empirical Realization of a Critical Point Description in Atomic Nuclei. *Physical Review Letters*, 2001, v. 87, 052503–052507.
10. Iachello F. and Arima A. The Interacting Boson Model. Cambridge University Press, Cambridge, England, 1987.
11. Arima A. and Iachello F. Interacting Boson Model of Collective States I. The Vibrational Limit. *Annals of Physics*, 1976,(N.Y.) v. 99, 253–317, Arima A. and Iachello F. Interacting Boson Model of Collective States II. The Rotational Limit. *Annals of Physics*, 1978,(N.Y.) v. 111, 201–238.
12. Casten R.F. Nuclear Structure from a Simple Prespective. Oxford University, Oxford, 1990.
13. Iachello F. Analytic Prescription of Critical Point Nuclei in a Spherical Axially Deformed Shape Phase Transtion. *Physical Review Letters*, 2001, v. 87, 052502–052506.
14. Iachello F. Dynamic Symmetries at The Critical Point. *Physical Review Letters*, 2000, v. 85 3580–3583.
15. Tonev D. et al. Transition Probabilities in 154Gd: Evidence for X(5) Critical Point Symmetry. *Physical Review*, 2004, v. C69, 034334–034339.
16. Dewald A. et al. Shape changes and test of the critical-point symmetry X(5) in N = 90 nuclei. *The European Physical Journal*, 2004, v. A20, 173–178.
17. Caprio M.A. et al. Low-Spin Structure of 156Dy Through -ray Spectroscopy. *Physical Review*, 2002, v. C66, 054310–054328.
18. Zhang J.Y. et al. Phase/shape coexistence in 152Sm in the geometric collective model. *Physical Review*, 1999, v. C60, 061304R–061308R.
19. Turken N. and Inci I. Comparing some predictions between Davidson-like potentials and interacting boson model: X(5) behavior of even-even 128-140Nd isotopes. *Physics of Atomic Nuclei*, 2008, v. 71, 1918–1925.
20. Bonatsos D. et al. Ground state bands of the E(5) and X(5) critical symmetries obtained from Davidson potentials through a variational procedure. *Physics Letters*, 2004, v. B584, 40–47.
21. Bonatsos D. et al. E(5) and X(5) Critical Point Symmetries Obtained From Davidson Potentials Through a Variational Procedure. *Physical Review*, 2004, v. C70, 024305–024314.
22. Caprio M.A. Effects of $\beta - \gamma$ coupling in transitional nuclei and the validity of the approximate separation of variables. *Physical Review*, 2005, v. C72, 054323–054333.
23. Rowe D.J. A computationally tractable version of the collective model. *Nuclear Physics*, 2004, v. A735, 372–392.
24. Rowe D.J., Turner P.S. and Repka J. Spherical harmonics and basic coupling coefficients for the group SO(5) in an SO(3) basis. *Journal of Mathematical Physics*, 2004, v. 45, 2761–2784.
25. Rowe D.J. and Turner P.S. The Algebraic Collective Model. *Nuclear Physics*, 2005, v. A753, 94–105.

Nuclear Potential Energy Surfaces and Critical Point Symmetries within the Geometric Collective Model

Khalaf A.M.[1], Aly H.F.[2], Zaki A.A.[2] and Ismail A.M.[2,3]

[1]Physics Department, Faculty of Science, Al-Azhar University, Cairo, Egypt. E-mail: ali_khalaf43@hotmail.com
[2]Hot Laboratories Center, Atomic Energy Authority, P.No. 13759, Cairo, Egypt.
[3]Physics Department, Faculty of Science and Arts, Bukairiyah, Qassim University, Kingdom Saudi Arabia.
Corresponding Author: E-mail: dr_ahmedph@yahoo.com

The critical points of potential energy surface (PES's) of the limits of nuclear structure harmonic oscillator, axially symmetric rotor and deformed γ-soft and discussed in framework of the general geometric collective model (GCM). Also the shape phase transitions linking the three dynamical symmetries are studied taking into account only three parameters in the PES's. The model is tested for the case of $^{238}_{92}$U , which shows a more prolate behavior. The optimized model parameters have been adjusted by fitting procedure using a simulated search program in order to reproduce the experimental excitation energies in the ground state band up to 6^+ and the two neutron separation energies.

1 Introduction

Shape phase transitions from one nuclear shape to another were first discussed in framework of the interacting boson model (IBM) [1]. The algebraic structure of this model is based upon U(6) and three dynamical symmetries arise involving the sub algebras U(5), SU(3) and O(6). There have been numerous recent studies of shape phase transitions between the three dynamical symmetries in IBM [2–9]. The three different phases are separated by lines of first-order phase transition, with a singular point in the transition from spherical to deformed γ-unstable shapes, which is second order. In the usual IBM-1 no triaxial shape appears.

Over the years, studies of collective properties in the framework of geometric collective model (GCM) [3, 10–12] have focused on lanthanide and actinide nuclei. In GCM the collective variables β (the ellipsoidal deformation) and γ (a measure of axial asymmetry) are used. The characteristic nuclear shapes occuring in the GCM are shown in three shapes which are spherical, axially symmetric prolate deformed (rotational) and axial asymmetry (γ -unstable). The shape phase transitions between the three shapes have been considered by the introduction of the critical point symmetries E(5) [13] and X(5) [14]. The dynamical symmetry E(5) describe the phase transition between a spherical vibrator (U(5)) and γ-soft rotor (O(6)) and the X(5) for the critical point of the spherical to axially deformed (SU(3)) transition. Also the critical point in the phase transition from axially deformed to triaxial nuclei, called Y(5) has been analyzed [15].

The main objective of this study is to analyze the importance of the critical points in nuclear shapes changes. The paper is organized as follows. In sec. 2 we survey the framework of the GCM and the method to analyze the PES's in terms of the deformation variables β and γ. In section 3 we study the behavior of the critical point. In section 4 we present the numerical result for realistic case to even-even ^{238}U nucleus and give some discussions. Finally in section 5, the conclusions of this work are made.

2 Potential Energy Surfaces in Geometric Collective Model

We start by writing the GCM Hamiltonian in terms of irreducible tensor operators of collective coordinates α's and conjugate momenta π as:

$$\begin{aligned} H = \frac{1}{2B_2}[\pi\times\pi]^{(0)} + C_2[\alpha\times\alpha]^{(2)} \\ + C_3[[\alpha\times\alpha]^{(2)}\times\alpha]^{(0)} \\ + C_4[\alpha\times\alpha]^{(0)}[\alpha\times\alpha]^{(0)} \end{aligned} \quad (1)$$

where B_2 is the common mass parameter of the kinetic energy term and C_2, C_3 and C_4 are the three stiffness parameters of collective potential energy. They are treated as adjustable parameters which have to be determined from the best fit to the experimental data, level energies, B(E2) transition strengths and two-neutron separation energy. The corresponding collective potential energy surface (PES) is obtained by transforming the collective coordinate $a_{2\nu}$ into the intrinsic coordinate $a_{2\nu}$. To separate the three rotational degree of freedom one only has to set

$$\alpha_{2\mu} = \sum_{\nu} D^{*2}_{\mu\nu}(\omega) a_{2\nu}. \quad (2)$$

Since the body axes are principle axes, the products of inertia are zero, which implies that $a_{21} = a_{2-1} = 0$ and $a_{22} = a_{2-2}$. The two remaining variables a_{20} and a_{22}, to gather with Eulerian angles ω, would completely describe the system replacing the five $\alpha_{2\mu}$. However, there is rather more direct physical significance in the variables β and γ defined by

$$a_{20} = \beta\cos\gamma \quad (3)$$

$$a_{22} = \frac{1}{\sqrt{2}}\beta \sin\gamma \tag{4}$$

where β is a measure of the total deformation of the nucleus and γ indicate the deviations from axial symmetry. In terms of such intrinsic parameters, we have

$$[\alpha \times \alpha]^{(0)} = \frac{\beta^2}{\sqrt{5}} \tag{5}$$

$$[[\alpha \times \alpha]^{(2)} \times \alpha]^{(0)} = -\sqrt{\frac{2}{35}}\,\beta^3 \cos 3\gamma. \tag{6}$$

The PES belonging to the Hamiltonian (1) then reads

$$E(\beta,\gamma) = C_2 \frac{1}{\sqrt{5}}\beta^2 - C_3\sqrt{\frac{2}{35}}\beta^3 \cos 3\gamma + C_4 \frac{1}{5}\beta^4. \tag{7}$$

The values of β and γ are restricted to the intervals $0 \le \beta \le \infty$, $0 \le \gamma \le \pi/3$. In other words the $\pi/3$ sector of the $\beta\gamma$ plane is sufficient for the study of the collective PES's.

3 Critical Point Symmetries

Minimization of the PES with respect to β gives the equilibrium value β_m defining the phase of the system. $\beta_m = 0$ corresponding to the symmetric phase and $\beta_m \neq 0$ to the broken symmetry phase. Since γ enters the potential (7) only through the $\cos 3\gamma$ dependence in the cubic term, the minimization in this variable can be performed separately. The global minimum is either at $\gamma_m = 0(2\pi/3, 4\pi/3)$ for $C_3 > 0$ or at $\gamma_m = \pi/3(\pi, 5\pi/3)$ for $C_3 < 0$. The second possibility can be expected via changing the sign of the corresponding β_m and simultaneously setting $\gamma_m = 0$. The phase can be described as follows:

1. For $C_3^2 < \frac{14C_2|C_4|}{\sqrt{5}}$, phase with $\beta_m = 0$ interpreted as spherical shape.
2. For $C_3^2 < \frac{14C_2|C_4|}{\sqrt{5}}, C_3 > 0$, phase with $\beta_m > 0, \gamma_m = 0$ interpreted as prolate deformed shape.
3. For $C_3^2 < \frac{14C_2|C_4|}{\sqrt{5}}, C_3 < 0$, phase with $\beta_m > 0, \gamma_m = \pi/3$ interpreted as oblate deformed shape.

For β non-zero the first derivative of equation (7) must be zero and the second derivative positive. This gives

$$\begin{aligned} \frac{4}{5}C_4\beta^2 - 3\sqrt{\frac{2}{35}}\,C_3\beta^3\cos 3\gamma + \frac{2}{\sqrt{5}}\,C_2 &= 0 \\ \frac{12}{5}\,C_4\beta^2 - 6\sqrt{\frac{2}{35}}\,C_3\beta^3\cos 3\gamma + \frac{2}{\sqrt{5}}\,C_2 &> 0 \end{aligned} \tag{8}$$

The solution of equation (8), yields $\beta_\pm = \frac{3}{4}\sqrt{\frac{5}{14}}(1 \pm r)e$ with $r = \sqrt{1-d}$, $d = \frac{112}{9\sqrt{5}}\frac{C_2C_4}{C_3^2}$ and $e = \frac{C_3}{C_4}$.

The minimum values of the potential are

$$E(\beta) = -\frac{135}{50176}(r \pm 1)^3(3r \mp 1)f \tag{9}$$

with $f = \frac{C_3^4}{C_4^3}$.

For $d > 1$ there is only one minimum located at $\beta = 0$. For $0 < d < 1$, minima are present both at non-zero β and at $\beta = 0$, with the deformed minimum lower $0 < d < 8/9$ and the undeformed minimum lower for $8/9 < d < 1$. For $d < 0$, the potential has both a global minimum and a saddle point at non-zero β. For harmonic vibrator shape $C_3 = C_4 = 0$, this yields

$$E(\beta) = \frac{C_2}{\sqrt{5}}\beta^2, \qquad C_2 > 0. \tag{10}$$

For γ-unstable shape, the solution for$\beta \neq 0$ are obtained if we set $C_3 = 0$ in equation (8). Then equation (8) gives

$$\frac{4}{5}C_4\beta^2 + \frac{2}{\sqrt{5}}\,C_2 = 0$$

or

$$\beta = \pm\sqrt{\frac{-\sqrt{5}}{2}\frac{C_2}{C_4}} \simeq \pm 1.057\sqrt{\frac{-C_2}{C_4}};$$

this requires C_4 and C_2 to have opposite sign. Since C_4 must be positive for bound solutions C_2 must be negative in deformed γ-unstable shape. That is the spherical — deformed phase transition is generated by a change in sign of C_2, while the prolate-oblate phase is corresponding to changing the sign of C_3. For symmetric rotor one needs with both a deformed minimum in β and a minimum in γ, at $\gamma = 0$ for prolate or $\gamma = \pi/3$ for oblate. For prolate shape this requires $C_3 > 0$, such a potential has a minimum in β at $\beta_\pm$ equation (7). For $\gamma = 0$ (to study the β-dependence), and providing that $C_2 > 0$ and $C_3 > 0$, then the critical point is located at $C_3^2 < 14C_2|C_4|/\sqrt{5}$.

In Fig. (1a) a typical vibrator is given, the minimum of the PES is at $\beta = 0$ and therefore the ground state is spherical. In

Table 1: The GCM parameters for shape-phase transition (a) from vibrator to rotor (b) from rotor to γ-soft.

	C_2	C_3	C_4
set (a)	1	0	0
	-0.25	0.7	10
	-1	1	20
	-2.5	1.7	29
set (b)	-3	2	40
	-4.2	1.5	80
	-4.5	1	120
	-5	0	170

Fig. (1b) a typical axially deformed prolate is given, where the minimum it as $\beta \neq 0$ and the ground state is deformed. In Fig. (1c) a case of γ-unstable shape is illustrated. Fig. (2a) gives the PES's calculated with GCM as a function of the shape poor rotor β for shape phase transition from spherical to prolate deformed and in Fig. (2b) from rotor to γ-soft. The model parameters are listed in Table (1).

For simplicity we write equation (7) when $\gamma = 0$ in form

$$E(\beta) = A_2\beta^2 + A_3\beta^3 + A_4\beta^4. \quad (11)$$

The extremism structure of the PES depends only upon the value A_2 as summarized in Table (2) and Fig. (3). For $A_2 < 0$ the potential has both a global minimum and a saddle point at non-zero β. For $A_2 > 0$, minima are present at both $\beta \neq 0$ and $\beta = 0$ with the deformed minimum lower for $A_2 = 109.066$ and the undeformed minimum lower for $A_2 = 161.265$. For $A_2 = 22.6$ there is only one minimum located at $\beta = 0$.

4 Application to $^{238}_{92}$U

We applied the GCM to the doubly even actinide nucleus ^{238}U. The optimized model parameter was adjusted by fitting procedure using a computer simulated search program in order to reproduce some selected experimental excitation energies $(2_1^+, 4_1^+, 6_1^+)$ and the two neutron separation energies. The PES versus the deformation parameter β for ^{238}U is illustrated in Fig. (4). The figure show that ^{238}U exhibit a deformed prolate shape.

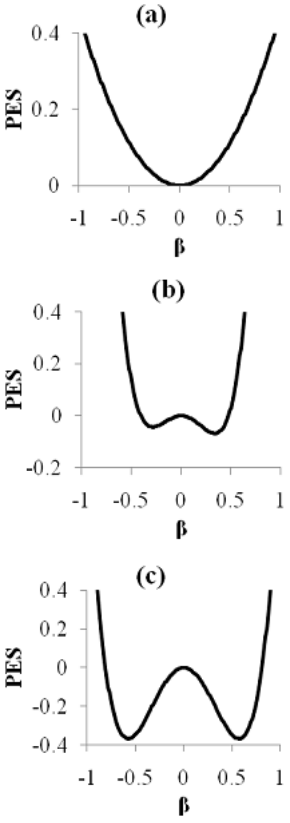

Fig. 1: Potential energy surface (PES's) in framework of GCM for three different shapes (a) harmonic vibrator shape ($C_2 = 1$, $C_3 = 0$, $C_4 = 0$) (b) strongly axially deformed prolate shape ($C_2 = -2.5$, $C_3 = 1.7$, $C_4 = 29$) (c) γ-unstable shape ($C_2 = -5$, $C_3 = 0$, $C_4 = 17$).

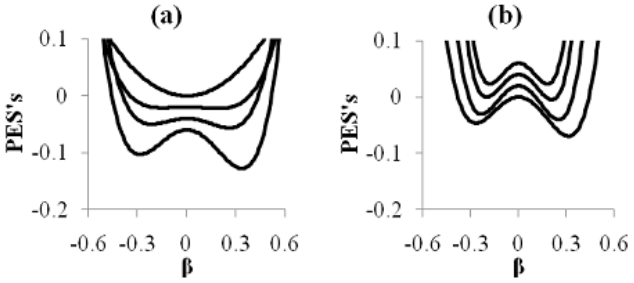

Fig. 2: Potential energy surface (PES's) in framework of GCM for two different shape transitions (a) from vibrator to rotor (b) from rotor to γ-soft rotor the set of parameters are listed in Table (1).

Table 2: Set of control parameters of the GCM to describe the nature of the critical points.

A_2	A_3	A_4
22.600	-1.120	0.234
66.412	-294.869	368.217
161.265	-935.148	1148.890
85.714	-573.709	960.000
109.066	-881.661	1603.589
0.000	-152.991	387.884
-15.581	-48.791	214.854
-22.098	-3.286	137.500

5 Conclusion

In this study we used the GCM to produce the PES's to investigate the occurrence of shape phase transitions. The critical point symmetries are obtained. The validity of the model is examined for ^{238}U. A fitting procedure was proposed to deforming the parameters of the geometric collective Hamiltonian for the axially symmetric deformed rotor.

Submitted on: September 21, 2013 / Accepted on: September 26, 2013

References

1. Iachello F. and Arima A. The Interacting Boson Model. Cambridge University Press, Cambridge, England, 1987.
2. Khalaf A.M. and Awwad T.M. A Theoretical Description of U(5)-SU(3) Nuclear Shape Transitions in the Interacting Boson Model. *Progress in Physics*, 2013, v. 1, 7–11.
3. Khalaf A.M. and Ismail A.M. The Nuclear Shape Phase Transitions Studied Within the Geometric Collective Model. *Progress in Physics*, 2013, v. 2, 51–55.

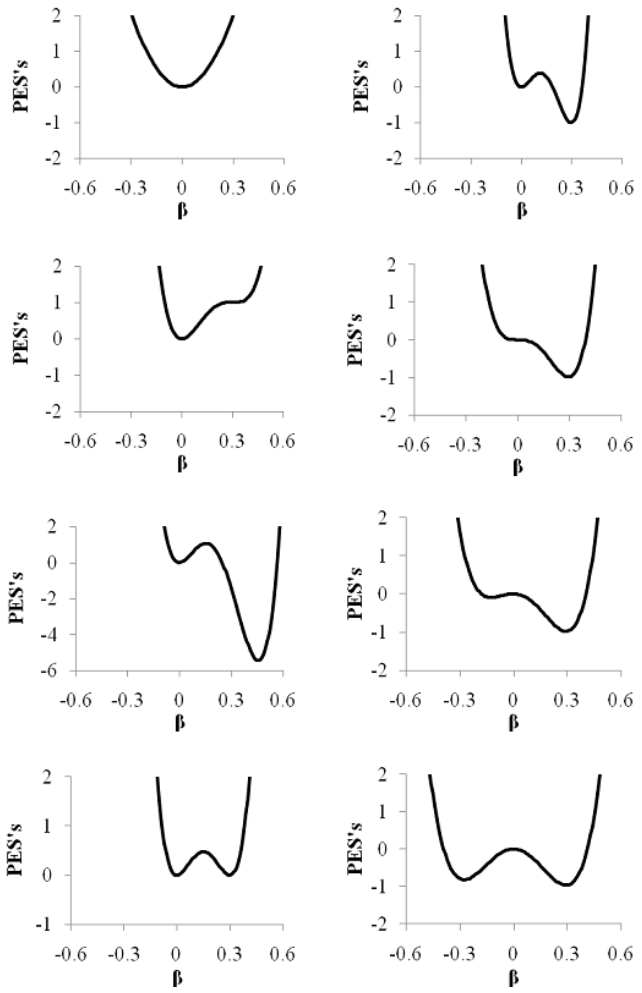

Fig. 3: Different shapes of PES's by varying the control parameters listed in Table (2).

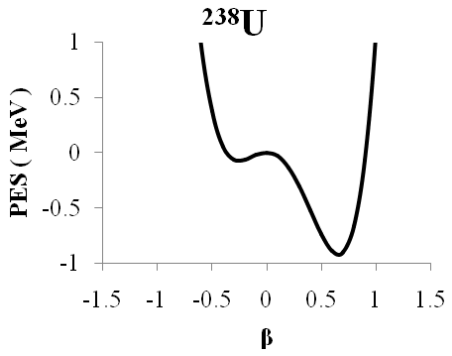

Fig. 4: The Potential energy surface (PES) as a function of deformation parameter β for ^{238}U and a cut through $\gamma = 0$ and $\gamma = \Pi/3$ are given with the parameters ($C_2 = -6.23928$, $C_3 = 18.63565$, $C_4 = 41.51437$).

4. Khalaf A.M. and Ismail A.M. Structure Shape Evolution in Lanthanide and Actinide Nuclei. *Progress in Physics*, 2013, v. 2, 98-104.

5. Zhang Y., Hau Z. and Liu Y.X. Distinguishing a First Order From a Second Order Nuclear Shape Phase Transition in The Interacting Boson Model. *Physical Review*, 2007, v. C76, 011305R–011308R.

6. Heinze S. et al. Evolution of spectral properties along the O(6)-U(5) transition in the interacting boson model. I. Level dynamics. *Physical Review*, 2006, v. C76, 014306–014316.

7. Liu Y.X., Mu L.Z. and Wei H. Approach to The Rotation Driven Vibrational to Axially Rotational Shape Phase Transition Along The Yrast Line of a Nucleus. *Physics Letters*, 2006, v. B633, 49–53.

8. Rosensteel G and Rowe D.J. Phase Transitions and Quasidynamical Symmetry in Nuclear Collective Models, III: The U(5) to SU(3) Phase Transition in the IBM. *Nuclear Physics*, 2005, v. A759, 92–128.

9. Casten R.F. and Zamfir N.V. Evidence for a Possible E(5) Symmetry in 134Ba. *Physical Review Letters*, 2000, v. 85, 3584–3586, Casten R.F. and Zamfir N.V. Empirical Realization of a Critical Point Description in Atomic Nuclei. *Physical Review Letters*, 2001, v. 87, 052503–052507.

10. Gneuss G., Mosel U. and Greiner W. A new treatment of the collective nuclear Hamiltonian. *Physics Letters*, 1969, v. B30, 397–399, Gneuss G., Mosel U. and Greiner W. On the relationship between the level-structures in spherical and deformed nuclei. *Physics Letters*, 1970, v. B31, 269–272.

11. Gneuss G. and Greiner W. Collective potential energy surfaces and nuclear structure. *Nuclear Physics*, 1971, v. A171, 449–479.

12. Troltenier D. Das Generalisierte Kollektivmodell. Frankfurt am Main, Germany, Report No. GSI-92-15, 1992.

13. Iachello F. Dynamic Symmetries at The Critical Point. *Physical Review Letters*, 2000, v. 85, 3580–3583.

14. Iachello F. Analytic Prescription of Critical Point Nuclei in a Spherical Axially Deformed Shape Phase Transtion. *Physical Review Letters*, 2001, v. 87, 052502–052506.

15. Iachello F. Phase Transitions in Angle Variables. *Physical Review Letters*, 2003, v. 91, 132502–132505.

Dynamical 3-Space: Observing Gravitational Wave Fluctuations and the Shnoll Effect using a Zener Diode Quantum Detector

David P. Rothall and Reginald T. Cahill

School of Chemical and Physical Sciences, Flinders University, Adelaide 5001, Australia
E-mail: David.Rothall@flinders.edu.au, Reg.Cahill@flinders.edu.au

Shnoll has investigated the non-Poisson scatter of measurements in various phenomena such as biological and chemical reactions, radioactive decay, photodiode current leakage and germanium semiconductor noise, and attributed the scatter to cosmophysical factors. A more recent model of reality leads to a description of space which is dynamic and fractal and exhibits reverberation effects, and which offers an explanation for the scatter anomaly. This paper is a correction to the work presented earlier which used data from a RF coaxial cable experiment, but had insufficient timing resolution to show the full effects of what Shnoll observed. Here we report a different way to produce the effects through studying current fluctuations in reverse biased zener diode gravitational wave detector with better timing resolution. The current fluctuations have been shown to be caused by dynamical 3-space fluctuations/turbulence, namely gravitational waves.

1 Introduction — Shnoll effect

For over half a century Simon Shnoll has studied the non-Poisson scatter anomalies in various phenomena such as biological and chemical reactions, radioactive decay, photodiode current leakage and germanium semiconductor noise. An example of this is Fig. 1, which shows a layered histogram of some 352,980 successive measurements of the α decay rate of a ^{239}Pu source [1] undertaken by Shnoll between May 28 — June 01, 2004. The layer lines taken every 6000 successive measurements show a fine structure which builds up over time instead of cancelling out as in the case of a typical random or Poisson distribution. This suggests that the radioactivity of ^{239}Pu takes on discrete (preferred) values, and is not completely random. It should be clarified here that the effects Shnoll studied in depth were those concerning the shapes of histograms taken using fewer measurements (usually between 60 and 100) instead of that of the non-Poisson scatter of measurements taken over a much larger data set as discussed in our previous paper [2]. Shnoll found that the shapes of histograms from either the same or different experiments correlated via both absolute (same time) and local (time delay due to Earth's rotation) time synchronism and that the phenomenon causing this had a fractal nature. Shnoll attributed the cause of this to cosmophysical factors, i.e. inhomogeneities in the "space-time continuum" [1, 4]. These inhomogeneities are "caused by the movement of an object in the inhomogeneous gravitational field", e.g. as the Earth rotates/orbits the Sun, as the moon orbits the Earth etc. While these inhomogeneities were not characterised by Shnoll there is a remarkable amount of evidence supporting this conclusion [1]. An experiment which studied the phase difference of two RF signals traveling through two coaxial cables [5] was reported to show similar non-Poisson characteristics to that of ^{239}Pu decay shown in Fig. 1.

An alternative model of reality leads to a description of space which is dynamic and fractal. The RF coaxial cable propagation experiment can be used to characterise gravitational waves. However the resolution of the data in the coaxial cable experiment proved to be insufficient to study changes in histogram shapes. It is reported here that a newer technique which studies the non-Poisson characteristics of the current fluctuations in zener diodes and may be used to study gravitational waves. This technique allows for faster recording of data (every second instead of every 5 seconds) and used much higher digital resolution.

2 Dynamical 3-space

An alternative explanation of the Shnoll effect has been proposed using the dynamical 3-space theory; see *Process Physics* [6]. This arose from modeling time as a non-geometric process, i.e. keeping space and time as separate phenomena, and leads to a description of space which is dynamic and fractal. It uses a uniquely determined generalisation of Newtonian Gravity expressed in terms of a velocity field $\boldsymbol{v}(\boldsymbol{r}, t)$, defined relative to an observer at space label coordinate $\boldsymbol{r}$, rather than the original gravitational acceleration field. The dynamics of space in the absence of vorticity, $\nabla \times \boldsymbol{v} = \boldsymbol{0}$, becomes*

$$\nabla\cdot\left(\frac{\partial \boldsymbol{v}}{\partial t} + (\boldsymbol{v}\cdot\nabla)\boldsymbol{v}\right) + \frac{5\alpha}{4}\left((trD)^2 - tr(D^2)\right) + ... = -4\pi G\rho, \quad (1)$$

where $D_{ij} = \partial v_i/\partial x_j$, and $\rho = \rho(\boldsymbol{r}, t)$ is the usual matter density. The 1st term involves the Euler constituent acceleration, while the $\alpha-$term describes the self interaction of space. Laboratory, geophysical and astronomical data suggest that α is

*The α term in (1) has recently been changed due to a numerical error found in the analysis of borehole data. All solutions are also altered by these factors. (1) also contains higher order derivative terms — see [7] .

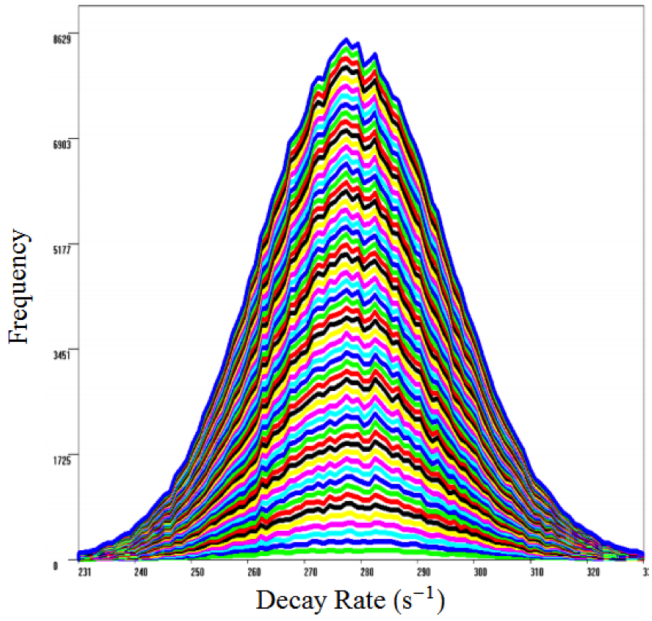

Fig. 1: Non-Poisson distribution of 352,980 measurements of ^{239}Pu α decay by Shnoll performed in 2004 (Fig. 2-2 of [1]). The layered histograms are taken every 6000 measurements. The x-axis denotes the number of decay events per second and the y-axis is the frequency of measurements.

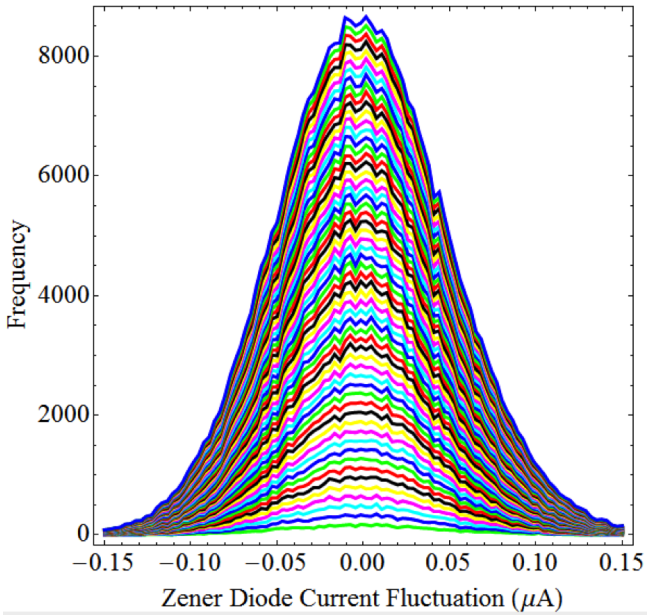

Fig. 2: Non-Poisson distribution of 376,101 measurements of zener diode current fluctuation (μA) observed from 20 — 27 Aug. 2013 in Adelaide. The layered histograms are taken every 6100 measurements to show a comparison with that of Fig.1.

the fine structure constant $\approx 1/137$. This velocity field corresponds to a space flow which has been detected in numerous experiments. In the spherically symmetric case and in the absence of matter $\rho = 0$, (1) contains solutions for black holes (spatial inflows) and an expanding universe (Hubble expansion) along with that for black holes embedded in an expanding universe [7]. Eqn.(1) also contains solutions for the inflow of space into a matter density. Perturbing the spatial inflow into matter (i.e. simulating gravitational waves) has shown to produce reverberations in which the wave generates trailing copies of itself [8]. This reverberation effect is caused by the non-linear nature of the flow dynamics evident in (1).

3 Zener diode quantum gravitational wave detector

A gravitational wave detector experiment performed in March 2012 measured the travel time difference of two 10MHz radio frequency (RF) signals propagating through dual coaxial cables [5]. This technique exploited the absence of the Fresnel drag effect in RF coaxial cables, at sufficiently low frequencies. This permitted the detection of gravitational waves at 1st order in v/c using one clock. The timing resolution of the results were however insufficient to study the effects Shnoll investigated, namely the changes in the histogram shapes over time.

A more recent experiment uses the current fluctuations in a reverse biased zener diode circuit. The circuit diagram is shown in Fig. 3. This detector exploits the discovery that the electron tunnelling current is not random, but caused by gravitational waves; namely fluctuations/turbulence in the passing dynamical 3-space [3]. A Fast Fourier Transform of the zener diode data was taken to remove low frequency artefacts, and then a histogram taken of the resultant 376,101 measurements (after inverse FFT) to generate the layered histogram plot shown in Fig. 2. Layer lines are inserted every 6100 measurements to show a comparison with the Shnoll plot in Fig. 1. Fig. 2 is remarkably comparable to Fig. 1, showng that the Shnoll effect is also present in zener diode experiments. The structure observed appears to build up over time instead of cancelling out and is also found to persist regardless of the time scale used for the phase difference, suggesting that the phenomenon causing this has a fractal nature as depicted in Fig.4. If this is indeed caused by a dynamical and fractal 3-space then the persisting structure observed in Figs. 1 and 2 correspond to regions of space passing the Earth that have preferred/discrete velocities, and not random ones, as randomly distributed velocities would result in a Poisson distribution, i.e. no features. A likely explanation for this is that the gravitational waves propagating in the 3-space inflow of the Earth or Sun could become phase locked due to the relative locations of massive objects [8]. This would cause reverberation effects, i.e. regions of space which have the same speed and direction, which then repeat over time. The reverberations would be detectable in many other experiments such as EM anisotropy, radiation decay, semiconductor noise generation etc. and could in the future be used to further characterise the dynamics of space.

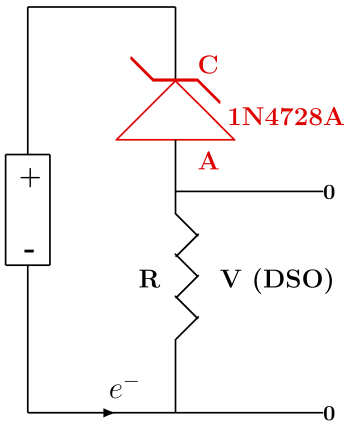

Fig. 3: Circuit of Zener Diode Quantum Gravitational Wave Detector, showing 1.5 AA battery, 1N4728A zener diode operating in reverse bias mode, and having a Zener voltage of 3.3 V, and resistor 10KΩ. Voltage V across resistor is measured and used to determine the space driven fluctuating tunneling current through the zener diode, [3]. Data is shown in Fig.2.

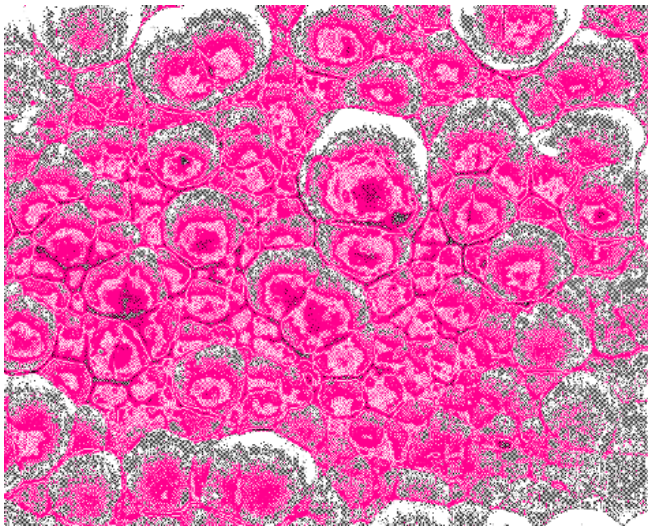

Fig. 4: Representation of the fractal wave data as revealing the fractal textured structure of the 3-space, with cells of space having slightly different velocities and continually changing, and moving wrt the earth with a speed of 500 km/s.

4 Conclusion

The data from a zener diode quantum gravitational wave experiment displays the non-Poisson characteristics Shnoll observed previously in radioactivity experiments. It is suggested that these two experiments (along with other work by Shnoll) are caused by the fractal nature of space, together with the reverberation effect from gravitational waves, as predicted by the Dynamical 3-Space theory.

5 Acknowledgments

Special thanks to Professor Simon Shnoll for permission to use data from his work — see ref [1] for details. Thanks also to Prof Simon Shnoll and Dr Dmitri Rabounski for drawing to our attention the limited digital resolution used in [2]. This report is from the Flinders University Gravitational Wave Detector Project, funded by an Australian Research Council Discovery Grant: *Development and Study of a New Theory of Gravity*.

Submitted on November 11, 2013 / Accepted on November 14, 2013

References

1. Shnoll S.E. Cosmophysical Factors in Stochastic Processes. American Research Press, Rehoboth, New Mexico, USA, 2012. Available from Progress in Physics website.
2. Rothall D.P. and Cahill R.T. Dynamical 3-space: gravitational wave detection and the Shnoll effect, *Progress in Physics*, 2013, v. 4, 44–47.
3. Cahill R.T. Nanotechnology quantum detectors for gravitational waves: Adelaide to London correlations observed. *Progress in Physics*, 2013, v. 4, 57–62.
4. Shnoll, S.E., Zenchenko T.A., Zenchenko K.I., Pozharskii E.V., Kolombet V.A. and Konradov A.A. Regular variation of the fine structure of statistical distributions as a consequence of cosmophysical agents. *Phys. Usp.*, 2000, v. 43(2), 205–209.
5. Cahill R.T. Characterisation of low frequency gravitational waves from dual RF coaxial-cable detector: fractal textured dynamical 3-space. *Progress in Physics*, 2012, v. 3, 3–10.
6. Cahill R.T. Process Physics: From Information Theory to Quantum Space and Matter. Nova Science Pub., New York, 2005.
7. Rothall D.P. and Cahill R.T. Dynamical 3-space: black holes in an expanding universe. *Progress in Physics*, 2013, v. 4, 25–31.
8. Cahill R.T. and Deane S.T. Dynamical 3-space gravitational waves: reverberation effects. *Progress in Physics*, 2013, v. 2, 9–11.

Kepler-47 Circumbinary Planets obey Quantization of Angular Momentum per Unit Mass predicted by Quantum Celestial Mechanics (QCM)

Franklin Potter

Sciencegems.com, 8642 Marvale Drive, Huntington Beach, CA 92646 USA. E-mail: frank11hb@yahoo.com

The Kepler-47 circumbinary system has three known planets orbiting its binary star barycenter and therefore can provide a precision test of the Quantum Celestial Mechanics (QCM) prediction of the quantization of angular momentum per unit mass in all gravitationally bound systems. Two of the planets are in the Habitable Zone (HZ), so system stability can be a primary concern. QCM may be a major contributor to the stability of this system.

1 Introduction

We report another precision test of quantum celestial mechanics (QCM) in the Kepler-47 circumbinary system that has three planets orbiting its two central stars. QCM, proposed in 2003 by H.G. Preston and F. Potter [1] as an extension of Einstein's general theory of relativity, predicts angular momentum per unit mass quantization states for bodies orbiting a central mass in all gravitationally bound systems with the defining equation in the Schwarzschild metric being

$$\frac{L}{\mu} = m\,\frac{L_T}{M_T}\,. \tag{1}$$

Here μ is the mass of the orbiting body with orbital angular momentum L and M_T is the total mass of the bound system with total angular momentum L_T. We determine that the quantization integers m are 4, 6, and 7, for the three circumbinary planets 47-b, -d, -c, respectively, with a linear regression fit $R^2 = 0.9993$. Note that in all systems we have considered, we assume that the orbiting bodies have been in stable orbits for at least a 100 million years.

In other two-star systems with one or two circumbinary planets, the two stars contributed more than 95% of the total angular momentum of the system. In Kepler-47, the three known planets are contributing at least 25% of the angular momentum, a significant fraction, so Kepler-47 provides an additional test of QCM.

As we determined in the paper cited above, in the Solar System the Oort Cloud dominates the total angular momentum, its contribution being nearly 60 times the angular momentum of the planets, but the value has large uncertainty. In the numerous multi-planetary systems around a single star for which we have checked the QCM angular momentum quantization restriction [2], not only do the planetary orbits contribute much more angular momentum than the star rotation, but also each was determined to require additional angular momentum contributions from more planets and/or the equivalent of an Oort Cloud.

We find also that Kepler-47 could have more angular momentum contributions beyond the angular momentum sum of the binary stars and the three planets.

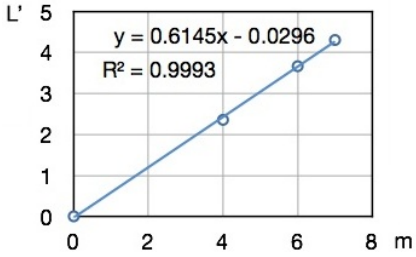

Fig. 1: Kepler-47 System m values predicted by QCM.

2 Results

W.F. Welsh, J.A. Orosz, et al. [3,4] have recently reported the properties of the Kepler-47 system:

- Stars A and B have masses 1.04 ± 0.06 $M_\odot$ and 0.36 $M_\odot$ with orbital period 7.45 days.
- Planet 47-b has mass < $2M_{Jup}$, orbital period 49.53 days and orbital eccentricity $e < 0.035$.
- Planet 47-c has mass < $28M_{Jup}$, orbital period 303.1 days and orbital eccentricity $e < 0.2$.
- Planet 47-d has orbital period 187.3 days, unknown eccentricity, and unknown mass value.

Planet-c is definitely within the Habitable Zone (HZ) and so is planet 47-d. As the authors state, Kepler-47 establishes that planetary systems can form and persist in the chaotic environment close to binary stars as well as have planets in the HZ around their host stars.

In order to use the angular momentum condition, one assumes that the orbiting body is at or near its QCM equilibrium orbital radius r and that the orbital eccentricity ϵ is low so that our nearly circular orbit approximation leading to the quantization equation holds true. Therefore, the L of the orbiting body will agree with its Newtonian value $L = \mu\sqrt{GM_T r(1-\epsilon^2)}$.

In Fig. 1 is shown a plot of $L' = L/\mu$ versus m for the three known planets in the Kepler-47 system. The circles about the data points contain the uncertainty bars for L'. The slope b of the line in this plot is used to predict the system's total angular momentum $L_T = bM_T$ multiplied by 10^{15} kg-m^2/s.

The QCM predicted value of 17.7×10^{44} kg-m^2/s is much larger than the estimated upper value of 12×10^{44} kg-m^2/s from the five bodies in orbit about the barycenter. Therefore, QCM predicts additional sources of angular momentum for this Kepler-47 system.

What are possible additional sources for the QCM predicted total angular momentum? There could be massive bodies at $m = 3, 5, 8, 9, \ldots$ However, massive bodies with sufficient orbital angular momentum at either $m = 3$ or $m = 5$ would have been detected already by their perturbation effects on the known planets, so the additional planetary angular momentum must be exterior to planet 47-c, i.e., will have $m > 7$. Perhaps new sources will be detected in the near future to provide another check on the QCM quantization condition.

3 Conclusions

The Kepler-47 system provides further evidence that angular momentum has a primary role in gravitationally bound systems at all scale sizes, particularly in determining the spacings of planetary orbits in solar systems, of satellites of planets [5], of planets in circumbinary systems, as well as determining physical properties of galaxies, clusters of galaxies, and the Universe.

Although the three known planets in Kepler-47 have an excellent fit to the QCM quantization condition, further orbiting bodies are predicted that could provide an additional test when they are detected. If they are located at orbital radii that do not agree with acceptable values, QCM will be challenged to explain the discrepancies.

Acknowledgements

The author thanks Sciencegems.com for encouragement and financial support.

Submitted on November 16, 2013 / Accepted on November 18, 2013

References

1. Preston H. G., Potter F. Exploring Large-scale Gravitational Quantization without h-bar in Planetary Systems, Galaxies, and the Universe. arXiv: gr-qc/030311v1.
2. Potter F. Multi-planet Exosystems All Obey Orbital Angular Momentum Quantization per Unit Mass predicted by Quantum Celestial Mechanics (QCM). *Progress in Physics*, 2013, v. 3, 60–61.
3. Welsh W. F., Orosz J. A., Carter J. A., Fabrycky D. C., and the *Kepler* Team. Recent Kepler Results On Circumbinary Planets. arXiv: 1308.6328.
4. Orosz J. A. The Confirmation of a Third Planet in the Kepler-47 Circumbinary System. http://nexsci.caltech.edu/conferences/KeplerII/agenda.shtml.
5. Potter F. Pluto Moons exhibit Orbital Angular Momentum Quantization per Mass. *Progress in Physics*, 2012, v. 4, 3–4.

Observed Gravitational Wave Effects: Amaldi 1980 Frascati-Rome Classical Bar Detectors, 2013 Perth-London Zener-Diode Quantum Detectors, Earth Oscillation Mode Frequencies

Reginald T. Cahill

School of Chemical and Physical Sciences, Flinders University, Adelaide 5001, Australia. E-mail: Reg.Cahill@flinders.edu.au

Amaldi *et al* in 1981 reported two key discoveries from the Frascati and Rome gravitational wave cryogenic bar detectors: (a) Rome events delayed by within a few seconds to tens of seconds from the Frascati events, and (b) the Frascati Fourier-analysed data frequency peaks being the same as the earth oscillation frequencies from seismology. The time delay effects have been dismissed as being inconsistent with gravitational waves having speed c. However using data from zener diode quantum detectors, from Perth and London, for January 1-3, 2013, we report the same effects, and in excellent agreement with the Amaldi results. The time delay effects appear to be gravitational wave reverberations, recently observed, and for gravitational wave speeds of some 500 km/s, as detected in numerous experiments. We conclude that the Amaldi *et al.* discoveries were very significant.

1 Introduction

On the basis of data from the new nanotechnology zener-diode quantum gravitational wave detectors [1] it is argued that the wave effects detected in 1980 by Amaldi *et al* [2,3], using two cryogenic bar detectors, located in Frascati and Rome, were genuine gravitational wave effects, together with earth oscillation effects, although not gravitational waves of the expected form.

The speed and direction of gravitational waves have been repeatedly detected using a variety of techniques over the last 125 years, and have a speed of some 500 km/s coming from a direction with RA $\sim$ 5 hrs, Dec $\sim 80^0$. These waves appear to be of galactic origin, and associated with the dynamics of the galaxy and perhaps the local cluster. This speed is that of the dynamical 3-space, which appears to have a fractal structure, and the significant magnitude waves are turbulence/fractal structure in that flowing space. The detection techniques include gas-mode Michelson interferometers, RF coaxial cable EM speed measurements, RF coaxial-cable - optical fiber RF/EM speed measurements, EM speed measurements from spacecraft Earth-flyby Doppler shifts, zener-diode quantum detectors, within Digital Storage Oscilloscopes, and in so-called Random Event Generators (REG) [1, 4, 5]. These zener diode devices have detected correlations between Adelaide and London, and between Perth and London, with travel time delays from 10 to 20 seconds, and with significant reverberation effects [1, 6]. The speed of some 500 km/s has also been observed as a time delay of some 500 ns in table-top zener-diode quantum detectors, separated by 25 cm in a S to N direction. The zener-diode gravitational wave quantum detectors operate by the process of the 3-space wave turbulence causing the quantum to classical transition, i.e. spatial localisation of the electron wave functions tunneling through a 10 nm quantum barrier, when the diode is operated in reverse bias. The earlier techniques rely on detecting EM radiation anisotropy.

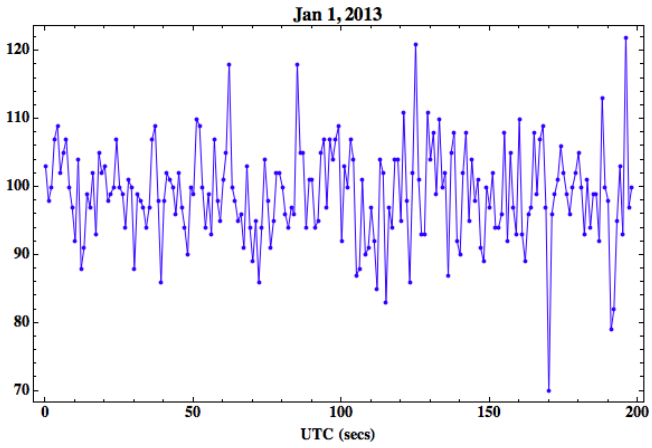

Fig. 1: Perth zener-diode quantum detector (REG) data, for January 1, 2013. The data points are at 1 s intervals. The data shows strong peaks at 5 - 30 s intervals, related to the reverberation effect [6]. This appears to be the time-delay effect detected between the Frascati and Rome cryogenic gravitational wave bar detectors [2, 3].

2 The Amaldi Frascati Rome gravitational wave detectors

Data was collected with two cryogenic resonant gravitational wave antennas operated simultaneously in Rome and Frascati. Coincidences were detected with pulses lasting about 1 second, and travel times differing from one second to twenty seconds ($\pm$0.5 s), with the NW Rome signal delayed relative to the Frascati events. These events were dismissed as gravi-

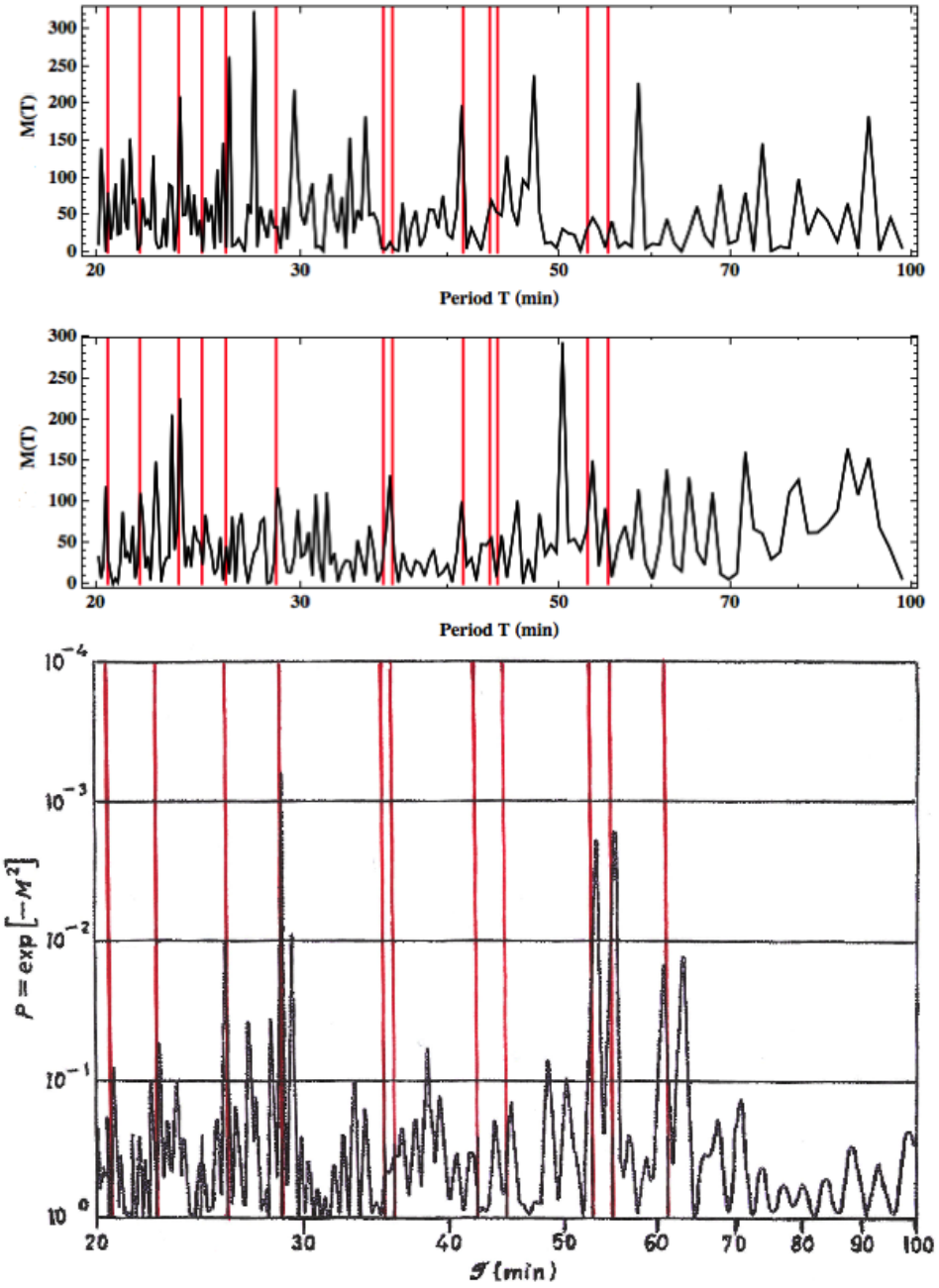

Fig. 2: Top: Power spectrum from Zener Diode detector in Perth, Jan 1-3, 2013. Middle: Power spectrum from Zener Diode detector in London, Jan 1-3, 2013. Bottom: Power spectrum from Frascati bar detector data, May 6-7, 1980, adapted from Amaldi *et al* [3]. Vertical lines (red) show various earth vibration periods, determined by seismology [9]. $M(T) = |F(T)|^2$ is the power spectrum, expressed as a function of period T, where $F(T)$ is the Fourier transform of the data time series. A 200 sec interval of the Perth data is shown in Fig.1. The spectra from all detectors show the same low frequency peaks, but with differing intensities. The peaks at 53.1 and 54.1 min equal the ${}_0S_2^{+1}$ and ${}_0S_2^{-1}$ Earth vibration modes.

tational wave events as the travel times, for the 20 km separation, far exceeded that expected if one assumes that gravitational waves travel at speed c, predicting travel times ∼0.1 ms. As well frequency analysis of the data revealed strong peaks at frequencies coinciding with known vibration frequencies of the earth, see bottom plot of Fig. 2. Amaldi *et al.* considered several mechanisms for the detection of such frequencies: (i) various instrumental couplings to the earth vibrations, (ii) gravitational field variations caused by a terrestrial source. However the very same results are obtained with the zener-diode quantum gravitational wave detectors.

3 Zener diode detectors

In [1] the discovery of the nanotechnology zener diode detection effect for gravitational waves was reported. This was established by detecting times delays between wave forms of 10-20 seconds for travel times Adelaide to London, and Perth to London, with that travel time variation following the earth's rotation with respect to the RA and Dec that had been reported in earlier experiments [4,5], and which displayed the sidereal effect, *viz* the earth time of the earth rotation phase was essentially fixed relative to sidereal time, i.e. the flow direction was fixed relative to the stars.

The zener diode detectors first used are known as Random Number Generators (RNG) or Random Event Generators (REG). There are various designs available from manufacturers, and all claim that these devices manifest hardware random quantum processes, as they involve the quantum to classical transition when a measurement, say, of the quantum tunneling of electrons through a nanotechnology potential barrier, ∼10 nm thickness, is measured by a classical/macroscopic system. According to the standard interpretation of quantum theory, the collapse of the electron wave function to one side or the other of the barrier, after the tunneling produces a component on each side, is purely a random event, internal to the quantum system. However that interpretation had never been tested experimentally, until [1]. Data from two REGs, located in Perth and London, was examined. The above mentioned travel times were then observed. The key features being a speed of ∼500 km/s, and strong reverberation effects, see Fig. 1.

This discovery revealed that current fluctuations through a zener diode in reverse bias mode are not random, and data from collocated zener diodes showed almost identical fluctuations [1]. Consequently the zener diode detectors can easily be increased in sensitivity by using zener diodes in parallel, with the sensitivity being proportional to the number of diodes used, see circuit diagram in [1]. That the quantum to classical transition, i.e. "collapse of the wave function", is induced by 3-space fluctuations, has deep implications for our understanding of quantum phenomena.

Using data from REG's located in Perth and London, for Jan. 1-3, 2013, and then doing a Fourier transform frequency analysis, we obtain the spectrum in the top two plots in Fig. 2. The unfiltered power spectra from the two REGs show remarkable similarity to each other, and to the spectrum from the Frascati data. Again the dominant frequencies correspond to known earth vibration frequencies [9], although there are long-period oscillations, common to all detectors, that are not known earth frequencies.

This new data shows that the time delays observed between Frascati and Rome are to be expected, because of the strong reverberation effects seen in the zener diode detector data. However the occurrence of the earth vibration frequencies is intriguing, and reveals new physics. Unlike the bar detectors it is impossible for any physical earth movement to mechanically affect the zener diodes, and so all detectors are responding to dynamical space fluctuations caused by the oscillations of the matter forming the earth. The key questions are: What causes this ongoing activation of the earth modes? Are they caused by earthquakes or by the fractal 3-space waves exciting the earth modes?

4 Conclusions

The discovery of the quantum detection of gravitational waves, showing correlations between well separated locations, that permitted the absolute determination of the 3-space velocity of some 500 km/s, in agreement with the speed and direction from a number of previous analyses, including in particular the NASA spacecraft Earth-flyby Doppler shift effect. This discovery enables a very simple and cheap nanotechnology zener-diode quantum gravitational wave detection technology, which will permit the study of various associated phenomena, such as solar flares, coronal mass ejections, earthquakes, eclipse effects, moon phase effects, non-Poisson fluctuations in radioactivity [7, 8], and other rate processes, and variations in radioactive decay rates related to distance of the earth from the Sun, as the 3-space fluctuations are enhanced by proximity to the sun. As an example of these possibilities we have confirmed that the Amaldi *et al* bar detectors did indeed detect gravitational wave events in 1980, but not of the form commonly expected, in particular gravitational waves do not travel at speed c, and there is no experimental or observational evidence supporting that claim.

5 Acknowledgements

This report is from the Flinders University Gravitational Wave Detector Project, Australian Research Council Discovery Grant: *Development and Study of a New Theory of Gravity*. Thanks to GCP and its director Dr Roger Nelson for the availability of extensive and valuable data from the REG international network: http://teilhard.global-mind.org/. Giovanni B. Bongiovanni, Turin, raised the earth vibration frequency effect observed using a zener diode detector, and also confirmed the strong correlations between collocated detectors.

Submitted on November 18, 2013 / Accepted on November 20, 2013

References

1. Cahill R. T. Nanotechnology quantum detectors for gravitational waves: Adelaide to London correlations observed. *Progress in Physics*, 2013, v. 4, 57–62.
2. Amaldi E., Coccia E., Frasca S., Modena I., Rapagnani P., Ricci F., Pallottino G. V., Pizzella G., Bonifazi P., Cosmelli C., Giovanardi U., Iafolla V., Ugazio S., and Vannaroni G. Background of gravitational-wave antennas of possible terrestrial origin — I. *Il Nuovo Cimento*, 1981, v. 4C (3), 295–308.
3. Amaldi E., Frasca S., Pallottino G. V., Pizzella G., Bonifazi P. Background of gravitational-wave antennas of possible terrestrial origin — II. *Il Nuovo Cimento*, 1981, v. 4C (3), 309–323.
4. Cahill R. T. Combining NASA/JPL one-way optical-fiber light-speed data with spacecraft Earth-flyby Doppler-shift data to characterise 3-space flow. *Progress in Physics*, 2009, v. 4, 50–64.
5. Cahill R. T. Characterisation of low frequency gravitational waves from dual RF coaxial-cable detector: fractal textured dynamical 3-space. *Progress in Physics*, 2012, v. 3, 3–10.
6. Cahill R. T. and Deane S.T. Dynamical 3-space gravitational waves: reverberation effects, *Progress in Physics*, 2013, v. 2, 9–11.
7. Shnoll S. E. Cosmophysical Factors in Stochastic Processes. American Research Press, Rehoboth, New Mexico, USA, 2012.
8. Rothall D. P. and Cahill R. T. Dynamical 3-Space: Observing Gravitational Wave Fluctuations and the Shnoll Effect using a Zener Diode Quantum Detector. *Progress in Physics*, 2014, v. 10 (1), 16–18.
9. Masters T. G. and Widmer R. Free oscillations: frequencies and attenuations. In: Ahrens I. J., Ed. Global Earth Physics, A Handbook of Physical Constants, AGU, 1995, 104–125.

LETTERS TO PROGRESS IN PHYSICS

Florentin Smarandache: A Celebration

Dmitri Rabounski

E-mail: rabounski@ptep-online.com

We celebrate Prof. Florentin Smarandache, the Associate Editor and co-founder of *Progress in Physics* who is a prominent mathematician of the 20th/21th centuries. Prof. Smarandache is most known as the founder of neutrosophic logic, which is a modern extension of fuzzy logics by introducing the neutralities and denials (such as "neutral A" and "non-A" between "A" and "anti-A"). He is also known due to his many discoveries in the filed of pure mathematics such as number theory, set theory, functions, etc. (see many items connected with his name in *CRC Encyclopedia of Mathematics*). As a multi-talented person, Prof. Smarandache is also known due to his achievements in the other fields of science, and also as a poet and writer. He still work in science, and continues his creative research activity.

Florentin Smarandache (born on December 10, 1954) — polymath, professor of mathematics, scientist, poet and writer (originally writting in Romanian, French, and English). He is a US citizen. He lives in the United States.

Florentin Smarandache was born in Bălceşti, a small village in province Vâlcea, Romania. His ancestors from father's side came to Romania from Greece, several generations before, but saved their Greek family name (which was romanized) over the centuries. He was the only child in the family.

In 1979, Florentin Smarandache was graduated from the Department of Mathematics at the University of Craiova (Romania). In 1997, the State University of Moldova at Kishinev bestowed upon him the PhD degree in mathematics. Then he continued his post-doctoral studies at various American Universities (such as University of Texas at Austin, University of Phoenix, etc.).

In the USA he worked as a software engineer for Honeywell (1990-1995), then as Adjunct Professor for Pima Community College (1995-1997). In 1997 he joined to the University of New Mexico, Gallup Campus, as Adjunct Professor. Then he was promoted to Associate Professor of Mathematics (2003), and to Full Professor (2008). During 2007-2009 he was the Chair of Department of Mathematics and Sciences.

During Ceausescu's dictatorship in Romania, Florentin Smarandache was enrolled into a conflict with the Romanian authorities. In 1986 he claimed a hungry strike for being refused to attend the International Congress of Mathematicians at the University of Berkeley. Then he published an open letter in the Notices of the American Mathematical Society, for the freedom of circulating of scientists. He thus became a political dissident in Romania. As a consequence, he was faired from the academic job, and survived during two years from private tutorship. Dr. Olof G. Tandberg, Foreign Secretary of Swedish Royal Academy, supported him by phone talking from Bucharest.

Not being allowed to publish, he tried to get his manuscripts out of the country through the French School of Bucharest and tourists, but for many of them he lost track. Finally, in September 1988, Florentin Smarandache escaped from Romania, then stayed for almost two years in Turkey, in a refugee camp. Here he kept in touch with the French Cultural Institutes that facilitated him the access to books and rencontres with personalities. Before leaving the country he buried some of his manuscripts in a metal box in his parents vineyard, near a peach tree, that he retrieved four years later, after the 1989 Revolution, when he returned for the first time to his native country. Other manuscripts, that he tried to mail to a translator in France, were confiscated by the secret police and never returned. He wrote hundreds of pages of the diaries about his life under the Romanian dictatorship, about

Prof. Florentin Smarandache

his being as a cooperative teacher in Morocco ("Professor in Africa", 1999), in the Turkish refugee camp ("Escaped... Diary From the Refugee Camp", vol.1, vol.2, 1994, 1998). In March 1990, Florentin Smarandache emigrated to the United States.

Florentin Smarandache is also known as the founder of "paradoxism" (established in 1980). This is the literary movement which has many followers in the world. Paradoxism is based on an excessive use of antitheses, antinomies, contradictions, paradoxes in creation paradoxes — both at the small level and the entire level of the work — making an interesting connection between mathematics, philosophy, and literature. He introduced paradoxist distiches, tautologic distiches, and dualistic distiches, which were inspired by the mathematical logic. The literary experiments were realized by him in the dramas: "Country of the Animals", "An Upside-Down World", "MetaHistory", "Formation of the New Man", and the others. Florentin Smarandache did many poetical experiments in the framework of his avant-garde. He published paradoxist manifestos: "Le Sens du Non-Sens" (1983), "Antichambres, Antipoésies, Bizarreries" (1984, 1989), "NonPoems" (1990), where he changed the French and respectively English linguistics clichés. While "Paradoxist Distiches" (1998) introduces new species of poetry with fixed form. Eventually he edited three International Anthologies on Paradoxism (2000-2004) with texts from about 350 writers from around the world in many languages. Twelve books were published that analyze his literary creation, including "Paradoxism's Aesthetics" by Titu Popescu (1995), and "Paradoxism and Postmodernism" by Ion Soare (2000).

Florentin Smarandache is also known as an artist working in the style of modernism. His experimental art albums comprises over-paintings, non-paintings, anti-drawings, superphotos, foreseen with a manifesto: "Ultra-Modernism?" and "Anti-manifesto".

In mathematics Prof. Smarandache introduced the degree of negation of an axiom or of a theorem in geometry: Smarandache geometries (1969), which can be partially Euclidean and partially non-Euclidean. He also introduced multi-structures (Smarandache n-structures, where a weak structure contains an island of a stronger structure), and multi-spaces (a combination of heterogeneous spaces). He introduced and developed many sequences and functions in number theory. Florentin Smarandache also generalized fuzzy logics to "nueutrosophic logic" and, similarly, he generalized fuzzy set to "neutrosophic set". Also, he suggested an extension of the classical probability and imprecise probability to "neutrosophic probability". Together with Dr. Jean Dezert (ONERA, France), he generalized Dempster-Shafer theory to a new theory of plausible and paradoxist fusion, which is now known as Dezert-Smarandache theory (2002). In 2004 he designed an algorithm for the unification of fusion theories (UFT) used in bioinformatics, robotics, and military.

In physics, Prof. Smarandache introduced a series of paradoxes (quantum Smarandache paradoxes). On the basis of neutrosophic logics, he also considered a theoretical possibility of a third form of matter, called as unmatter, which is a combination of matter and antimatter (2010). Based on his early 1972 publication (when he was a student in Romania), Prof. Smarandache suggested the hypothesis that "there is no speed barrier in the universe and one can construct any speed". This hypothesis was partially validated on September 22, 2011, when researchers at CERN experimentally proved that the muon neutrino particles travel with a speed greater than the speed of light. Upon his hypothesis he suggested a modification of Einstein's theory of relativity, where the relativistic paradoxes are only the observable effects registered by a particular observer, not the true reality. The speed of light in vacuum is thus considered to be a variable value, which is dependent on the type of synchronization of the particular observer. It is a constant for only the observer who uses light beams as the medium of synchronization. Therefore, the cosmological redshift and the other relativistic effects are true only for the social community of the observers whose picture of the world is "painted" on the basis of information obtained from the light signals.

In philosophy, Florentin Smarandache introduced neutrosophy (1995), which is a new generalization of Hegel's dialectic. Neutrosophy has a basis in his researches in mathematics and economics, such as "neutrosophic logic", "neutrosophic set", "neutrosophic probability", and "neutrosophic statistics". Neutrosophy is a new branch of philosophy that studies the origin, nature, and scope of neutralities, as well as their interactions with different ideational spectra. This theory considers every notion or an idea <A> together with its opposite or negation <Anti-A> and the spectrum of "neutralities" <Neut-A>. The <Neut-A> and <Anti-A> ideas together are referred to as <Non-A>. According to this theory every idea <A> tends to be neutralized and balanced by <Anti-A> and <Non-A> ideas as the state of equilibrium.

International Conference on Neutrosophy and Neutrosophic Logics was held in December 2001 at the University of New Mexico, USA. International Conference on Smarandache Type Notions in Number Theory was held in August 1997 at University of Craiova, Romania. International Conference on Smarandache Geometries was held in May 2003 at Griffith University in Queensland, Australia.International Conference on Smarandache Algebraic Structures was held in December 2004 at Loyola College in Madras, India.

Prof. Smarandache authored numeous monographs, and about 200 research papers published in about 50 scientific journals. He also was the editor of more than a hundred of scientific books authored by the other scientists. In addition to his scientific research, Prof. Smarandache gives lectures throughout the world for over many years. He was an invited lecturer at Bloomsburg University (USA, 1995), University of Berkeley (USA, 2003), NASA Langley Research Center (USA, 2004), Jadavpur University (India, 2004), NATO Ad-

vanced Studies Institute (Bulgaria, 2005), Institute of Biophysics (Russia, 2005), University Sekolah Tinggi Informatika and University Kristen Satya Wacana Salatiga (Indonesia, 2006), Minufiya University (Egypt, 2007), Universitatea din Craiova (Romania, (2009), Air Force Research Lab and Griffiss Institute (USA, 2009), Air Force Institute of Technology at Wright-Patterson AFB (USA, 2009), Air Force Research Lab of State University of NY Institute of Technology in Rome (NY, USA, 2009), COGIS (France, 2009), ENSIETA — National Superior School of Engineers and Study of Armament in Brest (France, 2010), Institute of Solid Mechanics and Commission of Acoustics (Romania, 2011), Guangdong University of Technology in Guangzhou (China, 2012), Okayama University (Japan, 2013), etc.

In 2011, Academia DacoRomana in Bucharest bestowed upon Prof. Smarandache the Doctor Honoris Causa degree. In the same year, Beijing Jiaotong University in China bestowed the Doctor Honoris Causa degree upon him as well.

We all, who know Prof Florentin Smarandache closely over decades, point out his benignity, enthusiasm, and scientific creativity. He never rests in mind, but always works on different fields of science, literature, and art. We wish him to be always full of energy, pink health, and to have happy life for many years.

Submitted on December 10, 2013 / Accepted on December 10, 2013

On Some General Regularities of Formation of the Planetary Systems

Anatoly V. Belyakov

E-mail: belyakov.lih@gmail.com

J. Wheeler's geometrodynamic concept has been used, in which space continuum is considered as a topologically non-unitary coherent surface admitting the existence of transitions of the input-output kind between distant regions of the space in an additional dimension. This model assumes the existence of closed structures (micro- and macrocontours) formed due to the balance between main interactions: gravitational, electric, magnetic, and inertial forces. It is such macrocontours that have been demonstrated to form — independently of their material basis — the essential structure of objects at various levels of organization of matter. On the basis of this concept in this paper basic regularities acting during formation planetary systems have been obtained. The existence of two sharply different types of planetary systems has been determined. The dependencies linking the masses of the planets, the diameters of the planets, the orbital radii of the planet, and the mass of the central body have been deduced. The possibility of formation of Earth-like planets near brown dwarfs has been grounded. The minimum mass of the planet, which may arise in the planetary system, has been defined.

1 Introduction

Wheeler's geometrodynamic concept, in which microparticles are considered as vortical oscillating deformations on a non-unitary coherent surface and the idea about transitions between distant regions of space in the form of Wheeler's "wormholes", made it possible to substantiate the existence of closed structures (micro- and macrocontours) acting at various levels of organization of matter [1–3].

These contours are material, based on the balance between main interactions: electrical, magnetic, gravitational, and inertial forces. They are not associated to the specific properties of the medium; they determine the important properties of objects and allow using analogies between objects of various scales.

Such approach allows using a model that best are independent of the properties of an object or medium. In this paper the concept is used to establish some of the basic laws of the formation of planetary systems. Here, as in paper [2], there is no need to consider the nature of the cosmological medium, i.e. protoplanetary nebula, from which the planets formed, and other specific features of the process. Idea of the planetary system consisting of some amount of macrocontours, from which planets formed, and the contours of a higher order integrating the planets and a central body was enough to get the general regularities.

2 Initial assumptions

As was shown earlier [1], from the purely mechanistic point of view the so-called *charge* only manifests the degree of the nonequilibrium state of physical vacuum; it is proportional to the momentum of physical vacuum in its motion along the contour of the vortical current tube. Respectively, the *spin* is proportional to the angular momentum of the physical vacuum with respect to the longitudinal axis of the contour, while the *magnetic interaction* of the conductors is analogous to the forces acting among the current tubes. It is given that the elementary unit of such tubes is a unit with the radius and mass equal to those of a classical electron (r_e and m_e).

It should be noted that in [1, 2] the expressions for the electrical and magnetic forces are written in a "Coulombless" form with charge replaced by electron limiting momentum.

In this case, the electrical and magnetic constants (ε_0 and μ_0) are expressed as follows:

$$\varepsilon_0 = m_e/r_e = 3.33 \times 10^{-16} \text{ kg/m}, \quad (1)$$

$$\mu_0 = 1/\varepsilon_0 c^2 = 0.0344 \text{ N}^{-1}, \quad (2)$$

where c is the velocity of light.

Thus, the electric constant ε_0 makes sense the linear density of the vortex tube current, and the magnetic constant μ_0 makes sense the reciprocal value of the interaction force between two elementary charges.

In [2] the relative comparison of various interactions have been carried out and the basic relationships were obtained, some of which are necessary for the understanding of this article.

1. *The balance of electric and magnetic forces* gives a geometric mean — a characteristic linear parameter that is independent of the direction of the vortex tubes and the number of charges:

$$R_s = (r_0 L)^{1/2} = (2\pi)^{1/2}\, c \times [sec] = 7.52 \times 10^8 \text{ m} \quad (3)$$

– a magnitude close to the Sun radius and the sizes of typical stars, where r_0, and L are the rotary radius or the distance between the vortex tubes (thread) and their length.

2. *The balance of gravitational and inertial (centrifugal) forces* gives the maximum gravitational mass of the object satisfying the condition (3):

$$M_m = \frac{R_s c^2}{\gamma} = fR_s\varepsilon_0 = 1.01 \times 10^{36} \text{ kg}. \quad (4)$$

3. *The balance of magnetic and gravitational forces* also results in a geometrical mean:

$$(r_0 L)^{1/2} = \left(\frac{\varepsilon}{f}\right)^{1/2} R_s, \quad (5)$$

where the ratio of the products $\varepsilon = (z_{g1}z_{g2})/(z_{e1}z_{e2})$ is an *evolutionary parameter*, which characterizes the state of the medium and its changes, as the mass carriers become predominant over the electrical ones and, as a matter of fact, shows how the material medium differs from vacuum. Here z_e and z_g are the relative values of charge and mass in the parameters of electron charge and mass, f — is the ratio of electrical-to-gravitational forces, which under the given conditions is expressed as follows:

$$f = \frac{c^2}{\varepsilon_0\gamma} = 4.16 \times 10^{42}, \quad (6)$$

where γ is the gravitational constant. In the general case, expression (5) gives a family of lengthy contours consisting of contra-directional closed vortex tubes (*mg-contours*).

4. The vortex tubes can consist, in their turn, of a number of parallel unidirectional vortex threads, whose stability is ensured by the *balance of magnetic and inertial forces* forming *mi-zones*.
5. Structurizations of the primary medium, where there is more than one pair of balanced forces, results in complication an originally unstructured mass by forming in it local *mi*-zones. In particular, the number of *mi*-zones in the object of arbitrary mass M_i will be:

$$z_i = \left(\frac{M_m}{M_i}\right)^{1/4}. \quad (7)$$

3 Planetary systems

Let us assume there is a cloud of the originally protoplanetary material having an evolutionary parameter ε, in which a planetary system with a central mass M_0 and planets with a mass m_p on a radius r_p, with a rotary velocity v_0 is being formed. Let us assume that the central body is a point-like mass, and the mass of the planet is formed of contours of total number z_p and axis sizes $d_p \times l_p$. Then the mass of the planet can be expressed as the total mass of contours:

$$m_p = z_p\varepsilon\varepsilon_0 l_p. \quad (8)$$

The characteristic size of the *mg*-contour by analogy to (5):

$$\left(l_p d_p\right)^{1/2} = \left(\frac{\varepsilon}{f}\right)^{1/2} R_s. \quad (9)$$

Suppose the number of *mg-contours* constituting the mass of the planet is proportional to the distance to the central body, i.e. a planet contour is a *structural unit for the contour of higher order* that integrates planet with the central body:

$$z_p = \frac{r_p}{d_p}. \quad (10)$$

This is true for a flat homogeneous disk of the initial nebula, where the *mg*-contour is *one-dimensional*, but in general, density of medium may be different and, of course, decrease toward the periphery. The protoplanetary disk may have a local rarefaction or condensation, i.e. have sleeves or be *flat-spiral*. Therefore, in general, we have:

$$z_p = \left(\frac{r_p}{d_p}\right)^n, \quad (11)$$

where the coefficient n reflects the "packaging" of contours in the model object (planet).

The orbital velocity of the planet can be expressed from the balance of centrifugal and gravitational forces:

$$v_0 = \left(\frac{\gamma M_0}{r_p}\right)^{1/2}. \quad (12)$$

On the other hand, we can use the analogy of the Bohr atom, where in the proton-electron system the orbital velocity of the electron at the radius of r_i is equal to

$$v_0 = c\left(\frac{r_e}{r_i}\right)^{1/2}. \quad (13)$$

Then for the contour integrating the planet with the central body, taking the parameter l_p as the unit of length, an analogous relation can be written:

$$v_0 = c\left(\frac{l_p}{r_p}\right)^{1/2}. \quad (14)$$

The number of *mg*-contour z_0 for the stable state of the object, as given in [2], should be taken equal to the number of *mi*-zones:

$$z_p = z_i = \left(\frac{M_m}{m_p}\right)^{1/4}. \quad (15)$$

Share further the dimensionless parameter: $M = M_0/M_m$, $m = m_p/M_m$, $v = v_0/c$, $r = r_p/R_s$, $l = l_p/R_s$, $d = d_p/R_s$, and $z = m^{-1/4}$. Taking into account (8-15), after transformations we obtain expressions describing the dependence of the planet mass on its orbit radius and mass of the central body:

$$m = \left(rM^2\right)^{4n/(5n-1)}, \quad (16)$$

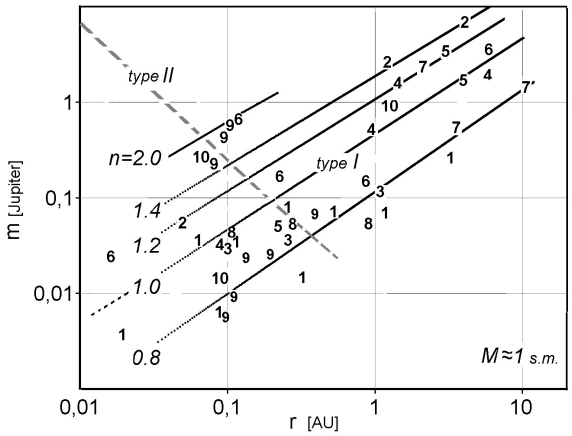

Fig. 1: Dependence of the mass of Type I planets on their orbital radius at $M \approx 1$ s.m. 1 — HD10180, 2 — HD125612, 3 — HD134606, 4 — HD160691, 5 — HD204313, 6 — HD75732, 7 — HD95128, 8 — HD31527, 9, 10 — KOI.

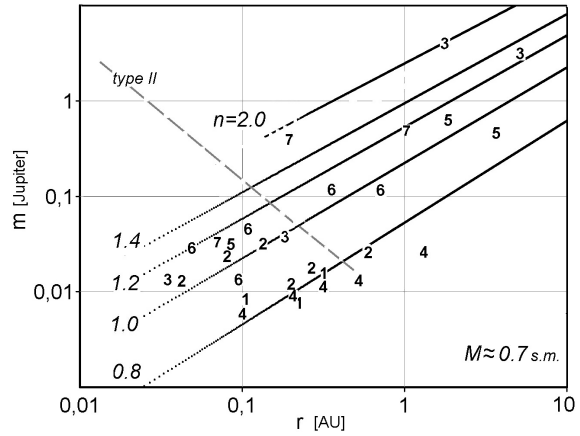

Fig. 2: Dependence of the mass of Type I planets on their orbital radius at $M \approx 0.7$ s.m. 1 — HD20794, 2 — HD40307, 3 — GJ676A, 4 — HD10700, 5 — HD181433, 6 — KOI 701, 7 — HIP57274.

proportions of *mg*-contour

$$d = \frac{m^{5/4}}{M^2}, \tag{17}$$

$$l = M, \tag{18}$$

and the value of the evolutionary parameter

$$\varepsilon = \frac{fm^{5/4}}{M}. \tag{19}$$

However, this model also admits a second case of orientation of *mg*-contour according to another to its axis. In this case an expression for z_p analogous to (11) can be written:

$$z_p = \left(\frac{r_p}{l_p}\right)^k; \tag{20}$$

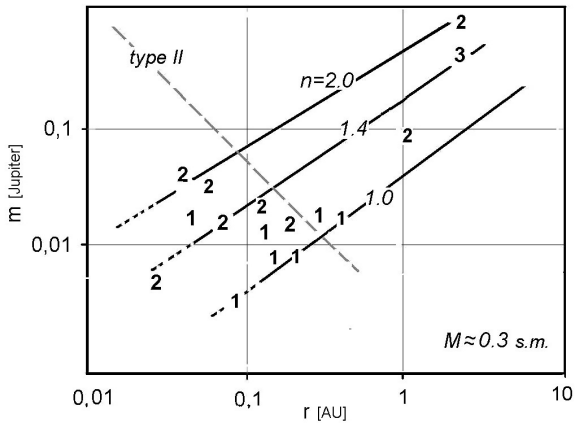

Fig. 3: Dependence of the mass of Type I planets on their orbital radius at $M \approx 0.3 \ldots 0.4$ s.m. 1 — GJ, 2 — Gliese, 3 — OGLE.

then relation $m(r)$ taking into account (15), (18), (20) will look as follows:

$$m = \left(\frac{M}{r}\right)^{4k}. \tag{21}$$

In this variant the emerging masses of planets quickly decrease to the periphery of the protoplanetary disk, and it can be assumed that such initial nebulae are *lenticular in nature*. We call planets corresponding relations of (16) and (20) as *Type I planets and Type II planets*, accordingly.

The actual data relating to the planets in extrasolar planetary systems having three or more planets plotted on diagrams in the coordinates of r — m, where r — the size of the major semiaxis, (Fig. 1-3).

The results of the site *http://www.allplanets.ru/index.htm* have been used. The numbers in the figures correspond to the position of the experimental points and point to the sections of the catalog of extrasolar planets.

The calculated dependencies $m(r)$ according with formula (16) converted to coordinates expressed in the masses of Jupiter and astronomical units by multiplying m by $M_m/1.87 \times 10^{27}$ and r by $R_s/1.5 \times 10^{11}$. These dependencies correspond to the period of planet formation, but several isolines n are shown, because the conditions of formation of the planets and their further evolution is unknown. A large scatter in the values is present on this and others diagrams; in this case it is inevitable. However, the dependence of the masses of extrasolar planets on their orbital radii and on the masses of central stars is revealed quite clearly in agreement with the expression (16). These regularities, i.e. increase in the mass of planets with increasing distance to the central star and with increasing the mass of central stars, also confirmed in [4–7] and others.

Types II planets do not fit into this pattern. In (Fig. 1-3) they would be located near the dashed line. They have masses of the order of the mass of Jupiter and greater than one and are in orbits close to the central star (hot Jupiters).

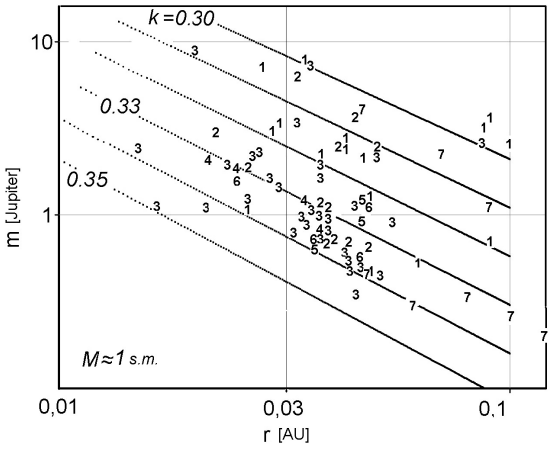

Fig. 4: Dependence of the mass of Type II planets on their orbital radius at $M \approx 1$ s.m. 1 — CoRoT, 2 — HAT-P, 3 — WASP, 4 — TrES, 5 — XO, 6 — OGLE, 7 — HD.

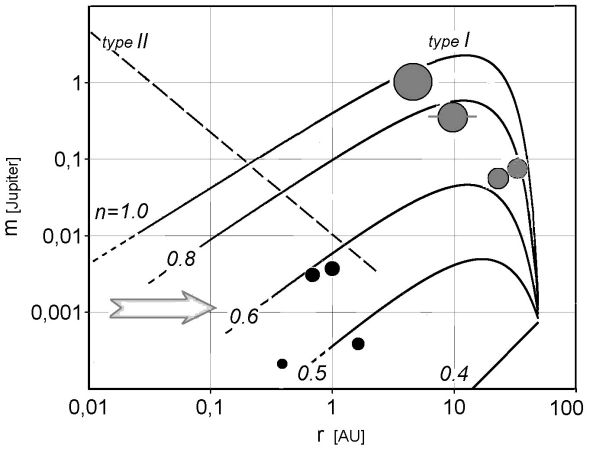

Fig. 6: Dependence of the mass of the solar system planets on their orbital radius.

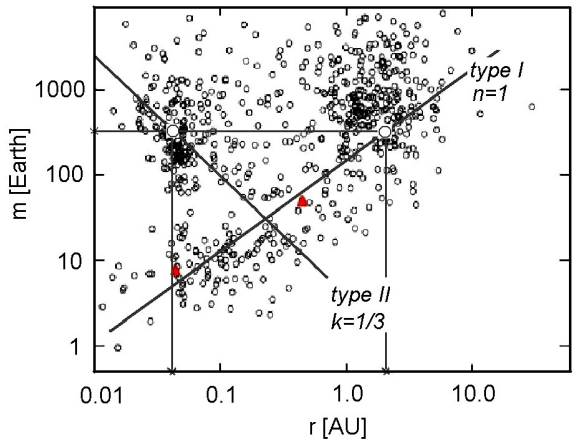

Fig. 5: The calculated dependence $m(r)$ on the background of distribution of all known extrasolar planets in the semimajor axis-mass parameter spaces. Triangles represent the planets of the system GJ 221. Masses are expressed in the masses of the Earth.

Figure 4 shows the actual data on extrasolar Type II planets, which are in agreement with the expression (21) at a coefficient k, whose value differs very little from 1/3. When comparing (11) and (20), given that $k \approx 1/3$, one comes to the conclusion that in this case *mg*-contour is *a three-dimensional* element. With decreasing the density of medium towards the periphery of the disc the dimension of *mg*-contour can be reduced.

These planets are mainly found in single-planet systems. The existence of systems of this type was unexpected for astrophysicists. It is supposed that their formation or dynamical history occurred in another way when the planets were formed on the periphery of the initial disc and then migrated to closer orbits [8]. In the framework of the proposed model the existence of such planetary systems *is natural*. Moreover, this situation by Type II occurs in systems of planetary satellites, such as the Earth-Moon, Neptune-Triton, and Pluto-Charon.

Figure 5, taken from the article [9], shows a large array of data on extrasolar planets in the coordinates r — m (star masses are different). In order to confirm these regularities isolines $m(r)$ by (16) and (21) at $M = 1$ s.m. superimposed on the diagram; they just pass through areas, where the planets are at the most grouped. Moreover, the model allows us to explain the presence of the large number of massive planets and indicate the area, where they are concentrated.

In paper [2] it is shown that for the central star there is a period of evolution when the number of *mg*-contours is equal to the number of *mi*-zones, which should correspond to the most *stable or balanced state*. It is this period is most favorable for the formation of the most massive planets. In this case, the evolutionary parameter ε receives the expression:

$$\varepsilon = fM^{11/12}. \tag{22}$$

Then, as it follows from (19) and (22),

$$m = M^{23/15}. \tag{23}$$

For the mass of the Sun $M = 2 \times 10^{-6}$. Then $m_p = (2 \times 10^{-6})^{23/15} M_m$ or 1.85×10^{27} kg, which is almost exactly the mass of Jupiter. Depending on the type of planetary system this mass can arise in orbit size of 0.038 au (hot Jupiters), or 2.3 au (cold Jupiter), (Fig. 5). More massive stars give rise greater mass of the planet.

Figure 6 shows the dependencies of $m(r)$ by (16) at different n and by (21) at $k = 1/3$ as well as the position of the planets in the solar system. Decrease in the value of index n with increasing radius and decreasing density of protoplanetary disk is interpreted by expression $n - (n - 0.4)r/50$, assuming that the disk was limited of radius 50 au wherein n was reduced to a value 0.4 at the periphery.

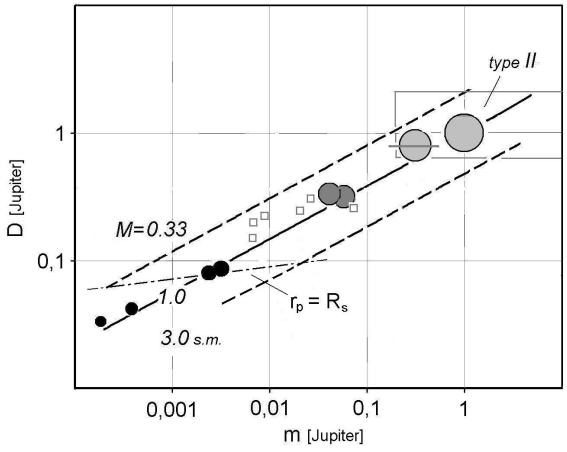

Fig. 7: Dependence of the diameter of the planets on their mass for Type I planets. The squares marked planets of the system Kepler-11. Rectangle roughly bounded region of massive Type II planets at $M \approx 1$. Dash-dot line shows the boundary of the minimum planetary masses, determined from the condition $r_p = R_s$ at $n = 1$.

In general, the initial protoplanetary cloud of the solar system would fit the flat model at $n \approx 1$ if it is assumed that the small planets were formed close to the Sun, but later moved to a more distant orbit under the influence of massive planets that were formed later. Detection of Earth-like planets that are very close to the central star [10, 16] confirms this assumption. It is also possible that the initial cloud had a low density on the orbits where small planets have been formed.

4 On the parameters of planets

For Type I planets calculations show that $d \gg l$, i.e. a *mg*-contour is actually a one-dimensional structure and when "packaging" it in a volume ratio of its linear dimensions, i.e. ratio of the diameters of planets averaged over density, taking into account (17), must meet the relationship:

$$D = d^{1/3} = m^{5/12} M^{-2/3}. \tag{24}$$

These parameters are here dimensionless and can be expressed as, for example, the parameters of Jupiter and the Sun.

Figure 7 shows the dimensionless dependence $D(m)$ by (24) for Type I planets reduced to the parameters of Jupiter and mass of the Sun. The planets of the solar system are located along a solid line. It also shows the position of the six planets of the sistem Kepler-11 having an intermediate density [11], which generally corresponds to the calculated dependence.

It is interesting to note that the expression (24) obtained solely on the basis of general provisions and being adequate to a wide range for Type I planets, in fact, coincides with the analogous dimensionless dependence derived by the authors in the paper [7]. However, this dependence was obtained by the authors by solving the equation of state, which describes the relationship between density, pressure, and temperature for the substance under conditions of thermodynamic equilibrium. The position of the terrestrial planets corresponds exactly to the general trend and confirms the assumption that these planets were formed by Type I near the Sun.

During evolution first planets were formed when ***the orbital angular momentum of the planet is compared to the rotational angular momentum of the central body***. Let us compare the corresponding expression: to the central body derived in [2] and, referring to (10), (12), (17), (19), at $n = 1$, analogous one to the planet:

$$M \frac{\varepsilon}{f} M_m c R_s = M^{7/10} \left(\frac{\varepsilon}{f} \right)^{6/5} M_m c R_s. \tag{25}$$

As follows from (25):

$$\varepsilon = f M^{3/2}, \tag{26}$$

and then one can obtain:

$$m = M^2, \tag{27}$$

$$r = 1, \tag{28}$$

Radius $r_p = R_s$ is the natural limit for *the minimum masses of Type I planets*. The outer planets, whose mass is *greater*, have the orbital angular momentum greater than the rotational angular momentum of the central star. With $M = 1$ s.m. $m_{p\,min} = 4 \times 10^{-12}$ $M_m = 4 \times 10^{24}$ kg, which just corresponds to the average mass of the terrestrial planets. Thus, in this model the existence of Earth-like planets near the central star is natural.

The size of the planets of type II can be estimated by the value of the orbital radius, having on a *mg*-contour, r/z. Keeping in mind the formula (20) at $k = 1/3$, and expressing r from (21), we obtain:

$$D \sim \frac{M}{m^{1/2}}, \tag{29}$$

There is a need additionally to take account the fact that the unit *mg*-contour is in this case not one-dimensional, and the mass of the model object is proportional to the parameter ε, formula (8). Thus, the relation (29) should be supplemented. Using (19) and moving from the mass ratio to the ratio of linear sizes the final expression gets the following forms:

– in the case of a three-dimensional *mg*-contour

$$D = \frac{M}{m^{1/2}} \left(m^{5/4} M^{-1} \right)^{1/3} = \frac{M^{2/3}}{m^{1/12}}; \tag{30}$$

– for the less dense medium, in the case of two-dimensional *mg*-contour, formula (30) takes the form:

$$D = \frac{M}{m^{1/2}} \left(m^{5/4} M^{-1} \right)^{1/2} = \frac{M^{1/2}}{m^{1/8}}; \tag{30a}$$

The obtained dimensionless relationships are generally in agreement with the actual laws. Figure 8 shows the dependence of $D(M)$, and Figure 9 shows the dependence of $D(m)$ calculated from formulas (30) and (30a) at different M, which are for illustrative purposes superimposed on the chart taken from the article [12].

In particular, it becomes clear both the existence of planets with similar sizes but sharply differing masses and having the same mass at various sizes. Planets with a relatively small mass, for example, GJ 1214b [13], Kepler-87c (they are shown in Figure 8 and 9), and others, formed probably by type II; their diameters varied greatly and correspond to the values, which are calculated by the option (30a).

The densities of Type I and Type II planets through their mass and the mass of a star in dimensionless units (in units of the Jupiter's mass and the Sun's mass), having in mind that $\rho \sim mD^{-3}$, have radically different character and can be expressed as follows:

$$\rho_1 = m^{-1/4} M^2, \tag{31}$$

$$\rho_2 = m^{5/4} M^{-2}, \tag{32}$$

$$\rho_{2a} = m^{5/8} M^{-3/2}. \tag{32a}$$

Of course, obtained dependences are not precise or definitive. They only reflect the general trends uniting the diameter of the planet to its mass and the mass of stars in the period of the formation of planetary systems. By equating the orbital angular momentum of the planet and the rotational angular momentum of the central body one can obtain the relations similar to (25-28) for Type II planets at $k = 1/3$:

$$M\left(\frac{\varepsilon}{f}\right) M_m c R_s = M^{3/2}\left(\frac{\varepsilon}{f}\right)^{1/2} M_m c R_s, \tag{33}$$

$$\varepsilon = fM, \tag{34}$$

$$m = M^{8/5}, \tag{35}$$

$$r = M^{-1/5}, \tag{36}$$

which determine their specific mass and orbital radius. At $M = 1$ s.m. $m_p = 7.6 \times 10^{-10} M_m = 7.6 \times 10^{26}$ kg or 0.4 Jupiter's masses, $r_p = 13.8\ R_s = 1.03 \times 10^{10}$ m or 0.07 au. The inner planets with a greater mass have angular momentum that *is less* than that of the central star.

As follows from (21) and (32) Type II planet masses decrease with increasing distance from the central star as well as their density decreases. This is illustrated by the planet Kepler 87c having a very low density with its orbital radius of 136 R_s or 0.68 au. Formation of the planets in more remote orbits it is unlikely, where the less often they exist, the more massive major planet [8].

Low-mass rocky planets of type II can not be formed near Sun's mass stars and having greater masses, but, as follows from (32), their formation is possible in the system of

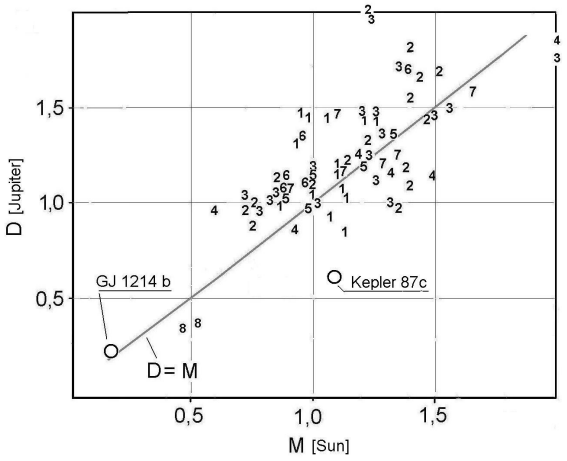

Fig. 8: Dependence of the diameter of the planets on the mass of the central star (masses of the planets are different). 1 — CoRoT, 2 — HAT-P, 3 — WASP, 4 — KOI, 5 — XO, 6 — TrES, 7 — OGLE, 8 — GJ.

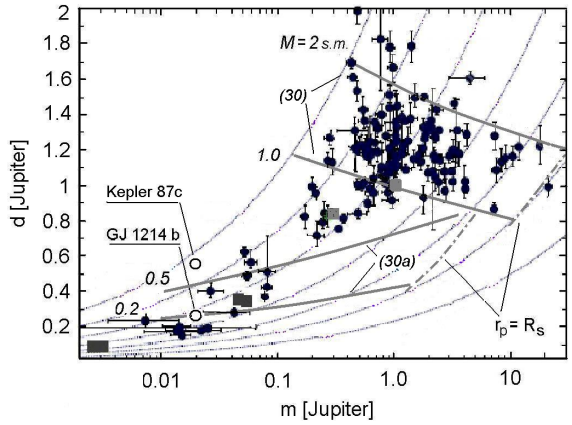

Fig. 9: The calculated dependences $D(m)$ of Type II planet on the background of distribution of known transit extrasolar planets in the planet mass-radius spaces. Squares shows the planets in the solar system. Dotted lines are lines of equal density — 0.1, 0.3, 0.9, 3.0, 9.0, 25.0, and 100 g/cm^3. Dash-dotted line limits the maximum masses of the planets, $k = 1/3$.

dwarf stars when $M < 1$ s.m. Indeed, another test of the correctness of the presented model may serve determination the masses of stars, at which planets with masses and sizes like the Earth can be formed. Let their mass is in the range from $0.001 \ldots 0.01$ Jupiter's mass and the density is $3 \ldots 5$ Jupiter's density.

Then for the Type I planets formula (31) gives: $M = 0.73 \ldots 1.26$ s.m. and for Type II planets formulas (32) and (32a) give: $M = 0.006 \ldots 0.032$ and $M = 0.019 \ldots 0.07$ s.m. The first solution is obvious and corresponds to the stars

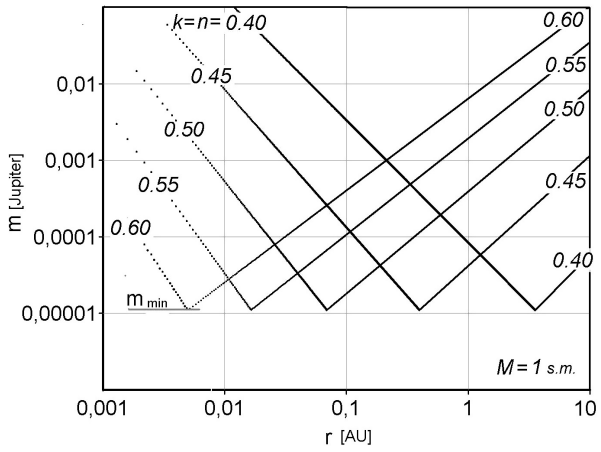

Fig. 10: Dependence of the mass of the planets on their orbital radius at $l = d$.

with a mass close to the mass of the Sun and the second solutions just correspond to the very low-mass stars — *brown dwarfs*.

This prediction proved to be correct. Indeed, recent observations have shown that is quite possible the formation of Earth-like planets around of brown dwarfs and there may be created suitable conditions for emergence of life [14]. These types of planetary systems even more preferable since no need planets to migrate to more distant (as in the case of the Earth) and the suitable masses of the brown dwarfs vary within a more wide range. The question arises whether there are conditions under which the formation of planets in the evolution of both types is equally probable?

It is logical to assume that in the initial period there had been rarefied initial spherical cloud around the central body, which is then transformed into or flatspiral disk, or lenticular in shape, from which Type I planets or Type II planets, respectively, have been formed. Hypothetically, this would correspond to the initial state of complete equality of conditions of planets formation in both types, i.e. $l = d = M$, $n = k$, masses of planets by (16) and (21) are equal.

Having in mind (16), (17), (21), we find:

$$n = k = 0.2\left(\frac{\lg\left(rM^2\right)}{\lg\left(M/r\right)} + 1\right), \tag{37}$$

$$m = M^{12/5}. \tag{38}$$

Thus, this mass depending on the coefficient n may occur at any orbit (Fig. 10). The size of the planet in this case is uncertain since dependences (24) and (30) are here incorrect. One can specify the maximum size of an object if mg-counters are packaged in a linear structure, $D_{max} = zl$. Since $z = m^{-1/4}$ and $l = M$, using (38), we obtain:

$$D_{max} = M^{2/5}. \tag{39}$$

Convergence coefficient values of n and k indicate a decrease formally in the density of medium in any variant evolution that, obviously, corresponds to the moust low mass. The average value of the coefficient equal to 0.5 at $M = 1$ s.m. corresponds to the orbital radius of 0.07 au, which coincides with the specific radius for Type II planets.

For the mass of the Sun, $m_{p\,lim} = 2.1 \times 10^{-14} M_m = 2.1 \times 10^{22}$ kg, $D_{p\,max} = 0.0053\, R_s = 3.9 \times 10^6$ m. It is unknown whether such planets form in reality. In any case, in the solar system there are no regular planet's masses less than $m_{p\,lim}$, except Pluto having a similar mass of 1.3×10^{22} kg, the status of which is uncertain. The same can be said of the satellite systems of the major planets. Masses less settlement not observed to date also among extrasolar planets.

The existence of lowest masses for the planets formed and, accordingly, their lowest diameters explains fact of rapid decrease of the planets having a small radius as well as existence of a maximum of the planetary radii specified in [15].

5 Conclusion

Planetary systems can be quite diverse as their structure depends on the initial composition of the protoplanetary cloud, mass and type of stars, formation history of the planetary system, and the random factors. Nevertheless, there are some general patterns.

There are two types of planetary systems. In the system of the first type planets are formed from flatspiral protoplanetary cloud. Masses of Type I planets increase to the periphery passing through their maximum (cold Jupiters) that occur in the distance from the center in the local condensations of the medium (the sleeves, spirals), supposedly, in later periods of the evolution. Earth-like planets are formed near the central star and maybe can migrate to the more remote orbits.

In the second type of planetary systems planets are formed from a protoplanetary cloud lenticular or elliptical type. The masses and densities of Type II planets decrease to the periphery of the disc. Massive planets (hot Jupiters) are formed in condensations near the central star; the formation of other planets in more distant orbits is unlikely. Low-mass rocky planets in these systems can be formed only at low-mass stars (brown dwarfs).

The possibility of the formation of Earth-like planets in the planetary systems of brown dwarfs has been predicted.

The regularities among the masses, sizes, orbital radii of the planets and masses of the central stars have been obtained.

Submitted on: July 03, 2013 / Accepted on: July 21, 2013

References

1. Belyakov A. V. Charge of the electron, and the constants of radiation according to J.A.Wheeler's geometrodynamic model. *Progress in Physics*, 2010, v. 4, 90–94.
2. Belyakov A. V. Evolution of Stellar Objects According to J. Wheeler's Geometrodynamic Concept. *Progress in Physics*, 2013, v. 1, 25–40.

3. Belyakov A. V. On the independent determination of the ultimate density of physical vacuum. *Progress in Physics*, 2011, v. 2, 27–29.
4. Stephane Udry. *Geneva University*, Debra Fischer. *San Francisco State University*, Didier Queloz. *Geneva University*. A Decade of Radial-Velocity Discoveries in the Exoplanet Domain.
5. Montet B. T., Crepp J. R. et al. The trends high-contrast imaging survey. iv. the occurrence rate of giant planets around m-dwarfs. 24 July 2013, arXiv: astro-ph/1307.5849 v1.
6. Jones M. I., Jenkins J. S. et al. Study of the impact of the post-MS evolution of the host star on the orbits of close-in planets. A giant planet in a close-in orbit around the RGB star HIP63242. June 2013, arXiv: astro-ph/1306.3939 v1.
7. Seager S., Kuchner M., Hier-Majumder C., Militzer B. Mass-Radius Relationships for Solid Exoplanets. 19 Jul 2007, arXiv: 0707.2895.
8. Steffen J. H., Ragozzine D. et al. Kepler constraints on planets near hot Jupiters. 10 May 2012, arXiv: astro-ph.EP/1205.2309 v1.
9. Arriagada P., Anglada-Escud G. et al. Two planetary companions around the K7 dwarf GJ 221: a hot super-Earth and a candidate in the sub-Saturn desert range. 9 May 2013, arXiv: astro-ph/1305.2203 v1.
10. Sanchis-Ojeda R., Rappaport S. et al. Transits and occultations of an earth-sized planet in an 8.5-hour orbit. 17 May 2013, arXiv: astro-ph/1305.4180 v1.
11. Lissauer J. J., Jontof-Hutter D. et al. All Six Planets Known to Orbit Kepler-11 Have Low Densities. 14 Jun 2013, arXiv: astro-ph/1303.0227 v2.
12. Sato B., Hartman J. D. et al. HAT-P-38b: A Saturn-Mass Planet Transiting a Late G Star. 24 Jan 2012, arXiv: astro-ph/1201.5075 v1.
13. Charbonneau D., Berta Z. K. et al. A super-Earth transiting a nearby low-mass star. http://fr.arxiv.org/ftp/arxiv/papers/0912/0912.3229.pdf. Nature 2009.
14. Ricci L., Testi L., Natta A., Scholz A., Gregorio-Monsalvo L. Alma observations of ρ-oph 102: grain growth and molecular gas in the disk around a young brown dwarf. 28 Nov 2012, arXiv: astro-ph.SR/1211.6743 v1.
15. Morton T. D., Swift J. The radius distribution of small planets around cool stars. 14 Mar 2013, arXiv: astro-ph/1303.3013 v1.
16. Charpinet S., Fontaine G. et al. A compact system of small planets around a former red-giant star. 22 Dec 2011, Nature, 480, 496–499.

LETTERS TO PROGRESS IN PHYSICS

The Liquid Metallic Hydrogen Model of the Sun and the Solar Atmosphere VIII. 'Futile' Processes in the Chromosphere

Joseph Luc Robitaille[1] and Pierre-Marie Robitaille[2]

[1]P.O. Box 21025, Columbus, Ohio, 43221.
[2]Department of Radiology, The Ohio State University, 395 W. 12th Ave, Columbus, Ohio 43210, USA.
robitaille.1@osu.edu

In the liquid metallic hydrogen solar model (LMHSM), the chromosphere is the site of hydrogen condensation (P.M. Robitaille. The Liquid Metallic Hydrogen Model of the Sun and the Solar Atmosphere IV. On the Nature of the Chromosphere. *Progr. Phys.*, 2013, v. 3, L15–L21). Line emission is associated with the dissipation of energy from condensed hydrogen structures, CHS. Previously considered reactions resulted in hydrogen atom or cluster addition to the site of condensation. In this work, an additional mechanism is presented, wherein atomic or molecular species interact with CHS, but do not deposit hydrogen. These reactions channel heat away from CHS, enabling them to cool even more rapidly. As a result, this new class of processes could complement true hydrogen condensation reactions by providing an auxiliary mechanism for the removal of heat. Such 'futile' reactions lead to the formation of activated atoms, ions, or molecules and might contribute to line emission from such species. Evidence that complimentary 'futile' reactions might be important in the chromosphere can be extracted from lineshape analysis.

In order to explain the occurrence of the dark lines in the solar spectrum, we must assume that the solar atmosphere incloses a luminous nucleus, producing a continuous spectrum, the brightness of which exceeds a certain limit. The most probable supposition which can be made respecting the Sun's constitution is, that it consists of a solid or liquid nucleus, heated to a temperature of the brightest whiteness, surrounded by an atmosphere of somewhat lower temperature.

Gustav Robert Kirchhoff, 1862 [1]

1 Introduction

During a solar eclipse, the flash spectrum associated with the chromosphere of the Sun becomes readily visible [2–5]. This spectrum is dominated by emission lines from hydrogen, most notably H-α, which gives rise to its characteristic color. However, the flash spectrum also contains a wide array of emission lines generated from neutral atoms, ions, or molecules [2–5]. Within the context of the Standard Solar Models (SSM) [6], these emission lines are produced by random temperature related excitation processes in this region of the Sun. Because the SSM adopt a gaseous solar body, the chromosphere is devoid of function and line emission does not help to account for structure.

In sharp contrast, within the Liquid Metallic Hydrogen Solar Model (LMHSM) [7, 8], the chromosphere is a site of hydrogen and proton capture, while the corona is responsible for harvesting electrons [8–12]. Condensation reactions have therefore been advanced to account for the production of emission lines in the chromosphere. These reactions facilitate the deposit of atomic hydrogen onto condensed hydrogen structures, CHS [9, 11, 12]. Line emission in the chromosphere is fundamentally linked to the dissipation of heat associated with exothermic condensation reactions. The role of condensation reactions in the chromosphere of the Sun has previously been presented in substantial detail [9, 11, 12]. For the sake of clarity, it is briefly readdressed herein.

One can consider an atom, A, reacting with hydrogen, H, to give rise to a molecular species, AH [8, 9, 11]. It should be possible for AH and CHS in the chromosphere to form an activated complex, CHS + AH $\rightarrow$ CHS-HA*. This would then be followed by an exothermic step involving the expulsion of an activated atom, CHS-HA* $\rightarrow$ CHS–H + A*, followed by the line emission from A*, A* $\rightarrow$ A + $h\nu$. In such a manner, a viable scheme is presented to account for line emission from neutral atoms, including those from hydrogen itself.

An analogous process could also be applied to a cation, A^{+n}, reacting with hydrogen, H, to give rise to a molecular species, AH^{+n}, where n=1, 2, etc [8, 9, 11]. Reaction of AH^{+n} with a condensed hydrogen structure (CHS) in the chromosphere leads to an activated complex, CHS + AH^{+n} $\rightarrow$ CHS-HA^{+n*}. This would then be followed by an exothermic step involving the expulsion of an activated ion, CHS-HA^{+n*} $\rightarrow$ CHS–H + A^{+n*}, followed by the line emission from the cation, A^{+n*}, A^{+n*} $\rightarrow$ A^+ + $h\nu$. Such reactions have been postulated to play an important role in the chromosphere and can explain the HeII lines, if HeH^+ triggers the condensation [8, 11]. When Ca^+ acts as the initial cation, such a mechanism can account for the strong CaII lines in the Sun [9].

2 'Futile' reactions

There is another class of reactions which may play a role in the Sun, but has previously been overlooked. It is possible for interactions to take place with condensed hydrogen structures, but without the net transfer of a hydrogen atom. This new set of 'futile' reactions is important for three reasons: 1) it offers new insight relative to line emission arising from neutral atoms and molecules, 2) it adds an important new mechanism, which can complement previous reactions [9, 11, 12], in describing spectroscopic linewidths in the chromosphere, and 3) it provides a mechanism which can facilitate condensation reactions in the chromosphere by offering yet another means to dissipate heat.

In biochemistry, futile reactions tend to be cyclic in nature. They involve chemical processes which do not lead to any useful work, but which are exothermic.

A classic example of a futile cycle would involve the reactions of fructose-6-phosphate in glycolysis and gluconeogenesis. During glycolysis, we have a reaction catalyzed by phosphofructokinase: fructose-6-phosphate + ATP → fructose-1,6-bisphosphate + ADP. The reaction is reversed in gluconeogenesis using fructose-1,6-bisphosphatase: fructose-1,6-bisphosphate + H_2O → fructose-6-phosphate + P_i. The overall reaction involves the simple wastage of ATP and energy dissipation without net work: ATP + H_2O→ ADP + P_i + heat. The cell, of course, had to work to make the ATP and as a result, such a cycle is truly futile.

Let us consider the simplest futile reaction in the chromosphere. A hydrogen atom, H, interacts directly with a condensed hydrogen structure to form a weak activated complex, CHS + H → CHS–H^*. But this time, the reaction is reversed and no hydrogen is deposited: CHS–H^* → CHS + H^*. This would then be followed by line emission from activated hydrogen H^*, H^* → H + $h\nu$, as hydrogen is allowed to relax back to the ground state. The reaction appears futile, as no net change has taken place. But on closer examination, it is noted that heat has been removed from the condensed hydrogen structure. As a result, though no additional condensation has occurred, such a futile process can cool the condensing structure, thereby facilitating its growth when other true condensation reactions [8–12] are occurring in parallel.

It is now readily apparent that a wide array of 'futile' processes may exist in the chromosphere. For instance, an atom, A, could react with hydrogen, H, to give rise to a molecular species, AH [8, 9, 11]. AH could interact with CHS in the chromosphere to form an activated complex, CHS + AH → CHS–HA^*. The reaction is reversed and no hydrogen is deposited: CHS–HA^* → CHS + AH^*. This would then be followed by line emission from the molecular species AH^*, AH^* → AH + $h\nu$. In such a manner, a viable scheme is presented to account for line emission from small neutral molecules, such as H_2, CaH, LiH, etc. Similar reactions could also be invoked which involve small molecules such as H_2O or NH_3. The result would be line emission from these molecular species.

The analysis of spectroscopic lineshapes in the Sun is an area of considerable complexity for current models. The wings and cores of many lines appear to change with altitude above the solar surface (see [3, 4, 8, 13] and references therein). Such findings suggest that the mechanism involved in line production might well involve both true condensation reactions and futile processes. As previously stated [8], it is unlikely that Stark mechanisms are truly responsible for the lineshapes we observe in the Sun.

Dedication

Dedicated to past, present, and future astronomers.

Submitted on: January 13, 2014 / Accepted on: January 15, 2014
First published online on: January 18, 2014

References

1. Kirchhoff G. The physical constitution of the Sun. In: *Researches on the Solar Spectrum and the Spectra of the Chemical Elements*. Translated by H.E. Roscoe, Macmillan and Co., Cambridge, 1862, p. 23.
2. Menzel D.H. A Study of the Solar Chromosphere. *Publications of the Lick Observatory*, University of California Press, Berkeley, CA, v. 17, 1931.
3. Thomas R.N. and Athay R.G. Physics of the Solar Chromosphere. Interscience Publishers, New York, N.Y., 1961.
4. Bray R.J. and Loughhead R.E. The Solar Chromosphere (The International Astrophysics Series), Chapman and Hall, London, U.K., 1974.
5. Zirin H. The mystery of the chromosphere. *Solar Phys.*, 1996, v. 169, 313–326.
6. Bahcall J.N. and Pinsonneault M.H. Standard solar models, with and without helium diffusion, and the solar neutrino problem. *Rev. Mod. Phys.*, 1992, v. 64, no.4, 885–926.
7. Robitaille P.M. Liquid metallic hydrogen: A building block for a liquid Sun. *Progr. Phys.*, 2011, v. 3, 60–74.
8. Robitaille P.M. Forty lines of evidence for condensed matter — The Sun on trial: Liquid metallic hydrogen as a solar building block. *Progr. Phys.*, 2013, v. 4, 90–142.
9. Robitaille P.M. The liquid metallic hydrogen model of the Sun and the solar atmosphere IV. On the nature of the chromosphere. *Progr. Phys.*, 2013, v. 3, L15–L21.
10. Robitaille P.-M. The LMH model of the Sun and the solar atmosphere V. On the nature of the corona. *Progr. Phys.*, 2013, v. 3, L22–L25.
11. Robitaille P.M. The liquid metallic hydrogen model of the Sun and the solar atmosphere VI. Helium in the chromosphere. *Progr. Phys.*, 2013, v. 3, L26–L28.
12. Robitaille P.M. The LMH model of the Sun and the solar atmosphere VII. Further insights into the chromosphere and corona. *Progr. Phys.*, 2013, v. 3, L30–L36.
13. Przybilla N. and Butler K. The solar hydrogen spectrum in non-local thermodynamic equilibrium. *Astrophys. J.*, 2004, v. 610, L61–L64.

LETTERS TO PROGRESS IN PHYSICS

Further Insight Relative to Cavity Radiation: A Thought Experiment Refuting Kirchhoff's Law

Pierre-Marie Robitaille

Department of Radiology, The Ohio State University, 395 W. 12th Ave, Columbus, Ohio 43210, USA.
robitaille.1@osu.edu

Kirchhoff's law of thermal emission demands that all cavities contain blackbody, or normal, radiation which is dependent solely on the temperature and the frequency of observation, while remaining independent of the nature of the enclosure. For over 150 years, this law has stood as a great pillar for those who believe that gaseous stars could emit a blackbody spectrum. However, it is well-known that, under laboratory conditions, gases emit in bands and cannot produce a thermal spectrum. Furthermore, all laboratory blackbodies are constructed from nearly ideal absorbers. This fact strongly opposes the validity of Kirchhoff's formulation. Clearly, if Kirchhoff had been correct, then laboratory blackbodies could be constructed of any arbitrary material. Through the use of two cavities in temperature equilibrium with one another, a thought experiment is presented herein which soundly refutes Kirchhoff's law of thermal emission.

If a space be entirely surrounded by bodies of the same temperature, so that no rays can penetrate through them, every pencil in the interior of the space must be so constituted, in regard to its quality and intensity, as if it had proceeded from a perfectly black body of the same temperature, and must therefore be independent of the form and nature of the bodies, being determined by temperature alone. . . In the interior therefore of an opake red-hot body of any temperature, the illumination is always the same, whatever be the constitution of the body in other respects.

Gustav Robert Kirchhoff, 1860 [1]

1 Introduction

Kirchhoff's law [1, 2] is generally considered to be the first amongst the laws governing thermal emission [3–6]. With its formulation, blackbody radiation achieved a magical presence within every cavity. Based on Kirchhoff's law, Planck believed that blackbody radiation had universal significance [6]. It is because of Kirchhoff that Boltzmann's and Planck's constants are viewed as sharing the same quality [5–10]. As such, the collapse of Kirchhoff's law [7–10] has great implication throughout physics. It touches not only condensed matter, but also the very makeup of the stars and our understanding of the microwave background (see [11–13] and references therein). Consequently, many refuse to accept that there can be problems with Kirchhoff's formulation. In so doing, they deny Balfour Stewart proper credit for correctly noting that the emissivity of a material is equal to its absorptivity at thermal equilibrium [14]. Furthermore, *cavity radiation is actually dependent on the nature of the enclosure* [7–10]. As such, a simple thought experiment is now presented which elegantly exposes the error in Kirchhoff's claims.

Cavity radiation revisited

Let us begin with a large perfectly absorbing enclosure - an ideal blackbody (Emissivity (ϵ) = 1, Reflectivity (ρ) = 0; at all temperatures and frequencies), as depicted in Fig. 1. The contents of this cavity are kept under vacuum. Within this outer cavity, let us place a somewhat smaller perfectly reflecting enclosure with 5 sides closed and 1 open ($\epsilon = 0$, $\rho = 1$; at all temperatures and frequencies). Guided by Max Planck [6], both cavities will be large compared to those dimensions which would require the consideration of diffraction. Since the inner cavity is perfectly reflecting, it will also be highly conducting, as good reflectors tend to be good conductors.*

Throughout his classic text on heat radiation [6], Planck makes use of perfectly reflecting enclosures. Therefore, it is appropriate to consider both the perfect emitter ($\epsilon = 1$) and the perfect reflector ($\epsilon = 0$) in this exercise.

At the onset, the experiment requires a mechanical means of closing the inner enclosure. This can be achieved with a mechanism which crosses the walls of the outer cavity while preserving the vacuum. The mechanism is allowed, because laboratory blackbodies are known to possess a small hole in their outer walls through which radiation is typically sampled.

Once this has been accomplished, place the perfectly absorbing enclosure ($\epsilon = 1$, $\rho = 0$), which contains the inner perfectly reflecting cavity ($\epsilon = 0$, $\rho = 1$), in a large helium bath at 4 K. The inner open cavity, is permitted to rest directly on the floor of the outer perfectly absorbing cavity (see Fig. 1). Under these conditions, the inner cavity will achieve temperature equilibrium with the outer cavity using conduction. Radiation inside the perfectly absorbing cavity will correspond

*For example, silver is amongst the best conductors with a resistivity of only ~1.6 x 10^{-8} Ω m at 300 K and of ~0.001 x 10^{-8} Ω m at 4 K [15]. It is also an excellent reflector in the infrared, our frequency range of interest.

Fig. 1: Schematic representation of our thought experiment. A large outer cavity acts as an ideal blackbody ($\epsilon = 1$, $\rho = 0$) and is initially immersed in a helium bath at 4 K. Within this cavity, a perfectly reflecting enclosure ($\epsilon = 0$, $\rho = 1$) rests of the floor with one of its sides initially remaining open.

to black radiation at 4 K. It will fill both the large cavity and the smaller open cavity.

When temperature equilibrium has been reached, permit the inner cavity to be sealed mechanically. At that moment, 4 K blackbody radiation has been trapped inside the smaller perfectly reflecting enclosure.

One can then permit the outer perfectly absorbing enclosure to rise in temperature to 300 K. It will now contain black radiation at that temperature. As for the perfectly reflecting enclosure, it will also move to 300 K, because it can reach temperature equilibrium through conduction (we can use any of 3 mechanisms to reach equilibrium - radiation, conduction, and convection). The inner cavity walls are thus also brought to 300 K. However, unlike the outer cavity which is filled with blackbody radiation at 300 K, the inner cavity remains filled with blackbody radiation at 4 K. Thereby, Kirchhoff's law is proven to be false.

Under these conditions, the only way to enable the inner cavity to hold 300 K blackbody radiation would be to permit a violation of the first and zeroth laws of thermodynamics. Namely, once temperature equilibrium has been reached through conduction, the inner cavity will not be allowed to spontaneously emit photons in search of a new radiative condition, while denying the zeroth law. Photons will not be created where no mechanism exists for their generation.*

In addition, the zeroth law of thermodynamics defines the conditions under which temperature equilibrium exists. These conditions refer to real objects. As long as the outer cavity is in temperature equilibrium with the bath/room and is in temperature equilibrium with the inner cavity; then by definition, the inner cavity is in temperature equilibrium with the bath/room. The nature of the field contained within the inner cavity is not covered by the zeroth law of thermodynamics. As is appropriate, the zeroth and first laws of thermodynamics must guide our judgment relative to Kirchhoff's formulation. Thermal equilibrium is defined as that condition which prevails in the absence of all net changes in conduction, convection, and radiation. Thus, thermal equilibrium has been met when the inner cavity reaches 300 K, despite the fact that it contains 4 K radiation, as there can no longer be any change in net conduction, convection, or radiation, across cavity walls. To argue otherwise implies that the temperature of an object depends on the radiation field it contains. This constitutes a direct violation of the zeroth law of thermodynamics which is independent of radiation fields.

Summary

In this thought experiment, two cavities have been considered and temperature equilibrium between them ensured using conduction. The perfectly absorbing cavity ends up holding perfectly black radiation at all temperatures because its emissivity is 1. But the situation is not the same for the inner cavity, as its emissivity is 0 at all temperatures.

Max Planck previously noted in his classic text on heat radiation that: *"... in a vacuum bounded by totally reflecting walls any state of radiation may persist"* [6, § 51]. In order to ensure that a perfectly reflecting cavity could contain black radiation, he inserted a small particle of carbon (see [9] for a detailed discussion). However, when Planck does so, it is as if he had lined the entire cavity with an excellent absorber, because the carbon particle was identical to graphite, a *nearly perfect absorber*, almost by definition [9]. Planck remains incapable of demonstrating that cavity radiation will always be black, independent of the nature of the walls [7–10].

When the temperature was brought to 300 K, the two cavities responded in different ways as a result of their inherent emissivities. The outer cavity has a perfect emissivity ($\epsilon = 1$) and is able to pump out additional photons, as required by Stefan's law [4]. Since Stefan's law has a fourth power dependence on temperature (T^4), the outer cavity now contains 3.2 x 10^7 times more photons than it did when its temperature was a 4 K. However, the radiation within the inner cavity *persists*, just as Max Planck stated. That is because this cavity lacks the physical mechanism to emit a photon. Until it is opened, it will forever contain black radiation which had cor-

*The emissivity of a material is defined relative to the emissivity of a blackbody at the temperature in question. Selecting an emissivity value for the surface of a cavity therefore implies thermal equilibrium by definition. Yet, in modeling the blackbody problem, computer simulations often perpetually pump photons into cavities, invoke reflection, and build up radiation until they achieve the blackbody spectrum. But real materials cannot act as perpetual sources of photons without dropping in temperature. Obviously, the temperature of a cavity which is already at equilibrium, by definition, cannot be allowed to drop. The pumping of ever more photons into an arbitrary cavity while invoking reflection as a means to justify the buildup of the blackbody spectrum is forbidden by the first law of thermodynamics [10].

responded to that initially produced by the outer cavity when it was at 4 K.

The perfectly absorbing cavity ends up holding perfect black radiation at all temperatures because its emissivity is 1. The perfectly reflecting cavity maintains 4 K radiation, because its emissivity is zero. There is no violation of the first law and the zeroth law guarantees the equilibrium arguments. It is permitted to utilize a perfectly reflecting ($\epsilon = 0$) cavity in this work using the same logic which allows the physics community to hypothesize that perfectly absorbing cavities ($\epsilon = 1$) exist. In reality, both objects cannot be found either in nature, or in the laboratory, over the range of frequencies and temperatures which might be of interest.

The discussion can be extended further to hypothesize, of course, that initial conditions (before the inner cavity was sealed) were at absolute zero. In that case, the inner cavity will always be devoid of radiation once it is closed. Should another initial condition be selected, then, when it is sealed, the inner cavity will contain black radiation at that temperature.

What becomes clear is that the radiation contained in the inner cavity can be made to be absolutely dependent on initial conditions (unrelated to final temperature) and dependent on the nature of the cavity walls. Stewart's law [8, 14] and not Kirchhoff's [1, 2] properly describes the relationship between emission and absorption under conditions of thermal equilibrium.

At the same time, it should be recognized that temperature equilibrium can be achieved without a detailed balance between emission and absorption. This can occur if there is net conduction, convection, or radiation into, or out of, an object whose temperature does not change. For instance, heat could enter through radiation and leave through conduction, while the temperature remains constant. Under these conditions, the object is under temperature equilibrium, but not under thermal equilibrium. Namely, its emission can be much less than its absorption, even if the temperature is not changing. When considering thermal equilibrium and the laws of emission *there must be no net conduction, convection, or radiation*.

This should sufficiently address, in the simplest form, the truth of Kirchhoff's formulation. Based on this presentation, Kirchhoff's law is not valid and the constants of Planck and Boltzmann are not universal.

Acknowledgment

Luc Robitaille is acknowledged for the preparation of Fig. 1.

Dedication

This work is dedicated to my first grandchild, Simone, as this thought experiment was envisioned on the day of her birth while I was driving alone from my home in Columbus to the hospital in Indiana.

Submitted on: January 13, 2014 / Accepted on: January 15, 2014
First published online on: January 18, 2014

References

1. Kirchhoff G. Über das Verhältnis zwischen dem Emissionsvermögen und dem Absorptionsvermogen. der Körper fur Wärme und Licht. *Poggendorfs Annalen der Physik und Chemie*, 1860, v. 109, 275–301. (English translation by F. Guthrie: Kirchhoff G. On the relation between the radiating and the absorbing powers of different bodies for light and heat. *Phil. Mag.*, 1860, ser. 4, v. 20, 1–21).
2. Kirchhoff G. Über den Zusammenhang zwischen Emission und Absorption von Licht und. Wärme. *Monatsberichte der Akademie der Wissenschaften zu Berlin*, sessions of Dec. 1859, 1860, 783–787.
3. Wien W. Über die Energieverteilung in Emissionspektrum eines schwarzen Körpers. *Ann. Phys.*, 1896, v. 58, 662–669.
4. Stefan J. Über die Beziehung zwischen der Warmestrahlung und der Temperature. *Sitzungsberichte der mathematisch naturwissenschaftlichen Classe der kaiserlichen Akademie der Wissenschaften*, Wien 1879, v. 79, 391–428.
5. Planck M. Über das Gesetz der Energieverteilung im Normalspektrum. *Annalen der Physik*, 1901, v. 4, 553–563 (English translation by ter Haar D.: Planck M. On the theory of the energy distribution law in the normal spectrum. The old quantum theory. Pergamon Press, 1967, 82–90; also Planck's December 14, 1900 lecture *Zur Theorie des Gesetzes der Energieverteilung in Normalspectrum*, which stems from this paper, can be found in either German, or English, in: Kangro H. Classic papers in physics: Planck's original papers in quantum physics. Taylor & Francis, London, 1972, 6–14 or 38–45).
6. Planck M. The theory of heat radiation. P. Blakiston's Son & Co., Philadelphia, PA, 1914.
7. Robitaille P.-M. On the validity of Kirchhoff's law of thermal emission. *IEEE Trans. Plasma Sci.*, 2003, v. 31, no. 6, 1263–1267.
8. Robitaille P.-M. A critical analysis of universality and Kirchhoff's law: A return to Stewart's law of thermal emission. *Progr. Phys.*, 2008, v. 3, 30–35.
9. Robitaille P.-M. Blackbody radiation and the carbon particle. *Progr. Phys.*, 2008, v. 3, 36–55.
10. Robitaille P.-M. Kirchhoff's law of thermal emission: 150 Years. *Progr. Phys.*, 2009, v. 4, 3–13.
11. Robitaille P.-M. Blackbody radiation and the loss of universality: Implications for Planck's formulation and Boltzmann's constant. *Progr. Phys.*, 2009, v. 4, 14–16.
12. Robitaille P.-M. Water, hydrogen bonding, and the microwave background. *Progr. Phys.*, 2009, v. 2, L5–L8.
13. Robitaille P.-M. Fourty lines of evidence for condensed matter - The Sun on trial: Liquid metallic hydrogen as a solar building block. *Progr. Phys.*, 2013, v. 4, 90–142.
14. Stewart B. An account of some experiments on radiant heat, involving an extension of Prévost's theory of exchanges. *Trans. Royal Soc. Edinburgh*, 1858, v. 22, no. 1, 1–20 (also found in Harper's Scientific Memoirs, edited by J.S. Ames: The Laws of Radiation and Absorption: Memoirs of Prévost, Stewart, Kirchhoff, and Kirchhoff and Bunsen, translated and edited by D.B. Brace, American Book Company, New York, 1901, 21–50).
15. Electrical Resistivity of Pure Metals. In, *CRC Handbook of Chemistry and Physics*, 2013–2014, CRC Press, Baca Raton, FL, p. 12-42.

ΔI=2 Nuclear Staggering in Superdeformed Rotational Bands

Madiha D. Okasha

Physics Department, Faculty of Science (Girls College), Al-Azhar University, Cairo, Egypt. E-mail: mady200315@yahoo.com

A four parameters model including collective rotational energies to fourth order is applied to reproduce the ΔI=2 staggering in transition energies in four selected super deformed rotational bands, namely, ^{148}Gd (SD6), ^{194}Hg (SD1, SD2, SD3). The model parameters and the spin of the bandhead have been extracted assuming various values to the lowest spin of the bandhead at nearest integer, in order to obtain a minimum root mean square deviation between calculated and the experimental transition energies. This allows us to suggest the spin values for the energy levels which are experimentally unknown. For each band a staggering parameter represent the deviation of the transition energies from a smooth reference has been determined by calculating the fourth order derivative of the transition energies at a given spin. The staggering parameter contains five consecutive transition energies which is denoted here as the five-point formula. In order to get information about the dynamical moment of inertia, the two point formula which contains only two consecutive transition energies has been also considered. The dynamical moment of inertia decreasing with increasing rotational frequency for $A \sim 150$, while increasing for $A \sim 190$ mass regions.

1 Introduction

The observation [1] of a very regular pattern of closely spaced γ-transitions in the spectrum of ^{152}Dy, which assigned to a rotational cascade between levels of spin ranging from $60\hbar$ to $24\hbar$ and excitation energy varying from ~ 30 to 12 MeV may adopt a superdeformed (SD) at high angular momentum. The moment of inertia of the associated band was found to be close to that of a rigid rotor with a 2:1 axis rotation. Now more than 350 settled superdeformed rotational bands (SDRB's), in more than 100 nuclei have been studied in nuclei of mass A ~ 30, 60, 80, 130, 150, 160, 190 [2, 3]. Such nuclei are associated with extremely large quadrupole $\beta_2 = 0.6$ in the mass A ~ 150 region and $\beta_2 = 0.47$ in the mass A ~ 190 region. Hence, they are expected to have a different structures to normal deformed nuclei.

Unfortunately, despite the rather large amount of experimental information on SDRB's, there are still a number of very interesting properties, which have not yet been measured. For example, the spin, parity and excitation energy relative to the ground state of the SD bands. The difficulty lies with observing the very weak discrete transitions which link SD levels with levels of normal deformation (ND). Several related approaches to assign the spins of SDRB's in terms of their observed γ-ray transition energies were proposed [4–10]. For all approaches an extrapolation fitting procedure was used.

It was found that some SDRB's show an unexpected ΔI=2 staggering in their γ-ray transition energies [11–20]. The SD energy levels are consequently separated into two sequences with spin values I, I+4, I+8, ...and I+2, I+6, I+10, ... respectively. The magnitude of splitting is found to be of some hundred eV to a few keV. Several theoretical explanation have been made. One of the earliest ones being based on the assumption of a C4 symmetry [21]. Also it was suggested that [22] the staggering is associated with the alignment of the total angular momentum along the axis perpendicular to the long deformation axis of a prolate nucleus. The staggering phenomenon was interpreted also as due to the mixing of a series of rotational bands differ by ΔI=4 [23] or arise from the mixing of two bands near yrast line [24] or by proposing phenomenological model [25, 26]. The main purpose of the present paper is to predict the spins of the bandhead of four SDRB's in A ~ 150 and A ~ 190 mass regions, and to examine the ΔI=2 staggering and the properties of the dynamical moments of inertia in framework of proposed four parameters collective rotational model.

2 Nuclear SDRB's in Framework of Four Parameters Collective Rotational Model

On the basis of collective rotational model [27] in adiabatic approximation, the rotational energy E for an axial symmetric nucleus can be expanded in powers of I(I+1), where I is the spin of state:

$$E(I) = A[I(I+1)]+B[I(I+1)]^2+C[I(I+1)]^3+D[I(I+1)]^4 \quad (1)$$

where A is the well-known rotational parameter for sufficiently small values of I and B, C, D are the corresponding higher order parameters. In the view of the above mentioned, it seems that the ground state energy bands of deformed even-even nucleus have quantum number K=0 (K is the projection of I along the symmetry axis), together with even parity and angular momentum. In SD nuclei, the experimentally determined quantities are the gamma ray transition energies between levels differing by two units of angular momentum, then we could obtain the reference transition energy

$$E_\gamma^{ref} = E(I)-E(I-2) \quad (2)$$

Table 1: The calculated adopted best parameters and the bandhead spins for the selected SD nuclei to investigate the $\Delta I = 2$ staggering.

SD-Band	A (keV)	B (keV) $\times 10^4$	C (keV) $\times 10^8$	D (keV) $\times 10^{12}$	I ($\hbar$)	E_γ (MeV)
^{148}Gd (SD-6)	4.33360	1.17108	0.001135	-0.04435	41	802.200
^{194}Hg (SD-1)	5.40524	-1.86747	0.000338	-0.00213	8	211.700
^{194}Hg (SD-2)	5.24253	-1.577380	0.003991	-0.00269	8	200.790
^{194}Hg (SD-3)	5.21638	-1.48121	0.0006129	-0.006501	9	222.000

$$\begin{aligned} E_\gamma^{ref} &= 2(2I-1)[A+2(I^2-I+1)B \\ &+ (3I^4-6I^3+13I^2-10I+4)C \\ &+ 4(I^6-3I^5+10I^4-15I^3+15I^2-8I+2)D]. \end{aligned} \quad (3)$$

The rotational frequency is not directly measurable but it is related to the observed excitation energy E.

Let us define the angular velocity of nuclear rotation as the derivative of the energy E with respect to the angular momentum I in analogy with classical mechanics. Instead of I it is convenient to use the quantum mechanical analogies $\sqrt{(I(I+1))}$

$$\hbar\omega = \frac{dE}{d\left(\sqrt{(I(I+1))}\right)} \quad (4)$$

$$\begin{aligned} &= 2A[I(I+1)]^{1/2} + B[I(I+1)]^{3/2} \\ &+ 6C[I(I+1)]^{5/2} + 8D[I(I+1)]^{7/2}. \end{aligned} \quad (5)$$

The rotational energy spectra can be discussed in terms of the dynamical moment of inertia calculated from the reciprocal second order derivative:

$$\frac{J^{(2)}}{\hbar^2} = \left(\frac{d^2E}{d\left(\sqrt{I(I+1)}\right)^2}\right)^{-1} \quad (6)$$

$$\begin{aligned} &= \Big([2A + 12B[I(I+1)] \\ &+ 30C[I(I+1)]^2 + 56D[I(I+1)]^3]\Big)^{-1}. \end{aligned} \quad (7)$$

The experimental $\hbar\omega$ and $J^{(2)}$ for the SDRB's are usually extracted from the observed energies of gamma transition between two consecutive transitions within the band from the following formulae:

$$\hbar\omega = [E_\gamma(I) + E_\gamma(I+2)]/4, \quad (8)$$

$$J^{(2)} = \frac{4}{E_\gamma(I+2) - E_\gamma(I)}. \quad (9)$$

We notice that $\hbar\omega$ and $J^{(2)}$ does not depend on the knowledge of the spin I, but only on the measured gamma ray energies.

In order to see the variation in the experimental transition energies $E_\gamma(I)$ in a band, we subtract from them a calculated reference. The corresponding five-point formula is the fourth order derivative of the transition energies at a given spin

$$\begin{aligned} \Delta^4 E_\gamma(I) &= \frac{1}{16}[E_\gamma(I+4) - 4E_\gamma(I+2) \\ &+ 6E_\gamma(I) - 4E_\gamma(I-2) + E_\gamma(I-4)]. \end{aligned} \quad (10)$$

One can easily see that $\Delta^4 E_\gamma(I)$ vanishes if our model contains two parameters A and B, due to the fact that the five-point formula is a normalized discrete approximation of the fourth derivatives of the function $E_\gamma(I)$. We define the staggering parameter $S^{(4)}(I)$ as the difference between the experimental transition energies and the auxiliary reference.

$$S^{(4)}(I) = 2^4[\Delta^4 E_\gamma^{exp}(I) - \Delta^4 E_\gamma^{ref}(I)] \quad (11)$$

3 Numerical Calculations and Discussions

The transition energies $E_\gamma(I)$ of equation (2) is used to fit the observed transition energies for our selected SDRB's with A, B, C, D and spin value of the bandhead I_0 as free parameters. I_0 is taken to the nearest integer of the fitting, the another fit is made to determine A, B, C and D by using a simulated search program [9] in order to obtain a minimum root mean square deviation

$$\chi = \left[\frac{1}{N}\sum_{i=1}^{N}\left(\frac{E_\gamma^{exp}(I) - E_\gamma^{Cal}(I)}{\triangle E_\gamma^{exp}(I)}\right)\right]^{1/2}$$

of the calculated transition energies E_γ^{Cal} from the measured energies E_γ^{exp}, where N is the number of data points considered, and ΔE_γ^{exp} is the uncertainty of the γ-transition energies. The experimental data for transition energies are taken from ref. [2]. Table (1) summarize the model parameters A, B, C, D and the correct bandhead lowest level spin I_0 and also the lowest γ- transition energies $E_\gamma(I_0 + 2 \rightarrow I_0)$ for our 4 SDRB's.

To investigate the appearance of staggering effects in the γ-transition energies of our selected SDRB's, for each band, the deviation of the γ-transition energies $E_\gamma(I)$ from a smooth reference (rigid rotor) was determined by calculating fourth-derivatives of $E_\gamma(I)$ (d^4E_γ/dI^4) at a given spin I by using the finite difference approximation. The resulting staggering parameters values against spin are presented in Figure (1). A significant ΔI=2 staggering was observed. At high spins the

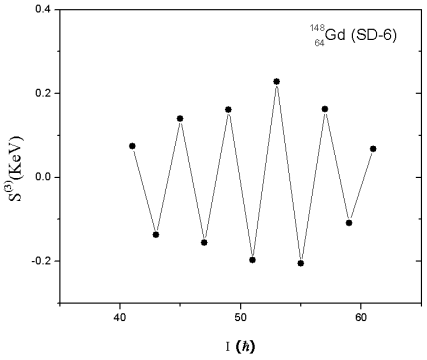

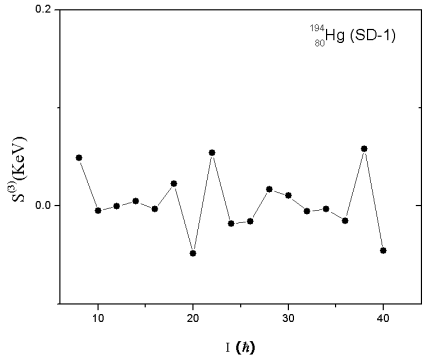

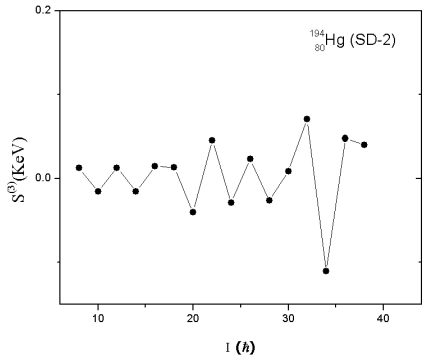

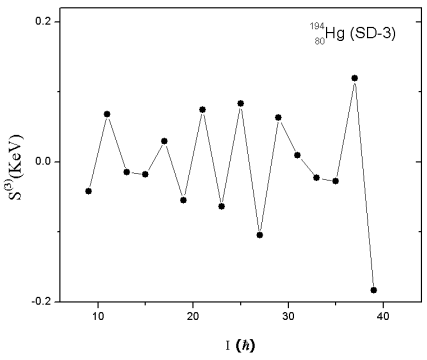

Fig. 1: The calculated $\Delta I = 2$ staggering parameters $S^{(4)}(I)$ obtained by five-point formula versus nuclear spin I for the SDRB's in ^{148}Gd and ^{194}Hg.

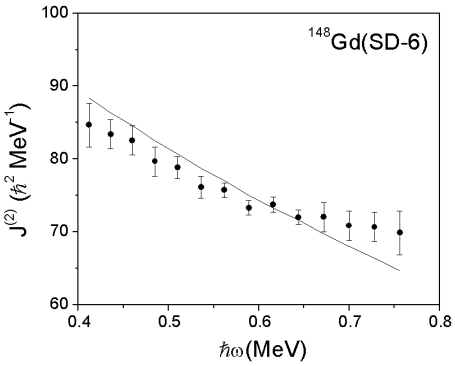

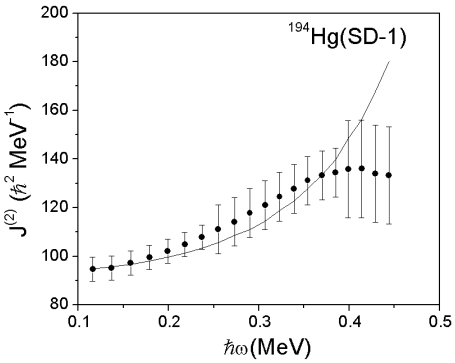

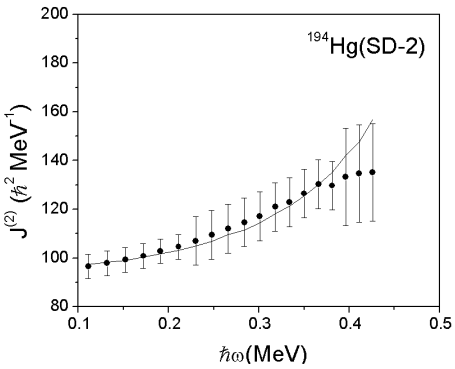

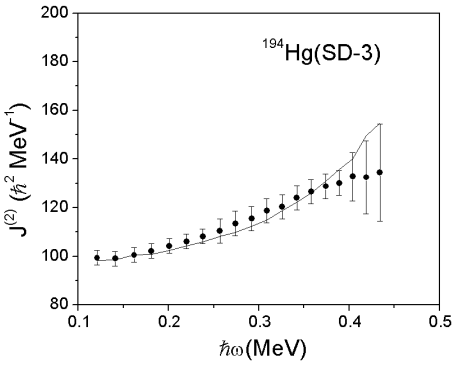

Fig. 2: The dynamical moment of inertia $J^{(2)}$ plotted as a function of the rotational frequency $\hbar\omega$ for the SDRB's in ^{148}Gd and ^{194}Hg nuclei. The solid curve represents the calculated results extracted from the proposed four parameters model. The experimental solid circles with error bars are presented for comparison.

ΔI=2 rotational band is perturbed and two ΔI=4 rotational sequences emerge with an energy splitting of some hundred eV. That is the E2 cascades obtained from our model exhibit for spins I, I+4, I+8, ... and I+2, I+6, I+10, ... staggering behavior.

The systematic behavior of the dynamic moment of inertia $J^{(2)}$ is very useful to understand the properties and structure of SDRB's. Our best fitted parameters were used to calculate the theoretical $J^{(2)}$. The evolution of the dynamical moment of inertia $J^{(2)}$ against rotational frequency $\hbar\omega$ are illustrated in Figure (2). It is seen that the agreement between the calculated (solid lines) and the values extracted from the observed data (closed circles) are excellent. For A∼190, the SDRB's have nearly the same $J^{(2)}$ which typically increase smoothly as rotational frequency increases due to gradual angular momentum alignment of a pair of nucleons occupying specific high-N intruder orbitals and the disappearance of pairing correlations. For A∼150 a smooth decrease of $J^{(2)}$ with increasing $\hbar\omega$ is reproduced well.

Submitted on January 02, 2014 / Accepted on January 10, 2014

References

1. Twin P.J., Nyak B.M. Observation of a Discrete-Line Superdeformed Band up to 60$\hbar$ in ^{152}Dy. *Physical Review Letters*, 1986, v. 57, 811–814.
2. Singh Balraj. Table of Superdeformed Nuclear Bands and Fission Isomers. *Nuclear Data Sheets*, 2006, v. 107, 1–224.
3. Singh Balraj, Zywine Roy, Richard B. Firestone. Table of Superdeformed Nuclear Bands and Fission Isomers. *Nuclear Data Sheets*, 2002, v. 97 (1), 241–592.
4. Draper J.E., Stephens F.S. et al. Spins in superdeformed bands in the mass 190 region. *Physical Review*, 1990, v. C42, R1791–R1795 .
5. Stephens F.S. Spin alignment in superdeformed rotational bands. *Nuclear Physics*, 1990, v. A520, c91–c104.
6. Becker J.A., Henry E.A. et al. Level spin for superdeformed nuclei near A=194. *Physical Review*, 1992, v. C46, 889–903.
7. Khalaf A.M., Allam M.A. and Sirag M.M. Bandhead Spin Determination and Moments of inertia of Superdeformed Nuclei in Mass Region 60-90 Using Variable Moment of inertia Model. *Egypt Journal of Physics*, 2010, v. 41(2), 13–27.
8. Khalaf A.M., Taha M.M. and Kotb M. Studies of Superdeformation in Gadolinium Nuclei Using Three-Parameters Rotational Formula. *Progress in Physics*, 2012, v. 4(2), 39–44.
9. Khalaf A.M. et al. Bandhead Spin Determination and Moments of inertia of Superdeformed Nuclei in Mass Region 60-90 Using Variable Moment of inertia Model. *Progress in Physics*, 2013, v. 3(2), 39–44.
10. Khalaf A.M., Sirag M.M. and Taha M.M. Spin Assignment and Behavior of Superdeformed Bands in A∼150 Mass Region. *Turkish Journal of Physics*, 2013, v. 37, 49–54.
11. Flibotte S. et al. ΔI=4 bifurcation in a superdeformed band: Evidence for a C_4 symmetry band. *Physical Review Letters*, 1993, v. 71, 4299–4302.
12. Cederwall B. et al. New features of superdeformed bands in ^{194}Hg. *Physica Scripta*, 1994, v. 72, 3150–3153.
13. Flibotte S., Hackman G. et al. Multi-particle excitations in the superdeformed ^{149}Gd nucleus. *Nuclear Physics*, 1995, v. A584, 373–396.
14. Carpenter M.P., Janssens R.V.F. Identification of the unfavored N=7 superdeformed band in ^{191}Hg. *Physical Review*, 1995, v. 51, 2400–2405.
15. Farris L.P., Henry E.A. et al. Neutron blocking and delayed proton pair alignment in superdeformed ^{195}Pb. *Physical Review*, 1996, v. C51, R2288–R2292.
16. Bernstein L.A. and Hughes J.R. Superdeformation in ^{154}Er. *Physical Review*, 1995, v. C52, R1171–R1174.
17. de Angelis G. and Wyss R. Spectroscopy in the second well of the^{148}Gd nucleus. Two quasiparticle and collective excitations. *Physical Review*, 1996, v. C53, 679–688.
18. Fischer S.M., Carpenter M.P. et al. Alignment additivity in the two-quasiparticle superdeformed bands of ^{192}Tl. *Physical Review*, 1996, v. C53, 2126–2133.
19. Semple A.T. and Nolan P.J. Energy Staggering in Superdeformed bands in ^{131}Ce, ^{132}Ce and ^{133}Ce. *Physical Review Letters*, 1996, v. 76, 3671–3674.
20. Haslip D.S., Flibotte1 S. and de France G. ΔI= 4 Bifurcation in Identical Superdeformed Bands. *Physical Review Letters*, 1997, v. 78, 3447–3450.
21. Hamamoto I. and Mottleson B. Superdeformed rotational bands in the presence of $_{44}$Y deformation. *Physics Letters*, 1994, v. B333, 294–298.
22. Pavlichenkov I.M. and Flibotte S. C_4 symmetry and bifurcation in superdeformed bands. *Physical Review*, 1995, v. C51, R460–R464.
23. Macchiavell A.O. et al. C_4 symmetry effects in nuclear rotational motion. *Physical Review*, 1995, v. C51, R1–R4.
24. Sun Y., Zhang Z. and Guidry M. ΔI = 4 Bifurcation without Explicit Fourfold Symmetry. *Physical Review Letters*, 1995, v. 75(1), 3398–3401.
25. Khalaf A.M. and Sirag M.M. Analysis of ΔI = 2 Staggering in Nuclear Superdeformed Rotational Bands. *Egypt Journal of Physics*, 2004, v. 35(2), 359–375.
26. Sirag M.M. Reexamination of ΔI = 2 Energy Staggering in Nuclear Superdeformed Rotational Bands. *Egypt Journal of Physics*, 2007, v. 35(1), 1–14.
27. Bohr A. and Mottelson B. Nuclear Structure. W. A. Benjamin Inc., New York 1975.

Lorentzian Type Force on a Charge at Rest

Rudolf Zelsacher

Infineon Technologies AG, Siemensstrasse 2 A-9500 Villach, Austria. E-mail: Rudolf.zelsacher2@infineon.com

A remarkable achievement of theoretical physics is the explanation of magnetic effects, described by the Lorentz force, to be corollaries of charge invariance, Coulombs Law and the Lorentz transformation. The relativistic explanation of magnetism is based essentially on the calculation of Coulomb forces between moving charges in the laboratory reference system. We will show presently that the ideas used for the relativistic explanation of magnetism also lead to a force on a charge at rest by moving charges, which we dub "Lorentzian type force on a charge at rest".

1 Introduction

1.1 Miscellaneous

We will follow very closely the chain of thought taken by Edward Mills Purcell in [1]. We will use the Gaussian CGS units in order to underline the close relationship between electric field $\mathbf{E}(x, y, z, t)$ and magnetic field $\mathbf{B}(x, y, z, t)$. We will use as our reference frame $F[x, y, z, t]$, the idealized laboratory inertial frame, abbreviated to lab, to describe the location of particles and fields at time t. We will use other reference systems like $F'[x', y', z', t']$ with axes parallel with respect to F, with the origins of these systems coinciding at $t = t' = 0$ and with F' being in uniform relative motion with respect to F in either the positive or negative x direction.

Table 1: Definition of symbols

symbol	description
F	inertial frame/system
$\mathbf{F}$	also for force
$\mathbf{p}$	momentum
q	charge
$\mathbf{B}$	magnetic field
$\mathbf{E}$	electric field
a	surface
S	surface
(x, y, z)	space coordinates
t	time
c	speed of light in vacuum
v	velocity
I	current
l	length
β	$\frac{v}{c}$
γ	$\frac{1}{\sqrt{1-\beta^2}}$
m	rest mass
$\hat{\mathbf{x}}, \hat{\mathbf{y}}, \hat{\mathbf{z}}, \hat{\mathbf{r}}$	unit vector in the indicated direction

1.2 The charge and the mass of moving charged particles

The conclusion of the experimental findings is that charge is quantized and invariant in all stages of relative motion, and can be calculated by Gauss's Law [1]

$$q' = q\,. \tag{1}$$

Mass changes with velocity, charge does not. The fact that mass changes with velocity finds its mathematical formulation through the introduction of relativistic momentum [2]

$$\mathbf{p} = m\mathbf{v}\gamma \tag{2}$$

and relativistic energy $E = mc^2\gamma$. Eq. 2 is the starting point for the derivation of forces in inertial systems connected by the Lorentz transformation.

1.3 The electric fields E in F arising from a point charge q at rest in F' and moving with v in F

The electric field $\mathbf{E}$ in F of a charge moving uniformly in F, at a given instant of time, is generally directed radially outward from its instantaneous position and given by [1]

$$\mathbf{E}(\mathbf{R}, \vartheta) = \frac{q\left(1-\beta^2\right)}{R^2\left(1-\beta^2\sin^2\vartheta\right)^{\frac{3}{2}}}\,\hat{\mathbf{R}}\,. \tag{3}$$

R is the length of $\mathbf{R}$, the radius vector from the instantaneous position of the charge to the point of observation; ϑ is the angle between the direction of motion of the charge q $\mathbf{v}\Delta t$ and $\mathbf{R}$. Eq. 3, multiplied by Q, tells us the force on a charge Q at rest in F caused by a charge q moving in F (q is at rest in F').

1.4 The relativistic explanation of magnetism

In Fig. 1 we have sketched the model given in [1] to explain magnetic effects by relativistic arguments. The calculation of the force on q gives

$$F'_y = \frac{dp'_y}{dt'} = qE' = \frac{2q}{\gamma_0 r'}\left(\gamma'_+\lambda_+ + \gamma'_-\lambda_-\right) = \frac{\gamma 4q\lambda v v_0}{r'c^2}. \tag{4}$$

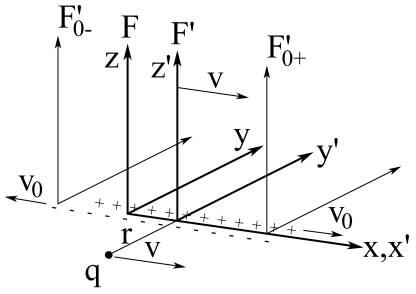

Fig. 1: We show a positive line charge distribution λ_+, stationary in reference frame F'_{0+}, moving in F in the positive x-direction with v_0, and a negative line charge distribution λ_- at rest in F'_{0-}, moving in F in the negative x-direction with v_0. A positive charge q, at rest in F', moves with v in F in the positive x-direction In F the electric fields sum up to **0** because by definition $\lambda_+ + \lambda_- = 0$. In F', the rest frame of charge q, there is an electric field **E' ≠ 0** due to fields transformed from the rest frame of λ_+ and λ_- to F'. The resulting force in F' on q, $d\mathbf{p}'/dt'$, is then transformed to F, the *lab* frame, where we observe the charge q.

The resulting force $d\mathbf{p}'/dt'$ on charge q in F' is transferred to F, the *lab* system, where we do the experiments, giving $F_y = \frac{dp_y}{dt} = \frac{dp'_y}{\gamma dt'}$, and has the value [1]

$$\mathbf{F} = \frac{4q\lambda v v_0}{rc^2}\,\hat{\mathbf{y}} = \frac{2qvI}{rc^2}\,\hat{\mathbf{y}} = \frac{qv}{c}\,\frac{2I}{rc}\,\hat{\mathbf{y}} \qquad (5)$$

with $\lambda = |\lambda_+| = |\lambda_-|$.

As was discovered well before the advent of relativity, the overall effect of currents on a moving charge can also be described completely by introducing the magnetic field **B** in the *lab* frame F and equating the Lorentz force to $d\mathbf{p}/dt$. The magnetic field **B** is calculated with Biot-Savart's Law. The main purpose of the derivation, which results in Eq. 5, is to explain how nature works, and to demonstrate how the physical entity "magnetic field" can be revealed using more fundamental physical laws, specifically Coulomb's law and the laws of special relativity [1].

2 Lorentzian type force on a test charge Q at rest

We consider now two very narrow wires isolated along their length, but connected at the ends, each having length 2a and lying in lab coaxial to the x-axis of F from $x = -a$ to $x = a$. In addition the system has a source of electromotive force applied so that a current I is flowing through the wires: in one of the wires I flows in the positive x direction and in the other wire I flows in the negative x direction. We also have in mind two wires forming a thermocouple or two superconducting wires. On the z-axis of F fixed (at rest) at (0, 0, h) a test charge Q is located.

The system is sketched in Fig. 2. We will now calculate the force $\mathbf{F}_{Lt}$ on the stationary test charge Q fixed at (0, 0, h)

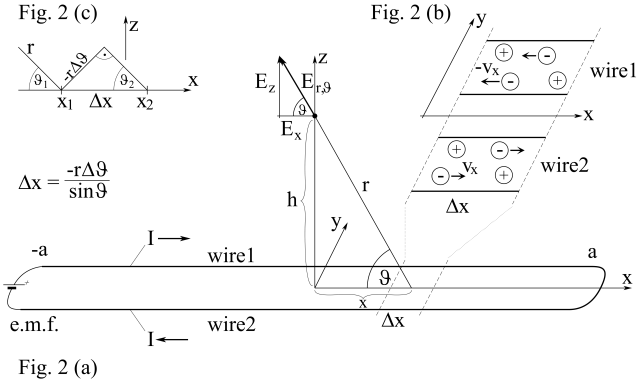

Fig. 2: (a) (b) (c): We show in Fig. 2(a) the two wires carrying the current I extended along the x axis of F from $x = -a$ to $x = a$ and the charge Q at rest in F at (0, 0, h). Additionally on the right-hand side a magnification of a small element Δx containing the two wires and labeled Fig. 2(b) can be seen. Fig. 2(b) shows some moving electrons and for each of these the nearest neighboring proton situated in the tiny element. We calculate the force on Q by precisely these pairs of charges. The effects of the other immobile electrons and protons of element Δx sum up to **0**. On the left-hand side another magnification of element Δx labeled Fig. 2(c) can be seen, showing some geometrical relations useful for integration.

due to the electrons of current I and their nearest stationary protons.

The two wires are electrically neutral before the current is switched on. Therefore after the current is switched on we have an equal number of N electrons and N protons in the system — the same number N, as with the current switched off. We look at the system at one instant of lab time t_0, after the current I is switched on and is stationary. We divide the wires into sections having lengths Δx_i. In each such element we consider the k_i electrons that make up the current I. For each of these k_i electrons e_{ij} with $j = 1, 2, \ldots k_i$, having velocity $\pm v_x$, which are defining the current I in Δx_i, we select the nearest neighboring stationary proton p_{ij} with $j = 1, 2, \ldots k_i$, with the restriction that the proton must lie in Δx_i. "Stationary" means that the charges retain their mean position over time. The effects on Q by the residual K_i stationary protons and K_i stationary electrons present in this element Δx_i sum up to **0**. The number of electrons and protons in the system is given by $N = \sum_i (K_i + k_i)$. For each charge of the mobile electron-stationary proton pairs present in Δx_i, we use the same $\mathbf{r}_i$ as the vector from each of the charges to Q. We use $\vartheta_i = \arcsin\frac{h}{r_i}$, the angle between the x-axis and $\mathbf{r}_i$, for each charge of the pairs of charges present in Δx_i. In Fig.3 we have sketched the situation for one pair of charges.

Referring to Fig. 2 we conclude that the line charge density λ and k_i, the number of current electrons moving with $|v_x|$ in Δx_i, and the line charge density λ and the k_i immobile

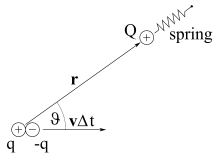

$$\mathbf{F}_Q = \frac{d\left(m\mathbf{v}_Q\gamma_Q\right)}{dt} =$$

$$-\frac{qQ}{r^2}\left(\frac{\left(1-\beta^2\right)}{\left(1-\beta^2\sin^2\vartheta\right)^{\frac{3}{2}}}-1\right)\hat{\mathbf{r}}+\mathbf{F}_{spring}=\mathbf{0}$$

$q \quad \mathbf{v}=\mathbf{0}$ at rest in laboratory

$-q \quad \mathbf{v}\neq\mathbf{0}$ moving in laboratory

$Q \quad \mathbf{v}_Q=\mathbf{0}$ at rest in laboratory

$$\beta=\frac{v^2}{c^2} \quad \gamma_Q=\left(1-\frac{v_Q{}^2}{c^2}\right)^{-\frac{1}{2}}$$

Fig. 3: We show a positive immobile charge q at rest in *lab* and a negative moving charge $-q$ moving in *lab* and the resulting electrical force on a positive charge Q at rest in *lab*. q and $-q$ are one of the pairs of charges that we select at time t_0 in Δx to calculate the effects of the current I on charge Q at rest in *lab*.

protons of Δx_i are both related by

$$k_i = \frac{|\lambda|\Delta x_i}{e} \tag{6}$$

with $e = 4.803^{-10}[esu]$. By doing so we replace the use of the relativistic length contraction by counting charges. We use the same distance $r_i(t_0)$ from Q to the k_i moving electrons and from Q to the k_i immobile protons. We now calculate the force on Q from exactly these charges, i.e. k_i electrons moving with $|v_x|$ and k_i immobile protons. In Figure 2(c) we sketched the model and some geometrical relations which are used below.

With

$$\Delta x = -\frac{r\Delta\vartheta}{\sin\vartheta} \tag{7}$$

and with

$$r = \frac{h}{\sin\vartheta} \tag{8}$$

we get

$$\Delta E_z = \frac{\lambda\left(1-\beta^2\right)\sin\vartheta\Delta\vartheta}{h\left(1-\beta^2\sin^2\vartheta\right)^{\frac{3}{2}}} - \frac{\lambda\sin\vartheta\Delta\vartheta}{h}. \tag{9}$$

Now we have to sum up over all elements Δx_i (or $\Delta\vartheta_i$). We do this by multiplying Eq. 9 by 4 and by integrating from $\vartheta = \frac{\pi}{2}$ to $\vartheta_{min} = \arctan\frac{h}{a}$. For the first term we substitute $u = \beta\cos\vartheta$ and use $\int \frac{du}{\left(a^2+u^2\right)^{\frac{3}{2}}} = \frac{u}{a^2\left(a^2+u^2\right)^{\frac{1}{2}}}$ and finally obtain

$$E_z = \frac{4\lambda\cos\vartheta_{min}}{h}\left(1-\frac{1}{\left(1-\beta^2\sin^2\vartheta_{min}\right)^{\frac{1}{2}}}\right) \approx$$

$$-\frac{2Iv_x\cos\vartheta_{min}\sin^2\vartheta_{min}}{hc^2}.$$

The force on Q, — the "Lorentzian type force on a charge at rest" — is then

$$\mathbf{F}_{Lt} = -\frac{Q\,2Iv_x\cos\vartheta_{min}\sin^2\vartheta_{min}}{hc^2}\,\hat{\mathbf{z}}; \tag{10}$$

q.e.d.

The force described by Eq. 10 is of the same order (e.g. for $\vartheta_{min} = \frac{\pi}{3}$) of magnitude as magnetic forces, as can be seen by comparing it to Eq. 5 (repeated below), but it acts on a charge Q which has zero velocity. Find Eq. 5 written again below

$$\mathbf{F} = \frac{4q\lambda v v_0}{rc^2}\,\hat{\mathbf{y}} = \frac{2qvI}{rc^2}\,\hat{\mathbf{y}} = \frac{qv}{c}\frac{2I}{rc}\,\hat{\mathbf{y}} \qquad \text{(5 repeated)} \tag{11}$$

for easier comparison with Eq. 10.

Discussion

Whenever new concepts and ideas are introduced in physics, it is to be expected that they not only adequately explain the existing findings, but also enable new predictions that are falsifiable by experimental means. The Lorentz force leaves no room for a force on a charge at rest caused by moving charges, because the velocity of the charge at rest is, of course, zero. But the ideas and methods of special relativity, when used to explain magnetism, show that such a force — a force of moving charges which are part of a neutral piece of matter containing the same number of electrons and protons — exerted on a charge at rest, a certain distance away of the above mentioned piece of matter, is possible. We have shown this by reproducing the derivation of magnetism by relativistic arguments given in [1] step-by-step and applying it to our system of wires and charges. We could have calculated the fields and forces on Q in a reference system F' where Q is at rest and transformed the result to F or lab to formally and completely reproduce the derivation of magnetism using relativity, resulting in Eq. 5 as shown in [1] and section 1.4. But as Q is at rest in lab, and therefore at rest in reference frame F, we have calculated the effects on Q due to moving charges directly in F using Eq. 3. Of course we then no longer need to transfer the rate of change of momentum to F because it is directly given in the frame F in which Q is at rest. In addition we have replaced the line charge variations in different reference frames due to the Lorentz-Fitzgerald length contraction used in [1] by defining pairs of moving current electrons and their nearest neighbor immobile protons to calculate the effects on the charge Q. In other words we have replaced the use of the Lorentz-Fitzgerald contraction by counting charges, and counting is relativistically invariant. The basic idea for the calculation of $\mathbf{F}_{Lt}$ manifestations is the use of pairs of moving and immobile charges. If the Lorentzian type force on a charge at rest cannot be found by experiment, and we have no hint that it exists, at least the derivation leading to Eq. 3, written down in [1], should be subject to a revision.

Acknowledgements

I am grateful to Thomas Ostermann for typesetting the equations and to Andrew Wood for correcting the English.

Submitted on January 14, 2014 / Accepted on January 24, 2014

References

1. Purcell E. M. Electricity and Magnetism. McGraw-Hill Book Company, New York, 1964.
2. Kittel C. et al. Mechanics. 2nd Edition, McGraw-Hill Book Company, New York, 1973.

Flow of Viscous Fluid between Two Parallel Porous Plates with Bottom Injection and Top Suction

Hafeez Y. Hafeez[1] and Chifu E. Ndikilar[2]

[1]Physics Department, Federal University Dutse, Nigeria. E-mail: hafeezyusufhafeez@gmail.com
[2] Physics Department, Federal University Dutse, Nigeria. E-mail: ebenechifu@yahoo.com

This paper deals with the problem of steady laminar flow of viscous incompressible fluid between two parallel porous plates with bottom injection and top suction. The flow is driven by a pressure gradient $\frac{\partial p}{\partial x}$ and uniform vertical flow is generated i.e. the vertical velocity is constant everywhere in the field flow i.e. $v = v_w = constant$. Also a solution for the small and large Reynold number is discussed and the graph of velocity profile for flow between parallel plates with the bottom injection and top suction for different values of Reynold numbers is drawn.

1 Introduction

The two dimensional steady laminar flow in channels with porous walls has numerous application in field of Science and Engineering through boundary layer control, transpiration cooling and biomedical enginering.

Berman (1953) was the first reasercher who studied the problem of steady flow in an incompressible viscous fluid through a porous channel with rectangular cross section, when the Reynold number is low and the pertubation solution assuming normal wall velocity to be equal was obtained [1].

Sellars (1955), extended problem studied by Berman by using very high Reynold numbers [2].

Yuan (1956) [3] and Terill (1964) [4] analysed the same problem assuming different normal velocity at the wall.

Terrill and Shrestha (1965) analysed the problem for a flow in a channel with walls of different permeabilities [5].

Green (1979) studied the flow in a channel with one porous wall [7].

In this paper, we considered the flow of an incompressible viscous fluid between two parallel porous plates with bottom injection and top suction and assume that the wall velocity is uniform.

2 Formulation of the problem

The study laminar flow of an incompressible viscous fluid between two parallel porous plates with bottom injection and top suction at walls and uniform cross flow velocity is considered. The well known governing equations of the flow are:

Continuity equation:

$$\frac{\partial u}{\partial x} + \frac{\partial v}{\partial y} = 0. \tag{1}$$

Momentum equations (without body force):

$$u\frac{\partial u}{\partial x} + v\frac{\partial u}{\partial y} = -\frac{1}{\rho}\frac{\partial p}{\partial x} + \nu\left(\frac{\partial^2 u}{\partial x^2} + \frac{\partial^2 u}{\partial y^2}\right), \tag{2}$$

$$u\frac{\partial v}{\partial x} + v\frac{\partial v}{\partial y} = -\frac{1}{\rho}\frac{\partial p}{\partial y} + \nu\left(\frac{\partial^2 v}{\partial x^2} + \frac{\partial^2 v}{\partial y^2}\right). \tag{3}$$

The flow between two porous plates at y=+h and y=-h, respectively is considered.THe flow is deriven by a pressure gradient $\frac{\partial p}{\partial x}$. It is assumeed that a uniform vertical flow is generated i.e the vertical velocity component is constant everywhere in the flow field i.e $v = v_w = constant$. Again the continuity equation shows that $u = u(y)$ only, the momentum equation (2) becomes:

$$v_w\frac{du}{dy} = -\frac{1}{\rho}\frac{dp}{dx} + \nu\frac{d^2u}{dy^2}. \tag{4}$$

Re-arranging eqn. (4), we have

$$\frac{d^2u}{dy^2} - \frac{v_w}{\nu}\frac{du}{dy} = \frac{1}{\mu}\frac{dp}{dx}. \tag{5}$$

Homogeneous part of eqn. (5) becomes

$$\frac{d^2u}{dy^2} - \frac{v_w}{\nu}\frac{du}{dy} = 0. \tag{6}$$

Eqn. (6) is differential equation, with auxiliary equation of

$$p^2 - \frac{v_w}{\nu}p = 0$$

with roots

$$p_1 = 0, p_2 = \frac{v_w}{\nu}.$$

The solution of eqn. (6) is of the form

$$u(y) = Ae^{p_1 y} + Be^{p_2 y},$$

where A and B are constant.

$$u(y) = A + Be^{\frac{v_w}{\nu}y} \tag{7}$$

For particular integral of eqn. (5), we set

$$u(y) = ay^2 + by + c, \tag{8}$$

where a, b, and c are constants.

$$\frac{du}{dy} = 2ay + b, \Rightarrow \frac{d^2u}{dy^2} = 2a \tag{9}$$

Substituting eqn. (9) in eqn. (5) we get

$$\left(2a - \frac{v_w}{\nu}b\right) - 2a\frac{v_w}{\nu}y = \frac{1}{\mu}\frac{dp}{dx}.$$

Comparing the co-efficients, we get

$$a = 0 \Rightarrow b = -\frac{\nu}{v_w}\frac{1}{\mu}\frac{dp}{dx}. \tag{10}$$

Now, eqn. (8) becomes

$$u(y) = -\frac{\nu}{v_w}\frac{1}{\mu}\frac{dp}{dx}y + c. \tag{11}$$

The final solution formes by adding eqn. (7) and eqn. (11)

$$u(y) = D + Be^{\frac{v_w}{\nu}y} - \frac{\nu}{v_w}\frac{1}{\mu}\frac{dp}{dx}y. \tag{12}$$

Since v_w is constant, the equation is linear. We retain the no-slip condition for the main flow.

$$u(+h) = u(-h) = 0$$

$$u(h) = D + Be^{\frac{v_w}{\nu}h} - \frac{\nu}{v_w}\frac{1}{\mu}\frac{dp}{dx}h \tag{13}$$

$$u(-h) = D + Be^{-\frac{v_w}{\nu}h} + \frac{\nu}{v_w}\frac{1}{\mu}\frac{dp}{dx}h. \tag{14}$$

Subtracting eqn. (14) from eqn. (13), we get

$$B = \frac{2\frac{\nu}{v_w}\frac{h}{\mu}\frac{dp}{dx}}{e^{\frac{v_w}{\nu}h} - e^{-\frac{v_w}{\nu}h}} = \frac{2\frac{\nu}{v_w}\frac{h}{\mu}\frac{dp}{dx}}{2\sinh\left(\frac{v_w}{\nu}h\right)} = \frac{\frac{\nu}{v_w}\frac{h}{\mu}\frac{dp}{dx}}{\sinh\left(\frac{v_w}{\nu}h\right)}. \tag{15}$$

Substituting eqn. (15) into eqn. (13), we get

$$D = -\frac{\frac{\nu}{v_w}\frac{h}{\mu}\frac{dp}{dx}e^{\frac{v_w}{\nu}h}}{\sinh\left(\frac{v_w}{\nu}h\right)} + \frac{\nu}{v_w}\frac{h}{\mu}\frac{dp}{dx}. \tag{16}$$

Eqn. (12) reduces to

$$u(y) = -\frac{\frac{\nu}{v_w}\frac{h}{\mu}\frac{dp}{dx}e^{\frac{v_w}{\nu}h}}{\sinh\left(\frac{v_w}{\nu}h\right)} + \frac{\nu}{v_w}\frac{h}{\mu}\frac{dp}{dx} + \frac{\frac{\nu}{v_w}\frac{h}{\mu}\frac{dp}{dx}e^{\frac{v_w}{\nu}y}}{\sinh\left(\frac{v_w}{\nu}h\right)} - \frac{\nu}{v_w}\frac{y}{\mu}\frac{dp}{dx}. \tag{17}$$

But wall Reynold number is $Re = \frac{v_w}{\nu}h$, $\frac{Re}{h} = \frac{v_w}{\nu} \Rightarrow \frac{h}{Re} = \frac{\nu}{v_w}$.

Re-arranging eqn. (17), we get

$$u(y) = -\frac{h^2}{Re}\frac{1}{\mu}\frac{dp}{dx}\left[\frac{y}{h} - 1 + \frac{e^{Re} - e^{Re\frac{y}{h}}}{\sinh(Re)}\right]. \tag{18}$$

The final solution of eqn. (5),

$$\frac{u(y)}{u_{max}} = \frac{2}{Re}\left[\frac{y}{h} - 1 + \frac{e^{Re} - e^{Re\frac{y}{h}}}{\sinh Re}\right]. \tag{19}$$

Where $u_{max} = \frac{h^2}{2\mu}(-\frac{dp}{dy})$ is the centerline velocity for imporous or poiseuille.

For very small Re (or small vertical velocity), then the last terms in the parentheses of of eqn. (19) can be expanded in a power series and $\sinh Re \approx Re$ i.e.

$$\frac{u(y)}{u_{max}} = \frac{2}{Re}\left[\frac{y}{h} - 1 + \frac{1 + Re + \frac{(Re)^2}{2} + .. - \left(1 + Re\frac{y}{h} + \frac{(Re)^2}{2}\frac{y^2}{h^2} + ..\right)}{Re}\right],$$

$$\frac{u(y)}{u_{max}} = \frac{2}{Re}\left[\frac{y}{h} - 1 + \frac{Re\left(1 + \frac{Re}{2} - \frac{y}{h} - \frac{Re}{2}\frac{y^2}{h^2}\right)}{Re}\right],$$

$$\frac{u(y)}{u_{max}} = 1 - \frac{y^2}{h^2}. \tag{20}$$

Eqn. (20) shows that, the poiseuille solution recovered.

For very large Re (or large vertical velocity), eqn. (19) can be written as

$$\frac{u(y)}{u_{max}} = \frac{2}{Re}\left[\frac{y}{h} - 1 + 2\frac{e^{Re} - e^{Re\frac{y}{h}}}{e^{Re} - e^{-Re}}\right],$$

$$\frac{u(y)}{u_{max}} = \frac{2}{Re}\left[\frac{y}{h} - 1 + 2\frac{1 - e^{-Re\left(1 - \frac{y}{h}\right)}}{1 - e^{-2Re}}\right].$$

For $Re \to \infty$ and $\frac{y}{h} > 1$, except for $y = +h$, we get

$$\frac{u(y)}{u_{max}} = \frac{2}{Re}\left[\frac{y}{h} - 1 + 2\right],$$

$$\frac{u(y)}{u_{max}} = \frac{2}{Re}\left[1 + \frac{y}{h}\right], \tag{21}$$

so that a straight line variation which suddenly drops to zero at the upper wall.

3 Discussion

The velocity profiles have been drawn for different values of Reynold numbers (i.e. Re = 0, 3, 5, 10). From Fig. (1), its observed that for $Re \geq 0$ in the region $-1 \leq y^* \leq 1$, the shapes change smoothly with Reynold numbers and the average velocity is decreasing and Reynold number increases; i.e. the friction factor increases as we apply more cross flow through the wall.

4 Conclusion

In the above analysis a class of solution of flow of viscous fluid between two parallel porous plates with bottom injection and top suction is presented when a cross flow velocity along the boundary is uniform, the convective acceleration is linear and the flow is deriven from pressure gradient.

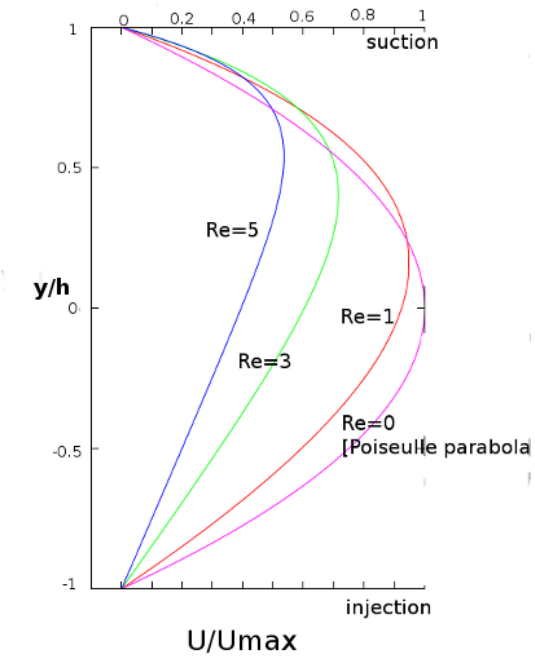

Fig. 1: Velocity profiles for flow between parallel plates with bottom injection and top suction for different values of Re.

Nomenclature

A,B,C,D: Constants
h: Height of the channel
P: Pressure
x: Axial distance
y:Lateral distance
v_w: Lateral wall velocity
u(x,y): Axial velocity component
v(x,y): Lateral velocity component
$y^* = \frac{y}{h}$: Dimensionless lateral distance
$Re = \frac{v_w h}{\nu}$: Wall Reynold number

Greek Symbols

μ: Shear viscosity
ν: Kinematic viscosity
ρ: Fluid density

Submitted on January 20, 2014 / Accepted on January 25, 2014

References

1. Berman A.S. Laminar flow in channels with porous walls. *Journal of Applied Physics*, 1953, v. 24, 1232.
2. Sellars J.R. Laminar flow in channels with porous walls at high suction Reynold number. *Journal of Applied Physics*, 1955, v. 26, 489.
3. Yuan S.W. Further Investigation of Laminar Flow in Channels with Porous Walls. *Journal of Applied Physics*, 1956, v. 27(3), 267–269.
4. Terrill R.M. Homotopy Analysis Solutions for the Asymmetric Laminar Flow in a Porous Channel with Expanding or Contracting Walls. *Aeronautical Quarterly*, 1964, v. 15, 299–310.
5. Terrill R.M., Shrestha G.M. Journal of Applied Mathematical Physics, 1965, v. 16, 470–482.
6. White F. Viscous fluid flow. 2nd edition, Mc Graw-Hill company, New York, 1991.
7. Green G.A. *Laminar flow through a channel with one porous wall*. Course project in Advanced fluid mechanics, 1979, Department of Chemical and Environmental Engineering.

Orbits in Homogeneous Time Varying Spherical Spacetime

Chifu E. Ndikilar

Physics Department, Federal University Dutse, P.M.B 7156, Dutse, Jigawa State, Nigeria. E-mail: ebenechifu@yahoo.com

The solution to Einstein's gravitational field equations exterior to time varying distributions of mass within regions of spherical geometry is used to study the behaviour of test particles and photons in the vicinity of the mass distribution. Equations of motion are derived and an expression for deflection of light in this gravitational field is obtained. The expresion obtained differs from that in Schwarzschild's field by a multiplicative time dependent factor. The concept of gravitational lens in this gravitational field is also studied.

1 Introduction

In [1], the covariant metric tensor exterior to a homogeneous time varying distribution of mass within regions of spherical geometry is defined as:

$$g_{00} = -\left[1 + \frac{2}{c^2} f(t,r)\right] \tag{1}$$

$$g_{11} = \left[1 + \frac{2}{c^2} f(t,r)\right]^{-1} \tag{2}$$

$$g_{22} = r^2 \tag{3}$$

$$g_{33} = r^2 \sin^2\theta \tag{4}$$

where $f(t,r)$ is a function dependent on the mass distribution within the sphere that experiences radial displacement. Einstein's gravitational field equations were constructed in [1] and an approximate expression for the analytical solution of the lone field equation was obtained as

$$f(t,r) \approx -\frac{k}{r} \exp\, i\omega\left(t - \frac{r}{c}\right) \tag{5}$$

where $k = GM_0$ with G being the universal gravitational constant and M_0 the total mass of the spherical body. ω is the angular frequency of the radial displacement of mass within the sphere.

In this article, we use this solution of Einstein's field equations to study the behaviour of light in the vicinity of a time varying spherical mass distribution.

2 Orbits in Time Varying Spherical Spacetime

In order to study the motion of planets and light rays in a homogeneous time varying spherical spacetime, there is need to derive the geodesic equations [2]. The Lagrangian (L) for this gravitational field can be defined using the metric tensor as:

$$L = \frac{1}{c}\left[-g_{00}\left(\frac{dt}{d\tau}\right)^2 - g_{11}\left(\frac{dr}{d\tau}\right)^2 - g_{22}\left(\frac{d\theta}{d\tau}\right)^2 - g_{33}\left(\frac{d\phi}{d\tau}\right)^2\right]^{\frac{1}{2}} \tag{6}$$

Assuming that the orbits remain permanently in the equatorial plane (as in Newtonian Theory), then $\theta = \frac{\pi}{2}$ and the Lagrangian reduces to

$$L = \frac{1}{c}\left[-g_{00}\left(\frac{dt}{d\tau}\right)^2 - g_{11}\left(\frac{dr}{d\tau}\right)^2 - g_{33}\left(\frac{d\phi}{d\tau}\right)^2\right]^{\frac{1}{2}} \tag{7}$$

or more explicitly as

$$L = \frac{1}{c}\left[\left(1 + \frac{2}{c^2} f(t,r)\right)\dot{t}^2 - \left(1 + \frac{2}{c^2} f(t,r)\right)^{-1} \dot{r}^2 - r^2\dot{\phi}^2\right]^{\frac{1}{2}} \tag{8}$$

where the dot denotes differentiation with respect to proper time (τ).

Now, using the Euler-Lagrange equations and considering the fact that in a gravitational field is a conservative field, it can be shown that the law of conservation of energy in this field is given as

$$\left(1 + \frac{2}{c^2} f(t,r)\right)\dot{t} = d\,(constant) \tag{9}$$

or more explicitly as

$$\left[1 - \frac{2GM}{rc^2} \exp\, i\omega\left(t - \frac{r}{c}\right)\right]\dot{t} = d \tag{10}$$

which differs from that in Schwarzschild's field by the exponential factor that describes the radial displacement of mass with time.

It can also be shown that the law of conservation of angular momemtum in this gravitational field is given as

$$r^2\dot{\phi} = h\,(constant) \tag{11}$$

which is the same as that in Schwarzschild's field.

Let $L = \varepsilon$, and equation (8) becomes

$$\varepsilon^2 = \left(1 + \frac{2}{c^2} f(t,r)\right)\dot{t}^2 - \frac{1}{c^2}\left[\left(1 + \frac{2}{c^2} f(t,r)\right)^{-1} \dot{r}^2 - r^2\dot{\phi}^2\right]. \tag{12}$$

Substituting equation (10) in (12) yields

$$\frac{1}{2}\left[\dot{r}^2 + r^2\dot{\phi}^2\left(1 + \frac{2}{c^2} f(t,r)\right)\right] + \varepsilon^2 f(t,r) = \frac{1}{2}c^2\left(d^2 - \varepsilon^2\right). \tag{13}$$

This is the Newtonian energy equation with a modification to the $\dot{\phi}^2$ term. It is similar to that obtained in Schwarzschild's field except for the time dependent radial diplacement. Also, using equation (11), it can be shown that

$$\dot{r} = \frac{dr}{d\phi}\frac{d\phi}{d\tau} = \dot{\phi}\frac{dr}{d\phi} = \frac{h}{r^2}\frac{dr}{d\phi}. \tag{14}$$

Now, let $u(\phi) = \frac{1}{r(\phi)}$ then

$$\dot{r} = -h\frac{du}{d\phi}. \tag{15}$$

Substituting equation (5) and (15) into equation (13) yields

$$\left(\frac{du}{d\phi}\right)^2 + u^2\left[1 - \frac{2k}{c^2}u\ \exp\ i\omega\left(t - \frac{1}{uc}\right)\right] + \frac{2\varepsilon^2 k}{h^2}u\ \exp\ i\omega\left(t - \frac{1}{uc}\right) = \frac{c^2}{h^2}\left(d^2 - \varepsilon^2\right) \tag{16}$$

It is worthnoting that integrating equation (16) directly leads to elliptical integrals which are ackward to handle; thus differentiating yields the following second order differential equation

$$\frac{d^2u}{d\phi^2} + u\left[1 - \frac{2k}{c^2}u\ \exp\ i\omega\left(t - \frac{1}{uc}\right)\right] - \frac{2k}{c^2}u^2\left(1 - \frac{1}{u}\right)\exp\ i\omega\left(t - \frac{1}{uc}\right) + \frac{2k\varepsilon^2}{h^2}\left(1 + \frac{1}{u^2}\right)\exp\ i\omega\left(t - \frac{1}{uc}\right) = 0. \tag{17}$$

This equation has additional terms not found in Schwarzschild's field.

3 Timelike Orbits and Precession

For timelike orbits $\varepsilon = 1$ and equation (17) becomes

$$\frac{d^2u}{d\phi^2} + u\left[1 - \frac{2k}{c^2}u\ \exp\ i\omega\left(t - \frac{1}{uc}\right)\right] - \frac{2k}{c^2}u^2\left(1 - \frac{1}{u}\right)\exp\ i\omega\left(t - \frac{1}{uc}\right) + \frac{2k}{h^2}\left(1 + \frac{1}{u^2}\right)\exp\ i\omega\left(t - \frac{1}{uc}\right) = 0. \tag{18}$$

Now as a first approximation, suppose $uc \gg 1$ and $k \ll h^2u^2$ then equation (8) reduces to

$$\frac{d^2u}{d\phi^2} + u = k\left[\frac{3}{c^2}u^2 + \frac{1}{c^2}u - \frac{1}{h^2}\right]\exp\ i\omega t. \tag{19}$$

The Newtonian equation for a spherical mass is

$$\frac{d^2u}{d\phi^2} + u = \frac{k}{h^2} \tag{20}$$

and that obtained in Schwarzschild's field is

$$\frac{d^2u}{d\phi^2} + u = \frac{k}{h^2} + \frac{3k}{c^2}u^2. \tag{21}$$

Apart from the first and second terms of equation (19) that are similar to Newton's equation and that in Schwarzschild's field, the other terms have terms dependent on the time rate of rotation of the mass content within the sphere [3].

Solution of the Newtonian equation (20) yields the well known conics

$$u_0 = \frac{1}{l}\left(1 + e\cos\theta\right) \tag{22}$$

where $l = \frac{h^2}{GM}$ and e is the eccentricity of the orbit. Attempting an approximate solution for equation (19) by substituting the Newtonian solution into the quadratic term in u on the right hand side and neglecting the term in u, a particular integral u_1 satisfies equation (19) such that

$$\frac{d^2u_1}{d\phi^2} + u_1 = k\left[\frac{3}{l^2c^2}\left(1 + e\cos\theta\right)^2 - \frac{1}{h^2}\right]\exp\ i\omega t. \tag{23}$$

Now suppose u_1 takes the form:

$$u_1 = A\ +\ B\phi\sin\phi\ +\ C\ \cos 2\phi \tag{24}$$

where A, B and C are constants, then it can be shown that

$$u_1 = \frac{k}{c^2}\left(\frac{3}{l^2} - \frac{1}{l} - \frac{1}{h^2}\right)\exp\ i\omega t + \frac{ke\phi}{2c^2}\left(\frac{3}{l^2} - \frac{1}{2l}\right)\sin 2\phi\ \exp\ i\omega t + \frac{ke^2}{l^2c^2}\cos 2\phi. \tag{25}$$

Then the approximate solution for u can be given as

$$u\ =\ u_0\ + u_1 \tag{26}$$

or

$$u = \frac{1}{l}\left(1 + e\cos\theta\right) + \frac{k}{c^2}\left(\frac{3}{l^2} - \frac{1}{l} - \frac{1}{h^2}\right)\exp\ i\omega t + \frac{ke\phi}{2c^2}\left(\frac{3}{l^2} - \frac{1}{2l}\right)\sin 2\phi\ \exp\ i\omega t + \frac{ke^2}{l^2c^2}\cos 2\phi. \tag{27}$$

Hence, this approximate solution introduces corrections to u_0 and hence depicts that the orbits of massive objects is only approximately elliptical and also accounts for the perihelion precession of planetary orbits in this gravitational field.

4 The Bending of Light

For null geodesics, $\varepsilon = 0$ and equation (17) yields

$$\frac{d^2u}{d\phi^2} + u = \left[\frac{3k}{c^2}\exp\ i\omega\left(t - \frac{1}{uc}\right)\right]u^2 + \left[\frac{k}{c^2}\exp\ i\omega\left(t - \frac{1}{uc}\right)\right]u. \tag{28}$$

In the limit of Special Relativity, equation (28) reduces to

$$\frac{d^2u}{d\phi^2} + u = 0. \tag{29}$$

The general solution of equation (29) is given as

$$u = \frac{1}{b}\sin(\phi - \phi_0) \tag{30}$$

where b is the closest approach to the origin (or impact parameter). This is the equation of a straight line as ϕ goes from ϕ_0 to $\phi_0 + \pi$. The straight line motion of light is the same as that predicted by Newtonian theory.

Now, solving the General Relativity problem (equation 28) by taking the general solution (u) to be a pertubation of the Newtonian solution, and setting $\phi_0 = 0$, then

$$u = u_0 + u_1 \tag{31}$$

where $u_0 = \frac{1}{b}\sin\phi$. Thus, u_1 satisfies the equation

$$\frac{d^2u_1}{d\phi^2} + u_1 = \frac{3k}{b^2c^2}\sin^2\phi \exp i\omega\left(t - \frac{b}{c\sin\phi}\right) + \frac{k}{bc^2}\sin\phi \exp i\omega\left(t - \frac{b}{c\sin\phi}\right). \tag{32}$$

Now, by considering a particular integral of the form

$$u_1 = A + B\sin^2\phi \tag{33}$$

and substituting in equation (32), it can be shown that

$$u_1 = \frac{2k}{b^2c^2}\left(1 - \frac{1}{2}\sin^2\phi\right)\exp i\omega\left(t - \frac{b}{c\sin\phi}\right) \tag{34}$$

and thus

$$u = \frac{1}{b}\sin\phi + \frac{2k}{b^2c^2}\left(1 - \frac{1}{2}\sin^2\phi\right)\exp i\omega\left(t - \frac{b}{c\sin\phi}\right). \tag{35}$$

Now, consider the deflection of a light ray from a star which just grazes the time varying homogeneous spherical mass (such as the Sun approximately); as in Fig. 1, then as $r \to \pm\infty$, $u \to 0$, so

$$0 = \frac{1}{b}\sin\phi + \frac{2k}{b^2c^2}\left(1 - \frac{1}{2}\sin^2\phi\right)\exp i\omega\left(t - \frac{b}{c\sin\phi}\right). \tag{36}$$

At the asymptotes, $\phi = -\psi_1$ and $\phi = \psi_2 + \pi$ and taking $\phi \ll 1$ then equation (36) reduces to

$$0 = \frac{1}{b}\psi_1 + \frac{2k}{b^2c^2}\exp i\omega\left(t + \frac{b}{c\psi_1}\right) \tag{37}$$

and

$$0 = \frac{1}{b}\psi_2 + \frac{2k}{b^2c^2}\exp i\omega\left(t + \frac{b}{c\psi_2}\right). \tag{38}$$

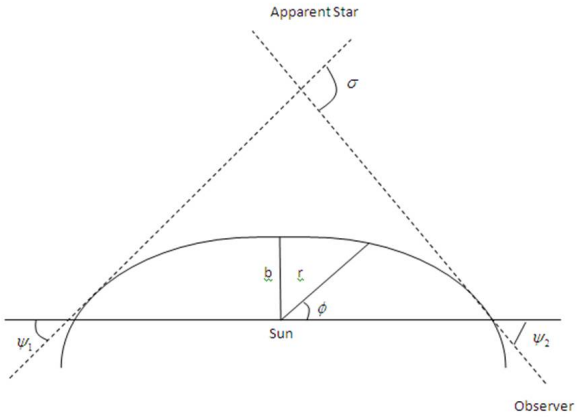

Fig. 1: Diagram showing the total deflection of light.

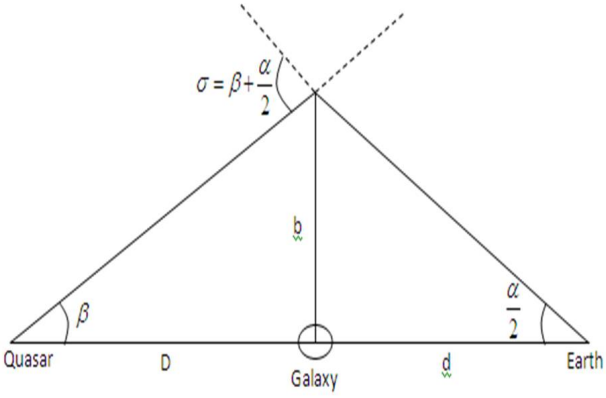

Fig. 2: Einstein's Ring.

The total deflection of light (σ) is given as

$$\sigma = \psi_1 + \psi_2$$

or

$$\sigma = \frac{2k}{bc^2}\left[\exp i\omega\left(t + \frac{b}{c\psi_1}\right) + \exp i\omega\left(t + \frac{b}{c\psi_2}\right)\right]. \tag{39}$$

Thus, the introduction of varying mass distribution with time introduces an exponential term in the deflection of light equation not found in static homogeneous spherical gravitational fields.

Now, as an example of the bending of light, let us consider a gravitational lens.

Consider a quasar directly behind a galaxy in our line of sight as shown in Fig. 2.

The distance of closest approach to the time varying spherical mass distribution corresponds to an angle (σ) given

as equation (39). From Fig. 2, considering that both α and β are small, it can be deduced that

$$\sigma = \frac{\alpha}{2} + \beta = \frac{b}{d} + \frac{b}{D} \tag{40}$$

and substituting equation (39) yields the impact parameter as

$$b = \left\{ \frac{2k}{c^2} \left(\frac{Dd}{D+d} \right) \left[\exp i\omega \left(t + \frac{b}{c\psi_1} \right) + \exp i\omega \left(t + \frac{b}{c\psi_2} \right) \right] \right\}^{\frac{1}{2}}.$$

Hence, the image of the quasar appears as a ring which subtends an angle

$$\alpha = \frac{2b}{d}$$

or

$$\alpha = \frac{2}{c} \left\{ \frac{Dd}{d(D+d)} \left[\exp i\omega \left(t + \frac{b}{c\psi_1} \right) + \exp i\omega \left(t + \frac{b}{c\psi_2} \right) \right] \right\}^{\frac{1}{2}}.$$

5 Conclusion

The results obtained in this study has paved the way for the theoretical study of homogeneous spherical mass distributions in which the mass content is varying with time. This will introduce correction terms found in Schwarzschild's static field. It is hoped that using this approach experimentally and astrophysically more satisfactory expressions and values will be obtained for gravitational phenomena in the universe.

Submitted on December 30, 2013 / Accepted on January 25, 2014

References

1. Chifu E.N. and Howusu S.X.K. Solution of Einstein's Geometrical Gravitational Field Equations Exterior to Astrophysically Real or Hypothetical Time Varying Distributions of Mass within Regions of Spherical Geometry. *Progress in Physics*, 2009, v. 3, 45–48.
2. Chifu E.N., Usman A. and Meludu O.C. Orbits in Homogeneous Oblate Spheroidal Gravitational Space-Time. *Progress in Physics*, 2009, v. 3, 49–53.
3. Weinberg S. Gravitation and Cosmology. J. Wiley, New York, 1972.

Exogenous Mechanism of the Time Sensor of Biological Clock

Takhir R. Akhmedov
333 S. Webster Ave, Suite 4, Norman, OK 73069. E-mail: TakhirAkhmedov@yandex.com

The problem of time sensor of a biological clock attracts interest of many scientists, and a great number of experiments are being conducted to study the influence of various physical and chemical factors on functioning of a biological clock. Analyzing publications and considering our own original results a physical exogenous mechanism of biological clock is formulated that adequately explains the obtained experimental data.

The problem of biological rhythms i.e. biorhythms (BR) with periodicity close to the periodicity of geophysical phenomena has been attracting interest of scientists for centuries. And a great number of experiments carried out on different organisms beginning from single-cell creatures and plants to animals and human beings confirm that biological organisms have the ability to measure time [1–6] and biological clocks (BC) really exist.

The central problem in this matter is explanation of how time sensor (TS) of a BC functions and of the very basic mechanism of TS. Attempts had been made to study the influence of different chemical and physical factors on the parameters of BC.

The most thoroughly studied rhythms are those with a period close to 24 hours. These are so called circadian rhythms (CR). Fewer works are devoted to lunar rhythms (LR) which are of periods around 29.53 and 14.77 days. A few works involve yearly rhythms, and there is information about a period of about 180 million years of the Earth‘s biosphere productivity [4].

In an attempt to determine the mechanism of TS influences of the following factors have been studied on the parameters of CR: illumination [7], light/darkness cycles [8], electrical and magnetic fields of the Earth [9, 10], and absence of such [11], temperature variations [12, 13], chemicals [14,15]. There were experiments in constant pressure and temperature environments [17].

The main properties of BC obtained from experiments are presented in [16]. The noteworthy fact is that the study of BC had been carried out on biological objects using parameters, which are the last stages of long chains of complex biochemical reactions and processes. In fact, in biological experiments researchers observe the motion of the “hands” of BC. Naturally, such observations do not allow revealing the mechanism of BCTS that controls the “hands” of the clock. Thus, the study of biological objects makes it impossible to draw conclusions about the specific stages where one or another factor begins to affect the biochemical chain of reaction. This means, it is difficult to come to a single conclusion, that the observed effects were the result of the action of a single factor on the mechanism of time BCTS. And, as J. Gustings noticed it is impossible to give an example of an isolated and studied biochemical system, which possesses the properties that would reveal the factor and the location of such factor’s influence on CR [14].

The summarized conclusion coming from broad experimental data is that physical and chemical factors, whose influence on BC have been studied, do not have any relationship with the mechanism of BCTS, but only play a synchronizing role. Namely, the factor whose influence is studied only affects the “hand” of the clock by force shifting it one way or another without affecting the actual mechanism behind the “face” of the clock, i.e. without changing the period of CR.

As a result the conclusion is drawn that the period of BC, particularly of CR, is independent from external factors. And thus this period of the rhythms must be defined by organisms independently from external factors, periodic or non-periodic, of physical or chemical nature. This hypothesis is based on three well known facts:

i. The difference of the period from 24 hours in experiments in constant conditions;

ii. Easiness of shifting the phase of the rhythms;

iii. Stability of the rhythm period during latitudinal shifts, that followed by the change of all geophysical factors determined by place and time.

But none of these facts can be accepted as a definite proof as it is established in scientific world [17].

Overall experimental data from studies of BCTS mechanism do not permit to arrive to a single conclusion regarding the physical foundation of BCTS. Therefore, presently the hypothesis of endogenous mechanism of BCTS is generally accepted. Though there are facts that may support a combined exogenous-endogenous mechanism [7]. Such attempts encourage search for processes (of physical or simple chemical nature) that would allow identifying possibly a single simple mechanism of BCTS.

Circadian periodicity of evaporation of water from a thermostated essel*

Initial experiments were carried out in 1974. During one of experiments (see the footnote) it became necessary to obtain a stable flow of water vapor of low intensity (1.4×10^{-5} kg/s).

*These experimental data had been obtained in 1974 by a group of physicists headed by Prof. M. A. Asimov. The author of the present article was a responsible leader for the experiments.

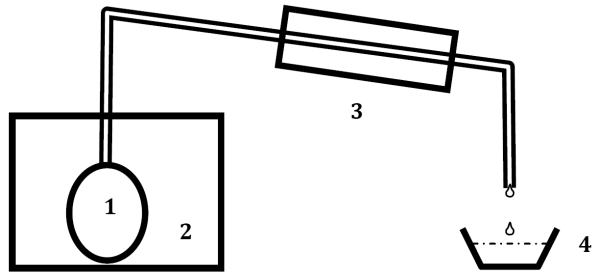

Fig. 1: (1) Container filled with distilled water; (2) Thermostated chamber with inside temperature of $103 \pm 0.1^{\circ}$C; (3) Cooling system; (4) Container where the water condensate was collected

For this, the experimental setup, schematics plotted on Fig. 1, had been assembled.

Container (1) with distilled water was placed into the thermostated chamber (2), where stable temperature at $103 \pm 0.1^{\circ}$C was maintained. Water was boiling inside the container (1). The water vapor went through the cooling system (3) and precipitated into the container (4). The mass of the evaporated/precipitated water was measured every 15 min and a set of 4 measurements had been plotted on the Fig. 2a and 2b. The experiments were carried out uninterruptedly by a number of series of 1 to 7 days of duration.

In order to thoroughly investigate the rate of water vaporization power supply of the thermostat was carefully stabilized, all containers and tubes and connections were thermally insulated, mass was carefully measured and stability of the temperature was closely monitored. The data coming from the measurements strongly suggested the existence of CR in the physical process of distilled water evaporation from a thermostated container.

Measurements were repeated 2001. Due to the limited resources and financial restrictions, the measurements were conducted for only 24 hours. The data collected in 2001 is plotted on Fig. 2b.

Simultaneously, external parameters were monitored. In the Fig. 3, these parameters were plotted vs. time of the day. Namely, temperature of the thermostated chamber T_{hot}, temperature of the liquid in cooling system T_{cold}, ambient temperature T_{amb}, atmospheric pressure p in mm Hg, relative humidity η, and voltage of the power supply were plotted vs. time. As it is clear from Fig. 3, no significant correlation was observed between external parameters and the mass of the evaporated/precipitated water*.

Lunar rhythm in the reaction of vapor conversion of methanol

The stable vapor flow of low intensity was necessary for studying of chemical reaction of vapor conversion of methanol. The reaction used in chemical industry to produce hydrogen is described by a formula:

$$CH_4 + 2H_2O \xrightarrow{450^{\circ}C} CO_2 + 4H_2 \qquad (1)$$

To investigate time dependence of the reaction speed there were provided stable flows of gaseous CH_4 and water vapor (deviations were $\pm 0.3\%$ and $\pm 3\%$, respectively).

The experiment had been carried out for 540 hours in October and November of 1974. In Fig. 4 the experimental measurements were plotted, y axis shows the fraction of residual methane in the converted dry gas at the output of the reactor.

Composition of the gas at the output was analyzed by the method of gas chromatography. Every 15 min three chromatographs were collected; results of 2-4 hour measurements

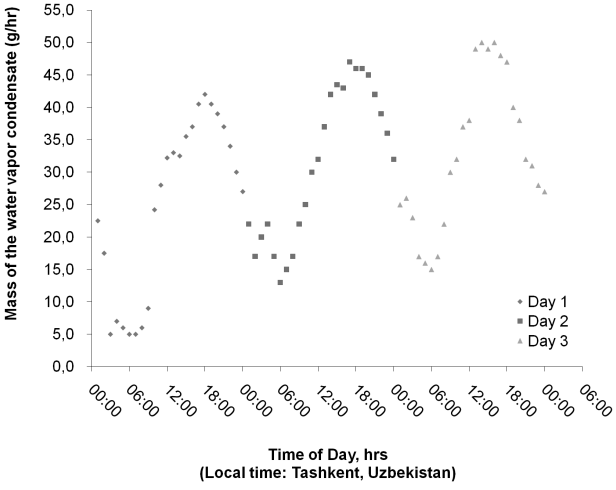

(a)

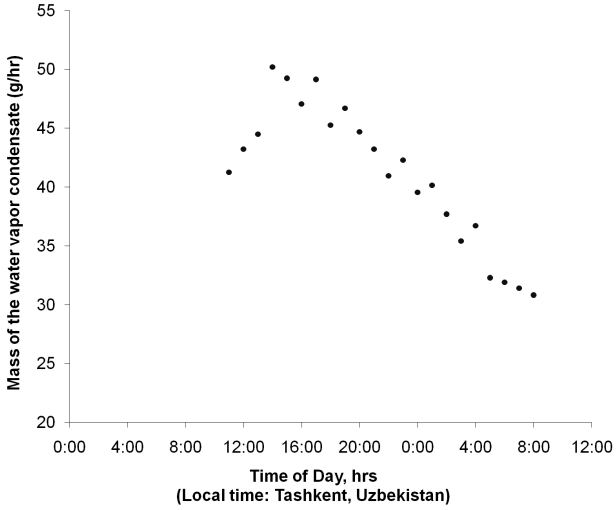

(b)

Fig. 2: Variation of the mass of collected water condensate vs. time of the day

*Experiment conducted in 2001 was made possible by generous technical assistance of Abdulaev Khikmat at the Biology Department of Tashkent State University.

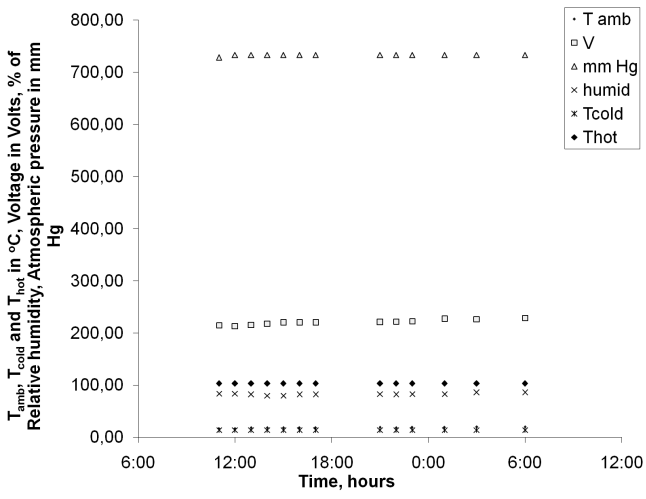

Fig. 3: Monitoring of external parameters of temperature of the thermostated chamber T_{hot}, temperature of the liquid in cooling system T_{cold}, ambient temperature T_{amb}, atmospheric pressure p in mm Hg, relative humidity η, and voltage of the power supply were plotted vs. time. Experiments were conducted in summer of 2001.

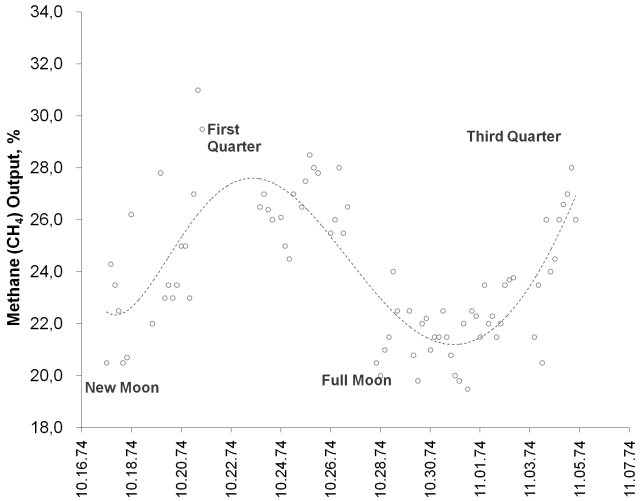

Fig. 4: Concentration of residual CH_4 in % in vapor conversion reaction output. (Experimental data presented in this figure were obtained in Tashkent State University, Uzbekistan by Docent M. A. Azimov's group, headed by Mr. Takhir R. Akhmedov in 1972–75)

were averaged and then plotted on the Fig. 4.

Results of these studies indicated on the existence of a lunar rhythm in the chemical reaction of vapor conversion of methanol at T = 450°C. This temperature is noticeably higher than temperature of any known living organism.

Discussion

A sum total of published experimental data and mentioned above original results of revealing of CR in water evaporation from a thermostated vessel (at T = 103°C), and LR in chemical reaction of vapor conversion of methanol (at T = 450°C) allowed to conclude that the mechanism of BCTS has exogenous nature.

Let's analyze changing of kinetic and potential energy of atoms/molecule on the surface of the Earth. An atom/molecule on the surface of the Earth takes part in following motions:

1. Spinning of the Earth around its own axis with the surface speed $V_1 = 465 \times \cos\alpha$ m/s, where α – is latitude;
2. Revolving with the Earth around the Sun with a linear speed of $V_2 = 3 \times 10^4$ m/s;
3. Moving with the Solar system around the center of the Galaxy with a linear speed of about $V_3 = 2.5 \times 10^5$ m/s;
4. Moving with the Galaxy from the center of the Universe with a linear speed of about $V_4 = 6 \times 10^5$ m/s [18];

It's known that total mechanical energy is the sum of kinetic energy KE and potential energy U:

$$E_{total} = KE + U \qquad (2)$$

And, if any of these components or both of them change according to a law, then the total energy will change according to the same law. And the change can be potentially affecting any physical, chemical or biological process.

The factors 1-3 cause changing of kinetic energy of atoms/molecules on the surface of the Earth with periods, respectively, 24 hours (CR), a year (year rhythm), 180 million years (the Galaxy "year" rhythm). The existence of the rhythms has been mentioned above. Analysis of the kinetic energy changing leads us to the following formula:

$$E_{max} - E_{min} = 2m \times V_T \times V_E \times \cos\alpha \qquad (3)$$

where m – mass of an atom/molecule, V_T – thermodynamic speed of an atom/molecule, V_E – the orbital speed of the Earth's surface on the equator, α – latitude.

Formula (3) evaluates the change of kinetic energy of H_2O molecule caused by orbital spinning of the Earth. Calculations show that the change of the kinetic energy is equivalent to the temperature change in the order of 1°C, which in turn explains the existence of a minimum/maximum of water evaporation from a thermostated vessel at 6 a.m./6 p.m. of the local time. Similar changes of energy in biological objects naturally lead to emerging of CR in them.

It should be underlined, that the argument I (differ of CR period from 24 hours), interpreted in the favor of endogenous mechanism of BCTS, actually proves exogenous character of the BCTS mechanism [15]. The argument II – easiness of shifting of CR phase in biological objects is not related to the mechanism of functioning of BC, but is the result of response of bio-objects to the external environmental factors, and the response is of biochemical nature.

The argument III – conservation of the rhythm during latitudinal shift – naturally follows from the above offered interpretation of the mechanism of BCTS. As the speed of an atom/molecule on the surface of the Earth is described by a formula:

$$V = V_T + V_E \cos\alpha \quad (4)$$

And for a given time zone during latitudinal shifting the BC of a studied object conserves circadian periodicity. But the shifting can be followed by a change of the amplitude. CR of bio-objects should disappear on the Poles of the Earth and in space (space stations).

As it's known, an atom/molecule besides kinetic energy possesses potential energy. E_{poten} in (2) for atoms/molecules on the surface of the Earth changes with a period equal to lunar rhythm, that is caused by displacement of celestial bodies in the system Sun-Earth-Moon. And temperature equivalent of the effect is of order of 10-20°C for the researched chemical reaction. The same mechanism of the energy changing may cause changing of daily global temperature [19].

Conclusions

1. The rhythms with periods close to geophysical rhythms (circadian rhythm, lunar rhythm, a year rhythm, and a rhythm of Earth's biosphere productivity-the Galaxy rhythm) have fundamental nature and take place not only in bio-objects, but also in physical and chemical processes at temperatures significantly higher then temperature of bio-objects.
2. The mechanism of time sensor of biological clock has exogenous nature.
3. The time sensor of biological clock is the changing of total energy E_{total} = KE + U of atoms/molecules on the surface of the Earth, caused by moving of the Earth in Space.
4. For global prove of the results and theoretical interpretation, experiments may be held to study the process of water evaporation from a thermostated vessel simultaneously in different places of the same latitude and/or longitude.

Submitted on December 6, 2013 / Accepted on December 9, 2013

References

1. Bunning E. Rhythms of Physiological Processes. FL, 1961.
2. Biological Clock. Trans. from Eng. with introduction by Shnol' S. E. Moscow, Mir, 1964 (further quoted as "*BC*").
3. Biological Rhythms. Vols. 1–2, Ed. Achhoff J. Moscow, Mir, 1984.
4. Malinovsky Yu. M. Dependence of the Earth's biosphere productivity on the Sun system position in Galaxy. *Problems of Space Biology*. Moscow, Nauka, 1973, v. 18.
5. Wilkins M. Influence of light on the rhythms of plants. In: *BC*, Moscow, Mir, 1964, 196.
6. Emme A. M. Biological clock. Novosibirsk, 1967.
7. Higo A. *Fed Proc.* 1977, v. 36 (2), 109.
8. Edmund L. N. etc. *Chronobiologia*, 1977, v. 4 (2), 109.
9. *Problems of Space Biology*. Moscow, Nauka, 1987, v. 37.
10. *Problems of Space Biology*. Moscow, Nauka, 1973, v. 18.
11. *Problems of Space Biology*. Moscow, Nauka, 1978, v. 37, 16.
12. Suinni B., Gustings J. In: *BC*, Moscow, Mir, 1964, 153.
13. Lukat K. *Expericutis*, 1978, v. 34 (4), 474.
14. Gustings J. Biochemical aspects of rhythms: phase shift, caused by chemical compounds. In: *BC*, Moscow, Mir, 1964, 220.
15. Brukmann K. J. *Interdiscipl. Cycle. Res.*, 1976, v. 7 (2), 149–170.
16. Pittendrigh C. S. Circadian rhythms and the circadian organization of living systems. In: *BC*, Moscow, Mir, 1964.
17. Brown F. Geophysical factors and problems of biological clock. In: *BC*, Moscow, Mir, 1964, 103.
18. Bakulin G. I. and others. General Course of Astronomy. Moscow, 1966.
19. Balling R. C. Jr. and Cerveny R. S. *Science*, 1995, v. 267, 1481–1482.

On the Effect of Lengthening Circadian Rhythm by Heavy Water

Takhir R. Akhmedov

333 S. Webster Ave, Suite 4, Norman, OK 73069. E-mail: TakhirAkhmedov@yandex.com

The problem of time sensor of biological clock (BC) attracts interest of many scientists, and a great number of experiments are being conducted to study the influence of various physical and chemical factors on functioning of BC. Special attention is drawn to studying the influence of heavy water (D_2O) on functioning of BC that always leads to lengthening of circadian rhythms (CR). This work presents theoretical consideration of lengthening of CR, when hydrogen (H_2) in water is replaced by deuterium (D_2), that is based on spacial difference of energy levels with similar principle quantum numbers.

The problem of the mechanism of time sensor (TS) of biological clock (BC), or biorhythms of periods close to periods of geophysical factors, attracts attention of scientists for a long time. The most thoroughly experimentally studied are circadian rhythms (CR) i.e. rhythms with a period close to 24 hours. And in a range of data about physical and chemical factors unfluence on CR there is a special case for the effects of D_2O on the rhythms. In [3, 4] it is noticed "that at present D_2O is the only matter, which always leads to lengthening of endogenous rhythms", and it is underlined, that theoretical interpretation of "the effect of heavy water" is based on the theory of reactions' absolute speeds, neglecting mass effects. However, the principle difference of H_2O and D_2O is the difference of masses of hydrogen and deuterium nuclei.

Consideration of the mass difference permits qualitave explanation of the lengthening of CR in biological objects, where H_2O is partially or completely replaced by D_2O.

Let's consider spacial distribution of energy levels of the same principle quantum number in atoms of hydrogen and deuterium. Taking into account the masses of the nuclei energy levels are separated by the distance.

$$r_{nH} = \frac{\alpha}{4\pi} \times \frac{1}{R_H} \times n^2 \qquad \text{in a hydrogen atom, and}$$

$$r_{nH} = \frac{\alpha}{4\pi} \times \frac{1}{R_D} \times n^2 \qquad \text{in a deuterium atom}$$

where α is fine structure constant, R_H and R_D are Rydberg constants for hydrogen and deuterium, respectively, n – the main quantum number [4].

In comparison with the similar levels of hydrogen atom in an atom of deuterium energy levels of the same principle quantum number are spatially shifted towards the nucleus by the value of

$$\Delta r = n^2 \times \frac{\alpha}{4\pi} \times \left(\frac{1}{R_H} - \frac{1}{R_D} \right)$$

Accepting that $\alpha = 7.397535 \times 10^{-3}$, $R_H = 109677.576\ \text{cm}^{-1}$ and $R_D = 109707.419\ \text{cm}^{-1}$, for $n = 1$, we have $r_1 = 1.3937 \times 10^{-12}$ cm. For example for $n = 10$, $r_{10} = 1.3937 \times 10^{-10}$ cm.

It is natural to assume, that the lower the energy threshold through which biochemical processes run in bio-objects the higher the sensitivity of the objects to the spatial shift of energy levels caused by the replacement of H_2 by D_2.

Thus, from above mentioned it follows that lengthening of CR by adding D_2O is caused by decreasing the possibility of biochemical processes running through the appropriate energy levels in deuterium atoms, which, being caused by mass difference, are spatially shifted towards the nucleus in comparison with analogous levels in hydrogen.

Submitted on December 6, 2013 / Accepted on December 9, 2013

References

1. Biological Rhythms. Ed. by Yu. Aschoff. Vols. 1–2, Moscow, Mir, 1984.
2. Biological Clock. Transl. from Eng. with introduction by Shnoll S. E.. Moscow, Mir, 1964.
3. Lobyshev V. I., Kalinchenko L. P. Isotope Effects in Biological Systems. Moscow, Nauka, 1978.
4. Dowse H. B. and Palmer J. D. The chronomutagenic effect of Deuterium Oxide on the period and entrainment of a biological rhythm. *Biological Bulletin*, 1972, vol. 143 (3), 513–524.
5. Shpolsky S. E. Atomic Physics. Vol. 1. Moscow, Nauka, 1973.

The Journal on Advanced Studies in Theoretical and Experimental Physics, including Related Themes from Mathematics

PROGRESS IN PHYSICS

A quarterly issue scientific journal, registered with the Library of Congress (DC, USA). This journal is peer reviewed and included in the abstracting and indexing coverage of: Mathematical Reviews and MathSciNet (AMS, USA), DOAJ of Lund University (Sweden), Zentralblatt MATH (Germany), Scientific Commons of the University of St. Gallen (Switzerland), Open-J-Gate (India), Referativnyi Zhurnal VINITI (Russia), etc.

Electronic version of this journal:
http://www.ptep-online.com

ISSN: 1555-5534 (print)
ISSN: 1555-5615 (online)

Standard Address Number: 297-5092
Printed in the United States of America

April 2014 **Vol. 10, Issue 2**

CONTENTS

Information for Authors and Subscribers

Progress in Physics has been created for publications on advanced studies in theoretical and experimental physics, including related themes from mathematics and astronomy. All submitted papers should be professional, in good English, containing a brief review of a problem and obtained results.

All submissions should be designed in LaTeX format using *Progress in Physics* template. This template can be downloaded from *Progress in Physics* home page http://www.ptep-online.com. Abstract and the necessary information about author(s) should be included into the papers. To submit a paper, mail the file(s) to the Editor-in-Chief.

All submitted papers should be as brief as possible. We accept brief papers, no larger than 8 typeset journal pages. Short articles are preferable. Large papers can be considered in exceptional cases to the section *Special Reports* intended for such publications in the journal. Letters related to the publications in the journal or to the events among the science community can be applied to the section *Letters to Progress in Physics*.

All that has been accepted for the online issue of *Progress in Physics* is printed in the paper version of the journal. To order printed issues, contact the Editors.

This journal is non-commercial, academic edition. It is printed from private donations. (Look for the current author fee in the online version of the journal.)

LETTERS TO PROGRESS IN PHYSICS

General Relativity Theory Explains the Shnoll Effect and Makes Possible Forecasting Earthquakes and Weather Cataclysms

Dmitri Rabounski and Larissa Borissova

E-mails: rabounski@ptep-online.com; borissova@ptep-online.com

The Shnoll effect manifests itself in the fine structure of the noise registered in very stable processes, where the magnitude of signal and the average noise remain unchanged. It is found in the periodic fluctuation of the fine structure of the noise according to the cosmic cycles connected with stars, the Sun, and the Moon. The Shnoll effect is explained herein, employing the framework of General Relativity, as the twin/entangled synchronization states of the observer's reference frame. The states are repeated while the observer travels, in common with the Earth, through the cosmic grid of the geodesic synchronization paths that connect his local reference frame with the reference frames of other cosmic bodies. These synchronization periods match the periods that are manifested due to the Shnoll effect, regardless of which process produces the noise. These synchronization periods are expected to exist in the noise of natural processes of any type (physics, biology, social, etc.) as well as in such artificial processes as computer-software random-number generation. This conclusion accords with what was registered according the Shnoll effect. The theory not only explains the Shnoll effect but also allows for forecasting fluctuations in the stock exchange market, fluctuations of weather, earthquakes, and other cataclysms.

1 The whole truth about the Shnoll effect

Fundamental misunderstandings of the Shnoll effect can be found in published articles as reported by journalists and scientists. Therefore, now is a good time to tell the whole truth about the Shnoll effect, to dot all the i's and to cross all the t's. We express our deep appreciation to Prof. Simon Shnoll, with whom we have enjoyed many years of friendly acquaintance and scientific collaboration.

The principal error in understanding the Shnoll effect is that some people think it is a periodical fluctuation of the magnitude of the signal that is measured. This is incorrect, since the magnitude of the signal and the average noise remain the same during the long-term measurements done by Shnoll and his workgroup. Further, such processes are specifically chosen for the study that are very stable in time. Simply put, nothing allegedly changes in the experiments which continue during days, months, and even years. The subject of the measurement is the *fine structure of the noise* registered in stable processes.

Every process contains noise. The noise originates due to the influence of random factors and satisfies the Gaussian distribution (i.e., the Gauss continuous distribution function of the probability of the measured value between any two moments of time). Gaussian distribution is attributed to any random process, such as noise, and is based on the averaging and smoothing of the noise fluctuation measured during a long enough interval of time. Nevertheless, if considering very small intervals of time, the real noise has a bizarre structure of the probability distribution function, which differs for each interval of time. Each of these real functions being considered "per se" cannot be averaged to a Gaussian curve. This is what Shnoll called the fine structure of noise and is the object of research studies originally conducted by Simon Shnoll, commencing in 1951–1954 to this day.

So, the magnitude of noise is measured in a very stable process during a long enough duration of time (days, months, and even years). Then the full row of the measured data is taken under study. The full duration of time is split into small intervals. A histogram of the probability distribution function is then created for each of the small intervals. Each interval of time has its own bizarre distribution function (form of the histogram) that differs from Gaussian function. Nevertheless, Shnoll found that "paired histograms," which have a very similar (almost identical) form, exist along the row of the measured data. That is, the histogram created for each interval of time has its own "twin" which has a similar form. The similar form was found in the histograms which were registered with the following periods of repetition connected with stars, the Sun, and the Moon:

- 24 hours = 1440 min (solar day);
- 365 days = 525 600 min (calendar year);
- 23 hours, 56 min = 1436 min (stellar day);
- 365 days, 6 hours, 9 min = 525 969 min (stellar year);
- 24 hours, 50 min = 1490 min (lunar day);
- 27 days, 7 hours, 43 min = 39 343 min (lunar month);
- 31 days, 19 hours, 29 min = 45 809 min (period of the lunar evection).

Also, aside as the similar forms of histograms, appearance the mirrored forms of histograms was registered by Shnoll with periods of:

- 720 min (half of the calendar/solar day);
- 182 days, 12 hours = 262 800 min (half of the calendar/solar year).

Shnoll called this phenomenon the "palindrome effect". It is one of Shnoll's newest findings: despite his having started the research studies in 1951, the possibility of the appearance of the mirrored forms of histograms only came to his attention in 2004. The "palindrome effect" was first registered in December 2007. Aside from these two periods of the "palindromes", a number of other palindrome cycles were found. However, certain circumstances have not allowed a continuation of these studies in full force yet.

As was shown by Shnoll after many experiments done synchronously at different locations from South Pole to North Pole, an appearance of the similar form (or the mirrored form) of the histograms does not depend on the geographical latitude, but depends only on the geographical longitude, i.e., the same *local time* at the point of observation. In other words, the Shnoll effect is manifested equally at any location on the Earth's surface, according to the local time, meaning the same locations of the celestial objects in the sky with respect to the visible horizon.

It is significant that the process producing the noise that we measure can be absolutely anything. Initially, in 1951, Shnoll started his research studies from measurements of the speed of chemical reactions in the aqueous solutions of proteins. Then many other biochemical processes attracted his attention. After decades of successful findings, he focused on such purely physical processes as α-decay and β-decay of the atomic nuclei. It was shown that not only all the random natural processes of different origins, but even artificial processes as random-number generation by computer software manifest the Shnoll effect. In other words, this is a fundamental effect.

That in a nutshell is the whole truth about the Shnoll effect. A detailed history of these research studies can be found in Shnoll's book [1], which also contains hundreds of references to the primary publications on this theme commencing in the 1950s to this day. A brief description of the Shnoll effect can also be found in his short presentation of 2006 [2].

A theoretical explanation of the Shnoll effect on the basis of General Relativity follows. But first, we need to explain two important misunderstandings which are popular among the general public.

2 The two most popular mistakes in the understandings of General Relativity

There are two main mistakes in the understanding of General Relativity. These mistakes originate due to the popular explanations of the theory provided by the reporters and other writers unfamiliar with the details of Riemannian geometry. The first is the prejudice that an absolute reference frame allegedly is impossible according to Einstein's theory. The second is the prejudice that Einstein's theory allegedly "prohibits" speeds of information transfer faster than the speed of light, including the instantaneous transfer of information.

These two prejudices originate due to the superficial explanation of Einstein's theory, which can be encountered in the majority of books on the subject. The superficial explanation limits the reader by the historical path in which Special Relativity and General Relativity were created, and by the simplest analysis of the basics of the theory of space-time-matter. As a result, the aforementioned two prejudices became widely popular among laymen as well as among the scientists who did not study the special aspects of Einstein's theory connected with these two problems.

Nevertheless there are a number of fundamental research studies that cover the aforementioned two problems in detail. While these research results may be unknown to reporters or the majority of the scientific community, relativists who work in the field of reference frames and observable quantities have long been aware of them.

So, in 1944 Abraham Zelmanov published his massive theoretical study [3], where he first determined physical observable quantities as the projections of four-dimensional quantities onto the line of time and the three-dimensional spatial section of the observer's reference frame. His mathematical apparatus for calculating physically observable quantities in the space-time of General Relativity then became known as the theory of chronometric invariants [4, 5]. Roger Penrose, Kip Thorne, and Stephen Hawking as young researchers visited Zelmanov in Sternberg Astronomical Institute (Moscow), and listened to his presentations about physical reference frames and observable quantities at his seminar. In particular, Zelmanov showed [3] that an absolute reference frame is allowed in a finite closed universe, if such a reference frame is linked to the global rotation or the global deformation of the universe.

Later, Zelmanov's followers also voiced, in their scientific presentations, the possibility of an absolute reference frame in a finite closed universe.

It should be noted that an absolute reference frame is impossible in the space-time of Special Relativity. This is because Special Relativity considers the simplified version of the four-dimensional pseudo-Riemannian space (space-time), which is always infinite, and also is free of curvature, rotation, and deformation. Therefore, an absolute reference frame is allowed only in the space-time of General Relativity, and only in those cosmological models where the universe exists as a finite closed volume of space, which rotates or deforms as a whole.

The second of the aforementioned prejudices claim that Einstein's theory allegedly "prohibits" the particles which travel faster than light. This claim is not true. The theoretical possibility of faster-than-light particles — tachyons — was

first considered in 1958 by Frank Tangherlini, in the space-time of Special Relativity. He presented this theoretical research in his PhD thesis [6] prepared under the supervision of Sidney Drell and Leonard Schiff, in the Department of Physics at Stanford University. A similar theory of tachyons in the framework of Special Relativity was suggested, independently of Tanglerlini, in 1979 by Torgny Sjödin [7] (he was a Swedish scientist working in Theoretical Physics Department at Vrije Universiteit in Brussels). The most important surveys on tachyons such as [8,9] referred to Tangherlini. Tachyons were first illuminated in the journal publications on the theory of relativity in a principal paper of 1960 [10], authored by Jakov Terletski. Then a more detailed paper [11] was published in 1962 by Bilaniuk, Deshpande, and Sudarshan. The term "tachyons" first appeared later, in 1967 by Gerald Feinberg [12]. See the newest historical survey and analysis of this problem in [13]. Detailed consideration of tachyons in the space-time of General Relativity was included in our books [14, 15].

The main problem with tachyons is that they cannot be registered by means of direct experimentation by a regular observer [16]. Really, regular observers synchronize their reference frames by light signals. In this case, as was already pointed out by Einstein, the speed of light is the ultimate maximum speed that can be registered by an observer: in this case superluminal displacements cannot be registered. More precisely, in reference frames synchronized by light signals, any superluminal displacement will still be registered as a light signal. See [16] or §1.15 of our book [14] for details. This problem arises not from the ideology of Einstein's theory (as many people erroneously think), but only from the general theory of physical experiments.

So, as was explained by international experts on reference frames, an absolute reference frame is allowed in the space-time of General Relativity, in a finite closed universe, if such a reference frame is linked to the global rotation or the global deformation of the universe. But an absolute reference frame is impossible in the space (space-time) of Special Relativity, because the space is infinite, and is free of rotation and deformation.

Faster-than-light particles (tachyons) are allowed in the space (space-time) of both Special Relativity and General Relativity. But superluminal speeds of such particles cannot be registered by a regular observer because his reference frame is synchronized to others by light signals. Such an observer will register any superluminal motion as motion with the speed of light.

Aside from the tachyon problem, there is also the problem of the instant transfer of information. We mean the instant transfer of information without applying quantum mechanics methods (we call it non-quantum teleportation). This problem was first investigated by us, in 1991–1995. These theoretical results were first published in 2001, in the first edition of our book [14]. A short explanation of the theory can also be found in our presentation [17].

The know-how of our theoretical research was that we considered the four-dimensional pseudo-Riemannian space (the space-time of General Relativity) without any limitations pre-imposed on the space geometry according to physical sense or philosophical concepts. In other words, we studied the space-time of General Relativity "per se". We found that, in addition to the regular state of space-time, a fully degenerate state is possible. From the point of view of a regular observer, whose home is our regular space-time, the fully degenerate space-time appears as a point: all four-dimensional (space-time) intervals, all three-dimensional intervals, and all intervals of time are zero therein. We therefore called the fully degenerate space-time *zero-space*. But this fact does not mean that zero-space is nonsense. Once the observer enters zero-space, he sees that the space and time intervals are nonzero therein.

We showed that zero-space is inhabited by light-like particles which are similar to regular photons. We called these particles *zero-particles*. Zero-particles travel in zero-space with the speed of light. But their motion is perceived by a regular observer as instantaneous displacement. This is one of the effects of relativity theory, which is due to the space-time geometry. We only see that particles travel instantaneously while they travel at the speed of light in their home space (zero-space), which appears to us, the external observers, as the space wherein all intervals of time and all three-dimensional intervals are zero.

We also showed that the regular relation between energy and momentum is not true for zero-particles. Zero-particles bear the properties of virtual photons, which are known from Quantum Electrodynamics (i.e., they transfer interactions between regular particles). This means that zero-particles play the rôle of virtual photons, which are material carriers of interaction between regular particles of our world.

Zero-space as a whole is connected to our regular space-time in every point: at every point of our regular space-time, we have full access to any location inside zero-space. Once a regular photon has entered into such a zero-space "gate" at one location of our regular space, it can be instantly connected to another regular photon which has entered into a similar "gate" at another location. This is a way for non-quantum teleportation of photons.

We also showed that zero-particles manifest themselves as standing light waves (stopped light) while zero-space as a whole is filled with the global system of the standing light waves (the world-hologram). This matches with what Lene Hau registered in the frozen light experiment [18, 19]: there, a light beam being stopped is "stored" in atomic vapor, remaining invisible to the observer until that moment of time when it is set free again in its regularly "travelling state". The complete theory of stopped light according to General Relativity was first given in 2011, in our presentations [20, 21], then again in 2012, in the third edition of our book [14]. The

obtained theoretical results mean that the frozen light experiment pioneered at Harvard by Lene Hau is an experimental "foreword" to the discovery of zero-particles and, hence, a way for non-quantum teleportation.

Until recently, teleportation has had an explanation given only by Quantum Mechanics [22]. It was previously achieved only in the strict quantum way: e.g., quantum teleportation of photons, in 1998 [23], and of atoms, in 2004 [24, 25]. Now the situation changes: with our theory we can find physical conditions for non-quantum teleportation of photons, which is not due to the probabilistic laws of Quantum Mechanics but according to the laws of General Relativity following the space-time geometry.

Thus, the instant transfer of information is allowed in the space-time of General Relativity (though the real speeds of the particles do not exceed the velocity of light). But this is impossible in the space-time of Special Relativity, because it is free of rotation and a gravitational field (whereas by contrast, the main physical condition of zero-space is a strong gravitational potential or a near-light-speed rotation).

Of course, the general reader cannot find all these important details in general-purpose books explaining Einstein's theory. Special skills in Riemannian geometry are needed to understand what has been written in the special publications that we surveyed herein. It is not surprising, therefore, that the majority of people are still puzzled by the aforementioned prejudices and misunderstandings about Einstein's theory.

3 General Relativity Theory explains the Shnoll effect: the scanning of the world-hologram along the Earth's path in the cosmos

As we shall set forth, the instantaneous synchronization of remote reference frames in our Universe via non-quantum teleportation has a direct connection with the Shnoll effect.

First, let us understand what is the Shnoll effect in terms of the theory of relativity.

The form of a histogram obtained as a result from a series of measurements of noise (note that the average magnitude of the noise remains the same) shows the fine structure of the countdown of the measured value, according to the structure of the physical coordinates and of the physical time of the observer. It does not matter which type of processes produces the registered noise; only the physical reference frame of the observer is substantial. In other words, the form of the histogram's resulting measurement of noise shows the fine structure of the physical coordinates and of the physical time of the observer. If two histograms' resulting measurements of noise taken at two different time intervals have the same form, then two of these different states of the same system that generates the noise are synchronized to each other. If these two synchronized states appear periodically in the moments of time associated with the same coordinates of a cosmic body on the celestial sphere, the two synchronized states are also synchronized with the cosmic body.

Therefore, we arrive at the following conclusion. In terms of relativity theory, the Shnoll effect means that the reference frame of a terrestrial observer is somehow synchronized with remote cosmic bodies. This synchronization is done at each moment of time with respect to coordinates connected with stars (cycles of the stellar day and the sidereal year), and with respect to the coordinates connected with the Sun (cycles of the solar day and the calendar year). Also, the synchronization condition (the form of the histogram) is repeated in the reversed mode in time at each of two opposite points in the Earth's orbit around the Sun, and at each of two opposite points of the observer's location with respect to stars (due to the daily rotation of the Earth): this is the "palindrome effect", including the half-year and half-day palindromes.

Now the second question arises. How is this synchronization accomplished? Regularly, and according to the initial suggestion of Einstein (which was introduced in the framework of Special Relativity), reference frames are synchronized by light signals. But in the case of experiments where the Schnoll effect was registered, the noise source and the measurement equipment were located in a laboratory building under a massive roof. So the laboratory is surely isolated from light signals and other (low-magnitude) electromagnetic radiations which come from stars... The answer comes from General Relativity.

First, as is known from General Relativity, two remote reference frames can be synchronized through the shortest path (known as geodesic line) connecting them in the space (space-time). A geodesic path can be paved between any two points at every fixed moment of time. If these points oscillate with respect to each other, the synchronized states are repeated with the period of the oscillation. In terms of a regular terrestrial observer, who is located on the surface of the Earth, this means that his reference frame can be synchronized with the reference frame of a celestial object, which is located in the depths of the cosmos, at any moment of time. Each single state (moment of time) of the synchronization has twin states of synchronization. The twin states are repeated due to the daily rotation and to the yearly rotation of the observer (at his location on the Earth's surface) with respect to stars*, with respect to the Sun, and also due to his cyclic motion with respect to the Moon. Thus the respective cycles of repetition of the synchronized twin states of the observer's reference frame (the cycles of appearance of the similar forms of histograms) must exist. The cycles of repetition of the twin states are, with precision, to the nearest minute:

*This refers to the International Celestial Reference System, which is the standard celestial coordinate system centered at the barycentre of the Solar System, with axes that are fixed with respect to objects in far-reaches of the cosmos. These coordinates are approximately the same as the equatorial coordinates on the celestial sphere. The International Celestial Reference System is defined by the measured positions of more than two hundred extragalactic objects (mainly quasars). It is the standard stellar reference system accepted by the International Astronomical Union.

- Solar day (24 hours = 1440 min), the period of daily rotation of the terrestrial observer together with the Earth with respect to the Sun;
- Calendar year (365 days = 525 600 min), the period of orbital revolution of the terrestrial observer together with the Earth around the Sun;
- Sidereal (stellar) day: 23 hours, 56 min = 1436 min. It is the period of daily rotation of the terrestrial observer, together with the Earth with respect to stars;
- Sidereal (stellar) year: 365 days, 6 hours, 9 min = 525 969 min. It is the period of orbital revolution of the terrestrial observer, together with the Earth around the Sun with respect to stars;
- Lunar day (24 hours, 50 min = 1490 min), the period between two observed moonrises. It is longer than a 24-hour solar day, because the Moon revolves around the Earth in the same direction that the Earth rotates around her own axis;
- Sidereal month: 27 days, 7 hours, 43 min = 39 343 min. It is the period of the Moon's revolution around the Earth with respect to stars;
- Period of the lunar evection (31 days, 19 hours, 29 min = 45 809 min), which is the period of the oscillatory deviation of the Moon's orbit from its average position with respect to the Earth.

Also, the cycles of reverse synchronization (appearance of the mirrored forms of histograms, that means the "palindrome effect") shall exist according to the half-periods:

- Half of the solar day (12 hours = 720 min);
- Half of the calendar year (182 days, 12 hours = 262 800 min);
- Half of the stellar day (11 hours, 58 min = 718 min);
- Half of the sidereal year (182 days, 15 hours, 5 min = 262 985 min);
- Half of the lunar day (12 hours, 25 min = 745 min);
- Half of the sidereal month (13 days, 15 hours, 52 min = 19 672 min);
- Half-period of the lunar evection (15 days, 21 hours, 45 min = 22 905 min).

Also there exist a number of other periods of appearance of the synchronized states of the observer's reference frame (appearance of the similar form of histograms), which manifest cyclic synchronization with some other celestial objects. We do not discuss them herein because of brevity of this presentation.

Second. Synchronization is possible not only of light signals or other electromagnetic signals moving at the speed of light. Instant synchronization of remote reference frames is possible in the space-time of General Relativity [14, 17]. This can be done through zero-space — the fully degenerate space-time. It will appear to a regular observer as a point; that is the necessary condition of non-quantum teleportation at any distance in our world. Therefore the "non-quantum teleportation channel" is constantly allowed between any two points of our space. Zero-particles — the particles that are hosted by zero-space — are material carriers in non-quantum teleportation. Zero-particles are standing light waves (i.e. stopped light), thus zero-space is filled with a global system of standing light waves — the world-hologram of non-quantum teleportation channels. According to space topology, there is univalent mapping of zero-space (the world-hologram) onto our regular space (our universe). This means that the local physical reference frame of a terrestrial observer, travelling together with the Earth in the cosmos, "scans" the world-hologram of teleportation channels.

Each point of the Earth's surface, including the observer's location, makes a daily revolution around the Earth's centre. The Earth revolves around the Sun at a speed of 30 km/sec. The Sun revolves, at a speed of 250 km/sec, around the centre of our Galaxy called the Milky Way. As a result, the observer located on the surface of the Earth travels in the Galaxy along the highly elongated double helix (which is like the DNA helix), through the cosmic grid of the "stargates" into the non-quantum teleportation channels which instantly synchronize his local reference frame with stars, the Sun, and other cosmic objects. Because of the cycles of the turbinal motion of the observer, each single stargate has its own twin respectively to the periods of the motion. The states of the observer's reference frame at these twin locations, due to entering into the same teleportation channel, are not only synchronized but also entangled with each other.*

The moments of a terrestrial observer's entering into the gate of the same teleportation channel are the same as the moments of repetition of the twin synchronized states of his local reference frame. Therefore, it is obvious that the appearance of the similar forms of histograms (and the appearance of the mirrored forms of histograms) manifests not only the synchronized (and, respectively, — reverse synchronized) twin states of the observer's reference frame, but also that these states are entangled with each other.

Such a synchronization occurs regardless of whether the observer sees the sky or is isolated in a laboratory building. It is done by zero-particles through zero-space, independently of the obstacles that can be met by electromagnetic signals in our regular space.

Recall, the Shnoll effect is periodic repetition of a similar form (or mirrored forms) of the histograms' resulting measurement of noise. Most of the periods that are expected according to the theory and listed above coincide with the periods registered by Shnoll and his workgroup [1]. These are the solar day (1440 min), the stellar day (1436 min), the calendar year (525 600 min), the stellar year (525 969 min),

*In a sense similar to the quantum entangled states, according to Quantum Mechanics.

the lunar day (1490 min), the lunar month (registered as the "near-27-day period"), and the period of the lunar evection (45 809 min). The mirrored forms of histograms were registered with periods of half of a solar day (720 min), and half of the calendar year (262 800 min), while analysis of the measurements is still under development. Nevertheless, there are enough coincidences of the theory with Shnoll's experimental data.

We therefore conclude that the Shnoll effect manifests the scanning of the world-hologram of the non-quantum teleportation channels along the Earth's path in the cosmos. So, the Shnoll effect has been explained according to General Relativity Theory.

It is important to understand the following: to find entangled moments of time (the "gates" into the same teleportation channel in the cosmos), it does not matter which stable process (which type of processes) produces the random noise that we register. Not only natural processes, but also the processes such as random-number generation by a computer's software will show the Shnoll effect, as well as such social phenomena as fluctuations in the stock exchange market. This means that the theoretical explanation that is given here on the basis of General Relativity provides a theoretical ground for a wide range of fundamental effects in physics, biology, geophysics, social behaviour and other fields of science. This fact leads us to a number of important sequels and applications, which can be achieved from further research studies of the Shnoll effect.

4 Forecasting earthquakes and other cataclysms on the basis of the scanning of the Earth's path in the cosmos

So, we have arrived at a conclusion that the Shnoll effect is a fundamental effect, which is explained according to General Relativity. Therefore, we expect the Shnoll effect to be found not just in noise that the terrestrial observer registers in such processes as biochemical reactions or nuclear decay. The noise of other terrestrial processes which have natural and artificial origin should also show the Shnoll effect. Because practical applications are important, the following important types of noise should be taken into account:

- Random mass migrations of people;
- Fluctuations in the stock exchange market;
- Fluctuations of the sickness rate among the masses of people, animals, and plants;
- Fluctuations of social unrest (local conflicts, etc.)
- Fluctuations of the Earth's crust — earthquakes;
- Fluctuations of weather (weather events and weather cataclysms);
- and many others.

Here within we've touched so far only on the last two items on this list. These are earthquakes and weather.

Our planet Earth is so large that earthquakes can be considered as the noise fluctuations of the Earth's crust, while weather events and weather cataclysms are the noise fluctuations in the atmosphere. Therefore, this is a proper background where the Shnoll effect should be manifested.

Indeed, there is a huge scientific study that shows the statistical behaviour of background earthquakes and weather events [26–32]. The study was done in the 1930–1940's. It was conducted by Nikolai Morozov, Hon. Member of the USSR Academy of Sciences.*

Morozov and his assistants analysed the observational data about the background earthquakes and weather events that were collected at all the world-known weather observatories and seismic stations of the world (located from the equator to the extreme north and south). The observational data were recorded throughout all periods of the systematic scientific observations, during the second half of the 19th century and the first half of the 20th century, which has then been accessed from yearbooks of the observatories and stations.

In addition to the statistical behaviour of the background earthquakes and weather events, Morozov found that air temperature, barometric pressure, humidity and other geophysical parameters depend on the height of the centre of our Galaxy (and other compact star clusters in our Galaxy) above the horizon. In other words, the weather factors depend on the stellar (sidereal) time at the point of observations. As a result, Morozov arrived at the following fundamental conclusion. All previous forecasts of earthquakes and weather cataclysms did not give satisfying results because the forecasters took into account only the influence of the Sun and Moon on the Earth's crust and the atmosphere (which influences were dated according to solar time), while the influence of objects in the farther-reaches of the cosmos, such as the centre of our Galaxy and other (as visible and invisible) compact stellar clusters, which are dated according to the stellar (sidereal) time, were not taken into account.

We can therefore say that Morozov's geophysical studies show that we can surely consider micro-earthquakes as random noise, which always exist in the Earth's crust. The same is true about weather where random noise is nothing but small fluctuations of air temperature, barometric pressure, humidity, etc.

A confirmation of the conclusion follows from Shnoll's experiments. Already by the 1980s, synchronous fluctuations of forms of the histograms (the Shnoll effect) were registered on the basis of seismic observations [33]. This means, according to our theoretical explanation herein, that the twin entangled synchronization states of the local physical reference frame of the terrestrial observer (the Shnoll effect, according to General Relativity) coincide with the seismic noise registered in the Earth's crust.

*This study was not continued after the death of its author, Prof. Morozov, in 1946.

Therefore, proceeding from our theoretical explanation of the Shnoll effect, we can forecast how, where, and when powerful earthquakes will appear in the Earth's crust; how, where, and when weather cataclysms will occur in the atmosphere. Essentially, here's how to go about doing it.

Two things are needed to understand this method. First, we need to understand that every real observer has his own local physical reference frame. The physical reference frame consists of real coordinate grids spanning over the real physical bodies around him (his real reference bodies), and also of the real clocks that are fixed on the real coordinate grids.* In the case of a terrestrial observer (us, for instance), the real coordinate grids and clocks are connected with the physical environment around us. Therefore, noise fluctuations of the environment mean noise fluctuations of the real physical measurement units of the observer.

Second, as follows from the theory of physical observable quantities in General Relativity, if the fine structure of noises in two physical reference frames match with each other, these two reference frames are synchronized with each other. Therefore, as we've shown above, the Shnoll effect manifests the twin/entangled states of the local physical reference frame of the observer. These twin/entangled states are instantly synchronized with each other, along with other cosmic bodies located along the entire synchronization path in the cosmos. If their physical reference frames are synchronized at a very close frequency, a resonance of noise fluctuations occurs. In this case, concerning seismic noise, a powerful earthquake occurs in the background of the noise from micro-earthquakes (that exist continuously and everywhere in the Earth's crust). Concerning the weather, this means that a weather cataclysm occurs in the background of noise fluctuations of the weather.

In other words, if one or more of the powerful cosmic bodies appear on the same path of synchronization with a terrestrial observer, noise fluctuations of these cosmic bodies become synchronized with the background noise of the observer's physical reference frame. A resonance occurs in the physical reference frame of the observer that is the local environment in the point of his observation. The background noise of the environment experiences a huge fluctuation: i.e., a powerful earthquake, a weather cataclysm, etc.

Thank to Morozov's geophysical studies we conclude that the Sun and the Moon are not the main "synchronizers" that cause a significant resonance in the physical reference frame of a terrestrial observer. We must therefore take into account the convergence of several "celestial synchronizers" of the Solar System and our Galaxy in one synchronization path.

Therefore, all that is required for forecasting earthquakes and weather cataclysms, according to our theoretical explanation of the Shnoll effect, is as follows.

1. First step — daily registrations of the basic noise fluctuations in different environments at different locations on the Earth. Analysis of the measurements, according to the histogram techniques that were used by Shnoll, in order to fix the details of the periods as determined by the Shnoll effect. In other words, this is the "scanning" of the local space of the planet in order to create the complex map of the background noise fluctuations of different environments of the Earth, according to solar time and stellar time;
2. Second step — creating a detailed list of the more or less powerful cosmic sources, which can be the main "synchronizers" affecting the physical reference frame of a terrestrial observer. The stellar (sidereal) coordinates of the cosmic sources, and their ephemerides will be needed in the third stage of the forecasting;
3. Third step — determining the moments of time when these celestial synchronizers converge on the same synchronization path, that is, their crossing the celestial meridian (hour circle) at approximately the same moment of time as the point of observation, then comparing these with the moments of time of the noise fluctuations registered due to the Shnoll effect (in the first step). As a result we will find those celestial synchronizers whose synchronization with the terrestrial environment produces the most powerful effect;
4. Fourth step — calculate further convergences of the most powerful synchronizers at every location on the Earth's surface. As a result, by taking into account the delay time of interaction rate in the respective terrestrial environment (the ground, the atmosphere, etc.), we will be able to forecast where and when the resonant states will occur in the Earth's crust (earthquakes) and in the atmosphere (weather cataclysms).

Forecasting the other events of the above list such as random mass migrations of people, fluctuations in the stock exchange market, fluctuations of the sickness rate, fluctuations of social unrest, and others, is possible analogously. The events predicted according to this method may have different periods of delay from the synchronization moment. The delay time depends on inertia in the medium that is being affected: the Earth's crust, atmosphere, interaction in the social medium, etc. Therefore, despite this, the moments of the resonant synchronization are the same for all processes that are registered at the point of observation; the resonant fluctuations will appear at different moments of time in different environments (including the technogenic environments and the social medium). Nevertheless the method of forecasting remains consistent for all the events around us.

So, forecasting powerful earthquakes and weather cataclysms is possible on the basis of our theoretical explanation of the Shnoll effect. Other practical applications of the the-

*See details about physical reference frames, and about physical observable quantities in Zelmanov's publications [3–5], or in our books [14, 15].

ory and experiment are also possible, but they are outside the scope of this short communication.

Acknowledgements

The authors are grateful to Prof. Simon Shnoll and his wife, Prof. Maria Kondrashova, for years of fruitful scientific collaboration and friendly acquaintance. We are also thankful to Prof. Joseph Hafele and Patrick Ivers for a discussion of these issues and useful tips.

Submitted on January 25, 2014 / Accepted on January 27, 2014

References

1. Shnoll S. E. Cosmophysical Factors in Stochastic Processes. American Research Press, Rehoboth (NM, USA), 2012.
2. Shnoll S. E. Changes in the fine structure of stochastic distributions as a consequence of space-time fluctuations. *Progress in Physics*, 2006, v. 2, issue 2, 39–45.
3. Zelmanov A. Chronometric Invariants. Dissertation, 1944. American Research Press, Rehoboth (NM, USA), 2006.
4. Zelmanov A. L. Chronometric invariants and accompanying frames of reference in the General Theory of Relativity. *Soviet Physics Doklady*, 1956, vol. 1, 227–230 (translated from *Doklady Academii Nauk USSR*, 1956, vol. 107, no. 6, 815–818).
5. Zelmanov A. L. On the relativistic theory of an anisotropic inhomogeneous universe. A 1957 Cosmogony Meeting thesis. *The Abraham Zelmanov Journal*, 2008, vol. 1, 33–63.
6. Tangherlini F. R. The velocity of light in uniformly moving frame. A dissertation. Stanford University, 1958. *The Abraham Zelmanov Journal*, 2009, vol. 2, 44–110.
7. Sjödin T. Synchronization in special relativity and related theories. *Nuovo Cimento B*, 1979, v. 51, 229–246.
8. Recami E. Classical tachyons and possible applications. *Rivista del Nuovo Cimento*, 1986, vol. 9, 1–178.
9. Liberati S., Sonego S., and Visser M. Faster-than-*c* signals, special relativity, and causality. *Annals of Physics*, 2002, vol. 298, 151–185.
10. Terletski Ya. P. The causality principle and the second law of thermodynamics. *Soviet Physics Doklady*, 1961, vol. 5, 782–785 (translated from *Doklady Academii Nauk USSR*, 1960, vol. 133, no. 2, 329–332).
11. Bilaniuk O.-M. P., Deshpande V. K., and Sudarshan E. C. G. "Meta" relativity. *American Journal of Physics*, 1962, vol. 30, no. 10, 718–723.
12. Feinberg G. Possibility of faster-than light particles. *Physical Review*, 1967, vol. 159, no. 5, 1089–1105.
13. Malykin G. B. and Malykin E. G. Tangherlini's dissertation and its significance for physics of the 21th century. *The Abraham Zelmanov Journal*, 2009, vol. 2, 121–143.
14. Rabounski D. and Borissova L. Particles Here and beyond the Mirror. Third expanded edition. American Research Press, Rehoboth (NM, USA), 2012. Re-printed in French as: Rabounski D. et Borissova L. Particules de l'Univers et au delà du Miroir. Traduit de l'anglais par Patrick Marquet, American Research Press, Rehoboth (NM, USA), 2012.
15. Borissova L. and Rabounski D. Fields, Vacuum, and the Mirror Universe. Svenska fysikarkivet, Stockholm, 2009. Re-printed in French as: Borissova L. et Rabounski D. Champs, Vide, et Univers miroir. Traduit de l'anglais par Patrick Marquet, American Research Press, Rehoboth (NM, USA), 2010.
16. Rabounski D. A blind pilot: who is a super-luminal observer? *Progress in Physics*, 2008, v. 4, issue 2, 171.
17. Borissova L. and Rabounski D. On the possibility of instant displacements in the space-time of General Relativity. *Progress in Physics*, 2005, v. 1, issue 1, 17–19.
18. Hau L. V. Frozen light. *Scientific American*, 17 July 2001, v. 285, no. 1, 52–59.
19. Hau L. V. Frozen light. *Scientific American Special Edition* "*The Edge of Physics*", 31 May 2003, 44–51.
20. Rabounski D. and Borissova L. A theory of frozen light according to General Relativity. A presentation delivered at the *2011 APS March Meeting*, held in March 21–25, 2011, in Dallas, Texas.
21. Rabounski D. and Borissova L. A theory of frozen light according to General Relativity. *The Abraham Zelmanov Journal*, 2011, v. 4, 3–27.
22. Bennett C. H., Brassard G., Crepeau C., Jozsa R., Peres A., and Wootters W. K. Teleporting an unknown quantum state via dual classical and Einstein-Podolsky-Rosen channels. *Physical Review Letters*, 1993, v. 70, 1895–1899.
23. Boschi D., Branca S., De Martini F., Hardy L., and Popescu S. Experimental realization of teleporting an unknown pure quantum state via dual classical and Einstein-Podolsky-Rosen Channels. *Physical Review Letters*, 1998, v. 80, 1121–1125.
24. Riebe M., Häffner H., Roos C. F., Hänsel W., Benhelm J., Lancaster G. P. T., Korber T. W., Becher C., Schmidt-Kaler F., James D. F. V., and Blatt R. Deterministic quantum teleportation with atoms. *Nature*, 2004, v. 429, 734–736.
25. Barrett M. D., Chiaverini J., Schaetz T., Britton J., Itano W. M., Jost J. D., Knill E., Langer C., Leibfried D., Ozeri R., and Wineland D. J. Deterministic quantum teleportation of atomic qubits. *Nature*, 2004, v. 429, 737–739.
26. Morozov N. A. On the possibility of a scientific prognosis of weather. *Bulletin de l'Académie des Sciences de l'URSS*, Série géographique et géophisique, 1944, tome VIII, no. 2–3, 63–71.
27. Morozov N. A. Influence of the central body of the galaxy and its other dark super-suns on the geophysical and meteorological phenomena that appear around us. *Archive of Russian Academy of Sciences*, fund 543 (personal fund of N. A. Morozov, Hon. Member of the USSR Academy of Sciences), folder 01, file 72 (188 pages).
28. Morozov N. A. On the cosmic factors affecting the frequency of earthquakes. *Ibidem*, file 96 (461 pages).
29. Morozov N. A. On the celestial influences on the frequency of earthquakes. *Ibidem*, file 98 (297 pages).
30. Morozov N. A. On the influence of the cosmic effects on the frequency of earthquakes. *Ibidem*, file 99 (110 pages).
31. Morozov N. A. Earthquakes: the cosmic studies. *Ibidem*, file 100 (282 pages).
32. Morozov N. A. Basics of Theoretical Meteorology and Geophysics. Manuscript of the book. *Ibidem*, files 128–139.
33. Shnoll S. E. Private communications with the authors.

On the Origin of Elementary Particle Masses

Johan Hansson

Department of Physics, LuleåUniversity of Technology, SE-971 87 Luleå, Sweden.

The oldest enigma in fundamental particle physics is: Where do the observed masses of elementary particles come from? Inspired by observation of the empirical particle mass spectrum we propose that the masses of elementary particles arise solely due to the self-interaction of the fields associated with a particle. We thus assume that the mass is proportional to the strength of the interaction of the field with itself. A simple application of this idea to the fermions is seen to yield a mass for the neutrino in line with constraints from direct experimental upper limits and correct order of magnitude predictions of mass separations between neutrinos, charged leptons and quarks. The neutrino interacts only through the weak force, hence becomes light. The electron interacts also via electromagnetism and accordingly becomes heavier. The quarks also have strong interactions and become heavy. The photon is the only fundamental particle to remain massless, as it is chargeless. Gluons gain mass comparable to quarks, or slightly larger due to a somewhat larger color charge. Including particles outside the standard model proper, gravitons are not exactly massless, but very light due to their very weak self-interaction. Some immediate and physically interesting consequences arise: i) Gluons have an effective range $\sim$1 fm, physically explaining why QCD has finite reach; ii) Gravity has an effective range $\sim$100 Mpc coinciding with the largest known structures, the cosmic voids; iii) Gravitational waves undergo dispersion even in vacuum, and have all five polarizations (not just the two of $m = 0$), which might explain why they have not yet been detected.

The standard model of particle physics [1–4] is presently our most fundamental *tested* [5] description of nature. Within the standard model there are some 18 parameters (several more if neutrinos are non-massless) which cannot be predicted but must be supplied by experimental data in a global best-fit fashion. There are coupling constants, mixing parameters, and, above all, values for the different fundamental particle masses. The theory is silent on where and how these parameters arise, and even more speculative theories, such as string theory, have so far not been able to predict (postdict) their values. Even if the Higgs particle is confirmed, and the Higgs mechanism [6] is validated in one form or another, it still does not explain "the origin of mass" as often erroneously stated. Unknown/incalculable parameters for particle masses are in the Higgs model replaced by equally unknown/incalculable coupling constants to the Higgs field; the higher the coupling, the larger the mass, while no coupling to the Higgs field gives massless particles like the photon and gluons. So nothing is gained in the *fundamental* understanding of masses. Fifteen of the free parameters in the standard model are due to the Higgs. Thirteen of them are in the fermion sector, and the Higgs interactions with the fermions are not gauge invariant so their strengths are arbitrary. So to make progress we must understand masses.

There is no hope of predicting elementary masses from renormalized quantum field theory as the very process of renormalization itself forever hides any physical mass-generating mechanism; the renormalized masses are taken as the experimentally measured values, *i.e.* any possible physical connection for predicting particle masses is lost. But surely, nature herself is not singular, the infinities appearing in quantum field theory instead arising from the less-than-perfect formulation of the theory. If a truly non-perturbative description of nature would be found it might be possible to calculate particle masses from first principles, but we still seem far from such a description.

In this article we will instead take a more phenomenological approach, but still be able to deduce a number of physical results and some interesting consequences.

From standard (perturbative) quantum field theory, the lowest order contribution to the self-mass is [7] (see Fig. 1)

$$\Delta m = \alpha \int \bar{u}\,\gamma_\mu K(1,2)\gamma^\mu\, u\, e^{ipx_{12}}\,\delta(s_{12}^2)\,\mathrm{d}^4x, \qquad (1)$$

where the loop integral is logarithmically UV divergent $\propto log(\frac{1}{r})$ as the cut-off radius $r \to 0$.* So (in perturbation theory) the contribution is divergent but as all gauge fields diverge in the same way, the *quotients* are finite. (Another way would be to assume that there exists a "shortest length" in nature that would serve as a natural cut-off and give finite integrals.) As an aside, as all expressions are relativistically invariant the usual relativistic factor $\gamma = 1/\sqrt{1 - v^2/c^2}$ is automatic if $v \neq 0$, *i.e.* if we are not in the rest frame of the particle.

*Also for a classical electron of radius r, $\Delta m = C\alpha \propto \alpha$, but there the coefficient is linearly divergent $C \propto 1/r$. Additionally, the classical result is exact, *i.e.* non-perturbative.

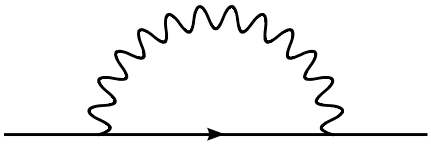

Fig. 1: Feynman diagram for self-mass contribution from a gauge field (squiggly line). Each vertex contributes one charge factor $\sqrt{\alpha} \propto q$.

We will thus imagine the following pragmatic scenario: a quantum field without any charges corresponds to a massless particle; when charges, q, are attached the mass is $m \propto q^2 \propto \alpha$, where α is the relevant coupling constant. This significantly reduces the number of *ad hoc* parameters. Also, the lagrangian can still be completely massless (as in the Higgs scenario), preserving attractive features such as gauge invariance that would be broken by explicit mass terms, the generation of mass being a secondary *physical* phenomenon.

So we get

$$m(electron) \propto \alpha_{QED} \tag{2}$$

$$m(quark) \propto \alpha_{QCD} \tag{3}$$

$$m(neutrino) \propto \alpha_{QFD} \tag{4}$$

where the dominating coupling constant is α_{QED} for quantum electrodynamics, α_{QCD} for quantum chromodynamics (strong interactions) and α_{QFD} for quantum flavordynamics (weak interactions).

If we now assume that all gauge fields give a contribution of roughly the same order of magnitude, so that the proportionality factors cancel up to a constant of order unity (coming from the different gauge groups), we get results for the quotients of elementary masses without having to know the exact (non-perturbative) contribution. Using the observed mass for the electron, and $\alpha_{QED} \sim 137^{-1}$, $\alpha_{QCD} \sim 1$, we get

$$m(quark) \simeq 50\,\mathrm{MeV}, \tag{5}$$

(although physical quark masses are notoriously hard to define [8]) and pretending as if we knew nothing of the electroweak theory (in order not to get entangled with the Higgs mechanism again), using the old Fermi theory for weak interactions (or quantum flavordynamics, QFD) as appropriate for the low energies where observations of physical masses are actually made, using the *physical* coupling derived from typical scattering cross sections or decay rates ($\tau^{-1} \propto \alpha^2$) , we get, using $\tau^{-1}_{QFD} \sim 10^6\mathrm{s}^{-1}$ (*e.g.* $\mu \to e\nu_\mu\bar{\nu}_e$) and $\tau^{-1}_{QED} \sim 10^{16}\mathrm{s}^{-1}$ (*e.g.* $\pi^0 \to \gamma\gamma$),

$$m(neutrino) \simeq 0.5 \times 10^{-5}\mathrm{MeV} \simeq 5\,\mathrm{eV}. \tag{6}$$

This is a *prediction* resulting from our simple assumption, compatible with upper limits from direct experiments, whereas in the Higgs model *no* predictions of masses are possible (being connected to free parameters).

We see that we immediately get the right hierarchy of masses, with the right magnitudes, which is encouraging considering the approximations made.

A clear indication of the relative effect of QED compared to QCD is seen in the case of pions: π^+ and π^- both have mass 139.6 MeV, while the neutral pion π^0 has a mass of 135 MeV. The small difference $\Delta m = 4.6$ MeV, attributable to QED, predicts a charge radius ∼1 fm, consistent with scattering experiments using pions.

One issue still remaining is why not $m(Z) \sim m(neutrino)$ or $m(W) \sim m(electron)$. We take it as a sign that the intermediate vector bosons W and Z really are not fundamental, but instead are composite [9, 10].

If we, disregarding renormalization issues, also include the graviton as the force carrier of gravity (which is expected to hold for weak gravitational fields) we see that QCD, QFD and gravity all should disappear exponentially at sufficiently large distances due to the non-zero physical masses of their force carrier particles, only electromagnetism (QED) having truly infinite reach as the physical mass of the photon is equal to zero, as the photon carries no charge. The range can be estimated by the Yukawa theory potential $e^{-\lambda mc/\hbar}/r$, giving $\lambda_{cutoff} \simeq \hbar/mc$. This gives for the gluon with bare mass zero (in the lagrangian), but physical mass $m(gluon) \neq 0$, the value $\lambda_{cutoff}(QCD) \simeq 0.3$ fm, which explains why QCD is only active within nuclei, although the bare mass $m = 0$ naively would give infinite reach as its coupling to the Higgs is zero. Despite what many thinks, this problem has not been solved [11].

For gravity, the same calculation leads to $\lambda_{cutoff}(gravity) \simeq 3 \times 10^8$ light-years, or 100 Mpc, which happens to coincide with the largest known structures in the universe, the cosmic voids [12]. The corresponding graviton mass is

$$m(graviton) \simeq 5 \times 10^{-32}\,\mathrm{eV}, \tag{7}$$

well in line with the experimental upper limits [13]. Another thing to keep in mind is that if/when gravity decouples, it will appear as if the universe accelerates when going from the coupled (decelerating) to the uncoupled (coasting) regime where distance $\geq \lambda_{cutoff}(gravity)$, perhaps making dark energy superfluous as explanation for cosmic "acceleration" [14, 15]. If masses really originate in this way it might be possible to include other interactions but the gravitational in an "equivalence principle", hence perhaps opening the door to a unified description of all interactions.

The relation $m(graviton) \neq 0$ has other peculiar effects: gravitational waves of different wavelengths (energies) would travel at different velocities, smearing them out, the longer the wavelength, the larger the effect. Also, not being strictly massless, gravitons (spin s=2) should have $2s + 1 = 5$ polarization states instead of the two conventionally assumed helicity states if massless. This might be why gravitational waves hitherto have escaped detection, as it would scramble their signature.

If we, just for the moment, tentatively reintroduce the perturbative running of coupling "constants" (renormalization group) we obtain $m(graviton) \to \infty$ as $r \to 0$ implying that (quantum) gravity gets a dynamical cutoff for small separations, as an increasingly more massive quantum is harder to exchange, effectively making the interaction of gravity disappear in that limit, perhaps showing a way out of the ultraviolet divergencies of quantum gravity in a way reminiscent of how massive vector bosons cured the Fermi theory.

We have not addressed the known replication of particles into three generations of seemingly identical, but more massive, variants, the most exactly studied from an experimental standpoint being the three charged leptons, *i.e.* (e, μ, τ), the electron and its heavier "cousins" the muon and tauon.*

A straightforward way would be to introduce some "generation charge" or quantum number, make *e.g.* a power-law ansatz and fit to the observed values of the charged leptons and deduce the masses of neutrinos and quarks in the higher generations. That would, however, not bring us any closer to a true understanding.

A more promising way could be to assume that the stable elementary particles of the first generation are exact soliton solutions to the relevant quantum field theory, or its dual [16], whereas unstable higher generation elementary particles would be solitary wave (particle-like, but not stable) solutions to the said quantum field theory. Unfortunately, there are no known exact 3+1 dimensional soliton solutions to quantum field theories, with non-trivial soliton scattering [16]. Another avenue would be to explore if Thom's "catastrophe theory" [17] (or other more general theories of bifurcation) applied to particle physics could spontaneously reproduce multiple generations, as it is known to include stable/unstable multiple solutions. Thom's theory states that all possible sudden jumps between the simplest attractors – points – are determined by the elementary catstrophes, and the equilibrium states of any dynamical system can in principle be described as attractors. As one attractor gives way for another the stability of the system may be preserved, but often it is not. It could be capable to generate masses spontaneously in a different and novel way compared to the Higgs mechanism. The different charges, *i.e.* coupling constants, could define the control surface, whereas the actual physical mass would define the behavior surface. Sudden bifurcations could signify decay of previously stable elementary particles.

To summarize, our simple and physically compelling assumption that particle masses are solely due to self-interactions: i) Directly and simply gives the correct mass hierarchy between neutrinos, electrons and quarks. ii) Reduces the number of *ad hoc* parameters in the standard model. iii) Qualitatively explains why the photon is the only massless fundamental particle, why QCD has short range, and why neutrinos are not strictly massless. iv) Gives testable predictions, *e.g.* regarding gravitons (gravitational waves).

*Are there additional generations? Data on the decay width of the Z indicate that there at least cannot be any additional light neutrinos. A fourth neutrino would have to be very massive $> m_Z/2 \simeq 45$ GeV. One might well ask if the generation structure is a true aspect of nature, or just a result of our incomplete understanding of the weak interaction [10].

Submitted on January 22, 2014 / Accepted on January 23, 2014

References

1. Glashow S. L. *Nucl. Phys.*, 1961, v. 22, 579.
2. Weinberg S. *Phys. Rev. Lett.*, 1967, v. 19, 1264.
3. Salam A. in Svartholm N., ed. Elementary Particle Physics: Relativistic Groups and Analyticity, Eight Nobel Symposium. Almqvist and Wiksell, 1968, p. 367.
4. Fritzsch H., Gell-Mann M., Leutwyler H. *Phys. Lett. B*, 1973, v. 47, 365.
5. Cahn R. N., Goldhaber G. The Experimental Foundations of Particle Physics, 2nd ed. Cambridge University Press, Cambridge, 2009.
6. Higgs P. *Phys. Rev. Lett.*, 1964, v. 13, 508.
7. Feynman R. P. *Phys. Rev.*, 1949, v. 76, 769.
8. Hansson J. *Can. J. Phys.*, 2002, v. 80, 1093. arXiv: hep-ph/0208137.
9. D'Souza I. A., Kalman C. S. Preons. World Scientific, Singapore, 1992.
10. Dugne J.-J., Fredriksson S., Hansson J. *Europhys. Lett.*, 2002, v. 60, 188. arXiv: hep-ph/0208135.
11. Clay Mathematics Institute Millennium Prize Problem: Yang-Mills, http://www.claymath.org/millennium/Yang-Mills-Theory/.
12. Lindner U. et al. *Astron. Astrophys.*, 1995, v. 301, 329.
13. Goldhaber A. S., Nieto M. M. *Rev. Mod. Phys.*, 2010, v. 82, 939.
14. Riess A. et al. *Astr. J.*, 1998, v. 116, 1009.
15. Perlmutter S. et al. *Ap. J.*, 1999, v. 517, 565.
16. Manton N.S. *Nonlinearity*, 2008, v. 21, T221.
17. Thom R. Stabilité Structurelle et Morphogenèse: Essai d'une Théorie Générale des Modèles. Benjamin, 1972. English trans. by Fowler D. H. Structural Stability and Morphogenesis: An Outline of a Theory of Models. Benjamin, 1975.

Extended Analysis of the Casimir Force

Bo Lehnert

Alfvén Laboratory, Royal Institute of Technology, SE-10044 Stockholm, Sweden. E-mail: Bo.Lehnert@ee.kth.se

There are several arguments for the conventional form of the Zero Point Energy frequency spectrum to be put in doubt. It has thus to be revised into that of a self-consistent system in statistical equilibrium where the total energy density and the equivalent pressure become finite. An extended form of the Casimir force is thereby proposed to be used as a tool for determining the local magnitude of the same pressure. This can be done in terms of measurements on the force between a pair polished plane plates consisting of different metals, the plates having very small or zero air gaps. This corresponds to the largest possible Casimir force. Even then, there may arise problems with other adhering forces, possibly to be clarified in further experiments.

1 Introduction

The vacuum is not merely an empty space. Due to quantum theory, there is a non-zero level of the ground state, the Zero Point Energy (ZPE) as described by Schiff [1] among others. An example of the related spectrum of vacuum fluctuations was given by Casimir [2], who predicted that two metal plates will attract each other when being separated by a sufficiently small air gap. This prediction was first confirmed experimentally by Lamoreaux [3].

In a number of investigations the author has called attention to the importance of ZPE in connection with fundamental physics, on both the microscopic and the macroscopic scales. This applies to revised quantum electrodynamics and its relation to massive elementary particle models [4–6], as well as to attempts of explaining the concepts of dark energy and dark matter of the expanding universe [7, 8].

This paper presents an extended analysis of the ZPE frequency spectrum and its effect on the Casimir force, thereby leading to proposed experimental investigations on the features of the same spectrum.

2 Frequency spectrum of the Zero Point Energy

The local Zero Point Energy density has to become derivable from the frequency spectrum of an ensemble of ZPE photons. Such a procedure has to be conducted in the same standard way as for statistical systems in general, as described by Terletskii [9] and Kennard [10] among others.

For a "gas" of ZPE photons the number of field oscillations per unit volume in the range $(\nu, \nu + \mathrm{d}\nu)$ becomes

$$\mathrm{d}n = \frac{8\pi}{c^3}\,\nu^2\,\mathrm{d}\nu. \tag{1}$$

This number can also be conceived to represent the various "rooms" to be populated by the photon frequency distribution.

In finding the corresponding self-consistent and fully determined contribution to the ZPE energy density, two points have to be taken into account:

- The quantized energy of every single photon is $E_0 = \frac{1}{2}h\nu$.
- The photon population of the frequency states has to be adapted to a statistical equilibrium, under the constraint of a finite and given total energy density. The latter corresponds to an average energy $\bar{E}_0 = \frac{1}{2}h\bar{\nu}$ per photon with a related average frequency $\bar{\nu}$.

Due to these points, the contribution to the energy density within the range $(\nu, \nu + \mathrm{d}\nu)$ becomes [7, 8]

$$\mathrm{d}u = \frac{4\pi h}{c^3}\,\nu^3 \exp\left(-\frac{\nu}{\bar{\nu}}\right). \tag{2}$$

Here the Boltzmann factor

$$P_B = \exp\left(-\frac{E_0}{\bar{E}_0}\right) = \exp\left(-\frac{\nu}{\bar{\nu}}\right) \tag{3}$$

is due to the probability of the various photon states in statistical equilibrium.

In the present isotropic state, the contribution to the pressure becomes $\mathrm{d}p = \mathrm{d}u/3$. The local ZPE pressure then has the total integrated value

$$p_0 = \frac{8\pi h\bar{\nu}^4}{c^3} \tag{4}$$

as obtained from relation (2).

In the earlier conventional analysis, the factor (3) has been missing, thus resulting in an infinite total ZPE energy density and pressure. Several investigators, such as Riess and Turner [11] as well as Heitler [12], have thrown doubt upon such an outcome. Attempts to circumambulate this irrelevant result by introducing cutoff frequencies either at the Planck length or at an arbitrary energy of 100 GeV, are hardly acceptable. This omission does not only debouch into a physically unacceptable result, but also represents an *undetermined* and not self-consistent statistical system [7, 8].

3 Experimental possibilities

The average frequency $\bar{\nu}$ appearing in the factor (3) is an important but so far not determined basic parameter. It may have a characteristic value in the environment of the Earth, or even of our galaxy. It should therefore be investigated if this para-

meter can be determined from experiments. This would require earlier experiments on the Casimir force to be extended. Two options are here proposed for such investigations, all using polished plane metal plates:

- Air gaps of a smaller width than those in earlier experiments, but being larger than the electromagnetic skin depth of the plates, would extend the measurable range. Thereby the insertion of insulating material of very small thickness may be tested.
- The largest possible Casimir force is expected to occur at a vanishing air gap. In this case the skin depth of the plates acts as an equivalent air gap. Even at this maximum Casimir force, other surface and sticking mechanisms such as by Van der Waals' forces may interfere with the measurements. To eliminate at least part of these difficulties, any magnetic alloy should be avoided as plate material in the first place. Further, as pointed out by N. Abramson [13] and G. Brodin [14], plates of different materials should be chosen to avoid microscopic matching of the metal structures. Possible choices of plate material are Ag, Cu, Au, Al, Mg, Mo, W, Zn, Ni, Cd, Sb, and Bi in order of decreasing electric conductivity.

As a device for measurement of the Casimir force, a weighting machine with two horizontal plates is proposed, in which the weight of the upper plate is outbalanced and a vertical Casimir force can be recorded.

4 The Casimir force

The Casimir force arises from the difference in pressure on the out- and insides of the metal plates. Whereas the full ZPE pressure acts at their outsides, there is a reduced pressure acting on their insides, due to the boundary condition which sorts out all frequencies below a limit $\hat{\nu}$. The latter corresponds to wavelengths larger than $\hat{\lambda} = c/\hat{\nu}$, as being further specified for the two options defined in Sec. 3. The net Casimir pressure thus becomes

$$\hat{p} = \int_0^\infty \mathrm{d}p - \int_{\hat{\nu}}^\infty \mathrm{d}p = \frac{4\pi h}{3c^3} \int_0^{\hat{\nu}} \nu^3 \exp\left(-\frac{\nu}{\bar{\nu}}\right) \mathrm{d}\nu \qquad (5)$$

due to the distribution (2). With $x = \nu/\bar{\nu}$ and $\hat{x} = \hat{\nu}/\bar{\nu}$ expression (5) obtains the form

$$\hat{p} = p_0 \, \Pi(\hat{x}) \qquad (6)$$

where p_0 is given by (4) and

$$\Pi = \int_0^{\hat{x}} x^3 \exp(-x) \, \mathrm{d}x = \\ = 1 - \left(1 + \hat{x} + \frac{1}{2}\hat{x}^2 + \frac{1}{6}\hat{x}^3\right) \exp(-\hat{x}) \, . \qquad (7)$$

4.1 Plates with an air gap

The first option concerns an air gap of the width a, being substantially larger than the skin depth of the plates at relevant frequencies. Then the frequencies smaller than $\hat{\nu} = c/2a$ and wavelengths larger than $\hat{\lambda} = 2a$ are excluded. In the limit of $\hat{x} \ll 1$, Π then approaches the value $\hat{x}^4/24$, and the net pressure becomes

$$\hat{p} \cong \frac{\pi h c}{48 a^4} \qquad (8)$$

being proportional to $1/a^4$ as earlier shown by Casimir [2].

For arbitrary values of $\hat{x} = c/2a\bar{\nu}$, the Casimir pressure (6) can then for various gap widths be studied as a function of $\bar{\nu}$. The set of obtained values of $\hat{p}$ then leads to information about the average frequency $\bar{\nu}$, within the limits of application of this option.

4.2 Plates with zero air gap

With the second option of a vanishing air gap, the sum of the skin depths at each plate plays the rôle of a total air gap. Using two plates of different metals having the electric conductivities σ_1 and σ_2, their skin depths at the frequency ν become [15]

$$(\delta_1, \delta_2) = \frac{1}{\sqrt{\pi \mu_0 \nu}} \left(\frac{1}{\sqrt{\sigma_1}} \, , \frac{1}{\sqrt{\sigma_2}} \right). \qquad (9)$$

The total skin depth can then be written as

$$\delta_1 + \delta_2 = \frac{2}{\sqrt{\pi \mu_0 \nu}} \frac{1}{\sqrt{\sigma_{12}}} \qquad (10)$$

where

$$\sigma_{12} = \frac{4 \, \sigma_1 \sigma_2}{\sigma_1 + \sigma_2 + 2\sqrt{\sigma_1 \sigma_2}}. \qquad (11)$$

In the limiting case where half a wavelength $\lambda/2 = c/2\nu$ is equal to the total skin depth (10), the corresponding frequency limit becomes

$$\hat{\nu} = \frac{\mu_0 \pi c^2 \sigma_{12}}{16} \, . \qquad (12)$$

Since λ varies as $1/\nu$ and $\delta_1 + \delta_2$ as $1/\sqrt{\nu}$, it is seen that all frequencies ν less than $\hat{\nu}$ are excluded by the boundary condition. Thus $\hat{\nu}$ represents the Casimir frequency limit, as in the analogous case of a nonzero air gap.

With p_0 given by (4), $\hat{p}$ and Π by (6) and (7), $\hat{\nu}$ by (12), and $\hat{x} = \hat{\nu}/\bar{\nu}$, the Casimir pressure $\hat{p}$ is obtained as a function of the average frequency $\bar{\nu}$ for a given effective conductivity (11) of a pair of plates. Examples are given by (Ag/Cu, Ni/Cd, Sb/Bi) for which $\sigma_{12} = (60.5, 14.1, 1.26) \times 10^6$ A/Vm and $\hat{\nu} = (134, 31.2, 2.79) \times 10^{16}$ s^{-1} and $\hat{\lambda} = (2.23, 9.60, 107) \times 10^{-10}$ m, respectively. The dependence of $\hat{p}$ on $\bar{\nu}$ for the three examples of metal plate combinations are demonstrated in Fig. 1. The left-hand part of the figure relates to large values of $\hat{x}$ for which $\hat{p}$ nearly includes the full pressure (4), and

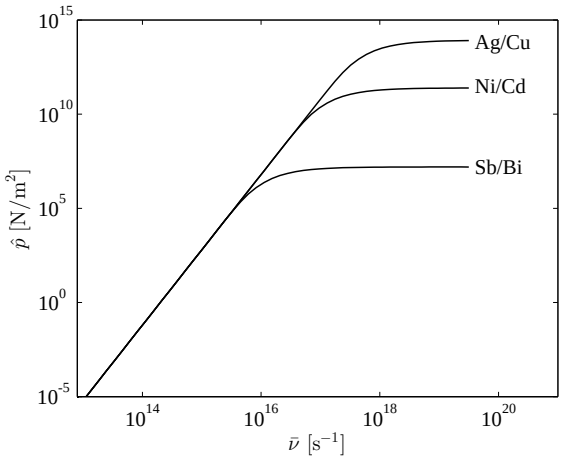

Fig. 1: Casimir pressure $\hat{p}$ as a function of the ZPE average frequency $\bar{\nu}$ for the three metal plate combinations Ag/Cu, Ni/Cd, and Sb/Bi.

for which there is a vanishing difference between the various plate combinations. The right-hand part of the same figure corresponds on the other hand to small $\hat{x}$ for which there is a difference due to the various values of resistivity and $\hat{\nu}$. This part leads to a pressure $\hat{p}$ having the asymptotic limit $(\pi h/3c^3)\,\hat{\nu}^4$ at large $\bar{\nu}$. To extend the range of resistivity dependent Casimir pressures in respect to $\bar{\nu}$, plates with even lower values of σ_{12} would have to be used. Provided that the Casimir force is the dominant one, the measured pressure $\hat{p}$ should thus be related to the same value of the average frequency $\bar{\nu}$, then being independent of the choice of metal combinations. This would, in its turn, lead to an identification of $\bar{\nu}$.

5 Conclusions

There are strong arguments for the frequency spectrum of the Zero Point Energy to be determined by means of a self-consistent system of statistical equilibrium in which there is a finite total pressure and a related finite average frequency. To investigate this state, an extended experimental analysis is proposed, based on the largest possible Casimir force which occurs on a pair of metal plates separated by a very small or even vanishing air gap. Provided that these forces become much stronger than those due to other possible adhering mechanisms, the proposed measurements may give an estimate of the average frequency defined in Section 2.

Submitted on January 30, 2014 / Accepted on February 7, 2014

References

1. Schiff L. I. Quantum Mechanics. McGraw-Hill Book Comp. Inc., New York-Toronto-London, 1949, Ch. IV, Sec. 13.
2. Casimir H. B. G. On the attraction between two perfectly conducting plates. *Proc. K. Ned. Akad. Wet.*, 1948, v. 51, 793–795.
3. Lamoreaux S. K. Demonstration of the Casimir force in the 0.6 to 6 μm Range. *Phys. Rev. Lett.*, 1997, v. 78, 5–8.
4. Lehnert B. Revised Quantum Electrodynamics. In Dvoeglazov V. V. (ed), Contemporary Fundamental Physics. Nova Science Publishers, Inc., New York, 2013.
5. Lehnert B. Potentialities of revised quantum electrodynamics. *Progress in Physics*, 2013, v. 4, 48–52.
6. Lehnert B. Mass-radius relations of Z and Higgs-like bosons. *Progress in Physics*, 2013, v. 10, 5–7.
7. Lehnert B. On dark energy and dark matter of the expanding universe. *Progress in Physics*, 2009, v. 2, 77–82.
8. Lehnert B. Dark energy and dark matter as due to zero point energy. *Journal of Plasma Physics*, 2013, v. 79, 324–334.
9. Terletskii Ya. P. Statistical Physics. North-Holland, Amsterdam and London, 1971, Ch. VI.
10. Kennard E. H. Kinetic Theory of Gases. McGraw-Hill Book Comp., Inc., First edition, New York and London, 1938, Sec. 226.
11. Riess A. G. and Turner M. S. From slowdown to speed-up. *Scientific American*, February 2004, 50–55.
12. Heitler W. The Quantum Theory of Radiation. Oxford: Clarendon Press, 1954, pp. 57 and 326.
13. Abramson N. Private communication 2012.
14. Brodin G. Private communication 2012.
15. Stratton J.A. Electromagnetic Theory. McGraw-Hill Book Comp., Inc., New York and London, 1941, p. 504.

Proton-Electron Mass Ratio: A Geometric Inference

Paulo R. Silva

Departamento de Física (Retired Associate Professor), Universidade Federal de Minas Gerais, Brazil
E-mail: prsilvafis@gmail.com

In this paper we propose that the inertial masses of the proton and of the electron can be associated to volumes of the unit cells of hyper-cubic lattices constructed in the momentum space. The sizes of the edges of these cells are given by the Planck's momentum in the case of the electron, and by a modified Planck's momentum in the case of the proton. We introduce a "conservation of information principle" in order to obtain the wave function which leads to this modified momentum. This modification is attributed to the curvature of the space-time, and in doing this, the concept of the entropy of a black hole has been considered. The obtained proton-electron mass ratio reproduces various results of the literature, and compares well with the experimental findings.

1 Introduction

The volumes of certain associated symmetric spaces have been used as a means to estimate the proton-electron mass ratio, besides the ratios among leptons and mesons masses [1–7]. Some of these papers [1–4] claim to present more consistent physical interpretations of the particles mass ratio, obtained through these geometric approaches. As was pointed out by González-Martin, Smilga [1,4] obtained a volume factor from the decomposition of $SO(3,3)$ with respect to the product group $SO(3,1) \times SO(2)$. He calculated this volume factor that when compared with the volume factor of the electron furnishes a proton-electron mass ratio very close to known experimental result. The same evaluation was done earlier by Wyler [7].

In this work we intend to pursue further on this subject, by associating the masses of the proton and of the electron to the volumes of unit cells in the momentum space, with each unit cell having its appropriate size. For appropriate size we mean that, the unit cell edge associated to the electron mass is given by a characteristic momentum of the Planck's scale. On the other hand the unit cell related to the proton mass is also evaluated with the aid of a Planck's scale momentum, but modified by the curvature of the space-time. The reason to establish such differences is that the electron is usually described through Quantum Electrodynamics (QED) [8], an abelian field theory. Meanwhile the proton is described by Quantum Chromodynamics (QCD) [9], a non-abelian field theory, and we propose that this feature introduces a curvature in space-time modifying the size of the cell of the momentum space.

2 A conjecture about the conservation of the information

If we consider a black hole of radius r, its entropy is given by the well known Bekenstein-Hawking [10–12] formula

$$S = \frac{A}{4} = \frac{\pi r^2}{L_{Pl}^2}, \tag{1}$$

where L_{Pl} is Planck's length.

Let us write a "law of the conservation of the information" in the form

$$S + I = C. \tag{2}$$

In (2), C is a constant. Now we propose to associate the quantity of information, I, to the logarithm of a density of probability Ψ^2, where Ψ is a wave function associated to this curved space-time. We have

$$\frac{\pi r^2}{L_{Pl}^2} + \ln(\Psi^2) = C. \tag{3}$$

Equation (3) leads to

$$\Psi = \Psi_0 \exp\left(-\frac{\pi r^2}{L_{Pl}^2}\right). \tag{4}$$

In order to better examine the content of Ψ it is convenient to interpret it as a ground-state wave function of a kind of one-dimensional harmonic oscillator. Inserting this function and its second derivative in a Schrödinger equation for a particle of mass M, we have

$$-\frac{\hbar^2}{2M}\left(\frac{\pi^2 r^2}{L_{Pl}^4}\right)\Psi + \frac{\hbar^2}{2M}\left(\frac{\pi}{L_{Pl}^2}\right)\Psi + V\Psi = \epsilon_0\Psi. \tag{5}$$

Making the identification of the "r-squared" and the "independent of r" terms, we have

$$\frac{1}{2}\frac{\hbar^2\pi^2}{ML_{Pl}^4} r^2 = \frac{1}{2} kr^2 = V(r) \tag{6}$$

and

$$\frac{\hbar^2\pi}{2ML_{Pl}^2} = \epsilon_0 = \frac{1}{2}\hbar\omega. \tag{7}$$

By taking

$$L_{Pl} = \frac{\hbar}{M_{Pl}} \quad \text{and} \quad M \equiv M_{Pl}, \tag{8}$$

we get

$$\hbar\omega = \pi M_{Pl}\, c^2 = <p> c \tag{9}$$

with

$$<p> = \pi M_{Pl}\, c. \tag{10}$$

We interpret (10) as the size of the unit cell in the curved momentum space. Equation (9) can be seen as the difference in energy levels in the curved space, namely $\hbar\omega$ being related to the emission (absorption) of a boson of momentum $<p>$.

3 Estimate of the proton-electron mass ratio

As was pointed out by Wesson [13], Einstein's Equivalence Principle (EEP) may be a direct consequence of an extra dimension. Yet according to Wesson, a null path in five space-time dimensions (5-D) can describe a massive particle which usually lives in four dimensions. This null path conditions in 5-D can encompass both the gravitational mass of this particle (related to its Schwarzschild radius) as well its inertial mass (related to its Compton length).

Partially inspired in Wesson work [13], we will assume that particle masses are tied to some type of unit cell in a five-dimensional momentum space lattice. First let us consider the electron. The field theory which deals with the electron is the (abelian) QED [8]. We imagine that the amount of inertial mass of the electron (m_e) is proportional to the five-dimensional volume of the unit cell in the momentum space lattice, which size is given by the Planck's characteristic momentum, namely

$$p = M_{Pl}\, c, \tag{11}$$

and

$$V_5 = p^5 = (M_{Pl}\, c)^5 . \tag{12}$$

Therefore we write

$$m_e = K V_5 = K\,(M_{Pl}\, c)^5 . \tag{13}$$

On the other hand the proton is a hadron which structure is described by QCD [9, 14], a non-abelian field theory. QCD has in common with General Relativity (GR), the fact that both are known to be non-linear theories. It seems that in evaluating the proton mass, a curved space-time must be considered. This leads to a modified size of the unit cell in the momentum space lattice. Looking at the wave function given by (4) and the structure of energy levels implied by it, we have obtained $<p>$ given by (10). But the curvature of a space seems not to be displayed by a mathematical object such as a volume. Then we propose that the inertial mass of the proton m_p is proportional to a five-surface area in the curved momentum space lattice, this surface area being a derivative from a six-volume. Therefore we write

$$<V_6> = <p>^6 \tag{14}$$

$$<S_5> = \frac{\mathrm{d}<V_6>}{\mathrm{d}<p>} = 6<p>^5 \tag{15}$$

and

$$m_p = K<S_5> = K\,6\pi^5\,(M_{Pl}\, c)^5 . \tag{16}$$

In writing (16) we have used (10), and considered that the proportionality constant K is the same as that used in determining the electron mass. By comparing (13) and (16), we finally obtain

$$\frac{m_p}{m_e} = 6\pi^5 \approx 1836.12. \tag{17}$$

The ratio given by (17) has been previously obtained by various authors, and compares relatively well with the experimental values (please see [1,3,4] and references cited in those papers).

Submitted on January 21, 2014 / Accepted on February 6, 2014

References

1. González-Martin G. arXiv: physics/0009066.
2. González-Martin G. arXiv: physics/0405094.
3. González-Martin G. *Revista Mexicana de Fisica*, 2003, v. 49 (3), 118.
4. Smilga W. arXiv: gen-ph/0505040v3.
5. Lenz F. *Phys. Rev.*, 1951, v. 82, 554.
6. Good J. *Phys. Lett. A*, 1970, v. 33, 383.
7. Wyler A. *C. R. Acad. Sc. Paris*, 1971, v. 217A, 186.
8. Ryder L. H. Quantum Field Theory. Cambridge Univ. Press, Cambridge, 1992.
9. Wilczek F. *Phys. Today*, 2000 (August), 22.
10. Bekenstein J. D. *Phys. Rev.D*, 1973, v. 7, 2333.
11. Hawking S. *Comm. Math. Phys.*, 1975, v. 43, 199.
12. Damour T. arXiv: hep-th/0401160.
13. Wesson P. S. arXiv: gen-ph/1301.0033v1.
14. Moriyasu K. An Elementary Primer For Gauge Theory. World Scientific, Singapore, 1983.

Memory of Living Beings and Its Three Characteristic Times

Paulo R. Silva

Departamento de Física (Retired Associate Professor), ICEx, Universidade Federal de Minas Gerais, Brazil
E-mail: prsilvafis@gmail.com

In this study we first evaluate the time between collisions related to the transport properties in liquid water, provided by the protons motion tied to the hydrogen bonds. As water is an essential substance for the establishment of life in the living beings, we take this time as the basic unit to measure some kinds of retention time related to their memory. Besides this, integration is an important feature associated to the operation of the memory. Then we consider two possible ways of doing integration and an average between them. One of these characteristic times, the Darwin time, is given by adding over the N basic units which forms the memory. The other possibility, the recent time, is obtained by considering a kind of time-like random walk running over the N basic units. Finally we perform a geometric average between these two times and call it generations' time. As a means to estimate these characteristic times, we take the number of protons contained in a volume of water compatible with the dimensions of the portion of the brain responsible by its memory.

1 Introduction

It seems that water is fundamental to the flourishing of life [1], and the hydrogen-bond kinetics [2] plays an important role in the establishment of the transport properties of this liquid. Besides this, living beings which exhibit the property of to replicate, must have this feature encoded in its memory. In electronic computers, electrical currents are the agents responsible for writing or deleting the information stored in its memory. In this paper we propose that, in the living beings case, the protonic currents do this job. In order to accomplish this we will treat protonic currents in close analogy with the electrical currents in metals.

First we will evaluate the averaged time between collisions for protonic currents and after we will use this time in an integration sense, in order to find characteristic times of persistency of the information registered in the living beings memories. By integration sense we mean that we are looking for physical properties which depend on the whole system, a kind of cooperative effect, or an emergent property of the collective of particles.

2 Electrical conductivity through protons

Drude formula for the electrical conductivity of metals can be written as

$$\sigma = \frac{e^2 n \tau}{M}\,, \tag{1}$$

where e is the quantum of electric charge, n is the number of charge carriers per unit of volume, τ is the average time between collisions and M is the mass of the charge carriers.

Besides this in reference [3], starting from Landauer's paradigm: conduction is transmission [4], the relation for the electrical conductivity can be put in the form

$$\sigma = \frac{e^2}{\pi \hbar \ell_0}\,. \tag{2}$$

where ℓ_0 is the size of the channel of conduction. In the case of the charge carrier being the proton, the maximum conductivity is reached when the length, ℓ_0, becomes equal to the reduced Compton wavelength of it, namely

$$\ell_0 = \frac{\hbar}{Mc}\,. \tag{3}$$

Inserting equation (3) into equation (2) we get

$$\sigma_{max} = \frac{e^2 M c}{\pi \hbar^2}\,. \tag{4}$$

Making the identification between the two relations for the electrical conductivity, namely equating equation (1) to equation (4), and solving for τ, we obtain for the maximum time between collisions the expression

$$\tau_{max} = \tau = \frac{M^2 c}{n \pi \hbar^2}\,. \tag{5}$$

It would be worth to evaluate numerically equation (5). In order to do this we consider that water molecules in the liquid state are relatively closed packed. Therefore by taking $n = 10^{29}\,\mathrm{m}^{-3}$, which seems to be an acceptable number for n, we get

$$\tau = 2.7 \times 10^{-7}\ \mathrm{s}. \tag{6}$$

This time interval is seven orders of magnitude greater than the time between collisions of electrons in metallic copper at room temperature [5].

3 Hydrogen bond and the transport properties of liquid water

As far we know, protonic currents have not been directly measured in water. Indeed, equation (5) for the maximum time between collisions, does not show explicit dependency on the quantum of electric charge e.

Meanwhile, from equation (27) of reference [5], we have

$$\lambda_{\mathrm{F}}^2 = \lambda_{\mathrm{C}}\,\ell\,. \tag{7}$$

In equation (7), λ_{F}, λ_{C} and ℓ, are respectively the Fermi and Compton wavelengths and the mean free path of the particle responsible by the transport property in water. Besides this, Luzar and Chandler [2] pointed out that: "In the hydrogen — bond definition employed by them, two water molecules separated by less than 3.5Å can be either bond or not bonded, depending upon their relative orientations. At large separations, a bond cannot be formed." This information comes from the first coordination shell of water, as measured by its oxygen-oxygen radial distribution function. We will idealize a lattice of water molecules, and by considering its Fermi length $\lambda_{\mathrm{F}} = 3.5$Å, and by taking λ_{C} equal to the reduced Compton length of the proton, we obtain from equation (7)

$$\ell = 6.2 \times 10^{-4}\ \mathrm{m}. \tag{8}$$

Equation (8) is an estimate of the proton mean free path in water. If we write

$$\ell = V_{\mathrm{F}}\tau \tag{9}$$

where V_{F} is a kind of Fermi velocity of the system and solving for V_{F}, we find after using equations (6) and (8)

$$V_{\mathrm{F}} \approx 2300\ \mathrm{m/s}. \tag{10}$$

We observe that this value of V_{F} is comparable with the speed of sound in water, approximately 1500 m/s. Therefore this time between collisions estimated for the proton motion performing the hydrogen bond in water seems to make some sense.

4 Three characteristic times tied to the living beings

Recently Max Tegmark [6] published a paper entitled *Consciousness as a State of Matter*. Tegmark was inspired in a work by Giulio Tononi [7]: *Consciousness as Integrated Information: A Provisional Manifesto*. According to Tegmark [6], Tononi [7] stated that for an information processing system to be conscious, it needs to have two distinct properties:

1. Have the ability to store a long amount of information;
2. This information must be integrated into unified whole.

Besides this, as was pointed out by Tegmark [6]: "Natural selection suggests that self-reproducing information processing systems will evolve integration if it is useful for them, regardless of whether they are conscious or not". In this work we are interested in look at the integrated effects with respect to time intervals, taking in account the great number N of basic units which compose the whole. By whole, we consider for instance, a substantial part of the brain of a living being responsible by its memory. We assume that the characteristic times are measured in terms of units of time-base. This unit will be taking as the time between collisions of the protons motion, related to the transport properties of water and associated to the hydrogen-bond dynamics.

4.1 Integrated time: first possibility

Let us to take a time-like string of N unit cells or basic units. We suppose that the time elapsed, τ_{R}, for the information sweep the whole string can be computed by considering a kind of Brownian motion on this time-like string. Then we can write

$$\tau_{\mathrm{R}} = N^{\frac{1}{2}}\tau. \tag{11}$$

Eighteen grams of liquid water occupies a volume of approximately 18 cm^3 and contains $2N_A$ protons, where N_A stands for Avogrado number. We assume that this volume corresponds to a portion of the human brain compatible with the size of the region of memory storage. As a means to estimate τ_{R}, let us put numbers in (11) and we get

$$\tau_{\mathrm{R}} = (2N_A)^{\frac{1}{2}}\,\tau \approx 3 \times 10^5\ \mathrm{s}. \tag{12}$$

The time interval, given by equation (12), corresponds approximately to the duration of 3.5 days and perhaps can be associated to the recent memory of the human brain. If the volume of the memory's device is ten times smaller, namely 1.8 cm^3, the value of τ_{R} is reduced to approximately one day.

As a means of comparison, we cite a statement quoted in a paper by S. Mapa and H. E. Borges [8] that a type of memory which they call working memory, may persist by one or more hours. Meanwhile, with chemical aids this time can be extended, as we can find in the words of Yassa and collaborators [9]: "We report for the first time a specific effect of caffeine on reducing forgetting over 24 hours".

4.2 Integrated time: second possibility

Another possibility to consider for the integrated time is assuming that the overall time is the sum over the basic time units. Thinking in this way it is possible to write

$$\tau_{\mathrm{D}} = N\tau\,. \tag{13}$$

If we take $(2N_A)/10$ protons of 1.8 grams of water, we obtain for τ_{D},

$$\tau_{\mathrm{D}} \approx 3.2 \times 10^{16} \approx 10^9\ \mathrm{years}. \tag{14}$$

We will call τ_{D} the Darwin's time. This choice can be based in the following reasoning. According to Joyce [10]: "The oldest rocks that provide clues to life's distant past are 3.6×10^9 years old and by that time cellular life seems already to be established!" Another interesting paper about the origins of life can be found in reference [11].

4.3 Third characteristic time

The two characteristic times we have discussed before were associated by us to the recent memory time τ_{R} (order of magnitude of one day) and the Darwin's time τ_{D} (order of magnitude of one billion of years), this last one related to the establishment of life on earth. We judge interesting to consider an-

other characteristic time corresponding to the geometric average of the two times we just described. We write

$$\tau_{\mathrm{G}} = (\tau_{\mathrm{D}}\tau_{\mathrm{R}})^{\frac{1}{2}} = N^{\frac{3}{4}}\,\tau\,. \tag{15}$$

Inserting $N = 1.2\times10^{23}$, the number of protons contained in $1.8\,\mathrm{cm}^3$ of water and the unit of time interval $\tau = 2.7\times10^{-7}$ s in equation (15), we obtain for the generations' time τ_{D} the value

$$\tau_{\mathrm{G}} = 1700\,\mathrm{years}. \tag{16}$$

If we estimate a mean lifetime of the human beings as 70 years, the above number corresponds to approximately 24 generations.

5 Analogy with the polymer physics

Two characteristic times we have described in this paper can be thought in analogy with polymer physics [12]. In four dimensions, the scaling relation of polymers reproduces that of a single random walk.

If we think about a time-like string of time-length τ_{D}, composed by "monomers" having the duration of a unit-time τ, we have after N steps the relation

$$\tau_{\mathrm{R}} = (\tau_{\mathrm{D}}\tau)^{\frac{1}{2}} = N^{\frac{1}{2}}\tau\,. \tag{17}$$

We remember that τ_{D} is given by equation (13). Therefore the Darwin's time τ_{D} corresponds to the time-length of the string and the recent time τ_{R} looks similar to the end to end distance (equivalent to the gyration radius of polymers).

6 Concluding remarks

This work has been developed through two steps. In the first one, an averaged time τ between collisions was calculated, taking in account the proton current associated to the hydrogen bond in liquid water. As the human body, in particular its brain, is constituted in great extension by this liquid, it seems that any physical process occurring in it must consider the relevancy of water in supporting this task. Perhaps the above reasoning could be extended to all living beings. The falsifiability of the calculated τ was verified by obtaining a kind of Fermi velocity which is comparable to the sound velocity in liquid water.

In the second step we considered an important property of memory, namely its integrability. By taking a number N of hydrogen bonds contained in a volume of water representative of the memory device of the living beings, we was able to associate two characteristic times to them. The integrability given by simple addition of unit-base time gives the Darwin time which grows linearly with N. Another kind of integration, a time-like random walk, leads to the recent memory time which grows with the square root of N. An intermediate time interval given by the geometric average of the last two ones was also evaluated and we call it generation's time.

Although this work may sound very speculative, we think that it perhaps could inspire other more robust research on the present subject.

Submitted on February 9, 2014 / Accepted on February 13, 2014

References

1. Atteberry J. Why is water vital to life? 10 August 2010. http://science.howstuffworks.com/environmental/earth/geophysics/water-vital-to-life.html.
2. Luzar A., and Chandler D. Hydrogen-bond kinetics in liquid water. *Nature*, v. 379, 4 January 1996, 55–57.
3. Silva P. R., Sampaio M., Nassif C., Nemes M. C. *Phys. Lett. A*, v. 358, 2006, 358–362.
4. Landauer R. *IBMJ Res. Dev.*, 1957, issue 1, 223.
5. Silva P.R. Electrical conductivity of metals: a new look at this subject. viXra: 1209.0071 (2012).
6. Tegmark M. Consciousness as a state of matter. arXiv: 1401.1219.
7. Tononi G. Consciousness as integrated information: a provisional manifesto. *Biol. Bull.*, 2008, 215–216. http://www.biobull.org/content/215/3/216.full.
8. Mapa S. and Borges H. E. Modelagem de um mecanismo para formação e evocação de memórias em criaturas artificiais. http://www.dca.fee.unicamp.br/~gudwin/courses/IA889/2011/IA889-05.pdf
9. Borota D., Murray E., Kiceli G., Chang A., Watabe J. M., Ly M., Toscano J. P., Yassa M. A. Post-study caffeine administration enhances memory consolidation in humans. *Nature Neuroscience*, 2014, v. 17, 201–203.
10. Joyce G. F. RNA evolution and the origin of life. *Nature*, 16 March 1989, v. 338, 217–224. http://www.its.caltech.edu/~bch176/Joyce1989.pdf
11. Damineli A. and Damineli D. S. C. Origens da vida. *Estudos Avançados*, 2007, v. 21(59), 263–284. http://dx.doi.org /10.1590/S0103-40142007000100022
12. De Gennes P.-G. Scaling Concepts in Polymer Physics. Cornell University Press, Ithaca (N.Y.), 1979.

New Experiments Call for a Continuous Absorption Alternative to Quantum Mechanics – The Unquantum Effect

Eric S. Reiter

251 Nelson Avenue, 94044 Pacifica, CA, USA. E-mail: eric@unquantum.net

A famous beam-split coincidence test of the photon model was performed with γ-rays instead of visible light. A similar test was performed to split α-rays. In both tests, coincidence rates greatly exceed chance, leading to an *unquantum* effect. In contradiction to quantum theory and the photon model, these new results are strong evidence of the long abandoned accumulation hypothesis, also known as the loading theory. Attention is drawn to assumptions applied to past key experiments that led to quantum mechanics. The history of the loading theory is outlined, and a few key experiment equations are derived, now free of wave-particle duality. Quantum theory usually works because there is a subtle difference between quantized and thresholded absorption.

1 Introduction

Since Einstein's photoelectric work of 1905, quantum mechanics (QM) has endured despite its bizarre implications because no strong experimental evidence has been put forth to refute it. Such new evidence is presented in detail here.

By QM and the photon model, a singly emitted photon of energy $h\nu_{\mathrm{L}}$ must not trigger two coincident detections in a beam-split coincidence test (see p. 50 in [1] and p. 39 in [2]) where h is Planck's constant of action, and ν_{L} is frequency of the electromagnetic wave. Beam-split coincidence tests of past have seemingly confirmed QM by measuring only an accidental chance coincidence rate [3–6].

Here, new beam-split coincidence experiments use γ-rays instead of visible light. The detectors employed have high "energy" resolution, whereby their pulse-height is proportional to ν_{L}. The γ-ray detection-pulses were within a full-height window, indicating we are not dealing with frequency down-conversion.

To measure such an *unquantum* effect implies that a fraction of pre-loaded energy was present in the detector molecules preceding the event of an incoming classical pulse of radiant energy. It is called the *accumulation hypothesis* or the *loading theory* [7–12] (see p. 47 in [12]). The pre-loaded energy came from previous absorption that did not yet fill up to a threshold. The unquantum tests give us a choice: we either give up an always-applicable *particle-energy conservation*, or give up *energy conservation* altogether. We uphold energy conservation.

A beam-split coincidence test compares an expected chance coincidence rate R_c to a measured experimental coincidence rate R_e. Prior tests [3–6] all gave $R_e/R_c = 1$. Past authors admitted that exceeding unity would contradict QM. These unquantum experiments are the only tests known to reveal $R_e/R_c > 1$. This clearly contradicts the one-to-one "Born rule" probability prediction of QM.

It is counterintuitive to attempt to contradict the photon model with what was thought to be the most particle-like form of light, γ-rays. Prior tests have only pitted QM against an overly classical model that did not consider a pre-loaded state. A beam-split coincidence test with γ-rays is fair to both the loading theory and photon theory. The loading theory takes h as a maximum. This idea of action allowed below h is algebraically equivalent to "Planck's second theory" of 1911 [9, 10, 14, 15]. There, Planck took action as a property of matter, not light (see p. 136 in [10]). The unquantum effect implies that it was a false assumption to think h is due to a property of light. The loading theory assumes light is quantized at energy $h\nu_{\mathrm{L}}$ only at the instant of emission, but thereafter spreads classically.

Similar new beam-split tests with α-rays, contradicting QM with $R_e/R_c > 1$, are also described herein. This is important because both matter and light display wave-particle duality, and its resolution requires experiment and theory for both.

2 Gamma-ray beam-split tests

In a test of unambiguous distinction between QM and the loading theory, the detection mechanism must adequately handle both time and energy in a beam-split coincidence test with two detectors, as shown in the following analysis. Surprisingly, discussions of pulse "energy" (height) resolution have not been addressed in past tests [3–6] which were performed with visible light, and one test with x-rays. Referring to Fig. 1 we will analyze a photomultiplier tube (PMT) pulse-height response to monochromatic visible light [16]. A single channel analyzer (SCA) is a filter instrument that outputs a window of pulse heights ΔE_{window} to be measured; LL is lower level and UL is upper level (italic symbols denote notation in figures). If we set LL to less than half E_{mean}, one could argue we favored the loading theory, because a down-conversion might take place that would record coincidences in both detectors. Also, if LL were set too low, one could argue we were recording false coincidences due to noise. If we set LL higher than half E_{mean}, one could argue we were

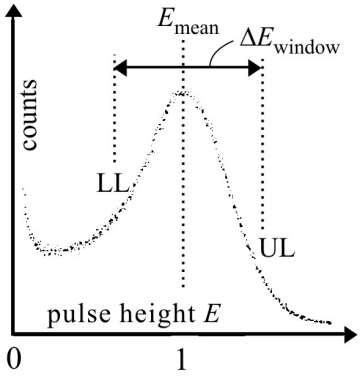

Fig. 1: PMT pulse-height response. Data according to [16].

Fig. 2: Two γ-ray detectors in tandem geometry; a demonstrator unit. Detector #1 was used with other components for data shown.

unfair to the loading theory by eliminating too many pulses that would have caused coincidences. Therefore a fair test requires high pulse-height resolution: $E_{mean} \gg \Delta E_{window}$. This criterion is not possible with a PMT or any visible light detector, but is easily met with γ-rays and scintillation detectors.

A high photoelectric effect detector-efficiency for the chosen γ-ray frequency was judged to enhance the unquantum effect, and this proved true. The single 88 keV γ-ray emitted in spontaneous decay from cadmium-109 (^{109}Cd), and detected with NaI(Tl) scintillators fit this criterion (see p. 717 [17]) and worked well. All radioisotopes used were low-level license-exempt.

A γ test of July 5, 2004 (see Fig. 6 in [18]) will be described in detail, and others briefly. After spontaneous decay by electron capture, ^{109}Cd becomes stable ^{109}Ag. ^{109}Cd also emits an x-ray, far below *LL*. We know that only one γ is emitted at a time, from a coincidence test with the γ source placed between two facing detectors that cover close to 4π solid angle (see p. 693 [19]). That test only revealed the chance rate, measured by

$$R_c = R_1 R_2 \tau , \qquad (1)$$

where R_1 and R_2 are the singles rates from each detector, and τ is the chosen time window within which coincident events are counted.

The test was performed with two detectors like those shown in Fig. 2, each being an NaI(Tl) crystal coupled to a PMT. The ^{109}Cd source was inside a tin collimator placed directly in front of detector #1, a custom made 4 mm thick 40×40 mm crystal. Directly behind detector #1 was detector #2, a 1.5″ Bicron NaI-PMT. We call this thin-and-thick detector arrangement tandem geometry. This test was performed inside a lead shield [20] that lowered the background rate 1/31. Referring to Fig. 3, components for each of the two detector channels are an Ortec 460 shaping amplifier, an Ortec 551 SCA, and an HP 5334 counter. For each detector channel, singles rates R_1 and R_2 were measured by calculating (counter pulses)/(test duration). A four channel Lecroy LT344 digital storage oscilloscope (DSO) with histogram software, monitored the analog pulses from each shaping amplifier on *Ch*1 (channel 1) and *Ch*2, and from the timing pulse outputs from each SCA on *Ch*3 and *Ch*4. Stored images of each triggered analog pulse assured that the number of misshaped pulses was well below 1%. Misshaped pulses can occur from pulse overlap and cosmic rays. This DSO can update pulse-height E and time difference Δt histograms after each triggered sweep. To assure exceeding particle-energy conservation, *LL* on each SCA window was set to $\sim 2/3$ of the ^{109}Cd γ characteristic pulse-height.

Data for this test is mostly from Fig. 4, a screen capture from the DSO. A control test with no source present is Δt histogram trace *B* of 16 counts/40.1 ks = 0.0004/s, a background rate to be subtracted. With τ taken as 185 ns, the chance rate from Eq. 1 was (291/s)(30/s)(185 ns) = R_c = 0.0016/s. From trace *A* and numbers on Fig. 4, R_e = 295/5.5 ks − 0.0004/s = 0.053/s. The unquantum effect was R_e/R_c = 33.5 times greater than chance. The described test is not some special case. Much critical scrutiny [18, 20] was taken to eliminate possible sources of artifact, including: faulty instruments, contamination by ^{113}Cd in the ^{109}Cd, fluorescence effects, cosmic rays, possibility of discovering stimulated emission, pile-up errors, and PMT artifacts. Hundreds of similar tests and repeats of various form have successfully defied QM. These tests include those with different sources (^{57}Co, ^{241}Am, pair-annihilation γ from ^{22}Na [21], ^{54}Mn, ^{137}Cs) and different detectors (NaI, high purity germanium, bismuth germinate, CsI), different geometries, and different collimator materials.

^{109}Cd was prepared in two chemical states of matter (see Fig. 11 in [18]). A salt state was prepared by evaporating an isotope solution. A metal state was prepared by electroplating the isotope in solution onto the end of a platinum wire. The unquantum effect from the salt state was 5 times greater than

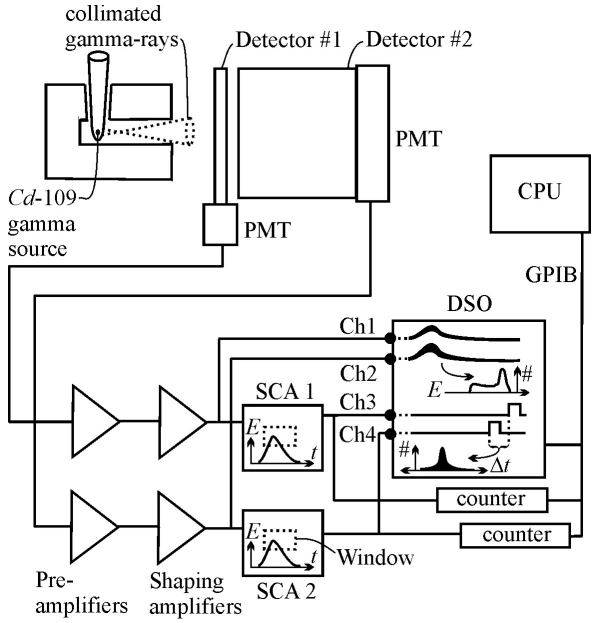

Fig. 3: γ-ray coincidence experiment.

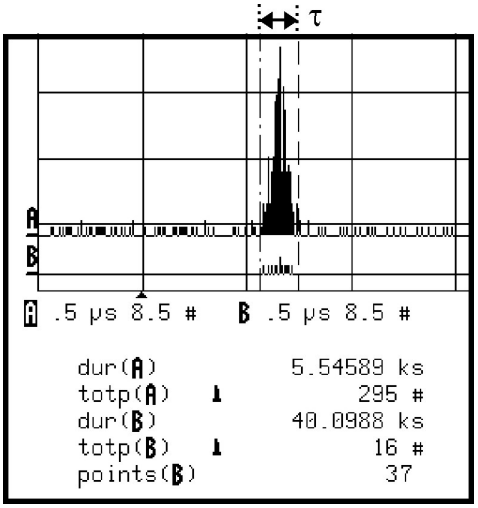

Fig. 4: γ-ray Δt from DSO.

from the metal state. This discovery measures how chemistry affects nuclear electron capture in isotope decay. We theorize that γ from the salt-crystaline source are more coherent and that the unquantum effect is enhanced by coherent waves. The singles spectrum did not measurably change with this chemical state change, so this sensitivity is due to the unquantum effect. A similar effect was reported [22] but was not nearly as sensitive or simple.

The unquantum effect is sensitive to distance (see Fig. 8–9 in [18]). A longer γ wavelength from ^{241}Am shows an enhanced unquantum effect when placed closer to the detectors, while a shorter γ wavelength from ^{137}Cs shows an enhanced effect when placed farther from the detector. Therefore, we can see how the spreading cone of a classical γ defines an area that matches the size of the microscopic scatterer (electron). We can measure how the short spatial and temporal qualities of a classical spreading γ wave-packet trigger the unquantum effect.

In addition to tandem geometry, a beam-split geometry was explored successfully. Different materials were tested to split an energy-fraction of a classical γ to one side, while the remaining ray passed through (see Fig. 12 in [18]). This beam-split geometry was developed into a spectroscopy whereby the pulse-height spectrum of the second detector was expanded. A non-shifted spectrum-peak indicates elastic Rayleigh scattering. A shifted spectrum-peak indicates non-elastic Compton scattering.

In beam-split geometry, crystals of silicon and germanium were explored with an apertured γ path to obtain angle resolution (see Fig. 13 in [18]). The unquantum effect varied with crystal orientation to reveal a new form of crystallography. This was not Bragg reflection from atomic planes, but rather from periodicity smaller than inter-atomic distance, perhaps electron-orbital structure.

The unquantum effect is sensitive to temperature of the beam-splitter (see Fig. 18 in [18]). A liquid nitrogen cooled slab of aluminum delivered a 50% greater unquantum effect, as expected.

Magnetic effects were explored with coincident deflected pulse-height analysis (see Fig. 14–16 in [18]) in beam-split geometry. A ferrite scatterer in a magnetic gap revealed enhanced Rayleigh scattering, indicating a stiff scatterer, as one would expect. A diamagnetic scatterer in a magnetic gap revealed enhanced Compton scattering, indicating a flexible scatterer, as expected.

The unquantum effect's increase/decrease response to several physical variables in the direction that made physical sense solidifies its fundamental validity. Each of the above mentioned modes of unquantum measurement represents a useful exciting discovery.

There is a simple way to measure the unquantum effect with a single NaI-PMT detector and a pulse-height analyzer [20]. Measure the ^{109}Cd sum-peak's count rate within a preset ΔE window that is set at twice 88 keV, and compare to chance. The result approached chance $\times 2$.

Our most impressive γ-split test [21] used ^{22}Na emitting a positron that annihilates into two 511 keV γ. The decay also emits a stronger γ that was caught in a third detector. In this triple-coincidence test $R_c = R_1 R_2 R_3 \tau_{12} \tau_{23}$. Only one from each pair of annihilation γ-rays were then captured by two detectors in tandem. Here $R_e/R_c = 963$. Energy $= h\nu$ is still true as a threshold value, but these experiments say there are no photons.

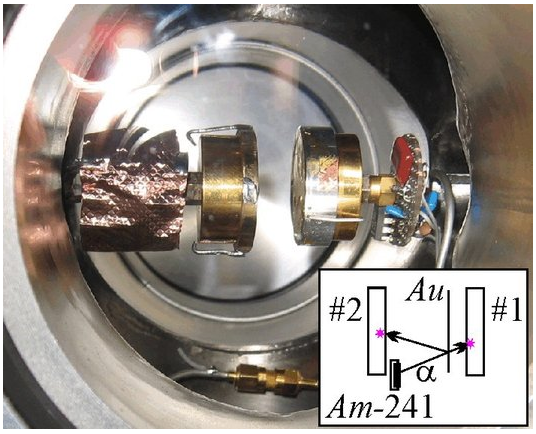

Fig. 5: α-split test in vacuum chamber.

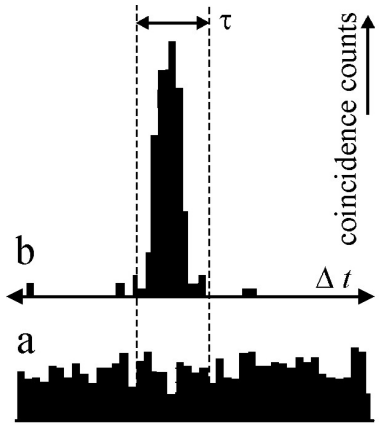

Fig. 6: α-ray Δt plots.

3 Alpha-ray beam-split tests

^{241}Am in spontaneous decay emits a single 5.5 MeV α-ray and a 59.6 keV γ. An α is a helium nucleus. This sounds like a particle, but consider a helium nuclear matter-wave. If the wave was probabilistic, the particle would go one way or another, and coincidence rates would only approximate chance. I performed hundreds of various tests in four vacuum chamber rebuilds. Two silicon Ortec surface barrier detectors with adequate pulse-height resolution were employed in a circuit nearly identical to Fig. 3. Fig. 5 shows the detectors and pre-amplifiers in the vacuum chamber. These tests were performed under computer CPU control by a program written in QUICKBASIC to interact with the DSO through a GPIB interface. Both SCA *LL* settings were at 1/3 of the characteristic α pulse-height, because it was found that an α-split usually maintains particle-energy conservation. The coincidence time-window was $\tau = 100$ ns. The Δt histograms of Fig. 6 were from DSO screen captures.

Data of Fig. 6-a was a two hour control test with the two detectors at right angles to each other and the ^{241}Am centrally located. Only the chance rate was measured, assuring that only one α was emitted at a time. This arrangement is adequate, and 4π solid angle capture is not practical with α. Any sign of a peak is a quick way to see if chance is exceeded. Background tests of up to 48 hours with no source gave a zero coincidence count.

Data of Fig. 6-b (Nov. 13, 2006) was from the arrangement of Fig. 5 using two layers of 24 carat gold leaf over the front of detector #1. Mounted on the rim of detector #2 were ^{241}Am sources, shaded to not affect detector #2. Every analog detector pulse in coincidence was perfectly shaped. $R_c = 9.8{\times}10^{-6}$/s, and $R_e/R_c = 105$ times greater than chance.

From collision experiments, the α requires $\sim$ 7 MeV per nucleon to break into components, and even more for gold [17]. It would take 14 MeV to create two deuterons. The only energy available is from the α's 5.5 MeV kinetic energy. So

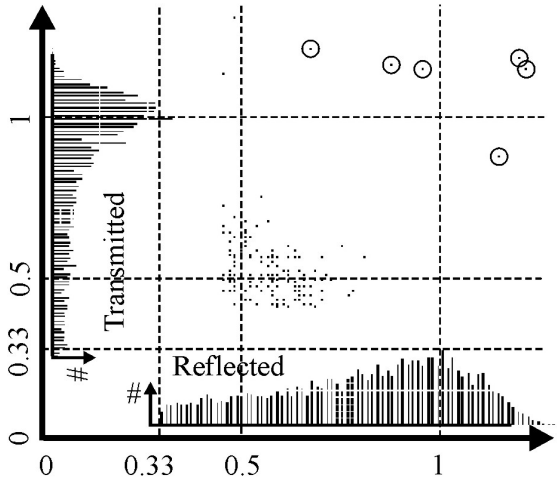

Fig. 7: Coincident α pulse-height pairs,

for any model of nuclear splitting there is not enough energy to cause a conventional nuclear split. Also plotted from the CPU program and data from the test of Fig. 6-b is data replotted in Fig. 7. Fig. 7 depicts pulse heights plotted as dots on a two dimensional graph to show coincident pulse heights from both detectors. The transmitted and reflected pulse-height singles spectra were carefully pasted into the figure. We can see that most of the a pulses (dots) are near the half-height marks; α usually splits into two lower kinetic-energy He matter-waves. Six dots, circled, clearly exceeded particle-energy conservation. Counting just these 6, we still exceed chance: $R_e/R_c = 3.97$. This is a sensational contradiction of QM because it circumvents the argument that a particle-like split, such as splitting into two deuterons, is somehow still at play.

In search for alternative explanations, we found none and conclude: an α matter-wave can split and continuous absorption can fill a pre-loaded state of He up to a detection thresh-

old. Also, the α-split test demonstrates how the loading theory applies to historical interference and diffraction tests with electrons, neutrons, and atoms [23, 24]. Several other materials were tested in transmission and reflection geometries to reveal the usefulness of this matter-wave unquantum effect in material science [21]. It is not necessary to use gold to exceed chance, but many materials tested just gave chance.

4 History of the loading theory and its misinterpretation

A believable report of such disruptive experimental results requires an accompanying historical and theoretical analysis.

Lenard [7, 8] recognized a pre-loaded state in the photoelectric (PE) effect with his trigger hypothesis. Most physicists ignored this idea in favor of Einstein's light quanta [25] because the PE equation worked. Planck (see Eq. 14 in [9], and p. 161 in [10]) explored a loading theory in a derivation of his black body law that recognized continuous absorption and explosive emission. Sommerfeld and Debye [11] explored an electron speeding up in a spiral around a nucleus during resonant light absorption. Millikan (see p. 253 in [13] described the loading theory, complete with its pre-loaded state in 1947, but assumed that its workings were "terribly difficult to conceive." In the author's extensive search, physics literature thereafter only treats a crippled version of the loading theory with no consideration of a pre-loaded state.

Most physics textbooks (e.g. [26], p. 79) and literature (e.g. [27]) routinely use photoelectric response time as evidence that the loading theory is not workable. Effectively, students are taught to think there is no such thing as a pre-loaded state. Using a known light intensity, they calculate the time an atom-sized absorber needs to soak up enough energy to emit an electron. One finds a surprisingly long accumulation time (the longest response time). They claim no such long response time is observed, and often quote $\sim$ 1 ns, the shortest response time from the 1928 work of Lawrence and Beams [28] (L&B). Such arguments unfairly compare a shortest experimental response time with a longest calculated response time. An absorber pre-loaded to near threshold explains the shortest response times. The longest response time from L&B was $\sim$ 60 ns. L&B did not report their light intensity, so it is not fair to compare their results to an arbitrary calculation. Energy conservation must be upheld, so an appropriate calculation is to measure the longest response time and the light intensity, assume the loading theory starting from an unloaded state, and calculate the effective size of the loading complex. The loading theory was the first and obvious model considered for our earliest experiments in modern physics. There is no excuse for the misrepresentation outlined here.

5 A workable loading theory

For brevity, the theory is elaborated for the charge matter-wave. If we develop three principles, we will find they explain both the quantum and unquantum experiments [29]:

1. de Broglie's wavelength equation is modified to the wavelength of a beat or standing-wave envelope-function of Ψ;
2. Planck's constant h, electron charge e, and mass constants like the electron mass m_e are maximum thresholds whereby emission is quantized but absorption is continuous and thresholded;
3. Ratios h/e, e/m, h/m, in our equations are conserved as the matter-wave expands and thins-out.

In de Broglie's derivation of his famous wavelength equation (see. p. 3 in [30])

$$\lambda_\Psi = \frac{h}{m_e v_p}\,, \tag{2}$$

he devised a frequency equation

$$h\nu_\Psi = m_e c^2, \tag{3}$$

and a velocity equation

$$v_p V_\Psi = c^2. \tag{4}$$

For equations (2–4), subscript Ψ is for either a matter-wave or a probabilistic wave, λ_Ψ is the phase wavelength, ν_Ψ the phase frequency, v_p the particle velocity, V_Ψ the phase velocity, and m_e the electron mass. Equations (3) and (4) remain widely accepted, but have serious problems. Equation (3) is only true when using ν_{L} instead of ν_Ψ to calculate a mass equivalent. If we measure v_p, λ_Ψ, and m_e for matter diffraction, equation (3) fails. Our experimental equations use h associated with kinetic energy, or momentum, not mass-equivalent energy.

As for equation (4), one might attempt to extract it from the Lorentz transformation equation of time by dimensional analysis, but its derivation independent of equations (2) or (3) has not been found by the author. Nevertheless, it describes an infinite V_Ψ in any particle's rest frame. Many physicists use equation (4) to justify the probability interpretation of QM, (see p. 89 in [31]) but this leads to "spooky action at a distance" we are all well aware of.

A much more reasonable frequency equation is the PE effect equation $h\nu_{\text{L}} = {}^1\!/_2\, m_e v_p^2$, with the work function not yet encountered. It is very reasonable to understand that something about charge is oscillating at the frequency of its emitted light, but just how to replace ν_{L} with a charge frequency requires insight. Recall the Balmer or Rydberg equation of the hydrogen spectrum in terms of frequency in its simplest form: $\nu_{\text{L}} = \nu_{\Psi 2} - \nu_{\Psi 1}$. Here ν_Ψ is frequency of a non-probabilistic Ψ matter-wave. The hydrogen atom is telling us that the relationship between ν_{L} and ν_Ψ is about difference-frequencies and beats. Consider that this difference-frequency property is fundamental to free charge as well as atomically bound charge. Beats, constructed from superimposing two sine waves are understood from a trigonometric identity to equal

an averaged Ψ wave modulated by a modulator wave M, as graphed in Fig. 8. If we take M as the coupling of light to charge we see that there are two beats per modulator wave, and we can write a relationship between light frequency and the frequency of charge beats: $2\nu_{\text{L}} = \nu_g$. Group velocity is commonly substituted for particle velocity, so $v_p = v_g$. Substituting the last two equations into the PE equation makes $h\nu_g = m_e v_g^2$. Groups are periodic, so we apply $\nu_g = v_g/\lambda_g$ to derive a wavelength equation (principle 1):

$$\lambda_g = \frac{h}{m_e v_g}\,. \tag{5}$$

Notice that both the PE equation and equation (5) have h/m_e. Recall several equations applicable to so-called "wave properties of particles": Lorentz force, PE, Compton effect, Aharonov-Bohm effect, others. They all have ratios like e/m, h/m, h/e. Examining $h/m_e \equiv Q_{h/m}$, if action is less than h and mass is less than m_e and the proportion is conserved, we would not be able to tell if those values went below our thresholds (h, m, e) while the charge-wave spreads out and diffracts (principles 2 & 3). Therefore we can write equation (5) as $\lambda_g = Q_{h/m}/v_g$ and the PE equation as $\nu_{\text{L}} = {}^1\!/_2\, Q_{m/h} v_g{}^2$. At threshold, $m_{group} = m_e$ and at sub-threshold we use Q ratios to emphasize wave nature (Q for quotient). To understand the PE effect without photons, visualize the pre-loaded state in the $Q_{m/h}$ ratio. Energy loads up to threshold and an electron is emitted explosively (principle 2); thereafter, the charge-wave can spread classically.

The Compton effect is often claimed to require QM treatment. A classical treatment is in Compton and Allison's book (see p. 232 in [12]) based upon a Bragg grating of envelopes from standing de Broglie waves. However, the envelopes were weak. If charge structures were inherently composed of beats of length d, it would naturally create a plausible Bragg grating. Use the Bragg diffraction equation $\lambda_{\text{L}} = 2d\sin(\phi/2)$, where ϕ is deflection angle. Substitute for d, λ_g from equation (5). Solve for v_g and insert into the Doppler shift equation $\Delta\lambda_{\text{L}}/\lambda_{\text{L}} = (v_g/c)\sin(\phi/2)$. Simplify using the trigonometric identity $\sin^2\theta = [1 - \cos(2\theta)]/2$ and $Q_{h/m}$ to yield

$$\Delta\lambda_{\text{L}} = \frac{Q_{h/m}}{c}(1 - \cos(\phi)),$$

the Compton effect equation.

Also related to the Compton effect are popular accounts of the test by Bothe and Geiger. The measured coincidence rate was not a one-to-one particle-like effect as often claimed, but rather the coincidence rate was $\sim 1/11$ [32].

What about quantized charge experiments? Measurements of e are performed upon ensembles of many atoms, such as in the Millikan oil drop experiment, and earlier by J. J. Thompson. Granted, electron detectors go click, but that is the same threshold effect demonstrated by the unquantum α-split experiments. From evidence of charge diffraction alone, it was a poor assumption to think charge was always quantized at e. Charge, capable of spreading out as a wave with a fixed e/m_e ratio for any unit of volume, loading up, and detected at threshold e, would remain consistent with our observations. Furthermore, the electron need not be relatively small. Chemists performing Electron Spin Resonance measurements often model the electron to be as large as a benzene ring. A QM electron would predict a smeared-out ESR spectrum.

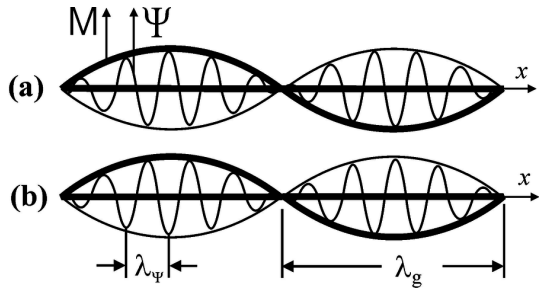

Fig. 8: Illustration of the concept of matter and antimatter. (a) Two positron beats. (b) Two electron beats.

The following is a list of famous experiments and principles re-analyzed with this newly developed Loading Theory (LT) by the author [29]: PE effect, Compton effect, shot noise, black body theory, spin, elementary charge quantization, charge & atom diffraction, uncertainty principle, exclusion principle, Bothe-Geiger experiment, Compton-Simon experiment, and the nature of antimatter, as envisioned in Fig. 8. The LT visualizes these fundamental issues, now free of wave-particle duality.

The LT supported by the unquantum effect easily resolves the enigma of the double-slit experiment. The wave of light or matter would load-up, and show itself as a click at a threshold.

These realizations lead to matter having two states: (1) a contained wave in a particle state, and (2) a spreading matter-wave that is not a particle at all, yet carries the wave-form matching a loading-up particle. One may protest by quoting experiments in support of QM, such as giant molecule diffraction, EPR tests, and quantum cryptography. My analysis of major flaws in such tests, and elaboration of topics outlined here, are freely viewable from my posted essays and at `www.unquantum.net`.

Submitted on October 11, 2013 / Accepted on February 23, 2014

References

1. Bohr N. Atomic physics and human knowledge. John Wiley and Sons Inc, New York, 1958.
2. Heisenberg W. The physical principles of the quantum theory. Dover Publications, Dover, 1930.
3. Givens M. P. An experimental study of the quantum nature of x-rays. *Philosophical Magazine*, 1946, v. 37, 335–346.
4. Brannen E., Ferguson H. The question of correlation between photons in coherent light rays. *Nature*, 1956, v. 4531, 481–482.

5. Clauser J. F. Experimental distinction between the quantum and classical field theoretic predictions for the photoelectric effect. *Physical Review D*, 1974, v. 9, 853–860.
6. Grainger P., Roger G., Aspect A. A new light on single photon interferences. *Annals of the New York Academy of Sciences*, 1986, v. 480, 98–107.
7. Lenard P. On cathode rays. Nobel lecture, *Nobel Lectures, Physics 1901-1921*, Elsevier Publishing Company, Amsterdam, 1967.
8. Lenard P. Ueber die lichtelektrische Wirkung. *Annalen der Physik*, 1902, v. 313(5), 149–198.
9. Planck M. Eine neue Strahlungshypothese. *Verhandlungen der Deutschen Physikalischen Gesellschaft*, 1911, v. 13, 138–148. Reprinted in: *Physikalische Abhandlungen und Vorträge*, Carl Schütte & Co, Berlin, 1958, v. 2, 249–259.
10. Planck M. The theory of heat radiation. Masius, M. (transl.) P. Blakiston's Son & Co., Philadelphia, 1914.
11. Debye P., Sommerfeld A. Theorie des lichtelektrischen Effektes vom Standpunkt des Wirkungsquantums. *Annalen der Physik*, 1913, v. 41, 872–930.
12. Compton A., Allison S. K. X-rays in theory and experiment. Van Nostrand, New York, 1935.
13. Millikan R.A. Electrons (+ and −) protons photons neutrons mesotrons and cosmic rays. University of Chicago Press, 1947.
14. Kuhn T. S. Black-body theory and the quantum discontinuity, 1894–1912. Oxford University Press, 1978, (see p. 235–264).
15. Whittaker E. A history of the theories of aether and electricity: the modern theories 1900–1926. Thomas Nelson and Sons, London, Edinburg, 1953, (see p. 103)
16. Flyckt S.-O., Mamonier C. Photomultiplier tubes principles and applications. Philips Photonics, Brive, France, 2002.
17. Evans R. The atomic nucleus. Tata McGraw Hill Publishing Company Limited, Bombay, New Delhi, 1955.
18. Reiter E. S. Photon violation spectroscopy. viXra: 1203.0094.
19. Knoll G. Radiation detection and measurement. John Wiley and Sons, Inc., New York, 1979.
20. Reiter E. S. A serious challenge to quantization. viXra: 1203.0092.
21. Reiter E. S. Particle violation spectroscopy. viXra: 1204.0032.
22. Kraushaar J. J., Wilson E. D., Bainbridge K. T. Comparison of the values of the disintegration constant of Be^7 in Be, BeO, and BeF_2. *Physical Review*, 1953, v. 90, 610–614.
23. Estermann I., Frisch R., Stern O. Monochromasierung der de Broglie-Wellen von Molekularstrahlen. *Zeitschrift fuer Physik*, 1932, v. A73, 348–365.
24. Berman P. R. Atom interferometry. Academic Press, San Diego, London, Boston, New York, Sydney, Tokyo, Toronto, 1997.
25. Einstein A. On a heuristic point of view concerning the production and transformation of light (title translated). *Annalen der Physik*, 1905, v. 17, 132–148.
26. Eisberg R. Fundamentals of modern physics. John Wiley and Sons, Inc., New York, 1961.
27. Gluck P., Saering B. No time lag in the photoelectric effect. *The Physics Teacher*, 2010, v. 48, 285–286.
28. Lawrence E., Beams J. The element of time in the photoelectric effect. *Physical Review*, 1928, v. 32, 478–485.
29. Reiter E. S. An understanding of the particle-like property of light and charge. viXra: 1203.0077.
30. de Broglie L. An introduction to the study of wave mechanics. E. P. Dutton, New York, 1930.
31. Born M. Atomic physics, fifth edition. Hafner Publishing Co., New York, 1951.
32. Shankland R. S. An apparent failure of the photon theory of scattering. *Physical Review*, 1936, v. 49, 8–13.

Staggering Phenomenon in Gamma Transitional Energies over Spin for Negative Parity States of Octupole Vibrational Nuclear Bands

A.M. Khalaf[1] and F.A. Altalhi[2]

[1]Physics Department, Faculty of Science, Al-Azhar University, Cairo, Egypt. E-mail: ali_khalaf43@hotmail.com
[2]Department of Science, Tabuk University, Ministry of Higher Education, Kingdom of Saudi Arabia. E-mail: Faltahi@hotmail.com

The negative parity states of octupole vibrational bands in Tungsten and Osmium nuclei have perturbed structure. To explore the $\Delta I = 1$ staggering, we plotted the gamma transitional energy over spin (EGOS) versus I^2. Such a plot exhibit large deviation from a linear $I(I+1)$ dependence $E(I) = A[I(I+1)]+B[I(I+1)]^2$ and effectively splits into two different curves for odd and even spin states and a staggering pattern is found. The odd-spin members $I^\pi = 1^-, 3^-, 5^-, \ldots$ were displaced relatively to the even-spin members $I^\pi = 2^-, 4^-, 6^-, \ldots$ i.e. the odd levels do not lie at the energies predicted by the pure rotator fit to the even levels, but all of them lie systematically above or all of them lie systematically below the predicted energies because the odd-spin states can be aligned completely, while the even-spin states can only be aligned partially. Also the $\Delta I = 1$ staggering effect has been clearly investigated by examining the usual backbeding plot.

1 Introduction

The properties of nuclear rotational bands built on octupole degrees of freedom have been extensively studied within various microscopic as will as macroscopic model approaches in nuclear structure [1–6]. It is will known that heavy nuclei have low-lying $K^\pi = 0^-$ octupole deformed bands [7,8]. Theoretical works of such bands have been presented in framework of cranked random phase approximation (RPA) [9, 10], the collective model [5], the interacting boson model (IBM) [3, 11], the variable moment of inertia (VMI) model [12] and the alpha particle cluster model [4, 13]. The IBM and the exotic cluster models address the existence of negative parity bands with $K^\pi \neq 0^-$.

Several staggering effects are known in nuclear spectroscopy. The $\Delta I = 2$ staggering has been observed and interpreted in superdeformed (SD) nuclei [14–22], where the levels with $I = I_0 + 2, I_0 + 6, I_0 + 10, \ldots$ are displaced relatively to the levels with $I = I_0, I_0 + 4, I_0 + 8, \ldots$, i.e. the level with angular momentum I is displaced relatively to its neighbors with angular momentum $I \pm 2$. There is another kind of staggering happening in SD odd-A nuclei, the $\Delta I = 1$ signature splitting in signature partners pairs [23].

The $\Delta I = 1$ Staggering in odd normal deformed (ND) nuclei is familiar for a long time [24–28], where the rotational bands with $K = 1/2$ separate into signature partners, i.e. the levels with $I = 3/2, 7/2, 11/2, \ldots$ are displaced relatively to the levels with $I = 1/2, 5/2, 9/2, \ldots$. In this paper, we will investigate another type of $\Delta I = 1$ energy staggering occurring in the negative parity octupole bands of even-even nuclei, where the levels with odd spin $I^\pi = 1^-, 3^-, 5^-, \ldots$ are displaced relatively to the levels with even spin $I^\pi = 2^-, 4^-, 6^-, \ldots$. This is more strikingly revealed when one makes the usual backbending plot of the energies in which the kinematic moment of inertia is plotted against the square of rotational frequency. The negative parity octupole band breaks into even and odd-spin bands with, however, very little backbending tendency.

2 Outline of the Theory of ΔI = 1 Energy Staggering

To analyze the $\Delta I = 1$ energy staggering in collective bands, several tests have been considered in the literature. In our analysis, the basic staggering parameter is the gamma transitional energy over spin (EGOS=$E_\gamma(I)/I$) of the transitional energies in a $\Delta I = 1$, where E(I) is the energy of the state of the spin I, and $E_\gamma(I)$ denotes the dipole transition energy

$$E_\gamma(I) = E(I) - E(I-1). \quad (1)$$

The level energies in a band can be more realistic parameterize by two-term rotational formula as a reference

$$E(I) = A[I(I+1)] + B[I(I+1)]^2. \quad (2)$$

The first two-term represents the perfect purely collective rigid rotational energy, where A denotes the inertial parameter $A = \hbar/2J$ (where J is the kinematic moment of inertia). The introduction of the second term is based on the assumption that, on rotation, the moment of inertia of the nucleus increases as does the quadratic function of the square of the angular velocity of rotation of the nucleus.

It is interesting to discuss the energy levels by plotting EGOS against spin. This is not helpful to identify the structure of the nucleus, but also to see clearly changes as a function of spin. For pure rotator, the energies of the yrast states are:

$$E(I) = A[I(I+1)]. \quad (3)$$

Then the $E2$ γ-ray energies are given by

$$E_\gamma(I) = A[4I - 2] \quad (4)$$

which yield

$$EGOS = A\left(4 - \frac{2}{I}\right). \quad (5)$$

Table 1: The adopted best model parameters A and B for our selected octupole vibrational bands.

	^{178}W	^{180}W	^{176}Os	^{178}Os	^{180}Os	^{182}Os
A (keV)	13.637	13.027	9.665	10.083	11.796	9.491
B (eV)	-13.821	-8.517	-2.223	-3.032	-8.607	0.140

In units of A, EGOS evolves from 3 for $I = 2$ up to 4 for high I, and so gradually increasing and asymptotic function of I.

EGOS for our proposed reference formula (2) is given by

$$EGOS = 2A + 4BI^2. \tag{6}$$

The EGOS when plotted against I^2, it represent a straight line of intercept 2A and slope 4B. Practically, the plot splits into two different curves for the odd and even spin states respectively. To see fine variation in the plot (EGOS & I^2), we use the staggering parameter

$$e(I) = EGOS - \left(2A + 4BI^2\right)_{\text{ref}} \tag{7}$$

where the unknown A and B are determined by minimizing the function F

$$F(I, A, B) = \sum_I |e(I)|^2. \tag{8}$$

The summation over spin in equation (8) is taken in step of $\Delta I = 1$. The function F has a minimum value when all its partial derivatives with respect to A and B vanish ($\partial F/\partial A = 0, \partial F/\partial B = 0$), this leads to

$$2nA + 4\sum_I I^2 B = \sum_I EGOS(I) \tag{9}$$

$$2\sum_I I^2 A + 4\sum_I I^4 B = \sum_I I^2 EGOS(I) \tag{10}$$

where n is the number of data points.

The behavior of the octupole band is most clearly illustrated by a conventional backbending plot. For each $\Delta I = 2$ value, the effective nuclear kinematic moment of inertia is plotted versus the square of the rotational frequency. If we consider the variation of the kinematic moment of inertia $J^{(1)}$ with angular momentum I, we can write

$$\frac{2J^{(1)}}{\hbar^2} = \frac{4I - 2}{E(I) - E(I-2)}. \tag{11}$$

Lets us define the rotational frequency $\hbar\omega$ as a derivative of the energy E(I) with respect to the angular momentum $[I(I+1)]^{1/2}$,

$$\hbar\omega = \frac{dE}{d[I(I+1)]^{1/2}} \tag{12}$$

usually we adopt the relation

$$(\hbar\omega)^2 = \frac{4(I^2 - I + 1)}{(2J^{(1)}/\hbar^2)^2}. \tag{13}$$

3 Numerical Calculation and Discusion

Our selected octupole bands are namely: ^{178}W, ^{180}W, ^{176}Os, ^{178}Os, ^{180}Os and ^{182}Os. The optimized model parameters A and B for each nucleus have been adjusted by using a compuer simulation search program to fit the calculated theoretical energies $E^{cal}(I_i)$, with the corresponding experimental ones $E^{exp}(I_i)$. The procedure of fitting is repeated for several trail values A and B to minimize the standard quantity χ which represent the root mean square deviation

$$\chi = \left[\frac{1}{N}\sum_{i=1}^{N}\left(\frac{E^{exp}(I_i) - E^{Cal}(I_i)}{\triangle E^{exp}(I_i)}\right)^2\right]^{1/2}$$

where N is the number of data points and $\Delta E^{exp}(I_i)$ are the experimental errors. The best optimized parameters are listed in table (1). The negative parity octupole bands have several interesting characteristics, the most obvious of which is the staggering effect. In this paper the $\Delta I = 1$ staggering is evident on a plot of staggering parameter $e(I)$ against I^2 and illustrated in figure (1), the band effectively splits into an odd- and even-spin sequence with a slight favoring in energy for the odd-spin states. In terms of an alignment of the angular momentum of the octupole vibration, the odd energy favoring can be understood since the odd-spin states can be aligned completely ($I \sim R + 3$, where $R = 0, 2, 4, \ldots$ is the collective rotation), while the even spins can only be aligned partially ($I \sim R + 2$). As expected from a good rotor model, the γ-ray transition energy $E_\gamma(I)$ increases with increasing the angular momentum I. It is found in some rotational deformed nuclei that the transition energy decreases with increasing I, this anomalous behavior is called nuclear backbending. In order to represent this backbending, one prefers to plot twice the kinematic moment of inertia $2J^{(1)}/\hbar^2$ versus the square of the rotational frequency $(\hbar\omega)^2$. Figure (2) shows the backbending plot for our selected octupole bands. It is seen that the bands are essentially separate into odd and even spin sequences which shows the effects of rotation alignment. The increase in Coriolis effects is due to the lowering of the Fermi level, then these effects depress the odd spin states relative to the even spin states. When the Coriolis effects are large compered with the octupole correlations effected through the residual interaction, it becomes inappropriate to identify these bands as octupole bands (decoupled two quasiparticle bands). These are bands in which the intrinsic spin has been aligned with the rotational spin through the decoupling action of the Coriolis force.

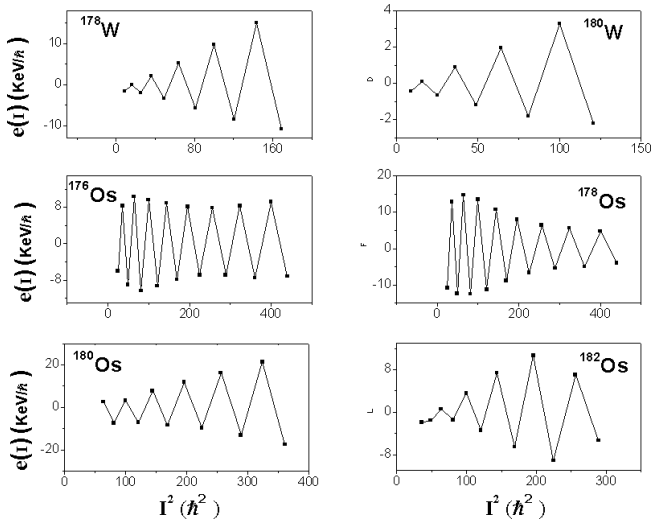

Fig. 1: The odd-even $\Delta I = 1$ energy staggering parameters $e(I)$ versus I^2 for negative parity states of octupole vibrational bands in doubly even nuclei ^{178,180}W and ^{176,178,180,182}Os.

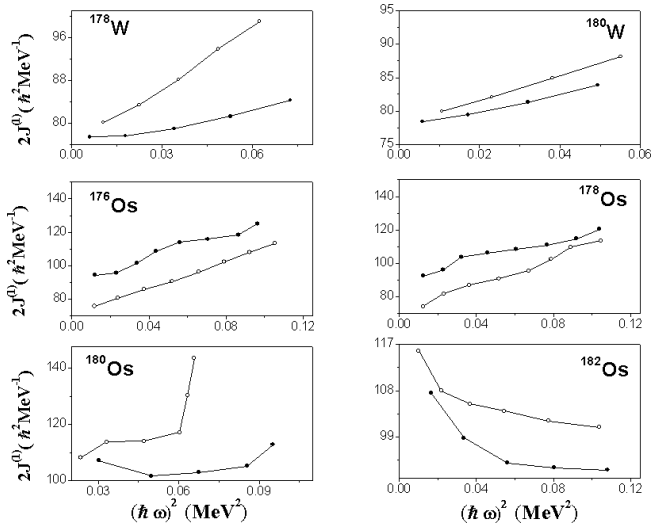

Fig. 2: Plot of twice Kinematic moment of inertia $2J^{(1)}$ against the square of the rotational frequency $(\hbar\omega)^2$ for the negative parity bands in ^{178,180}W and ^{176,178,180,182}Os isotopes.

4 Conclusion

In negative parity octupole bands of even-even W/Os nuclei, the levels with odd spins $I^\pi = 1^-, 3^-, 5^-, ...$ are displaced relatively to the levels with even spins $I^\pi = 2^-, 4^-, 6^-, ...$ The effect is called $\Delta I = 1$ staggering and its magnitude is clearly larger than the experimental errors. The phase and amplitude of the splitting is due to rotation particle Corialis coupling. Our proposed two terms formula provided us with information about the effective moment of inertia.

Submitted on February 11, 2014 / Accepted on February 23, 2014

References

1. Ahmed I. and Butler B.M. Octupole Shapes in Nuclei *Annual Review of Nuclear and Particle Science*, 1993, v. 43, 71–814.
2. Denisov V.Yu. and Dzyublik A.Ya. Collective states of even-even and odd nuclei with $\beta_2, \beta_3, ..., \beta_N$ deformations. *Nuclear Physics*, 1995, v. A589 17–57.
3. Zamfir N.V. and Kusnezov D. Octupole Correlations in the Transitional octinides and the spdf interacting boson Model. *Physical Review*, 2001, v. C63 054306–054315 and Octupole Correlations in U and Pu Nuclei. *Physical Review*, 2001, v. C67 014305–014313.
4. Shneidman T.M., et al. Cluster interpretation of parity splitting in alternating parity bands. *Physics Letters*, 2002, v. B526 322–328, and Cluster interpretation of properties of alternating parity bands in heavy nuclei. *Physical Review*, 2003, v. C67 014313–014325.
5. Minkov N., et al. Parity shift and beat staggering structure of octupole bands in a collective model for quadrupole–octupole-deformed nuclei. *Journal of Physics G: Nuclear and Particle Physics*, 2006, v. 32 497–510.
6. Hinde D. and Dasgupta M. Insights into the dynamics of fusion forming heavy elements. *Nuclear Physics*, 2007, v. A787 176–183.
7. Butler P.A. and Nazarewicz W. Intrinsic reflection asymmetry in atomic nuclei. *Review of Modern Physics*, 1996, v. 68 349–421.
8. Stefan Frauendorf. Spontaneous symmetry breaking in rotating nuclei. *Review of Modern Physics*, 2001, v. 73 463–514.
9. Ward D. et al. Rotational bands in ^{238}U. *Nuclear Physics*, 1996, v. A600 88–110.
10. Hackman G. High-spin properties of octupole bands in ^{240}Pu and ^{248}Cm. *Physical Review*, 1998, v. C57 R1056–R1059.
11. Cottle P.D. and Zamfir N.V. Octupole states in deformed actinide nuclei with the interacting boson approximation. *Physical Review*, 1998, v. C58 1500–1514.
12. Lenis D. and Dennis Bonatsos. Parameter-free solution of the Bohr Hamiltonian for actinides critical in the octupole mode. *Physics Letters*, 2006, v. B633 474–478.
13. Buck B., Merchant A.C. and Perez S.M. Negative parity bands in even–even isotopes of Ra, Th, U and Pu. *Journal of Physics G: Nuclear and Particle Physics*, 2008, v. 35 085101–085102.
14. Flibotte S., et al. $\Delta I = 4$ bifurcation in a superdeformed band: Evidence for a C_4 symmetry band. *Physical Review Letters*, 1993, v. 71 4299–4302.
15. Cederwall B, et al. New features of superdeformed bands in ^{194}Hg. *Physica Scripta*, 1994, v. 72 3150–3153.
16. Haslip1 D.S., Flibotte1 S. and de France G. $\Delta I = 4$ Bifurcation in Identical Superdeformed Bands. *Physical Review Letters*, 1997, v. 78 3447–3450.
17. Hamamoto I. and Mottleson B. Superdeformed rotational bands in the presence of $_4$4Y deformation. *Physics Letters*, 1994, v. B333 294–298.
18. Pavlichenkov I.M. and Flibotte S. C_4 symmetry and bifurcation in superdeformed bands. *Physical Review*, 1995, v. C51 R460–R464.
19. Khalaf A.M., Taha M.M., and Kotb M. Studies of Superdeformation in Gadolinium Nuclei Using Three-Parameters Rotational Formula. *Progress in Physics*, 2012, v. 8 (4), 39–44.
20. Khalaf A.M. and Sirag M.M. Analysis of $\Delta I = 2$ Staggering in Nuclear Superdeformed Rotational Bands. *Egypt Journal of Physics*, 2004, v. 35 (2), 359–375.
21. Sirag M.M. Reexamination of $\Delta I = 2$ Energy Staggering in Nuclear Superdeformed Rotational Bands. *Egypt Journal of Physics*, 2007, v. 38 (1), 1–14.
22. Madiha D. Okasha. ΔI=2 Nuclear Staggering in Superdeformed Rotational Bands. *Progress in Physics*, 2014, v. 10 (1), 41–44.

23. Khalaf A.M., et al. ΔI = 1 Signature Splitting in Signature Partners of Odd Mass Superdeformed Nuclei. *Progress in Physics*, 2013, v. 9 (3), 39–43.

24. Stephens F.S. Spin alignment in superdeformed rotational bands. *Nuclear Physics*, 1990, v. A520 c91–c104.

25. Toki H. and Faessler A. Asymmetric rotor model for decoupled bands in transitional odd-mass nuclei. *Nuclear Physics*, 1975, v. A253 231–252.

26. Khalaf A.M. High Spin Properties in Deformed Nuclei Using Weak Coupling Model. *Indian Journal of pure and Applied Physics*, 1986, v. 24 469–471.

27. Khalaf A.M. Nuclear Backbending and Evidence for Particle Core Coupling in Even-Even Nuclei. *Indian Journal of pure and Applied Physics*, 1986, v. 24 530–535.

28. Khalaf A.M. and Hegazi A.N. Theoretical Investigation of Potential Spectra for Axially Symetric Nuclei. *Proceedings of the Mathematical and Physical Society of Egypt*, 1984, v. 57 (2), 95–104.

A Model for the Expansion of the Universe

Nilton Penha Silva
Departmento de Física (Retired Professor), Universidade Federal de Minas Gerais, Belo Horizonte, MG, Brazil
Email: nilton.penha@gmail.com

One introduces an ansatz for the expansion factor $a(t) = e^{(H(t)t-H_0T_0)/\beta}$ for our Universe in the spirit of the FLRW model; β is a constant to be determined. Considering that the ingredients acting on the Universe expansion ($t > 4\times10^{12}\ s \approx 1.3\times10^{-5}\ Gyr$) are mainly matter (baryons plus dark matter) and dark energy, one uses the current measured values of Hubble constant H_0, the Universe current age T_0, matter density parameter $\Omega_m(T_0)$ and dark energy parameter $\Omega_\Lambda(T_0)$ together with the Friedmann equations to find $\beta = 0.5804$ and that our Universe may have had a negative expansion acceleration up to the age $T_\star = 3.214\ Gyr$ (*matter era*) and positive after that (*dark energy era*), leading to an eternal expansion. An interaction between matter and dark energy is found to exist. The deceleration $q(t)$ has been found to be $q(T_\star) = 0$ and $q(T_0) = -0.570$.

1 Introduction

The Cosmological Principle states that the Universe is spatially homogeneous and isotropic on sufficiently large scale [1–4] and [7]. This is expressed by the Friedmann spacetime metric:

$$ds^2 = \mathfrak{R}^2(t)\,d\psi^2+\mathfrak{R}^2(t)f_k^2(\psi)\left(d\theta^2 + sin^2\theta\,d\phi^2\right)-c^2dt^2, \quad (1)$$

where ψ, θ and ϕ are comoving space coordinates ($0 \le \psi \le \pi$, $for\ closed\ Universe$, $0 \le \psi \le \infty$, $for\ open\ and\ flat\ Universe$, $0 \le \theta \le \pi$, $0 \le \phi \le 2\pi$), t is the proper time shown by any observer clock in the comoving system. $\mathfrak{R}(t)$ is the scale factor in units of distance; actually $\mathfrak{R}(t)$ is the *radius of curvature* of the Universe. The proper time t may be identified with the cosmic time. In terms of the usual expansion factor

$$a(t) = \frac{\mathfrak{R}(t)}{\mathfrak{R}(T_0)}, \quad (2)$$

being T_0 the current age of the Universe, equation (1) becomes

$$\begin{aligned} ds^2 = {} & \mathfrak{R}^2(T_0)\,a^2(t) \\ & \left(d\psi^2 + f_k^2(\psi)\left(d\theta^2 + sin^2\theta\,d\phi^2\right)\right) - c^2dt^2, \end{aligned} \quad (3)$$

$f_k^2(\psi)$ assumes the following expressions:

$$f_k^2(\psi)\begin{cases} f_1^2(\psi) = sin^2\psi & \text{(closed Universe)} \\ f_0^2(\psi) = \psi^2 & \text{(flat Universe)} \\ f_{-1}^2(\psi) = sinh^2\psi & \text{(open Universe)} \end{cases} \quad (4)$$

The expansion process one will be considering here is the one started by the time of $4\times10^{12}\ s \approx 1.3\times10^{-5}\ Gyr$ when the so called *matter era* began. Right before that, the Universe went through the so called *radiation era*. In this paper one considers only the role of the matter (baryonic and non-baryonic) and the dark energy.

2 Einstein's field equations

Let one uses Einstein's Field Equations [5], with the inclusion of the Λ "cosmological constant" term.

$$G_{\mu\nu} = R_{\mu\nu} - \frac{1}{2}g_{\mu\nu}\,R = \frac{8\pi G}{c^4}\left(T_{\mu\nu} + T^\Lambda_{\mu\nu}\right) \quad (5)$$

where $g_{\mu\nu}$ is the metric tensor, $R_{\mu\nu}$ is the Ricci tensor, R is the Ricci scalar curvature, $T_{\mu\nu}$ is the energy-momentum tensor, and, $T^\Lambda_{\mu\nu}$ the dark-energy-momentum tensor,

$$T^\Lambda_{\mu\nu} = \rho_\Lambda c^2 g_{\mu\nu}, \quad (6)$$

$$\rho_\Lambda = \frac{\Lambda c^2}{8\pi G}; \quad (7)$$

Λ is the "cosmological constant", which will be here allowed to vary with time. The metric tensor for the metric above, equation (3), is

$$(g_{\mu\nu}) = \begin{pmatrix} \mathfrak{R}^2(t) & 0 & 0 & 0 \\ 0 & \mathfrak{R}^2(t)f_k^2(\psi) & 0 & 0 \\ 0 & 0 & \mathfrak{R}^2(t)f_k^2(\psi)sin^2\theta & 0 \\ 0 & 0 & 0 & -c^2 \end{pmatrix} \quad (8)$$

where

$$\mathfrak{R}(t) = \mathfrak{R}(T_0)\,a(t). \quad (9)$$

The Ricci tensor is given by

$$R_{\mu\nu} = \partial_\lambda\Gamma^\lambda_{\mu\nu} - \partial_\nu\Gamma^\lambda_{\mu\lambda} + \Gamma^\eta_{\mu\nu}\Gamma^\lambda_{\eta\lambda} - \Gamma^\eta_{\mu\lambda}\Gamma^\lambda_{\eta\nu} \quad (10)$$

where the Christoffel symbols $\Gamma^\lambda_{\mu\nu}$ are

$$\Gamma^\lambda_{\mu\nu} = \frac{1}{2}g^{\lambda\sigma}\left(\partial_\mu g_{\sigma\nu} + \partial_\nu g_{\sigma\mu} - \partial_\sigma g_{\mu\nu}\right). \quad (11)$$

The Ricci scalar curvature is given by

$$R = g^{\mu\nu}R_{\mu\nu}\,, \quad (12)$$

and the energy-momentum tensor is

$$T_{\mu\nu} = \left(\rho_m + \frac{1}{c^2}p_m\right)u_\mu u_\nu + p_m g_{\mu\nu}\,, \tag{13}$$

where ρ_m is the matter density and p_m is the matter pressure, both only time dependent. By making straightforward calculations, one gets

$$\begin{aligned} R &= 6\left(\frac{k}{\Re^2(T_0)a^2(t)} + \frac{1}{c^2}\left(\left(\frac{\dot{a}(t)}{a(t)}\right)^2 + \frac{\ddot{a}(t)}{a(t)}\right)\right) \\ &= 6\left(K(t) + \frac{1}{c^2}\left(\left(\frac{\dot{a}(t)}{a(t)}\right)^2 + \frac{\ddot{a}(t)}{a(t)}\right)\right). \end{aligned} \tag{14}$$

Here $K(t)$ is Gaussian curvature at cosmic time t:

$$K(t) = \frac{k}{\Re^2(t)} = \frac{k}{\Re^2(T_0)\,a^2(t)}. \tag{15}$$

The Einstein's field equations are

$$\begin{aligned} &G_{ii} = \frac{8\pi G}{c^4}\left(T_{ii} + T^{\Lambda}_{ii}\right) \;\leftrightarrow \\ &-\left(c^2K(t) + \left(\frac{\dot{a}(t)}{a(t)}\right)^2 + 2\frac{\ddot{a}(t)}{a(t)}\right) = 8\pi G\left(\frac{1}{c^2}\,p_m - \rho_\Lambda\right) \end{aligned} \tag{16}$$

and

$$\begin{aligned} &G_{tt} = \frac{8\pi G}{c^4}\left(T_{tt} + T^{\Lambda}_{tt}\right) \;\leftrightarrow \\ &3\left(c^2K(t) + \left(\frac{\dot{a}(t)}{a(t)}\right)^2\right) = 8\pi G\,(\rho_m + \rho_\Lambda) \end{aligned} \tag{17}$$

where $i = (\psi, \theta, \phi)$; all off-diagonal terms are null. The equation of state for dark energy is

$$p_\Lambda = -\rho_\Lambda c^2. \tag{18}$$

Simple manipulation of equations above leads to

$$\frac{\ddot{a}(t)}{a(t)} = -\frac{4\pi G}{3}\left(\rho_m + 3\frac{1}{c^2}p_m - 2\rho_\Lambda\right), \tag{19}$$

$$\left(\frac{\dot{a}(t)}{a(t)}\right)^2 + c^2K(t) = \frac{8\pi G}{3}\,(\rho_m + \rho_\Lambda)\,. \tag{20}$$

Equations (19-20) are known as Friedmann equations. Having in account that

$$\frac{\dot{a}(t)}{a(t)} = H(t), \tag{21}$$

$$\frac{\ddot{a}(t)}{a(t)} = \dot{H}(t) + H^2(t), \tag{22}$$

where $H(t)$ is time dependent Hubble parameter, and that pressure $p_m = 0$ (matter is treated as dust), one has

$$\dot{H}(t) + H^2(t) = \frac{8\pi G}{3}\left(-\frac{1}{2}\,\rho_m + \rho_\Lambda\right), \tag{23}$$

$$c^2K(t) + H^2(t) = \frac{8\pi G}{3}\,(\rho_m + \rho_\Lambda)\,, \tag{24}$$

or

$$\frac{\dot{H}(t)}{H^2(t)} + 1 = \frac{1}{\rho_{crit}}\left(-\frac{1}{2}\,\rho_m + \rho_\Lambda\right), \tag{25}$$

$$\frac{c^2K(t)}{H^2(t)} + 1 = \frac{1}{\rho_{crit}}\,(\rho_m + \rho_\Lambda)\,, \tag{26}$$

where

$$\rho_{crit} = \frac{3H^2(t)}{8\pi G} \tag{27}$$

is the so called critical density. From equations (25-26) one obtains, after simple algebra,

$$\rho_m = \frac{1}{4\pi G}\left(c^2K(t) - \dot{H}(t)\right), \tag{28}$$

$$\rho_\Lambda = \frac{1}{4\pi G}\left(\frac{1}{2}\,c^2K(t) + \frac{3}{2}H^2(t) + \dot{H}(t)\right), \tag{29}$$

or,

$$\Omega_m = \left(\frac{2}{3}\frac{c^2K(t)}{H^2(t)} - \frac{2}{3}\frac{\dot{H}(t)}{H^2(t)}\right), \tag{30}$$

$$\Omega_\Lambda = \left(\frac{1}{3}\frac{c^2K(t)}{H^2(t)} + \frac{2}{3}\frac{\dot{H}(t)}{H^2(t)} + 1\right), \tag{31}$$

where $\Omega_m = \rho_m/\rho_{crit}$ and $\Omega_\Lambda = \rho_\Lambda/\rho_{crit}$ are, respectively, the cosmological matter and dark energy density parameters.

The Ricci scalar curvature stands as

$$R = 6\left(K(t) + \frac{1}{c^2}\left(2H^2(t) + \dot{H}(t)\right)\right). \tag{32}$$

3 The ansatz

Now let one introduces the following ansatz for the expansion factor:

$$a(t) = e^{(H(t)t\,-\,H_0T_0)/\beta} \tag{33}$$

where T_0 is the current age of the Universe, $H_0 = H(T_0)$ is the Hubble constant, and β is a constant parameter to be determined. From equations (21-23) one obtains

$$H(t) = H_0\left(\frac{t}{T_0}\right)^{\beta-1} \tag{34}$$

$$\dot{H}(t) = H(t)\frac{1}{t}\,(\beta - 1)\,. \tag{35}$$

By inserting equations (34-35) into equation (25) one has:

$$\frac{\beta - 1}{H_0 t}\left(\frac{t}{T_0}\right)^{1-\beta} + 1 = \frac{1}{\rho_{crit}}\left(-\frac{1}{2}\,\rho_m + \rho_\Lambda\right) \tag{36}$$

$$\frac{\beta - 1}{H_0T_0}\left(\frac{t}{T_0}\right)^{-\beta} = -\frac{1}{2}\,\Omega_m + \Omega_\Lambda - 1 \tag{37}$$

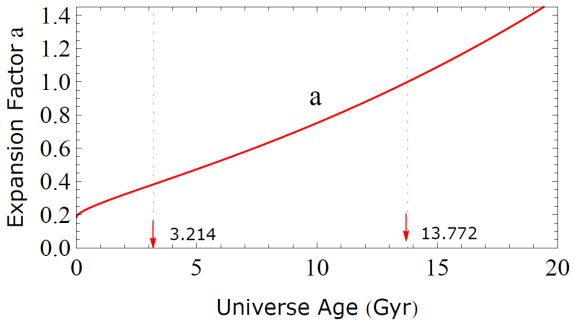

Fig. 1: $a(t) = e^{\frac{1}{\beta}\left(\left(\frac{t}{T_0}\right)^{\beta}-1\right)H_0T_0}$

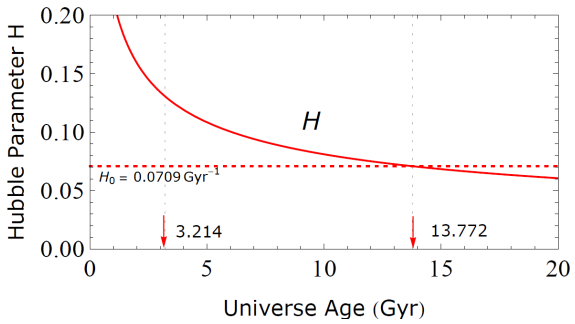

Fig. 2: $H(t) = H_0\left(\frac{t}{T_0}\right)^{\beta-1}$

Since β is assumed to be a constant, and, that $\Omega_m(T_0)$, $\Omega_\Lambda(T_0)$ and $H(T_0) = H_0$ are measured quantities, one has for $t = T_0$,

$$\frac{\beta-1}{H_0T_0} = -\frac{1}{2}\,\Omega_m(T_0) + \Omega_\Lambda(T_0) - 1 \tag{38}$$

which solved for β gives

$$\beta = 1 + H_0T_0\left(-\frac{1}{2}\Omega_m(T_0) + \Omega_\Lambda(T_0) - 1\right) = 0.5804. \tag{39}$$

where

$$H_0 = 69.32\ kms^{-1}Mpc^{-1} = 0.0709\ Gyr^{-1},$$

$$T_0 = 13.772\ Gyr,$$

$\Omega_m(T_0) = 0.2865$ and $\Omega_\Lambda(T_0) = 0.7135$ [6].

The plot of the expansion acceleration

$$\ddot{a}(t) = \left(\dot{H}(t) + H^2(t)\right)a(t) \tag{40}$$

as function of t = *age of the Universe* reveals that for $t < T_\star$, the acceleration is *negative* and for $t > T_\star$, the acceleration is *positive*. See Figure (4). This means that when the Universe is younger than $T_\star$, the regular gravitation overcomes dark energy, and after $T_\star$, dark energy overcomes gravitation. The result is an eternal positive accelerated expansion after $T_\star = 3.214\ Gyr$. See ahead.

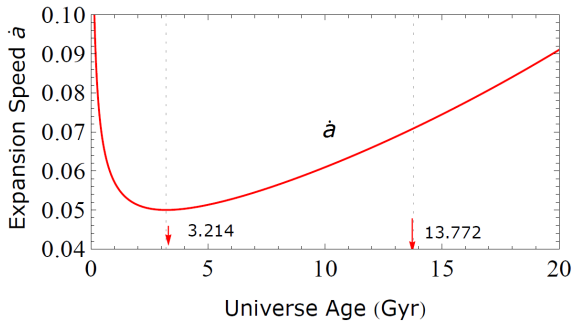

Fig. 3: $\dot{a}(t) = a(t)\,H_0\left(\frac{t}{T_0}\right)^{\beta-1}$

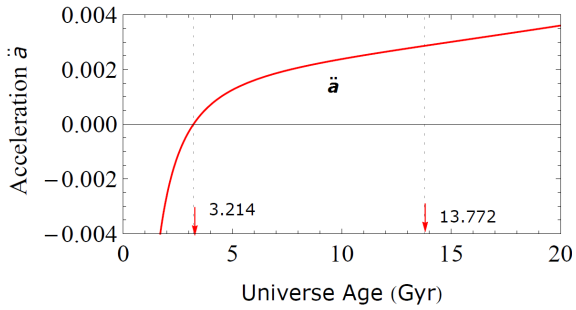

Fig. 4: $\ddot{a}(t) = a(t)\left(H_0\left(\frac{t}{T_0}\right)^{\beta} - (1-\beta)\,\frac{1}{t}\right)H_0\left(\frac{t}{T_0}\right)^{\beta-1}$

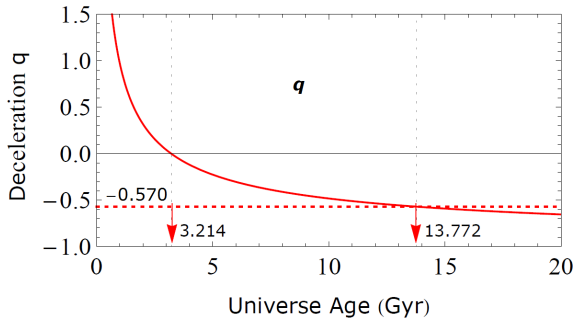

Fig. 5: $q(t) = -\left(1 + \frac{1}{H_0T_0}\,(\beta-1)\left(\frac{t}{T_0}\right)^{-\beta}\right)$

In fact, by setting equation (40) to zero and just solving it for t,

$$H(t)\frac{1}{t}(\beta-1) + H^2(t) = 0, \tag{41}$$

one gets

$$t = T_\star = T_0\left(\frac{1-\beta}{H_0T_0}\right)^{\frac{1}{\beta}} = 3.214\ Gyr\,. \tag{42}$$

From equation (26), one writes

$$\frac{c^2k}{\Re^2(t)H^2(t)} = \Omega_m + \Omega_\Lambda - 1. \tag{43}$$

The known recently measured values of $\Omega_m(T_0)$ and $\Omega_\Lambda(T_0)$ [6] do not allow one to say, from above equation, that the

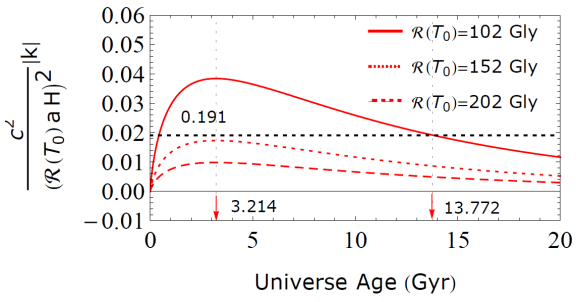

Fig. 6: Left hand side of equation (43) is plotted for some values of $\Re(T_0)$. At the current Universe age $T_0 = 13.772\,Gyr$, the right side of the referred equation has the margin of error equal to ±0.0191.

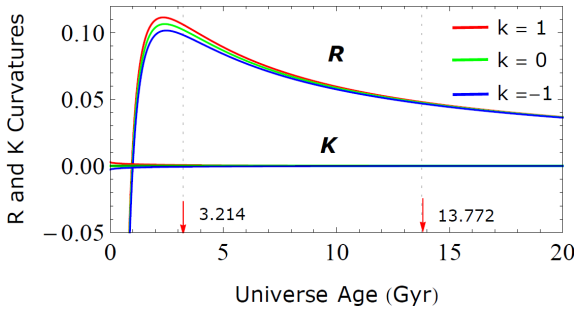

Fig. 7: Gaussian curvature $K(t) = \frac{k}{\left(\Re(T_0)a(t)\right)^2}$ and Ricci scalar curvature $R(t) = 6\left(K(t) + \frac{1}{c^2}H(t)\left(2H(t) + \frac{1}{t}(\beta-1)\right)\right)$.

Universe is clearly flat ($k = 0$). The referred measured values have a margin of error:

$$\Omega_\Lambda(T_0) = 0.7135 \begin{cases} +0.0095 \\ -0.0096 \end{cases}$$

$$\Omega_m(T_0) = 0.2865 \begin{cases} +0.0096 \\ -0.0095 \end{cases}$$

Considering also the margin of errors of the other measured parameters [6], one cannot distinguish between $k = 1$, -1 or 0. The match between both sides of equations (43) requires that, the today's curvature radius of the Universe be $\Re(T_0) > 100\,Gly$, in the context of this paper. See Figure (6).

The so called deceleration parameter is

$$\begin{aligned} q(t) &= -\frac{\ddot{a}(t)a(t)}{\dot{a}^2(t)} = -\left(\frac{\dot{H}(t)}{H^2(t)} + 1\right) \\ &= -\left(1 + \frac{\beta-1}{H_0T_0}\left(\frac{t}{T_0}\right)^{-\beta}\right) \end{aligned} \tag{44}$$

which, at current Universe age is $q(T_0) = -0.570$. See Figure (5).

The expansion scalar factor $a(t)$, Hubble parameter $H(t)$, expansion speed $\dot{a}(t)$, expansion acceleration $\ddot{a}(t)$, and the deceleration parameter $q(t)$ are plotted in Figures (1-5).

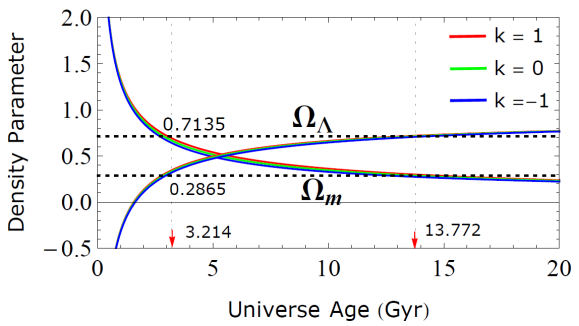

Fig. 8: Matter and dark energy density parameters for $k = 1, 0, -1$: $\Omega_m(t) = \frac{2}{3H^2(t)}\left(c^2K(t) - (\beta-1)\frac{H(t)}{t}\right)$; $\Omega_\Lambda(t) = \frac{1}{3H^2(t)}\left(c^2K(t) + 2(\beta-1)\frac{H(t)}{t} + 3H^2(t)\right)$. The radius of curvature is taken as $\Re(T_0) = 102\,Gly$.

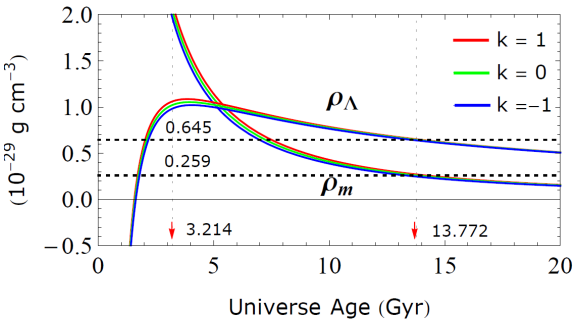

Fig. 9: Matter and dark energy densities for $k = 1, 0, -1$:
$\rho_m(t) = \frac{2}{8\pi G}\left(c^2K(t) - (\beta-1)\frac{H(t)}{t}\right)$;
$\rho_\Lambda(t) = \frac{1}{8\pi G}\left(c^2K(t) + 2(\beta-1)\frac{H(t)}{t} + 3H^2(t)\right)$.
The radius of curvature is taken as $\Re(T_0) = 102\,Gly$.

The sequence of Figures (7-10) shows the Gaussian $K(t)$ and R curvatures, matter density parameter $\Omega_m(t)$, dark energy density parameter $\Omega_\Lambda(t)$, matter density $\rho_m(t)$, dark energy density $\rho_\Lambda(t)$ and cosmological dark energy $\Lambda(t)$.

The time derivatives of $\rho_\Lambda(t)$ and $\rho_m(t)$ reveal interesting detail of the model in question:

$$\dot{\rho}_m + 3H\left(\rho_m + \frac{1}{c^2}p_m\right) = \dot{\rho}_m + 3H\rho_m = -Q \tag{45}$$

$$\dot{\rho}_\Lambda + 3H\left(\rho_\Lambda + \frac{1}{c^2}p_\Lambda\right) = \dot{\rho}_\Lambda = Q \tag{46}$$

$$Q = 2H\left(\frac{1}{t^2}(\beta-2)(\beta-1) + 3\dot{H} - c^2K\right) \tag{47}$$

where $p_m = 0$ and $p_\Lambda = -\rho_\Lambda c^2$. This implies that

$$\dot{\rho}_m + \dot{\rho}_\Lambda = -3H\rho_m. \tag{48}$$

The two perfect fluids interact with each other. In Figure (11) one shows the plots for $\dot{\rho}_m$, $\dot{\rho}_\Lambda$ and $\dot{\rho}_m + \dot{\rho}_\Lambda$ as functions of cosmic time.

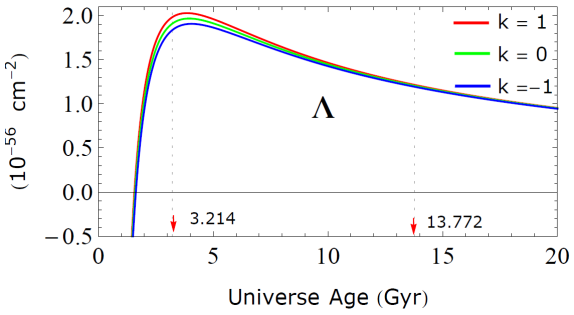

Fig. 10: Dark energy $\Lambda(t)$, in units of cm^{-2} for $k = 1, 0, -1$. $\Lambda(t) = \frac{1}{c^2} 8\pi G \rho_\Lambda(t)$. The radius of curvature is taken as $\Re(T_0) = 102\, Gly$. The result for $\Lambda(t)$ satisfies the following inequality: $|\Lambda| < 10^{-42} cm^{-2}$ [4].

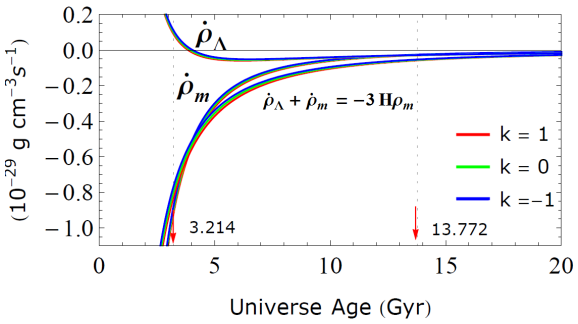

Fig. 11: Time derivatives of ρ_Λ, ρ_m and of the sum $\rho_\Lambda + \rho_m$ for $k = 1, 0, -1$. The radius of curvature is taken as $\Re(T_0) = 102\, Gly$.

4 Conclusion

The expression for the expansion factor $a(t) = e^{\frac{H_0 T_0}{\beta}\left(\left(\frac{t}{T_0}\right)^\beta - 1\right)}$, where $\beta = 0.5804$, constitutes a model for the expansion of the Universe for $t > 4 \times 10^{12} s \approx 1.3 \times 10^{-5} Gyr$ in which gravity dominates up to the Universe age of $T_* = 3.214\, Gyr$ and after that dark energy overcomes gravity and that persists forever. The acceleration of expansion is negative in the first part (*matter era*) and positive after that (*dark energy era*). The mathematical expressions for dark energy and matter densities indicate a clear interaction between the two perfect fluids (dark energy and matter). The classical deceleration parameter $q(t)$ is found to have the value $q(T_0) = -0.570$ for the current Universe age and the current radius of curvature should be $\Re(T_0) > 100\, Gly$.

Submitted on March 2, 2014 / Accepted on March 4, 2014

References

1. Raine, D. An Introduction to the Science Of Cosmology. Institute of Physics Publishing Ltd, 2001.
2. Peacock, J.A. Cosmological Physics. Cambridge University Press, 1999.
3. Harrison, E.R. Cosmology: The Science of the Universe. Cambridge University Press, 2nd ed. 2000.
4. Islam J.N. An Introduction to Mathematical Cosmology. Cambridge University Press. 2002.
5. Baryshev, Y.V. Expanding space: The root of conceptual problems of the cosmological physics. arXiv: gr-qc/0810.0153. 2008
6. Bennett, C.L. et al. Nine-Year Wilkinson Microwave Anisotropy Probe (WMAP) Observations: Final Maps and Results. arXiv: astro-ph.CO. 2013.
7. Ellis, G.F.R. et al. Relativistic Cosmology. Cambridge University Press, 2012.

Binding Energy and Equilibrium of Compact Objects

Massimo Germano

Department of Basic and Applied Sciences for Engineering (SBAI), University of Rome "La Sapienza", Via Antonio Scarpa 14 00162, Rome, Italy. E-mail: massimo.germano@uniroma1.it

The theoretical analysis of the existence of a limit mass for compact astronomic objects requires the solution of the Einstein's equations of general relativity together with an appropriate equation of state. Analytical solutions exist in some special cases like the spherically symmetric static object without energy sources that is here considered. Solutions, i.e. the spacetime metrics, can have a singular mathematical form (the so called Schwarzschild metric due to Hilbert) or a nonsingular form (original work of Schwarzschild). The former predicts a limit mass and, consequently, the existence of black holes above this limit. Here it is shown that, the original Schwarzschild metric permits compact objects, without mass limit, having reasonable values for central density and pressure. The lack of a limit mass is also demonstrated analytically just imposing reasonable conditions on the energy-matter density, of positivity and decreasing with radius. Finally the ratio between proper mass and total mass tends to 2 for high values of mass so that the binding energy reaches the limit m (total mass seen by a distant observer). As it is known the negative binding energy reduces the gravitational mass of the object; the limit of m for the binding energy provides a mechanism for stable equilibrium of any amount of mass to contrast the gravitational collapse.

1 Introduction to nonsingular Schwarzschild metric

The fate of extremely compact objects in the universe is ruled by the particular solutions of the Einstein's equations. As it is true that no all the mathematical theorems and statements have a corresponding meaning in the physical world, at the same time there is not a general rule, other than the verification by means of experimental and observational data, to establish, a priori, which mathematical solution must be discarded and which must be accepted.

In the case of the basic static model for compact objects, in the theory up to date the collapse is ruled by a specific solution (called Schwarzschild solution but not given explicitly by Schwarzschild, coming from the Hilbert's interpretation instead) that contains mathematical and thus physical singularities leading to a mass limit for ordinary compact objects and to the consequent black hole hypothesis (generalization to rotating or charged objects contains as well the features of singularity and horizon surface and it is not necessary in this context).

However, a different interpretation of the solution (nonsingular), particularly the original Schwarzschild solution, cannot be excluded if the completely different consequences (the nonexistence of mass limit and thus of black holes) are not yet demonstrated to be inconsistent with observational data.

1.1 Possible solutions to the static problem

Karl Schwarzschild in 1916 [1, eq. 14, page 194] gave an exact solution in vacuum to Einstein's field equation determining the line element for systems with static spherical symmetry (in units such that $c = G = 1$):

$$ds^2 = \left(1-\frac{\alpha}{R(r)}\right)dt^2 - \frac{dR(r)^2}{1-\frac{\alpha}{R(r)}} - R(r)^2\left(d\theta^2 + \sin^2\theta\, d\phi^2\right), \quad (1)$$

where α is a constant depending on the value of the mass, that can be obtained from the newtonian limit, and

$$R(r) = (r^3 + \sigma)^{1/3} \quad (2)$$

where σ (indicated with ρ in the original article) is a second constant to be determined and r is the same radial variable of the spherically symmetric Minkowski spacetime. Mathematically, there are two possible solutions that satisfy Einstein's field equation in vacuum ($R_{\mu\nu} = 0$): one is given by the class of infinite values of $R(r)$ such that [2, 3]

$$R(r) = (|r - r_0|^n + \alpha^n)^{1/n} \quad (3)$$

with arbitrary r_0 and $r \neq r_0$, the other is given by setting

$$R(r) = r. \quad (4)$$

It is worth to note that all the solutions of the class (3) can be obtained one from another by means of a simple coordinate transformation as must be in general relativity, while the solution (4) cannot be obtained from (3) and viceversa with a simple coordinate transformation. So, since the actual solution must be of course unique, the actual solution must be chosen among the form (3) and the form (4). At this stage, the only request that $R_{\mu\nu} = 0$ cannot discriminate about these solutions, additional considerations must be examined: in the

following it will be shown that, since $R(r)$ is related to the Gaussian curvature, it cannot be set equal to the radial coordinate r as in (4) because this brings to unphysical consequences.

The choices made, for example, by Schwarzschild [1] ($r_0 = 0$, $r > r_0$, $n = 3$), by Brillouin [4] ($r_0 = 0$, $r > r_0$, $n = 1$) and by Droste [5] ($r_0 = \alpha$, $r > r_0$, $n = 1$) belong to the class of solutions of the first kind (3); all the solutions of this class share the same constant α in the denominator (or, like in the Droste's solution, the additional condition for validity that $r > \alpha$) that prevents the metric to become singular and to change signature so that they could be called a class of "nonsingular" solutions.

The other possibility is the "singular" solution (4), due to the contribution by Hilbert [6], leading to the so called "Schwarzschild Solution", that from now on will be called Schwarzschild-Hilbert or "singular" solution, that sets $n = 1$, $r_0 = \alpha$ in (3), so that $\sigma = 0$ in (2) i.e. $R = r$; this is similar to the Droste's solution but with no limitation on r so that $0 \leqslant r \leqslant \infty$. The line element in this case is the well known Schwarzschild (-Hilbert) metric

$$ds^2 = \left(1 - \frac{\alpha}{r}\right)dt^2 - \frac{dr^2}{1 - \dfrac{\alpha}{r}} - r^2\left(d\theta^2 + \sin^2\theta\, d\phi^2\right), \qquad (5)$$

where r is (supposed to be) the usual radial coordinates (but it is actually related to the Gaussian curvature as it will be shown later) running from zero to infinity and α is determined from the Newtonian potential in the limit $r \to \infty$, so that $\alpha = 2m$ where m is the mass in geometrized units while its complete expression would be $m = GM/c^2$.

The consequences of the line element (5) are well known, among them the existence of an "event horizon", a not removable singularity in $r = 0$, the change in the sign of the g_{00} and g_{11} elements of the metric when $0 \leqslant r \leqslant 2m$ and the existence of a mass limit for equilibrium of massive neutron cores [7] and the consequent black hole hypothesis.

There is an open question about if there is an actual difference between all these solutions, leading to different physical consequences. An example of this discussion can be find on references [2, 3, 8, 9].

The present article will not enter deep into the question, instead it must be intended as a contribute for understanding the possible physical consequences, on compact objects, applying the nonsingular metric (1 and 2).

1.2 Some characteristics of the Schwarzschild metric

This article, will start from a "nonsingular" solution, the one given by K. Schwarzschild [1] (1 and 2) (from now on, simply, Schwarzschild solution), that set (eq. 13 in [1])

$$\sigma = \alpha^3 = 8m^3 \qquad (6)$$

so that the line element of the Schwarzschild Solution (1), using the coordinate r, becomes

$$ds^2 = \left(1 - \frac{\alpha}{(r^3+\sigma)^{1/3}}\right)dt^2 - \frac{r^4(r^3+\sigma)^{-4/3}}{1 - \dfrac{\alpha}{(r^3+\sigma)^{1/3}}}dr^2 - \\ - (r^3+\sigma)^{2/3}\left(d\theta^2 + \sin^2\theta d\phi^2\right), \qquad (7)$$

where σ has been explicitly left in order to compare all the subsequent formulas for this Schwarzschild metric (7) to the ones derived from the Schwarzschild-Hilbert metric (5), by simply setting $\sigma = 0$.

A first glance at the metric (7) indicates that there is no singularity at $r = 2m$, no "event horizon" and no change of sign (and of nature of the light cone) in the g_{00} and g_{11} elements of the metric. The "problem" has been moved to the origin $r = 0$ with the choice $\sigma = \alpha^3$. Moreover, the behavior of Schwarzschild metric, at the origin, is totally different from the one of Schwarzschild-Hilbert metric: in this latter, indeed, the presence of r in the denominator produces a mathematical, and consequently physical, not removable singularity, in the former there is just a smooth vanishing of the g_{00} and g_{11} metric elements, since in Schwarzschild metric (7)

$$\lim_{r\to 0} g_{00} = 0; \qquad \lim_{r\to 0} g_{11} = 0. \qquad (8)$$

It worths to note that the expression of the "time" element g_{00} in the limit $r \to 0$ is analogous to the limit $r \to 2m$ of the same element in metric (5), so that there is a coordinate time (time measured by a distant observer) going to infinite while a radially ingoing object would approach $r = 0$.

Both singular (4) and nonsingular (3) class of solutions give similar results in the weak field limit, that is the limit where all the experimental proofs for general relativity are performed. For example, Schwarzschild, applied his metric (7) to solve the problem of the observed anomaly in the perihelion of Mercury. He found the exact solution ([1] eq.18 p.195) and noticed that the approximate Einstein's solution is the exact one by substituting the Einstein radial coordinate r with $(r^3+\alpha^3)^{1/3} = r(1+\alpha^3/r^3)^{1/3}$; since the term within parenthesis differs from 1 by a quantity of the order of 10^{-12}, the actual level of precision of the measurements cannot make a distinction between the two kind of metrics. Quite a different behavior appears in the strong field limit as it will be shown later.

1.3 Different nature of r and different centers of spherical symmetry for the two kind of metrics

The further analysis to discriminate among these two kind of metrics involves the nature of the r coordinate that represents two very different quantities in the two metrics. In effect can be demonstrated that, in the Schwarzschild metric (1), r is the usual radial coordinate analogue of the coordinate in

Minkowski space and $r = 0$ is the actual center of the configuration with a finite curvature: in the derivation of metric (1), Schwarzschild never changes the nature of r (see [1] eq.7) that corresponds to the radial coordinate of the Minkowski space. $r = 0$ corresponds to the center of the distribution and this is demonstrated if one looks at a curvature invariant, the Kretschmann scalar, that is maximized at $r = 0$ as it is required. In effect, considering the nonsingular Schwarzschild solution, its expression is

$$R_{kr} = R_{\mu\nu\lambda\xi}R^{\mu\nu\lambda\xi} = \frac{12\alpha^2}{\left(r^3+\alpha^3\right)^2} \tag{9}$$

that has a maximum finite value in $r = 0$ of $R_{kr}(0) = 12/\alpha^4$.

At the same time, the Gaussian Curvature is defined by

$$K_S = \frac{R_{1212}}{g} = \frac{1}{R^2} = \frac{1}{(r^3+\alpha^3)^{2/3}} \tag{10}$$

so that for $r = 0 \Rightarrow K_S = 1/\alpha^2$ so K_S is finite at the center.

On the other side, the r of the Schwarzschild-hilbert metric (5) it is not the radial coordinate neither a distance at all but it is, actually, the square of the inverse of the Gaussian curvature of a spherically symmetric geodesic surface in the spatial section of the spacetime manifold because

$$K_{SH} = \frac{R_{1212}}{g} = \frac{1}{r^2}\,. \tag{11}$$

Where are the centers of spherical distribution for the two kind of metric? The answer to this question can be given by the quantity that represents the *proper distance* $R_p(r) = \int g_{11}dr$.

In the Schwarzschild-Hilbert case (5),

$$\begin{aligned} R_p(r) &= \int g_{11}dr = \int \frac{1}{\sqrt{1-\dfrac{\alpha}{r}}}\,dr = \\ &= \sqrt{r}\,\sqrt{r-\alpha} + \alpha\ln\left[2\left(\sqrt{r}+\sqrt{r-\alpha}\right)\right] + C \end{aligned} \tag{12}$$

where C is a constant. The center r_c of the distribution is found setting the proper distance equal to zero ($R_p(r_c) = 0$) that happens for $r_c = \alpha$ and $C = -\alpha\ln\left(2\sqrt{\alpha}\right)$. Finally the expression for the proper distance is [2, 3]

$$R_p(r) = \sqrt{r}\,\sqrt{r-\alpha} + \alpha\ln\left(\frac{\sqrt{r}+\sqrt{r-\alpha}}{\sqrt{\alpha}}\right). \tag{13}$$

So, in the Schwarzschild-Hilbert metric $\alpha \equiv 2m < r \leqslant \infty$, while the range of the proper distance is $0 \leqslant R_p \leqslant \infty$, there is no meaning for $r \leqslant 2m$ coherently with its nature connected with the Gaussian curvature and the center of the distribution is $r_c = 2m$.

This means that, if is given a Minkowski spacetime, where $\mathbf{E}^3$ is its Euclidean space, the center of the spherical symmetry is $r_c = 0$ and r coincides with the proper distance R_p and with the radius of Gaussian curvature R_G, $r = R_p = R_G$, considering the metric manifold $\mathbf{M}^3$, that is the spatial part of Schwarzschild-Hilbert spacetime, then the central point $R_p(r_c) = 0$ corresponds to the point $r_c = 2m$ in $\mathbf{E}^3$ that is any point on a spherical surface centered in $r = 0$ with radius $r = 2m$. Only in this way there is a one to one correspondence between all points of $\mathbf{E}^3$ and $\mathbf{M}^3$.

In the Schwarzschild case (7) instead,

$$\begin{aligned} R_p(r) &= \int g_{11}dr = \int \sqrt{\frac{r^4\left(r^3+\alpha^3\right)^{-\frac{4}{3}}}{1-\dfrac{\alpha}{\left(r^3+\alpha^3\right)^{\frac{1}{3}}}}}\,dr = \\ &= \left(r^3+\alpha^3\right)^{-\frac{1}{3}} \times \sqrt{\left(r^3+\alpha^3\right)^{\frac{4}{3}} - \alpha\left(r^3+\alpha^3\right)} + \\ &+ \alpha\ln\left[2\left(r^3+\alpha^3\right)^{\frac{1}{6}} + 2\sqrt{\left(r^3+\alpha^3\right)^{\frac{1}{3}} - \alpha}\right] + C. \end{aligned} \tag{14}$$

The center of the distribution r_c if found setting $R_p(r_c) = 0$ that is for $r_c = 0$ and $C = -\alpha\ln\left(2\sqrt{\alpha}\right)$ so that the expression for the proper distance is

$$\begin{aligned} R_p(r) &= \left(r^3+\alpha^3\right)^{-\frac{1}{3}}\sqrt{\left(r^3+\alpha^3\right)^{\frac{4}{3}} - \alpha\left(r^3+\alpha^3\right)} + \\ &+ \alpha\ln\left[\frac{\left(r^3+\alpha^3\right)^{\frac{1}{6}} + \sqrt{\left(r^3+\alpha^3\right)^{\frac{1}{3}} - \alpha}}{\sqrt{\alpha}}\right]. \end{aligned} \tag{15}$$

In conclusion, in Schwarzschild metric (1) r is the actual radial coordinate that goes from 0 to ∞ (whole manifold) and $r = 0$ is recognized to be the center where the Kretschmann scalar is maximized (9) and the Gaussian Curvature $K_S(r) = 1/R(r)^2$ is finite since it goes from $K_S(0) = 1/\alpha^2$ to $K_S(\infty) = 0$. In Schwarzschild-Hilbert metric, (5) instead, r has nothing to do with the radial coordinate or distance but it is actually related to the Gaussian curvature $K_{SH} = 1/r^2$ and it is defined only from $2m$ to ∞ as recognized by Droste [5].

2 Metric inside matter and equilibrium equations

Let's consider a mass of degenerate matter (without source of energy [10]) in a finite volume, the full treatment consists in solving Einstein's equations (equilibrium equations) together with an appropriate equation of state for the matter. There are well known studies dedicated to the analysis of equilibrium in the strong field limit, for massive compact objects in the environment of the singular Schwarzschild-Hilbert metric, where neutron massive cores of neutron stars have been considered, imposing different equations of state for the neutron matter.

Anyway, all these different equations of state, from the pioneer and fundamental work of Oppenheimer and Volkoff [7] to the more realistic models [11] [12], share an important common characteristic: all these models, applied to the singular metric (5), predict some theoretical upper limit to a

mass in equilibrium due to the intrinsic relativistic effect of the metric itself, and a consequent final collapse above this limit. The difference between these approaches regards the value of the limit that can change from 0.7 solar masses in the Oppenheimer-Volkoff (O-V) model to few solar masses in the other models [13]. Above these limits nothing can stop the object from the final collapse inside its "Schwarzschild" radius $2m$ and then, because of the changing of sign, up to a not avoidable final singularity, where curvature reaches an infinite value and the known physics meets its limits.

In this article, one of these models will be considered, in particular the O-V model in the environment of the nonsingular Schwarzschild metric (7) in the form valid inside the matter. The O-V model is not quite realistic because it considers the neutrons as a Fermi gas; however, no matter which model is considered, all the models predict a limit to the mass because of the singular metric, while it will be shown that in a nonsingular metric even the O-V model, that otherwise gives the sharper limit to the mass (≈ 0.7 of solar mass), does not show it, instead it gives the equilibrium radius for any value of the mass.

The procedure will follow the original one given by Oppenheimer and Volkoff so that the results can be directly compared. The difference will be that the nonsingular Schwarzschild metric inside matter will be applied instead of the singular one and the equations derived from the latter can be obtained from the former setting $\sigma = 0$.

Let's consider the static metric (7) with spherical symmetry, valid in empty space and set the g_{00} and g_{11} elements in the general exponential form:

$$ds^2 = e^{\nu(r)}dt^2 - e^{\lambda(r)}dr^2 - \left(r^3+\sigma\right)^{2/3}\left(d\theta^2+\sin^2\theta d\phi^2\right). \quad (16)$$

Solving Einstein's equations (see Appendix A) the metric inside the matter is found:

$$ds^2 = \left(1-\frac{2m(r)}{\left(r^3+8m^3\right)^{1/3}}\right)dt^2 - \frac{r^4\left(r^3+8m^3\right)^{-4/3}}{1-\dfrac{2m(r)}{\left(r^3+8m^3\right)^{1/3}}}\,dr^2 - \left(r^3+8m^3\right)^{2/3}\left(d\theta^2+\sin^2\theta d\phi^2\right). \quad (17)$$

The system of equilibrium equations becomes:

$$\left.\begin{aligned}\frac{dp(r)}{dr} &= -\frac{(p(r)+\varrho(r))\left[m(r)+4\pi\left(r^3+\sigma\right)p(r)\right]}{\dfrac{\left(r^3+\sigma\right)^{4/3}}{r^2}\left[1-\dfrac{2m(r)}{\left(r^3+\sigma\right)^{1/3}}\right]}\\ \frac{dm(r)}{dr} &= 4\pi\varrho(r)r^2\end{aligned}\right\}. \quad (18)$$

where $\sigma = 8m^3$ and

$$m(r) = \frac{1}{2}\left(r^3+8m^3\right)^{1/3}\left(1-e^{-\lambda}\frac{r^4}{\left(r^3+8m^3\right)^{4/3}}\right).$$

If one sets $\sigma = 0$ in the first equation of (18), then the Tolman-Oppenheimer-Volkoff equation (A-4) can be obtained; equations (18) together with an equation of state $\varrho = \varrho(p)$ constitute the system to be integrated.

3 Equation of state and numerical integration

Following the procedure by Oppenheimer and Volkoff [7], the matter is considered to consist of particles with rest mass μ_0 obeying Fermi statistics, neglecting thermal energy and forces between them; the equation of state can be put in the parametric form

$$\varrho = K\left(\sinh(t) - t\right),$$

$$p = \frac{1}{3}K\left(\sinh(t) - 8\sinh(t/2) + 3t\right),$$

where $K = \pi\mu_0^4c^5(4h^3$ and $t = 4\log(\hat{p}/\mu_0c + [1+(\hat{p}/\mu_0c)^2]^{1/2})$ where $\hat{p}$ is the maximum momentum in the Fermi distribution related to the proper particle density $N/V = 8\pi\hat{p}^3/(3h^3)$.

Setting $K = 1/4\pi$ the units of length a and of mass b are fixed such that, for neutron gas,

$$a = \frac{1}{\pi}\left(\frac{h}{\mu_0c}\right)^{2/3}\frac{c}{(\mu_0G)^{1/2}} = 1.36\times10^6\text{cm} \quad (19)$$

and $b = c^2a/G = 1.83\times10^{34}$g.

Finally the system of adimensional equations, renaming the adimensional mass $m(r) \equiv u(r)$, to be integrated are

$$\left.\begin{aligned}\frac{du}{dr} &= r^2\left(\sinh(t)-t\right)\\ \frac{dt}{dr} &= -\frac{4(\sinh(t)-2\sinh(t/2))}{\dfrac{r^3+8m^3}{r^2}\left[\left(r^3+8m^3\right)^{1/3}-2u\right]}\times\\ &\times\frac{\left[\frac{1}{3}\left(r^3+8m^3\right)(\sinh(t)+8\sinh(t/2)+3t)+u\right]}{\cosh(t)-4\cosh(t/2)+3}\end{aligned}\right\}. \quad (20)$$

This system is the analogous of the system integrated by Oppenheimer and Volkoff ([7], Eqs. 18 and 19) which can be obtained setting $\sigma \equiv \alpha^3 \equiv 8m^3 = 0$.

The procedure followed by Oppenheimer and Volkoff first fixes the value t_0 for the parameter t when $r = 0$ (determining central energy density and pressure), then the equations in [7] are numerically integrated for several finite values of t_0. Another boundary condition can be obtained setting of $u(0) \equiv u_0 = 0$. The equations are integrated till a value of $r = r_b$ for which t (and consequently the pressure) drops to 0, representing the border radius of the matter distribution; the corresponding value $u(r_b) = m$ is then, the value of the mass that can stay in equilibrium with a radius r_b and the imposed central density.

In the original paper (O-V) the first 4 results for t_0 equal to 1, 2, 3 and 4 are reported in a table (table I in [7], reported

Table 1: Comparison with Oppenheimer Volkoff table [7]; numbers not in parenthesis are in units a and b defined in (19).

	$m(M_s)$	$t_0(\varrho_0(10^{14}\mathrm{g/cm^3}))$	r_b (km)
O-V	0.033 (0.30)	1.000 (1.014)	1.550 (21.1)
Eqs. (20)	0.033 (0.30)	1.006 (1.033)	1.506 (20.49)
O-V	0.066 (0.60)	2.000 (9.418)	0.980 (13.33)
Eqs. (20)	0.066 (0.60)	1.835 (6.923)	1.001 (13.61)
O-V	0.078 (0.71)	3.000 (40.62)	0.700 (9.52)
Eqs. (20)	0.078 (0.71)	2.166 (12.376)	0.861 (11.71)

here in table 1) together with an asymptotic value: the characteristics of the results is that, starting from $t_0 = 1$, the mass is increasing for increasing t_0 (the central density) but soon, for $t_0 = 3$, the mass reaches its maximum value calculated to be $M_{max} = 0.71$ solar masses.

Increasing further t_0, causes a decreasing of values for the mass (see [7], Fig. 1) so, for $m < M_{max}$ there are two values for central density but only the lower value must be considered to describe stable neutron stars; the maximum mass is thus considered the maximum possible mass for a stable equilibrium configuration of neutron stars with a Fermi equation of state as obtained by Oppenheimer and Volkoff. Different equations of state give different values of the maximum mass (till some units of solar masses) but anyway, as it will be seen later, a limit exists and is due to the use of the singular metric.

In our case, the equations to be integrated (20) came from the Schwarzschild nonsingular metric (17) so results can be quite different: in particular, there is an additional parameter that is the constant mass m, as seen by a distant observer. The integration procedure must then be modified: first, the parameter m is set and a prove of integration is performed starting from a low value of the central parameter t_0; integration on r ends at $r = r_b$, the border radius, where $t(r_b) = 0$ (null pressure): if the starting value t_0 is set too low, then the resulting mass would be $u(r_b) < m$. If this would be the case, then it would be necessary to increase t_0 to the minimum value such that $u(r_b) = m$. This minimum value t_0 together with m fixed and r_b found, will be the correct values for central density and pressure, mass and radius of the configuration in stable equilibrium.

For low values of the mass, i.e. for weak gravitational fields, results are expected to be similar to those of O-V while for increasing mass values the nonsingular metric should lead to results very different from those resulting from the singular one. In table I, the results are compared with the first three values of O-V table. It can be noted that for the lower mass (0.30 M_s), almost the same values are obtained for central density and radius, while on increasing the mass, the two approaches diverge and the nonsingular one leads to a "softer" equilibrium, with lower central density and greater radius, with respect to the O-V calculation.

If the mass is further increased, the two metrics behave in a complete different way: the O-V equations show a decreasing mass and a mass above the maximum found limit $0.71M_s$ cannot be sustained in equilibrium. On conversely, the nonsingular Schwarzschild metric will permit equilibrium for increasing masses and will not have a limit mass. The central density indeed will meet a maximum limit and, then, will decrease for increasing masses. At the same time the radius, instead of continuously decreasing for increasing masses as in O-V case, will show a minimum to keep the equilibrium configuration.

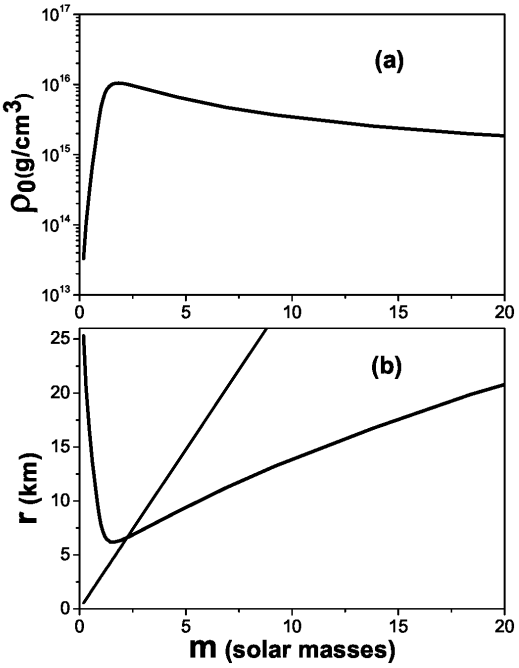

Fig. 1: Central density and equilibrium radius vs. mass: (a) central density shows a maximum; (b) equilibrium radius shows a minimum, straight line represents the so called Schwarzschild radius for that mass.

Let's first consider the behavior of various parameters for low masses: in Fig. 1 values of central density ρ_0 and radius r_b for low masses (up to 20 solar masses) are plotted; turning zones are clearly visible before the value of 2 solar masses in which the central density reaches a maximum and the radius a minimum. In particular, the central density reaches the maximum value of $1.048 \times 10^{16}\mathrm{g\ cm^{-3}}$ at 1.84 solar masses while the radius reaches the minimum value of 6.172 km at 1.47 solar masses. It can be noted, in Fig. 1(b), that, in this zone, the equilibrium radius of the mass is below the value $r_b < 2m$ where $2m$ here is the constant in the denominator of the nonsingular metric and not a limit like the so called "Schwarzschild" radius for the singular metric.

The behavior of ρ_0 and r_b is, thus, totally different from the results obtained by Oppenheimer and Volkoff for the equilibrium with the singular metric; an interpretation for this behavior could derive from recalling the concept of proper mass

M^p, linked to the concept of gravitational binding energy E_B: the total mass m, i.e. the mass seen by a distant observer, is defined by $m = \int_0^{r_b} 4\pi\varrho(r)r^2dr$ but if one integrates the energy-density ϱ over the proper "local" volume, the proper mass M^p of the system can be defined.

The proper volume element $d\tau$ is defined from $d\tau^2 = g_{ij}dx^i dx^j$ where $i, j = 1, 2, 3$ are only spatial coordinates. The proper volume from the O-V singular metric (5) then is $d\tau_S = 4\pi r^2(1 - 2m/r)^{-1/2}dr$ and the proper volume from the actual Schwarzschild nonsingular metric (7) $d\tau_N S = 4\pi r^2(1 - 2m/(r^3 + \sigma)^{1/3})^{-1/2}dr$; coherently can be defined respectively as two proper masses M^P:

$$M_S^P = \int_0^{r_b} \varrho 4\pi r^2(1 - 2m/r)^{-1/2}dr \qquad (21)$$

and

$$M_{NS}^P = \int_0^{r_b} \varrho 4\pi r^2(1 - 2m/(r^3 + \sigma)^{1/3})^{-1/2}dr. \qquad (22)$$

The physical meaning of proper mass is connected with the difference $M^P - m = E_B$ where E_B is the gravitational binding energy ([14] p. 126). In Fig. 2 the completely different behavior of the binding energy is shown, in the cases of singular solution and nonsingular solution: in the first case, the binding energy increases dramatically (together with the increasing of the central density to unphysical values) and above the maximum mass limit of about 0.7 solar masses the function becomes multivalued.

On the other side, in the nonsingular case, the binding energy increases smoothly with increasing mass and does not indicate any mass limit. In Fig. 2 only low mass values are reported but it will be shown later that, in the nonsingular case, the binding energy for higher mass values increases linearly with the mass and, considering that the ratio M^P/m in Fig. 3 tends $\to 2$, the binding energy tends to the value m of the rest mass.

Central (ϱ_0) and average $\varrho_{AV} \equiv M/(\frac{4}{3}\pi r_b^3)$ densities have a similar behavior: starting from values of $\varrho_0(0.184M_s) = 3.29 \times 10^{13} g/cm^3$ and $\varrho_{AV}(0.184M_s) = 5.40 \times 10^{12} g/cm^3$, reaching the maximum values of $\varrho_0(1.84M_s) = 1.0476 \times 10^{16} g/cm^3$ and $\varrho_{AV}(2.30M_s) = 3.688 \times 10^{15} g/cm^3$ and finally reaching the values for the last considered mass, $\varrho_0(3.68 \times 10^6 M_s) = 1.243 \times 10^{10} g/cm^3$ and $\varrho_{AV}(3.68 \times 10^6 M_s) = 8.687 \times 10^9 g/cm^3$.

Behavior evidences the presence of a maximum for both the densities and a decreasing for increasing masses: the central density converges to the average density values which decrease because volume grows with radius with an higher power than the mass.

Integration of the system (20) admits solution with an equilibrium radius for any amount of mass: in Fig. 3, higher values of mass are considered till, as an example, a value around 4 million of solar masses as it is supposed to be concentrated in the Milky Way's center.

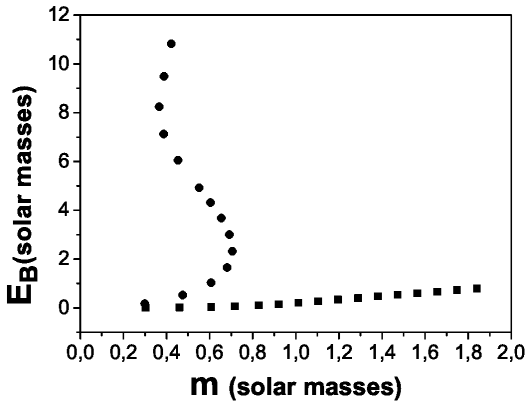

Fig. 2: Gravitational binding energy vs. mass: comparison between Oppenheimer-Volkoff results [7] (multivalued line with circles) and this article results (squares).

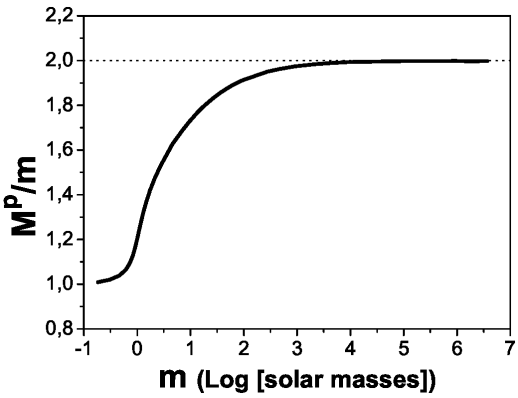

Fig. 3: Ratio between proper mass and mass vs. mass logarithm: limit tends to value 2 corresponding to an efficiency of 100% of mass conversion in gravitational binding energy

Together with the density decreasing with mass, there is another peculiar behavior, the one referred to the ratio of proper mass on mass: in Fig. 3 it is shown that this ratio tends to the value 2, meaning that there ia a 100% efficiency in converting mass into binding energy. The total mass of the compact object includes both the rest-mass energy and the negative binding energy so that the mass of the collapsed object is smaller than the sum of the component particles [15]. For neutron stars this mass deficit can be as large as 25% [16] but here it increases till 100% above 1 thousand of solar masses (depending on the equation of state) and this can be the mechanism to support stable equilibrium for such objects.

4 Inequality for nonexistance of a limit mass

Numerical results show that there is not a mass limit for equilibrium. This result can be seen also analytically trying to find an upper limit for the mass, independently from the specific equation of state. This limit exists in the case of singular

metric and it is possible to see that this limit does not exist in the case of nonsingular metric following the procedure expressed, for example, by R.M. Wald [14, p. 130].

A first less sharp limit exists for the singular metric as necessary condition for the metric to be static: a metric is said to be static if it is stationary and, in addition, exists a spacelike hypersurface Σ (orthogonal to the timelike Killing vector field ξ^α); in order for Σ to be spacelike the necessary condition for staticity is that the radial element of the metric g_{11} would be greater than zero (in the following calculation, it will be used the Wald notation of $g_{11} \equiv h(r)$ and $g_{00} \equiv f(r)$, with the Suffix S to indicate the expression from the singular metric and NS for the nonsingular one).

So for the two metrics (5) and (7) it will be

$$h_S(r) = \left(1 - \frac{2m(r)}{r}\right)^{-1} \tag{23}$$

and

$$h_{NS}(r) = r^4\left(r^3 + \sigma\right)^{-4/3}\left(1 - \frac{2m(r)}{(r^3+\sigma)^{1/3}}\right)^{-1}. \tag{24}$$

The necessary condition for stability implies that, for a given mass M and equilbrium radius r_b, $h(r_b) > 0$ so, it clearly requires a limit for M only in the singular case, that is $M < r_b/2$ (eq. 6.2.32 in [14]) while, in the nonsingular case, $h_{NS}(r_b) > 0$ is always satisfied for any value of M and r_b (considering that $\sigma \equiv 8M^3$).

This limit for M (for the singular metric) can be sharpened using the condition $g_{00} \equiv f(r) \geqslant 0$ that imposes the Killing field ξ^α to be timelike everywhere. The term $f(r)$ has the form, for the singular and nonsingular metric, respectively

$$\left.\begin{aligned} f_S(r) &= \left(1 - \frac{2m(r)}{r}\right) \\ f_{NS}(r) &= \left(1 - \frac{2m(r)}{(r^3+\sigma)^{1/3}}\right) \end{aligned}\right\}. \tag{25}$$

Since $f(r)$ must be greater than zero everywhere, it could seem that it would be necessary to know the specific equation of state for matter but, actually, the only conditions that must be assumed are very basic i.e. the density must be such that $\varrho \geqslant 0$ and $d\varrho/dr \leqslant 0$ while there is no need for whatsoever assumption about pressure P.

Applying these conditions, the following inequalities are obtained (see Appendix B): in the singular case it is found an upper mass limit

$$M \leqslant \frac{4}{9}\, r_b\,, \tag{26}$$

in the nonsingular case, instead, the following inequality is found:

$$1 - \left(\frac{8M^3}{r_b^3 + 8M^3}\right)^{\frac{1}{3}} \geqslant \frac{1}{9}\left(1 - \frac{8M^3}{r_b^3 + 8M^3}\right). \tag{27}$$

Since it is always true that $0 \leqslant 8M^3/(r_b^3 + 8M^3) \leqslant 1$, the inequality for the nonsingular case (27), i.e. the condition of stability, is always satisfied for any values of both M and r_b so that there is no upper limit for the mass, to have equilibrium, whatever would be the, reasonable, equation of state.

5 Conclusions

In conclusion, the application of the class of nonsingular static spherically symmetric metrics (particularly the Schwarzschild solution [1]) to the problem of hydrostatic equilibrium gives completely different solutions from those of the singular case. In this latter, there is a mass limit (whose value depends from the specific state equation) for dense cores of degenerate matter: above this limit, nothing can stop the configuration from a final gravitational collapse with formation of event horizon and inner physical singularity. In the case of nonsingular metric (that does not include the possibility of an event horizon) instead, the equilibrium is always reached whatever would be the amount of mass.

The application with a Fermi gas state equation, as in the Oppenheimer-Volkoff work [7], shows that central density has the same behavior, for increasing mass, than average density i.e. a maximum (with reasonable physical value), before reaching the 2 solar masses and then a decreasing. The equilibrium radius of the system shows a minimum before the 2 solar masses then grows with increasing masses but remaining well below the so called "Schwarzschild radius" for that mass which, in the nonsingular metric environment, is not the dimension of an event horizon but only a parameter connecting the general relativistic metric with the newtonian one. Proper mass of the system tends to the limit of twice the mass. This means that the negative binding energy tends to the limit of m counterbalancing the gravitational mass m. This is a mechanism that can stop gravitational collapsing and that can sustain stable equilibrium.

Considering experimental observations, weak field experiments give same results, within errors, for the singular and nonsingular metrics, while for strong fields, the nonsingular metric admits stable configuration of greater amount of mass while singular metrics admits black hole formation. Few observational, indirect, evidences for black holes existence have been performed in years but it seems that an alternative hypothesis of very compact degenerate matter configurations, permitted by nonsingular metrics, could be compatible with observations: let's consider, for example, a single nonrotating compact object of 9.2 solar masses (m=1 in units of (19)), in the singular metric, it would be a black hole, no matter of which state equation is used, and a "Schwarzschild radius" $r_s = 27.17$ km would define the horizon event whose surface would have an infinite gravitational redshift and would surround a pointlike singularity.

The application of nonsingular metric (with a Fermi equation of state) instead, would give a very compact object, of

radius $r_b = 13.23$km, made by ordinary (degenerate) matter with a central density $\varrho_0 = 13.23 \times 10^{15} g/cm^3$; the density value is not far from the ordinary nuclear density, moreover a more realistic state equation would keep density value within reasonable physical limit.

Gravitational redshift factor $f = \sqrt{-g_{11}}$ (the ratio between wavelength observed at infinity and wavelength emitted at distance r) at the surface of the matter configuration would be $f = 1.165$. This redshift would correspond, in the black hole case, to a redshift of a photon emitted ad distance $r = r_s f^2/(f^2 - 1) = 3.8 r_s$. This difference, theoretically, could be observable but total luminosity would be so faint not to permit direct observations while indirect observations due to, for example, the accretion disk surrounding these compact objects, would be very similar. The existence of compact massive (several solar masses) objects could justify why observed emissions from individuated neutron stars and black hole candidates are so similar [17] despite the totally different characteristics of a hard surface and an event horizon.

Recent observations involving magnetic fields of quasars also put in doubt the existence of inner super-massive black holes [18]. It must be remarked that at the state of the art there is still no observational proof of a black hole event horizon [19].

Lack of single compact objects of very great mass it is due more to mechanism of formation of such object than to some mass limit, anyway in the galactic's centers there is gravitational evidence for compact objects of millions of solar masses. Let's resume how it would be such an object in the nonsingular model with a Fermi gas state equation (others EOS would not change the qualitative features): considering an object 3.6 millions of solar masses, it would have a radius of about $58,000$ km that is the half percent of its estimated "Schwarzschild radius" in the black hole hypothesis, a central density $\varrho_0 = 1.24 \times 10^{10} g/cm^3$ and a central pressure $P_0 = 7.3 \times 10^{16}$ Pa both smoothly decreasing outward.

Sagittarius A, the radio point source associated with the dark mass located at the center of the Milky Way, is the best studied black hole candidate to date, but till now has not be possible to verify or to exclude the presence of a horizon [20]. The horizon existence has been inferred because a surface emission, to remain undetected, would require large radiative efficiencies, greater than 99.6% [21] anyway, this is actually the phenomenon predicted by the application of nonsingular metric, because, as seen in Fig. 3, the limit value of 2 for the ratio M^P/M means an efficiency limit of about 100%. This could be justified, actually, by a not exotic object having a hard surface, emissions and gravitational effects compatible with observations, and that could be permitted because the contribution of the negative binding energy.

Submitted on February 16, 2014 / Accepted on February 24, 2014

References

1. Schwarzschild K. Über das Gravitationsfeld eines Massenpunktes nach der Einsteinschen Theorie (On the Gravitational Field of a Mass Point According to Einstein's Theory), *Sitzungsber. Preuss. Akad. Wiss., Phys. Math. Kl.*, 1916, v. 1916a, 189–196.
2. Crothers S.J. The Schwarzschild solution and its implications for gravitational waves: Part I. *SPESIF-2009* (Space, Propulsion and Energy Sciences International Forum 2009), Huntsville, AL, Von Braun Center, February 24-27, 2009; http://viXra.org/abs/1405.0326
3. Crothers S.J. The Schwarzschild solution and its implications for gravitational waves: Part II. *SPESIF-2009* (Space, Propulsion and Energy Sciences International Forum 2009), Huntsville, AL, Von Braun Center, February 24-27, 2009; http://viXra.org/abs/1405.0325
4. Brillouin M. The singular points of Einstein's universe. *J. Phys. Radium*, 1923, v. 23, 43–46.
5. Droste J. The field of a single centre in Einstein's theory. *Ned. Acad. Wet.*, 1917, v. 19, 197–215.
6. Hilbert D. Die Grundlagen der Phisik. *Nachr. Ges. Wis. Göttingen Math. Phys. Kl.*, 1915, 395–407.
7. Oppenheimer J.R., Volkoff G.M. On massive neutron cores. *Phys. Rev.*, 1939, v. 55, 374–381.
8. Abrams L.S. Black holes: the legacy of Hilbert's error. *Can. J. Phys.*, 1989, v. 67, 919–934.
9. Stavroulakis N. On a paper by J. Smaller and B. Temple. *Ann. Fond. de Broglie*, 2002, v. 27(3), 511–519.
10. Landau L. On the theory of stars. *Physik. Zeits. Sowjetunion*, 1932, v. 1, 285–288.
11. Rhoades C.E., Ruffini R. Maximum mass of a neutron star. *Phys. Rev. Lett.*, 1974, v. 32, 324–327.
12. Srinivasan G. The maximum mass of neutron stars. *Bull. Astr. Soc. India.*, 2002, v. 30, 523–547.
13. Hartle J.B., Sabbadini A.G. The equation of state and bounds on the mass of nonrotating neutron star. *Astrophys. J.*, 1977, v. 213, 831–835.
14. Wald R.M. General Relativity. The University of Chicago Press, Chicago, 1984.
15. Alécian E., Morsink S.M. The effect of neutron star gravitational binding energy on gravitational radiation-driven mass-transfer binaries. *Astrophys. J.*, 2004, v. 614, 914–921.
16. Cook G.B., Shapiro S.L., Teukolsky S.A. Rapidly rotating neutron stars in general relativity realistic equation of state. *Astrophis. J.*, 1994, v. 424, 823–845.
17. Ed. Maccarone J., Fender R. P., Ho L.C. From X-ray Binaries to Quasars: Black Holes on all Mass Scales. Springer, the Netherlands, 2005.
18. Schild R.E., Leiter D.J. Black hole or MECO? decided by a thin luminous ring structure deep within Quasar Q0957+561. *J. of Cosmology*, 2010, v. 6, 1400–1437.
19. Abramowicz M.A., Kluzniak W., Lasota, J.P. No observational proof of black hole event-horizon. *Astronomy and Astrophysics*, 2002, v. 396, L31–L34.
20. Broderick A.E., Narayan R. On the Nature of the Compact Dark Mass at the Galactic Center. *Astrophys. J.*, 2006, v. 638 (1), L21–L24.
21. Broderick A.E., Loeb A., Narayan R. The event horizon of Sagitarius A. *Astrophys. J.*, 2009, v. 701, 1357–1366.
22. Tolman R.C. Relativity Thermodynamics and Cosmology. University Press, Oxford, 1934.

Appendix A

The only non vanishing components of the Einstein Tensor G are G^0_0, G^1_1 and $G^2_2 = G^3_3$. Considering a matter that supports no transverse stresses and has no mass motion then the energy momentum components are [22] $T^1_1 = T^2_2 = T^3_3 = -p$ and $T^0_0 = \varrho$ where p is the pressure and ϱ is the macroscopic energy density measured in proper coordinates. So Einstein's equations are

$$G^0_0 = 8\pi T^0_0 = 8\pi\varrho = e^{-\lambda}\left[\frac{\lambda' r^2}{r^3+\sigma} - \frac{r^4}{(r^3+\sigma)^2} - \right.$$
$$\left. - \frac{4r\sigma}{(r^3+\sigma)^2}\right] + \frac{1}{(r^3+\sigma)^{2/3}} \qquad \text{(T00)}$$

$$G^1_1 = 8\pi T^1_1 = 8\pi p = e^{-\lambda}\left[\frac{\nu' r^2}{r^3+\sigma} + \frac{r^4}{(r^3+\sigma)^2}\right] -$$
$$- \frac{1}{(r^3+\sigma)^{2/3}} \qquad \text{(T11)}$$

$$G^2_2 = 8\pi T^2_2 = e^{-\lambda}\left[\frac{(\nu'-\lambda')r^2}{2(r^3+\sigma)} - \frac{\lambda'\nu'}{4} + \frac{\nu'^2}{4} + \right.$$
$$\left. + \frac{2r\sigma}{(r^3+\sigma)^2} + \frac{\nu''}{2}\right] + \frac{1}{(r^3+\sigma)^{2/3}} \qquad \text{(T22)}$$

where p, ϱ, λ and ν are functions of r and the primes indicates a differentiation with respect to r. Since $T^1_1 = T^2_2$ then $(T^1_1 - T^2_2)\times 2/r = 0$ and from equations (T00) it is easy to verify that

$$\frac{d}{dr}\left(-T^1_1\right) + \left(T^0_0 - T^1_1\right)\frac{\nu'}{2} = \left(T^1_1 - T^2_2\right)\frac{2}{r} = 0 \qquad \text{(A-1)}$$

so that this latter equation can be read

$$\frac{dp}{dr} = -\frac{p+\varrho}{2}\,\nu'. \qquad \text{(A-2)}$$

Equations (T00), (T11) and (A-2) constitute the system of equations to be solved and correspond to the ones in Oppenheimer Volkoff article [7, Eqs. 4,3 and 5] if σ is set equal to 0; an opportune equation of state $\varrho = \varrho(p)$ must also be included in the system.

Eliminating ν' in (T11) and (A-2), the hydrostatic equilibrium equation in exponential form is

$$\frac{dp}{dr} = -\frac{p+\varrho}{2}\times$$
$$\times\left[8\pi p\, e^{\lambda}\frac{(r^3+\sigma)}{r^2} + e^{\lambda}\frac{(r^3+\sigma)^{1/3}}{r^2} - \frac{r^2}{(r^3+\sigma)}\right]. \qquad \text{(A-3)}$$

If it is set $\sigma = 0$ and the singular metric (5) (inside the matter) is considered where $e^{\lambda(r)} = (1-2m(r)/r)^{-1}$ (and consequently $m(r) = \frac{1}{2}r(1-e^{-\lambda})$) then the Tolman-Oppenheimer-Volkoff equilibrium equation is obtained

$$\frac{dp}{dr} = -\frac{(p(r)+\varrho(r))\left[m(r)+4\pi r^3 p(r)\right]}{r^2\left(1-\dfrac{2m(r)}{r}\right)}. \qquad \text{(A-4)}$$

In our case (A-3) instead, it is possible to give the correct physical meaning to $m(r)$ setting, for the nonsingular metric inside the matter,

$$e^{\lambda(r)} = \frac{(r^3+\sigma)^{-4/3}}{1-\dfrac{2m(r)}{(r^3+\sigma)^{1/3}}}\, r^4; \qquad \text{(A-5)}$$

in effect, at the border $r = r_b$ there will be continuity with the metric in vacuum (7) and (6) so that

$$e^{\lambda(r_b)} = e^{\lambda} = \frac{r^4(r^3+8m^3)^{-4/3}}{1-\dfrac{2m}{(r^3+8m^3)^{1/3}}}$$

and $m(r_b)$ will assume its value m as seen by an external observer

$$m(r_b) = \frac{1}{2}\left(r_b^3+8m^3\right)^{1/3}\left(1-e^{-\lambda}\frac{r_b^4}{\left(r_b^3+8m^3\right)^{4/3}}\right) = m. \qquad \text{(A-6)}$$

Finally the Schwarzschild metric inside the matter (in continuity with (7) where it is set $\alpha = 2m(r)$ and $\sigma = 8m^3$ so that $\sigma = \alpha^3$ outside the matter) will be

$$ds^2 = \left(1-\frac{2m(r)}{(r^3+8m^3)^{1/3}}\right)dt^2 -$$
$$- \frac{r^4\left(r^3+8m^3\right)^{-4/3}}{1-\dfrac{2m(r)}{(r^3+8m^3)^{1/3}}}\,dr^2 - \qquad \text{(A-7)}$$
$$- \left(r^3+8m^3\right)^{2/3}\left(d\theta^2+\sin^2\theta d\phi^2\right).$$

So, with $e^{\lambda(r)}$ given by (A-5), the equilibrium equation (A-3) (that is the merging of the two Einstein's equations (T11) and (A-2)) and the other Einstein's equation (T00) will become respectively

$$\left.\begin{aligned}\frac{dp(r)}{dr} &= -\frac{(p(r)+\varrho(r))\left[m(r)+4\pi(r^3+\sigma)p(r)\right]}{\dfrac{\left(r^3+\sigma\right)^{4/3}}{r^2}\left[1-\dfrac{2m(r)}{(r^3+\sigma)^{1/3}}\right]}\\ \frac{dm(r)}{dr} &= 4\pi\varrho(r)r^2\end{aligned}\right\}, \qquad \text{(A-8)}$$

where $\sigma = 8m^3$.

Appendix B

Pressure P can be eliminated from Einstein's equations considering that $G^1_1 - G^2_2 = 0$, this, together with the definition of $h(r)$ (23) leads to the following equation for the singular metric (using the notation by Wald, eq. 6.2.34 in [14])

$$\frac{d}{dr}\left[r^{-1}h_S(r)^{-1/2}\frac{df_S^{1/2}(r)}{dr}\right] = \\ = \left[f_S(r)h_S(r)\right]^{1/2}\frac{d}{dr}\left[\frac{m(r)}{r^3}\right] \tag{B-1}$$

while, for the nonsingular metric

$$\frac{d}{dr}\left[(r^3+\sigma)^{-1/3}h_{NS}(r)^{-1/2}\frac{df_{NS}(r)^{1/2}}{dr}\right] = \\ = \frac{(r^3+\sigma)^{2/3}}{r^2}\left[f_{NS}(r)h_{NS}(r)\right]^{1/2}\frac{d}{dr}\left[\frac{m(r)}{r^3+\sigma}\right]. \tag{B-2}$$

The right sides for both equations are proportional to the derivative with respect to r of the average density, so because the condition $d\varrho/dr \leqslant 0$, the left sides must be both less or equivalent to 0. Integrating the inequalities for the left sides, inward from the border r_b to a generic radius r we obtain

$$\frac{1}{rh_S^{1/2}(r)}\frac{df_S(r)^{1/2}}{dr} \geqslant \frac{M}{r_b^3}, \tag{B-3}$$

$$\frac{1}{(r^3+\sigma)^{1/3}h_{NS}^{1/2}(r)}\frac{df_{NS}^{1/2}(r)}{dr} \geqslant \frac{M}{r_b^3+\sigma}. \tag{B-4}$$

These inequalities can be integrated again inward from r_b to 0. The condition $d\varrho/dr \leqslant 0$ implies that $m(r)$ cannot be smaller than the value it would have for a uniform density star so, for the singular case, $m(r) \geqslant Mr^3/r_b^3$ and, for the nonsingular one, $m(r) \geqslant M(r^3+\sigma)/(r_b^3+\sigma)$, so that inequalities (B-3 and B-4) become: for the singular case (Wald, eq. 6.2.39)

$$f_S^{1/2}(0) \leqslant \frac{3}{2}\left(1-\frac{2M}{r_b}\right)^{1/2} - \frac{1}{2} \tag{B-5}$$

and for the nonsingular case

$$f_{NS}^{1/2}(0) \leqslant \frac{3}{2}\left(1-\frac{2M}{(r_b^3+\sigma)^{1/3}}\right)^{1/2} - \frac{1}{2}\left(1-\frac{2M\sigma^{2/3}}{r_b^3+\sigma}\right) \tag{B-6}$$

(as usual for $\sigma = 0$ the two cases are equivalent). Finally, the condition $f^{1/2}(0) \geqslant 0$ implies that, for the singular case, the necessary condition for staticity involves a maximum limit for the mass: from (B-5)

$$M \leqslant \frac{4}{9}\, r_b\,. \tag{B-7}$$

For the nonsingular case instead, the stability condition implies, from (B-6) and inserting the value $\sigma \equiv 8m^3$, the inequality

$$1-\left(\frac{8M^3}{r_b^3+8M^3}\right)^{\frac{1}{3}} \geqslant \frac{1}{9}\left(1-\frac{8M^3}{r_b^3+8M^3}\right). \tag{B-8}$$

Addendum to "Phenomenological Derivation of the Schrödinger Equation"

Fernando Ogiba
E-mail: Ogiba@cpovo.net

This addendum to the article [1] is crucial for understanding how the complex effective action, despite its derivation based on classical concepts, prevents quantal particles to move along extreme action trajectories. The reason relates to homogenous, isotropic and unpredictable impulses received from the environment. These random impulses allied to natural obedience to the dynamical principle imply that such particles are permanently and randomly passing from an extreme action trajectory to another; all of them belonging to the ensemble given by the stochastic Hamilton-Jacobi-Bohm equation. Also, to correct a wrong interpretation concerning energy conservation, it is shown that the remaining energy due to these permanent particle-medium interactions (absorption-emission phenomena) is the so-called quantum potential.

1 Introduction

The central subject of the article [1] is: Quantal particles (such as electrons), due to its interactions with the environment, move in accordance with the complex effective action

$$S_{eff} = S + i\frac{\hbar}{2}\ln P \tag{1}$$

which was obtained following the classical Hamilton's dynamical principle but considering the motion as a whole, that is, taking averages. The resulting canonical equations coincide with those extracted from the Schrödinger equation writing $\psi = \sqrt{P}\exp(iS/\hbar)$, namely:

$$\frac{\partial S}{\partial t} + \frac{\nabla S \cdot \nabla S}{2m} + V + Q = 0 \tag{2}$$

and

$$\frac{\partial P}{\partial t} + \nabla \cdot \left(P\frac{\nabla S}{m}\right) = 0\,, \tag{3}$$

where

$$Q = \frac{\hbar^2}{8m}\frac{\nabla P \cdot \nabla P}{P^2} - \frac{\hbar^2}{4m}\frac{\nabla \cdot \nabla P}{P} \tag{4}$$

is the quantum potential which, visibly, is the remaining energy of two distinct concurrent phenomena.

The main motivation for writing this addendum concerns the result

$$\int P\left(i\frac{\hbar}{2}\frac{1}{P}\frac{\partial P}{\partial t}\right)d^3r = 0 \tag{5}$$

which is not the expression of energy conservation, as argued in connection with Eg. 23 of the article. In true, the null value of this average means that the involved energy (the enclosed quantity) does not remain in the particle; it is radiation, as will be shown. In doing this, it is necessary to explain how Q — as an energy resulting from the particle-medium interactions — agrees with the energy conservation required by the so-called quantum equilibrium.

Also, in the mentioned article the meaning of the effective action (1) is not so clear. It was derived supposing a particle over a possible trajectory; what, in view of the results, must be true. On the other hand, a continuous trajectory of elementary particles is an experimentally discredited concept. So, there must be a link between these two opposing points of view. In true, there is, as will be seen. Indeed, it will be shown that quantal particles occupies, sequentially and instantly, just one point over different trajectories which are randomically chosen in the ensemble (2). This means that quantal particles don't move along extreme action trajectories but occupy trajectories (permited by the dynamical principle) just for a moment.

The interacting medium — primarily responsible for quantum effects — is the zero-point field (ZPF) which, according to the classical description of the Casimir's experiment, is viewed as a homogeneous and isotropic distribution of electromagnetic waves pervading all space. As the phases of these waves are randomically distributed in the range $[0, 2\pi]$, then electrical charged particles (balanced or not) are permanently receiving unpredictable impulses. This has two main consequences: First, the accelerated charged particles radiate all the absorbed energy. Second, the unpredictable impulses prevent quantal particles to follow predictable paths. Even so, the overall motion obeys the Hamilton's principle which is founded on trajectories. How can all this happen?

2 The quantum potential and the ensemble of virtual trajectories

The answer to the above question lay in the fact that the natural behavior of any moving particle, at any time, is obeying the classical dynamical principle. This must be interpreted as follows: In the absence of random forces, they move along extreme action trajectories. However, in the case of particles which are significantly affected by the ZPF the situation is drastically modified. Indeed, homogeneous, isotropic and random forces (including beck reaction forces) are not part of the traditional classical description of the motion.

Here, it will be proved that the quantal motion occurs as follows: Immediately before any particle-field random inter-

action the particle is over a given trajectory (obedience to the dynamical principle), but upon receiving an unpredictable impulse it is withdrawing from this trajectory to an unpredictable place. Again, in the new position it continues obeying the dynamical principle; that is, the particle is over another trajectory. As this is a permanent process, then the particle occupies these possible trajectories only instantly (virtual trajectories). In a sense, we can say that the unpredictable impulse has created initial conditions (arbitrary) for a new trajectory.

In the light of the foregoing, at each position actually occupied by the particle pass an infinite number of such virtual trajectories. This assumption is in agreement with the following facts: First, Eq. (2) represents an ensemble of unpredictable trajectories; $P(\mathbf{x}, t)$ — preserving its uniqueness — can take any value at $\mathbf{x}$. Moreover, ∇P is not deterministic. Second, energy and momentum in quantum mechanics are independent of coordinates. This means that everywhere there are equivalent ensembles of partial derivatives $\partial S/\partial t$ and ∇S — requiring continuous virtual functions S — which on average give the corresponding observed quantities. This statement implies the same uncertainty everywhere (non locality). Thirty, Probability density, classically, is defined over trajectories; it is canonically conjugate to the action function S (this remains valid in the equations above). Over extreme action trajectories $\partial P/\partial t = 0$ (we know where the particle is at the time t). Therefore, if $\partial P/\partial t \neq 0$, then it means that the particle was "banned" from its trajectory.

To formally prove that the trajectories represented by the virtual ensemble (2) are instantly visited by the particle, it is necessary finding a valid expression which leads to the idea that such trajectories (or momenta ∇S) are randomly chosen (or induced) where the particle is. This is better made after knowing the meaning of the quantum potential.

If a moving particle is not actuated by random forces, then, given the potential V and the initial conditions, we can predict its extreme action trajectory. However, the presence of random forces — exactly like that found in the ZPF — modify this classical way to see the motion. This rupture relates to the fact that now there is only a probability of finding the particle at a given position at the time t.

Whenever a particle is removed from a given position by random forces, the probability of find it there is diminished. Consequently, as probability is a conserved quantity, this decrease of probability leads to the emergence of an outgoing compensatory probability current. Formally, following standard techniques and considering the ZPF properties, at each position there is a diffusion of probability density currents ($P\mathbf{v}$), in such a way that

$$\frac{\partial P}{\partial t} + \nabla \cdot (P\mathbf{v}) = 0\,. \tag{6}$$

In true, $P\mathbf{v}$ represents all possible local outflows of matter whose velocities $\mathbf{v}$ have the directions of the vectors ∇P. Therefore, all currents obey

$$P\mathbf{v} = \alpha \nabla P, \tag{7}$$

where α is a proportionality factor, to be determined.

Being the matter-field interaction conservative, then there is no net momentum transfer to the particle. This implies that the average probability density current is zero, i.e.

$$\int P\,(P\mathbf{v})\; d^3r = \int P\,(\alpha \nabla P)\; d^3r = 0\,. \tag{8}$$

Integrating the second form by parts and considering that $P \to 0$ at infinity, we find that its null value is plenty satisfied if α is a constant. In true, it is an imaginary diffusion constant because there is no effective dislocation of matter in all directions (this is a single-particle description). In fact, in accordance with the imaginary part of the effective action (1), the unpredictable impulses received by the particle are given by

$$m\mathbf{v} = \nabla \left(i\,\frac{\hbar}{2}\,\ln P \right) = i\,\frac{\hbar}{2}\,\frac{\nabla P}{P}\,, \tag{9}$$

which, compared with (7), implies that $\alpha = i\hbar/2m$.

The consequent average kinetic energy induced by the ZPF on the particle is

$$\langle T_{ZPF} \rangle = \int P \left(\frac{1}{2}\, m|\mathbf{v}|^2 \right) d^3r\,, \tag{10}$$

which considering (9), reads

$$\langle T_{ZPF} \rangle = \frac{\hbar^2}{8m} \int \frac{(\nabla P)^2}{P}\; d^3r. \tag{11}$$

However, the implicated acceleration makes the electrical charge radiates. So, we must appeal to the general rule concerning accelerated charged particles, namely: The change in the kinetic energy in the absorption-emission process is equal to the work done by the field minus the radiated energy. This is the energy conservation implicit in the determination of the Abraham-Lorentz back reaction force.

Therefore, varying the average kinetic energy, that is, taking the functional derivative of (11) with respect to P, we find that the remaining energy due to particle-field interactions is

$$\delta\langle T_{ZPF} \rangle = \frac{\hbar^2}{8m} \left(\frac{\nabla P \cdot \nabla P}{P^2} - 2\,\frac{\nabla \cdot \nabla P}{P} \right), \tag{12}$$

where, therefore, the first term relates to absorption of radiation, and the second to emission.

Coincidentally, this remaining energy is the quantum potential (4) which, therefore, is the expression of the required energy conservation implied in the so-called quantum equilibrium.

At this point we have sufficient valid information to prove that extreme action trajectories are randomly chosen at each position actually occupied by the particle.

Indeed, the probability density conservation (6), considering (9), reads

$$\frac{\partial P}{\partial t} + i\,\frac{\hbar}{2m}\nabla^2 P = 0\,, \tag{13}$$

which has the shape of a diffusion equation; local diffusion of probability density currents or virtual outflows of matter at the actual particle position.

The validity of this equation is unquestionable. In fact, it is absolutely equivalent to Eq. (3), or

$$\frac{\partial(\psi^*\psi)}{\partial t} + i\,\frac{\hbar}{2m}\,\nabla\cdot(\psi^*\,\nabla\psi - \psi\,\nabla\,\psi^*) = 0\,, \tag{14}$$

as can be proven from $|\nabla\psi|^2 = -\psi^*\nabla\psi$ and the parameterized forms of S and P in terms of ψ.

Very important, the equations (13) and (3) represent the same diffusion at each position $\mathbf{x}$ actually occupied. Equivalently, these two ways of expressing probability conservation contain implicitly all possibilities for the particle flow at $\mathbf{x}$. As Eq. (3) expresses this in terms of ∇S, then ∇S must represent all possible momenta at $\mathbf{x}$. However, as these partial derivatives require continuous action functions, then there pass multiple virtual trajectories. One of them infallibly will be occupied, but only for a moment because in the next position the same phenomenon is repeated.

In this sence, the obedience to the dynamical principle, implicit in the effective action (1), is traduced as follows: At a given time the particle is over a trajectory represented by the action S (real part), but at this very moment there is a choice for the next motion, which is dictated by the probability dependent local action (imaginary part). In other words, the imaginary part chose the next action function (S) representing another trajectory to be occupied during an infinitesimal time; and so on.

Now, it is possible to correct the interpretation given to (5) in the article [1]. Just rewrite Eq. (13) in the energy form

$$i\,\frac{\hbar}{2}\frac{1}{P}\frac{\partial P}{\partial t} = \frac{\hbar^2}{4m}\frac{\nabla\cdot\nabla P}{P}\,, \tag{15}$$

which implies that

$$\int_{all} P\left(i\,\frac{\hbar}{2}\frac{1}{P}\frac{\partial P}{\partial t}\right)d^3r = \int_{all} P\left(\frac{\hbar^2}{4m}\frac{\nabla\cdot\nabla P}{P}\right)d^3r = 0\,. \tag{16}$$

Being the second member of (15) the emitted energy of the balance (12), then the result (5) means that the involved energy doesn't remain in the particle.

3 Conslusion

The subsequent particle's positions, randomly chosen in the interactions, are on different trajectories. Therefore, there are continuous trajectories, but never followed by quantal particles. They simply represent the obedience to the mechanical principle, regardless of where the particle is. Nevertheless, as these virtual trajectories are inherent to the Schrödinger picture, then it is expected that they — properly determined and used as statistical tools - can give the same predictions. However, the convenience of such procedure needs to be better discussed.

On the other hand, were highlighted permanent emissions and absorptions of radiation, meaning that particles are actuated by forces and back reaction forces, which, on average, are zero. This explains why the interactions become transparent in the quantum description. Nevertheless, speculating, these permanent absorptions and emissions of electromagnetic waves (a delicate asymmetry accompanying particles everywhere) may be important to interpret certain properties of matter.

Submitted on March 3, 2014 / Accepted on March 11, 2014

References

1. Ogiba F. Phenomenological derivation of the Schrödinger equation. *Prog. Phys.*, 2011, no.4, 25–28.

Views about the "Oxford Questions". Wave Function Collapse and Schrödinger's Cat: Are They Real Scientific Topics or Plain Fictions?

Spiridon Dumitru

Department of Physics (retired), "Transilvania" University, B-dul Eroilor 29, 500036 Braşov, Romania
E-mail: s.dumitru42@yahoo.com

Motivated by the recently published "Oxford Questions" we review the foundational character of the wave function collapse theme. We show that the respective theme, as well as its twin analogue represented by the Schrödinger's cat problem, are not real scientific topics but plain and rather trivial fictions. Consequently, we suggest that the related items of the "Oxford Questions" have to be perceived with some epistemic caution.

1 Introduction

The newly diffused *The Oxford Questions on the Foundations of Quantum Physics* [1], known also as "*Oxford Questions*, aims to formulate "*a list of main open questions about the foundations of quantum physics*". Within the respective list, the issue "*whether or not the 'collapse of the wave packet' is a physical process*" is approached in "*several Oxford Questions: in particular, 1b, 2a, 2c, 3a, 3c and 5a*". The issue is mainly brought into attention in 3c: "*How can the progressive collapse of the wave function be experimentally monitored?*".

It is expected that, in the future, the Oxford Questions will stimulate more or less extensive studies in both advanced and pedagogic research. Previous to these studies, it is important to examine the correctness of the items gathered in the Oxford Questions, particularly the ones pertaining to the above-mentioned quantum collapse. Such an examination is intended in this short paper, by using some ideas noted in some of our recent works. Section 2 is focused on the theme of Wave Function Collapse. Additionally, in Section 3, we examine the case of Schrödinger's Cat Thought Experiment which in fact is a twin analogue of the Wave Function Collapse. We find that both the Wave Function Collapse and the Schrödinger's Cat Thought Experiment are not real scientific topics but only pure fictions.

The present paper ends in Section 4 with some closing thoughts, particularly with the suggestion that, for real science, the invalidated Oxford Questions items have to be regarded as needless.

2 On the wave function collapse

Historically speaking, the Wave Function Collapse concept was brought into scientific debate by the conflict between the following two suppositions:

$\mathbf{s}_1$ The old opinion that a Quantum Measurement of a (sub)atomic observable should be regarded as a single sampling (trial) which gives a unique deterministic value. ■

$\mathbf{s}_2$ The agreement, enforced by theoretical considerations, is such that to describe such an observable one should resort to probabilistic (non-deterministic) entities represented by an operator together with a wave function. ■

To avoid conflict between suppositions $\mathbf{s}_1$ and $\mathbf{s}_2$ it was in diffused the thesis that, during a Quantum Measurement, the corresponding wave function collapses into a particular eigenfunction associated with a unique (deterministic) eigenvalue of the implied operator. Such a thesis has led to the Wave Function Collapse concept regarded as a true dogma. The respective concept was assumed, in different ways and degrees, within a large number of mainstream publications (see [2–8] and references therein). But, as a rule, the previously mentioned assumptions were (and still are) not accompanied with adequate elucidations concerning the initial correctness of the alluded concept in relation to the natural themes of Quantum Mechanics.

Now, explicitly or implicitly, the Oxford Questions [1] put forward the problems:

$\mathbf{p}_1$ Whether or not the "collapse of the wave packet" is a physical process. ■

$\mathbf{p}_2$ How can the progressive collapse of the wave function be experimentally monitored? ■

$\mathbf{p}_3$ According to which theoretical scheme, justified by physical reality alone, can a Wave Function Collapse be described properly? (This is in the situation [6] where a whole "*zoo of collapse models*" have already been invented. ■

In order to generate significant remarks on the above-mentioned Oxford Questions problems $\mathbf{p}_1$–$\mathbf{p}_3$, now we wish to bring into attention some ideas prefigured and to a certain extent argued in our recent paper [9, 10]. We mainly pointed out the ephemeral character (i.e. caducity) of the Wave Function Collapse concept. Basically our argumentations are grounded on the following indubitable facts. Mathematically, a quantum observable (described by a corresponding opera-

tor) is a true random variable. Then, in a theoretical framework, such a variable must be regarded as endowed with a spectra of eigenvalues. For a given quantum state/system the mentioned eigenvalues are associated with particular probabilities incorporated within the wave function of the mentioned state/system. Consequently, from an experimental perspective, a measurement of a quantum observable requires an adequate number of samplings finished through a significant statistical group of data/outcomes. That is why one can conclude that the supposition $\mathbf{s}_1$ of the Wave Function Collapse concept appears as a false premise while the whole respective concept proves oneself to be a useless fiction.

The previously noted conclusion can be consolidated indirectly by mentioning the quantum-classical probabilistic similarity (see [11–14]) among quantum mechanical observables and macroscopic random variables, studied within the thermodynamic theory of fluctuations. On the whole, a macroscopic random variable is characterized by a continuous spectra of values associated with an intrinsic probability density. Then, for measuring a macroscopic random variable, a single experimental sampling delivering a unique value (result) is worthless. Such a sampling is not described as a collapse of the mentioned probability density. Similarly, a quantum measurement must not be represented as a wave function collapse. Moreover, a true experimental evaluation of a macroscopic random variable requires an adequate lot of samplings finished through a statistical set of individual results. A plausible model for a theoretical description of the alluded evaluation can be done [14–16] through an information transmission process. In the respective model, the measured system appears as an information source while the measuring device plays the role of an information transmission channel to the recorder of measurement data. As part of the mentioned measuring process, the quantum mechanical operators (describing quantum observables) preserve their mathematical expressions. Additionally, the transmission to the the recorder of quantum probabilistic attributes is described by means of linear transformations for probability density and current(associated with the corresponding wave function).

Taking into account the above mentioned indubitable arguments, we think that in natural perception the "collapse of the wave function" cannot be considered as a physical process. Consequently, the Wave Function Collapse concept does not have the qualities of a real scientific topic, it being only a purely trivial and worthless fiction. Moreover, the above noted problems $\mathbf{p}_2$ and $\mathbf{p}_3$ make no sense. That is why the further studies expected to be raised by the Oxford Questions would be more appropriate if ignoring all the elements regarding the Wave Function Collapse concept.

3 As regards the Schrödinger's cat

Subsidiarily to the above considerations about the Wave Function Collapse concept, some remarks can be brought into question [9] concerning the famous Schrödinger's Cat Thought Experiment. The essential element in the respective experiment is represented by a single decay of a radioactive atom (which, through some macroscopic machinery, kills the cat). But the individual lifetime of a single decaying atom is a random variable. That is why the mentioned killing decay is in fact a twin analogue of the above mentioned single sampling taken into account in supposition $\mathbf{s}_1$ of the Wave Functions Collapse concept. So, the previous considerations reveal the notifiable fact that is useless (even forbidden) to design experiments or actions that rely solely on a single deterministic sampling of a random variable (such is the decay lifetime). Accordingly, the Schrödinger's Cat Thought Experiment appears as a twin analogue of the Wave Functions Collapse i.e. as a fiction (figment) and a deontology without any real scientific value.

The previously mentioned fictional character of the Schrödinger's Cat Thought Experiment can be argued once more by observation [9] that it is possible to imagine a macroscopic thought-experiment completely analogous with Shrödinger's quantum one. Within the respective analogue, a cousin of Schrödinger's cat can be killed through launching a single macroscopic ballistic projectile. More specifically, the killing macroscopic machinery is activated by the reaching of the projectile in a probable hitting point. But the respective point has characteristics of a true macroscopic (non-quantum) random variable. Consequently, the launching of a single projectile is a false premise, similar to the supposition $\mathbf{s}_1$ of the Wave Function Collapse concept. Add here the known fact that within the practice of traditional artillery (operating only with macroscopic ballistic projectiles but not with propelled missiles) designed for an expected destruction of a military objective, one uses a considerable (statistical) number of projectiles but not a single one. So the whole situation with a macroscopic killing projectile is completely analogous with the Schrödinger's Cat Thought Experiment which uses a single quantum radioactive decay. Therefore, the acknowledged classical experiment makes clear once more the fictional character of the Schrödinger's Cat Thought Experiment.

According to the above-noted remarks, certain things must be regarded as being worthless, i.e. allegations such as: *"the Schrödinger's cat thought experiment remains a topical touchstone for all interpretations of quantum mechanics"*. Note that such or similar allegations can be found in many science popularization texts, e.g. in the ones disseminated via the Internet.

4 Closing thoughts

Through the contents of the previous sections, we have brought into attention a few significant remarks regarding the themes of the Wave Function Collapse and the Schrödinger's Cat Thought Experiment. Through the respective remarks, we argue that the mentioned themes are not real scientific

topics but pure and trivial fictions. So we find that the Oxford Questions have an important, prolonged drawback and, consequently, their invalidated items have to be regarded as needless things for science.

Submitted on February 27, 2014 / Accepted on March 12, 2014

References

1. Briggs G.A.D., Butterfield J.N., Zeilinger A. The Oxford Questions on the foundations of quantum physics. *Proc. Royal Soc. A*, 2013, v.469, 20130299; arXiv:1307.1310.
2. Stamatescu I.-O. Wave function collapse. In: *Compendium of Quantum Physics*, Springer, 2009, 813–822.
3. Ghirardi C. Collapse theories. The Stanford Encyclopedia of Philosophy. Winter 2011 Edition, http://plato.stanford.edu/archives/win2011
4. Omnes R. Decoherence and wave function collapse. *Foundations of Physics*, 2011, v.41, 1857–1880; arXiv: 1105.0831.
5. Weinberg S. Collapse of the state vector. *Phys. Rev. A*, 2012, v.85, 062116; arXiv: 1109.6462.
6. Bassi A., Lochan K., Satin S., Singh T.P., and Ulbricht H. Models of wave-function collapse, underlying theories, and experimental tests. arXiv: 1204.4325.
7. Cowan C.W., Tumulka R. Epistemology of wave function collapse in quantum physics. arXiv: 1307.0827.
8. Bassi A., Ulbricht H. Collapse models: from theoretical foundations to experimental verifications. arXiv:1401.6314.
9. Dumitru S. Caducity of idea about wave function collapse as well new views on Schrödinger's cat and quantum measurements. *Progress in Physics*, 2013, v.9, no.2, 63–68.
10. Dumitru S. Annotations regarding the Oxford Questions. arXiv: 1311.2581.
11. Dumitru S. Fluctuations and thermodynamic inequalities. *Physica Scripta*, 1974, v.10, 101–103.
12. Dumitru S. The Planck and Boltzmann constants as similar generic indicators of stochasticity: some conceptual implications of quantum-nonquantum analogies. *Physics Essays*, 1993, v.6, 5–20.
13. Dumitru S., Boer A. Fluctuations in the presence of fields — phenomenological Gaussian approximation and a class of thermodynamic inequalities. *Phys. Rev. E*, 2001, v.64, 021108; arXiv: cond-mat/0011444.
14. Dumitru S. Reconsideration of the uncertainty relations and quantum measurements, *Progress in Physics*, 2008, v.4, no.2, 50–68; arXiv:1205.3892.
15. Dumitru S. Phenomenological theory of recorded fluctuations. *Physics Letters A*, 1974, v.48, 109–110.
16. Dumitru S., Boer A. On the measurements regarding random observables. *Romanian Journal of Physics*, 2008, v.53, 1111–1116; http://www.nipne.ro/rjp/2008_53_9-10.html

The Electron and Proton Planck-Vacuum Coupling Forces and the Dirac Equation

William C. Daywitt

National Institute for Standards and Technology (retired), Boulder, Colorado, U.S.A.
E-mail: wcdaywitt@me.com

This short paper derives the electron and proton Planck-vacuum coupling forces so that both the electron and proton, and their antiparticles, possess a Compton radius and obey the Dirac equation.

1 Introduction

The Dirac equation can be expressed as [1] [2]

$$e_*^2\left(i\frac{\partial}{\partial ct}+\boldsymbol{\alpha}\cdot i\nabla\right)\psi = mc^2\beta\psi \tag{1}$$

where in the Planck vacuum (PV) theory the coefficients e_*^2 and mc^2 are particle-PV coupling constants associated with the polarization and curvature forces

$$\frac{(\pm e_*)(-e_*)}{r^2} = \mp\frac{e_*^2}{r^2} \qquad \text{and} \qquad \frac{mm_*G}{r_*r} = \frac{mc^2}{r} \tag{2}$$

where $(\pm e_*)$ and mc^2 are the charge and rest mass energy of the free-space Dirac particles and $(-e_*)$ refers to the separate Planck particles making up the PV continuum. G is Newton's gravitational constant, m_* and r_* are the mass and Compton radius of the Planck particles, and e_* is the massless bare charge. The 'Dirac particles' refer in the present paper to the electron and proton and their respective antiparticles.

The coupling constants in (1) and (2) are presently associated with the rest-frame coupling forces [3]

$$F(r) = \mp\frac{e_*^2}{r^2} - \frac{mc^2}{r} \tag{3}$$

but there is a problem. The negative polarization force in (3) is due to the positive charge in $(\pm e_*)$ of (2) and yields the equation

$$-e_*^2\left(i\frac{\partial}{\partial ct}+\boldsymbol{\alpha}\cdot i\nabla\right)\psi = mc^2\beta\psi \tag{4}$$

which, because of the negative sign, is not a Dirac equation. Thus these coupling forces do not lead to a Dirac particle in the positron and proton cases — nor can they produce their corresponding Compton radii $r_c = e_*^2/mc^2$ from (3), where $F(r_c)$ must vanish. So there is something wrong with these coupling forces and, to resolve the problem, it is necessary to look more closely at the foundation of the PV theory.

2 Single superforce

The two observations: "investigations point towards a compelling idea, that all nature is ultimately controlled by the activities of a single *superforce*", and "[a living vacuum] holds the key to a full understanding of the forces of nature" ; come from Paul Davies' popular 1984 book [4, p.104] entitled "*Superforce: The Search for a Grand Unified Theory of Nature*". This living vacuum consists of a "seething ferment of virtual particles", and is "alive with throbbing energy and vitality". These statements form the foundation of the PV theory [5] [6] that, among other things, derives the primary constants associated with Newton's constant $G\,(=\,e_*^2/m_*^2)$, Planck's reduced constant $\hbar\,(=\,e_*^2/c)$, and the fine structure constant $\alpha\,(=e^2/e_*^2)$.

The single-superforce idea is taken here to mean that the superforces associated with General relativity [5] and the Newton and Coulomb forces have the same magnitude. In particular it is assumed that

$$\frac{m_*^2G}{r_*^2} = \frac{c^4}{G} = (\pm)\frac{e_*^2}{r_*^2} \tag{5}$$

where the first, second, and third ratios are the superforces for Newton's gravitational force and General relativity, and the free-space forces and superforces associated with the Coulomb force.

Equating the first and second ratios in (5) leads to

$$\frac{c^4}{G} = (\pm)\frac{m_*c^2}{r_*} \tag{6}$$

where, since c^4 and G are positive-definite constants, the negative sign in (6) must refer to some other aspect of the ratio — this other aspect is the c^4/G association with the two-term particle-PV coupling forces. Equating the second and third ratios in (5) and using (6) yields

$$(\pm)\frac{m_*c^2}{r_*} = (\pm)\frac{e_*^2}{r_*^2} \tag{7}$$

both sides of which are coupling forces.

Equating the first and third ratios in (5) gives

$$G = \frac{e_*^2}{m_*^2} \tag{8}$$

as the definition of the secondary constant G in terms of the primary constants e_*^2 and m_*^2.

Using the curvature and polarization forces in (7), the two-term coupling forces take the form

$$F(r_*) = (\pm)\frac{e_*^2}{r_*^2}(\pm)\frac{m_*c^2}{r_*} \tag{9}$$

where the proper choice of the plus and minus signs leads to coupling forces consistent with the existence of a Compton radius. Thus the proper choice is

$$F(r_*) = \pm\left(\frac{e_*^2}{r_*^2} - \frac{m_*c^2}{r_*}\right) \tag{10}$$

defining coupling forces that vanish at the Compton radius ($r_* = e_*^2/m_*c^2$) of the Planck particle. The vanishing of (10) reveals a basic property of the PV state that establishes how the stable free-space particle interacts with the vacuum — i.e., via a two-term coupling force that generates a characteristic Compton radius ($r_c = e_*^2/mc^2$) for the particle.

For the free-space electron and proton and their antiparticles, the results of the previous paragraph suggest that their coupling forces should be

$$F(r) = \pm\left(\frac{e_*^2}{r^2} - \frac{m_ec^2}{r}\right) = \begin{cases}\text{electron}\\ \text{positron}\end{cases} \tag{11}$$

and

$$F(r) = \mp\left(\frac{e_*^2}{r^2} - \frac{m_pc^2}{r}\right) = \begin{cases}\text{proton}\\ \text{antiproton}\end{cases} \tag{12}$$

where the plus and minus signs correspond to the particles indicated on the right of the braces, and the subscripts 'e' and 'p' refer to the electron and proton respectively. These coupling forces replace the problematic forces in (3). The radius r in these equations is the radius from the free-space Dirac particle to the separate particles of the PV.

The vanishing of equations (10)–(12) leads to the important string of Compton relations

$$r_em_ec^2 = r_pm_pc^2 = r_*m_*c^2 = e_*^2 \quad (= c\hbar) \tag{13}$$

relating the Dirac particles to the Planck particles.

3 Conclusions and comments

The forces (11) and (12) vanish at the electron and proton, and their respective antiparticle, Compton radii

$$r_e = \frac{e_*^2}{m_ec^2} \qquad \text{and} \qquad r_p = \frac{e_*^2}{m_pc^2} \tag{14}$$

and lead to the Dirac equations

$$\pm e_*^2\left(i\frac{\partial}{\partial ct} + \boldsymbol{\alpha}\cdot i\nabla\right)\psi = \pm mc^2\beta\psi\,. \tag{15}$$

Dividing through by $\pm mc^2$ gives

$$r_c\left(i\frac{\partial}{\partial ct} + \boldsymbol{\alpha}\cdot i\nabla\right)\psi = \beta\psi \tag{16}$$

where the Compton radius r_c ($= e_*^2/mc^2$) and m now represent any of the Dirac particles ($r_c = r_e, r_p$).

The particle-PV potential energy associated with the coupling forces in (11) and (12) is defined as

$$V(r) = -\int_{r_c}^{r} |F(r)|\,dr \tag{17}$$

for $r \leqslant r_c$, resulting in (using (13))

$$\frac{V(r)}{mc^2} = \frac{r_c}{r} - 1 - \ln\frac{r_c}{r} \tag{18}$$

where $V(r_c) = 0$. The potential increases as the Dirac-particle cores ($\pm e_*, m$) are approached (as r decreases), making the negative energy vacuum susceptible to free-space (where the cores reside) perturbations. This susceptibility leads to an internal vacuum structure for the Dirac particles; where, in the "The Dirac Proton and its Structure" calculations [6] [7], quantitative confirmation for the preceding Dirac-particle calculations is provided.

Submitted on March 6, 2014 / Accepted on March 17, 2014

References

1. Daywitt W.C. Understanding the Dirac Equation and the Electron-Vacuum System. *Progress in Physics*, 2013, no. 4, 78.
2. Daywitt W.C. The Electron-Vacuum Coupling Force in the Dirac Electron Theory and its Relation to the Zitterbewegung. *Progress in Physics*, 2013, no. 3, 25.
3. Daywitt W.C. Particles and Antiparticles in the Planck Vacuum Theory. *Progress in Physics*, 2011, no. 1, 55.
4. Davies P. *Superforce: the Search for a Grand Unified Theory of Nature*. Simon and Schuster, Inc., New York, 1984.
5. Daywitt W.C. The Planck Vacuum. *Progress in Physics*, 2009, no. 1, 20. See also www.planckvacuum.com.
6. Daywitt W.C. The Proton and its Structure. This paper has been submitted the the Canadian "*Applied Physics Research*" Journal for publication. See also www.planckvacuum.com.
7. Barut A.O. and Bracken A.J. Zitterbewegung and the Internal Geometry of the Electron. *Phys. Rev. D*, 1981, v. 23, no. 10.

Further Insight Relative to Cavity Radiation II: Gedanken Experiments and Kirchhoff's Law

Pierre-Marie Robitaille

Department of Radiology, The Ohio State University, 395 W. 12th Ave, Columbus, Ohio 43210, USA.
E-mail: robitaille.1@osu.edu

Kirchhoff's law of thermal emission states that cavity radiation must always be black, or normal, irrespective of the nature of the walls. Arbitrary cavity radiation must be solely dependent upon the equilibrium temperature and the frequency of observation. Despite such theoretical claims, it is well established that laboratory blackbodies are not constructed from arbitrary materials, but rather from nearly perfect absorbers of radiation over the frequency of interest. In the laboratory, arbitrary cavities do not contain black radiation. This experimental fact stands in direct conflict with Kirchhoff's formulation. Nonetheless, Kirchhoff's law of thermal emission endures, in part, due to Gedanken experiments whose errors in logic are difficult to ascertain. In this work, thought experiments are discussed in order to expose some logical shortcomings. It will be demonstrated that Kirchhoff's law cannot be supported in this context.

If a space be entirely surrounded by bodies of the same temperature, so that no rays can penetrate through them, every pencil in the interior of the space must be so constituted, in regard to its quality and intensity, as if it had proceeded from a perfectly black body of the same temperature, and must therefore be independent of the form and nature of the bodies, being determined by temperature alone... In the interior therefore of an opake red-hot body of any temperature, the illumination is always the same, whatever be the constitution of the body in other respects.

Gustav Robert Kirchhoff, 1860 [1]

1 Introduction

Recently, the validity of Kirchhoff's law [1, 2] and the universality of the laws of thermal emission [3–6] have been brought into question [7–13]. This reformulation of an established thermodynamic principle has repercussions throughout the fields of physics and astronomy. The issues at hand not only concern our understanding of the nature of the stars [14] and the microwave background [15], but also the universality endowed upon Boltzmann's and Planck's constants [12]. Thus, although 150 years have passed since Kirchhoff's law was formulated [1, 2], it is appropriate to carefully reconsider its authenticity. In this respect, the author has argued against the validity of this law of thermal emission [7–13].

Stewart's law [16], not Kirchhoff's [1, 2], properly accounts for the equivalence between emissivity and absorptivity in thermal equilibrium. Unlike his contemporaries [1,2,6], Stewart [16] does not require that all radiation within cavities be black, or normal. In this work, the variable nature of cavity radiation is affirmed by addressing a Gedanken experiment which is often invoked to justify Kirchhoff's law, either in the classroom or within textbooks.

2 Experiment I: Two ideal cavities

In this experiment, two cavities of the same dimensions are imagined to exist in an empty universe at the same temperature (see Fig. 1A). In order to ensure that the heat contained within each cavity cannot escape, let us surround the exterior of these enclosures with an adiabatic wall. The interior of each cavity is then placed under vacuum to prevent convective processes. The inner surface of the first enclosure (cavity 1) is comprised of an ideal, or perfect, emitter (Emissivity (ϵ) = 1, Reflectivity (ρ) = 0; at the frequency of interest). The interior of cavity 2 is constructed from an ideal, or perfect, reflector ($\epsilon = 0$, $\rho = 1$; at the frequency of interest). For pedagogical purposes, a perfectly adiabatic structure is selected for the inner wall of cavity 2. The cavities are in temperature equilibrium with a third object in the same universe, which is also surrounded by an adiabatic wall.

The physics community currently maintains that, under these conditions, both cavities must contain black radiation, in accordance with Kirchhoff's law [1,2], despite the fact that the second cavity, being fully adiabatic, acts as a perfect reflector and, hence, is unable to emit a single photon. How can it be argued that cavity 2 is filled with black radiation?

Let the two cavities come into contact with one another and place a small hole between them, as displayed in Fig. 1B. When this occurs, photons must cross from cavity 1 (perfectly emitting) into cavity 2 (perfectly reflective). Yet, if cavity 2 is devoid of black radiation, it will not be able to transfer a photon back into the first cavity. As a result, since the first cavity would be losing net photons into the second cavity, its energy content or temperature would drop. Conversely, the energy content of the second cavity would rise. This cannot be permitted according to the zeroth law of thermodynamics, since all three objects are already at the same temperature. Consequently, it is argued that the perfectly reflecting cavity

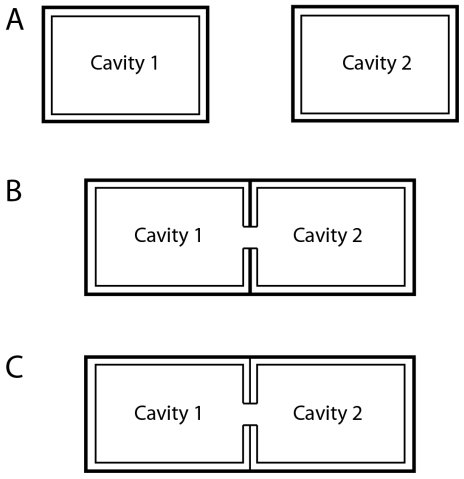

Fig. 1: Schematic representation of our thought experiments. A) Two cavities are presented. Cavity 1 is constructed from a perfect emitter ($\epsilon = 1$, $\rho = 0$) surrounded by an adiabatic wall. Cavity 2 represents a perfect reflector ($\epsilon = 0$, $\rho = 1$). In this case, we assume that both the inner lining and the outer wall are fully adiabatic. B) The cavities displayed in A are brought together and a small hole is made between them in order to permit radiation to flow from one enclosure into the other. C) Two cavities are presented which again have been brought in contact with one another. The inner surface of cavity 1 is constructed from graphite, or soot, and is assumed to act as a perfect emitter ($\epsilon = 1$, $\rho = 0$). The inner surface of cavity 2 is constructed from silver which is assumed to act as a perfectly reflector ($\epsilon = 0$, $\rho = 1$). Both cavities are surrounded by adiabatic walls. However, when the two cavities are brought together, the adiabatic walls between them are removed. This allows for direct thermal contact of the two inner surfaces. A small hole is included to permit radiation to move from one enclosure into the other.

must have contained black radiation all along, such that radiative equilibrium could always be maintained and that the temperature of the cavities can remain intact.

The error in such arguments must be found in permitting net energy to be transferred from cavity 1 into cavity 2. This cannot be allowed, simply based on the zeroth law of thermodynamics, if both cavities are said to be at the same temperature. A logical misstep must have been made in this thought experiment. The two cavities must not have been properly conceived.

The problem can be attributed to the inner surface of the second cavity and in the fact that both cavities must be surrounded by an adiabatic wall to prevent the emission of photons into the surrounding empty universe. This was central to maintaining the energy/temperature stability of each subsystem.

In designing the second cavity from a perfectly adiabatic wall, a physical regimen has been adopted which has no relationship to the best reflectors. Adiabatic walls are immune to all thermal processes. As a consequence, scientists who invoke their use in this setting, fail to recognize that such walls cannot be characterized with a temperature. Thus, if Kirchhoff's law is invalid and there are actually no photons within cavity 2, one cannot even set a temperature for the second system. By default, adiabatic walls cannot store energy within themselves. Namely, in addition to being perfectly reflective, they cannot support thermal conduction or electron flow. This stands in direct opposition to the known properties of the best reflectors and real heat shields.*

In reality, all good reflectors are also good conductors. As a case in point, silver constitutes a very efficient reflector in the infrared, but it is also one of the best electrical and thermal conductors.†

Since the formulation of a law of physics must depend upon the proper characterization of the physical world, one must be careful not to invoke a mathematical or physical regimen which has lost all relation to reality. The use of a fully adiabatic perfectly reflecting cavity has not allowed for sufficient degrees of freedom in which to store energy, as it cannot sustain any phonons within its walls. The only degree of freedom which might be available to such a cavity would rest in its ability to contain a radiation field. However, can cavity 2 actually have the ability to spontaneously generate such a field, despite its complete lack of phonons and perfect reflection, simply driven by a law of physics which is currently under question?

As cavity 2 is perfectly reflecting, the proper conclusion remains that it cannot self-generate a single photon. Thus, it should initially be devoid of a radiation field. Because it also cannot hold any energy in its adiabatic walls, cavity 2 cannot be characterized by *any* temperature.

Consequently, at the beginning of the experiment, cavity 2 cannot be in thermal equilibrium with cavity 1. Therefore, cavity 1 is allowed to transfer photons into cavity 2, simply because there is no thermal equilibrium initially. The temperature of cavity 1 must drop, as it pumps photons into cavity 2. Thus, cavity 1 falls out of thermal equilibrium with the third object, and Kirchhoff's law has not been proven.

Obviously, there are shortcomings in cavity 2. As such, the cavities should be redesigned, such that the validity of Kirchhoff's law can be assessed from a slightly different perspective.

*Superconducting magnets for MRI utilize heat shields in their interior that may well represent the closest example of an adiabatic shield in nature. Such shields are typically made from a highly reflective and conductive metal. They are suspended in the interior of the cryostat using very thin and insulating fiberglass rods which act to help eliminate all conductive thermal contact between the shield and other portions of the magnet system (i.e. the liquid helium Dewar containing the magnet windings, other heat shields, the liquid nitrogen Dewar, the outer casing of the magnet, etc.). These heat shields are typically suspended in a vacuum environment. This is done in order to minimize any convective contact between the shield and the rest of the magnet.

†Silver is amongst the best conductors with a resistivity of only $\sim 1.6 \times 10^{-8}$ Ω m at 300 K and of $\sim 0.001 \times 10^{-8}$ Ω m at 4 K [17]. It is also an excellent reflector in the infrared, our frequency range of interest.

3 Experiment II: Two cavities in thermal contact

Once again, each cavity is surrounded, under vacuum, with an adiabatic wall such that heat radiation cannot be lost into the universe and the temperature of each cavity can be maintained. As before, these two cavities are in temperature equilibrium with a third object in the same universe, which is also surrounded by an adiabatic wall.

The inner surface of cavity 1, the perfectly emitting cavity, will be constructed from graphite, or soot. These materials are known to be very good physical examples of blackbodies in the laboratory [18–21]. Departure from physical reality will consist solely in assuming that the emissivity of the inner surface is perfect ($\epsilon = 1, \rho = 0$).

Silver will be used to line the inner surface of cavity 2. This metal is perhaps the best known reflector in the laboratory. In parallel fashion, a single departure is made from physical reality, namely in assuming that the reflectivity of the silver interior will be perfect ($\epsilon = 0, \rho = 1$), much like the second cavity in section 2.

Each cavity has a total energy which is now equal to the sum of the energy it contains in the photons it encloses and in the phonons which exists in its walls.* In this sense, each cavity is given access to only two possible degrees of freedom: 1) the vibrational/phonon system in its walls and 2) the radiation field.

Since the systems must be in thermal equilibrium, net conduction is forbidden in accordance with the requirements set forth by Max Planck [6, p. 23].

Let us now bring the two cavities together. But this time, before making the small hole, let us remove the adiabatic outer wall from that section of the cavities which come into direct contact. In this manner, thermal conduction can occur between the two cavities, if necessary. Finally, let us make the small hole and permit cavity 1 to transfer a photon into cavity 2 (see Fig. 1C).

Under these conditions, if a photon from cavity 1 enters cavity 2, an identical quantum of energy instantly propagates from the second perfectly reflecting cavity, through conduction and phonon action, into the walls of the first cavity. In a sense, cavity 1 has instantly converted this phonon into the photon it just expelled. As a result, cavity 1 has simply acted as a transformer of energy. It has taken phonon energy from cavity 2, created a photon, and sent energy back into cavity 2. Cavity 1 has not lost any net photons. The total energy of each system does not change and the zeroth law is not violated.

Thus, when a small hole is made between the two enclosures, each cavity eventually becomes filled with blackbody radiation when thermal equilibrium is reestablished. This conclusion has previously been demonstrated mathematically [9] and was recognized long ago in the laboratory. The net result is that no net energy has been exchanged. The temperature does not change, and no laws of thermodynamics have been violated. Yet, for the period of time when photon and phonon transfer was occurring, the entire system fell out of thermal equilibrium, even if temperature equilibrium was being maintained. Eventually however, thermal equilibrium is re-established and both cavities are filled with black radiation.

Over the course of this experiment, something very important has occurred in cavity 2. The energy which this cavity contained has been redistributed amongst its two degrees of freedom. Although the net temperature of cavity 2 has not changed, phonon energy has been lost to the radiation field. This simple observation has consequences in physics, as it signifies that the law of equipartition which characterizes so much of statistical thermodynamics cannot hold. The energy of a system is not necessarily distributed equally between all of its available degrees of freedom.

It could be argued, of course, that a behavior has been demanded from real materials which can never exist. This is a question of how closely physical reality can be modeled. Is it a more grievous error to assume 1) that a perfectly adiabatic cavity can exist, a material which cannot emit photons, cannot sustain conduction in any form, or be associated with any temperature, or 2) that graphite and silver come to represent two 'perfect' examples of emissivity and reflectivity, respectively?

Relative to this question, it is clear that the construction of a perfectly reflecting cavity from an ideally adiabatic wall (Experiment I) constitutes the greater departure from physical reality. Adiabatic surfaces, with their inability to emit any photons and their incapability of sustaining thermal or electrical conduction simply are not approached by anything in nature. It is impossible to state that a truly adiabatic wall is at any given temperature, as temperature in the physical world must be associated with energy content and adiabatic walls contain none. They represent a convenient intellectual concept and offer very little relative to properly modeling physical reality. For this reason, their use results in the finding that all cavities must be filled with blackbody radiation, even if their walls lack the physical ability to emit a single photon. Obviously, a logical conflict has been produced which highlights that our model has deviated too far from physical reality. As a result, it is unlikely that such a model (Experiment I) provides a proper proving ground relative to the validity of Kirchhoff's formulation.

Conversely, it is known that laboratory blackbodies constructed from graphite, or soot (carbon black, lampblack), can reach rather high emissivities over certain frequencies [18–21]. The requirement that these materials can come to have an emissivity of 1 is very close to reality. At the same time, silver can manifest an excellent reflectivity over certain frequencies. Silver surfaces are the best reflectors known. As a result, the assumption that silver can exhibit a reflectivity of 1, is not very far from experimental fact. In this regard,

*For the purpose of this discussion, the energy associated with the electrons in conduction bands, or any other degree of freedom, can be neglected, as these do not provide additional insight into this problem.

it must be concluded that Experiment II constitutes a much better representation of nature. It is known that laboratory blackbodies are always made from near perfect emitters of radiation, like graphite or soot [10, 11]. They are never made of excellent reflectors, such as silver [10, 11].

The silver cavity was initially devoid of any radiation, precisely because it can emit none. It is only when it is placed in contact with a perfectly absorbing cavity, that the energy contained in its vibrational degrees of freedom can be transformed into a radiation field. This directly highlights that Kirchhoff's formulation cannot be correct. We do not find an equal ability to construct blackbody cavities in the laboratory irrespective of the nature of the walls. Silver cavities cannot hold black radiation unless they have been subjected to the action of a perfect absorber [9].

4 Conclusions

When properly analyzed, Gedanken experiments reveal that Kirchhoff's law of the thermal emission cannot be valid. The proper analysis of cavity radiation must be open to realistic treatments of energy balance within real materials. When this is correctly accomplished, cavity radiation becomes absolutely dependent on the nature of the enclosure. Phonon transfer can balance photon transfer. As such, Kirchhoff's law holds no validity, either mathematically, in the experimental setting, or in the context of thought experiments [7–13]. Cavity radiation is not always black, but is absolutely dependent on the nature of the enclosure. As demonstrated in Experiment II, two cavities can be at the same temperature, but not contain identical radiation. The introduction of black radiation into opaque enclosures absolutely depends on the presence, or action, of a perfect emitter. Based on this presentation, the constants of Planck and Boltzmann are not universal [12].

Beyond Kirchhoff's law, the analysis of cavity radiation leads to the conclusion that the equipartition theorem cannot be valid across all systems. The amount of energy associated with a given degree of freedom at temperature equilibrium is not necessarily equal to that contained in all other degrees of freedom. The zeroth law of thermodynamics, by which temperature is defined, is not concerned with radiation fields, but simply temperature equilibrium. If two objects are at the same temperature, they are by definition in thermal equilibrium, provided that their is no net emission, conduction, and convection taking place in the systems of interest.

In Experiment II, a system is initially placed under temperature and thermal equilibrium. It then is allowed to remain under temperature equilibrium, while it temporarily falls out of thermal equilibrium, as the small hole is created to enable the exchange of phonons and photons. At any time, if the two cavities are physically separated and the hole filled, they would immediately regain both temperature and thermal equilibrium. At that point, the second cavity would contain an arbitrary number of photons and not black radiation. It is only if cavity 1 is given sufficient time to act that cavity II will contain black radiation. However, the action of the first cavity was absolutely critical to this transformation. A perfect emitter had to be present. It is not simply a question of time, but of physical action by a perfect emitter.

Experiment II is indicating that it is not necessarily possible to equilibrate the energy contained within the degrees of freedom within real materials. Under these conditions, equipartition cannot hold. Equipartition requires that all degrees of freedom have the same ability to contain energy. This cannot be correct. The most compelling example is illustrated by the hydrogen and hydroxyl bonding systems within water [14]. The force constants in these two systems are drastically different. As a result, the hydrogen bonding system is likely to be filled with energy at temperatures just above absolute zero (~3K). This is the reason, in fact, why the microwave background which surrounds the Earth does not vary in intensity in response to seasonal changes [14]. Equipartition is also invalid in the photosphere, where dramatic differences in the energy content of the translational and vibrational degrees of freedom are likely to exist [22].

Throughout his treatise on heat radiation [6], Max Planck invoked a carbon particle, which he surmised to act as a simple catalyst (see [10] for a detailed review). However, he inserted a perfect emitter into his cavity. This particle could then fill the cavity with black radiation, provided that it was placed in physical contact with the energy source to be converted. It did not matter how much carbon was inserted, as this only governs the time involved. For this reason, when Planck introduced the carbon particle into his cavity [6], it was as if he had lined it completely with carbon [10]. He had not demonstrated that all cavities contained black radiation, only that all perfectly emitting cavities are black.

Acknowledgment

Sylvain Bréchet is recognized for valuable insight relative to phonon transfer during conduction. Luc Robitaille is acknowledged for the preparation of Fig. 1.

The first draft of this work was completed at the home of Professor Lawrence J. Berliner immediately following a discussion which took place at my poster (H1.00227 — The Sun on Trial) during the APS March Meeting. Larry and his wife Barbara are recognized for their unceasing encouragement and for welcoming me into their Denver home.

Dedication

This work is dedicated to my father, Noel Antoine Robitaille (born on December 22, 1929). He devoted his life to the practice of family and emergency medicine, delivering over 800 babies and tending the medical needs of the communities in which he resided, both in Canada and Iowa. He retired on August 30, 2013, at the age of nearly 84, after having, for

many years, served at his small clinic in LaPorte City and making visits to the local nursing home. A few years ago, as he walked with nostalgia in the cemetery of his village, he recalled how so many buried there were once his patients and friends. His daughter-in-law, to help lighten the atmosphere, had inquired: "So Noel, do you think you were a good doctor?"

In February 2014, he passed the 50 year anniversary of receiving the rare privilege, as a white man, to be named an honorary Indian Chief — "Kitchitouagegki". He was the first named by any of the Three First Nations: The Council of Three Fires (Ojibway, Odawa, and Potawatomi). In describing the honor conferred upon him, Allen Toulouse recalled, *"His presence contributed to reducing the infant mortality rate of the Sagamok First Nation (Reducing the number of deaths during pregnancy for both the mothers and their babies). He also made many actions to improve the conditions of the people of Sagamok — including having running water and wells installed in the reserve in the early 1960s"* [23]. It appears that his elevation to Chief represents *"the first official case of a First Nation bestowing this honor upon a Caucasian medical doctor in North-American history"* [23].

Fig. 2: Noel Antoine Robitaille, honorary chief "Kitchitouagegki". Photo courtesy of Allen Toulouse and Christine Robitaille.

Submitted on: March 17, 2014 / Accepted on: March 19, 2014
First published online on: March 19, 2014

References

1. Kirchhoff G. Über das Verhältnis zwischen dem Emissionsvermögen und dem Absorptionsvermögen der Körper fur Wärme und Licht. *Poggendorfs Annalen der Physik und Chemie*, 1860, v. 109, 275–301. (English translation by F. Guthrie: Kirchhoff G. On the relation between the radiating and the absorbing powers of different bodies for light and heat. *Phil. Mag.*, 1860, ser. 4, v. 20, 1–21).
2. Kirchhoff G. Über den Zusammenhang zwischen Emission und Absorption von Licht und Wärme. *Monatsberichte der Akademie der Wissenschaften zu Berlin*, sessions of Dec. 1859, 1860, 783–787.
3. Wien W. Über die Energieverteilung in Emissionspektrum eines schwarzen Körpers. *Ann. Phys.*, 1896, v. 58, 662–669.
4. Stefan J. Über die Beziehung zwischen der Wärmestrahlung und der Temperatur. *Sitzungsberichte der mathematisch naturwissenschaftlichen Classe der kaiserlichen Akademie der Wissenschaften*, Wien 1879, v. 79, 391–428.
5. Planck M. Über das Gesetz der Energieverteilung im Normalspektrum. *Annalen der Physik*, 1901, v. 4, 553–563.
6. Planck M. The theory of heat radiation. P. Blakiston's Son & Co., Philadelphia, PA, 1914.
7. Robitaille P.-M. On the validity of Kirchhoff's law of thermal emission. *IEEE Trans. Plasma Sci.*, 2003, v. 31, no. 6, 1263–1267.
8. Robitaille P.M. Robitaille P. M. L. An analysis of universality in blackbody radiation. *Progr. Phys.*, 2006, v. 2, 22–23; arXiv:physics 0507007.
9. Robitaille P.-M. A critical analysis of universality and Kirchhoff's law: A return to Stewart's law of thermal emission. *Progr. Phys.*, 2008, v. 3, 30–35.
10. Robitaille P.-M. Blackbody radiation and the carbon particle. *Progr. Phys.*, 2008, v. 3, 36–55.
11. Robitaille P.-M. Kirchhoff's law of thermal emission: 150 Years. *Progr. Phys.*, 2009, v. 4, 3–13.
12. Robitaille P.-M. Blackbody radiation and the loss of universality: Implications for Planck's formulation and Boltzmann's constant. *Progr. Phys.*, 2009, v. 4, 14–16.
13. Robitaille P.-M. Further Insight Relative to Cavity Radiation: A Thought Experiment Refuting Kirchhoff's Law. *Progr. Phys.*, 2014, v. 10(1), 38–40.
14. Robitaille P.-M. Water, hydrogen bonding, and the microwave background. *Progr. Phys.*, 2009, v. 2, L5–L8.
15. Robitaille P.-M. Fourty lines of evidence for condensed matter — The Sun on trial: Liquid metallic hydrogen as a solar building block. *Progr. Phys.*, 2013, v. 4, 90–142.
16. Stewart B. An account of some experiments on radiant heat, involving an extension of Prévost's theory of exchanges. *Trans. Royal Soc. Edinburgh*, 1858, v. 22, no. 1, 1–20.
17. Electrical Resistivity of Pure Metals. In, *CRC Handbook of Chemistry and Physics*, 2013–2014, CRC Press, Baca Raton, FL, p. 12–42.
18. Touloukian Y.S., DeWitt D.P. Thermal radiative properties of nonmetallic solids. Vol. 8 in: Thermophysical Properties of Matter, IFI/Plenum, New York, 1972.
19. Burchell T.D. Thermal properties and nuclear energy applications. In: Graphite and Precursors, Gordon and Breach Science Publishers, Amsterdam, The Netherlands, 2001, 87–109.
20. Harris L. The optical properties of metal blacks and carbon blacks. MIT and The Eppley Foundation for Research, Monograph Ser., 1, New Port, R.I., Dec. 1967.
21. Pierson H.O. Handbook of Carbon, Graphite, Diamond and Fullerenes. Noyes Publications, Park Ridge, NJ, 1993, p. 109.
22. Robitaille P.-M. On the Temperature of the Photosphere: Energy Partition in the Sun. *Progr. Phys.*, 2011, v. 3, 89–92.
23. Toulouse A. Sagamok Anishinabek News, Dec. 2013, p. 13. http://issuu.com/sagamok/docs/sagamok_news_december_digital_versi (Accessed online 3/8/2013).

Electrical Conductivity of Metals: A New Look at this Subject

Paulo Roberto Silva

Departmento de Física (Retired Associate Professor), ICEx, Universidade Federal de Minas Gerais, Belo Horizonte, MG, Brazil. E-mail: prsilvafis@gmail.com

Various parameters tied to the electrical conductivity of typical metals are estimated and are expressed in terms of universal constants. It happens that they are close to those found in metallic copper at room temperature. The fact that the realization of the model occurs at room temperature is explained by using the Landauer's erasure principle. The averaged collision time of the electron of conduction is also thought as a particle lifetime. Finally an analogy is established between the motion of the electron of conduction and the cosmological constant problem, where a spherical surface of radius equal to the electron mean free path has been thought as a surface horizon for the charge carriers.

1 Introduction

Highly purified water is a bad electrical conductor. However, the addition of small amounts of sodium chloride (NaCl) to this liquid, can increase its electrical conductivity in a substantial way. At the ambient temperature (295K), the water's dielectric constant of 80, permits the Na+ and Cl- ions to move freely through the liquid and this feature can account for the change in its conductive behavior. It seems that the concentration of free charge carriers has the most relevant role in determining the electrical conductivity of the substances. But what to say about electrical conductivity in metals? Isolated metallic atoms have their inner electrons belonging to closed shells and hence tightly bound to their corresponding atomic nucleus. However the electrons of the outer most shell are weakly bonded to its respective nucleus. When arranged in a crystal lattice structure, the bond weakness of these outer electrons is enhanced due to the interactions among neighbor atoms of the lattice, so that the electrons of conduction are free to travel through the whole crystal. Resistance to their motion is due to the thermal vibrations (phonons) and defects provoked by the presence of impurities and lattice dislocations. In a perfect crystal at zero absolute temperature, these free electrons can be described by using the quantum mechanical formalism of the Bloch waves [1, 2]. The concentration of free electrons plays an important role in the description of the electrical conductivity in metals.

2 Evaluation of typical parameters tied to the electrical conductivity of metals

A possible way to estimate the concentration of conduction electrons in a typical good metal will be next presented. An alternative form to estimate the Casimir force between two parallel uncharged metallic plates separated by a close distance d was developed in reference [3]. There, we considered the cutting of a cubic cavity of edge d in a metallic block. We imagined that the free electrons in metal as a gas of non-relativistic particles confined by the vacuum pressure in the interior of a cubic box of edge equal to d. On the other hand as was pointed out by Jaffe [12], the Casimir force can be calculated without reference to the vacuum fluctuations, and like other observable effects in QED, it vanishes as the fine structure constant α goes to zero.

In reference [3], we treated a non-relativistic Fermi gas confined by the vacuum pressure B and found the relation

$$Bd^3 = \frac{2}{5} E_{av}\,, \tag{1}$$

where E_{av} stands for the average energy of the gas. Meanwhile it is convenient to consider that an equivalent way to treat the problem is by taking in account the electromagnetic interaction through the dependence of the energy levels of the system on the fine structure constant α. We reproduce here some steps of the reasons outlined in reference [3]. One of the simplest models which exhibits energy levels dependence on the fine structure α is the Bohr atom, namely

$$E_n = -\frac{\alpha^2 mc^2}{2n^2} = -\frac{E_1}{n^2}\,. \tag{2}$$

By taking the maximum occupied energy level equal to $\frac{N}{2}$, we get the maximum energy E_M of the system

$$E_M = -\frac{4E_1}{N^2}\,. \tag{3}$$

The average energy could be estimated as

$$E_F = \frac{2}{N}\int_1^{\frac{N}{2}} (-)\, E_1\, n^{-2} dn = \frac{2}{N}\, E_1\, \frac{2-N}{N}\,. \tag{4}$$

In the limit, as $N \gg 1$, we have

$$E_{av} = -\,2\,\frac{E_1}{N}\,. \tag{5}$$

Now let us estimate the vacuum pressure. We have

$$Bd^3 = -\frac{2}{5}\frac{\alpha^2 mc^2}{N} = \frac{2}{5}\, E_{av}\,. \tag{6}$$

By taking $p_0 = \frac{\alpha mc}{2}$ and $\lambda_0 = \frac{h}{p_0} = \frac{2h}{\alpha mc}$, it is possible to make the choice

$$N = \frac{d}{\lambda_0} = \frac{\alpha mcd}{2h}. \quad (7)$$

Inserting equation (7) into equation (6), we obtain

$$B = -\frac{8}{5\pi}\frac{\alpha\pi^2\hbar c}{d^4}. \quad (8)$$

Therefore we notice that by making the choice indicated by equation (7), the explicit dependence of B on the electron mass m and on the maximum quantum number N has disappeared. The alternative way we have used in order to treat the Casimir force problem, permit us to calculate a typical density of charge carriers in good metals. Let us write

$$nd^3 = \frac{4\pi}{3} N^3 3! = 8\pi N^3. \quad (9)$$

In equation (9), we have considered the volume of a sphere in the N-space, and the possible number of permutations among the N_x, N_y and N_z quantum numbers. Putting equation (7) into equation (9) we obtain

$$n = \pi\left(\frac{\alpha mc}{h}\right)^3. \quad (10)$$

Numerical evaluation of equation (10) gives $n = 8.56 \times 10^{28}\,\mathrm{m}^{-3}$, which could be compared with $8.45 \times 10^{28}\,\mathrm{m}^{-3}$, the density of charge carriers in metallic copper [1, 2]. Meanwhile the Fermi energy of metals could be expressed as [1, 4]

$$E_F = \frac{h^2}{8m}\left(\frac{3n}{\pi}\right)^{\frac{2}{3}}. \quad (11)$$

Inserting equation (10) into equation (11), we get

$$E_F = \frac{3^{\frac{2}{3}}}{8}\alpha^2 mc^2. \quad (12)$$

Numerical estimate of equation (12) gives $E_F = 7.07\,\mathrm{eV}$, which naturally is very close to the value found in metallic copper.

In order to proceed further, let us compute the electrical conductivity of a typical good metal. To do this we first suppose that we have n scatters per unit of volume and by considering a prism shaped tube having longitudinal size equal to the electron mean free path ℓ, width ℓ_F equal to half of the Fermi wavelength of the electron, and thickness ℓ_C equal to half of its Compton wavelength. If we consider that the electrical conductivity always happens in a regime of charge neutrality, the number of scatters per unit of volume will be equal to the number density of charge carriers, and we can write

$$n\ell_F\ell_C\ell = n\frac{h}{2mv_F}\frac{h}{2mc}v_F\tau = 1. \quad (13)$$

In equation (13), ℓ_C stands for the wavelength of a photon with a momentum related to the creation of a electron-positron pair and this corresponds to a minimum thickness of the prism, which also implies in a maximum τ, the average time between collisions. From equation (13) we obtain the relation

$$n\tau = \frac{m^2c}{\pi^2\hbar^2}. \quad (14)$$

Now, Drude formula for the electrical conductivity σ is given by (Kittel [1])

$$\sigma = \frac{e^2 n\tau}{m}. \quad (15)$$

Inserting $n\tau$ of equation (14) into equation (15), we obtain

$$\sigma = \frac{e^2 mc}{\pi^2\hbar^2}. \quad (16)$$

Numerical estimate of the electrical resistivity ρ, gives $\rho = \frac{1}{\sigma} = 1.57 \times 10^{-8}\Omega\mathrm{m}$ which can be compared with the resistivity of the metallic copper measured at the temperature of 295 K, namely $\rho_{copper} = 1.70 \times 10^{-8}\Omega\mathrm{m}$. From equation (10) and equation (14) we also obtain the averaged time between collisions

$$\tau = \frac{1}{\alpha^3}\frac{4h}{\pi mc^2}. \quad (17)$$

Numerical estimate of equation (17) gives $\tau = 2.65 \times 10^{-14}\mathrm{s}$. This umber must be compared with the value estimated of $\tau_{copper} = 2.5 \times 10^{-14}\mathrm{s}$, for copper at the room temperature as quoted by Allen [2]. It is also interesting to write formulas for the Fermi velocity v_F and the electron mean free path ℓ. We have

$$v_F = \left(\frac{2E_F}{m}\right)^{\frac{1}{2}} = \frac{3^{\frac{1}{3}}}{2}\alpha c, \quad (18)$$

and

$$\ell = v_F\tau = \frac{3^{\frac{1}{3}}2h}{\alpha^2\pi mc}. \quad (19)$$

These relations for the quantities associated to the electrical conduction in typical metals are exhibited in table 1, as well their respective numerical estimates and are also compared with the corresponding ones quoted for copper at the room temperature.

3 Realization at the room temperature: a possible explanation

It is an intriguing question why a model describing the electrical conductivity of a typical good metal just realizes itself in copper crystals at room temperature. The answer to this question could be elaborated through these reasons.

- As was pointed out by Jacobs [9], Landauer's erasure principle [8] states that: whenever a single bit of information is erased, the entropy in the environment to which the information storing system is connected must increase at least $k_B \ln 2$, where k_B is the Boltzmann's constant;

- A free electron in a metal travels in average a distance equal to its mean free path, with a constant velocity v_F, until to collide with the ionic vibrations (phonons). In the collision process, the free electron looses its memory.

We think that we may associate to the Fermi energy E_F, a string of length equal to its Fermi wavelength, composed by unit cells having a length equal to the Compton wavelength of the electron. Let us to introduce a quasi-particle with a mass-energy μc^2 defined as

$$\mu c^2 = E_F \frac{v_F}{c} . \tag{20}$$

As we can see from equation (20), this quasi-particle has a mass-energy equal to the Fermi energy divided by the number of cells in the string. Defining

$$\Delta F = \Delta U - T\Delta S = \frac{1}{2}\mu c^2 - k_B \ln 2 . \tag{21}$$

And after making the requirement that

$$\Delta F|_{T=T^\star} = 0 , \tag{22}$$

we obtain the relation

$$E_F^3 = \left(k_B T^\star\right)^2 2\,(\ln 2)^2\, mc^2 . \tag{23}$$

Putting $E_F = 7.1\text{eV}$ (table 1) and $mc^2 = 0.511\text{MeV}$ in equation (23) and solving for $k_B T^\star$, we find

$$k_B T^\star = 26\ meV \tag{24}$$

The above number for the characteristic temperature $T^\star$ must be compared with $k_B T_{Room} = 25\,\text{meV}$. Therefore the obtained result for the characteristic temperature given by equation (24) seems to make sense to the fact that the realization of the model for the electrical conductivity of good metals to happen for copper crystals at the room temperature.

4 Three characteristic lenghts and the grow of a polymer chain

In a paper dealing with the cosmological constant problem [6], the time evolution of the universe world line was compared with the growing of a polymer chain by making use of a Flory-like free energy. It is possible to think the electron mean free path as the length of a polymer chain, composed by monomers of size equal to the Compton wavelength of electron. Within this analogy, the radius of gyration of the chain is identified with the Fermi wavelength of electron. We consider as in the de Gennes derivation [7] two contributions for the Flory's free energy. The first term which goes proportional to $\frac{N^2}{R^d}$, corresponds to a repulsive-like monomer-monomer interaction. A second term which comes from an entropic contribution, namely a logarithm of a Gaussian distribution (a signature of a random walk process) goes as $\frac{R^2}{(N\lambda_C)^2}$. We write

$$F = \frac{N^2\lambda_C^d}{R^d} + \frac{R^2}{N\lambda_C^2} , \tag{25}$$

where F is a Flory-like free energy, λ_C is the Compton length, N is the number of monomers in the chain, and d is the space-time dimension. Setting $\ell = N\lambda_C$ and minimizing equation (25) relative to R, we obtain for the radius of gyration R_g the relation

$$R_g = \ell^{\frac{3}{2+d}} \lambda_C^{\frac{d-1}{2+d}} . \tag{26}$$

We identify $R_g(d = 4)$ with the Fermi length of the electron, λ_F. We have

$$\lambda_F = (\ell\lambda_C)^{\frac{1}{2}} . \tag{27}$$

We observe that equation (27) , relating the three characteristics lengths of the problem, agrees with the upper bound to the electron mean free path found in reference [13]. Please see equation (21) of the cited reference. It is worth to notice that the agreement between both calculations occurs just when the radius of gyration is evaluated in the space-time dimension $d = 4$.

5 High temperature behaviour of the collision time

It would be interesting to evaluate a relation expressing the high temperature behavior of the collision time appearing in the Drude formula for the electrical conductivity. By considering a viscous force which depends linearly on the velocity, the power dissipated by this force can be written as

$$\frac{dE}{dt} = -F_{viscous} v = -\frac{1}{\tau} pv . \tag{28}$$

The power dissipated by this viscous force acting on the charge carrier will appear as an increasing in the internal energy of the lattice and we write

$$\frac{dU}{dt} = -\frac{dE}{dt} = \frac{1}{\tau} pv . \tag{29}$$

By taking

$$p = \frac{\hbar}{2R} \text{ and } vdt = dR , \tag{30}$$

where the first relation in equation (30) comes from the uncertainty principle, we get

$$dU = \frac{\hbar}{2\tau}\frac{dR}{R} . \tag{31}$$

Performing the integration of equation (31) between the limits $R_0 = \frac{\hbar}{mc}$ and $R_1 = \frac{\hbar}{mv_F}$, we obtain

$$\Delta U = \frac{\hbar}{2\tau} \ln \frac{c}{v_F} . \tag{32}$$

Now, let us consider an entropy variation given by

$$\Delta S = k_B \ln 2^D = D k_B \ln 2 . \tag{33}$$

In equation (33), we have written an entropy variation similar to that considered in applying the Landauer's erasure principle [8], but here putting $D = 4$, by taking in account the four dimensions of the space-time. Taking the extremum of the free energy, namely writing

$$\Delta F = \Delta U - T\Delta S = 0\,, \tag{34}$$

and solving for τ, we have

$$\tau = \frac{\hbar}{8k_BT}\ln\frac{c}{v_F}\,. \tag{35}$$

In the case of copper $\left(v_F = 1.57\times10^6\mathrm{m\ s^{-1}}\right)$ at the room temperature ($T = 300\,\mathrm{K}$), we find

$$\tau_{copper}\,(300\,\mathrm{K}) = 2.4\times10^{-14}\mathrm{s}. \tag{36}$$

As we can see in table 1, the result of equation (36) is very close to the room temperature mean collision time of the electrons of conduction in copper, as quoted in the literature.

6 Average collision time as a particle lifetime

There are two characteristics linear momenta that we can associate to the free electrons responsible for the electrical conductivity in good metals. They are: the Fermi momentum mv_F and the Compton momentum mc. By taking into account that the free electron has a fermionic character, we will write a non-linear Dirac-like equation describing the "motion" of this particle. We have

$$\frac{\partial\Psi}{\partial x} - \frac{1}{c}\frac{\partial\Psi}{\partial t} = \frac{mv_F}{\hbar}\Psi - \frac{mc}{\hbar}\left|\Psi^\star\Psi\right|\Psi\,. \tag{37}$$

We see that equation (37) contains only first order derivatives of the field Ψ. Besides this, the field Ψ has not a spinorial character. Making the two sides of equation (37) equal to zero and solving for $|\Psi^\star\Psi|$, we get

$$\left|\Psi^\star\Psi\right| = \frac{v_F}{c} = \frac{3^{\frac{1}{3}}}{2}\,\alpha\,. \tag{38}$$

In obtaining equation (38), we also used the result for v_F shown in table 1. On the other hand in the collision process, the free electron loss its memory. We may think that this feature looks similar to the annihilation of a particle- antiparticle pair, each of mass-energy equal to E_F. Putting this thing in a form of the uncertainty principle yields

$$2E_F\Delta t = \frac{h}{2} \quad\text{or}\quad \frac{h\nu}{2} = 2E_F\,. \tag{39}$$

Solving equation (39) for ν, we get

$$\nu = \frac{1}{\Delta t} = 4\frac{E_F}{h} = \frac{3^{\frac{2}{3}}}{2h}\alpha^2mc^2. \tag{40}$$

By combining the results of equation (38) and equation(40) we obtain the line width Γ tied to the "particle" decay

$$\Gamma = \nu\left|\Psi^\star\Psi\right| = \frac{3}{4h}\,\alpha^3mc^2\,. \tag{41}$$

Finally the "particle" lifetime τ is given by

$$\tau = \frac{1}{\Gamma} = \frac{4h}{3\alpha^3mc^2}\,. \tag{42}$$

Comparing τ giving by equation (42) with the time between collisions shown in table 1, we verify that the present result displays the number 3 in the denominator, instead of the number π which appears in table 1.

Table 1: Formulas related to the electrical conductivity of typical metals, in terms of universal constants (this work). Numerical estimates of them are compared with those quoted for Copper at room temperature.

Formula	Numerical estimates	Copper at room temperatures
$n = \pi\left(\frac{\alpha mc}{h}\right)^3$	$8.56\times10^{28}\,\mathrm{m^{-3}}$	$8.45\times10^{28}\,\mathrm{m^{-3}}$ [1,2]
$E_F = \frac{3^{\frac{2}{3}}}{8}\,\alpha^2mc^2$	7.07 eV	7.0 eV [1]
$\rho = \frac{1}{\sigma} = \frac{\pi^2\hbar^2}{e^2mc}$	$1.57\times10^{-8}\,\Omega\mathrm{m}$	$1.70\times10^{-8}\,\Omega\mathrm{m}$ [1,2]
$\tau = \frac{1}{\alpha^3}\frac{4h}{\pi mc^2}$	$2.65\times10^{-14}\,\mathrm{s}$	$2.5\times10^{-14}\,\mathrm{s}$ [2,5]
$v_F = \frac{3^{\frac{1}{3}}}{2}\,\alpha c$	$1.6\times10^6\,\mathrm{m\ s^{-1}}$	$1.6\times10^6\,\mathrm{m\ s^{-1}}$ [1]
$\ell = \frac{3^{\frac{1}{3}}2h}{\alpha^2\pi mc}$	419Å	400Å [5]

7 Analogy with the cosmological constant problem

In this section we assume, for simplicity, that $\hbar = c = k_B = 1$. One worth point we can consider now is the analogy that can be made with the cosmological constant problem. Hsu and Zee [10] have proposed an effective action A_{eff} as a means to deal with the cosmological constant problem. They wrote

$$A_{eff} = -\left(\Lambda L^4 + \frac{M_P^4}{\Lambda}\right) + \text{independent of }\Lambda\text{-terms}, \tag{43}$$

where M_P is the Planck mass, L is the radius of the event horizon of the universe and Λ is the cosmological constant. Taking the extremum of this action they got

$$\Lambda = \left(\frac{M_P}{L}\right)^2. \tag{44}$$

We could think A_{eff} above as a four-dimensional representation of a kind of free energy, where the first term plays the role of the internal energy and the second one is related to the entropy S. The absolute temperature is taken to be equal to one. We propose that

$$\Omega \sim \exp\left(\frac{M_P^4}{\Lambda}\right) \tag{45}$$

with

$$S = \ln \Omega. \tag{46}$$

On the other hand, there is a proposal [11] that the universe can be considered as a black hole with its entropy being evaluated by counting the number of cells contained in the area of its event horizon (the holographic principle), namely

$$S_{universe} \sim \left(\frac{L}{L_P}\right)^2 = L^2 M_P^2 . \tag{47}$$

By considering the two equivalent ways of the entropy evaluation, from equation (46) and equation (47) relations, we can write

$$L^2 M_P^2 = \frac{M_P^4}{\Lambda}, \tag{48}$$

which reproduces the results of Hsu and Zee [10], please see equation (44). Turning to the problem of the electrical conductivity in good metals, let us consider for instance in a copper crystal an electron of the conduction band which just suffered a collision. In the absence of an external electric field, all the directions in the space have equal probability to be chosen in a starting new free flight. Therefore if we take a sphere centered at the point where the electron has been scattered, with a radius equal to the electron mean free path, the surface of this sphere may be considered as an event horizon for the phenomena. Any electron starting from this center will be on average scattered when striking the event horizon, loosing the memory of its previous free flight. Besides this, all the lattice sites of the metallic crystal are treated on equal footing, due to the translational symmetry of the system. Based on the previous discussion and inspired on the black hole physics, let us to define the entropy related on the event horizon for the electron of conduction in metals. We write

$$S_{Metal} = \pi \left(\frac{\ell}{w}\right)^2, \tag{49}$$

where ℓ is the electron mean free path and w is the equivalent to the Planck length of the problem. It is possible to write an action analogous to that of Hsu and Zee [10], in order to describe the electrical conductivity in metals. We have

$$A_{Metal} \sim \left(\Lambda_M \ell^4 + \frac{1}{\Lambda w^4}\right). \tag{50}$$

Making the equality between the two ways of writing the entropy, namely equaling the entropy of a surface horizon of radius ℓ and ultra-violet cutoff w with the last term of equation(50), we get

$$\pi \left(\frac{\ell}{w}\right)^2 = \frac{1}{\Lambda_M w^4}, \tag{51}$$

which leads to

$$\Lambda_M^{\left(-\frac{1}{4}\right)} = \pi^{\frac{1}{4}} (\ell w)^{\frac{1}{2}}. \tag{52}$$

Upon to identify $\Lambda_M^{\left(-\frac{1}{4}\right)}$ with the Fermi wavelength of the electron λ_F and w with its Compton wavelength λ_C, we obtain

$$\lambda_F = \pi^{\frac{1}{4}} (\ell \lambda_C)^{\frac{1}{2}}. \tag{53}$$

Relation (53) must be compared with equation (27).

Submitted on March 14, 2014 / Accepted on March 17, 2014

References

1. Kittel C. Introduction to Solid State Physics. 5th Ed, Wiley, 1976, Chapter 6.
2. Allen P.B. Electrical Conductivity. *The Physics Teacher*, v. 17(6), September 1979, 362–366.
3. Silva P.R. Casimir force: an alternative treatment. arXiv: 0901.0908.
4. Tipler P.A. Modern Physics. Worth Pub. Inc., New York, 1978, Chapter 9.
5. Halliday D. et al. Fundamentals of Physics, 3th Edition, Extended Version, Wiley, 1988, Chapter 28.
6. Silva P.R. Cosmological constant and polymer physics. *Braz. J. Phys.*, 2008, v. 38, 587–590; arXiv: 0812.4007.
7. de Gennes P-G. Scaling Concepts in Polymer Physics. Cornell University Press, 1979, Chapter 1.
8. Landauer R. *IBM J. Res. Develop.*, 1961, v. 5, 183.
9. Jacobs K. arXiv: quant-ph/0512105.
10. Hsu S. and Zee A. arXiv: hep-ph/0406142.
11. Susskind L. The world as a hologram. arXiv: hep-th/9409089.
12. Jaffe R.L. *Phys. Rev. D*, 2005, v. 72, 021301.
13. Silva P.R. et al. Quantum conductance and electric resistivity. *Phys. Lett. A*, 2006, v. 358, 358–362.

LETTERS TO PROGRESS IN PHYSICS

On the Equation which Governs Cavity Radiation

Pierre-Marie Robitaille

Department of Radiology, The Ohio State University, 395 W. 12th Ave, Columbus, Ohio 43210, USA
E-mail: robitaille.1@osu.edu

In this work, the equation which properly governs cavity radiation is presented. Given thermal equilibrium, the radiation contained within an arbitrary cavity depends upon the nature of its walls, in addition to its temperature and its frequency of observation. With this realization, the universality of cavity radiation collapses. The constants of Planck and Boltzmann can no longer be viewed as universal.

Science enhances the moral value of life, because it furthers a love of truth and reverence...

Max Planck, Where is Science Going? 1932 [1]

When Max Planck formulated his law [2, 3], he insisted that cavity radiation must always be black or normal [3, Eqs. 27, 42], as first proposed by Gustav Robert Kirchhoff [4, 5]. The laws of thermal emission [2–7] were considered universal in nature. Based on Kirchhoff's law [4, 5], cavity radiation was said to be independent of the nature of the walls and determined solely by temperature and frequency. Provided that the cavity walls were opaque, the radiation which it contained was always of the same nature [2–5]. All cavities, even those made from arbitrary materials, were endowed with this property.

Cavity radiation gained an almost mystical quality and Planck subsequently insisted that his equation had overarching consequences throughout physics. The constants contained within his formulation, those of Planck and Boltzmann (h and k), became fundamental to all of physics, leading to the development of Planck length, Planck mass, Planck time, and Planck temperature [3, p. 175].

However, it can be demonstrated that cavity radiation is not universal, but depends on the nature of the cavity itself [8–15]. As such, the proper equation governing cavity radiation is hereby presented.

It is appropriate to begin this treatment by considering Kirchhoff's law [3, Eqs. 27, 42]:

$$\frac{\epsilon_\nu}{\kappa_\nu} = f(T, \nu)\,, \tag{1}$$

where $f(T, \nu)$ is the function presented by Max Planck [3, Eq. 300].* In order to avoid confusion, Eq. 1 can be expressed by using the currently accepted symbols for emissive power, E, and absorptivity, κ_ν:

$$\frac{E_\nu}{\kappa_\nu} = f(T, \nu)\,. \tag{2}$$

As Eq. 1 was hypothesized to be applicable to all cavities, we can adopt the limits of two extremes, namely the "perfect absorber" and the "perfect reflector".†

First, the condition under which Kirchhoff's law is often presented, the "perfectly absorbing" cavity, can be considered (emissivity $(\epsilon_\nu) = 1$, absorptivity $(\kappa_\nu) = 1$, reflectivity $(\rho_\nu) = 0$; at the frequency of interest, ν). In setting κ_ν to 1, it is apparent that the mathematical form of the Eq. 1 remains valid. Second, if a "perfectly reflecting" cavity is utilized ($\epsilon_\nu = 0$, $\kappa_\nu = 0$, $\rho_\nu = 1$), it is immediately observed that, in setting κ_ν to 0, Eqs. 1 and 2 become undefined. Max Planck also recognized this problem, but chose to ignore its consequences (see § 48, 49). Yet, this simple mathematical test indicates that arbitrary cavities cannot be black, as Kirchhoff's law cannot be valid over all conditions.

It is also possible to invoke Stewart's law of thermal emission [16] which states that, under conditions of thermal equilibrium, the emissivity and absorptivity are equal:

$$\epsilon_\nu = \kappa_\nu\,. \tag{3}$$

Therefore, Eq. 2 can be expressed as follows:

$$E_\nu = \epsilon_\nu \cdot f(T, \nu)\,. \tag{4}$$

Once again, this expression never states that all cavities contain black radiation. Rather, at thermal equilibrium, cavities contain raditation which will be reduced in intensity from the Planck function by an amount which manifests the lower

*Note that Max Planck refers to ϵ_ν as the "emissionskoeffizienten" [3, §26], which M. Masius translates as the "coefficient of emission". Today, the emission coefficient is also known as the emissivity of a material. Unfortunately, it is also referred to by the symbol ϵ_ν and this can lead to unintended errors in addressing the law of emission. In Eq. 1, dimentional analysis (see [3, Eq. 300]) reveals that Max Planck is referring to the emissive power, denoted by E, and not to emissivity, usually denoted by ϵ_ν. Still, at other points within "The Theory of Heat Radiation" (e.g. see §49) he utilizes the symbol, E, to refer to emissive power or "the radiation emitted". To further complicate the question, in his Eq. 27, Max Planck refers to κ_ν as the "absorptionskoeffizienten" which M. Masius translates at the "coefficient of absorption". In this case, dimentional analysis reveals that he is indeed referring to absortivity, κ_ν, and not to the absorptive power, A, of the medium.

†Perfectly absorbing or reflecting cavities do not exist in nature. Nonetheless, they are hypothesized to exist in mathematical treatments of blackbody radiation (see [3]).

emissivity of the material involved. It is evident that a lower emissivity is tied to a higher reflectivity, but the effect of reflection has not been properly included in Kirchhoff's law.

For any material, the sum of the emissivity and reflectivity is always equal to 1. This constitutes another formulation of Stewart's law [10, 16] which can also be expressed in terms of emissivity or absorptivity:

$$\epsilon_\nu + \rho_\nu = \kappa_\nu + \rho_\nu = 1\,. \tag{5}$$

With simple rearrangement, it is well known that absorptivity, κ_ν, and emissivity, ϵ_ν, can be expressed as:

$$\epsilon_\nu = \kappa_\nu = 1 - \rho_\nu. \tag{6}$$

As such, let us substitute these relations into Eq. 2:

$$\frac{E_\nu}{(1-\rho_\nu)} = f(T,\nu)\,. \tag{7}$$

With simple rearrangement, the law for arbitrary cavity radiation under conditions of thermal equilibrium, arises:

$$E_\nu = f(T,\nu) - \rho_\nu \cdot f(T,\nu)\,. \tag{8}$$

This law is now properly dependent on the nature of the cavity walls, because it includes the reflectivity observed in real materials.

Note that this expression is well known. Planck, for instance, presents it in a slightly modified form [3, § 49]. However, he choses to dismiss its consequences. Still, it is evident that when a cavity is constructed from a material which is "perfectly absorbing", the second term in Eq. 8 makes no contribution ($\rho_\nu \cdot f(T,\nu) = 0$) and the emissive power is simply determined by the Planck function. If the cavity walls are "perfectly reflecting", Eq. 8, unlike Eq. 1 and 2, does not become undefined, but rather, equal to 0. For all other situations, the radiation contained within a cavity will be dependent on the manner in which the reflection term is driven. This will be discussed seperately.

Dedication

This work is dedicated to our mothers on whose knees we learn the most important lesson: love.

Submitted on: March 25, 2014 / Accepted on: March 26, 2014
First published online on: March 26, 2014 / Revised on: December 26, 2014

References

1. Planck M. The new science — 3 complete works: Where is science going? The universe in the light of modern physics; The philosophy of physics. [Translated from the German by James Murphy and W.H. Johnston], Meridian Books, New York, 1959.
2. Planck M. Über das Gesetz der Energieverteilung im Normalspektrum. *Annalen der Physik*, 1901, v. 4, 553–563.
3. Planck M. The theory of heat radiation. P. Blakiston's Son & Co., Philadelphia, PA, 1914; (Available in English and German within "The History of Modern Physics: 1800–1950", (G. Holton et al., Eds), V. 11, The American Institute of Physics, 1988).
4. Kirchhoff G. Über das Verhältnis zwischen dem Emissionsvermögen und dem Absorptionsvermogen. der Körper fur Wärme und Licht. *Poggendorfs Annalen der Physik und Chemie*, 1860, v. 109, 275–301. (English translation by F. Guthrie: Kirchhoff G. On the relation between the radiating and the absorbing powers of different bodies for light and heat. *Phil. Mag.*, 1860, ser. 4, v. 20, 1–21).
5. Kirchhoff G. Über den Zusammenhang zwischen Emission und Absorption von Licht und. Wärme. *Monatsberichte der Akademie der Wissenschaften zu Berlin*, sessions of Dec. 1859, 1860, 783–787.
6. Wien W. Über die Energieverteilung in Emissionspektrum eines schwarzen Körpers. *Ann. Phys.*, 1896, v. 58, 662–669.
7. Stefan J. Über die Beziehung zwischen der Warmestrahlung und der Temperature. *Sitzungsberichte der mathematischnatur Wissenschaftlichen Classe der kaiserlichen Akademie der Wissenschaften*, Wien 1879, v. 79, 391–428.
8. Robitaille P.-M. On the validity of Kirchhoff's law of thermal emission. *IEEE Trans. Plasma Sci.*, 2003, v. 31, no. 6, 1263–1267.
9. Robitaille P.M. Robitaille P. M. L. An analysis of universality in blackbody radiation. *Progr. Phys.*, 2006, v. 2, 22–23; arXiv: physics 0507007.
10. Robitaille P.-M. A critical analysis of universality and Kirchhoff's law: A return to Stewart's law of thermal emission. *Progr. Phys.*, 2008, v. 3, 30–35.
11. Robitaille P.-M. Blackbody radiation and the carbon particle. *Progr. Phys.*, 2008, v. 3, 36–55.
12. Robitaille P.-M. Kirchhoff's law of thermal emission: 150 Years. *Progr. Phys.*, 2009, v. 4, 3–13.
13. Robitaille P.-M. Blackbody radiation and the loss of universality: Implications for Planck's formulation and Boltzmann's constant. *Progr. Phys.*, 2009, v. 4, 14–16.
14. Robitaille P.-M. Further Insight Relative to Cavity Radiation: A Thought Experiment Refuting Kirchhoff's Law. *Progr. Phys.*, 2014, v. 10(1), 38–40.
15. Robitaille P.-M. Further Insight Relative to Cavity Radiation II: Gedanken Experiments and Kirchhoff's Law. *Progr. Phys.*, 2014, v. 10(2), 116–120.
16. Stewart B. An account of some experiments on radiant heat, involving an extension of Prévost's theory of exchanges. *Trans. Royal Soc. Edinburgh*, 1858, v. 22, no. 1, 1–20.

The Journal on Advanced Studies in Theoretical and Experimental Physics, including Related Themes from Mathematics

PROGRESS IN PHYSICS

A quarterly issue scientific journal, registered with the Library of Congress (DC, USA). This journal is peer reviewed and included in the abstracting and indexing coverage of: Mathematical Reviews and MathSciNet (AMS, USA), DOAJ of Lund University (Sweden), Zentralblatt MATH (Germany), Scientific Commons of the University of St. Gallen (Switzerland), Open-J-Gate (India), Referativnyi Zhurnal VINITI (Russia), etc.

Electronic version of this journal:
http://www.ptep-online.com

Postal Address

Department of Mathematics and Science,
University of New Mexico,
705 Gurley Ave., Gallup, NM 87301, USA

ISSN: 1555-5534 (print)
ISSN: 1555-5615 (online)

Standard Address Number: 297-5092
Printed in the United States of America

July 2014 **Vol. 10, Issue 3**

CONTENTS

Information for Authors and Subscribers

Progress in Physics has been created for publications on advanced studies in theoretical and experimental physics, including related themes from mathematics and astronomy. All submitted papers should be professional, in good English, containing a brief review of a problem and obtained results.

All submissions should be designed in LaTeX format using *Progress in Physics* template. This template can be downloaded from *Progress in Physics* home page http://www.ptep-online.com. Abstract and the necessary information about author(s) should be included into the papers. To submit a paper, mail the file(s) to the Editor-in-Chief.

All submitted papers should be as brief as possible. We accept brief papers, no larger than 8 typeset journal pages. Short articles are preferable. Large papers can be considered in exceptional cases to the section *Special Reports* intended for such publications in the journal. Letters related to the publications in the journal or to the events among the science community can be applied to the section *Letters to Progress in Physics*.

All that has been accepted for the online issue of *Progress in Physics* is printed in the paper version of the journal. To order printed issues, contact the Editors.

This journal is non-commercial, academic edition. It is printed from private donations. (Look for the current author fee in the online version of the journal.)

Gravitational Wave Experiments with Zener Diode Quantum Detectors: Fractal Dynamical Space and Universe Expansion with Inflation Epoch

Reginald T. Cahill

School of Chemical and Physical Sciences, Flinders University, Adelaide 5001, Australia.

The discovery that the electron current fluctuations through Zener diode *pn* junctions in reverse bias mode, which arise via quantum barrier tunnelling, are completely driven by space fluctuations, has revolutionized the detection and characterization of gravitational waves, which are space fluctuations, and also has revolutionized the interpretation of probabilities in the quantum theory. Here we report new data from the very simple and cheap table-top gravitational wave experiment using Zener diode detectors, and reveal the implications for the nature of space and time, and for the quantum theory of "matter", and the emergence of the "classical world" as space-induced wave function localization. The dynamical space possesses an intrinsic inflation epoch with associated fractal turbulence: gravitational waves, perhaps as observed by the BICEP2 experiment in the Antarctica.

1 Introduction

Physics, from the earliest days, has missed the existence of space as a dynamical and structured process, and instead took the path of assuming space to be a geometrical entity. This failure was reinforced by the supposed failure of the earliest experiment designed to detect such structure by means of light speed anisotropy: the 1887 Michelson-Morley experiment [1]. Based upon this so-called "null" experiment the geometrical modelling of space was extended to the spacetime geometrical model. However in 2002 [2, 3] it was discovered that this experiment was never "null": Michelson had assumed Newtonian physics in calibrating the interferometer, and a re-analysis of that calibration using neo-Lorentz relativity [4] revealed that the Newtonian calibration overestimated the sensitivity of the detector by nearly a factor of 2000, and the observational data actually indicated an anisotropy speed up to ±550 km/s, depending of direction. The spacetime model of course required that there be no anisotropy [4]. The key result of the neo-Lorentz relativity analysis was the discovery that the Michelson interferometer had a design flaw that had gone unrecognized until 2002, namely that the detector had zero sensitivity to light speed anisotropy, unless operated with a dielectric present in the light paths. Most of the more recent "confirmations" of the putative null effect employed versions of the Michelson interferometer in vacuum mode: vacuum resonant cavities, such as [5].

The experimental detections of light speed anisotropy, via a variety of experimental techniques over 125 years, shows that light speed anisotropy detections were always associated with significant turbulence/fluctuation wave effects [6, 7]. Repeated experiments and observations are the hallmark of science. These techniques included: gas-mode Michelson interferometers, RF EM Speeds in Coaxial Cable, Optical Fiber Michelson Interferometer, Optical Fiber / RF Coaxial Cables, Earth Spacecraft Flyby RF Doppler Shifts and 1st Order Dual RF Coaxial Cables. These all use classical phenomena.

However in 2013 the first direct detection of flowing space was made possible by the discovery of the Nanotechnology Zener Diode Quantum Detector effect [8]. This uses waveform correlations between electron barrier quantum tunnelling current fluctuations in spatially separated reverse-biased Zener diodes: gravitational waves. The first experiments discovered this effect in correlations between detectors in Australia and the UK, which revealed the average anisotropy vector to be 512 km/s, RA=5.3 hrs, Dec=81°S (direction of Earth through space) on January 1, 2013, in excellent agreement with earlier experiments, particularly the Spacecraft Earth-Flyby RF Doppler Shifts [9].

Here we elaborate the very simple and cheap table-top gravitational wave experiments using Zener diode detectors, and reveal the implications for the nature of space and time, and for the quantum theory of "matter", and the emergence of the "classical world" as space-induced wave function localization. As well we note the intrinsic inflation epoch of the dynamical 3-space theory, which arises from the same dynamical term responsible for bore hole g anomalies, flat spiral galaxy rotation plots, black holes and cosmic filaments. This reveals the emerging physics of a unified theory of space, gravity and the quantum [10].

2 Quantum gravitational wave detectors

The Zener diode quantum detector for gravitational waves is shown in Fig. 1. Experiments reveal that the electron current fluctuations are solely caused by space fluctuations [8]. Fig. 5, top, shows the highly correlated currents of two almost collocated Zener diodes. The usual interpretations of quantum theory, see below, claim that these current fluctuations should be completely random, and so uncorrelated, with the randomness intrinsic to each diode. Hence the Zener diode experiments falsifies that claim. With these correlations the detector S/N ratio is then easily increased by using diodes in parallel, as shown in Fig. 1. The source of the "noise" is,

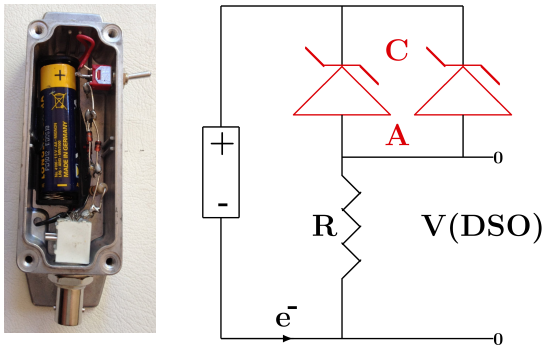

Fig. 1: Right: Circuit of Zener Diode Gravitational Wave Detector, showing 1.5V AA battery, two 1N4728A Zener diodes operating in reverse bias mode, and having a Zener voltage of 3.3V, and resistor R= 10KΩ. Voltage V across resistor is measured and used to determine the space driven fluctuating tunnelling current through the Zener diodes. Correlated currents from two collocated detectors are shown in Fig. 5. Left: Photo of detector with 5 Zener diodes in parallel. Increasing the number of diodes increases the S/N ratio, as the V measuring device will produce some noise. Doing so demonstrates that collocated diodes produce in-phase current fluctuations, as shown in Fig. 5, top, contrary to the usual interpretation of probabilities in quantum theory.

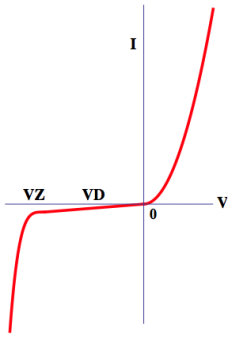

Fig. 2: Current-Voltage (IV) characteristics for a Zener Diode. $VZ = -3.3V$ is the Zener voltage, and $VD \approx -1.5V$ is the operating voltage for the diode in Fig. 1. $V > 0$ is the forward bias region, and $V < 0$ is the reverse bias region. The current near VD is very small and occurs only because of wave function quantum tunnelling through the potential barrier, as shown in Fig. 3.

in part, space induced fluctuations in the DSO that measures the very small voltages. When the two detectors are separated by 25 cm, and with the detector axis aligned with the South Celestial Pole, as shown in Fig. 4, the resulting current fluctuations are shown in Fig. 5, bottom, revealing that the N detector current fluctuations are delayed by $\sim 0.5\ \mu$s relative to the S detector.

The travel time delay $\tau(t)$ was determined by computing the correlation function between the two detector voltages

$$C(\tau, t) = \int_{t-T}^{t+T} dt'\, S_1(t' - \tau/2)\, S_2(t' + \tau/2)\, e^{-a(t'-t)^2}. \quad (1)$$

The fluctuations in Fig. 5 show considerable structure at the μs time scale (higher frequencies have been filtered out by the DSO). Such fluctuations are seen at all time scales, see [11], and suggest that the passing space has a fractal structure, illustrated in Fig. 7. The measurement of the speed of passing space is now elegantly and simply measured by this very simple and cheap table-top experiment. As discussed below those fluctuations in velocity are gravitational waves, but not with the characteristics usually assumed, and not detected despite enormous effects. At very low frequencies the data from Zener diode detectors and from resonant bar detectors reveal sharp resonant frequencies known from seismology to be the same as the Earth vibration frequencies [12–14]. We shall now explore the implications for quantum and space theories.

3 Zener diodes detect dynamical space

The generalized Schrödinger equation [15]

$$i\hbar \frac{\partial \psi(\boldsymbol{r}, t)}{\partial t} = -\frac{\hbar^2}{2m} \nabla^2 \psi(\boldsymbol{r}, t) + V(\boldsymbol{r}, t)\, \psi(\boldsymbol{r}, t) - \\ - i\hbar \left(\boldsymbol{v}(\boldsymbol{r}, t) \cdot \nabla + \frac{1}{2} \nabla \cdot v(\boldsymbol{r}, t) \right) \psi(\boldsymbol{r}, t) \quad (2)$$

models "quantum matter" as a purely wave phenomenon. Here $\boldsymbol{v}(\boldsymbol{r}, t)$ is the velocity field describing the dynamical space at a classical field level, and the coordinates $\boldsymbol{r}$ give the relative location of $\psi(\boldsymbol{r}, t)$ and $\boldsymbol{v}(\boldsymbol{r}, t)$, relative to a Euclidean embedding space, also used by an observer to locate structures. At sufficiently small distance scales that embedding and the velocity description is conjectured to be not possible, as then the dynamical space requires an indeterminate dimension embedding space, being possibly a quantum foam [10]. This minimal generalization of the original Schrödinger equation arises from the replacement $\partial/\partial t \to \partial/\partial t + \boldsymbol{v}.\nabla$, which ensures that the quantum system properties are determined by the dynamical space, and not by the embedding coordinate system, which is arbitrary. The same replacement is also to be implemented in the original Maxwell equations, yielding that the speed of light is constant only with respect to the local dynamical space, as observed, and which results in lensing from stars and black holes. The extra $\nabla \cdot \boldsymbol{v}$ term in (2) is required to make the hamiltonian in (2) hermitian. Essentially the existence of the dynamical space in all theories has been missing. The dynamical theory of space itself is briefly reviewed below.

A significant effect follows from (2), namely the emergence of gravity as a quantum effect: a wave packet analysis shows that the acceleration of a wave packet, due to the space terms alone (when $V(\boldsymbol{r}, t) = 0$), given by $\boldsymbol{g} = d^2<\boldsymbol{r}>/dt^2$ [15]

$$\boldsymbol{g}(\boldsymbol{r}, t) = \frac{\partial \boldsymbol{v}}{\partial t} + (\boldsymbol{v} \cdot \nabla)\, \boldsymbol{v}. \quad (3)$$

That derivation showed that the acceleration is independent

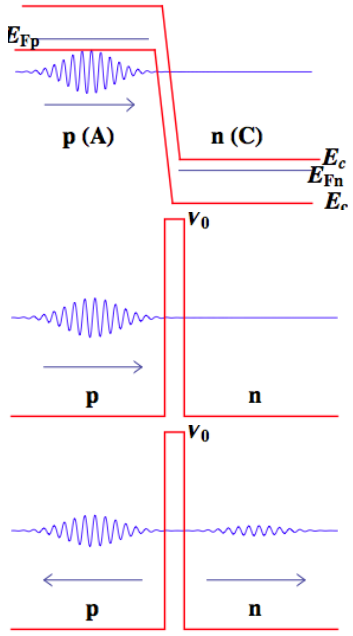

Fig. 3: Top: Electron before tunnelling, in reverse biased Zener diode, from valence band in doped p semiconductor, with hole states available, to conduction band of doped n semiconductor. A and C refer to anode and cathode labelling in Fig. 1. E_c is bottom of conduction bands, and E_v is top of valence bands. E_{Fp} and E_{Fn} are Fermi levels. There are no states available in the depletion region. Middle: Schematic for electron wave packet incident on idealized effective interband barrier in a pn junction, with electrons tunnelling A to C, appropriate to reverse bias operation. Bottom: Reflected and transmitted wave packets after interaction with barrier. Energy of wave packet is less than potential barrier height V_0. The wave function transmission fluctuations and collapse to one side or the other after barrier tunnelling is now experimentally demonstrated to be caused by passing space fluctuations.

of the mass m: whence we have the first derivation of the Weak Equivalence Principle, discovered experimentally by Galileo. The necessary coupling of quantum systems to the fractal dynamical space also implies the generation of masses, as now the waves are not propagating through a structureless Euclidean geometrical space: this may provide a dynamical mechanism for the Higgs phenomenology.

4 Quantum tunnelling fluctuations

It is possible to understand the space driven Zener diode reverse-bias-mode current fluctuations. The operating voltage and energy levels for the electrons at the pn junction are shown schematically in Figs.2 and 3. For simplicity consider wave packet solutions to (2) applicable to the situation in Fig. 3, using a complete set of plane waves,

$$\psi(\boldsymbol{r},t) = \int d^3\boldsymbol{k}\, d\omega\, \psi(\boldsymbol{k},\omega)\, \exp(i\boldsymbol{k}\cdot\boldsymbol{r} - i\omega t). \qquad (4)$$

Then the space term contributes the term $\hbar\boldsymbol{v}\cdot\boldsymbol{k}$ to the equations for $\psi(\boldsymbol{k},\omega)$, assuming we can approximate $\boldsymbol{v}(\boldsymbol{r},t)$ by a constant over a short distance and interval of time. Here $\boldsymbol{k}$ are wave numbers appropriate to the electrons. However the same analysis should also be applied to the diode, considered as a single massive quantum system, giving an energy shift $\hbar\boldsymbol{v}\cdot\boldsymbol{K}$, where $\boldsymbol{K}$ is the much larger wavenumber for the diode. Effectively then the major effect of space is that the barrier potential energy is shifted: $V_0 \to V_0 + \hbar\boldsymbol{v}\cdot\boldsymbol{K}$. This then changes the barrier quantum tunnelling amplitude, $T(V_0 - E) \to T(V_0 + \hbar\boldsymbol{v}\cdot\boldsymbol{K} - E)$, where E is the energy of the electron, and this amplitude will then be very sensitive to fluctuations in $\boldsymbol{v}$.

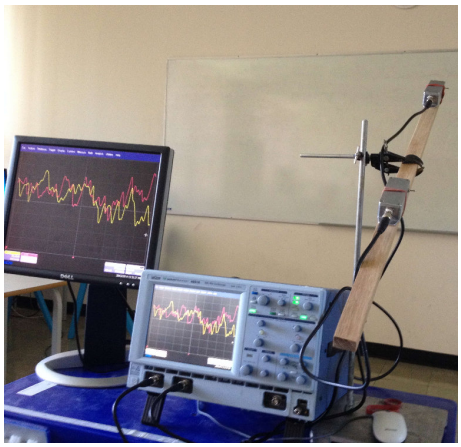

Fig. 4: Zener diode gravitational wave detector, showing the two detectors orientated towards south celestial pole, with a separation of 50cm. The data reported herein used a 25cm separation. The DSO is a LeCroy Waverunner 6000A. The monitor is for lecture demonstrations of gravitational wave measurements of speed and direction, from time delay of waveforms from S to N detectors.

Quantum theory accurately predicts the transition amplitude $T(V_0 - E)$, with $|T|^2 i$ giving the average electron current, where i is the incident current at the pn junction. However quantum theory contains no randomness or probabilities: the original Schrödinger equation is purely deterministic: probabilities arise solely from *ad hoc* interpretations, and these assert that the actual current fluctuations are purely random, and intrinsic to each quantum system, here each diode. However the experimental data shows that these current fluctuations are completely determined by the fluctuations in the passing space, as demonstrated by the time delay effect, herein at the μs time scale and in [8] at the 10-20 sec scale. Hence the Zener diode effect represents a major discovery regarding the so called interpretations of quantum theory.

5 Alpha decay rate fluctuations

Shnoll [16] discovered that the α decay rate of ^{239}Pu is not completely random, as it has discrete preferred values. The same effect is seen in the histogram analysis of Zener diode tunnelling rates [18]. This α decay process is another exam-

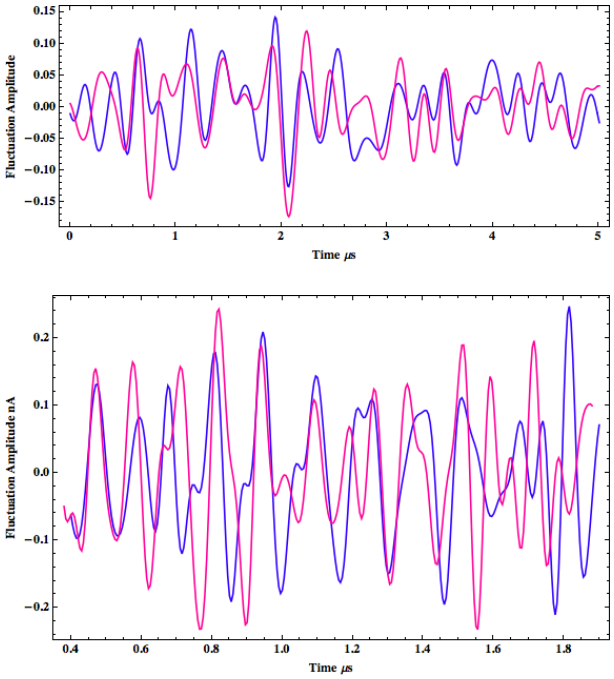

Fig. 5: Top: Current fluctuations from two collocated Zener diode detectors, as shown in Fig. 1, separated by 3-4 cm in EW direction due to box size, revealing strong correlations. The small separation may explain slight differences, revealing a structure to space at very small distances. Bottom: Example of Zener diode current fluctuations (nA), about a mean of ~3.5 μA, when detectors separated by 25cm, and aligned in direction RA=5hrs, Dec=-80°, with southerly detector signal delayed in DSO by 0.48 μs, and then showing strong correlations with northerly detector signal. This time delay effect reveals space traveling from S to N at a speed of approximately 476km/s, from maximum of correlation function $C(\tau, t)$, with time delay τ expressed as a speed. Data has been smoothed by FFT filtering to remove high and low frequency components. Fig. 6, top, shows fluctuations in measured speed over a 15 sec interval.

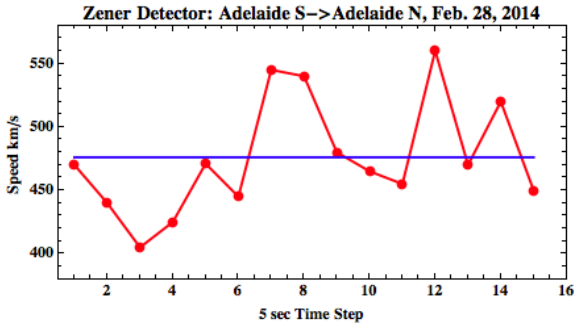

Fig. 6: Average projected speed, and projected speed every 5 sec, on February 28, 2014 at 12:20 hrs UTC, giving average speed = 476 ± 44 (RMS) km/s, from approximately S → N. The speeds are effective projected speeds, and so do not distinguish between actual speed and direction effect changes. The projected speed = (actual speed)/cos[a], where a is the angle between the space velocity and the direction defined by the two detectors, and cannot be immediately determined with only two detectors. However by varying direction of detector axis, and searching for maximum time delay, the average direction (RA and Dec) may be determined. As in previous experiments there are considerable fluctuations at all time scales, indicating a fractal structure to space.

ple of quantum tunnelling: here the tunnelling of the α wave packet through the potential energy barrier arising from the Coulomb repulsion between the α "particle" and the residual nucleus, as first explained by Gamow in 1928 [17]. The analysis above for the Zener diode also applies to this decay process: the major effect is the changing barrier height produced by space velocity fluctuations that affect the nucleus energy more than it affects the α energy. Shnoll also reported correlations between decay rate fluctuations measured at different locations. However the time resolution was ~60 sec, and so no speed and direction for the underlying space velocity was determined. It is predicted that α decay fluctuation rates with a time resolution of ~1 sec would show the time delay effect for experiments well separated geographically.

6 Reinterpretation of quantum theory

The experimental data herein clearly implies a need for a reinterpretation of quantum theory, as it has always lacked the dynamical effects of the fractal space: it only ever referred to the Euclidean static embedding space, which merely provides a position labelling. However the interpretation of the quantum theory has always been problematic and varied. The main problem is that the original Schrödinger equation does not describe the localization of quantum matter when measured, e.g. the formation of spots on photographic films in double slit experiments. From the beginning of quantum theory a metaphysical addendum was created, as in the Born interpretation, namely that there exists an almost point-like "particle", and that $|\psi(\boldsymbol{r}, t)|^2$ gives the probability density for the location of that particle, whether or not a measurement of position has taken place. This is a dualistic interpretation of the quantum theory: there exists a "wave function" as well as a "particle", and that the probability of a detection event is completely internal to a particular quantum system. So there should be no correlations between detection events for different systems, contrary to the experiments reported here. To see the failure of the Born and other interpretations consider the situation shown in Fig. 3. In the top figure the electron state is a wave packet $\psi_1(\boldsymbol{r}, t)$, partially localized to the left of a potential barrier. After the barrier tunnelling the wave function has evolved to the superposition $\psi_2(\boldsymbol{r}, t) + \psi_3(\boldsymbol{r}, t)$: a reflected and transmitted component. The probability of the electron being detected to the LHS is $\|\psi_2(\boldsymbol{r}, t)\|^2$, and to the RHS is $\|\psi_3(\boldsymbol{r}, t)\|^2$, the respective squared norms. These values do indeed predict the observed average reflected and transmitted electron currents, but make no prediction about the fluctuations that lead to these observed averages. As well, in the Born interpretation there is no mention of a collapse of the wave function to one of the states in the linear combina-

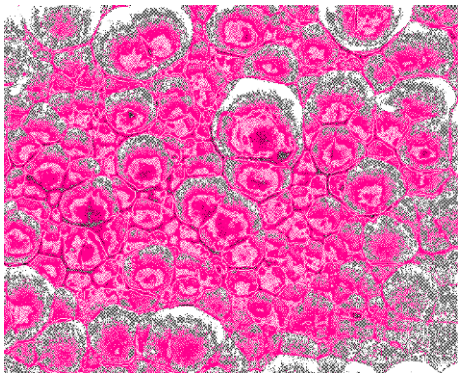

Fig. 7: Representation of the fractal wave data as revealing the fractal textured structure of the 3-space, with cells of space having slightly different velocities and continually changing, and moving wrt the Earth with a speed of ~500 km/s.

tion, as a single location outcome is in the metaphysics of the interpretation, and not in any physical process.

This localization process has never been satisfactorily explained, namely that when a quantum system, such as an electron, in a de-localized state, interacts with a detector, i.e. a system in a metastable state, the electron would put the combined system into a de-localized state, which is then observed to localize: the detector responds with an event at one location, but for which the quantum theory can only provide the expected average distribution, $|\psi(\boldsymbol{r},t)|^2$, and is unable to predict fluctuation details. In [10] it was conjectured that the de-localized electron-detector state is localized by the interaction with the dynamical space, and that the fluctuation details are produced by the space fluctuations, as we see in Zener diode electron tunnelling and α decay tunnelling. Percival [19] has produced detailed models of this wave function collapse process, which involved an intrinsic randomness, and which involves yet another dynamical term being added to the original Schrödinger equation. It is possible that this randomness may also be the consequence of space fluctuations.

The space driven localization of quantum states could give rise to our experienced classical world, in which macroscopic "matter" is not seen in de-localized states. It was the inability to explain this localization process that gave rise to the Copenhagen and numerous other interpretations of the original quantum theory, and in particular the dualistic model of wave functions and almost point-like localized "particles".

7 Dynamical 3-space

If Michelson and Morley had more carefully presented their pioneering data, physics would have developed in a very different direction. Even by 1925/26 Miller, a junior colleague of Michelson, was repeating the gas-mode interferometer experiment, and by not using Newtonian mechanics to attempt a calibration of the device, rather by using the Earth aberration effect which utilized the Earth orbital speed of 30 km/s to set the calibration constant, although that also entailed false assumptions. The experimental data reveals the existence of a dynamical space. It is a simple matter to arrive at the dynamical theory of space, and the emergence of gravity as a quantum matter effect as noted above. The key insight is to note that the emergent matter acceleration in (3), $\partial\boldsymbol{v}/\partial t + (\boldsymbol{v}\cdot\nabla)\boldsymbol{v}$, is the constituent Euler acceleration $\boldsymbol{a}(\boldsymbol{r},t)$ of space

$$\begin{aligned}\boldsymbol{a}(\boldsymbol{r},t) &= \lim_{\Delta t\to 0}\frac{\boldsymbol{v}(\boldsymbol{r}+\boldsymbol{v}(\boldsymbol{r},t)\Delta t, t+\Delta t)-\boldsymbol{v}(\boldsymbol{r},t)}{\Delta t}\\ &= \frac{\partial\boldsymbol{v}}{\partial t}+(\boldsymbol{v}\cdot\nabla)\boldsymbol{v}\end{aligned} \tag{5}$$

which describes the acceleration of a constituent element of space by tracking its change in velocity. This means that space has a structure that permits its velocity to be defined and detected, which experimentally has been done. This then suggests that the simplest dynamical equation for $\boldsymbol{v}(\boldsymbol{r},t)$ is

$$\begin{aligned}&\nabla\cdot\left(\frac{\partial\boldsymbol{v}}{\partial t}+(\boldsymbol{v}\cdot\nabla)\boldsymbol{v}\right)=-4\pi G\rho(\boldsymbol{r},t);\\ &\nabla\times\boldsymbol{v}=0\end{aligned} \tag{6}$$

because it then gives $\nabla\cdot\boldsymbol{g}=-4\pi G\rho(\boldsymbol{r},t)$; $\nabla\times\boldsymbol{g}=0$, which is Newton's inverse square law of gravity in differential form. Hence the fundamental insight is that Newton's gravitational acceleration field $\boldsymbol{g}(\boldsymbol{r},t)$ is really the acceleration field $\boldsymbol{a}(\boldsymbol{r},t)$ of the structured dynamical space*, and that quantum matter acquires that acceleration because it is fundamentally a wave effect, and the wave is refracted by the accelerations of space.

While the above lead to the simplest 3-space dynamical equation this derivation is not complete yet. One can add additional terms with the same order in speed spatial derivatives, and which cannot be *a priori* neglected. There are two such terms, as in

$$\nabla\cdot\left(\frac{\partial\boldsymbol{v}}{\partial t}+(\boldsymbol{v}\cdot\nabla)\boldsymbol{v}\right)+\frac{5\alpha}{4}\left((trD)^2-tr(D^2)\right)+\ldots=-4\pi G\rho \tag{7}$$

where $D_{ij}=\partial v_i/\partial x_j$. However to preserve the inverse square law external to a sphere of matter the two terms must have coefficients α and $-\alpha$, as shown. Here α is a dimensionless space self-interaction coupling constant, which experimental data reveals to be, approximately, the fine structure constant, $\alpha=e^2/\hbar c$ [21]. The ellipsis denotes higher order derivative terms with dimensioned coupling constants, which come into play when the flow speed changes rapidly with respect to distance. The observed dynamics of stars and gas clouds near the centre of the Milky Way galaxy has revealed the need for such a term [22], and we find that the space dynamics then requires an extra term:

$$\nabla\cdot\left(\frac{\partial\boldsymbol{v}}{\partial t}+(\boldsymbol{v}\cdot\nabla)\boldsymbol{v}\right)+\frac{5\alpha}{4}\left((trD)^2-tr(D^2)\right)+$$

*With vorticity $\nabla\times\boldsymbol{v}\neq 0$ and relativistic effects, the acceleration of matter becomes different from the acceleration of space [10].

$$+\delta^2\,\nabla^2\left((trD)^2 - tr(D^2)\right) + \ldots = -4\pi G\rho \qquad (8)$$

where δ has the dimensions of length, and appears to be a very small Planck-like length, [22]. This then gives us the dynamical theory of 3-space. It can be thought of as arising via a derivative expansion from a deeper theory, such as a quantum foam theory [10]. Note that the equation does not involve c, is non-linear and time-dependent, and involves non-local direct interactions. Its success implies that the universe is more connected than previously thought. Even in the absence of matter there can be time-dependent flows of space.

Note that the dynamical space equation, apart from the short distance effect - the δ term, there is no scale factor, and hence a scale free structure to space is to be expected, namely a fractal space. That dynamical equation has back hole and cosmic filament solutions [21,22], which are non-singular because of the effect of the δ term. At large distance scales it appears that a homogeneous space is dynamically unstable and undergoes dynamical breakdown of symmetry to form a spatial network of black holes and filaments [21], to which matter is attracted and coalesces into gas clouds, stars and galaxies.

We can write (8) in non-linear integral-differential form

$$\frac{\partial u}{\partial t} = -\frac{(\nabla u)^2}{2} + G\int d^3r' \frac{\rho(\boldsymbol{r}',t) + \rho_{DM}(\boldsymbol{v}(\boldsymbol{r}',t))}{|\boldsymbol{r}-\boldsymbol{r}'|} \qquad (9)$$

on satisfying $\nabla\times\boldsymbol{v} = 0$ by writing $\boldsymbol{v} = \nabla u$. Effects on the Gravity Probe B (GPB) gyroscope precessions caused by a non-zero vorticity were considered in [24]. Here ρ_{DM} is an effective "dark density" induced by the 3-space dynamics, but which is not any form of actual matter,

$$\rho_{DM}(\boldsymbol{v}(\boldsymbol{r},t)) = \frac{1}{4\pi G}\left(\frac{5\alpha}{4}\left((trD)^2 - tr(D^2)\right) + \right.$$
$$\left. + \delta^2\,\nabla^2\left((trD)^2 - tr(D^2)\right)\right). \qquad (10)$$

8 Universe expansion and inflation epoch

Even in the absence of matter (6) has an expanding universe solution. Substituting the Hubble form $\boldsymbol{v}(\boldsymbol{r},t) = H(t)\boldsymbol{r}$, and then using $H(t) = \dot{a}(t)/a(t)$, where $a(t)$ is the scale factor of the universe for a homogeneous and isotropic expansion, we obtain the exact solution $a(t) = t/t_0$, where t_0 is the age of the universe, since by convention $a(t_0) = 1$. Then computing the magnitude-redshift function $\mu(z)$, we obtain excellent agreement with the supernova data, and without the need for 'dark matter' nor 'dark energy' [20]. However using the extended dynamics in (8) we obtain $a(t) = (t/t_0)^{1/(1+5\alpha/2)}$ for a homogeneous and isotropic expansion, which has a singularity at $t = 0$, giving rise to an inflationary epoch. Fig. 8 shows a plot of $da(t)/dt$, which more clearly shows the inflation. However in general this space expansion will be turbulent:

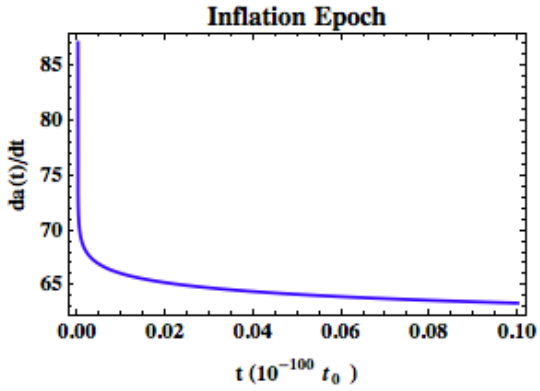

Fig. 8: Plot of $da(t)/dt$, the rate of expansion, showing the inflation epoch. Age of universe is $t_0 \approx 14 * 10^9$ years. On time axis $0.01 \times 10^{-100} t_0 = 4.4 \times 10^{-83}$ secs. This inflation epoch is intrinsic to the dynamical 3-space.

gravitational waves, perhaps as seen by the BICEP2 experiment in the Antarctica. Such turbulence will result in the creation of matter. This inflation epoch is an *ad hoc* addition to the standard model of cosmology [26]. Here it is intrinsic to the dynamics in (8) and is directly related to the bore hole g anomaly, black holes without matter infall, cosmic filaments, flat spiral galaxy rotation curves, light lensing by black holes, and other effects, all without the need for "dark matter".

9 Zener diodes and REG devices

REGs, Random Event Generators, use current fluctuations in Zener diodes in reverse bias mode, to supposedly generate random numbers, and are used in the GCP network. However the outputs, as shown in [8], are not random. GCP data is available from http://teilhard.global-mind.org/. This data extends back some 15 years and represents an invaluable resource for the study of gravitational waves, and their various effects, such as solar flares, coronal mass ejections, earthquakes, eclipse effects, moon phase effects, non-Poisson fluctuations in radioactivity [16], and variations in radioactive decay rates related to distance of the Earth from the Sun [23], as the 3-space fluctuations are enhanced by proximity to the Sun.

10 Earth scattering effect

In [8] correlated waveforms from Zener diode detectors in Perth and London were used to determine the speed and direction of gravitational waves, and detected an Earth scattering effect: the effective speed is larger when the 3-space path passes deeper into the Earth, Fig. 9. Eqn. (9) displays two kinds of waveform effects: disturbances from the first part, $\partial u/\partial t = -(\nabla u)^2/2$; and then matter density and the "dark matter" density effects when the second term is included. These later effects are instantaneous, indicating in this theory, that the universe (space) is highly non-locally

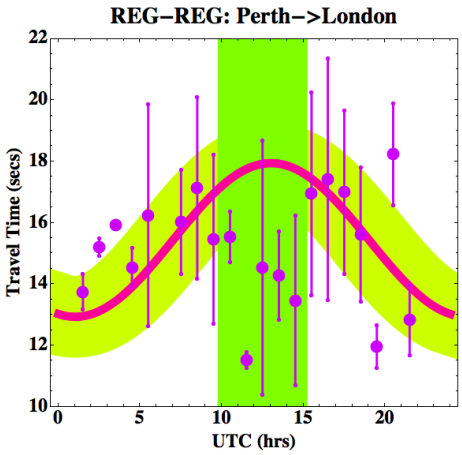

Fig. 9: Travel times from Zener Diode detectors (REG-REG) Perth-London from correlation delay time analysis, from [8]. The data in each 1 hr interval has been binned, and the average and rms shown. The thick (red line) shows best fit to data using plane wave travel time predictor, see [8], but after excluding those data points between 10 and 15hrs UTC, indicated by vertical band. Those data points are not consistent with the plane wave fixed average speed modelling, and suggest a scattering process when the waves pass deeper into the Earth, see [8]. This Perth-London data gives space velocity: 528 km/s, from direction RA = 5.3 hrs, Dec = 81°S. The broad band tracking the best fit line is for +/- 1 sec fluctuations, corresponding to speed fluctuation of +/- 17km/s. Actual fluctuations are larger than this, as 1st observed by Michelson-Morley in 1887 and by Miller in 1925/26.

connected, see [10], and combine in a non-linear manner with local disturbances that propagate at the speed of space. The matter density term is of course responsive for conventional Newtonian gravity theory.

However because these terms cross modulate the "dark matter" density space turbulence can manifest, in part, as a speed-up effect, as in the data in Fig. 9. Hence it is conjectured that the Earth scattering effect, manifest in the data, affords a means to study the dynamics arising from (10). That dynamics has already been confirmed in the non-singular space inflow black holes and the non-singular cosmic filaments effects, which are exact analytic solutions to (8) or (9). Indeed by using data from suitably located Zener diode detectors, for which the detected space flow passes through the centre of the Earth, we could be able to study the black hole located there, i.e. to perform black hole scattering experiments.

11 Gravitational waves as space flow turbulence

In the dynamical 3-space theory gravity is an emergent quantum effect, see (3), being the quantum wave response to time varying and inhomogeneous velocity fields. This has been confirmed by experiment. In [12] it was shown that Zener diodes detected the same signal as resonant bar gravitational wave detectors in Rome and Frascati in 1981. These detectors respond to the induced $g(\boldsymbol{r}, t)$, via (3), while the Zener diode detectors respond directly to $\boldsymbol{v}(\boldsymbol{r}, t)$. As well the Zener diode data has revealed the detection of deep Earth core vibration resonances known from seismology, but requiring superconductor seismometers. The first publicized coincidence detection of gravitational waves by resonant bar detectors was by Weber in 1969, with detectors located in Argonne and Maryland. These results were criticized on a number of spurious grounds, all being along the lines that the data was inconsistent with the predictions of General Relativity, which indeed it is, see Collins [27]. However in [7] it was shown that Weber's data is in agreement with the speed and direction of the measured space flow velocity. Data collected in the experiments reported in [8] revealed that significant fluctuations in the velocity field were followed some days later by solar flares, suggesting that these fluctuations, via the induced $g(\boldsymbol{r}, t)$, were causing solar dynamical instabilities. This suggests that the very simple Zener diode detection effect may be used to predict solar flares. As well Nelson and Bancel [25] report that Zener diode detectors (REGs) have repeatedly detected earthquakes. The mechanism would appear to be explained by (9) in which fluctuations in the matter density $\rho(\boldsymbol{r}, t)$ induce fluctuations in $\boldsymbol{v}(\boldsymbol{r}, t)$, but with the important observation that this field decreases like $1/\sqrt{r}$, unlike the g field which decreases like $1/r^2$. So in all of the above examples we see the link between time dependent gravitational forces and the fluctuations of the 3-space velocity field. A possibility for future experiments is to determine if the incredibly sensitive Zener diode detector effect can directly detect primordial gravitational waves from the inflation epoch, 3-space turbulence, as a background to the local galactic 3-space flow effects.

12 Conclusions

We have reported refined direct quantum detection of 3-space turbulence: gravitational waves, using electron current fluctuations in reverse bias mode Zener diodes, separated by a mere 25cm, that permitted the absolute determination of the 3-space velocity of some 500 km/s, in agreement with the speed and direction from a number of previous analyzes that involved light speed anisotropy, including in particular the NASA spacecraft Earth-flyby Doppler shift effect, and the first such Zener diode direct detections of space flow using correlations between Perth and London detectors in 2013. The experimental results reveal the nature of the dominant gravitational wave effects; they are caused by turbulence / fluctuations in the passing dynamical space, a space missing from physics theories, until its recent discovery. This dynamical space explains bore hole anomalies, black holes without matter infall, cosmic filaments and the cosmic network, spiral galaxy flat rotation curves, universe expansion in agreement with supernova data, and all without dark matter nor dark energy, and a universe inflation epoch, accompanied

by gravitational waves. Quantum tunnelling fluctuations have been shown to be non-random, in the sense that they are completely induced by fluctuations in the passing space. It is also suggested that the localization of massive quantum systems is caused by fluctuations in space, and so generating our classical world of localized objects, but which are essentially wave phenomena at the microlevel. There is then no need to invoke any of the usual interpretations of the quantum theory, all of which failed to take account of the existence of the dynamical space. Present day physics employs an embedding space, whose sole function is to label positions in the dynamical space. This [3]-dimensional embedding in a geometrical space, while being non-dynamical, is nevertheless a property of the dynamical space at some scales. However the dynamical space at very small scales is conjectured not to be embeddable in a [3]-geometry, as discussed in [10].

Received on March 11, 2014 / Accepted on March 24, 2014

References

1. Michelson A. A., Morley E. W. On the relative motion of the earth and the luminiferous ether. *Am. J. Sci.*, 1887, v. 34, 333–345.
2. Cahill R. T., Kitto K. Michelson-Morley Experiments Revisited. *Apeiron*, 2003, v. 10 (2), 104–117.
3. Cahill R. T. The Michelson and Morley 1887 Experiment and the Discovery of Absolute Motion. *Progress in Physics*, 2005 v. 3, 25–29.
4. Cahill R. T. Dynamical 3-Space: Neo-Lorentz Relativity. *Physics International*, 2013, v. 4 (1), 60–72.
5. Braxmaier C., Müller H., Pradl O., Mlynek J., Peters O. Tests of Relativity Using a Cryogenic Optical Resonator. *Phys. Rev. Lett.*, 2001, v. 88, 010401.
6. Cahill R. T. Discovery of Dynamical 3-Space: Theory, Experiments and Observations - A Review. *American Journal of Space Science*, 2013, v. 1 (2), 77–93.
7. Cahill R. T. Review of Gravitational Wave Detections: Dynamical Space. *Physics International*, 2014, v. 5 (1), 49–86.
8. Cahill R. T. Nanotechnology Quantum Detectors for Gravitational Waves: Adelaide to London Correlations Observed. *Progress in Physics*, 2013, v. 4, 57–62.
9. Cahill R. T. Combining NASA/JPL One-Way Optical-Fiber Light-Speed Data with Spacecraft Earth-Flyby Doppler-Shift Data to Characterise 3-Space Flow. *Progress in Physics*, 2009, v. 4, 50–64.
10. Cahill R. T. Process Physics: From Information Theory to Quantum Space and Matter. Nova Science Pub., New York, 2005.
11. Cahill R. T. Characterisation of Low Frequency Gravitational Waves from Dual RF Coaxial-Cable Detector: Fractal Textured Dynamical 3-Space. *Progress in Physics*, 2012, v. 3, 3–10.
12. Cahill R. T. Observed Gravitational Wave Effects: Amaldi 1980 Frascati-Rome Classical Bar Detectors, 2013 Perth-London Zener-Diode Quantum Detectors, Earth Oscillation Mode Frequencies. *Progress in Physics*, 2014, v. 10 (1), 21–24.
13. Amaldi E., Coccia E., Frasca S., Modena I., Rapagnani P., Ricci F., Pallottino G. V., Pizzella G., Bonifazi P., Cosmelli C., Giovanardi U., Iafolla V., Ugazio S., Vannaroni G. Background of Gravitational-Wave Antennas of Possible Terrestrial Origin - I. *Il Nuovo Cimento*, 1981, v. 4C (3), 295–308.
14. Amaldi E., Frasca S., Pallottino G. V., Pizzella G., Bonifazi P. Background of Gravitational-Wave Antennas of Possible Terrestrial Origin - II. *Il Nuovo Cimento*, 1981, v. 4C (3), 309–323.
15. Cahill R. T., Dynamical Fractal 3-Space and the Generalised Schrödinger Equation: Equivalence Principle and Vorticity Effects. *Progress in Physics*, 2006, v. 1, 27–34.
16. Shnoll S. E. Cosmophysical Factors in Stochastic Processes. American Research Press, Rehoboth, NM, 2012.
17. Gamow G. Zur Quantentheorie des Atomkernes. *Z. Physik*, 1928, v. 51, 204.
18. Rothall D. P., Cahill R. T. Dynamical 3-Space: Observing Gravitational Wave Fluctuations with Zener Diode Quantum Detector: the Shnoll Effect. *Progress in Physics*, 2014, v. 10 (1), 16–18.
19. Percival I. Quantum State Diffusion. Cambridge University Press, Cambridge, 1998.
20. Cahill R. T., Rothall D. Discovery of Uniformly Expanding Universe. *Progress in Physics*, 2012, v. 1, 63–68.
21. Rothall D. P., Cahill R. T. Dynamical 3-Space: Black Holes in an Expanding Universe. *Progress in Physics*, 2013, v. 4, 25–31.
22. Cahill R. T., Kerrigan D. Dynamical Space: Supermassive Black Holes and Cosmic Filaments. *Progress in Physics*, 2011, v. 4, 79–82.
23. Jenkins J. H., Fischbach E., Buncher J. B., Gruenwald J. T., Krause, D. E., Mattes J. J. Evidence for Correlations Between Nuclear Decay Rates and Earth-Sun Distance. *Astropart. Phys.*, 2009, v. 32, 42.
24. Cahill R. T. Novel Gravity Probe B Frame Dragging Effect. *Progress in Physics*, 2005, v. 3 (1), 30–33.
25. Nelson R. D., Bancel P. A. Anomalous Anticipatory Responses in Networked Random Data, Frontiers of Time: Retrocausation - Experiment and Theory. *AIP Conference Proceedings*, 2006, v. 863, 260–272.
26. Guth A. H. The Inflationary Universe: A Possible Solution to the Horizon and Flatness Problems. *Phys. Rev.*, 1981, v. D23, 347. OCLC 4433735058.
27. Collins H. Gravity's Shadow: The Search for Gravitational Waves. University of Chicago Press, Chicago, 2004.

Chrome of Baryons

Gunn Quznetsov

gunn@mail.ru, quznets@yahoo.com

Chromes of quarks are changed under the Cartesian turns. And the Lorentz's transformations change chromes and grades of quarks. Baryons represent one of ways of elimination of these noninvariancy.

Introduction

According to the quark model [1], the properties of hadrons are primarily determined by their so-called valence quarks. For example, a proton is composed of two up quarks and one down quark. Although quarks also carry color charge, hadrons must have zero total color charge because of a phenomenon called color confinement. That is, hadrons must be "colorless" or "white". These are the simplest of the two ways: three quarks of different colors, or a quark of one color and an antiquark carrying the corresponding anticolor. Hadrons with the first arrangement are called baryons, and those with the second arrangement are mesons.

1 Cartesian rotation

Let α be any real number and

$$\begin{aligned} x'_0 &:= x_0, \\ x'_1 &:= x_1\cos(\alpha) - x_2\sin(\alpha); \\ x'_2 &:= x_1\sin(\alpha) + x_2\cos(\alpha); \\ x'_3 &:= x_3; \end{aligned} \tag{1}$$

Since j_A is a 3+1-vector then from [2, p. 59]:

$$\begin{aligned} j'_{A,0} &= -\varphi^\dagger\beta^{[0]}\varphi, \\ j'_{A,1} &= -\varphi^\dagger\left(\beta^{[1]}\cos(\alpha) - \beta^{[2]}\sin(\alpha)\right)\varphi; \\ j'_{A,2} &= -\varphi^\dagger\left(\beta^{[1]}\sin(\alpha) + \beta^{[2]}\cos(\alpha)\right)\varphi; \\ j'_{A,3} &= -\varphi^\dagger\beta^{[3]}\varphi. \end{aligned} \tag{2}$$

Hence if for φ':

$$\begin{aligned} j'_{A,0} &= -\varphi'^\dagger\beta^{[0]}\varphi', \\ j'_{A,1} &= -\varphi'^\dagger\beta^{[1]}\varphi'; \\ j'_{A,2} &= -\varphi'^\dagger\beta^{[2]}\varphi'; \\ j'_{A,3} &= -\varphi'^\dagger\beta^{[3]}\varphi', \end{aligned}$$

and

$$\varphi' := U_{1,2}(\alpha)\,\varphi$$

then

$$\begin{aligned} U^\dagger_{1,2}(\alpha)\beta^{[0]}U_{1,2}(\alpha) &= \beta^{[0]}, \\ U^\dagger_{1,2}(\alpha)\beta^{[1]}U_{1,2}(\alpha) &= \beta^{[1]}\cos\alpha - \beta^{[2]}\sin\alpha; \\ U^\dagger_{1,2}(\alpha)\beta^{[2]}U_{1,2}(\alpha) &= \beta^{[2]}\cos\alpha + \beta^{[1]}\sin\alpha; \\ U^\dagger_{1,2}(\alpha)\beta^{[3]}U_{1,2}(\alpha) &= \beta^{[3]}; \end{aligned} \tag{3}$$

from [2, p. 62]: because

$$\rho_A = \varphi^\dagger\varphi = \varphi'^\dagger\varphi',$$

then

$$U^\dagger_{1,2}(\alpha)\,U_{1,2}(\alpha) = 1_4. \tag{4}$$

If

$$U_{1,2}(\alpha) := \cos\frac{\alpha}{2}\cdot 1_4 - \sin\frac{\alpha}{2}\cdot\beta^{[1]}\beta^{[2]}$$

i.e.:

$$U_{1,2}(\alpha) = \begin{bmatrix} e^{-i\frac{1}{2}\alpha} & 0 & 0 & 0 \\ 0 & e^{i\frac{1}{2}\alpha} & 0 & 0 \\ 0 & 0 & e^{-i\frac{1}{2}\alpha} & 0 \\ 0 & 0 & 0 & e^{i\frac{1}{2}\alpha} \end{bmatrix} \tag{5}$$

then $U_{1,2}(\alpha)$ fulfils to all these conditions (3), (4).

Then let

$$\begin{aligned} x'_0 &:= x_0, \\ x'_1 &:= x_1\cos(\alpha) - x_3\sin(\alpha), \\ x'_2 &:= x_2, \\ x'_3 &:= x_1\sin(\alpha) + x_3\cos(\alpha). \end{aligned} \tag{6}$$

Let

$$U_{1,3}(\alpha) := \cos\frac{\alpha}{2}\cdot 1_4 - \sin\frac{\alpha}{2}\cdot\beta^{[1]}\beta^{[3]}.$$

In this case:

$$U_{1,3}(\alpha) = \begin{bmatrix} \cos\frac{1}{2}\alpha & \sin\frac{1}{2}\alpha & 0 & 0 \\ -\sin\frac{1}{2}\alpha & \cos\frac{1}{2}\alpha & 0 & 0 \\ 0 & 0 & \cos\frac{1}{2}\alpha & \sin\frac{1}{2}\alpha \\ 0 & 0 & -\sin\frac{1}{2}\alpha & \cos\frac{1}{2}\alpha \end{bmatrix} \tag{7}$$

and

$$\begin{aligned} U^\dagger_{1,3}(\alpha)\beta^{[0]}U_{1,3}(\alpha) &= \beta^{[0]}, \\ U^\dagger_{1,3}(\alpha)\beta^{[1]}U_{1,3}(\alpha) &= \beta^{[1]}\cos\alpha - \beta^{[3]}\sin\alpha, \\ U^\dagger_{1,3}(\alpha)\beta^{[2]}U_{1,3}(\alpha) &= \beta^{[2]}, \\ U^\dagger_{1,3}(\alpha)\beta^{[3]}U_{1,3}(\alpha) &= \beta^{[3]}\cos\alpha + \beta^{[1]}\sin\alpha. \end{aligned} \tag{8}$$

If

$$\varphi' := U_{1,3}(\alpha)\,\varphi$$

and

$$j'_{A,k} := \varphi'^{\dagger}\beta^{[k]}\varphi'$$

where ($k \in \{0,1,2,3\}$) then

$$\begin{aligned} j'_{A,0} &= j_{A,0}, \quad (9)\\ j'_{A,1} &= j_{A,1}\cos\alpha - j_{A,3}\sin\alpha, \quad (10)\\ j'_{A,2} &= j_{A,2},\\ j'_{A,3} &= j_{A,3}\cos\alpha + j_{A,1}\sin\alpha. \end{aligned}$$

Then let

$$\begin{aligned} x'_0 &:= x_0,\\ x'_1 &:= x_1,\\ x'_2 &= \cos\alpha\cdot x_2 + \sin\alpha\cdot x_3, \quad (11)\\ x'_3 &= \cos\alpha\cdot x_3 - \sin\alpha\cdot x_2. \end{aligned}$$

Let

$$U_{3,2}(\alpha) = \cos\frac{\alpha}{2}\cdot 1_4 - \sin\frac{\alpha}{2}\cdot\beta^{[3]}\beta^{[2]}$$

In this case:

$$U_{3,2}(\alpha) = \begin{bmatrix} \cos\frac{1}{2}\alpha & i\sin\frac{1}{2}\alpha & 0 & 0\\ i\sin\frac{1}{2}\alpha & \cos\frac{1}{2}\alpha & 0 & 0\\ 0 & 0 & \cos\frac{1}{2}\alpha & i\sin\frac{1}{2}\alpha\\ 0 & 0 & i\sin\frac{1}{2}\alpha & \cos\frac{1}{2}\alpha \end{bmatrix}, \quad (12)$$

and

$$\begin{aligned} U^{\dagger}_{3,2}(\alpha)\beta^{[0]}U_{3,2}(\alpha) &= \beta^{[0]},\\ U^{\dagger}_{3,2}(\alpha)\beta^{[1]}U_{3,2}(\alpha) &= \beta^{[1]},\\ U^{\dagger}_{3,2}(\alpha)\beta^{[0]}U_{3,2}(\alpha) &= \beta^{[0]}\cos\alpha + \beta^{[3]}\sin\alpha, \quad (13)\\ U^{\dagger}_{3,2}(\alpha)\beta^{[3]}U_{3,2}(\alpha) &= \beta^{[3]}\cos\alpha - \beta^{[2]}\sin\alpha \end{aligned}$$

If

$$\varphi' := U_{3,2}(\alpha)\varphi$$

and

$$j'_{A,k} := \varphi'^{\dagger}\beta^{[k]}\varphi'$$

where ($k \in \{0,1,2,3\}$) then

$$\begin{aligned} j'_{A,0} &= j_{A,0},\\ j'_{A,1} &= j_{A,1}, \quad (14)\\ j'_{A,2} &= j_{A,2}\cos\alpha + j_{A,3}\sin\alpha,\\ j'_{A,3} &= j_{A,3}\cos\alpha - j_{A,1}\sin\alpha. \end{aligned}$$

2 Lorentzian rotation

Let v be any real number such that $-1 < v < 1$.

And let:

$$\alpha := \frac{1}{2}\ln\frac{1-v}{1+v}.$$

In this case:

$$\begin{aligned} \cosh\alpha &= \frac{1}{\sqrt{1-v^2}},\\ \sinh\alpha &= -\frac{v}{\sqrt{1-v^2}}. \quad (15) \end{aligned}$$

Let

$$\begin{aligned} x'_0 &:= x_0\cosh\alpha - x_1\sinh\alpha, \quad (16)\\ x'_1 &:= x_1\cosh\alpha - x_0\sinh\alpha,\\ x'_2 &:= x_2,\\ x'_3 &:= x_3. \end{aligned}$$

Let

$$U_{1,0}(\alpha) = \cosh\frac{\alpha}{2}\cdot 1_4 - \sinh\frac{\alpha}{2}\cdot\beta^{[1]}\beta^{[0]}.$$

That is:

$$U_{1,0}(\alpha) := \begin{bmatrix} \cosh\frac{1}{2}\alpha & \sinh\frac{1}{2}\alpha & 0 & 0\\ \sinh\frac{1}{2}\alpha & \cosh\frac{1}{2}\alpha & 0 & 0\\ 0 & 0 & \cosh\frac{1}{2}\alpha & -\sinh\frac{1}{2}\alpha\\ 0 & 0 & -\sinh\frac{1}{2}\alpha & \cosh\frac{1}{2}\alpha \end{bmatrix}. \quad (17)$$

In this case:

$$\begin{aligned} U^{\dagger}_{1,0}(\alpha)\beta^{[0]}U_{1,0}(\alpha) &= \beta^{[0]}\cosh\alpha - \beta^{[1]}\sinh\alpha, \quad (18)\\ U^{\dagger}_{1,0}(\alpha)\beta^{[1]}U_{1,0}(\alpha) &= \beta^{[1]}\cosh\alpha - \beta^{[0]}\sinh\alpha,\\ U^{\dagger}_{1,0}(\alpha)\beta^{[2]}U_{1,0}(\alpha) &= \beta^{[2]},\\ U^{\dagger}_{1,0}(\alpha)\beta^{[3]}U_{1,0}(\alpha) &= \beta^{[3]}. \end{aligned}$$

If

$$\varphi' := U_{1,0}(\alpha)\varphi$$

and

$$j'_{A,k} := \varphi'^{\dagger}\beta^{[k]}\varphi'$$

where ($k \in \{0,1,2,3\}$) then

$$\begin{aligned} j'_{A,0} &= j_{A,0}\cosh\alpha - j_{A,1}\sinh\alpha, \quad (19)\\ j'_{A,1} &= j_{A,1}\cosh\alpha - j_{A,0}\sinh\alpha,\\ j'_{A,2} &= j_{A,2},\\ j'_{A,3} &= j_{A,3}. \end{aligned}$$

Then let

$$\begin{aligned} x'_0 &:= x_0\cosh\alpha - x_2\sinh\alpha, \quad (20)\\ x'_1 &:= x_1,\\ x'_2 &:= x_2\cosh\alpha - x_0\sinh\alpha,\\ x'_3 &:= x_3. \end{aligned}$$

Let

$$U_{2,0}(\alpha) := \cosh\frac{\alpha}{2}\cdot 1_4 - \sinh\frac{\alpha}{2}\cdot\beta^{[2]}\beta^{[0]}. \qquad (21)$$

That is:

$$U_{2,0}(\alpha) = \begin{bmatrix} \cosh\frac{1}{2}\alpha & -i\sinh\frac{1}{2}\alpha & 0 & 0 \\ i\sinh\frac{1}{2}\alpha & \cosh\frac{1}{2}\alpha & 0 & 0 \\ 0 & 0 & \cosh\frac{1}{2}\alpha & i\sinh\frac{1}{2}\alpha \\ 0 & 0 & -i\sinh\frac{1}{2}\alpha & \cosh\frac{1}{2}\alpha \end{bmatrix}.$$

In this case:

$$\begin{aligned} U^{\dagger}_{2,0}(\alpha)\beta^{[0]}U_{2,0}(\alpha) &= \beta^{[0]}\cosh\alpha - \beta^{[2]}\sinh\alpha, \qquad (22)\\ U^{\dagger}_{2,0}(\alpha)\beta^{[1]}U_{1,0}(\alpha) &= \beta^{[1]},\\ U^{\dagger}_{2,0}(\alpha)\beta^{[2]}U_{1,0}(\alpha) &= \beta^{[2]}\cosh\alpha - \beta^{[0]}\sinh\alpha,\\ U^{\dagger}_{2,0}(\alpha)\beta^{[3]}U_{2,0}(\alpha) &= \beta^{[3]}. \end{aligned}$$

If

$$\varphi' := U_{2,0}(\alpha)\varphi$$

and

$$j'_{A,k} := \varphi'^{\dagger}\beta^{[k]}\varphi'$$

where ($k \in \{0,1,2,3\}$) then

$$\begin{aligned} j'_{A,0} &= j_{A,0}\cosh\alpha - j_{A,1}\sinh\alpha, \qquad (23)\\ j'_{A,1} &= j_{A,1},\\ j'_{A,2} &= j_{A,2}\cosh\alpha - j_{A,0}\sinh\alpha,\\ j'_{A,3} &= j_{A,3}. \end{aligned}$$

Then let

$$\begin{aligned} x'_0 &:= x_0\cosh\alpha - x_3\sinh\alpha, \qquad (24)\\ x'_1 &:= x_1,\\ x'_2 &:= x_2,\\ x'_3 &:= x_3\cosh\alpha - x_0\sinh\alpha. \end{aligned}$$

Let

$$U_{3,0}(\alpha) := \cosh\frac{\alpha}{2}\cdot 1_4 - \sinh\frac{\alpha}{2}\cdot\beta^{[3]}\beta^{[0]}.$$

That is:

$$U_{3,0}(\alpha) = \begin{bmatrix} e^{\frac{1}{2}\alpha} & 0 & 0 & 0 \\ 0 & e^{-\frac{1}{2}\alpha} & 0 & 0 \\ 0 & 0 & e^{-\frac{1}{2}\alpha} & 0 \\ 0 & 0 & 0 & e^{\frac{1}{2}\alpha} \end{bmatrix}. \qquad (25)$$

In this case:

$$\begin{aligned} U^{\dagger}_{3,0}(\alpha)\beta^{[0]}U_{3,0}(\alpha) &= \beta^{[0]}\cosh\alpha - \beta^{[3]}\sinh\alpha, \qquad (26)\\ U_{3,0}(\alpha)\beta^{[1]}U_{3,0}(\alpha) &= \beta^{[1]},\\ U_{3,0}(\alpha)\beta^{[2]}U_{3,0}(\alpha) &= \beta^{[2]},\\ U_{3,0}(\alpha)\beta^{[3]}U_{3,0}(\alpha) &= \beta^{[3]}\cosh\alpha - \beta^{[0]}\sinh\alpha. \end{aligned}$$

If

$$\varphi' := U_{3,0}(\alpha)\varphi$$

and

$$j'_{A,k} := \varphi'^{\dagger}\beta^{[k]}\varphi'$$

where ($k \in \{0,1,2,3\}$) then

$$\begin{aligned} j'_{A,0} &= j_{A,0}\cosh\alpha - j_{A,3}\sinh\alpha, \qquad (27)\\ j'_{A,1} &= j_{A,1},\\ j'_{A,2} &= j_{A,2}.\\ j'_{A,3} &= j_{A,3}\cosh\alpha - j_{A,0}\sinh\alpha. \end{aligned}$$

3 Equation of motion

Function φ submits to the following equation [2, p. 82]:

$$\begin{aligned} &\tfrac{1}{\mathrm{c}}\partial_t\varphi - \left(\mathrm{i}\Theta_0\beta^{[0]} + \mathrm{i}\Upsilon_0\beta^{[0]}\gamma^{[5]}\right)\varphi =\\ &= \Bigg(\sum_{\nu=1}^{3}\beta^{[\nu]}\left(\partial_\nu + \mathrm{i}\Theta_\nu + \mathrm{i}\Upsilon_\nu\gamma^{[5]}\right) +\\ &\quad +\mathrm{i}M_0\gamma^{[0]} + \mathrm{i}M_4\beta^{[4]} -\\ &\quad -\mathrm{i}M_{\zeta,0}\gamma^{[0]}_{\zeta} + \mathrm{i}M_{\zeta,4}\zeta^{[4]} -\\ &\quad -\mathrm{i}M_{\eta,0}\gamma^{[0]}_{\eta} - \mathrm{i}M_{\eta,4}\eta^{[4]} +\\ &\quad +\mathrm{i}M_{\theta,0}\gamma^{[0]}_{\theta} + \mathrm{i}M_{\theta,4}\theta^{[4]}\Bigg)\varphi. \end{aligned}$$

That is:

$$\begin{aligned} &\Bigg(\sum_{\nu=0}^{3}\beta^{[\nu]}\left(\partial_\nu + \mathrm{i}\Theta_\nu + \mathrm{i}\Upsilon_\nu\gamma^{[5]}\right) +\\ &\quad +\mathrm{i}M_0\gamma^{[0]} + \mathrm{i}M_4\beta^{[4]} -\\ &\quad -\mathrm{i}M_{\zeta,0}\gamma^{[0]}_{\zeta} + \mathrm{i}M_{\zeta,4}\zeta^{[4]} -\\ &\quad -\mathrm{i}M_{\eta,0}\gamma^{[0]}_{\eta} - \mathrm{i}M_{\eta,4}\eta^{[4]} +\\ &\quad +\mathrm{i}M_{\theta,0}\gamma^{[0]}_{\theta} + \mathrm{i}M_{\theta,4}\theta^{[4]}\Bigg)\varphi = 0. \end{aligned} \qquad (28)$$

Like coordinates x_5 and x_4 [2, p. 83] here are entered new coordinates y^β, z^β, y^ζ, z^ζ, y^η, z^η, y^θ, z^θ such that

$$\begin{aligned} -\frac{\pi\mathrm{c}}{\mathrm{h}} &\le y^\beta \le \frac{\pi\mathrm{c}}{\mathrm{h}}, -\frac{\pi\mathrm{c}}{\mathrm{h}} \le z^\beta \le \frac{\pi\mathrm{c}}{\mathrm{h}},\\ -\frac{\pi\mathrm{c}}{\mathrm{h}} &\le y^\zeta \le \frac{\pi\mathrm{c}}{\mathrm{h}}, -\frac{\pi\mathrm{c}}{\mathrm{h}} \le z^\zeta \le \frac{\pi\mathrm{c}}{\mathrm{h}},\\ -\frac{\pi\mathrm{c}}{\mathrm{h}} &\le y^\eta \le \frac{\pi\mathrm{c}}{\mathrm{h}}, -\frac{\pi\mathrm{c}}{\mathrm{h}} \le z^\eta \le \frac{\pi\mathrm{c}}{\mathrm{h}},\\ -\frac{\pi\mathrm{c}}{\mathrm{h}} &\le y^\theta \le \frac{\pi\mathrm{c}}{\mathrm{h}}, -\frac{\pi\mathrm{c}}{\mathrm{h}} \le z^\theta \le \frac{\pi\mathrm{c}}{\mathrm{h}}. \end{aligned}$$

and like $\widetilde{\varphi}$, [2, p. 83] let:

$$\begin{aligned} &[\varphi]\left(t,\mathbf{x},y^\beta,z^\beta,y^\zeta,z^\zeta,y^\eta,z^\eta,y^\theta,z^\theta\right) := \qquad (29)\\ &:= \varphi(t,\mathbf{x})\times\exp\Big(\mathrm{i}(y^\beta M_0 + z^\beta M_4 + y^\zeta M_{\zeta,0} + z^\zeta M_{\zeta,4} +\\ &\quad +y^\eta M_{\eta,0} + z^\eta M_{\eta,4} + y^\theta M_{\theta,0} + z^\theta M_{\theta,4})\Big). \end{aligned}$$

In this case if

$$\begin{gathered}([\varphi],[\chi]) := \\ := \int_{-\frac{\pi c}{h}}^{\frac{\pi c}{h}} dy^{\beta} \int_{-\frac{\pi c}{h}}^{\frac{\pi c}{h}} dz^{\beta} \int_{-\frac{\pi c}{h}}^{\frac{\pi c}{h}} dy^{\zeta} \int_{-\frac{\pi c}{h}}^{\frac{\pi c}{h}} dz^{\zeta} \times \\ \times \int_{-\frac{\pi c}{h}}^{\frac{\pi c}{h}} dy^{\eta} \int_{-\frac{\pi c}{h}}^{\frac{\pi c}{h}} dz^{\eta} \int_{-\frac{\pi c}{h}}^{\frac{\pi c}{h}} dy^{\theta} \int_{-\frac{\pi c}{h}}^{\frac{\pi c}{h}} dz^{\theta} \times \\ \times \quad [\varphi]^{\dagger}[\chi]\end{gathered} \tag{30}$$

then

$$\begin{aligned}([\varphi],[\varphi]) &= \rho_{\mathcal{A}}, \\ \left([\varphi],\beta^{[s]}[\varphi]\right) &= -\frac{j_{\mathcal{A},k}}{\mathrm{c}},\end{aligned} \tag{31}$$

and in this case from (28):

$$\begin{gathered}\left(\sum_{\nu=0}^{3}\beta^{[\nu]}\left(\partial_{\nu}+\mathrm{i}\Theta_{\nu}+\mathrm{i}\Upsilon_{\nu}\gamma^{[5]}\right)+\right. \\ +\gamma^{[0]}\partial_{y}^{\beta}+\beta^{[4]}\partial_{z}^{\beta}- \\ -\gamma_{\zeta}^{[0]}\partial_{y}^{\zeta}+\zeta^{[4]}\partial_{z}^{\zeta}- \\ -\gamma_{\eta}^{[0]}\partial_{y}^{\eta}-\eta^{[4]}\partial_{z}^{\eta}+ \\ \left.+\gamma_{\theta}^{[0]}\partial_{y}^{\theta}+\theta^{[4]}\partial_{z}^{\theta}\right)[\varphi]=0.\end{gathered} \tag{32}$$

Because

$$\gamma_{\eta}^{[0]}=\begin{bmatrix}0&0&0&i\\0&0&-i&0\\0&i&0&0\\-i&0&0&0\end{bmatrix},\ \eta^{[4]}=\mathrm{i}\begin{bmatrix}0&0&0&-i\\0&0&i&0\\0&i&0&0\\-i&0&0&0\end{bmatrix}; \tag{33}$$

$$\gamma_{\theta}^{[0]}=\begin{bmatrix}0&0&-1&0\\0&0&0&1\\-1&0&0&0\\0&1&0&0\end{bmatrix},\ \theta^{[4]}=\mathrm{i}\begin{bmatrix}0&0&1&0\\0&0&0&-1\\-1&0&0&0\\0&1&0&0\end{bmatrix}; \tag{34}$$

$$\gamma_{\zeta}^{[0]}=\begin{bmatrix}0&0&0&-1\\0&0&-1&0\\0&-1&0&0\\-1&0&0&0\end{bmatrix},\ \zeta^{[4]}=\mathrm{i}\begin{bmatrix}0&0&0&1\\0&0&1&0\\0&-1&0&0\\-1&0&0&0\end{bmatrix}; \tag{35}$$

then from (32):

$$\begin{gathered}\sum_{\nu=0}^{3}\beta^{[\nu]}\left(\partial_{\nu}+\mathrm{i}\Theta_{\nu}+\mathrm{i}\Upsilon_{\nu}\gamma^{[5]}\right)[\varphi]+ \\ +\gamma^{[0]}\partial_{y}^{\beta}[\varphi]+\beta^{[4]}\partial_{z}^{\beta}[\varphi]+ \\ +\left(\begin{bmatrix}0&0&-\partial_{y}^{\theta}&\partial_{y}^{\zeta}-i\partial_{y}^{\eta}\\0&0&\partial_{y}^{\zeta}+i\partial_{y}^{\eta}&\partial_{y}^{\theta}\\-\partial_{y}^{\theta}&\partial_{y}^{\zeta}-i\partial_{y}^{\eta}&0&0\\\partial_{y}^{\zeta}+i\partial_{y}^{\eta}&\partial_{y}^{\theta}&0&0\end{bmatrix}+\right. \\ \left.+\mathrm{i}\begin{bmatrix}0&0&\partial_{z}^{\theta}&\partial_{z}^{\zeta}+i\partial_{z}^{\eta}\\0&0&\partial_{z}^{\zeta}-i\partial_{z}^{\eta}&-\partial_{z}^{\theta}\\-\partial_{z}^{\theta}&-\partial_{z}^{\zeta}-i\partial_{z}^{\eta}&0&0\\-\partial_{z}^{\zeta}+i\partial_{z}^{\eta}&\partial_{z}^{\theta}&0&0\end{bmatrix}\right) \\ \times[\varphi]=0.\end{gathered} \tag{36}$$

Let a Fourier transformation of

$$[\varphi]\left(t,\mathbf{x},y^{\beta},z^{\beta},y^{\zeta},z^{\zeta},y^{\eta},z^{\eta},y^{\theta},z^{\theta}\right)$$

be the following;

$$\begin{gathered}[\varphi]\left(t,\mathbf{x},y^{\beta},z^{\beta},y^{\zeta},z^{\zeta},y^{\eta},z^{\eta},y^{\theta},z^{\theta}\right)= \\ =\sum_{w,p_1,p_2,p_3,n^{\beta},s^{\beta},n^{\zeta},s^{\zeta},n^{\eta},s^{\eta},n^{\theta},s^{\theta}} c(w,p_1,p_2,p_3,n^{\beta},s^{\beta}, \\ n^{\zeta},s^{\zeta},n^{\eta},s^{\eta},n^{\theta},s^{\theta})\times \\ \times\exp\left(-\mathrm{i}\frac{\mathrm{h}}{\mathrm{c}}(wx_0+p_1x_1+p_2x_2+p_3x_3+\right. \\ +n^{\beta}y^{\beta}+s^{\beta}z^{\beta}+n^{\zeta}y^{\zeta}+s^{\zeta}z^{\zeta}+ \\ \left.+n^{\eta}y^{\eta}+s^{\eta}z^{\eta}+n^{\theta}y^{\theta}+s^{\theta}z^{\theta})\right).\end{gathered} \tag{37}$$

Let in (36) $\Theta_{\nu}=0$ and $\Upsilon_{\nu}=0$.

Let us design:

$$\begin{gathered}G_0 := \left(\sum_{\nu=0}^{3}\beta^{[\nu]}\partial_{\nu}+\gamma^{[0]}\partial_{y}^{\beta}+\beta^{[4]}\partial_{z}^{\beta}-\right. \\ -\gamma_{\zeta}^{[0]}\partial_{y}^{\zeta}+\zeta^{[4]}\partial_{z}^{\zeta}- \\ -\gamma_{\eta}^{[0]}\partial_{y}^{\eta}-\eta^{[4]}\partial_{z}^{\eta}+ \\ \left.+\gamma_{\theta}^{[0]}\partial_{y}^{\theta}+\theta^{[4]}\partial_{z}^{\theta}\right).\end{gathered} \tag{38}$$

that is:

$$\begin{gathered}G_0= \\ \begin{bmatrix}-\partial_0+\partial_3&\partial_1-\mathrm{i}\partial_2&\partial_y^{\beta}-\partial_y^{\theta}&\partial_y^{\zeta}-i\partial_y^{\eta}\\\partial_1+\mathrm{i}\partial_2&-\partial_0-\partial_3&\partial_y^{\zeta}+i\partial_y^{\eta}&\partial_y^{\beta}+\partial_y^{\theta}\\\partial_y^{\beta}-\partial_y^{\theta}&\partial_y^{\zeta}-i\partial_y^{\eta}&-\partial_0-\partial_3&-\partial_1+\mathrm{i}\partial_2\\\partial_y^{\zeta}+i\partial_y^{\eta}&\partial_y^{\beta}+\partial_y^{\theta}&-\partial_1-\mathrm{i}\partial_2&-\partial_0+\partial_3\end{bmatrix} \\ +\mathrm{i}\begin{bmatrix}0&0&\partial_z^{\beta}+\partial_z^{\theta}&\partial_z^{\zeta}+i\partial_z^{\eta}\\0&0&\partial_z^{\zeta}-i\partial_z^{\eta}&\partial_z^{\beta}-\partial_z^{\theta}\\-\partial_z^{\beta}-\partial_z^{\theta}&-\partial_z^{\zeta}-i\partial_z^{\eta}&0&0\\-\partial_z^{\zeta}+i\partial_z^{\eta}&-\partial_z^{\beta}+\partial_z^{\theta}&0&0\end{bmatrix}\end{gathered} \tag{39}$$

$$\begin{gathered}G_0[\varphi]=-\mathrm{i}\frac{\mathrm{h}}{\mathrm{c}}\sum_{w,p_1,p_2,p_3,n^{\beta},s^{\beta},n^{\zeta},s^{\zeta},n^{\eta},s^{\eta},n^{\theta},s^{\theta}}\check{g}(w, \\ p_1,p_2,p_3,n^{\beta},s^{\beta},n^{\zeta},s^{\zeta},n^{\eta},s^{\eta},n^{\theta},s^{\theta}) \\ \sum_{k=0}^{3}c_k(w,p_1,p_2,p_3,n^{\beta},s^{\beta},n^{\zeta},s^{\zeta},n^{\eta},s^{\eta},n^{\theta},s^{\theta})\times \\ \times\exp\left(-\mathrm{i}\frac{\mathrm{h}}{\mathrm{c}}(wx_0+p_1x_1+p_2x_2+p_3x_3+\right. \\ +n^{\beta}y^{\beta}+s^{\beta}z^{\beta}+n^{\zeta}y^{\zeta}+s^{\zeta}z^{\zeta}+ \\ \left.+n^{\eta}y^{\eta}+s^{\eta}z^{\eta}+n^{\theta}y^{\theta}+s^{\theta}z^{\theta})\right).\end{gathered} \tag{40}$$

Here

$$c_k(w, p_1, p_2, p_3, n^\beta, s^\beta, n^\zeta, s^\zeta, n^\eta, s^\eta, n^\theta, s^\theta)$$

is an eigenvector of

$$\breve{g}(w, p_1, p_2, p_3, n^\beta, s^\beta, n^\zeta, s^\zeta, n^\eta, s^\eta, n^\theta, s^\theta)$$

and

$$\begin{aligned}&\breve{g}(w, p_1, p_2, p_3, n^\beta, s^\beta, n^\zeta, s^\zeta, n^\eta, s^\eta, n^\theta, s^\theta) := \\ &:= \beta^{[0]}w + \beta^{[1]}p_1 + \beta^{[2]}p_2 + \beta^{[3]}p_3 + \\ &+\gamma^{[0]}n^\beta + \beta^{[4]}s^\beta - \gamma^{[0]}_\zeta n^\zeta + \zeta^{[4]}s^\zeta - \\ &-\gamma^{[0]}_\eta n^\eta - \eta^{[4]}s^\eta + \gamma^{[0]}_\theta n^\theta + \theta^{[4]}s^\theta.\end{aligned} \tag{41}$$

Here

$$\{c_0, c_1, c_2, c_3\}$$

is an orthonormalized basis of the complex4-vectors space.

Functions

$$\begin{aligned}&c_k(w, p_1, p_2, p_3, n^\beta, s^\beta, n^\zeta, s^\zeta, n^\eta, s^\eta, n^\theta, s^\theta)\times \\ &\times\exp\Big(-\mathrm{i}\frac{\mathrm{h}}{\mathrm{c}}(wx_0 + p_1x_1 + p_2x_2 + p_3x_3 + \\ &+n^\beta y^\beta + s^\beta z^\beta \ + \\ &+n^\zeta y^\zeta + s^\zeta z^\zeta + +n^\eta y^\eta + s^\eta z^\eta + n^\theta y^\theta + s^\theta z^\theta)\Big)\end{aligned} \tag{42}$$

are eigenvectors of operator G_0.

4 Chromes under Lorentz's and Cartesian transformations

$$\varphi^\zeta_y := c(w, \mathbf{p}, f)\exp\Big(-\mathrm{i}\frac{\mathrm{h}}{\mathrm{c}}(wx_0 + \mathbf{px} + \gamma^{[0]}_\zeta f y^\zeta)\Big)$$

is *a red lower chrome function,*

$$\varphi^\zeta_z := c(w, \mathbf{p}, f)\exp\Big(-\mathrm{i}\frac{\mathrm{h}}{\mathrm{c}}(wx_0 + \mathbf{px} - \mathrm{i}\zeta^{[4]}f z^\zeta)\Big)$$

is *a red upper chrome function,*

$$\varphi^\eta_y := c(w, \mathbf{p}, f)\exp\Big(-\mathrm{i}\frac{\mathrm{h}}{\mathrm{c}}(wx_0 + \mathbf{px} + \gamma^{[0]}_\eta f y^\eta)\Big)$$

is *a green lower chrome function,*

$$\varphi^\eta_z := c(w, \mathbf{p}, , f)\exp\Big(-\mathrm{i}\frac{\mathrm{h}}{\mathrm{c}}(wx_0 + \mathbf{px} - \mathrm{i}\eta^{[4]}f z^\eta)\Big)$$

is *a green upper chrome function,*

$$\varphi^\theta_y := c(w, \mathbf{p}, f)\exp\Big(-\mathrm{i}\frac{\mathrm{h}}{\mathrm{c}}(wx_0 + \mathbf{px}+\gamma^{[0]}_\theta f y^\theta)\Big)$$

is *a blue lower chrome function,*

$$\varphi^\theta_z := c(w, \mathbf{p}, s^\theta)\exp\Big(-\mathrm{i}\frac{\mathrm{h}}{\mathrm{c}}(wx_0 + \mathbf{px} - \mathrm{i}\theta^{[4]}f z^\theta)\Big)$$

is *a blue upper chrome function.*

Operator $-\partial^\zeta_y\partial^\zeta_y$ is called *a red lower chrome operator*, $-\partial^\zeta_z\partial^\zeta_z$ is *a red upper chrome operator,* $-\partial^\eta_y\partial^\eta_y$ is called *a green lower chrome operator*, $-\partial^\eta_z\partial^\eta_z$ is *a green upper chrome operator,* $-\partial^\theta_y\partial^\theta_y$ is called *a blue lower chrome operator*, $-\partial^\theta_z\partial^\theta_z$ is *a blue upper chrome operator*.

For example, if φ^ζ_z is a red upper chrome function then

$$\begin{aligned}-\partial^\zeta_y\partial^\zeta_y\varphi^\zeta_z &= -\partial^\eta_y\partial^\eta_y\varphi^\zeta_z = -\partial^\eta_z\partial^\eta_z\varphi^\zeta_z = \\ &= -\partial^\theta_y\partial^\theta_y\varphi^\zeta_z = -\partial^\theta_z\partial^\theta_z\varphi^\zeta_z = 0\end{aligned}$$

but

$$-\partial^\zeta_z\partial^\zeta_z\varphi^\zeta_z = -\left(\frac{\mathrm{h}}{\mathrm{c}}f\right)^2\varphi^\zeta_z.$$

Because

$$G_0[\varphi] = 0$$

then

$$UG_0U^{-1}U[\varphi] = 0.$$

If $U = U_{1,2}(\alpha)$ then $G_0 \to U_{1,2}(\alpha)G_0U^{-1}_{1,2}(\alpha)$ and $[\varphi] \to U_{1,2}(\alpha)[\varphi]$.

In this case:

$\partial_1 \to \partial'_1 := (\cos\alpha\cdot\partial_1 - \sin\alpha\cdot\partial_2)$,
$\partial_2 \to \partial'_2 := (\cos\alpha\cdot\partial_2 + \sin\alpha\cdot\partial_1)$,
$\partial_0 \to \partial'_0 := \partial_0$,
$\partial_3 \to \partial'_3 := \partial_3$,
$\partial^\beta_y \to \partial^{\beta\prime}_y := \partial^\beta_y$,
$\partial^\beta_z \to \partial^{\beta\prime}_z := \partial^\beta_z$,
$\partial^\zeta_y \to \partial^{\zeta\prime}_y := \left(\cos\alpha\cdot\partial^\zeta_y - \sin\alpha\cdot\partial^\eta_y\right)$,
$\partial^\eta_y \to \partial^{\eta\prime}_y := \left(\cos\alpha\cdot\partial^\eta_y + \sin\alpha\cdot\partial^\zeta_y\right)$,
$\partial^\zeta_z \to \partial^{\zeta\prime}_z := \left(\cos\alpha\cdot\partial^\zeta_z + \sin\alpha\cdot\partial^\eta_z\right)$,
$\partial^\eta_z \to \partial^{\eta\prime}_z := \left(\cos\alpha\cdot\partial^\eta_z - \sin\alpha\cdot\partial^\zeta_z\right)$,
$\partial^\theta_y \to \partial^{\theta\prime}_y := \partial^\theta_y$,
$\partial^\theta_z \to \partial^{\theta\prime}_z := \partial^\theta_z$.

Therefore,

$$\begin{aligned}-\partial^{\zeta\prime}_z\partial^{\zeta\prime}_z\varphi^\zeta_z &= \left(f\frac{\mathrm{h}}{\mathrm{c}}\cos\alpha\right)^2\cdot\varphi^\zeta_z, \\ -\partial^{\eta\prime}_z\partial^{\eta\prime}_z\varphi^\zeta_z &= \left(-\sin\alpha\cdot f\frac{\mathrm{h}}{\mathrm{c}}\right)^2\varphi^\zeta_z.\end{aligned}$$

If $\alpha = -\frac{\pi}{2}$ then

$$\begin{aligned}-\partial^{\zeta\prime}_z\partial^{\zeta\prime}_z\varphi^\zeta_z &= 0, \\ -\partial^{\eta\prime}_z\partial^{\eta\prime}_z\varphi^\zeta_z &= \left(f\frac{\mathrm{h}}{\mathrm{c}}\right)^2\varphi^\zeta_z.\end{aligned}$$

That is under such rotation the red state becomes the green state.

If $U = U_{3,2}(\alpha)$ then $G_0 \to U_{3,2}(\alpha) G_0 U_{3,2}^{-1}(\alpha)$ and $[\varphi] \to U_{3,2}(\alpha)[\varphi]$.

In this case:

$\partial_0 \to \partial'_0 := \partial_0$,
$\partial_1 \to \partial'_1 := \partial_1$,
$\partial_2 \to \partial'_2 := (\cos\alpha \cdot \partial_2 + \sin\alpha \cdot \partial_3)$,
$\partial_3 \to \partial'_3 := (\cos\alpha \cdot \partial_3 - \sin\alpha \cdot \partial_2)$,
$\partial_y^\beta \to \partial_y^{\beta\prime} := \partial_y^\beta$,
$\partial_y^\zeta \to \partial_y^{\zeta\prime} := \partial_y^\zeta$,
$\partial_y^\eta \to \partial_y^{\eta\prime} := \left(\cos\alpha \cdot \partial_y^\eta - \sin\alpha \cdot \partial_y^\theta\right)$,
$\partial_y^\theta \to \partial_y^{\theta\prime} := \left(\cos\alpha \cdot \partial_y^\theta + \sin\alpha \cdot \partial_y^\eta\right)$,
$\partial_z^\beta \to \partial_z^{\beta\prime} := \partial_z^\beta$,
$\partial_z^\zeta \to \partial_z^{\zeta\prime} := \partial_z^\zeta$,
$\partial_z^\eta \to \partial_z^{\eta\prime} := \left(\cos\alpha \cdot \partial_z^\eta - \sin\alpha \cdot \partial_z^\theta\right)$,
$\partial_z^\theta \to \partial_z^{\theta\prime} := \left(\cos\alpha \cdot \partial_z^\theta + \sin\alpha \cdot \partial_z^\eta\right)$.

Therefore, if φ_y^η is a green lower chrome function then

$$-\partial_z^{\eta\prime}\partial_z^{\eta\prime}\varphi_y^\eta = \left(\frac{\mathrm{h}}{\mathrm{c}}\cos\alpha \cdot f\right)^2 \cdot \varphi_y^\eta,$$
$$-\partial_y^{\theta\prime}\partial_y^{\theta\prime}\varphi_y^\eta = \left(\frac{\mathrm{h}}{\mathrm{c}}\sin\alpha \cdot f\right)^2 \cdot \varphi_y^\eta.$$

If $\alpha = \pi/2$ then

$$-\partial_z^{\eta\prime}\partial_z^{\eta\prime}\varphi_y^\eta = 0,$$
$$-\partial_y^{\theta\prime}\partial_y^{\theta\prime}\varphi_y^\eta = \left(\frac{\mathrm{h}}{\mathrm{c}}f\right)^2 \cdot \varphi_y^\eta.$$

That is under such rotation the green state becomes blue state.

If $U = U_{3,1}(\alpha)$ then $G_0 \to U_{3,1}(\alpha) G_0 U_{3,1}^{-1}(\alpha)$ and $[\varphi] \to U_{3,1}(\alpha)[\varphi]$.

In this case:

$\partial_0 \to \partial'_0 := \partial_0$,
$\partial_1 \to \partial'_1 := (\cos\alpha \cdot \partial_1 - \sin\alpha \cdot \partial_3)$,
$\partial_2 \to \partial'_2 := \partial_2$,
$\partial_3 \to \partial'_3 := (\cos\alpha \cdot \partial_3 + \sin\alpha \cdot \partial_1)$,
$\partial_y^\beta \to \partial'_3 := \partial_y^\beta$,
$\partial_y^\zeta \to \partial_y^{\zeta\prime} := \left(\cos\alpha \cdot \partial_y^\zeta + \sin\alpha \cdot \partial_y^\theta\right)$,
$\partial_y^\eta \to \partial_y^{\eta\prime} := \partial_y^\eta$,
$\partial_y^\theta \to \partial_y^{\theta\prime} := \left(\cos\alpha \cdot \partial_y^\theta - \sin\alpha \cdot \partial_y^\zeta\right)$,
$\partial_z^\beta \to \partial_z^{\beta\prime} := \partial_z^\beta$,
$\partial_z^\zeta \to \partial_z^{\zeta\prime} := \left(\cos\alpha \cdot \partial_z^\zeta - \sin\alpha \cdot \partial_z^\theta\right)$,
$\partial_z^\eta \to \partial_z^{\eta\prime} := \partial_z^\eta$,
$\partial_z^\theta \to \partial_z^{\theta\prime} := \left(\cos\alpha \cdot \partial_z^\theta + \sin\alpha \cdot \partial_z^\zeta\right)$.

Therefore,

$$-\partial_z^{\zeta\prime}\partial_z^{\zeta\prime}\varphi_z^\zeta = -\left(f\frac{\mathrm{h}}{\mathrm{c}}\cos\alpha\right)^2 \cdot \varphi_z^\zeta,$$

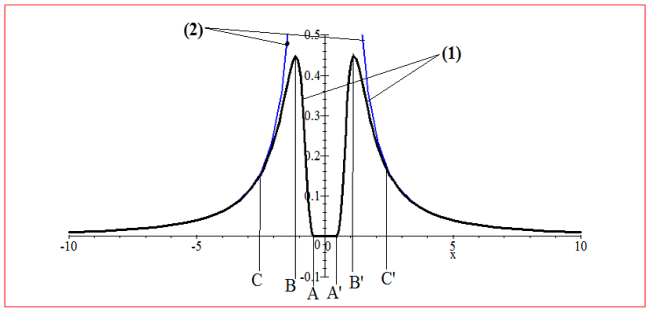

Fig. 1:

$$-\partial_z^{\theta\prime}\partial_z^{\theta\prime}\varphi_z^\zeta = -\left(\sin\alpha \cdot f\frac{\mathrm{h}}{\mathrm{c}}\right)^2 \varphi_z^\zeta.$$

If $\alpha = \pi/2$ then

$$-\partial_z^{\zeta\prime}\partial_z^{\zeta\prime}\varphi_z^\zeta = 0,$$
$$-\partial_z^{\theta\prime}\partial_z^{\theta\prime}\varphi_z^\zeta = -\left(f\frac{\mathrm{h}}{\mathrm{c}}\right)^2 \varphi_z^\zeta.$$

That is under such rotation the red state becomes the blue state. Thus at the Cartesian turns chrome of a state is changed.

One of ways of elimination of this noninvariancy consists in the following. Calculations in [2, p. 156] give the grounds to assume that some oscillations of quarks states bend time-space in such a way that acceleration of the bent system in relation to initial system submits to the following law (Fig. 1):

$$g(t, \mathbf{x}) = \mathrm{c}\lambda / \left(\mathbf{x}^2 \cosh^2\left(\lambda t/\mathbf{x}^2\right)\right).$$

Here the acceleration plot is line (1) and the line (2) is plot of $\lambda/\mathbf{x}^2$.

Hence, to the right from point C' and to the left from point C *the Newtonian gravitation law* is carried out.

AA' is *the Asymptotic Freedom Zone*.

CB and $B'C'$ is *the Confinement Zone.*

Let in the potential hole AA' there are three quarks φ_y^ζ, φ_y^η, φ_y^θ. Their general state function is determinant with elements of the following type: $\varphi_y^{\zeta\eta\theta} := \varphi_y^\zeta \varphi_y^\eta \varphi_y^\theta$. In this case:

$$-\partial_y^\zeta \partial_y^\zeta \varphi_y^{\zeta\eta\theta} = \left(\frac{\mathrm{h}}{\mathrm{c}}f\right)^2 \varphi_y^{\zeta\eta\theta}$$

and under rotation $U_{1,2}(\alpha)$:

$$-\partial_y^{\zeta\prime}\partial_y^{\zeta\prime}\varphi_y^{\zeta\eta\theta} = \left(\frac{\mathrm{h}}{\mathrm{c}}f\right)^2 \left(\gamma_\zeta^{[0]}\cos\alpha - \gamma_\eta^{[0]}\sin\alpha\right)^2 \left(\varphi_y^\zeta \varphi_y^\eta \varphi_y^\theta\right)$$
$$= \left(\frac{\mathrm{h}}{\mathrm{c}}f\right)^2 \varphi_y^{\zeta\eta\theta}.$$

That is at such turns the quantity of red chrome remains.

As and for all other Cartesian turns and for all other chromes.

Baryons $\Delta^- = ddd$, $\Delta^{++} = uuu$, $\Omega^- = sss$ belong to such structures.

If $U = U_{1,0}(\alpha)$ then $G_0 \to U_{1,0}^{-1\ddagger}(\alpha) G_0 U_{1,0}^{-1}(\alpha)$ and $[\varphi] \to U_{1,0}(\alpha)[\varphi]$.

In this case:

$\partial_0 \to \partial'_0 := (\cosh\alpha \cdot \partial_0 + \sinh\alpha \cdot \partial_1)$,
$\partial_1 \to \partial'_1 := (\cosh\alpha \cdot \partial_1 + \sinh\alpha \cdot \partial_0)$,
$\partial_2 \to \partial'_2 := \partial_2$,
$\partial_3 \to \partial'_3 := \partial_3$,
$\partial_y^\beta \to \partial_y^{\beta\prime} := \partial_y^\beta$,
$\partial_y^\zeta \to \partial_y^{\zeta\prime} := \partial_y^\zeta$,
$\partial_y^\eta \to \partial_y^{\eta\prime} := \left(\cosh\alpha \cdot \partial_y^\eta - \sinh\alpha \cdot \partial_z^\theta\right)$,
$\partial_y^\theta \to \partial_y^{\theta\prime} := \left(\cosh\alpha \cdot \partial_y^\theta + \sinh\alpha \cdot \partial_z^\eta\right)$,
$\partial_z^\beta \to \partial_z^{\beta\prime} := \partial_z^\beta$,
$\partial_z^\zeta \to \partial_z^{\zeta\prime} := \partial_z^\zeta$,
$\partial_z^\eta \to \partial_z^{\eta\prime} := \left(\cosh\alpha \cdot \partial_z^\eta + \sinh\alpha \cdot \partial_y^\theta\right)$,
$\partial_z^\theta \to \partial_z^{\theta\prime} := \left(\cosh\alpha \cdot \partial_z^\theta - \sinh\alpha \cdot \partial_y^\eta\right)$.

Therefore,

$$-\partial_y^{\eta\prime}\partial_y^{\eta\prime}\varphi_y^\eta = \left(1 + \sinh^2\alpha\right) \cdot \left(\frac{\mathrm{h}}{\mathrm{c}} f\right)^2 \varphi_y^\eta,$$

$$-\partial_z^{\theta\prime}\partial_z^{\theta\prime}\varphi_y^\eta = \sinh^2\alpha \cdot \left(\frac{\mathrm{h}}{\mathrm{c}} f\right)^2 \varphi_y^\eta.$$

Similarly chromes and grades change for other states and under other Lorentz transformation.

One of ways of elimination of this noninvariancy is the following:

Let

$$\varphi_{yz}^{\zeta\eta\theta} := \varphi_y^\zeta \varphi_y^\eta \varphi_y^\theta \varphi_z^\zeta \varphi_z^\eta \varphi_z^\theta.$$

Under transformation $U_{1,0}(\alpha)$:

$$-\partial_z^{\theta\prime}\partial_z^{\theta\prime}\varphi_{yz}^{\zeta\eta\theta} = -\left(\mathrm{i}\frac{\mathrm{h}}{\mathrm{c}} f\right)^2 \varphi_{yz}^{\zeta\eta\theta}.$$

That is a magnitude of red chrome of this state doesn't depend on angle α.

This condition is satisfied for all chromes and under all Lorentz's transformations.

Pairs of baryons

$$\{p = uud, n = ddu\},$$
$$\left\{\Sigma^+ = uus, \Xi^0 = uss\right\},$$
$$\left\{\Delta^+ = uud, \Delta^0 = udd\right\}$$

belong to such structures.

Conclusion

Baryons represent one of ways of elimination of the chrome noninvariancy under Cartesian and under Lorentz transformation.

Submitted on April 4, 2014 / Accepted on April 9, 2014

References

1. Amsler C. et al. (Particle Data Group). Review of particle physics — quark model. *Physics Letters B*, 2008, v. 667, 1.
2. Quznetsov G. Final Book on Fundamental Theoretical Physics. American Research Press, Rehoboth (NM), 2011.

CKM and PMNS Mixing Matrices from Discrete Subgroups of SU(2)

Franklin Potter

Sciencegems.com, 8642 Marvale Drive, Huntington Beach, CA 92646 USA E-mail: frank11hb@yahoo.com

One of the greatest challenges in particle physics is to determine the first principles origin of the quark and lepton mixing matrices CKM and PMNS that relate the flavor states to the mass states. This first principles derivation of both the PMNS and CKM matrices utilizes quaternion generators of the three discrete (i.e., finite) binary rotational subgroups of SU(2) called [3,3,2], [4,3,2], and [5,3,2] for three lepton families in R^3 and four related discrete binary rotational subgroups [3,3,3], [4,3,3], [3,4,3], and [5,3,3] represented by four quark families in R^4. The traditional 3×3 CKM matrix is extracted as a submatrix of the 4×4 CKM4 matrix. The predicted fourth family of quarks has not been discovered yet. If these two additional quarks exist, there is the possibility that the Standard Model lagrangian may apply all the way down to the Planck scale.

1 Introduction

The very successful Standard Model (SM) local gauge group $SU(2)_L \times U(1)_Y \times SU(3)_C$ defines an electroweak (EW) interaction part and a color interaction part. Experiments have determined that the left-handed EW isospin flavor states are linear superpositions of mass eigenstates. One of the greatest challenges in particle physics is to determine the first principles origin of the quark and lepton mixing matrices CKM and PMNS that relate the flavor states to the mass states.

In a recent article [1] I derived the lepton PMNS mixing matrix by using the quaternion (i.e., spinor) generators of three specific discrete (i.e., finite) binary rotational subgroups of the EW gauge group $SU(2)_L \times U(1)_Y$, one group for each lepton family, while remaining within the realm of the SM lagrangian. All the derived PMNS matrix element values are within the 1σ range of the empirically determined absolute values.

The three lepton family groups, binary rotational groups called [3,3,2], [4,3,2], and [5,3,2], (or 2T, 2O, and 2I), have discrete rotational symmetries in R^3. Each group has two degenerate basis states which must be taken in linear superposition to form the two orthogonal fermion flavor states in each family, i.e., (ν_e, e), (ν_μ, μ), and (ν_τ, τ).

In order to have a consistent geometrical approach toward understanding the SM, I have proposed in a series of articles [2–4] over several years that the quark flavor states represent discrete binary rotational groups also. However, one must move up one spatial dimension from R^3 to R^4 and use the related four discrete binary rotational subgroups [3,3,3], [4,3,3], [3,4,3], and [5,3,3], (or 5-cell, 16-cell, 24-cell, and 600-cell), for the quarks, thereby dictating four quark families. Recall that both R^3 and R^4 are subspaces of the unitary space C^2.

Therefore, following up the success I had deriving the neutrino PMNS matrix, the CKM mixing matrix should be derivable by using the same geometrical method, i.e., based upon the quaternion generators of the four groups of specific discrete rotational symmetries. In this quark case, however, first one determines a 4×4 mixing matrix called CKM4 and then extracts the appropriate 3×3 submatrix as the traditional CKM matrix.

These seven closely-related groups representing specific discrete rotational symmetries dictate the three known lepton families in R^3 and four related quark families in R^4, the fourth quark family still to be discovered. That is, neither leptons nor quarks are to be considered as point objects at the fundamental Planck scale of about 10^{-35} meters. If this geometrical derivation of both the PMNS and CKM mixing matrices is based upon the correct reason for the mixing of flavor states to make the mass states, then one must reconcile the empirical data with the prediction of a fourth quark family.

My proposal that leptons are 3-D entities and that quarks are 4-D entities has several advantages. There is a clear distinction between leptons and quarks determined by inherent geometrical properties such as explaining that leptons do not experience the color interaction via $SU(3)_C$ because gluons and quarks would involve 4-D rotations associated with the three color charges defined in R^4. Also, one now has a geometrical reason for there being more than one family of leptons and of quarks. In addition, the mass ratios of the fundamental fermions are determined by the group relationships to the j-invariant of the Monster Group. These physical properties and many other physical consequences are discussed in my previous papers.

2 Review of the PMNS matrix derivation

This section reviews the mathematical procedure used in my 2013 derivation [1] of the PMNS matrix from first principles. One constructs the three SU(2) generators, the U_1 = j, U_2 = k, and the U_3 = i, (i.e., the Pauli matrices in quaternion form), from the three quaternion generators from each of the discrete subgroups [3,3,2], [4,3,2], and [5,3,2]. As you know, the three Pauli matrices, i.e., the quaternions i, j, and k, can generate all rotations in R^3 about a chosen axis or, equivalently, all rotations in the plane perpendicular to this axis. For example,

Table 1: Lepton Family Quaternion Generators U_2

Fam.	Grp.	Generator	Factor	Angle°
ν_e,e	332	$-\frac{1}{2}i-\frac{1}{2}j+\frac{1}{\sqrt{2}}k$	-0.2645	105.337
ν_μ,μ	432	$-\frac{1}{2}i-\frac{1}{\sqrt{2}}k+\frac{1}{2}j$	0.8012	36.755
ν_τ,τ	532	$-\frac{1}{2}i-\frac{\phi}{2}j+\frac{\phi^{-1}}{2}k$	-0.5367	122.459

the quaternion k is a binary rotation by 180° in the i-j plane.

The complete mathematical description [5] for the generators operating on the unit vector x in R^3 extending from the origin to the surface of the unit sphere S^2 is given by $R_s = i\,x\,U_s$ where s = 1, 2, 3 and

$$U_1 = j,\;\; U_2 = -icos\frac{\pi}{q} - jcos\frac{\pi}{p} + ksin\frac{\pi}{h},\;\; U_3 = i, \qquad (1)$$

with h = 4, 6, 10 for the three lepton flavor groups [p,q,2], respectively. Their U_2 generators are listed in Table 1.

My three lepton family binary rotational groups, [3,3,2], [4,3,2], and [5,3,2], all have generators U_1 = j and U_3 = i, but each U_2 is a different quaternion generator operating in R^3. One obtains the correct neutrino PMNS mixing angles from the linear superposition of their U_2's by making the total U_2 = k, agreeing with SU(2). This particular combination of three discrete angle rotations is now equivalent to a rotation in the i-j plane by the quaternion k.

The sum of all three U_2 generators should be k, so there are three equations for the three unknown factors, which are determined to be: -5.537, 16.773, and -11.236. Let the quantity $\phi = (\sqrt{5}+1)/2$, the golden ratio. The resulting angles in Table 1 are the arccosines of these factors (normalized), i.e., their projections to the k-axis, but they are twice the rotation angles required in R^3, a property of quaternion rotations.

Using one-half of these angles produces

$$\theta_1 = 52.67^\circ,\; \theta_2 = 18.38^\circ,\; \theta_3 = 61.23^\circ, \qquad (2)$$

resulting in mixing angles

$$\theta_{12} = 34.29^\circ,\; \theta_{13} = -8.56^\circ,\; \theta_{23} = -42.85^\circ. \qquad (3)$$

The absolute values of these mixing angles are all within the 1σ range of their values for the normal mass hierarchy [6–11] as determined from several experiments:

$$\theta_{12} = \pm 34.47^\circ,\; \theta_{13} = \pm 8.73^\circ,\; \theta_{23} = \pm(38.39^\circ - 45.81^\circ). \qquad (4)$$

The experimental 1σ uncertainty in θ_{12} is about 6%, in θ_{13} about 14%, and θ_{23} has the range given. The ± signs arise from the squares of the sines of the angles determined by the experiments.

For three lepton families, one has the neutrino flavor states ν_e, ν_μ, ν_τ, and the mass states ν_1, ν_2, ν_3, related by the PMNS matrix V_{ij}

$$\begin{bmatrix} \nu_e \\ \nu_\mu \\ \nu_\tau \end{bmatrix} = \begin{bmatrix} V_{e1} & V_{e2} & V_{e3} \\ V_{\mu 1} & V_{\mu 2} & V_{\mu 3} \\ V_{\tau 1} & V_{\tau 2} & V_{\tau 3} \end{bmatrix} \begin{bmatrix} \nu_1 \\ \nu_2 \\ \nu_3 \end{bmatrix}.$$

The PMNS entries are the products of the sines and cosines of the derived angles (3) using the standard parametrization of the matrix, producing:

$$\begin{bmatrix} 0.817 & 0.557 & -0.149e^{-i\delta} \\ -0.413 - 0.084e^{i\delta} & 0.605 - 0.057e^{i\delta} & -0.673 \\ -0.383 + 0.090e^{i\delta} & 0.562 + 0.061e^{i\delta} & 0.725 \end{bmatrix}.$$

For direct comparison, the empirically estimated PMNS matrix for the *normal hierarchy* of neutrino masses is

$$\begin{bmatrix} 0.822 & 0.547 & -0.150 + 0.038i \\ -0.356 + 0.0198i & 0.704 + 0.0131i & 0.614 \\ 0.442 + 0.0248i & -0.452 + 0.0166i & 0.774 \end{bmatrix}$$

Comparing the V_{e3} elements from each, the phase angle δ is confined to be $0^\circ \le \delta \le \pm 14.8^\circ$, an angle in agreement with the T2K collaboration value of $\delta \approx 0$ but quite different from other proposed $\delta \approx \pi$ values.

3 The CKM4 matrix derivation

The success of the above geometrical procedure for deriving the lepton PMNS matrix by using the quaternion generators from the 3 discrete binary rotation groups demands that the same approach should work for the quark families in R^4 using the 4 discrete binary rotation groups [3,3,3], [4,3,3], [3,4,3], and [5,3,3]. If this procedure succeeds in deriving the CKM matrix elements as a 3×3 submatrix of CKM4, then a fourth sequential quark family, call its quark states b' and t', exists in Nature.

These 4 binary rotational groups for the quark family flavors each have rotation subgroups of SO(4) = SO(3) × SO(3), and they also have the double covering SU(2) × SU(2). The SO(4) is the rotation group of the unit hypersphere S^3 in R^4, with every 4-D rotation being simultaneous rotations in two orthogonal planes.

The only finite (i.e., discrete) quaternion groups are [12]

$$2I,\;\; 2O,\;\; 2T,\;\; 2D_{2n},\;\; 2C_n,\;\; 1C_n\,(n\;odd) \qquad (5)$$

with the 2 in front meaning binary (double) group, the double cover of the normal 3-D rotation group by SU(2) over SO(3). Mathematically, the 4 discrete binary groups for the quark families each can be identified as (L/L_K; R/R_K) with the homomorphism $L/L_K = R/R_K$. Here L and R are specific discrete groups of quaternions and L_K and R_K are their kernels.

P. DuVal [13] established that one only needs the cyclic groups $2C_n$ and $1C_n$ when considering the four discrete rotational symmetry groups, i.e., the ones I am using for the

quark families. Essentially, vertices on the 4-D regular polytope can be projected to be a regular polygon on each of the two orthogonal planes in R^4.

There will be 6 quaternion generators for each of the 4 groups, producing simultaneous rotations in two orthogonal planes. The two sets of Pauli matrices for producing continuous rotations can be identified as i, j, k, and another i, j, k, but they act on the two different S^2 spheres, i.e, in the two orthogonal planes. One can consider this 4-D rotational transformation as the result of a bi-quaternion operation [14], or equivalently, a bi-spinor or Ivanenko-Landau-Kähler spinor or Dirac-Kähler spinor operation.

For three quark families, one has the "down" flavor states d', s', b', and their mass states d, s, b, related by the CKM matrix. This quark mixing matrix for the left-handed components is defined in the standard way as

$$V = U_L D_L^{\dagger}, \tag{6}$$

but for four quark families the mathematics is a little different, for one must consider the bi-quaternion case in which there will be Bogoliubov mixing [14], producing two subfactors for each component, i.e.,

$$U_L = W^u_{14,23} W^u_{12,34}, \quad D_L = W^d_{14,23} W^d_{12,34} \tag{7}$$

with the W^u and W^d factor on the right mixing the 1st and 2nd generations and, separately, mixing the 3rd and 4th generations. The Bogoliubov mixing in the factor on the left mixes the 1st and 4th generations and, separately, the 2nd and 3rd generations. Therefore, the CKM4 matrix derives from

$$V_{CKM4} = U_L D_L^{\dagger} = W^u_{14,23} W^u_{12,34} (W^d_{14,23} W^d_{12,34})^{\dagger}. \tag{8}$$

The product $W^u_{12,34} W^{d\dagger}_{12,34}$ is given by

$$W^u_{12,34} W^{d\dagger}_{12,34} = \begin{bmatrix} x_1 & y_1 & 0 & 0 \\ z_1 & w_1 & 0 & 0 \\ 0 & 0 & x_2 & y_2 \\ 0 & 0 & z_2 & w_2 \end{bmatrix}.$$

The upper left block is an SU(2) matrix that mixes generations 1 and 2 while the lower right block is an SU(2) matrix that mixes generations 3 and 4. Each 2x2 block relates the rotation angles and the phases via

$$\begin{bmatrix} x & y \\ z & w \end{bmatrix} = \begin{bmatrix} cos\theta\, e^{i\alpha} & -sin\theta\, e^{i\beta} \\ sin\theta\, e^{i\gamma} & cos\theta\, e^{i\delta} \end{bmatrix}.$$

The 4×4 matrix that achieves the Bogoliubov mixing has four possible forms for the four possible isospin cases obeying SU(2) × SU(2): (0, 0), (1/2, 0), (0, 1/2), and (1/2, 1/2). The (1/2, 1/2) is the one for equal, simultaneous, isospin 1/2 rotations in the two orthogonal planes for CKM4:

$$W^{u,d}_{14,23} = \frac{1}{\sqrt{2}} \begin{bmatrix} 1 & 0 & -1 & 0 \\ 0 & 1 & 0 & -1 \\ 1 & 0 & 1 & 0 \\ 0 & 1 & 0 & 1 \end{bmatrix}.$$

Table 2: Quark Family Discrete Group Assignments for U_2

Fam.	Grp.	Generator	Angle°	Factor	Angle°
u,d	333	exp[2πi/5]	72	1.132	81.504
c,s	433	exp[2πi/8]	45	1.132	50.940
t,b	343	exp[2πi/12]	30	1.132	33.960
t',b'	533	exp[2πi/30]	12	1.132	13.584

Multiplying out these three 4×4 bi-quaternion mixing matrices, one determines that

$$V_{CKM4} = \frac{1}{2} \begin{bmatrix} x_1 + x_2 & y_1 + y_2 & x_1 - x_2 & y_1 - y_2 \\ z_1 + z_2 & w_1 + w_2 & z_1 - z_2 & w_1 - w_2 \\ x_1 - x_2 & y_1 - y_2 & x_1 + x_2 & y_1 + y_2 \\ z_1 - z_2 & w_1 - w_2 & z_1 + z_2 & w_1 + w_2 \end{bmatrix}$$

in which the phases $\alpha, \beta, \gamma, \delta$ have been ignored.

One determines the angles θ_1 and θ_2 from the quaternion generators of the 4 discrete binary rotation groups for the quark families. Projections of each of the four discrete symmetry 4-D entities onto the two orthogonal planes produces a regular polygon [5, 13] with the generator iexp[2πj/h], as given in Table 2, where the h values are 5, 8, 12, 30, for the [3,3,3], [4,3,3], [3,4,3], and [5,3,3], respectively.

Again, we need to determine the contribution from each group generator that will make the sum add to 180°, i.e., make their collective action produce the rotation $U_2 = k$. Expanding out the exponentials in terms of sines and cosines reveals four unknowns but only two equations. Alternately, because the four rotation angles sum to only 159°, we can use the same factor for each group, i.e., the ratio 180°/159° = 1.132.

In the last column of Table 2 are the normalized angles which are twice the angle required. Therefore, taking the appropriate half-angle differences produces the mixing angles

$$\theta_1 = 15.282^{\circ}, \quad \theta_2 = 10.188^{\circ}. \tag{9}$$

Substituting the cosines and sines of these two derived angles into the CKM4 matrix form above produces a mixing matrix symmetrical about the diagonal. Remember that I have ignored up to eight possible phases in the 2x2 blocks.

$$V_{CKM4} = \begin{bmatrix} 0.9744 & 0.2203 & 0.0098 & 0.0433 \\ 0.2203 & 0.9744 & 0.0433 & 0.0098 \\ 0.0098 & 0.0433 & 0.9744 & 0.2203 \\ 0.0433 & 0.0098 & 0.2203 & 0.9744 \end{bmatrix}.$$

One can compare the upper left 3×3 submatrix to the most recent *estimated absolute values* [7]

$$V_{CKM} = \begin{bmatrix} 0.9745 & 0.2246 & 0.0036 \\ 0.2244 & 0.9736 & 0.0415 \\ 0.0088 & 0.0407 & 0.9991 \end{bmatrix}.$$

Note that most of these estimated V_{CKM} values are probably good to within a few percent but some could have uncertainties as large as 10% or more.

Of concern are my low values of 0.2203 for V_{us} and V_{cd}. However, according to the Particle Data Group (2013) there are two possible values [7]: 0.2253 and 0.2204, the latter from tau decays. Also, my derived symmetric CKM4 matrix V_{ub} value is high while the V_{td} value is reasonable, i.e., V_{td} at 0.0098 compares well with the estimated value of 0.0088.

The V_{tb} element of CKM4 is 0.9744, quite a bit smaller than the suggested 0.9991 V_{tb} value for the 3×3 CKM matrix. However, if one imposes the unitarity condition on the rows and columns of the extracted CKM, the new value for this V_{tb} matrix element would be 0.999, in agreement.

My final comment is that if one calculates CKM using only the first three quark groups [3,3,3], [4,3,3], and [3,4,3], the resulting 3×3 CKM matrix will disagree significantly with the known CKM matrix. Therefore, one cannot eliminate a fourth quark family when discrete rotational subgroups of SU(2) are considered.

4 Discussion

In the SM the EW symmetry group is the Lie group $SU(2)_L \times U(1)_Y$. This local gauge group operating on the lepton and quark states works extremely well, meaning that all its predictions agree with experiments so far. However, in this context there is no reason for Nature to have more than one fermion family, and certainly no reason for having 3 lepton families and at least 3 quark families. As far as I know, the normal interpretation of the SM provides no answer that dictates the actual number of families, although the upper limit of 3 lepton families with low mass neutrinos is well established via Z^0 decays and via analysis of the CMB background.

My geometrical approach with *discrete* symmetries alters the default reliance upon SU(2) and its continuous symmetry transformations, for I utilize discrete binary rotational subgroups of SU(2) for the fundamental fermion states, a different subgroup for each lepton family and for each quark family. In this scenario one can surmise that the enormous success of the SM occurs because $SU(2)_L \times U(1)_Y$ is acting like a mathematical "cover group" for the actual underlying discrete rotations operating on the lepton states and quark states.

Assuming that the above matrix derivations are correct, the important question is: Where is the b' quark of the predicted 4th quark family? In 1992 I predicted a top quark mass of about 160 GeV, a b' quark mass of 65–80 GeV, and a t' quark at a whopping 2600 GeV. These mass predictions were based upon the mass ratios being determined by the j-invariant function of elliptic modular functions and of fractional linear transformations, i.e., Möbius transformations. Note that all seven discrete groups I have for the fermions are related to the j-invariant and Möbius transformations, which have direct connections to numerous areas of fundamental mathematics.

With a predicted b' mass that is much smaller than the top quark mass of 173.3 GeV and even smaller than the W mass at 80.4 GeV, one would have expected some production of the b' at LEP, Fermilab, and the LHC. Yet, no clear indication of the b' quark has appeared.

Perhaps the b' quark has escaped detection at the LHC and lies hidden in the stored data from the runs at 7 TeV and 8 TeV. With a mass value below the W and Z masses, the b' quark must decay via flavor changing neutral current (FCNC) decay channels [16] such as b' → b + γ and b' → b + gluon. The b' could have an average lifetime too long for the colliders to have detected a reasonable number of its decays within the detector volumes and/or the energy and angle cuts. However, the b' quark and t' quark would affect certain other decays that depend upon the heaviest "top" quark in a box diagram or penguin diagram.

Another possibility is that a long lifetime might allow the formation of the quarkonium bound state b'-anti-b', which has its own specific decay modes, to bb-bar, gg, $\gamma\gamma$, and WW* → $\nu\nu\ell\ell$. Depending upon the actual quarkonium bound state, the spin and parity $J^{PC} = 0^{++}$ or 0^{-+}.

And finally, there is an important theoretical problem associated with the mismatch of three lepton families to four quark families, e.g., the famous triangle anomalies do not cancel in the normal manner. Perhaps my fundamental leptons and quarks, being extended particles into 3 and 4 dimensions, respectively, can avoid this problem which occurs for point particles. Someone would need to work on this possibility.

5 The bigger picture!

We know that the SM is an excellent approximation for understanding the behavior of leptons, quarks, and the interaction bosons in the lower energy region when the spatial resolution is less than 10^{-24} meters. At smaller distance scales, perhaps one needs to consider a discrete space-time, for which the discrete binary rotation groups that I have suggested for the fundamental particles would be appropriate. Quite possibly, with this slight change in emphasis to discrete subgroups of the local gauge group, the SM lagrangian will hold true all the way down to the Planck scale.

If indeed the SM applies at the Planck scale, then one can show [2] that the Monster group dictates all of physics! The surprising consequence: The Universe *is* mathematics and is *unique*. Indeed, we humans are mathematics!

This connection to the Monster Group is present already in determining the lepton and quark mass ratios, which are proportional to the j-invariant of elliptic modular functions, the same j-invariant that is the partition function for the Monster Group in a quantum field theory [17].

The mathematics of these discrete groups does even more for us, for there is a direct connection [2] from the lepton

groups [3,3,2], [4,3,2], [5,3,2], and the quark groups [3,3,3], [4,3,3], [3,4,3], [5,3,3], in R^3 and R^4, respectively, via special quaternions called icosians to the discrete space R^8. One then brings in another R^8 for relativistic space-time transformations. The two spaces combine into a 10-D discrete space-time obeying the discrete symmetry transformations of "Weyl" SO(9,1) = Weyl $E_8 \times$ Weyl E_8. This proposed *unique* connection to "Weyl" SO(9,1) was a surprise to me because one has two 8-D spaces combining to make a 10-D space-time! Its direct and unique relationship to the SM certainly is a welcome replacement to the 10^{500} ways for M-theory.

Finally, among the advantages to having a fourth family of quarks is a possible explanation of the baryon asymmetry of the Universe (BAU). From the CKM and the PMNS matrices, one learns that the predicted CP violation (CPV) is at least 10 orders of magnitude too small to explain the BAU. That is, the important quantity called the Jarlskog value is much too small. But a 4th quark family resolves this issue [18] because substituting the fourth quark family mass values into the Jarlskog expression increases the CPV value by more than 10^{13}! Voilà. One now has penguin diagrams distinguishing the particle and antiparticle decays with sufficient difference to have the particle Universe we experience.

6 Conclusion

The quark mixing matrix CKM4 has been derived using four quark families. Using quaternion generators from four specific related discrete binary rotational groups [3,3,3], [4,3,3], [3,4,3], and [5,3,3], I have derived the quark CKM4 and its CKM submatrix. However, neither quark of the 4th quark family has been detected at the colliders. Their appearance could mean that the Standard Model lagrangian might be a good approximation to the ultimate lagrangian all the way down to the Planck scale if space-time is discrete.

Acknowledgements

The author wishes to thank Sciencegems.com for financial support and encouragement.

Submitted on April 2, 2014 / Accepted on April 10, 2014

References

1. Potter, F. Geometrical Derivation of the Lepton PMNS Matrix Values. *Progress in Physics*, 2013, v. 9 (3), 29–30.
2. Potter, F. Our Mathematical Universe: I. How the Monster Group Dictates All of Physics. *Progress in Physics*, 2011, v. 7 (4), 47–54.
3. Potter, F. Unification of Interactions in Discrete Spacetime. *Progress in Physics*, 2006, v. 2 (1), 3–9.
4. Potter, F. Geometrical Basis for the Standard Model. *International Journal of Theoretical Physics*, 1994, v. 33, 279–305.
5. Coxeter, H. S. M. Regular Complex Polytopes. Cambridge University Press, Cambridge, 1974.
6. An, F. P. *et al*. (Daya Bay Collaboration). Spectral Measurement of Electron Antineutrino Oscillation Amplitude and Frequency at Daya Bay. *Physical Review Letters*, 2014, v. 112, 061801. arXiv:1310.6732.
7. Beringer, J. *et al*. (Particle Data Group). The Review of Particle Physics: V_{ud}, V_{us}, the Cabbibo Angle, and CKM Unitarity. *Physical Review*, 2012 and 2013 partial update, v. D86, 010001, 6–7.
8. Capozzi, F., Fogli, G. J., *et al*. Status of three-neutrino oscillation parameters, circa 2013. arXiv:1312.2878v1.
9. Fogli, G. I. Global analysis of neutrino masses, mixings and phases: Entering the era of leptonic CP violation searches. *Physical Review*, 2012, v. D86, 013012. arXiv:1205.5254v3.
10. Forero, D. V., Tortola, M., Valle, J. W. F. Global status of neutrino oscillation parameters after Neutrino–2012. *Physical Review*, 2012, v. D86, 073012. arXiv:1205.4018.
11. T2K Collaboration, Abe, K. *et al*. Indication of Electron Neutrino Appearance from an Accelerator-produced Off-axis Muon Neutrino Beam. *Physical Review Letters*, 2011, v. 107, 041801. arXiv:1106.2822.
12. Conway, J. H., Smith, D. A. On Quaternions and Octonions: Their Geometry, Arithmetic, and Symmetry. A.K. Peters, Wellesley, Massachusetts, 2003.
13. Du Val, P. Homographies, Quaternions, and Rotations. Oxford University Press, Oxford, 1964.
14. Jourjine, A. Scalar Spin of Elementary Fermions. *Physics Letters*, 2014, v. B728, 347–357. arXiv:1307.2694.
15. Beringer, J. *et al*. (Particle Data Group). The Review of Particle Physics: Neutrino Mass, Mixing and Oscillations. *Physical Review*, 2012 and 2013 partial update, v. D86, 010001, 46–48.
16. Arhrib, A., Hou, W.S. CP Violation in Fourth Generation Quark Decays. *Physical Review*, 2009, v. D80, 076005. arXiv:0908.0901v1.
17. Witten, E. Three-Dimensional Gravity Reconsidered. arXiv:0706.3359.
18. Hou, W. S. Source of CP Violation for the Baryon Asymmetry of the Universe. *International Journal of Modern Physics*, 2011, v. D20, 1521–1532. arXiv:1101.2161v1.

Superluminal Velocities in the Synchronized Space-Time

Sergey Yu. Medvedev
Department of Physics, Uzhgorod National University
54, Voloshyna str., Uzhgorod 88000, Ukraine. E-mail: medvefiz@gmail.com

Within the framework of the non-gravitational generalization of the special relativity, a problem of possible superluminal motion of particles and signals is considered. It has been proven that for the particles with non-zero mass the existence of anisotropic light barrier with the shape dependent on the reference frame velocity results from the Tangherlini transformations. The maximal possible excess of neutrino velocity over the absolute velocity of light related to the Earth (using the clock with instantaneous synchronization) has been estimated. The illusoriness of the acausality problem has been illustrated and conclusion is made on the lack of the upper limit of velocities of signals of informational nature.

1 Introduction

In the special relativity (SR) the velocity of establishing connection between two events "1" and "2" (particle motion, information transfer, quantum teleportation and so on) could not exceed the velocity of light c in vacuum. The attempts to overcome such a prohibition encounter the problem of causality principle violation, namely, if in the initial inertial reference frame (IRF) K a signal moves with the superluminal velocity $u > c$, then exists such IRF K' that moves with the velocity $v < c$, but $\mathbf{v} \cdot \mathbf{u} > c^2$, in which the event-effect "2" anticipates the event-cause "1", $t'_2 < t'_1$ (while in the K IRF $- t_2 > t_1$). In some papers (see, e.g. [1]) the extreme paradoxicalness of this problem, namely, the appearance of the acausal loops, when the cyclic process terminates at the point of its beginning, but before its beginning, is discussed. The absurdity of acausality leads one to the conclusion about the existence of the isotropic light barrier, i.e. in the space of the possible velocities of particles and signals that realize the cause-and-effect relationship the velocity vectors lie inside the sphere of the radius c. In other words, the 4-interval between the cause-and-effect events could be the time-like one only. The event-effect must be inside the light cone of the future event-cause. All the mentioned above follows from the Lorentz transformations (LT).

Below, however, we will show that the causality principle violation is illusory, and the assumption about the possibility of the appearance of the acausal loop is wrong. This problem is discussed in detail in Sect. 6, while here we will indicate only the important fact noted by Leonid I. Mandelstam in his SR-related lectures [2]: the time involved in LT is measured by the clock synchronized by the light signals with *a priori* assumption about the light velocity invariance. The consequence of such synchronization (in fact, the consequence of the light velocity invariance postulate) is the relativity of simultaneity: the spatially split events, simultaneous in one IRF, are not simultaneous in the other one, i.e. $t'_2 \neq t'_1$ at $t_2 = t_1$. Mandelstam in the same lectures explained also that in case of using the clock with instantaneous synchronization at the spatially split points the simultaneity of events will be absolute. Hence the irrefutable logical conclusion follows about the non-invariance of the velocity of light measured using the clock with instantaneous synchronization (because from the light velocity invariance the simultaneity relativity follows). The principal possibility of such synchronization was proven in the works by Vitaliy L. Ginzburg and his followers (see, e.g. [3]). Namely, the clock at the points "1" and "2" could be synchronized by means of a photo relays switched on by the light spot that moves from "1" to "2" with the velocity $V = \omega R$ at the light source rotation with the angular velocity ω (the light source being located at the distance R). Since the product ωR could be, in principle, unrestrictedly large, $\omega R \gg c$, then $V \gg c$ as well, i.e. such synchronization can be considered almost instantaneous. For instance, the above light spot produced by the emission of the *NP*.0532 pulsar in the Crab nebula moves the Earth surface with the velocity $V = 1.2 \times 10^{22}$ m/s ($\omega = 200$ rad/s, $R = 6 \times 10^{19}$ m). Another way of almost instantaneous synchronization was realized in Marinov's experiments [4, 5] on measuring the velocity of the Earth with respect to the ether (see below Sect. 3).

Note that in the classical physics the clock at the spatially split points is considered synchronized just by the instantaneous signals. As shown below, to explain the lack of interference in the Michelson-Morley (MM) experiment [6] there was no necessity to change the above synchronization and, thus, discard such a fundamental property of time as the absolute simultaneity of the spatially split events. The theoretical model of relativistic processes for the case of instantaneously synchronized clock was developed, mainly, in the Frank R. Tangherlini's Ph.D thesis [7, 8] (see also [9]). In this model, the existence of a dedicated absolute inertial reference system (AIRF), in which the velocity of light is isotropic, is postulated. It seems most naturally to represent this reference system as resting with respect to the ether. Note that the lack of the ether does not follow from the MM experiment, this experiment failed only to find its presence for the reason explained in Sect. 2. The second postulate of this theory is the

invariance of the average velocity of light at the motion along the closed contour, just this property of the light velocity follows with the necessity from the MM experiment and all the following interference experiments, in which the light either passed twice the same distance or moved around a closed loop (see, e.g. [10, 11]). The following space-time transformations (i.e. the Tangherlini transformations, TT) [7, 8] are obtained from the above postulates:

$$x' = \gamma(x - vt), \qquad y' = y, \qquad z' = z; \tag{1}$$

$$t' = \frac{t}{\gamma}, \qquad \gamma = \left(1 - \frac{v^2}{c^2}\right)^{-1/2}. \tag{2}$$

Here (x, y, z, t) are the coordinates and time of the point event in AIRF K, whereas (x', y', z', t') are those in the IRF K' that moves with the velocity v along the X-axis in AIRF K.

A detailed discussion of the above transformations as well as the new ways of their deriving could be found in [12–19]. Relation (2) demonstrates the absolute simultaneity: from the condition $\Delta t = 0$ follows that $\Delta t' = 0$ as well. Therefore, one may, similarly to [18, 19], call TT the "synchronized transformations".

One may call the TT-based theory the "non-gravitational SR generalization" (see Sect. 7 below).

As shown in the pioneer work [7, 8], the main experimentally verified LT and TT consequences coincide (since they do not depend on the way of synchronizing the clock). In particular, both TT and LT equally successfully explain the MM experiment [6] and all the following interference experiments. The same results are obtained by calculating the momentum-energy characteristics as well (see below equations (29) and (30)).

Only the values of velocities (and other physical values determined by the time derivative) differ. In Sect. 2, the transformation properties of the velocity characteristics in the Tangherlini theory (TTh) are described and the "coefficient of recalculation" of these characteristics from TTh to SR and *vice versa* is obtained. These results are used in Sect. 3 to obtain the theoretical estimates of the possibility of the excess of the neutrino velocity u' (with respect to the Earth) over the absolute velocity of light c, i.e. the velocity of light with respect to AIRF. It is proved in Sect. 4 that the particle having a non-zero rest mass cannot go before the light when moving in the same direction in any IRF. Its velocity u' may only exceed the absolute velocity of light c, i.e. the situation may occur when $c < u'(\theta') < c'(\theta')$, where c' is the velocity of light with respect to IRF K'. Thus, in TTh the light barrier (isotropic in SR) appears to be anisotropically deformed, and the degree of such deformation depends on the velocity v of IRF K'. The light cone undergoes the similar deformation (see Sect. 4). It is explained in Sect. 5 why the mass of the particle moving with the velocity exceeding the absolute velocity of light c remains real (unlike the tachyon mass in SR). Section 6 is dedicated to the discussion of the properties of time in TTh and SR. The illusoriness of the problem of violation of the causality principle in SR and, hence, that of prohibition of motion with superluminal velocity have been found. The final remarks and conclusions are presented in Sect. 7.

2 Transformational properties of the velocity characteristics in the Tangherlini theory

Let $\mathbf{u} = (u_x; u_y; u_z)$ be the vector of the velocity of the particle with respect to AIRF K. Let us determine the value and direction of the velocity $\mathbf{u}'$ in IRF K' that moves with the velocity v along the X-axis in AIRF K. From TT (1), (2) we obtain [7, 8]:

$$u'_x = \gamma^2(u_x - v), \qquad u'_y = \gamma u_y, \qquad u'_z = \gamma u_z. \tag{3}$$

Hence, the below expressions for the velocity $u' \equiv |\mathbf{u}'|$ and angle $\theta' = (\widehat{\mathbf{u}', \mathbf{v}})$ follow from here:

$$u'(\mathbf{u}, \mathbf{v}) = \frac{\sqrt{(\mathbf{u} - \mathbf{v})^2 - \left(\frac{\mathbf{u}\times\mathbf{v}}{c}\right)^2}}{1 - \frac{v^2}{c^2}}, \tag{4}$$

$$\cos\theta' = \frac{\cos\theta - \frac{v}{u}}{\sqrt{\left(\cos\theta - \frac{v}{u}\right)^2 + \left(1 - \frac{v^2}{c^2}\right)\sin^2\theta}}. \tag{5}$$

If we use LT to calculate the velocity projections in IRF K', we obtain:

$$\tilde{u}'_x = \frac{u - v}{1 - \frac{uv\cos\theta}{c^2}}, \; \tilde{u}'_y = \frac{u_y}{\gamma\left(1 - \frac{uv\cos\theta}{c^2}\right)}, \; \tilde{u}'_z = \frac{u_z}{\gamma\left(1 - \frac{uv\cos\theta}{c^2}\right)}. \tag{6}$$

Here and below "$\sim$" denotes characteristics calculated from LT.

As seen, each of projections of the vector $\mathbf{u}'$ is obtained by multiplying the relevant projection of the vector $\tilde{\mathbf{u}}'$ onto the same "coefficient of recalculation"

$$\chi = \frac{1 - \frac{\mathbf{u}\cdot\mathbf{v}}{c^2}}{1 - \frac{v^2}{c^2}}; \tag{7}$$

$$u'_x = \tilde{u}'_x\chi, \qquad u'_y = \tilde{u}'_y\chi, \qquad u'_z = \tilde{u}'_z\chi. \tag{8}$$

Hence, two conclusions result here:

1. The directions of the vectors $\mathbf{u}'$ and $\tilde{\mathbf{u}}'$ coincide.
2. The value of the velocity in TTh is obtained by multiplying this value in SR u' by χ: $u' = \chi\tilde{u}'$, where

$$\tilde{u}'(\mathbf{u}, \mathbf{v}) = \frac{\sqrt{(\mathbf{u} - \mathbf{v})^2 - \left(\frac{\mathbf{u}\times\mathbf{v}}{c}\right)^2}}{1 - \frac{\mathbf{u}\cdot\mathbf{v}}{c^2}}. \tag{9}$$

The nature of the coefficient χ is easy to understand: it arises due to the difference in the ways of synchronizing the clock in SR and TTh. As the consequence of this difference, we obtain the following relation between the time intervals in

TTh and SR for the particle that moves with the velocity **u** in AIRF K (see Sect. 6):

$$dt' = \frac{d\tilde{t}'}{\chi}. \tag{10}$$

Thus, the time interval between two events (in the same IRF) differs dependent of the way of the clock synchronization. What time is more adequate to the physical reality — t' or $\tilde{t}'$? The answer to this question is discussed below in Sect. 6.

Using the reverse TT, one may express the coefficient χ through $\mathbf{u}'$ and $\mathbf{v}$ (and through $\tilde{\mathbf{u}}'$, $\mathbf{v}$):

$$\chi = 1 - \frac{\mathbf{u}' \cdot \mathbf{v}}{c^2} = \frac{1}{1 + \frac{\tilde{\mathbf{u}}' \cdot \mathbf{v}}{c^2}}. \tag{11}$$

Consider an important particular case: i.e. the transformational properties of the velocity of light. If in AIRF K the light propagates with the velocity c at the angle θ with respect to the X-axis, then we obtain from (4) and (5):

$$c'(v,\theta) = c\frac{1 - \frac{v}{c}\cos\theta}{1 - \frac{v^2}{c^2}}, \tag{12}$$

$$\cos\theta' = \frac{\cos\theta - \frac{v}{c}}{1 - \frac{v}{c}\cos\theta}. \tag{13}$$

From (13) we obtain:

$$\cos\theta = \frac{\cos\theta' + \frac{v}{c}}{1 + \frac{v}{c}\cos\theta'}. \tag{14}$$

Relations (13) and (14) coincide with the relevant SR formulae. Inserting (14) into (12) we obtain [7, 8]:

$$c'(v,\theta') = \frac{c}{1 + \frac{v}{c}\cos\theta'}. \tag{15}$$

In the 1^{st} degree of expansion in v/c, expression (15) coincides with that resulted from the Galilean velocity addition:

$$c'(v,\theta') = c - v\cos\theta' + o\left(\frac{v^2}{c^2}\right). \tag{16}$$

Formula (15) describes the anisotropy of the velocity of light in IRF K'. Such anisotropy was observed in [20, 21]. Note that formula (15) does not contradict the postulate of the light velocity invariance in SR, what is meant here are the two different velocities differing in the way of synchronizing the clock they are determined by. It is easy to state that formula (15) explains the lack of interference in the MM experiment [6] since the time of the "back and forth" motion is

$$t_{\uparrow\downarrow} = t_{\uparrow} + t_{\downarrow} = \frac{L}{c'(\theta')} + \frac{L}{c'(\theta' + \pi)} = \frac{2L}{c} = \text{invar}. \tag{17}$$

Formula (15) enables one to understand how the ether "hided" from Michelson (more exactly, it did not allow him to find it), i.e. at adding the reverse velocities in (17) the "ether terms" are mutually abolished. The reader has to recognize the methodological value of formula (15), since it indicates that the lack of interference in the MM experiment could be explained not postulating the assumption about the independence of the velocity of light on the observer's motion velocity. All the difficulties in the time behavior in SR seat in this assumption.

3 Estimation of the possible excess of the absolute velocity of light in IRF related to the Earth

Let us use equation (4) to obtain the estimate of the possible excess of the neutrino velocity over the absolute velocity of light. Let v and u be the velocity of the Earth and that of neutrino with respect to AIRF K (conditionally speaking, with respect to the ether), respectively, u' be the neutrino velocity value with respect to the Earth. According to Marinov's measurements [4, 5]

$$v = (360 \pm 40)\ \text{km/s}. \tag{18}$$

The same estimate follows from the analysis of the experimental data on the light velocity anisotropy [20, 21].

Let us assume that the velocity u is very close to the velocity of light c: $u = c - \delta$, $\delta \ll c$. Taking also into account that $v \ll c$, we obtain from (4) to the accuracy of the first-order values over v/c and δ/c:

$$\frac{u' - c}{c} = -\frac{v}{c}\cos\theta - \frac{\delta}{c}, \qquad \theta = (\widehat{\mathbf{u}, \mathbf{v}}). \tag{19}$$

At the neutrino energies of the order of GeV, taking into account the smallness of the neutrino rest mass (several eV), $\delta \ll v$. Then

$$\frac{u' - c}{c} = -\frac{v}{c}\cos\theta. \tag{20}$$

The maximal value of the above excess is reached at $\theta = \pi$:

$$\left(\frac{u' - c}{c}\right)_{MAX} = (121 \pm 13.3) \times 10^{-5}, \tag{21}$$

This is approximately 50 times larger than the infamous CERN result [22] obtained with a technical mistake that, obviously, could not be considered the contestation of theoretical estimates (20) and (21). It is important to achieve the correct confirmation of estimates (20) and (21) for the sake of the further progress of physics. To do this it is necessary to ensure the clock synchronization close to instantaneous. One may also use the "light synchronization" (GPS) that is more convenient technically, but in this case one has to take into account in (15) the difference of velocities of electromagnetic signals propagating in the opposite directions.

Note that in case of the use of the clock synchronized "according to Einstein" we may obtain from (9) for the situation under discussion:

$$\frac{\tilde{u}' - c}{c} = -\left(\frac{v}{c}\cos\theta\right)^2 \qquad \Rightarrow \qquad \tilde{u}' < c, \tag{22}$$

i.e. the "superluminal" motion would not be observed as is true according to SR.

Note a specific circumstance: the estimate (20) could be obtained from the Galilean velocity addition $\mathbf{u}' = \mathbf{u} - \mathbf{v}$, despite the fact that the velocities $\mathbf{u}'$ and $\mathbf{u}$ are relativistic. This is due to the fact that the Tangherlini transformations are the less correction of the Galilean transformations (GT) than the Lorentz ones. To make the velocity addition law (3)–(5) (that follows from TT) coincide in the first order with the Galilean one, the fulfillment of the condition $v \ll c$ is sufficient, whereas formulae (6) and (9) coincide with the Galilean ones only when $u \ll c$ and $v \ll c$, and this is demonstrated by formula (22).

4 Anisotropic deformation of the light barrier and light cone in the Tangherlini theory

It follows from (4) and (15) that the velocities of the particle u' and light c' in IRF K' that moves with respect to the ether may exceed the absolute velocity of light c. However, the following holds true:

Statement 1 *The velocity u' of the particle with a non-zero rest mass is always less than the velocity c' of light that moves in the same direction:*

$$u'(\theta') < c'(\theta') \tag{23}$$

Proof. Using formulae (4), (9), (11) and (15), we obtain:

$$\frac{u'(\theta')}{c'(\theta')} = \frac{\tilde{u}'}{c}\,\frac{1+\frac{v}{c}\cos\theta'}{1+\frac{\tilde{u}'v}{c^2}\cos\theta'} = \frac{1+\frac{v}{c}\cos\theta'}{\frac{c}{\tilde{u}'}+\frac{v}{c}\cos\theta'}. \tag{24}$$

Since always $c > \tilde{u}'$, it follows from (24) that $\frac{u'(\theta')}{c'(\theta')} < 1$, i.e. *quod erat demonstrandum*.

Thus, it follows from TT that in IRF K' that moves with respect to the ether with the velocity v an anisotropically deformed light barrier appears:

$$u' < \frac{c}{1+\frac{v}{c}\cos\theta'}.$$

Only in AIRF K ($v = 0$) this barrier takes a form of an absolute SR barrier. In other IRTs, the value of deformation depends on the velocity v of IRF with respect to the ether. Therefore, even in case when the velocity of particle exceeds, according to (20), the absolute velocity of light, it will not overcome the light barrier, this barrier is simply such deformed that the motion with the velocity exceeding the absolute velocity of light ($c < u' < c'$) becomes possible. Therefore, one has not to expect the "vacuum" Cherenkov effect. If the neutrino outruns its self-radiation, then, according to Kohen-Glashow calculations [23], it would lose almost its total energy for the production of a pair of particles, which has not been observed experimentally.

Thus, for the particle with the non-zero mass, even at $u' > c$, the term "superluminal motion" is conditional.

To obtain the equation that describes the light "quasi-cone" in TTh, we will use the non-invariant metric tensor [7, 8]:

$$g'_{\mu\nu}(v) = \begin{pmatrix} 1 & -\frac{v}{c} & 0 & 0 \\ -\frac{v}{c} & \frac{v^2}{c^2}-1 & 0 & 0 \\ 0 & 0 & -1 & 0 \\ 0 & 0 & 0 & -1 \end{pmatrix}. \tag{25}$$

The invariant 4-interval is:

$$dS'^2 = g'_{\mu\nu}dx'^{\mu}dx'^{\nu} = g_{\mu\nu}dx^{\mu}dx^{\nu} = \\ = c^2dt^2 - (dx^2+dy^2+dz^2). \tag{26}$$

For the light "quasi-cone" we obtain the following equation:

$$ct' - \frac{v}{c}x' = \pm\sqrt{x'^2+y'^2+z'^2}. \tag{27}$$

At $v \ll c$, this "quasi-cone" transforms into the SR light cone. Taking into account relation (15), equation (27) should be written in a form:

$$c'(\theta')t' = \pm\sqrt{x'^2+y'^2+z'^2}, \tag{28}$$

and this vindicates the use of the term "light quasi-cone".

5 Energy and momentum of the "superluminal" particle

Let us ascertain that at the "superluminal" motion, i.e. at $u' > c$, the mass of the particle remains real. According to TT (1), (2), one may obtain the following expressions for the momentum $\mathbf{P}'$ and energy E':

$$\mathbf{P}' = \frac{m\mathbf{u}'}{\sqrt{\chi^2 - \left(\frac{u'}{c}\right)^2}} = \tilde{\mathbf{P}}', \tag{29}$$

$$E' = \frac{\chi mc^2}{\sqrt{\chi^2 - \left(\frac{u'}{c}\right)^2}} = \tilde{E}'. \tag{30}$$

These expressions were obtained in [7, 8] from the extreme action principle with the certain-type Lagrangian. In [17], the same expressions were obtained by means of the two simpler methods: a) by using the notion "proper time" and b) by applying TT to the 4-vector of energy-momentum. It is easy to show that the Statement 1 provides the positiveness of the radicand expression in (29) and (30), including that at $u' > c$. Hence, there is no necessity to postulate the imaginary character of the rest mass m (in contrary to the tachyon hypothesis in SR).

6 Notion of time in TTh and SR. Acausality illusoriness

Let us discuss now the difference of the properties of time in TTh and SR resulting from the difference of the ways of the clock synchronizing. The TT set (1), (2) does not form a group, but, substituting:

$$t' \to \tilde{t}' = t' - \frac{v}{c^2}x', \tag{31}$$

we obtain the time part of LT:

$$\tilde{t}' = \gamma\left(t - \frac{v}{c^2}\,x\right) \tag{32}$$

(the co-ordinate parts in TT and LT are the same).

The Lorentz transformations form a group and, therefore, seem to be more preferred than TT. However, is it correct to call the time the value $\tilde{t}'$ that is a linear combination of the time t' and co-ordinate x'? One may call the quantity $\tilde{t}'$ the "quasi-time", and the derivative with respect to $\tilde{t}'$ the radius-vector $\mathbf{r}'$ – the "quasi-velocity". Then the second SR postulate sounds as follows: "the quasi-velocity of light is invariant". This coincides with the second TTh postulate, since the quasi-velocity of light equals to the average velocity of light when moving along the closed contour.

Let us express the relation between the intervals dt' and $d\tilde{t}'$ through the velocities v and $u'_x = dx'/dt'$. From (31) we obtain:

$$d\tilde{t}' = \left(1 - \frac{vu'_x}{c^2}\right)dt' = \left(1 - \frac{\mathbf{v}\cdot\mathbf{u}'}{c^2}\right)dt' = \chi dt' \tag{33}$$

and this explains the relation between the velocities in TTh and SR (see Section 2).

In IRF related to the Earth ($v \approx 360$ km/s), deviation of the coefficient χ from unit is insufficient (i.e. it is about 10^{-3}). However, for the precise measuring the velocities with announced error less than 10^{-3} (as in the CERN experiment [22] on finding the superluminal neutrino motion) this difference should be taken into account. Of particular consideration is the situation of the "superluminal" motion, i.e. when $u' > c$. It is seen from (2) that at $dt > 0$ the condition $dt' > 0$ always holds true as well, i.e. the time in TTh, as it has been always in physics, varies in any IRF towards one side, i.e. from the past to the future. No "backward time motion" does exist. As regards the interval $d\tilde{t}'$, it follows from (33) that given the fulfillment of the condition $\mathbf{v}\cdot\mathbf{u}' > c^2$ this interval becomes negative, i.e. $d\tilde{t}' < 0$ (at $dt' > 0$). This allows one to understand the illusoriness of the so-called problem of violation of the causality principle in SR: the illusion of the acausality arises due to neglecting the difference in the velocities of light in case of the opposite directions. Let us dwell upon this problem in more detail. Let the superluminal signal propagate in IRF K' along the X-axis from the point "1" to the point "2". According to the instantaneously synchronized clock, the motion time interval is $\Delta t' = t'_2 - t'_1$. If one uses the light synchronization (GPS) with fixing at the point "3" the light signals emitted at the points "1" and "2" (let us consider for simplicity that $x_3 = (x_1 + x_2)/2$), then the motion time interval is:

$$\Delta\tilde{t}' = \tilde{t}'_2 - \tilde{t}'_1 = \Delta t' - \frac{Lv}{c^2}, \qquad L = x_2 - x_1. \tag{34}$$

Thus, at $Lv/c^2 > \Delta t'$ (that is equal to the condition $u'v > c^2$) the "acausality" takes place, i.e. $\tilde{t}'_2 < \tilde{t}'_1$. Everything is extremely simple here, i.e. the light signal from the event-effect "2" is detected earlier than the light signal from the event-cause "1" due to the fact that the signal from the event-cause "1" moves (along the IRF motion direction) for a time longer than the total time of the superluminal motion and the reverse (i.e. in the opposite to the IRF motion) light beam motion from the point "2" to the point "3". The acausality illusion vanishes, if one, formulating the causality principle, clearly states the things implied as well, i.e. the event-effect always occurs later than the event-cause according to the clock with the instantaneous synchronization.

Perception of the illusoriness lifts the ban on the superluminal motion: the velocity of the signals of the informational origin (in particular, the quantum teleportation) could be arbitrarily large.

It is easy to understand that the assumption about the possibility of appearance of the acausal loop is wrong. Indeed, the intervals $\Delta t'$ and $\Delta\tilde{t}'$ between the events taking place at the same point coincide. Therefore, it follows from $\Delta t' > 0$ for the cyclic process that $\Delta\tilde{t}' > 0$ as well.

Note that in TTh, as seen from (2), the experimentally proven delay of time also exists. However, unlike SR, this delay depends not on the relative velocity of the two reference frames, but on the velocity of motion of a given IRF with respect to the ether. For the two reference systems K'_1 and K'_2 moving with the same velocities in the opposite directions $\mathbf{v}'$ and $\mathbf{v}'' = -\mathbf{v}'$ the time varies similarly, i.e. $t'' = t'$, though their relative velocity $2v'/(1-(v'/c)^2)$ could be as much as desired large.

Obviously, the clock paradox doesn't take place in TTh.

7 Final comments and conclusions

The above discussion allows one to conclude that TTh is a wider theory than SR, however, all the TTh results almost coincide with those of SR in the cases when one may neglect the non-invariance of the velocity of light (this is a kind of application of the Bohr's correspondence principle). In IRF related to the Earth, this condition holds true very frequently. Just due to this, such a brilliant agreement of the SR calculations with a huge number of experimental data does exist. However, the motion with the superluminal velocities is out of the SR competence. As it had been shown above, the apparent violation of the causality principle at the superluminal velocities in SR is due to neglecting the light velocity difference in case of motion in opposite directions. Therefore, no restrictions on the velocity of particles and signals are imposed by the causality principle. However, as proven in Statement 1, when comparing the velocity of particle with the non-zero mass u' with that of the light c' in the arbitrary reference frame, condition $u' < c'$ is always valid (though in this case u' could be arbitrarily large, including the case $u' > c$).

In the case of the non-local correlation interaction between the "entangled states" of the quantum objects, the ve-

locity of its propagation is not restricted at all. The experimental excess of this velocity over the velocity of light has been observed for the first time in the paper by Alan Aspect et al. [24] devoted to the correlation of the photon pairs polarized states. The theoretical justification of the possibility of information transfer with the superluminal velocity could be easily found, say, in [25]. The possibility of the technical realization of the superluminal signals in the communication networks is discussed in [26] in the section with the characteristic name "Superluminal communications".

Submitted on April 06, 2014 / Accepted on April 07, 2014
Received after revision on April 21, 2014

References

1. Barashenkov V.S. Tachyons: particles moving with velocities greater than the speed of light. *Review Soviet Physics Uspekhi*, 1975, v. 17 (5), 774–782.
2. Mandelshtam L. I. Lectures on the Physical Principles of Relativity Theory (1933–1934). In: Rytov S. M. (ed.). Academician L. I. Mandelshtam. Lectures on Optics, Relativity Theory and Quantum Mechanics. Nauka, Moscow, 1972. Pages 83–285. (In Russian).
3. Bolotovskii B. M., Ginzburg V. L. The Vavilov-Cerenkov effect and the Doppler effect in the motion of sources with superluminal velocity in vacuum. *Soviet Physics Uspekhi*, 1972, v. 15 (2), 184–192.
4. Marinov S. Measurement of the laboratory's absolute velocity. *General Relativity and Gravitation*, 1980, v. 12 (1), 57–66.
5. Marinov S. New measurement of the Earth's absolute velocity with the help of the "Coupled Shutters" experiment. *Progress in Physics*, 2007, v. 3 (1), 31–37.
6. Michelson A. A., Morley E. W. On the relative motion of the Earth and the luminiferous ether. *American Journal of Science*, 1887, v. 34 (203), 333–345.
7. Tangherlini F. R. The velocity of light in uniformly moving frames. A dissertation. Stanford University, 1958. *The Abraham Zelmanov Journal*, 2009, v. 2, 44–110.
8. Malykin G. B., Malykin E. G. Tangherlini's dissertation and its significance for physics of the 21th century. *The Abraham Zelmanov Journal*, 2009, v. 2, 121–147.
9. Tangherlini F. R. Light travel times around a closed Universe. *Nuovo Cimento B*, 1994, v. 109 (9), 929–951.
10. Kennedy R. J., Thorndike E. M. Experimental establishment of the relativity of time. *Physical Review*, 1932, v. 43 (3), 400–418.
11. Ragul'skii V. V. An experimental study of the optical isotropy of space. *Soviet Physics Uspekhi*, 1997, v. 40 (9), 972–974.
12. Malykin G. B. Para-Lorentz transformations. *Soviet Physics Uspekhi*, 2009, v. 52 (3), 263–266.
13. Chavarga M. M. Relative motion of solitons in the light-carrying ether. *Uzhhorod National University Scientific Herald. Series Physics*, 2000, v. 7, 174–194. (In Ukrainian).
14. Obukhov Yu. A., Zakharchenko N. N. The light-carrying ether and the violation of the principle of relativity. *Physical Though of Russia*, 2001, v. 3, 71–83. (In Russian).
15. Kupryaev N. V. Extended representation of the Lorentz transformations. *Russian Physical Journal*, 1999, v. 42 (7), 592–597.
16. Chepick A. M. Absolute. Main principles (to discussion). *Modern Problems of Statistical Physics*, 2007, v. 6, 111–134. (In Russian).
17. Medvedev S. Yu., Halamba I. F. About some consequences from the Tangherlini transformations. *Uzhhorod National University Scientific Herald. Series Physics*, 2012, v. 31, 174–184. (In Ukrainian)
18. Homem G. On Abreu's theory of space and time and new measurements of absolute velocities. arXiv: physics/0212050 [physics.gen-ph].
19. Homem G. Physics in a synchronized space-time. In: Projecto de Final de Curso da LEFT 2002/2003 orientado por prof. de Abreu Rodrigo, 2003. 38 Pages.
20. Smoot G. F., Gorenstein M. V., Muller R. A. Detection of anisotropy in the Cosmic Blackbody Radiation. *Physical Review Letters*, 1977, v. 39 (14), 898–901.
21. Gurzadayan V. G. et.al. Probing the light speed anisotropy with respect to the Cosmic Microwave Background Radiation dipole. *Modern Physics Letters A*, 2005, v. 20 (1), 19.
22. Adam T. et.al. Measurement of the neutrino velocity with the OPERA detector in the CNGS beam. arXiv: 1109.4897 [hep-ex].
23. Cohen A. G., Glashow S. L. Pair creation constrains superluminal neutrino propagation. *Physical Review Letters*, 2011, v. 107 (18), 181803.
24. Aspect A., Dalibard J., Roger G. Experimental test of Bell's inequalities using time-varying analyzers. *Physical Review Letters*, 1982, v. 49 (25), 804–1807.
25. Gadomsky O. N., Altunin K. K. Quantum teleportation and resonance information transfer from one atom to another at arbitrary interatomic distances. *Russian Physical Journal*, 2000, v. 43 (11), 893–898.
26. Kadomtsev B. B. Dynamics and information. *Soviet Physics Uspekhi*, 1994, v. 37 (5), 425–499.

On the Equation which Governs Cavity Radiation II

Pierre-Marie Robitaille

Department of Radiology, The Ohio State University, 395 W. 12th Ave, Columbus, Ohio 43210, USA
E-mail: robitaille.1@osu.edu

In this work, the equation which properly governs cavity radiation is addressed once again, while presenting a generalized form. A contrast is made between the approach recently taken (P. M. Robitaille. On the equation which governs cavity radiation. *Progr. Phys.*, 2014, v. 10, no. 2, 126–127) and a course of action adopted earlier by Max Planck. The two approaches give dramatically differing conclusions, highlighting that the derivation of a relationship can have far reaching consequences. In Planck's case, all cavities contain black radiation. In Robitaille's case, only cavities permitted to temporarily fall out of thermal equilibrium, or which have been subjected to the action of a perfect absorber, contain black radiation. Arbitrary cavities do not emit as blackbodies. A proper evaluation of this equation reveals that cavity radiation is absolutely dependent on the nature of the enclosure and its contents. Recent results demonstrating super-Planckian thermal emission from hyperbolic metamaterials in the near field and emission enhancements in the far field are briefly examined. Such findings highlight that cavity radiation is absolutely dependent on the nature of the cavity and its walls. As previously stated, the constants of Planck and Boltzmann can no longer be viewed as universal.

Science enhances the moral value of life, because it furthers a love of truth and reverence...

Max Planck, Where is Science Going? 1932 [1]

1 Introduction

The equation which governs radiation in an arbitrary cavity has been presented [2, Eq. 8] by combining Kirchhoff's law of thermal emission [3, 4] with Stewart law [5, 6]:

$$E_\nu = f(T, \nu) - \rho_\nu \cdot f(T, \nu), \quad (1)$$

where E_ν corresponds to the frequency dependent emissive power, ρ_ν to the frequency dependent reflectivity, and f(T, ν) to the function defined by Max Planck [2, 7, 8].* This expression is valid under assumptions made by the German scientist in neglecting the effects of diffraction and scattering [8, §2]. At the same time, it implies that all materials used to assemble blackbodies will act as Lambertian emitters/reflectors. The total emission will vary with the cosine of the polar angle in accordance with Lambert's Law (see e.g. [9, p. 19] and [11, p. 22–23]). Planck assumes that white reflectors, which are Lambertian in nature, can be utilized in the construction of blackbodies (e.g. [8, §61, §68, §73, §78]). But very few materials, if any, are truly Lambertian emitters/reflectors.

*The emissivity of an object, ϵ_ν, is equal to its emissive power, E, divided by the emissive power of a blackbody of the same shape and dimension. Similarly, the reflectivity, ρ_ν, can be taken as the reflected portion of the incoming radiation, divided by the total incoming radiation, as often provided by a blackbody [9, 10]. Like emissivity, the reflectivity of an object is an intrinsic property of the material itself. Once measured, its value does not depend on the presence of incident radiation. As a result, Eq. 1 can never be undefined, since ρ_ν can only assume values between 0 and 1. For a perfect blackbody, $\rho_\nu = 0$ and $\epsilon_\nu = 1$.

Consequently, a fully generalized form of Eq. 1 must take into account that all of these conditions might not necessarily be met:

$$E_{\nu,\theta,\phi} = f(T, \nu, \theta, \phi, s, d, N) - \rho_{\nu,\theta,\phi} \cdot f(T, \nu, \theta, \phi, s, d, N), \quad (2)$$

where θ and ϕ account for the angular dependence of the emission and reflection in real materials, s and d account for the presence of scattering and diffraction, respectively, and N denotes the nature of the materials involved.

Since laboratory blackbodies must be Lambertian emitters [11, p. 22–23], they are never made from materials whose emissivity is strongly directional. This explains why strong specular reflectors, such as silver, are not used to construct blackbodies. It is not solely that this material is a poor emitter. Rather, it is because all reflection within blackbodies must be diffuse or Lambertian, a property which cannot be achieved with polished silver.

It should also be noted that when Eq. 1 was presented in this form [2], the reflectivity term was viewed as reducing the emissive power from arbitrary cavities. There was nothing within this approach which acted to drive the reflection. Within the cavity, the absorptivity must equal the emissivity. Hence, any photon which left a surface element to arrive at another must have been absorbed, not reflected. The overall probability of emission within the cavity must equal the probability of absorption under thermal equilibrium. This precludes the buildup of reflective power and, thereby, prevents a violation of the 1^{st} law of thermodynamics.

However, are there any circumstances when the reflection term can be driven? In order to answer this question, it is valuable to return to the work of Max Planck [8].

2 Max Planck's treatment of reflection

In his derivation of Eq. 1,* Max Planck had also sought to remove the undefined nature of Kirchhoff's law, when expressed in term of emission and absorption [8, §45–49]. However, in order to address the problem, he actively placed the surface of interest in contact with a perfect emitter [8, §45–49]. In so doing, Planck permitted a perfectly emitting body to drive the reflection and, thereby, build the radiation within his cavities, noting in §49 that *"the amount lacking in the intensity of the rays actually emitted by the walls as compared with the emission of a black body is supplied by rays which fall on the wall and are reflected there"*. In §45, he had informed the reader that the second medium was a blackbody. It is for this reason that Planck insists that all cavities must contain black radiation.

Thus, despite the advantage of expressing Eq. 1 in terms of reflection, Planck abandoned the relationship he had presented in §49 [8], as reflection became inconsequential if it could be driven by a carbon particle. He subsequently summarized *"If we now make a hole in one of the walls of a size $d\sigma$, so small that the intensity of the radiation directed towards the hole is not changed thereby, then radiation passes through the hole to the exterior where we shall suppose there is the same diathermanous medium as within. This radiation has exactly the same properties as if $d\sigma$ were the surface of a black body, and this radiation may be measured for every color together with the temperature T"* [8, §49].

The problem of radiation emitted by an arbitrary cavity had not been solved, because Planck ensured, throughout his *Theory of Heat Radiation* [8], that he could place a minute particle of carbon within his perfectly reflecting cavities in order to release the "stable radiation" which he sought [12]. He advanced that the carbon particle simply had a catalytic role [8, 12]. In fact, since he was placing a perfect emitter within his cavities at every opportunity [8, 12], he had never left the confines of the perfectly absorbing cavity, as represented by materials such as graphite or soot. His cavities all contained black radiation as a direct result. Perhaps this explains why he did not even number Eq. 1 in his derivation. Since he was driving reflection, all cavities contained the same radiation and Eq. 1 had no far reaching consequences.

Planck's approach stands in contrast to the derivation of Eq. 1 presented recently [2]. In that case, particles of carbon are never inserted within the arbitrary cavities. Instead, the emissivity of an object is first linked by Stewart's law [5,6] to its reflectivity, before a cavity is ever constructed

$$\epsilon_\nu + \rho_\nu = \kappa_\nu + \rho_\nu = 1\,. \qquad (3)$$

*Planck obtains $I = E + (1 - A)I = E + RI$, where E corresponds to emitted power, $R(= \epsilon)$ is the fraction of light reflected and $I(= f(T, \nu))$ is the blackbody brightness which, in Planck's case, also drives the reflection [8, §49]. This is because he places a carbon particle inside the cavity to produce the black radiation.

This is how the emissivity of a real material is often measured in the laboratory. The experimentalist will irradiate the substance of interest with a blackbody source and note its reflectivity. From Stewart's law (Eq. 3), the emissivity can then be easily determined.

It is only following the determination of the emissivity and reflectivity of a material that the author constructs his arbitrary cavity. As such, the recent derivation of Eq. 1 [2], does not require that materials inside the cavity can drive the reflectivity term to eventually "build up" a blackbody spectrum. This is a fundamental distinction with the derivation provided by Max Planck [8, §49].

The emissivity of a material is defined relative to the emissivity of a blackbody at the same temperature. To allow, therefore, that reflectivity would "build up" black radiation, within an arbitrary cavity in the absence of a perfect emitter, constitutes a violation of the first law of thermodynamics (see [2] and references therein). Planck himself must have recognized the point, as he noted in §51 of his text that *"Hence in a vacuum bounded by perfectly reflecting walls any state of radiation may persist"* [8].

Consequently, one can see a distinction in the manner in which Eq. 1 has been applied. This leads to important differences in the interpretation of this relationship. For Planck, all cavities contain black radiation, because he has insisted on placing a small carbon particle within all cavities. The particle then actively drives the reflection term to produce black radiation.

In contrast, in the author's approach, arbitrary cavity radiation will never be black, because a carbon particle was not placed within the cavity. Emissivity and reflectivity are first determined in the laboratory and then the cavity is constructed. That cavity will, therefore, emit a radiation which will be distinguished from that of a blackbody by the presence of reflectivity. This term, unlike the case advocated by Max Planck, acts to decrease the net emission relative to that expected from a blackbody.

In this regard, how must one view arbitrary cavities and which approach should guide physics? Answers to such questions can only be found by considering the manner in which blackbodies are constructed and utilized in the laboratory.

3 Laboratory blackbodies

Laboratory blackbodies are complex objects whose interior surfaces are always manufactured, at least in part, from nearly ideal absorbers of radiation over the frequency of interest (see [13], [14, p. 747–759], and references therein). This fact alone highlights that Kirchhoff's law cannot be correct. Arbitrary cavities are not filled with blackbody radiation. If this was the case, the use of specialized surfaces and components would be inconsequential. Blackbodies could be made from any opaque material. In practice, they are never constructed from surfaces whose emissive properties are poor and whose

emissivity/reflectivity are far from Lambertian.

Sixty years ago, De Vos summarized black body science as follows: *"Resuming, it must be concluded that the formulae given in the literature for the quality of a blackbody can be applied only when the inner walls are reflecting diffusely to a high degree and are heated quite uniformly"* [15]. De Vos was explicitly stating that mathematical rules only apply when a cavity is properly constructed. Even if the temperature was uniform, the walls must have been diffusely reflecting. Everything was absolutely dependent on the nature of the walls. Lambertian emitters/reflectors had to be utilized. Specialized materials were adopted in the laboratory, in sharp contrast to Kirchhoff's claims (see [2] and references therein).

At the same time, there is another feature of laboratory blackbodies which appears to have been overlooked by those who accept universality and Planck's use of reflection to produce black radiation.

Laboratory blackbodies (see [13], [14, p. 747–759], and references therein) are *heated* devices: *"In photometry and pyrometry often use is made of blackbodies i.e. opaque hollow bodies which are provided with one or more small holes and whose walls are heated uniformly"* [15]. They tend to be cylindrical or spherical objects heated in a furnace, by immersion in a bath of liquid (water, oil, molten metal), through electrical means like conduction (where resistive elements are placed in the walls of the cavity) and induction (where electromagnetic fields are varied), and even by electron bombardment [13–15].

The question becomes, when does the heating in a laboratory blackbody stop? For most experiments, the answer is never. Once the desired temperature is achieved, additional heat continues to be transferred to the blackbody with the intent of maintaining its temperature at the desired value. The consequences of this continual infusion of energy into the system are ignored. Since temperature equilibrium has been achieved, scientists believe that they have now also reached the conditions for thermal equilibrium. The two, however, are completely unrelated conditions.

4 Theoretical considerations

As an example, an object can maintain its temperature, if it is heated by conduction, or convection, and then radiates an equivalent amount of heat away by emission. In that case, it will be in temperature equilibrium, but completely out of thermal equilibrium. For this reason, it is clear that heated cavities cannot be in thermal equilibrium during the measurements, as this condition demands the complete absence of *net* conduction, convection, or radiation (neglecting the amount of radiation leaving from the small hole for discussion purposes).

Planck touched briefly on the subject of thermal equilibrium in stating, *"Now the condition of thermodynamic equilibrium required that the temperature shall be everywhere the same and shall not vary with time. Therefore in any given arbitrary time just as much radiant heat must be absorbed as is emitted in each volume-element of the medium. For the heat of the body depends only on the heat radiation, since, on account of the uniformity in temperature, no conduction of heat takes place"* [8, §25]. Clearly, if the experimentalists were adding energy into the system in order to maintain its temperature, they could not be in thermal equilibrium, and they could not judge what the effect of this continual influx of energy might be having on the radiation in the cavity.

4.1 Consequences of preserving thermal equilibrium

Consider an idealized isothermal cavity in thermal equilibrium whose reflection has not been driven by adding a carbon particle. Under those conditions, the emissivity and absorptivity of all of its surface elements will be equal. Then, one can increase the temperature of this cavity, by adding an infinitesimal amount of heat. If it can be assumed that the walls of the cavity all reach the new temperature simultaneously, then the emissivity of every element, ϵ_ν, must equal the absorptivity of every element, κ_ν, at that instant. The process can be continued until a much higher temperature is eventually achieved, but with large numbers of infinitesimal steps. Under these conditions, reflection can play no part, as no energy has been converted to photons which could drive the process. All of the energy simply cycles between emission and absorption. The cavity will now possess an emissive power, E, which might differ substantially from that set forth by Kirchhoff for all cavities. In fact, at the moment when the desired temperature has just been reached, it will simply correspond to

$$E_\nu = \epsilon_\nu \cdot f(T, \nu)\,, \tag{4}$$

because the emissivity of a material remains a fundamental property at a given temperature. This relationship will deviate from the Planckian solution by the extent to which ϵ_ν deviates from 1.

4.2 Consequences of violating thermal equilibrium

At this stage, an alternative visualization can be examined. It is possible to assume that the influx of energy which enters the system is not infinitesimal, but rather, causes the emissivity of the cavity to temporarily become larger than its absorptivity. The cavity is permitted to move out of thermal equilibrium, if only for an instant. Under these conditions, the temperature does not necessarily increase. The additional energy can simply be converted, through emission, to create a reflective component. Thermal equilibrium is violated. Emissivity becomes greater than absorptivity and the difference between these two values enters a reflected pool of photons. A condition analogous to

$$\epsilon_\nu = \kappa_\nu + \delta\rho_\nu \tag{5}$$

has been reached, where $\delta\rho_\nu$ is that fraction of the reflectivity which has actually been driven.

The emissive power might still not be equal to the Kirchhoff function in this case, depending on the amount of photons that are available from reflection. If one assumes that the radiation inside the cavity must be governed in the limiting case by the Planck function, then the emissive power under these circumstances will be equal to the following:

$$E_\nu = (\epsilon_\nu + \delta\rho_\nu) \cdot f(T, \nu) . \quad (6)$$

The cavity is still not filled with blackbody radiation, as the reflective term has not yet been fully driven. Nonetheless, the process can be continued until $\delta\rho_\nu = \rho_\nu$ and the reflective component has been fully accessed. At the end of the process, Eq. 3 becomes valid in accordance to Stewart's Law [5, 6]. The temperature has not yet increased, but the energy which was thought to heat the cavity has been transformed to drive the reflective component.

Finally, thermal equilibrium can be re-established by limiting any excess heat entering the system. The reflected photons will bounce back and forth within the cavity. Balfour Stewart referred to these photons as "bandied" [5] and, for historical reasons, the term could be adopted. Thus, given enough transfer of energy into the system, and assuming that the material is able to continue to place excess emitted photons into the reflected pool, then eventually, the cavity might become filled with black radiation, provided that emission and reflection are Lambertian. In that case, the Planckian result is finally obtained:

$$E_\nu = (\epsilon_\nu + \rho_\nu) \cdot f(T, \nu) . \quad (7)$$

In practice, when a blackbody is being heated, some reflected photons will always be produced at every temperature, as the entire process is typically slow and never in thermal equilibrium. However, for most materials, the introduction of photons into the reflected pool will be inefficient, and the temperature of the system will simply increase. That is the primary reason that arbitrary cavities can never contain black radiation. Only certain materials, such as soot, graphite, carbon black, gold black, platinum black, etc. will be efficient in populating the reflected pool over the range of temperatures of interest. That is why they are easily demonstrated to behave a blackbodies. Blackbodies are not made from polished silver, not only because it is a specular instead of a diffuse reflector, but because that material is inefficient in pumping photons into the reflected pool. With silver, it is not possible to adequately drive the reflection through *excessive* heating. The desired black radiation cannot be produced.

In order to adequately account for all these effects, it is best to divide the reflectivity between that which eventually becomes bandied, $\delta\rho_{\nu,b}$, and that which must be viewed as unbandied, $\delta\rho_{\nu,ub}$:

$$\rho_\nu = \delta\rho_{\nu,b} + \delta\rho_{\nu,ub} . \quad (8)$$

The unbandied reflection is that component which was never driven. As such, it must always be viewed as subtracting from the maximum emission theoretically available, given applicability of the Planck function. With this in mind, Eq. 1 can be expressed in terms of emissive power in the following form:

$$E_\nu = (1 - \delta\rho_{\nu,ub}) \cdot f(T, \nu) , \quad (9)$$

where one assumes that the Planckian conditions can still apply in part, even if not all the reflectivity could be bandied. In a more general sense, then the expression which governs the radiation in arbitrary cavities can be expressed as:

$$E_\nu = (1 - \delta\rho_{\nu,\theta,\phi,ub}) \cdot f(T, \nu, \theta, \phi, s, d, N) . \quad (10)$$

In this case, note that $f(T, \nu, \theta, \phi, s, d, N)$ can enable thermal emission to exceed that defined by Max Planck. The specialized nature of the materials utilized and the manner in which the cavity is physically assembled, becomes important. In this regard, Eqs. 1, 9, and 10, do not simply remove the undefined nature of Kirchhoff's formulation when considering a perfect reflector, but they also properly highlight the central role played by reflectivity in characterizing the radiation contained within an arbitrary cavity.

5 Discussion

Claims that cavity radiation must always be black or normal [7, 8] have very far reaching consequences in physics. Should such statements be true, then the constants of Planck and Boltzmann carry a universal significance which provide transcendent knowledge with respect to matter. Planck length, mass, time, and temperature take on real physical meaning throughout nature [8, §164]. The advantages of universality appear so tremendous that it would be intuitive to protect such findings. Yet, universality brings with it drawbacks in a real sense, namely the inability to properly discern the true properties of real materials.

Moreover, because of Kirchhoff's law and the associated insistence that the radiation within a cavity must be independent of the nature of the walls, a tremendous void is created in the understanding of thermal emission. In this respect, Planckian radiation remains the only process in physics which has not been linked to a direct physical cause. Why is it that a thermal photon is actually emitted from a material like graphite or soot?

This question has not yet been answered, due to the belief that Kirchhoff's law was valid. Thus, Kirchhoff's law has enabled some to hope for the production of black radiation in *any* setting and in a manner completely unrelated to real processes taking place within graphite or soot. It is for this reason that astronomers can hold that a gaseous Sun can produce a thermal spectrum. Such unwarranted extensions of physical reality are a direct result of accepting the validity of Kirchhoff's formulation. Real materials must invoke the same mechanism to produce thermal photons. Whatever happens

within graphite and soot to generate a blackbody spectrum must also happen on the surface of the Sun.

The belief that arbitrary materials can sustain black radiation always results from an improper treatment of reflection and energy influx. In Max Planck's case, this involved the mandatory insertion of a carbon particle within his cavities. This acted to drive reflection. In the construction of laboratory blackbodies, it involves departure from thermal equilibrium as the inflow of energy enables the emissivity to drive the reflection. In the belief that optically thick gases can emit blackbody radiation [16], it centers upon the complete dismissal of reflection and a misunderstanding with respect to energy inflow in gases [17].

Relative to the validity of Kirchhoff's Law, it is also possible to gain insight from modern laboratory findings. Recent experiments with metamaterials indicate that super-Planckian emission can be produced in the near field [18–20]. Such emissions can exceed the Stefan-Boltzmann law by orders of magnitude [18–20].

Guo et al. summarize the results as follows: *"The usual upper limit to the black-body emission is not fundamental and arises since energy is carried to the far-field only by propagating waves emanating from the heated source. If one allows for energy transport in the near-field using evanescent waves, this limit can be overcome"* [18]. Beihs et al. states that, *"Accordingly, thermal emission is in that case also called super-Planckian emission emphasizing the possibility to go beyond the classical black-body theory"* [19].

Similar results have been obtained, even in the far-field, using a thermal extraction device [21, 22]. In that case, the spatial extent of the blackbody is enhanced by adding a transparent material above the site of thermal emission. A fourfold enhancement of the far-field emission could thus be produced. In their *Nature Communications* article, the authors argue that this does not constitute a violation of the Stefan-Boltzmann law, because the effective "emitting surface" is now governed by the transmitter, which is essentially transparent [21]. However, this was not the position advanced when the results were first announced and the authors wrote: *"The aim of our paper here is to show that a macroscopic blackbody in fact can emit more thermal radiation to far field vacuum than* $P = \sigma T^4 S$ *"* [22].

In the end, the conclusion that these devices do not violate the Stefan-Boltzmann relationship [21] should be carefully reviewed. It is the opaque surface of an object which must be viewed as the area which controls emission. Kirchhoff's law, after all, refers to opaque bodies [3, 4]. It is an extension of Kirchhoff's law beyond that previously advanced to now claim that transparent surface areas must now be considered to prevent a violation of the laws of emission.

In this regard, Nefedov and Milnikov have also claimed that super-Planckian emission can be produced in the far-field [23]. In that case, they emphasize that Kirchhoff's law is not violated, as energy must constantly flow into these systems. There is much truth in these statements. Obviously, modern experiments [18–23] fall short of the requirements for thermal equilibrium, as the cavities involved are heated to the temperature of operation. But given that all laboratory blackbodies suffer the same shortcomings, the production of super-Planckian emission in the near and far fields [18–23] cannot be easily dismissed. After all, in order for Planck to obtain a blackbody spectrum in every arbitrary cavity, he had to drive the reflection term, either by injecting a carbon particle or by permitting additional heat to enter the system, beyond that required at the onset of thermal equilibrium.

An interesting crossroads has been reached. If one assumes that modern experiments cannot be invoked, as they require an influx of conductive energy once temperature equilibrium has been reached, then the same restriction must be applied to all laboratory blackbodies. Yet, in the absence of bandied reflection, very few cavities indeed would adhere to Kirchhoff's law. In fact, many cavities can never be filled with black radiation, even if one attempts to drive the reflection term. That is because certain materials are not conducive to emission and prefer to increase their temperature rather than drive reflection. Arbitrary cavities do not contain black radiation, and that is the measure of the downfall of Kirchhoff's law.

Taken in unison, all of these observations, even dating back to the days of Kirchhoff himself, highlight that the universality of blackbody radiation has simply been overstated. The emissive characteristics of a cavity are absolutely dependent on the nature of the cavity walls (see [13], [14, p. 747–759], and references therein). This has broad implications throughout physics and astronomy.

Dedication

This work is dedicated to our mothers on whose knees we learn the most important lesson: love.

Submitted on: April 28, 2014 / Accepted on: April 29, 2014
First published online on: May 1, 2014 / Revised on: December 26, 2014

References

1. Planck M. The new science – 3 complete works: Where is science going? The universe in the light of modern physics; The philosophy of physics. [Translated from the German by James Murphy and W.H. Johnston], Meridian Books, New York, 1959.
2. Robitaille P.-M. On the equation with governs cavity radiation. *Progr. Phys.*, v. 2, no. 2, 126–127.
3. Kirchhoff G. Über das Verhältnis zwischen dem Emissionsvermögen und dem Absorptionsvermogen. der Körper fur Wärme und Licht. *Poggendorfs Annalen der Physik und Chemie*, 1860, v. 109, 275–301. (English translation by F. Guthrie: Kirchhoff G. On the relation between the radiating and the absorbing powers of different bodies for light and heat. *Phil. Mag.*, 1860, ser. 4, v. 20, 1–21).
4. Kirchhoff G. Über den Zusammenhang zwischen Emission und Absorption von Licht und. Wärme. *Monatsberichte der Akademie der Wissenschaften zu Berlin*, sessions of Dec. 1859, 1860, 783–787.
5. Stewart B. An account of some experiments on radiant heat, involving an extension of Prévost's theory of exchanges. *Trans. Royal Soc.*

Edinburgh, 1858, v. 22, no. 1, 1–20 (also found in Harper's Scientific Memoirs, edited by J. S. Ames: The Laws of Radiation and Absorption: Memoirs of Prévost, Stewart, Kirchhoff, and Kirchhoff and Bunsen, translated and edited by D. B. Brace, American Book Company, New York, 1901, 21–50).

6. Robitaille P.-M. A critical analysis of universality and Kirchhoff's law: A return to Stewart's law of thermal emission. *Progr. Phys.*, 2008, v. 3, 30–35.
7. Planck M. Über das Gesetz der Energieverteilung im Normalspektrum. *Annalen der Physik*, 1901, v. 4, 553–563.
8. Planck M. The theory of heat radiation. P. Blakiston's Son & Co., Philadelphia, PA, 1914.
9. Modest M.F. Radiative Heat Transfer. McGraw-Hill, New York, 1993, pp. 26–ff.
10. Palmer J.M. The Measurement of Transmission, Absorption, Emission, and Reflection, in: Handbook of Optics (2^{nd} Ed.), Part II, M. Bass, Ed., McGraw-Hill, NY, 1994.
11. Burns D.A. and Ciurczak E.W. Handbook of Near-Infrared Analysis (3rd Edition), CRC Press, Boca Raton, Fl, 2008.
12. Robitaille P.-M. Blackbody radiation and the carbon particle. *Progr. Phys.*, 2008, v. 3, 36–55.
13. Robitaille P.-M. Kirchhoff's law of thermal emission: 150 Years. *Progr. Phys.*, 2009, v. 4, 3–13.
14. DeWitt D. P. and Nutter G. D. Theory and Practice of Radiation Thermometry. John Wiley and Sons Inc., New York, NY, 1988.
15. de Vos J.C. Evaluation of the quality of a blackbody. *Physica*, 1954, v. 20, 669–689.
16. Finkelnburg W. Conditions for blackbody radiation in gases. *J. Opt. Soc. Am.*, 1949, v. 39, no. 2, 185–186.
17. Robitaille P.M. Blackbody radiation in optically thick gases? *Progr. Phys.*, 2014, v. 10, no. 3, submitted for publication.
18. Guo Y., Cortez C.L., Molesky S., and Jacob Z. Broadband super-Planckian thermal emission from hyperbolic metamaterials. *Appl. Phys. Let.*, 2012, v. 101, 131106.
19. Biehs S.A., Tschikin M., Messina R. and Ben-Abdallah P. Super-Planckian near-field thermal emission with phonon-polaritonic hyperbolic metamaterials. *Appl. Phys. Let.*, 2013, v. 102, 131106.
20. Petersen S.J., Basu S. and Francoeur M. Near-field thermal emission from metamaterials. *Photonics and Nanostructures — Fund. Appl.*, 2013, v. 11, 167–181.
21. Yu Z., Sergeant N.P., Skauli T., Zhang G., Wang H., and Fan S. Enhancing far-field thermal emission with thermal extraction. *Nature Comm.*, 2013, DOI: 10.1038/ncomms2765.
22. Yu Z., Sergeant N., Skauli T., Zhang G., Wang H. and Fan S. Thermal extraction: Enhancing thermal emission of finite size macroscopic blackbody to far-field vacuum. 4 Nov 2012, arXiv:1211.0653v1 [physics.optics].
23. Nefedov I.S. and Melnikov L.A. Super-Planckian far-zone thermal emission from asymmetric hyperbolic metamaterials. 14 Feb 2014, axXiv:1402.3507v1 [physics.optics].

Digital Gamma-Neutron Discrimination with Organic Plastic Scintillator EJ 299-33

Sheth Nyibule[1], Eric Henry[2], Jan Tõke[2], Wojtek Skulski[1], Wolf-Udo Schröder[2,1]

[1]Department of Physics and Astronomy, University of Rochester, P.O Box 270171,14627, Rochester, New York. E-mail: sochieng@pas.rochester.edu
[2]Department of Chemistry, University of Rochester, P.O Box 270216,14627, Rochester, New York. E-mail: schroeder@chem.rochester.edu

The neutron/gamma pulse shape discrimination (PSD) is measured for the newly discovered plastic scintillator EJ 299-33 using a fast digitizer DDC10. This plastic scintillator (EJ 299-33) discovered by Lawrence Livermore National Laboratory(LLNL) is now commercially available by Eljen Technology. Some of its properties include light output emission efficiency of 56/100 (of Anthracene), wavelength of maximum emission of 420 nm, C:H ratio of 1:1.06 and density of 1.08 g/cm^3. The PSD between neutrons and gamma rays in this plastic scintillator is studied using a 5.08-cm diameter by 5.08-cm thick sample irradiated by a neutron-gamma source AmBe-241 and employing charge integration method. The results show that EJ 299-33 has a very good PSD, having a figure of merit of approximately 0.80, 2.5 and 3.09 at 100 KeVee, 450 KeVee and 750 KeVee light outputs respectively. The performance of this new material is compared to that of a liquid scintillator with a well proven excellent PSD performance NE213, having a figure of merit of 0.93, 2.95 and 3.30 at 100 KeVee, 450 KeVee and 750 KeVee respectively. The PSD performance of EJ 299-33 is found to be comparable to that of NE 213.

1 Introduction

For several years efforts to develop plastic scintillators with efficient neutron/gamma discrimination yielded little success [1, 2]. Plastic scintillators are preferred over liquid scintillators for a number of attractive features including low cost, self-containment, and ease of machining. This is why the invention of the plastic scintillator EJ 299-33 [3], with a very good PSD capability has generated a great interest in the community [4–8].

Applications of this type of scintillator in complex nuclear physics experiments or in homeland security and nonproliferation and safeguards are now possible. The goal of this paper is to report our recent off-line evaluation of PSD capability of EJ 299-33.

2 Experimental method

The experiment was performed at Nuclear Science Research Laboratory in Rochester. This experiment was done prior to our in-beam experiment at Laboratori Nazionali del Sud (LNS) in Catania [8]. It was meant to test the response of the organic plastic scintillator EJ 299-33, the same scintillator used in the in-beam experiment. Our results from the in-beam experiments have since been published elsewhere [8].

The experiment was done using a fast digital signal processing module, DDC10 made by SkuTek instruments [9]. The DDC10 is fashioned with 10 analog inputs, each of which is capable of a 14bit analog to digital conversions operating at 100 Ms/s. The neutron/gamma study was performed using neutron-gamma source AmBe-241, shielded with a 5.0-cm lead block which reduced the γ rates to a magnitude comparable to that of neutrons, to irradiate the 5.08-cm diameter $\times$ 5.08-cm thick EJ 299-33 sample. The plastic scintillator EJ 299-33 was coupled to the photomultipler(PMT) Hamamatsu R7724 and PMT base of ELJEN model VD23N-7724 operated at 1750 Volts. The liquid scintillator NE-213 was however coupled to PMT XP-2041 operated at 1750 Volts.

In order to separate neutrons from γ-rays, integration is performed in two parts of the pulse from the digital waveforms. The first integration is done from the beginning of the pulse rise time and the other integration is done over the tail part. These two integrals are designated Q_{total} and Q_{tail} respectively. The ratio between them is used to separate neutrons from γ-rays. Thus PSD is defined as

$$PSD = \frac{Q_{tail}}{Q_{total}} . \quad (1)$$

The point where the tail begins can be optimized for better neutron/gamma separation. For this case, the tail begins 40-ns after the rise time.

The quantitative evaluation of PSD was made using figures of merit (FOM) defined below.

$$FOM = \frac{\Delta X}{(\delta_{gamma} + \delta_{neutron})} , \quad (2)$$

where ΔX is the separation between the gamma and neutron peaks, and δ_{gamma} and $\delta_{neutron}$ are the full width at half maximum of the corresponding peaks (see Figs. 2A-F). The separation, ΔX was calculated as the difference between the mean delayed light fraction $\frac{Q_{tail}}{Q_{total}}$, for neutrons and gamma-rays taken as a normal distribution in PSD over a specified energy range [3]

A reference parameter to define a good PSD in the tested sample is arrived at by noting that a reasonable definition

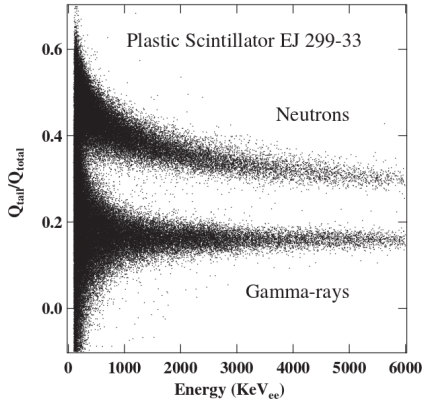

Fig. 1A: Pulse shape discrimination patterns for γ-rays and neutrons obtained using charge integration method for the plastic scintillator EJ 299-33.

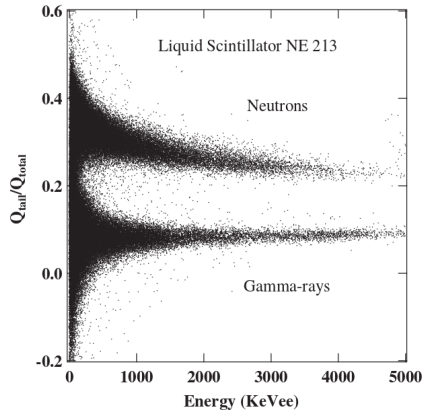

Fig. 1B: Pulse shape discrimination patterns for γ-rays and neutrons obtained using charge integration method for the liquid scintillator NE213.

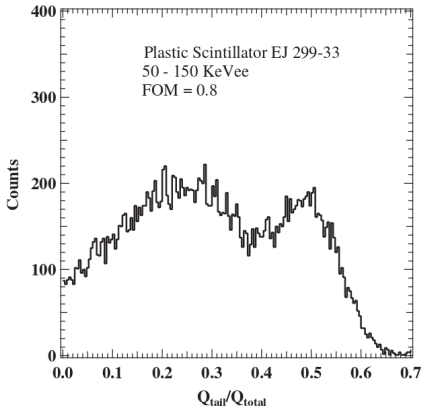

Fig. 2A: PID pattern obtained with organic plastic scintillator EJ 299-33 showing n/γ separation for the light output cut 50-150 KeVee.

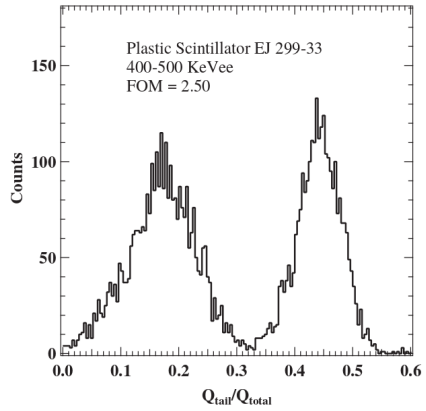

Fig. 2B: PID pattern obtained with organic plastic scintillator EJ 299-33 showing n/γ separation for the light output cut 400-500 KeVee.

for well separated Gaussian distributions of similar populations sizes is $\Delta X > 3(\sigma_{gamma} + \sigma_{neutron})$, where σ is the standard deviation for each corresponding peak. Considering that full width at half maximum for each peak is related to the standard deviation by the expression, FWHM$\approx$2.36σ, FOM$\geq 3(\sigma_{gamma} + \sigma_{neutron})/2.36(\sigma_{gamma} + \sigma_{neutron}) \approx 1.27$ is considered a good PSD [3].

3 Experimental results

The main experimental results are represented in Figs. 1A-1B and Figs. 2A-2F. The quality of PSD achieved with the plastic scintillator EJ 299-33 is illustrated in Fig. 1A, where one observes a very good separation of intensity ridges due to γ-rays (effectively recoil electrons) and neutrons(effectively recoil protons). Fig. 1B illustrates similar result but for the standard liquid scintillator NE 213 with proven excellent PSD capability for purposes of comparison. As one observes in 1A-B, the degree of separation of neutrons from γ-rays for the EJ 299-33 and NE 213 is comparable. This excellent PSD capability is what makes this new scintillator unique among the plastic scintillators and is a welcome feature from the point of neutron detection and identification in the presence of gamma-ray background.

The quality of particle identification(PID) i.e. separation of neutrons and γ-rays is further evidenced by the figure of merit(FOM) as illustrated in Figs. 2A-2C for EJ 299-33 for the energy cuts 100 KeVee, 450 KeVee and 750 KeVee respectively, as indicated by the labels. Figs. 2D-2F show similar results but this case for the liquid scintillator NE 213 included for the purpose of comparison. In order to calculate the FOM, we make energy cut and project only the points within the energy cut along the y-axis. The resulting plot has a PSD along the x-axis and counts on the y-axis as shown in Figs. 2A-2F. The obtained figures of merit suggest the per-

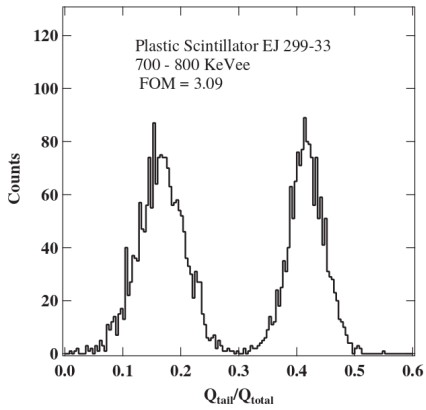

Fig. 2C: PID pattern obtained with organic plastic scintillator EJ 299-33 showing n/γ separation for the light output cut 700-800 KeVee.

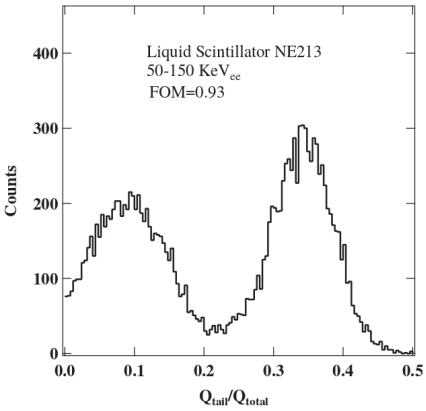

Fig. 2D: PID pattern obtained with organic liquid scintillator NE213 showing n/γ separation for the light output cut 50-150 KeVee.

formance of the standard liquid scintillator NE 213 and the new plastic scintillator are comparable. This results suggest that the replacement of liquid scintillators by plastic scintillators for applications challenged by the well known problems of liquids such as toxicity, flammability, high freezing points, among others is now possible [3, 4].

4 Summary

The results show excellent PSD capability of the new plastic scintillator EJ 299-33 to a level useful for practical applications in complex nuclear physics experiments, nuclear forensics etc. Along with its good charged particle identification [8], EJ 299-33 is expected to provide a viable alternative to the widely used CsI(Tl)detetctor.

Acknowledgements

The work was supported by the U.S. Department of Energy Grant no. DE-FG02-88ER40414.

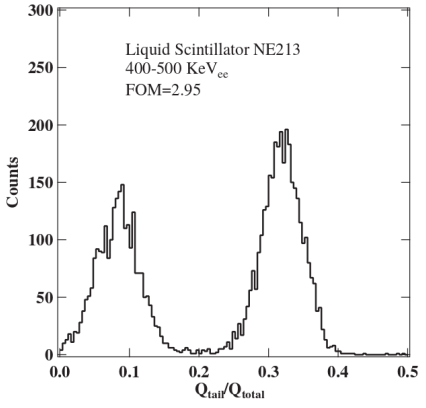

Fig. 2E: PID pattern obtained with organic liquid scintillator NE213 showing n/γ separation for the light output cut 400-500 KeVee.

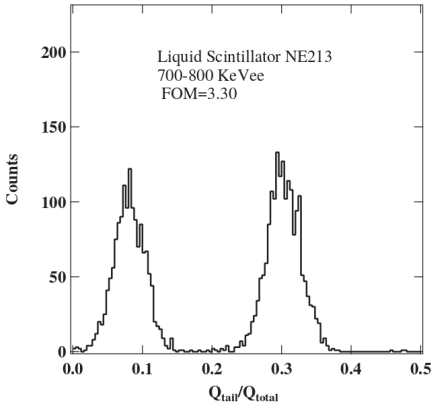

Fig. 2F: PID pattern obtained with organic liquid scintillator NE213 showing n/γ separation for the light output cut 700-800 KeVee.

Submitted on April 17, 2014 / Accepted on April 26, 2014

References

1. Birks J. B. The theory and Practice of Scintillation Counting. Pergamon Press, London, 1963.
2. Knoll G. F. Radiation Detection and Measurements. John Wiley and Sons, Inc. 2007.
3. Zaitzeva N., Benjamin L. P., Iwona P., Andrew G., Paul H. M., Leslie C., Michele F., Nerine C., Stephen P. *Nuclear Instruments and Methods in Physics Research*, 2012, v. A668, 88–93.
4. Pozzi S. A., Bourne M. M., Clarke S. *Nuclear Instruments and Methods in Physics Research*, 2013, v. A723, 19–23.
5. Cester D., Nebbia G., Pino F., Viesti G. *Nuclear Instruments and Methods in Physics Research*, 2014, v. A748, 33–38.
6. Preston R. M., Eberhard J. E., Tickner J. R. *Journal of Instrumentation*, 2013, issue 8, P12005.
7. Favalli A. *IEEE Nuclear Science*, 2013, v. 60, 1053.
8. Nyibule S., Henry E., Tõke J.,Schöder U. W. *Nuclear Instruments and Methods in Physics Research*, 2013, v. A728, 36–39.
9. http://www.skutek.com

LETTERS TO PROGRESS IN PHYSICS

Blackbody Radiation in Optically Thick Gases?

Pierre-Marie Robitaille
Department of Radiology, The Ohio State University, 395 W. 12th Ave, Columbus, Ohio 43210, USA.
robitaille.1@osu.edu

In this work, the claim that optically thick gases can emit as blackbodies is refuted. The belief that such behavior exists results from an improper consideration of heat transfer and reflection. When heat is injected into a gas, the energy is primarily redistributed into translational degrees of freedom and is not used to drive emission. The average kinetic energy of the particles in the system simply increases and the temperature rises. In this respect, it is well-know that the emissivity of a gas can drop with increasing temperature. Once reflection and translation are properly considered, it is simple to understand why gases can never emit as blackbodies.

Supposing all the above conditions to have been verified, then the physicist's picture of the external universe has only one further requirement to fulfill. Throughout its whole composition it must be free from everything in the nature of a logical incoherence. Otherwise the researcher has an entirely free hand. [Intellectual freedom]... is not a mere arbitrary flight into the realms of fancy.

Max Planck, Where is Science Going? 1932 [1]

1 Introduction

In the laboratory, blackbodies are specialized, heated, and opaque enclosures, whose internal radiation is determined by the Planckian function [2, 3]. Not all cavities contain this type of radiation, even if Kirchhoff's law of thermal emission had dictated such an outcome [4, 5]. There are demonstrable shortfalls in Kirchhoff's ideas [6–15] and arbitrary cavities are not black. Everything is very much dependent on the nature of the walls [6–15].

Nonetheless, if can be shown that the interior of a cavity is lined with a nearly ideal absorber, or subjected to the action of a carbon particle [8–10], then it can support black body radiation [15]. It is also possible, under special circumstances, to drive the reflectivity of a cavity through a temporary violation of thermal equilibrium [15]. Under those conditions, a cavity, if it has walls which can support Lambertian radiation, might also come to be filled with black radiation. These are unique settings which do not ratify Kirchhoff's claims [15].

In its proper formulation, the law which governs radiation in arbitrary cavities [14, 15] under the limits set by Max Planck [2, 3], combines the laws of Kirchhoff [4, 5] and Stewart [16] (see Eq. 1 and 9 in [15]). These solutions include the effect of reflectivity, which can act to produce substantial deviations from the behavior expected for cavity radiation, as advanced in 1860 [4, 5]. That real materials possess reflectivity implies that they cannot generate a blackbody spectrum without driving this reflective component [15].

2 Optically thick gases

Finkelnburg [17] advocated that optically thick gases can also produce blackbody radiation [3–6], since he did not properly consider reflection and energy transfer within a gas. Real gases can never meet the requirements for generating a blackbody spectrum, as they possess both convection and reflection.

Relative to the claim that optically thick gases [17] can sustain blackbody radiation [2, 3], the arguments advanced [17] fail to properly address the question. It is easy to demonstrate that, if reflection is not considered, cavity radiation will always be black, independent of the nature of the walls [8–10, 15]. However, real materials, including gases, possess reflection. As a direct consequence, this property must be included.

In his classic paper [17], Finkelnburg makes the suggestion that even if gases are transparent at certain frequencies, they can come to absorb slightly over all frequencies because *"a thermally excited gas by necessity is ionized to a certain, though occasionally small degree"*. He continues, *"As a consequence of this ionization, a continuous spectrum resulting from the stopping of the free discharge electrons in the fields of the positive ions covers the whole spectral region. The same applies (with largely varying intensity) for a number of continuous spectra beyond the series limits where the emission results from recombination of free electrons with ions into different excited states of atoms. Even if any broadening of the discrete lines or bands emitted by the gas is disregarded the absorption coefficient of every luminous gas thus is different from zero for 'all' wave-lengths"* [17]. In this respect, Finkelnburg has overlooked that internal reflection within the gas is also likely to be different from zero at all wavelengths.

Finkelnburg failed to properly address the reflection. That is why he advocated that optically thick gases could emit as blackbodies. He made the assumption that surface reflectivity was negligible in a gas [17]. Yet, since gases have no surfaces,

there can be little relevance in such statements.

The reality remains that all gases possess internal reflection over certain wavelengths and that this characteristic cannot be distinguished from emissivity.* Unlike the transmissivity, the reflective properties of a gas remain independent of path length and is an ever present property which cannot be ignored. Photons can be reflected within a gaseous system, even if no surface exists. This is not the same as if the photons were emitted because reflection is a driven phenomenon which involves an external source to drive the departure from thermal equilibrium [15].

It has recently been argued that, in order to obtain black radiation in an arbitrary cavity, the reflectivity of a material must be driven [15]. While gases cannot be characterized by reflectivity, since they do not have a surface, they do possess internal reflection. In order for a gas to gain a blackbody appearance, it is this reflection which must be driven.

Yet, there are only two ways in which reflection can be driven. The first method, adopted by Max Planck, involves placing a small carbon particle within the cavity of interest [15]. Obviously, this cannot be achieved when considering optically dense gases in space. The second method involves driving the reflection, by the addition of energy [15], without an associated change in temperature.†

For a gas to emit like a blackbody, it must be possible to channel energy into this system and produce an excess of emission over absorption. This must occur in a manner which can serve to drive reflection [16], rather than promote convection and increase temperature. However, within a gas, this is extremely unlikely to occur. Gases are known to increase their temperature in response to the inflow of energy. They do not easily increase their emissivity [18]. In fact, the emissivities of some gases are known to drop with increasing temperature, directly confirming this conclusion [18, p. 214–217]. Gases primarily respond to energy by channeling it into translational (not simply in their vibrational, rotational, or electronic) degrees of freedom. Gases increase their average kinetic energy, hence their temperature. When confronted with heat, the atoms of a gas do not simply conserve their kinetic energy in order to promote emission. Therefore, gases can never act as blackbodies, since they can easily access convection. This situation is completely unlike a solid, like graphite, which cannot invoke convection to deal with the influx of energy. Planck insisted that blackbodies have rigid walls [3]. There can be no convection.

As a side note, all experiments on pure gases on Earth involve some form of container. This places the gas within the confines of an enclosure, which though not necessarily opaque to photons, will act to permit gaseous atoms to experience collisional broadening. Such an effect can dramatically alter the conclusions reached, when studying gases in the laboratory versus how gases behave in the unbounded conditions of space. It is not possible for Finkelnburg to assert that *"Even if any broadening of the discrete lines or bands emitted by the gas is disregarded the absorption coefficient of every luminous gas thus is different from zero for 'all' wavelengths"* [4], as the experimentalist who is studying a gas remains restricted to his container and the effects which it imposes on his conclusions. Obviously, if no broadening of the lines can be observed, then the gas under study is even further from approaching the blackbody spectrum. If broadening does not occur, then the lines, by definition, remain sharp and this implies no absorption between the bands.

3 Discussion

When the interaction between a photon and a gas is considered, one must include the effect of reflection or scattering. Such processes are ignored in all derivations which lead to the conclusion that gases can act as blackbodies, when they are sufficiently optically thick [17]. A gaseous atom can interact briefly with a photon and this can result in diffuse reflection or scattering. This term prevents any mathematical proof that all gases, given sufficient optical thickness, can act as blackbodies. The proper equations for radiation in thermal equilibrium with an enclosure, even in the illogical scenario that a gas can be in thermal equilibrium with a self-provided enclosure, involves reflection [15]. The momentary loss of thermal equilibrium, associated with the injection of an infinitesimal amount of heat into a gas, is seldom associated with increased emissivity and the ability to drive reflection [15]. Rather, the additional energy is channeled towards the translational degrees of freedom.

Gases can easily support convection. That is why no gas can ever behave as a blackbody, even when "optically thick".

Long ago, Sir William Huggins and his wife, Margaret Lindsay Huggins [19], demonstrated that planetary nebula can manifest extremely sharp lines in spite of their great spatial extent [20, p. 87]. These findings provide strong evidence that astronomical gases do not emit as blackbodies.

As previously emphasized [6–15], condensed matter is absolutely required for the production of a thermal spectrum.

Dedication

This work is dedicated to Larry and Winifred, in thanksgiving for their friendship and encouragement.

Submitted on: May 1, 2014 / Accepted on: May 4, 2014
First published online on: May 7, 2014

*When monitoring a gas, it is impossible to ascertain whether a photon which reaches the detector from the *"interior of the gas"* has been directly produced by emission, or whether the photon has undergone one or more reflections before arriving at the detector.

†This second method relies on a temporary departure from thermal equilibrium. In the case of real cavities, a situation such as $\epsilon_\nu = \kappa_\nu + \delta\rho_\nu$ must be considered, where ϵ_ν corresponds to emissivity, κ_ν to absorptivity, and $\delta\rho_\nu$ to that fraction of the reflectivity which has been driven [15]. In a gas, we can reformulate this relationship in terms of emissive and absorptive powers, E and A, and obtain $E = A + \delta R \cdot I$, where δR is the fraction of the internal reflection which has been driven by some function, I [15].

References

1. Planck M. The new science — 3 complete works: Where is science going? The universe in the light of modern physics; The philosophy of physics. [Translated from the German by James Murphy and W.H. Johnston], Meridian Books, New York, 1959, p. 45.
2. Planck M. Über das Gesetz der Energieverteilung im Normalspektrum. *Annalen der Physik*, 1901, v. 4, 553–563.
3. Planck M. The Theory of Heat Radiation. P. Blakiston's Son & Co., Philadelphia, PA, 1914.
4. Kirchhoff G. Über das Verhältnis zwischen dem Emissionsvermögen und dem Absorptionsvermogen. der Körper fur Wärme und Licht. *Poggendorfs Annalen der Physik und Chemie*, 1860, v. 109, 275–301. (English translation by F. Guthrie: Kirchhoff G. On the relation between the radiating and the absorbing powers of different bodies for light and heat. *Phil. Mag.*, 1860, ser. 4, v. 20, 1–21).
5. Kirchhoff G. Über den Zusammenhang zwischen Emission und Absorption von Licht und. Wärme. *Monatsberichte der Akademie der Wissenschaften zu Berlin*, sessions of Dec. 1859, 1860, 783–787.
6. Robitaille P.-M. On the validity of Kirchhoff's law of thermal emission. *IEEE Trans. Plasma Sci.*, 2003, v. 31, no. 6, 1263–1267.
7. Robitaille P.M. Robitaille P. M. L. An analysis of universality in blackbody radiation. *Progr. Phys.*, 2006, v. 2, 22–23; arXiv:physics 0507007.
8. Robitaille P.-M. A critical analysis of universality and Kirchhoff's law: A return to Stewart's law of thermal emission. *Progr. Phys.*, 2008, v. 3, 30–35.
9. Robitaille P.-M. Blackbody radiation and the carbon particle. *Progr. Phys.*, 2008, v. 3, 36–55.
10. Robitaille P.-M. Kirchhoff's law of thermal emission: 150 years. *Progr. Phys.*, 2009, v. 4, 3–13.
11. Robitaille P.-M. Blackbody radiation and the loss of universality: Implications for Planck's formulation and Boltzmann's constant. *Progr. Phys.*, 2009, v. 4, 14–16.
12. Robitaille P.-M. Further insight relative to cavity radiation: A thought rxperiment refuting Kirchhoff's law. *Progr. Phys.*, 2014, v. 10(1), 38–40.
13. Robitaille P.-M. Further insight relative to cavity radiation II: Gedanken experiments and Kirchhoff's law. *Progr. Phys.*, 2014, v. 10(2), 116–120.
14. Robitaille P.M. On the equation which governs cavity radiation. *Progr. Phys.*, 2014, v. 10, no. 2, 126–127.
15. Robitaille P.M. On the equation which governs cavity radiation II. *Progr. Phys.*, 2014, v. 10, no. 3, 157–162.
16. Stewart B. An account of some experiments on radiant heat, involving an extension of Prévost's theory of exchanges. *Trans. Royal Soc. Edinburgh*, 1858, v. 22, no. 1, 1–20.
17. Finkelnburg W. Conditions for blackbody radiation of gases. *J. Opt. Soc. Am.*, 1949, v. 39, no. 2, 185–186.
18. DeWitt D. P. and Nutter G. D. Theory and Practice of Radiation Thermometry. John Wiley and Sons Inc., New York, NY, 1988.
19. Becker B.J. Dispelling the myth of the able assistant: Margaret and William Huggins at work in the Tulse Hill Observatory, in *Creative Couples in the Sciences*, (H.M. Pycior, N.G. Slack, and P.G. Abir-Am, eds.), 1996, Rutgers University Press, 88–111.
20. Watts W.M. and Huggins W. An Introduction to the Study of Spectrum Analysis. Longmans, Green, and Co., London, 1904.

Black Hole Structure in Schwarzschild Coordinates

David Proffitt

Sheerness, UK. E-mail: proffittcenter@gmail.com

In the analysis of the interior region of both stationary and rotating black holes, it is customary to switch to a set of in-falling coordinates to avoid problems posed by the coordinate singularity at the event horizon. I take the view here that to understand the physics of black holes, we need to restrict ourselves to bookkeeper or Schwarzschild coordinates of a distant observer if we are to derive measurable properties. I show that one can derive interesting properties of black holes that might explain some of the observational evidence available without the necessity of introducing further ad hoc conjectures.

1 The Schwarzschild black hole

Birkhoff's theorem [1] assures us that for any non-rotating spherically symmetric distribution of matter, the gravitational effect on any test mass is solely due to whatever mass lies closer to the center of symmetry. This allows us to infer what happens inside the event horizon, by comparing a hypothetical distribution of matter that is identical but with all mass outside the point of interest removed, with that of (say) a collapsing star. Making no further assumptions, let the density at any point inside the event horizon be $\rho_{initial}(r)$ where r is the reduced distance from the center of symmetry. Now consider a test mass m at a distance r_p from the center of a black hole, but inside an event horizon of radius r_{eh}. Now compare this in a thought experiment with a similar test mass m with an identical distribution of mass but with all mass at a distance greater than r_p set to zero. Clearly, our test mass in both cases will head towards the origin, but so too will every other particle that makes up the mass distribution $\rho_{initial}$ but is not yet at the origin. In our thought experiment, the spherical mass distribution will become increasingly compressed with our test particle riding on the collapsing surface. A point in time will be reached in our thought experiment where the mass enclosed by the collapsing surface becomes a black hole in its own right. To a distant observer, the test mass can then never in a finite time cross the event horizon formed by this newly created black hole. This will be true in our thought experiment, and thus must be equally true in the original black hole. At this point in time, to have formed a black hole, we must have

$$r' = \frac{2Gm'}{c^2},$$

where m' is the total mass enveloped by a surface with a radius of r'. As the test mass was at an arbitrary distance from the origin, this will become equally true for every point within the event horizon of the original black hole. As a consequence, the eventual distribution of mass must be such that for all r less than r_{eh}

$$r = \frac{2G}{c^2}\int_0^r 4\pi r^2 \rho(r)\, dr$$

with $\rho(r)$ being the eventual mass distribution function. This relation is satisfied by

$$\rho(r) = \frac{c^2}{8\pi G r^2}.$$

The black hole has a density inside its outer event horizon that is inversely proportional to the square of the (reduced) distance from the origin.

2 The Kerr black hole

In Boyer-Lindquist coordinates [2], there is a spherical inner event horizon for a Kerr black hole [3]; also in the limit of zero rotation, these coordinates, not surprisingly, reduce to Schwarzschild coordinates. The curvature tensors at the surfaces of the (inner) event horizons seem very different but are in fact identical. To understand this, see section 3, below. Therefore, in Boyer-Lindquist coordinates, both the Kerr black hole and the Schwarzschild black hole, have identical gravitational fields at their respective event horizons and therefore identical internal structure as a consequence of the holographic principal [4]. Let us clarify this: they are identical in Boyer-Lindquist coordinates but not from a viewing platform here on earth. From here, the spinning black hole will have an event horizon that appears as an oblate spheroid.

3 Comparing infinities

Consider two men with infinite piles of money, but with one having additional small piles of money. Which is the richer? Clearly they are equal. This was an example using scalar quantities, but let us extend this to vectors. Two vectors each have an infinite component but one of them has additional non-zero components at right angles. Which is the larger? Convert to polar coordinates to see that again they are equal. The same is true for tensors. Consider first two tensors each with one large and equal (but not infinite) component, but one tensor having small non-zero additional components (the other having all other components at zero). Now scale all components to the size of the largest by dividing through by the largest component. Then let the largest component increase without limit. The largest component remains at unity

whilst all other components approach zero. Thus we are left with two identical tensors.

4 Consequences

With this solution, every point inside a black hole is sitting on a local event horizon, where, to a distant observer, time stands still, and so no two points inside a black hole will ever move closer together. Consequently, the black hole must be truly rigid in a way that no other physical object can be; it then follows directly from consideration of the Ehrenfest paradox [5] that the angular velocity of a black hole can never increase — it is fixed at birth. When a black hole increases in mass, it must also increase in angular momentum in order to keep the angular velocity constant up to the maximum speed of rotation set by the periphery being unable to exceed the speed of light, which thus limits the ultimate size a black hole can grow to. We thus formulate a new fifth law of black hole dynamics: **it is never possible to change the angular velocity of a black hole**. Rigidity means that black holes cannot be deformed by any outside processes, so it is difficult to comprehend a process that will allow black holes to coalesce. Ignoring this problem, it can be seen that the limitations of the laws of black hole dynamics severely restrict the possible outcomes whenever two black holes meet.

5 Observational justification

No definitive experimental evidence to confirm these results is produced at this time, but observe that with stellar black holes we would expect that at creation they would have to have a typical mass range of 3–30 solar masses. One would also expect them to be created with high spin due to the conservation of the angular momentum of the collapsing (spinning) star. This limits the maximum mass that a stellar mass black hole could ever grow to. This may apparently be justified by current observations but leaves the unanswered question of how supermassive black holes are ever formed. I suggest that although black holes may never merge, neutron stars can, and with counter-rotating neutron stars, this can give rise to a stellar mass black hole with exceptionally low spin. These black holes are not so limited in growth as normal stellar mass black holes and could grow to become supermassive. All measurements to date suggest that the spin rates for supermassive black holes are extremely high; that is they are approaching the end of their growth phase.

6 Counterarguments

In general relativity, any convenient system of coordinates can be used and is valid [6]. I suggest that as far as observational data goes, Schwarzschild coordinates are the most appropriate as these alone can correlate with observations. Two different coordinate systems — Schwarzschild and infalling coordinates — give very different results in the vicinity of a black hole horizon and yet we know that they must describe the same reality for different observers. Understanding the relation between these two results is therefore crucial to accepting the validity of this result. Consider twins, one of whom descends towards the event horizon of a black hole. We accept that one, the traveler, will appear to be slowing down due the gravitational effect on the passage of time. However, the traveler sees the opposite: time for the stay at home twin seems to speed up. There is nothing fictitious or illusory about this — if the traveler returns home, he will certainly be younger than his twin. Depending upon how close to the event horizon he travels, he could be many days or years younger. In principal, he could be 100,000 years younger and still not have crossed the event horizon. (Apart from the technical difficulties, we are assuming eternal life.) So when does the traveler cross the event horizon. By his own watch, it may be just a few hours but for the stay at home twin it will be eternity. So the traveler does arrive at the real singularity at the center, but for the stay at home twin, this is after the Universe has ceased to exist. Both are real but only one produces a measurable outcome.

Acknowledgements

I thank Anna Proffitt for many challenging discussions leading to this work.

Submitted on May, 19, 2014 / Accepted on May 21, 2014

References

1. Johansen N. V., Ravndal F. On the discovery of Birkhoff's theorem. arXiv:physics/0508163, 2005
2. Bondi H. Boyer–Lindquist coordinates. *Review of Modern Physics*, 1957, v. 29 (3), 423–428.
3. Kerr R. P. The Kerr and Kerr-Schwarzschild metrics. In: *The Kerr Spacetime*. Cambridge Univ. Press, Cambridge, 2009, pp. 38–72.
4. Susskind L., Lindesay J., and Scarpetta G. An Introduction to Black Holes, Information and the String Revolution. Hologr. Universe, 2014, pp. 1–200.
5. Ehrenfest P. Gleichförmige Rotation starrer Körper und Relativitätstheorie. *Physikalische Zeitschrift*, 1909, Bd. 10, 918.
6. Einstein A. How I Constructed the Theory of Relativity. Translated by M. Morikawa. *Association of Asia Pacific Physical Societies* (*AAPPS*) *Bulletin*, 2005, v. 15, no. 2, 17–19.

Drude-Schwarzschild Metric and the Electrical Conductivity of Metals

Paulo Roberto Silva

Departmento de Física (Retired Associate Professor), ICEx, Universidade Federal de Minas Gerais, Belo Horizonte, MG, Brazil.
E-mail: prsilvafis@gmail.com

Starting from a string with a length equal to the electron mean free path and having a unit cell equal to the Compton length of the electron, we construct a Schwarzschild-like metric. We found that this metric has a surface horizon with radius equal to the electron mean free path and its Bekenstein-like entropy is proportional to the number of squared unit cells contained in this spherical surface. The Hawking temperature is inversely proportional to the perimeter of the maximum circle of this sphere. Also, interesting analogies on some features of the particle physics are examined.

1 Introduction

Drude model of the electrical conductivity of metals [1, 2], considers that in this medium the free electrons (the electrons in conductors) undergo Brownian motion with an average characteristic time τ between collisions. Due to the Pauli's exclusion principle, only the electrons with energies which are close to the Fermi energy participate in the conduction phenomena. These electrons travel freely on average by a distance called electron mean free path equal to $\ell = v_F\tau$, where v_F is the Fermi velocity.

Meanwhile, let us note the following feature of black hole physics [3]: an observer at a distance greater than R_S (the Schwarzschild or the surface horizon radius) of the black hole's origin, does not observe any process occurring inside the region bounded by this surface.

Going back to the phenomena of electrical conductivity in metals. let us consider (for instance in a copper crystal) an electron in the conduction band which just suffered a collision. In the absence of an external electric field, all the directions in space have equal probability to be chosen in a starting new free flight. Therefore if we take a sphere centered at the point where the electron have been scattered, with radius equal to the electron mean free path, the surface of this sphere may be considered as an event horizon for this process. Any electron starting from this center will be, on average, scattered when striking the event horizon, losing the memory of its previous free flight. Besides this, all lattice sites of the metallic crystal are treated on equal footing, due to the translational symmetry of the system.

This analogy between two branches of physics, general relativity (GR) and the electrical conduction in metals (ECM), will be considered in the present work. As we will see, we are going to use the GR tools to evaluate some basic quantities related to ECM. We are also going to use some concepts related to the study of particle lifetimes in particle physics (PP).

2 The electron mean free path as a Schwarzschild radius

Let us consider a string of length ℓ (coinciding with the electron mean free path), composed by N unit cells of size equal to the Compton wavelength of the electron (λ_C). Associating a relativistic energy pc to each of these cells, we have an overall kinetic energy K given by

$$K = Npc = \frac{\ell}{\lambda_C}pc = \left(\frac{\ell mc^2}{h}\right)p. \tag{1}$$

In a paper entitled: "Is the universe a vacuum fluctuation?", E.P. Tryon [4] considers a universe created from nothing, where half of the mass-energy of a created particle just cancels its gravitational interaction with the rest of matter in the universe. Inspired by the Tryon proposal we can write

$$K + U = 0 \tag{2}$$

implying that

$$U = -K = -\left(\frac{\ell mc^2}{h}\right)p. \tag{3}$$

However, we seek for a potential energy which depends on the radial coordinate r, and by using the uncertainty relation $p = \frac{h}{r}$, we get

$$U = -\left(\frac{\ell mc^2}{r}\right). \tag{4}$$

Next we deduce a metric, in the curved space, which is governed by the potential energy defined in (4). We follow the procedure established in reference [5]. A form of equivalence principle was proposed by Derek Paul [6], and when it is applied to the potential energy (4) yields

$$\hbar d\omega = dU = \frac{\ell mc^2}{r^2}dr. \tag{5}$$

Now we consider de Broglie relation

$$\hbar\omega = 2mc^2. \tag{6}$$

Dividing (5) by (6) yields

$$\frac{d\omega}{\omega} = \frac{\ell}{2r^2}dr. \tag{7}$$

Performing the integration of (7) between the limits ω_0 and ω, and between R and r, we get

$$\omega = \omega_0 \exp\left(-\frac{\ell}{2}\left(\frac{1}{r}-\frac{1}{R}\right)\right) \tag{8}$$

and

$$\omega^2 = \omega_0^2 \exp\left(-\ell\left(\frac{1}{r}-\frac{1}{R}\right)\right). \tag{9}$$

Making the choice $R = \ell$, leads to

$$\omega^2 = \omega_0^2 \exp\left(1-\frac{\ell}{r}\right) \tag{10}$$

Then we construct the auxiliary metric

$$d\sigma^2 = \omega^2 dt^2 - k^2 dr^2 - r^2\left(d\theta^2 + \sin^2\theta d\phi^2\right). \tag{11}$$

In (11) we take k^2, such that

$$\frac{k^2}{k_0^2} = \frac{\omega_0^2}{\omega^2}. \tag{12}$$

Relation (12) is a reminiscence of the time dilation and space contraction of special relativity. Now we seek for a metric which becomes flat in the limit $r \to \infty$. This can be accomplished by defining [7]

$$\omega^2 = \ln\left(\frac{\omega^2}{\omega_0^2}\right), \quad \text{and} \quad k^2 = \frac{1}{\omega^2}. \tag{13}$$

Making the above choices we can write

$$ds^2 = \left(1-\frac{\ell}{r}\right)dt^2 - \left(1-\frac{\ell}{r}\right)^{-1} dr^2 - r^2\left(d\theta^2+\sin^2\theta d\phi^2\right). \tag{14}$$

We observe that (14) is the Schwarzschild metric, where ℓ is just the Schwarzschild radius of the system.

3 A Schwarzschild-like metric

In the last section we deduced a metric where the so called Schwarzschild radius is just the conduction's electron mean free path. But that construction seems not to be totally satisfactory, once the viscous character of the fluid embedding the charge carriers has not yet been considered. By taking separately in account the effect of the viscous force, we can write

$$m\frac{dv}{dt} = -\frac{p}{\tau^*}. \tag{15}$$

In (15), τ^* is a second characteristic time, which differs from the first one τ that was defined in the previous section. Pursuing further we write

$$vdt = dr, \quad \text{and} \quad p = \frac{h}{r}. \tag{16}$$

Upon inserting (16) into (15), and multiplying (15) by v and integrating, we get the decreasing change in the kinetic energy of the conduction's electron as

$$\Delta K_{qt} = -\frac{h}{\tau^*}\ln\left(\frac{r}{R}\right), \tag{17}$$

where R is some radius of reference.

Next, by defining $\Delta U_{qt} = -\Delta K_{qt}$, we have the total potential energy U_t, namely

$$U_t = U + \Delta U_{qt} = -\frac{mc^2\ell}{r} + \frac{h}{\tau^*}\ln\left(\frac{r}{R}\right). \tag{18}$$

In the next step, we consider the equivalence principle [6] and de Broglie frequency to a particle pair, writing

$$\frac{dU}{2mc^2} = \frac{d\omega}{\omega} = \frac{\ell}{2}\left(\frac{dr}{r^2}\right) + \frac{1}{2}\left(\frac{dr}{r}\right). \tag{19}$$

Upon integrating we get

$$\omega = \omega_0 \exp\left(-\frac{\ell}{2r} + \frac{1}{2}\ln\left(\frac{er}{\ell}\right)\right). \tag{20}$$

In obtaining (20), we have also made the choices

$$mc^2\tau^* = h, \quad \text{and} \quad \frac{r}{R} = \frac{er}{\ell}. \tag{21}$$

Squaring (20), yields

$$\omega^2 = \omega_0^2 \exp\left(-\frac{\ell}{r} + \ln\left(\frac{er}{\ell}\right)\right). \tag{22}$$

Defining

$$\omega^2 = \ln\left(\frac{\omega^2}{\omega_0^2}\right), \quad \text{and} \quad k^2 = \frac{1}{\omega^2}, \tag{23}$$

we finally get

$$ds^2 = \left(\ln\left(\frac{er}{\ell}\right)-\frac{\ell}{r}\right)dt^2 - \left(\ln\left(\frac{er}{\ell}\right)-\frac{\ell}{r}\right)^{-1} dr^2 - r^2 d\Omega^2. \tag{24}$$

Relation (24) is a Schwarzschild-like metric [5], that displays the same qualitative behavior like that describing the Schwarzschild geometry. We also have used in (24) a compact form of writing the solid angle differential, namely $d\Omega$ (please compare with the last term of eq. (11)).

4 Average collision time as a particle lifetime

There are two characteristics linear momenta that we can associate to the free electrons responsible for the electrical conductivity of metals. They are the Fermi momentum mv_F and the Compton momentum mc. By taking into account the fermionic character of the electron, we will write a non-linear

Dirac-like equation describing the "motion" of this particle. We have [8]

$$\frac{\partial\psi}{\partial x} - \frac{1}{c}\frac{\partial\psi}{\partial t} = \frac{mv_F}{\hbar}\psi - \frac{mc}{\hbar}|\psi^*\psi|\psi. \tag{25}$$

We see that eq. (25) contains only first order derivatives of the field ψ. Besides this, the field ψ exhibits not a spinorial character. Taking the zero of (25) and solving for $|\psi^*\psi|$, we get

$$|\psi^*\psi| = \frac{v_F}{c}. \tag{26}$$

On the other hand in the collision process, the conduction's electron loss its memory. We may think that this feature looks similar to the annihilation of a particle-anti particle pair, each of mass-energy equal to E_F. Putting this in a form of the uncertainty principle yields

$$2E_F\Delta t = \frac{h}{2} \quad \text{or} \quad \frac{h\nu}{2} = 2E_F. \tag{27}$$

Solving equation (27) for ν, we get

$$\nu = \frac{1}{\Delta t} = 4\frac{E_F}{h}. \tag{28}$$

By combining the results of (28) and (26) we obtain the line width Γ tied to the "particle" decay

$$\Gamma = \nu|\psi^*\psi| = \frac{4E_F v_F}{hc}. \tag{29}$$

The averaged time between collisions τ is then given by

$$\tau = \frac{1}{\Gamma} = \frac{hc}{4E_F v_F}. \tag{30}$$

Now, let us compare the two characteristic times appearing in this work. By considering (21) and (30), we get

$$\frac{\tau}{\tau^*} = \frac{1}{2}\left(\frac{c}{v_F}\right)^3 \tag{31}$$

and the electron mean free path

$$\ell = v_F\tau = \frac{1}{2}\left(\frac{c}{v_F}\right)^2\frac{h}{mc}. \tag{32}$$

Evaluating the number of unit cells in the string of size ℓ, we have

$$N = \frac{\ell}{\lambda_C} = \frac{mc^2}{4E_F}. \tag{33}$$

It is also possible to define an effective gravitational constant G_W as

$$\ell = 2\frac{G_W Nm}{c^2} = \frac{G_W m^2}{2E_F}. \tag{34}$$

Taking $M = Nm$, we can write

$$2\frac{G_W M}{c^2} = \ell = \frac{G_W m}{v_F^2}, \tag{35}$$

which leads to

$$M = \frac{1}{2}m\left(\frac{c}{v_F}\right)^2. \tag{36}$$

In order to better numerically evaluate the quantities we have described in this work, let us take

$$E_F = \frac{1}{4}\alpha^2 mc^2. \tag{37}$$

This value for E_F [eq. (37)], is representative of the Fermi energy of metals, namely it is close to the Fermi energy of the copper crystal. Using (37) as a typical value of E_F, we get

$$\left(\frac{c}{v_F}\right)^2 = \frac{2}{\alpha^2}. \tag{38}$$

Inserting (38) into the respective quantities we want to evaluate, we have

$$\ell = \frac{h}{\alpha^2 mc}, \quad \tau = \frac{\sqrt{2}h}{\alpha^3 mc^2}, \quad M = \frac{m}{\alpha^2}. \tag{39}$$

Putting numbers in (39) yields

$$\ell = 453\ \text{Å},\ \tau = 2.93\ 10^{-14}\text{s},\ M = 9590\ \frac{\text{MeV}}{\text{c}^2}. \tag{40}$$

It would be worth to evaluate the strength of G_W. We have

$$G_W M^2 \sim 10^{-8}\hbar c. \tag{41}$$

We notice that M is approximately equal to ten times the proton mass.

5 The event horizon temperature and entropy

To obtain the Hawking [9, 11, 12] temperature of this model, we proceed following the same steps outlined in reference [5]. First, by setting $t \to i\tau$, we perform Wick rotation on the metric given by (24). We write

$$ds^2 = -\left(yd\tau^2 + y^{-1}dr^2 + r^2d\Omega^2\right), \tag{42}$$

where y is given by

$$y = \ln\left(\frac{er}{\ell}\right) - \frac{\ell}{r}. \tag{43}$$

Now, let us make the approximation

$$y^{\frac{1}{2}} \sim \ell^{-\frac{1}{2}}\left(r\ln\left(\frac{er}{\ell}\right) - \ell\right)^{\frac{1}{2}} = \ell^{-\frac{1}{2}}u^{\frac{1}{2}}. \tag{44}$$

In the next step we make the change of coordinates

$$Rd\alpha = \ell^{-\frac{1}{2}}u^{\frac{1}{2}}d\tau, \quad \text{and} \quad dR = \ell^{\frac{1}{2}}u^{-\frac{1}{2}}dr. \tag{45}$$

Upon integrating, taking the limits between 0 and 2π for α, from 0 to β for τ, and from ℓ to r for r, we get

$$R = \ell^{\frac{1}{2}}u^{\frac{1}{2}}, \quad \text{and} \quad R\,2\pi = \ell^{-\frac{1}{2}}u^{\frac{1}{2}}\beta. \tag{46}$$

Finally from (46), we find the temperature T of the horizon of events, namely

$$T \equiv \frac{1}{\beta} = \frac{1}{2\pi\ell}. \tag{47}$$

Once we are talking about event's horizon, it would be worth to evaluate the Bekenstein [10–12] entropy of the model. Let us write

$$\Delta F = \Delta U - T\Delta S. \tag{48}$$

In (48), we have the variations of the free energy F, the internal energy U, and the entropy S. In an isothermal process, setting $\Delta F = 0$, and taking $\Delta U = Nmc^2$, and inserting T given by (47), we have

$$\Delta F = \left(\frac{\ell}{\lambda_C}\right)mc^2 - \frac{hc}{2\pi\ell}\Delta S = 0 \tag{49}$$

which leads to

$$\Delta S = 2\pi\left(\frac{\ell}{\lambda_C}\right)^2. \tag{50}$$

The entropy of the event's horizon is then (putting $S_0 = 0$)

$$S = S_0 + \Delta S = 2\pi\left(\frac{\ell}{\lambda_C}\right)^2. \tag{51}$$

6 Conclusion

Therefore the analogy developed in this work between black hole physics and the electrical conductivity of metals is very encouraging. This feature was discussed in a previous paper [8] where the connection with the cosmological constant problem [13] has also been considered

Submitted on May 19, 2014 / Accepted on May 23, 2014

References

1. Kittel C. Introduction to Solid State Physics. 5^{th} Edition, Wiley, 1976, Chapter 6.
2. Silva P.R. et al, Quantum conductance and electric resistivity, Phys. Lett. A, 2006, v. 358, 358–362.
3. Damour T. arXiv: hep-th/0401160.
4. Tryon E.P. Nature, 1973, v. 246, 396.
5. Silva P.R. arXiv: 1302.1491.
6. Paul D. Amer. J. Phys., 1980, v. 48, 283.
7. Jacobson T. arXiv: gr-qc/0707.3222.
8. Silva P.R. Progress in Physics, 2014, v. 10, issue 2, 121–125.
9. Hawking S.W. Commun. Math. Phys., 1975, v. 43, 199.
10. Bekenstein J.D. Phys. Rev. D, 1973, v. 7, 2333.
11. Zee A. Quantum Field Theory in a Nutshell. Princeton University Press, 2003.
12. Silva P.R. arXiv: gr-qc/0605051.
13. Hsu S. and Zee A. arXiv: hep-th/0406142.

Why the Proton is Smaller and Heavier than the Electron

William C. Daywitt

National Institute for Standards and Technology (retired), Boulder, Colorado. E-mail: wcdaywitt@me.com

This paper argues that the proton is smaller and heavier (more massive) than the electron because, as opposed to the electron, the proton is negatively coupled to the Planck vacuum state. This negative coupling appears in the coupling forces and their potentials, in the creation of the proton and electron masses from their massless bare charges, and in the Dirac equation. The mass calculations reveal: that the source of the zero-point electric field is the primordial zero-point agitation of the Planck particles making up the Planck vacuum; and that the Dirac-particle masses are proportional to the root-mean-square random velocity of their respective charges.

1 Introduction

The Planck vacuum (PV) is an omnipresent degenerate continuum of negatively charged Planck particles, each of which is represented by $(-e_*, m_*)$, where e_* is the massless bare charge and m_* is the Planck mass [1]. Associated with each of these particles is a Compton radius $r_* = e_*^2/m_*c^2$. This vacuum state is a negative energy state separate from the free space in which the proton and electron exist. That is, the proton and electron do not propagate through the Planck particles within the PV, but their charge- and mass-fields do penetrate that continuum.

The proton and electron cores denoted by (e_*, m_p) and $(-e_*, m_e)$ are "massive" bare charges. The two cores are "shrouded" by the local response of the PV that surrounds them and gives the proton and electron their so-called structure [2]. These two particles are referred to here as Dirac particles because they are stable, possess a Compton radius, $r_p\,(= e_*^2/m_pc^2)$ and $r_e\,(= e_*^2/m_ec^2)$ respectively, and obey the Dirac equation. They are connected to the PV state via the three Compton relations

$$r_em_ec^2 = r_pm_pc^2 = r_*m_*c^2 = e_*^2 \qquad (= c\hbar) \tag{1}$$

which are derived from the vanishing of the coupling equations in (2).

In their rest frames the Dirac particles exert a two-term coupling force on the PV that takes the form [3]

$$F(r) = \mp\left(\frac{e_*^2}{r^2} - \frac{mc^2}{r}\right) = \mp\frac{e_*^2}{r^2}\left(1 - \frac{r}{r_c}\right) \tag{2}$$

where the $\mp$ sign refers to the proton and electron respectively. The force vanishes at the Compton radius $r_c\,(= e_*^2/mc^2)$ of the particles, where m is the corresponding mass. The PV response to the forces in (2) is the pair of Dirac equations

$$\mp e_*^2\left(i\frac{\partial}{\partial ct} + \boldsymbol{\alpha}\cdot i\nabla\right)\psi = \mp mc^2\,\beta\psi \tag{3}$$

(with the Compton radius $\frac{\mp e_*^2}{\mp mc^2} = r_c$) which describe the dynamical motion of the free Dirac particles.

The potential defined in the range $r \leqslant r_c$

$$V(r) = \int_r^{r_c} F(r)dr \qquad \left(F(r) = -\frac{dV(r)}{dr}\right) \tag{4}$$

leads to (with the help of (1))

$$\frac{V(r)}{mc^2} = \mp\left(\frac{r_c}{r} - 1 - \ln\frac{r_c}{r}\right) \tag{5}$$

with

$$V_p(r \leqslant r_p) \leqslant 0 \qquad \text{and} \qquad V_e(r \leqslant r_e) \geqslant 0\,. \tag{6}$$

For $r \ll r_c$, the potentials become

$$V_p(r) = -\frac{e_*^2}{r} = \frac{(e_*)(-e_*)}{r} \ll 0 \tag{7}$$

and

$$V_e(r) = +\frac{e_*^2}{r} = \frac{(-e_*)(-e_*)}{r} \gg 0 \tag{8}$$

where the final $(-e_*)$ in (7) and (8) refers to the Planck particles at a radius r from the stationary Dirac particle at $r = 0$. The leading (e_*) and $(-e_*)$ in (7) and (8) give the free proton and electron cores their negative and positive coupling potentials.

Equations (6)–(8) show that the proton potential is negative relative to the electron potential — so the proton is more tightly bound than the electron. Thus the Compton relations in (1) imply that the proton is smaller and heaver than the electron. These results follow directly from the fact that the proton has a positive charge, while the electron and the Planck particles in the PV have negative charges.

The masses of the proton and electron [4] [5] are the result of the proton charge $(+e_*)$ and the electron charge $(-e_*)$ being driven by the random zero-point electric field $\mathbf{E}_{\rm zp}$, which is proportional to the Planck particle charge $(-e_*)$ of the first paragraph. A nonrelativistic calculation (Appendix A) describes the random motion of the proton and electron charges as

$$\frac{2\,\ddot{\mathbf{r}}_\pm}{3} = \mp\left(\frac{\pi}{2}\right)^{1/2}\frac{c^2}{r_c}\,\mathbf{I}_{\rm zp} \tag{9}$$

where the upper and lower signs refer to the proton and electron respectively, r_c to their respective Compton radii, and where $\mathbf{I}_{\rm zp}$ is a random variable of zero mean and unity mean square. The radius vector $\mathbf{r}$ [NOT to be confused with the radius r of equations (2) thru (8)] represents the random excursions of the bare charge about its average position at $\langle \mathbf{r} \rangle = 0$. The $2/3$ factor on the left comes from the planar motions (Appendix A) of the charges $\pm e_*$ that create the Dirac masses $m_\pm$. The $\mp$ sign on the right side of (9) is the result of the $\mp$ sign on the right side of the potentials in (5).

After the charge accelerations in (9) are "time integrated" and their root-mean-square (rms) calculated [5], the following Dirac masses emerge (with the help of (1))

$$\frac{m_\pm}{m_*} = \frac{2}{3}\frac{\left\langle \ddot{\mathbf{r}}_\pm^2 \right\rangle^{1/2}}{c} \tag{10}$$

where $m_\pm$ are the derived masses whose sources are the driven charges — consequently the average center of charge and the average center of mass are the same. Equations (10) and (1) lead to the following ratios

$$\frac{\left\langle \ddot{\mathbf{r}}_+^2 \right\rangle^{1/2}}{\left\langle \ddot{\mathbf{r}}_-^2 \right\rangle^{1/2}} = \frac{m_p}{m_e} = \frac{r_e}{r_m} \approx 1800 \tag{11}$$

where the rms random velocity of the proton charge is 1800 times that of the electron charge because of the proton's negative coupling potential.

2 Summary and comments

The negative and positive potentials in (6)–(8) imply that the proton is smaller and heavier than the electron. Furthermore, these two facts are manifest in the $\mp$ signs of the random motion of the bare charges that create, with the help of the zero-point field $\mathbf{E}_{\rm zp}$, the Dirac masses $m_\pm$.

In the PV theory, the radian-frequency spectrum of the zero-point electric field is approximately $(0, c/r_*)$, where the upper limit is the Planck frequency $c/r_* (\sim 10^{43}$ rad/s). On the other hand, the rms accelerations and velocities associated with the random variables $\ddot{\mathbf{r}}$ and $\dot{\mathbf{r}}$ in (9)–(11) are predominately associated with the two decades

$$\frac{c}{100 r_*}\,, \quad \frac{c}{10 r_*}\,, \quad \frac{c}{r_*} \tag{12}$$

at the top of that spectrum [6]. Thus the continuous creation of the Dirac masses $m_\pm$ takes place in a "cycle time" approximately equal to $200\pi r_*/c \sim 10^{-41}$ sec, rapid enough for the masses in (2) and (3) to be considered constants of the motion described by (3).

The theory of the PV model suggests that the proton and electron are stable particles because the PV response to the coupling forces in (2), i.e. the Dirac equation in (3) with $r_c = e_*^2/mc^2$, maintains the separate identities of the two coupling constants e_*^2 and mc^2. In other words, the charge and mass of the free Dirac particle are separate characteristics of the motion in (3), even though the $m_\pm$ are derived from the random motion of the bare charges $\pm e_*$.

Appendix A: Dirac masses

The nonrelativistic planewave expansion (perpendicular to the propagation vector $\widehat{\mathbf{k}}$) of the zero-point electric field that permeates the free space of the Dirac particles is [1] [5]

$$\mathbf{E}_{zp}(\mathbf{r}, t) = -e_* \mathrm{Re} \sum_{\sigma=1}^{2} \int d\Omega_k \int_0^{k_{c*}} dk\, k^2 \widehat{\mathbf{e}}_\sigma \left(\frac{k}{2\pi^2}\right)^{1/2} \times \exp\left[i\left(\mathbf{k}\cdot\mathbf{r} - \omega t + \Theta\right)\right] \tag{A1}$$

where $(-e_*)$ refers to the negative charge on the separate Planck particles making up the PV, $k_{c*} = \sqrt{\pi}/r_*$ is the cutoff wavenumber (due to the fine granular nature of the PV [7]), $\widehat{\mathbf{e}}_\sigma$ is the unit polarization vector perpendicular to $\widehat{\mathbf{k}}$, and Θ is the random phase that gives the field its stochastic nature.

Equation (A1) can be expressed in the more revealing form

$$\mathbf{E}_{zp}(\mathbf{r}, t) = \left(\frac{\pi}{2}\right)^{1/2} \left(\frac{-e_*}{r_*^2}\right) \mathbf{I}_{\rm zp}(\mathbf{r}, t) \tag{A2}$$

where $\mathbf{I}_{\rm zp}$ is a random variable of zero mean and unity mean square; so the factor multiplying $\mathbf{I}_{\rm zp}$ (without the negative sign) is the rms zero-point field. This equation provides direct theoretical evidence that the zero-point field has its origin in the primordial zero-point agitation of the Planck particles (thus the ratio $-e_*/r_*^2$) within the PV. The random phase Θ in (A1) is a manifestation of this agitation.

The random motion of the massless charges that lead to the Dirac masses m_p and m_e are described by [4] [5]

$$\pm e_* \frac{2\,\ddot{\mathbf{r}}_\pm}{3} = \frac{c^2}{r_c} r_*^2 \mathbf{E}_{\rm zp} = \left(\frac{\pi}{2}\right)^{1/2} \frac{c^2}{r_c}\left(-e_* \mathbf{I}_{\rm zp}\right) \tag{A3}$$

which yield the accelerations in (9). The upper and lower signs in (A3) and (9) refer to the proton and electron respectively. The $2/3$ factor is related to the two-dimensional charge motion in the $\widehat{\mathbf{e}}_\sigma$ *plane*. The physical connection leading to these equations is the particle-PV coupling $\mp e_*^2$ in (2).

Finally, there is a detailed (uniform and isotropic at each frequency) spectral balance between the radiation absorbed and re-radiated by the driven dipole $\pm e_* \mathbf{r}$ in (A3); so there is no net change in the spectral energy density of the zero-point field as it continuously creates the proton and electron masses [5] [8].

Submitted on June 7, 2014 / Accepted on June 12, 2014

References

1. Daywitt W.C. The Planck Vacuum. *Progress in Physics*, 2009, v. 1, 20.
2. Daywitt W.C. The Dirac Proton and its Structure. This paper is to be published in the International Journal of Advanced Research in Physical Science (IJARPS). See also www.planckvacuum.com.

3. Daywitt W.C. The Electron and Proton Planck-Vacuum Forces and the Dirac Equation. *Progress in Physics*, 2014, v. 2, 114.
4. Daywitt W.C. The Source of the Quantum Vacuum. *Progress in Physics*, 2009, v. 1, 27. In the first line of the last paragraph in Appendix A of this paper "$p = \hbar/r_L$" should read "$m\gamma c = \hbar/r_L$".
5. Puthoff H.E. Gravity as a Zero-Point-Fluctuation Force. *Phys. Rev. A*, 1989, v. 39, no. 5, 2333–2342.
6. Daywitt W.C. Neutron Decay and its Relation to Nuclear Stability. To be published in *Galilean Electrodynamics*. See also www.planckvacuum.com.
7. Daywitt W.C. The Apparent Lack of Lorentz Invariance in Zero-Point Fields with Truncated Spectra. *Progress in Physics*, 2009, v. 1, 51.
8. Boyer T.H. Random Electrodynamics: the Theory of Classical Electrodynamics with Classical Electrodynamic Zero-Point Radiation. *Phys. Rev. D*, 1975, v. 11, no. 4, 790–808.

The Dichotomous Cosmology with a Static Material World and Expanding Luminous World

Yuri Heymann

3 rue Chandieu, 1202 Geneva, Switzerland. E-mail: y.heymann@yahoo.com

The dichotomous cosmology is an alternative to the expanding Universe theory, and consists of a static matter Universe, where cosmological redshifts are explained by a tired-light model with an expanding luminous world. In this model the Hubble constant is also the photon energy decay rate, and the luminous world is expanding at a constant rate as in de Sitter cosmology for an empty Universe. The present model explains both the luminosity distance versus redshift relationship of supernovae Ia, and ageing of spectra observed with the stretching of supernovae light curves. Furthermore, it is consistent with a radiation energy density factor $(1 + z)^4$ inferred from the Cosmic Microwave Background Radiation.

1 Introduction

Our model is inspired by the tired-light theory that was first proposed by [1] to explain cosmological redshifts, which has been subject to other investigations [2–4]. Generally, tired-light models describe a static Universe; however, in the present model only the matter component of the Universe is static, and the luminous component is expanding. The idea of a static Universe was proposed in Einstein's cosmological model [5], which is the first of the relativist cosmologies. Einstein had to introduce a cosmological constant to make his Universe static; otherwise it would have collapsed due to the gravitational field. Einstein came to the conclusion that his cosmology describes a spatially finite spherical Universe, as he encountered a degeneracy of coefficient $g_{\mu\nu}$ at infinity. Also, Poisson's equation, $\nabla^2\Phi = 4\pi G\rho$, where Φ is the scalar potential and ρ the matter density, played an important role in Einstein's cosmology. As Einstein's wrote in [5]: "It is well known that Newton's limiting condition of the constant limit for Φ at spatial infinity leads to the view that the density of matter becomes zero at infinity."

Let us do a simple thought experiment for inertial bodies in an infinite Universe that is isotropic and has no edge in Newton's absolute Euclidean space. Imagine you are a galaxy, there is a galaxy on your left and on your right, and both exert a gravitional force of same magnitude on you; the two forces would offset and you would not move from your position. From this view, based on the principle of inertia in an absolute Euclidean space, each galaxy in an isotropic Universe would be in this position of equilibrium, and the Universe would be static overall. However, for galaxy clusters where the cluster has an edge, we would expect that the galaxies will end up merging.

De Sitter introduced the concept of "relativity of inertia" based on his analysis of the degeneracy of the $g_{\mu\nu}$ at infinity in Einstein cosmology [6]. To overcome this problem, de Sitter found a solution by extending Einstein's cosmology in three-dimensional space to the four dimensional Minkowski space-time — a world of hyperboloid shape — and with no matter. De Sitter's cosmological model is a solution to Einstein's field equation applied to a vacuum, with a positive vacuum energy density, and describes an expanding Universe. Contemporary cosmological models based on general relativity such as the ΛCDM assume a uniform distribution of matter in space, but the effect of the deformation of space-time due to massive bodies may be preponderant only locally, hence this hypothesis may not be valid. In special relativity, light moves along the geodesics of the Minkowski space-time, whereas matter is confined in the three-dimensional Euclidean space. From the equivalence principle in curved space-time, an inertial particle and a pulse of light both follow the same geodesic. Contrary to Newtonian physics which describes interactions between bodies, general relativity is often employed to describe the dynamics of light, such as the deflection of light, or the event horizon of black holes. In contrast, the theory of general relativity does not establish such a dichotomy beteween matter and light; based on the weak field approximation of general relativity [7], Newton's laws are a good approximation of the properties of physical space only when the gravitational field is weak. As a matter of fact, in the present cosmological model, the luminous portion of the Universe is expanding at a constant rate as in the de Sitter cosmology in a flat Universe; this is also the condition required in order for the model to match the luminosity distance versus redshift relationship of supernovae Ia. The dichotomous cosmology differs in the sense that it is the light wavelength that gets stretched due to a tired-light process and not space itself that expands.

The present model describes the dynamics of light using two transformations. First, we allow a time-varying light wavefront in order to accomodate the stretching of light's wavelength when photons lose energy. Second, a time dilation is incorporated into the model in order for the light wavefront to stay at the celerity of light. A consequence of this

model is the "time-dilation effect" (a.k.a. the ageing of spectra) observed for supernovae light curves [8] with a stretching of the light curves by a factor $(1+z)$. In addition, the expanding luminous world is consistent with the radiation energy density factor $(1+z)^4$ inferred from the CMBR (Cosmic Microwave Background Radiation).

2 Light ageing model

In the tired-light cosmology where redshifts are explained by a decay of the photon energy, the following equation replaces the cosmological redshift equation of the expanding Universe theory:

$$1+z = \frac{\lambda_{obs}}{\lambda_{emit}} = \frac{E(z)}{E_0}, \tag{1}$$

where λ_{obs} and λ_{emit} are the observed and emitted light wavelength respectively, E_0 the photon energy at reception, and $E(z)$ the photon energy when emitted at redshift z.

A simple law of decay of the photon energy is considered:

$$\frac{\dot{E}}{E} = -H, \tag{2}$$

where E is the photon energy, and H the decay of photon energy. From now on we assume that the decay rate of photon energy is constant over time and is always equal to H_0.

By integrating (2) we get:

$$E(t) = E_0 \exp(-H_0 t), \tag{3}$$

where t is the time which is equal to zero time of observation, and E_0 the photon energy at reception.

Let us apply the following change of coordinates $T = t_0 - t$, where T is the light travel time when looking back in the past and t_o the present time. Hence, (3) can be rewritten as follows:

$$E(T) = E_0 \exp(H_0 T), \tag{4}$$

where T is the light travel time when looking back in the past from the earth.

It is shown below that a constant decay rate for the photon energy conforms to the supernovae luminosity distance versus redshift relationship.

3 Light travel time with respect to the point of emission and luminosity distance

Here, we consider a set of two transformations to describe the photon energy decay. During this process the number of light wave cycles is constant, but due to the stretching of light wavelengths when photons lose energy we allow a superluminal light wavefront, resulting in an expansion. Then a time dilation is applied in order to maintain the speed of light at the celerity with respect to the emission point. The velocity of the light wavefront before time dilation is expressed as follows:

$$v(t) = c\frac{E_{emit}}{E(t)}, \tag{5}$$

where E_{emit} is the photon energy at emission, $E(t)$ the photon energy at time t, and c the celerity of light. We note that in (5) the light wavefront is at the speed of light at the point of emission.

In order to maintain the light wavefront at the speed of light with respect to the emission point, the following time dilation is applied:

$$\frac{\delta t'}{\delta t} = \frac{E_{emit}}{E(t)}, \tag{6}$$

where $\frac{\delta t\prime}{\delta t}$ is a time scale factor between time t' and time t. The light travel time with respect to the point of emission is:

$$T' = \int_{-T}^{0} \frac{\delta t'}{\delta t} dt = \int_{-T}^{0} \frac{E_{emit}}{E(t)} dt, \tag{7}$$

where T' is the light travel time with respect to the point of emission, and T the light travel time with time-varying speed of light.

Introducing (3) into (7) we get:

$$T' = \frac{E_{emit}}{E_0} \int_{-T}^{0} \exp(H_0 t) dt. \tag{8}$$

Integrating (8) we obtain:

$$T' = \frac{E_{emit}}{E_0} \frac{1}{H_0} \left(1 - \exp(-H_0 T)\right). \tag{9}$$

By substitution of (4) into (9), we get:

$$T' = \frac{E_{emit}}{E_0} \frac{1}{H_0} \left(1 - \frac{E_0}{E_{emit}}\right). \tag{10}$$

Introducing (1) into (10) we get:

$$T' = \frac{z}{H_0}. \tag{11}$$

After the time dilation (6), the light wavefront is at the speed of light, hence the luminosity distance is expressed as follows:

$$\frac{dr_L}{dT'} = c. \tag{12}$$

By integrating (12) between 0 and T' we get the following equation:

$$r_L(T') = cT'. \tag{13}$$

By combining (11) and (13) we get the following relationship between luminosity distance and redshifts:

$$r_L = \frac{c}{H_0} z. \tag{14}$$

Ultimately, we find the linear relationship between luminosity distance and redshifts which is observed in supernovae Ia data. A rectilinear plot of the luminosity distance versus redshift of slope of 14.65 where the luminosity distance is

expressed in *Gly* (billion light years) was obtained in [9] using the redshift adjusted distance modulus [10] which is based on photon flux. The corresponding decay rate of photon energy which is the inverse of the slope from (11) is equal to $H_0 = 2.16 \times 10^{-18}\, sec^{-1}$ or $67.3\, km\, s^{-1}\, Mpc^{-1}$.

To compute the luminosity distance, the light travel time with respect to the emission point must be used. In the luminosity distance the light wavefront is maintained at the speed of light with respect to the emission point where the time dilation is equal to unity. For an indication of distances of an object with respect to the observer, the light travel time with respect to the point of observation is used for which the time dilation is equal to unity.

4 Light travel time with respect to the observer

The light travel time measured with respect to the observer is the light travel time obtained with a time dilation equal to unity at the point of observation. In this scenario, the velocity of the light wavefront before time dilation is as follows:

$$v(t) = c\frac{E_0}{E(t)}\,, \tag{15}$$

Thus, the time-dilation effect is:

$$\frac{\delta t_0}{\delta t} = \frac{E_0}{E(t)}\,, \tag{16}$$

where $\frac{\delta t_0}{\delta t}$ is a time scale factor between present time t_0 and time t.

Therefore, the light travel time with respect to the observer is:

$$T_0 = \int_{-T}^{0} \frac{\delta t_0}{\delta t} dt = \int_{-T}^{0} \frac{E_0}{E(t)} dt\,, \tag{17}$$

where T_0 is the light travel time with respect to the point of observation, and T the light travel time with time-varying speed of light.

Introducing (3) into (17) and integrating we get:

$$T_0 = \frac{1}{H_0}\left(1 - \exp(-H_0 T)\right)\,, \tag{18}$$

Introducing (4) into (18) we get:

$$T_0 = \frac{1}{H_0}\left(1 - \frac{E_0}{E_{emit}}\right). \tag{19}$$

Finally, introducing (1) into (19):

$$T_0 = \frac{1}{H_0}\frac{z}{(1+z)}\,. \tag{20}$$

We note that in (20) when redshift tends to infinity, the light travel time with respect to the observer converges towards $1/H_0$. This is the farthest distance from which light can reach an observer in the Universe. There is a squeezing effect by the factor (1+z) for the light travel time when measured with respect to the point of observation instead of the point of emission. This squeezing of light travel time is due to the fact that time dilation is relative to the reference point in time from which the light wavefront is measured.

5 Equivalence in the de Sitter cosmology for an expanding Universe

The de Sitter cosmology is dominated by a repulsive cosmological constant Λ which in a flat Universe yields an expansion rate of the Universe H that does not vary over time.

In this cosmology, the luminosity distance is calculated as follows:

$$\frac{dr_L}{dT} = c + H\, r_L \tag{21}$$

with boundary condition $r_L = 0$ at $T = 0$, where r_L is the luminosity distance, T the light travel time between emission and observation of the light source, and H the Hubble constant at time T.

By integrating (21) we get:

$$r_L = \frac{c}{H_0}\left(\exp(H\, T) - 1\right)\,. \tag{22}$$

Because $dt = \frac{da}{H\, a}$, where a is the scale factor, the light travel time versus redshift is as follows:

$$T = \int_{1/(1+z)}^{1} \frac{da}{H\, a} = \frac{1}{H}\ln(1+z)\,. \tag{23}$$

Eqs. (22) and (23) yield:

$$r_L = \frac{c}{H}\, z\,, \tag{24}$$

which is the same equation as (14).

A measure of distance is obtained by calculating the corresponding the distance if there were no expansion of the Universe, which we call the Euclidean distance. Consider a photon at a Euclidean distance y from the observer, moving towards the observer. Hence:

$$\frac{dy}{dt} = -c + Hy\,. \tag{25}$$

By setting time zero at a reference T_b in the past, we get $t = T_b - T$; therefore, $dt = -dT$. Hence, (25) becomes:

$$\frac{dy}{dT} = c - Hy\,, \tag{26}$$

with boundary condition $y(T = 0) = 0$.

Solving (26) we get:

$$y = \frac{c}{H}\left(1 - \exp(-HT)\right)\,. \tag{27}$$

By substitution of (23) into (27) we get:

$$y = \frac{c}{H}\frac{z}{(1+z)}\,, \tag{28}$$

which is the same equation as (20) where $T_0 = \frac{y}{c}$.

We have shown that de Sitter cosmology is the equivalent to our light ageing model in an expanding Universe. In the de Sitter cosmology, the cosmological constant Λ corresponding to a positive vacuum energy density sets the expansion rate $H = \sqrt{\frac{1}{3}\Lambda}$ for a flat Universe, which is the photon energy decay rate of light traveling in vacuum.

6 Radiation density and the CMBR

The CMBR was a prediction of the work of George Gamow, Ralph Alpher, Hans Bethe and Robert Herman on the Big Bang nucleosynthesis [11, 12], and was discovered later in 1964 by Penzias and Wilson. It is believed that the CMBR is the remnant radiation of a primordial Universe made of plasma, and that galaxies are formed by gravitational collapse of this plasma phase. Here, we investigate a requirement for the CMBR to originate from a hot plasma.

From Wien's displacement law for thermal radiation from a black body, there is an inverse relationship between the wavelength of the peak of the emission spectrum and its temperature is expressed as follows:

$$\lambda_p T = b\,, \tag{29}$$

where λ_p is the peak wavelength and T the absolute temperature.

From this law we get:

$$\lambda_{obs} T_0 = \lambda_{emit} T_{emit}\,, \tag{30}$$

where T_0 is the temperature of the black body spectrum today, which is 2.7 K for the CMBR, and T_{emit} the temperature of the emitting plasma.

Hence:

$$T_{emit} = T_0 \frac{\lambda_{obs}}{\lambda_{emit}} = T_0(1+z)\,. \tag{31}$$

From the Stefan-Boltzmann's law, the energy flux radiating from a black body is as follows:

$$\text{Flux} = \sigma T^4\,, \tag{32}$$

where σ is the Stefan-Boltzmann constant, and T the temperature of the black body.

Combining (31) and (32), we find that the energy flux of the source of a black body that is redshifted is of order $(1+z)^4$. Hence, the energy flux of the emitting black body must be diluted by a factor $(1+z)^4$. For an expanding luminous phase, the photon flux is diluted by a factor $(1+z)^3$. Because photons lose energy as the light wavelength is stretched, another factor $(1+z)$ must be accounted for, and the resulting energy flux is diluted by a factor $(1+z)^4$. This is the required condition for the redshifted spectrum of a black body to be a black body spectrum itself. It appears that our cosmology with an expanding luminous world is consistent with the radiation energy density inferred from the CMBR.

7 Conclusion

The dichotomous cosmology is inspired by the tired-light model and consists of a static material world and an expanding luminous world. In this model the luminous world is expanding at a constant rate as in de Sitter cosmology. The model consists of two transformations, respectively: (1) to compensate for the stretching of the light's wavelength when the photon loses energy, we allow a time-varying light wavefront; (2) a time-dilation effect is incorporated into the model in order for the light wavefront to stay at the speed of light. This model explains both the luminosity distance versus redshift relationship of supernovae Ia, and "time-dilation effect" observed with the stretching of supernovae light curves. Furthermore, it is consistent with a radiation energy density factor $(1+z)^4$ inferred from the CMBR. This alternative cosmology only differs from the expanding Universe theory from the viewpoint that it is the light wavelength that is stretched due to a tired light process and not space itself that expands.

Submitted on June 8, 2014 / Accepted on June 10, 2014

References

1. Zwicky F. Red shift of spectral lines. *Proc. Nat. Acad. Sci.*, 1929, v. 15 773–779.
2. Pecker, J.-C. and Vigier, J.-P. A possible tired-light mechanism. *Observational Cosmology, edited by A. Hewitt, G. Burbidge, and L.Z. Fang*, 1987. p. 507.
3. Sorrell W.H. Misconceptions about the Hubble recession law. *Astrophysics and Space Science*, 2009, v. 323 205–211.
4. Shao M.H. The energy loss of photons and cosmological redshift. *Physics Essays*, 2013, v. 26 183–190.
5. Einstein A. Kosmologische Betrachtungen zur allgemeinen Relativitatstheorie. Koniglich Preussische Akademie der Wissenschaften (Berlin). Sitzungsberichte (1917). Engl. tr.: Cosmological considerations in the General Theory of Relativity. The Collected Papers of Albert Einstein, Volume 6, Princeton University Press, 1997. p. 421.
6. De Sitter W. On the relativity of inertia. Remarks concerning Einstein's latest hypothesis. *Koninklijke Nederlandsche Akademie van Wetenschappen Proceedings*, 1917, v. 19 1217–1225.
7. Carroll S.M. An Introduction to General Relativity Spacetime and Geometry. Addison Wesley, 2004. p. 153.
8. Blondin S., Davis T.M., Krisciunas K., Schmidt B.P., Sollerman J., Wood-Vasey W.M., Becker A.C., Challis P., Clocchiatti A., Damke G., Filippenko A.V., Foley R.J., Garnavich P.M., Jha S.W., Kirshner R.P., Leibundgut B., Li W., Matherson T., Miknaitis G., Narayan G., Pignata G., Rest A., Riess A.G., Silverman J.M., Smith R.C., Spyromilion J., Stritzinger M., Stubbs C.W., Suntzeff N.B., Tonry J.L., Tucker B.E., and Zenteno A. Time dilation in Type Ia Supernovae spectra at high redshift. *The Astrophysical Journal*, 2008, v. 682 724–736.
9. Heymann Y. On the Luminosity Distance and the Hubble Constant. *Progress in Physics*, 2013, v. 3 5–6.
10. Heymann Y. Redshift Adjustment to the Distance Modulus. *Progress in Physics*, 2012, v. 1 6–7.
11. Alpher R.A., Bethe H. and Gamow G. The origin of chemical elements. *Physical Review*, 1948, v. 73 803–804.
12. Alpher R.A and Herman R.C. On the relative abundance of the elements. *Physical Review*, 1948, v. 74 1737–1742.

LETTERS TO PROGRESS IN PHYSICS

Tractatus Logico-Realismus: Surjective Monism and the Meta-Differential Logic of the Whole, the Word, and the World

Indranu Suhendro

The Zelmanov Cosmological Group; Secretary of the Abraham Zelmanov Journal
for General Relativity, Gravitation, and Cosmology

"Surjective Monism" is a creation of a whole new stage after: 1) "Primitive Monism" of Leibniz, Pascal, and to some extent also the dualist Descartes. 2) "Reflexive-Geometric-Substantival Monism" of Spinoza's geometric "Tractatus" and "Ethics", which Einstein embraced, loved and lived, and its variants which he deemed more profound than Kantianism and which one can see very profoundly present in the scientific creation and philosophy of Zelmanov. 3a) "Machian Empirico-Monism" (as formulated in its final form by Bogdanov) along with "Pavlovian Material Monism" (a form defined as supposedly strict "materialistic ontology" in close connection with the school of Sechenov and Pavlov). 3b) "Russellian Neutral-Primitive Monism" (used in process philosophy). Thus "Surjective Monism" finally goes beyond Husserlian Phenomenology, Substantivalism, Psychologism, Existentialism, Picture/Logo Theory and the Analytical Philosophy of Mind and Language (of Wittgenstein's "Tractatus" and its "Language Game Theory" sublimation). It also complements Smarandachean Neutrosophic Logic and Multi-Space Theory. In the above, 3a) and 3b) simply ran developmentally parallel and somewhat competing in history.

Dedicated to the vastly profound intellection, memory, and solitude of A. L. Zelmanov (1913–1987), fountainhead of the celebrated Zelmanov Cosmological School; and to the closely following centennial anniversary of Einstein's General Theory of Relativity (1915–2015)

1 OMNUS: "Omnetic Reality" and the Summary-Quiddity of Surjective Monism (the Surjective Monad Theory of Reality)

In condensed form, we can present our Reality Theory — Surjective Monism — as the following singular meta-differential picture, i.e., "Qualon-Logos" ("OMNUS" or "Metanon"):

$$M : N(U(g, dg)) \sim S \, .$$

1.1 Reality is absolutely ONE, one-in-itself, beyond concrete and abstract count, beyond even the oft-defined "phenomena" and "noumena" (the way most philosophical abstractions define or attempt them self-limitedly); such that

1.2 Between Reality (M), i.e., Reality-in-itself, and Phenomenality (O) there $BE(S)$ — in the four-fold, asymmetric, anholonomic, meta-categorical (meta-differential) Unity of Sight and Sense (i.e., "Universum" (U) of Surject-Reality (g) and Surjectivity-Quality (dg)) of Surjective Monism — (capitalized with emphasis) a Surjective-Reflexive, Omnetic-Ontometric, Verizontal-Horizontal, Meta-Differential, Diffeo-Unitic Meta-Picture of Reality and Phenomenality, of Being and Existence, of Surject and Reflex, of the Verizon and the Horizon, of Onticity and Epistemicity, of Unity, Unicity, and Multiplicity, of the Infinite, the Infinitesimal, and the (Trans-) Finite, of the Whole, the Word, and the World, of Eidos, Nous, Noema, and Plaeroma, i.e., of the most fundamental "Qualon" (N) (Reality as its own Quality — "Qualicity"); such that

1.3 That which is meta-categorically between Phenomenality and Reality is EXISTENCE (X), i.e., Existence-in-itself: the reflexive Mirror and Boundary and the meta-differential Horizon, while that which is between Reality and Phenomenality is BEING (M:), i.e., Being-in-itself: the surjective Reality, Unity, and Difference (the Qualon) and the meta-differential Verizon; such that

1.4 The meta-categorical Distance between Reality and Phenomenality is Different from that between Phenomenality and Reality: $OM \neq MO$ — unless by way of Surjection (Reality's singular Exception, just Reality is, in itself, the "surjective-diffeonic" Exception of itself); such that

1.5 Reality contains all things phenomenal but these contain Reality not; such that

1.6 Reality is meta-categorically Different from all differences and similarities — and Different still; such that

1.7 If Reality were not SUCH, Reality and Non-Reality (Unreality), Being and Non-Being, Existence and Non-Existence would be absolutely NOT, once and for-ever, which is meta-categorically absurd.

As such Reality, as outlined in Surjective Monism, has 7 (seven) meta-differential ontic-epistemic levels. In addition, Reality possesses 4 (four) asymmetric, anholonomic, meta-categorical logical modalities/foliages encompassing:

M1. Meta-Onticity of (A, non-A, non-non-A, and none of these);

M2. Meta-Ergodicity of (without, within, within-the-within, without-the-without);

M3. Meta-Universality of (the material Universe, the abstract Universe, the Universe-in-itself, Reality);

M4. Meta-Epistemicity of (thought, anti-thought, Unthought, Reality).

In the above surdetermination and most direct presentation of Reality, the Whole Object ([O]bject, Surject, Qualon) that intrinsically (in the utmost eidetic-noetic sense) transcends and overcomes all logical predication (transitive and intransitive) between object and subject — as well as between occasionalism and substantivalism, i.e., between existentialism and essentialism — is uniquely determined by the meta-differential "Qualon-Logos" ("Metanon") of [O]bject = (Surject, Prefect, Abject, Subject, Object), through the unified qualitative-quantitative ontological-cosmological triplicity of Surjectivity, Reflexivity, and Projectivity.

2 ONTOMETRICITY: "Ontometric Reality", Unified Field Theory (Geometrization of Space-Time and Substance, i.e., Fields, Matter, and Motion), and the Ultimate Nature of the Physico-Mathematical Universe

Our fundamental "ontometric picture" of physical reality is embodied in the following purely geometric (and kinemetric) equation:

$$(DD - R)\, U(g, dg) = 0\,,$$

where DD is a differential wave operator and R is the very peculiar "ontometric spin-curvature" — both are built from the fundamental generalized asymmetric metric tensor (g) and connection form (W), in such a way that there is no point x in our space not dependent on the kinemetric pairs (x, dx) and (g, dg) —, and U is the wave function of the Universe — again as a kinemetric function of the metric and its differential. This way, there is no geometric point in our space that is merely embedded in it; rather it serves as a fundamental, fully geometric (and fully kinemetric) "ontometric meta-point" — constituting already fully geometric and intrinsic charge, mass, magnetic moment, and spin-curvature — for which the space, derived from it, is correspondingly emergent as a meta-space of geometrized fields — the "ontometric meta-space" of geometrically emergent and unified gravity, electromagnetism, chromodynamics, and superfluidity (matter) along with the fundamental properties of chronometricity, kinemetricity, and orthometricity.

This section, just as the above introductory description, is again a condensed form of our peculiar views on the nature of physical reality as outlined in, e.g., "Spin-Curvature and the Unification of Fields in a Twisted Space" and several other unified field theories referred to therein, such as "A Four-Dimensional [Meta-]Continuum Theory of Space-Time and the Classical Physical Fields" — as well as the more recent superfluidity geometrization model "A Hydrodynamical Geometrization of Matter and Chronometricity in [Extended] General Relativity". These are generally theoretical meta-pictures where I have attempted a theoretical "ontometric" meta-continuum picture of cosmophysical reality aimed at unifying gravitation, electromagnetism, and chromodynamics on one hand, and superfluidity, chirality, spin-curvature, matter, and motion — self-realizably along with Zelmanov's chronometricity, kinemetricity, and orthometricity — on the other, as also independently and quintessentially alluded to in our works cited above. Particularly, we will here outline a fresh summary of the nature of Universe whose ontological and epistemological reality would be most satisfactory to the sense of the profound Zelmanov school of scientific creation. Our common aim, as a scientific group and as a whole — in the tradition of Zelmanov — is not simply to "think differently" (a slogan readily laden with post-modern cliche nowadays), but also to be meta-categorically "different from all differences and similarities, and different still" in the truest and most qualified epistemic sense of science and scientific creation.

As a reminder, a present-day category of approaches to unification (of the physical fields) lacks the ultimate epistemological and scientific characteristics as I have always pointed out elsewhere. This methodological weakness is typical of a lot of post-modern "syllogism physics" (and ultimately the solipsism of such scientism in general). Herein, we shall once again make it clear as to what is meant by a true unified field theory in the furthest epistemological-scientific-dialectical sense, which must inevitably include also the most general (and natural) kinemetric unity of the observer and physical observables, i.e., "ontometricity".

Herein, I shall state my points very succinctly. Apart from the avoidance of absolutely needless verbosity, this is such as to also encompass the scientific spirit of Albert Einstein, who tirelessly and independently pursued a pure kind of geometrization of physics as demanded by the real geometric quintessence of General Relativity, and that of Abraham Zelmanov, who formulated his theory of chronometric invariants and a most all-encompassing classification of inhomogeneous, anisotropic general relativistic cosmological models and who revealed a fundamental preliminary version of the kinemetric monad formalism of General Relativity for the unification of the observer and observables in the cosmos.

Thus, we can very empathically state the following:

1. A true unified field theory must not start with an arbitrarily concocted Lagrangian density (with merely the appearance of the metric determinant $\sqrt{-g}$ together with a sum of variables inserted by hand), for this is merely a way to embed — and not construct from first principles — a variational density in an *ad hoc* given space (manifold). In classical General Relativity, the case of pure vacuum, i.e., $R_{\alpha\beta} = 0$, there is indeed a rather unique Lagrangian density: the space-time integral over $R\sqrt{-g}$, the variation of which gives $R_{\alpha\beta} = 0$. Now, precisely because there is only one purely geometric integrand here, namely the Ricci curvature scalar R (apart from the metric volume term $\sqrt{-g}$, this renders itself a valid geometric-variational reconstruction of vacuum General Relativity, and it is a mere tautology: thus it is valid rather in a secondary sense (after the underlying Riemannian geometry of General Relativity is encompassed). Einstein indeed did not primarily construct full General Relativity this way. In the case of classical General Relativity with matter and fields, appended to the pure gravitational Lagrangian density are the matter field and non-geometrized interactions (such as electromagnetism), giving the relevant energy-momentum tensor: this "integralism procedure" (reminiscent of classical Newtonian-Lagrangian dynamics) is again only tautologically valid since classical General Relativity does not geometrize fields other than the gravitational field. Varying such a Lagrangian density sheds no further semantics and information on the deepest nature of the manifold concerned.

2. Post-modern syllogism physics — including string theory and other toy-models (a plethora of "trendy salad approaches") — relies too heavily on such an arbitrary procedure. Progress associated with such a mere approach — often with big-wig politicized, opportunistic claims –, seems rapid indeed, but it is ultimately a mere facade: something which Einstein himself would scientifically, epistemologically abhore (for him, in both the pure Spinozan and Kantian sense).

3. Thus, a true unified field theory must build the spin-curvature geometry of space-time, matter, and physical fields from scratch (first principles). In other words, it must be constructed from a very fundamental level (say, the differential tetrad and metricity level), i.e., independently of mere embedding and variationalism. When one is able to construct the tetrad and metricity this way, he has a pure theory of kinemetricity for the universal manifold M: his generally asymmetric, anholonomic metric $g_{\alpha\beta}$, connection W, and curvature R will depend on not just the coordinates but also on their generally non-integrable (asymmetric) differentials:

$$M(x, dx) \to M(g, dg) \to W(g, dg) \to R(g, dg)\,.$$

In other words, it becomes a multi-fractal first-principle geometric construction, and the geometry is a true chiral meta-continuum. This will then be fully capable of producing the true universal equation of motion of the unified fields as a whole in a single package (including the electromagnetic Lorentz equation of motion and the chromodynamic Yang-Mills equation of motion) and the nature of pure geometric motion — kinemetricity — of the cosmos will be revealed. This, of course, is part of the the emergence of a purely geometric energy-momentum tensor as well. The ultimate failure of Einstein's tireless, beautiful unification efforts in the past was that he could hardly arrive at the correct geometric Lorentz equation of motion and the associated energy-momentum tensor for the electromagnetic field (and this is not as many people, including specialists, would understand it). In my past works (with each of my theories being independent and self-contained), I have shown how all this can be accomplished: one is with the construction of an asymmetric metric tensor whose anti-symmetric part gives pure spin and electromagnetism, and whose differential structure gives an anholonomic, asymmetric connection uniquely dependent on x and dx (and hence x and the world-velocity u, giving a new kind of Finslerian space), which ultimately constructs matter (and motion) from pure kinemetric scratch. Such a unified field theory is bound to be scale-independent (and metaphorically saying, "semi-classical"): beyond (i.e., truly independent of) both quantum mechanical and classical methods.

4. Such is the ultimate epistemology — and not just methodology — of a scientific construct with real mindful power (intellection, and not just intellectualism), i.e., with real scientific determination. That is why, the subject of quantum gravity (or quantum cosmology) will look so profoundly different to those rare few who truly understand the full epistemology and the purely geometric method of both our topic (on unification) and General Relativity. These few are the true infinitely self-reserved ones (truly to unbelievable lengths) and cannot at all be said to be products of the age and its trends. Quantizing space-time (even using things like the Feynman path-integrals and such propagators) in (extended) General Relativity means nothing if somewhat alien procedures are merely brought (often in disguise) as part of a mere embedding procedure: space-time is epistemologically and dialectically not exactly on the same footing as quantum and classical fields, matter, and energy (while roughly sharing certain parallelism with these things); rather, it must categorically, axiomatically qualify these things. Even both quantum mechanically and classically it is evident that material things possessed of motion and energy are embedded in a configuration space, but the space-time itself cannot be wholly found in these constituents. In the so-called "standard model", for example, even when quarks are arrived at as being material constituents "smaller than atoms", one still has no further (fundamental) information of the profounder things a quark necessarily contains, e.g., electric charge, spin, magnetic moment, and mass. In other words, the nature of both electromagnetism and matter is not yet understood in such a way. At the profoundest level, things cannot merely be embedded in

space-time nor can space-time itself be merely embedded in (and subject to) a known quantum procedure. Geometry is geometry: purer, greater levels of physico-mathematical reality reside therein, within itself, and this is such only with the first-principle construction of a new geometry of spin-curvature purely from scratch — not merely synthetically from without — with the singular purpose to reveal a complete kinemetric unity of the geometry itself, which is none other than motion and matter at once. Again, such a geometry is scale-independent, non-simply connected, anholonomic, asymmetric, inhomogeneous: it ultimately has no "inside" nor "outside" (which, however, goes down to saying that there are indeed profound internal geometric symmetries).

5. Thus, the mystery (and complete insightful understanding) of the cosmos lies in certain profound scale-independent, kinemetric, internal symmetries of the underlying geometry (i.e., meta-continuum), and not merely in *ad hoc* projective, embedding, and variational procedures (including the popular syllogism of "extra dimensions").

3 On the Furthest-Qualified Metaphysics, Phenomenology, Ontology, and Cosmology

We have, in our time, very fortunately witnessed the heroic emergence of a class of neutral, vast generalizations ("neutrosophies", to use the Smarandachean term, after the pioneering logician, mathematician, and polymath F. Smarandache) of logic and dialectics — worked out entirely by very few original, profound minds of genuine universal character — aiming at envisioning a much better future for humanity in the cosmos, e.g., scientific, psychological, social, and economic terms, thus forming an inspirational surge beyond the blatant superficialities and tyranny of certain politically, inter-subjectively established paradigms often masquarading as the "true scientific method" and "objectivity". The inherently flawed assumptions of these misleading paradigms, as such, can be seen only with clear independent epistemicity (true, objective knowledge, even "un-knowledge", on the horizon of things), and not in terms of methodology alone (which can often be fabricated and imitated), as to how they are chiefly non-epistemic — thus ultimately pseudo-scientific and pseudo-objective — trends that pretend that certain ontically and epistemically intricate matters are already settled by "consensus" of the majority.

All this is crucially taking place in the incessant, highly nervous background of science and certain peculiar scientific affairs of today (as Thomas Kuhn has indicated just what the "tectonic rims" of science might be), just as it has always appeared historically, and will always appear as such, to rescue the state-of-the art of science from "usual human tendencies towards promulgating corruption" at very critical epistemological junctions. The common objective of these generalizations is to form a broader window — a truly open window pretty much without cumbersome curtains indeed — for a more genuine outlook on the landscape of science and humanity.

Having said the above, I hereby applaud any lone epistemic effort — among other such lone efforts — in the direction of a new reality theory and a new semantics theory aimed at, e.g., a new neutral synthesis of ubiquitous doctrines such as substantivalism and occasionalism, as well as absolutism and relativism, for cosmology and cosmogony. Such a work, to the one who knows "how corrugated, discrete, and paradoxical landscapes in the cosmos can be", is a pure dialectical enjoyment in itself, in the solitary niche where true epistemic minds often hide their solitary effulgence and brilliance. Therein, one is obliged to outline a genuine solution to the persistent, often popularly misunderstood problems and challenges in scientific epistemology from the ancient epochs of the Greeks and the Indians (the Sanskrit/Vedic "Indo-Aryans"), through the medieval ages of the Perso-Arabic — and then pan-Hellenic European — civilization and Renaissance, to the most recent eras of modernism, post-modernism, and scientism.

However, the reader should be aware that behind this simple appraisal a supposedly genuine thought aimed at a conscious stationing (dialectical synthesis) of phenomena constitutes a train of further in-going paradoxical thoughts. Thus, let us do a brief (and yet dense), crucial, signaling surgery on the manifold of thoughts of modernism, post-modernism, and scientism (including critical post-modernism) — as to why such intellectual strands ultimately fail to transcend anything real — and on the dialectical anatomy ("cosmogony") of the problems of the world in general.

Keep in mind, once and for all, that, despite diverse causes, the root of this meta-situation can be traced back to the cosmic "superset" as to whether the world we inhabit is essentially autonomous in itself or extraneously governed by some kind of intelligence. Further independent epistemic qualifications (including disqualifications) can be applied to these options as new horizons are encompassed. This should suffice to underline what is crucial in any original reality (and linguistics) theory, among other similar and dissimilar epistemically sincere proposals ranging from absolute agnosticism to a further sense of knowing and enlightenment.

I'd like to re-identifty, in my own words, the very problem that any genuine reality theory has to deal with in terms of scientific epistemology as follows (as I have stated elsewhere on past occasions, especially in my work on a new kind of Reality theory, namely "The Surjective Monad Theory of Reality" or "Surjective Monism", and on my seminal address "On Meta-Epistemic Determination of Quality and Reality in Scientific Creation"). Despite many conscious and conspicuous attempts at elevating the use of process-synthetic philosophy and integralism to a "new" key paradigm at the critical crossroads between world affairs and individual well-being, many thinkers have not developed the first-principle logical-dialectical tool needed to solve fundamental existential and

phenomenological problems in modern philosophy (that is to say, since Kant and Copernicus), be it one that directly or indirectly underlies the pure workings of science. This way, the complete surgical tool of meta-logic is still missing from their hands, and so true determination — in the profoundest sense of the word "determination" — is absent. Thus, the purported newness [and trend] of post-modern paradigms do not really constitute a first-principle philosophical newness: it is merely a magnified old-nostalgic trace of process-integralism, an issue contested by the likes of Russell and Whitehead (philosophically, scientifically, and morally) at the critical, dehumanizing, life-shearing onset of last century's two world-wars as well as the cold war (which continues to prevail under the surface of history, precisely as a dialectical part of epistemicity and historicity, not mere hermeneutics, linguistics, and history).

This is precisely why mere post-modern visions of revisionist holism and inter-subjective facticity (somewhat akin to Gestalt psychology) — both as a natural scientific-revisionist investigation and a purportedly broader philosophical picture — still suffer from the contingency (that is, reflexes, conditions, and associations) of [their] embedding solipsistic sphere, when this on-going contingency ought to be categorically deconstructed in the first place, and not merely highlighted in the light of further arbitrary psychological associationism put forth arbitrarily as "objective science" (such as the "second-hand" inclusion of the convenient psychologism and propaganda that "syntax-only science supersedes semantics").

Thus, while such an approach may be sufficiently inspirational for a psychological reform within a known, ultimately defective established scientific, political, and cultural system, it is not yet an adequate framework for genuine humanistic revolution and logical determination. A genuine thinker should look for a meta-language, a meta-paradigm for science; one that is free of the usual kinds of pretense and bigotry we encounter from time to time in the history of thought, especially modern thought: a journey from Cartesian dualism to Spinozaic monism to Berkeleyan psychologism via the weary intellectual bridges of Hume, Kant, Hegel, Husserl, Heidegger, and Wittgenstein (both the analytic young Wittgenstein and the post-modern old Wittgenstein).

Or else, much of humanity has forgotten — or is simply absolutely, blissfully, complacently ignorant of — the essence of what Max Planck and Ernst Mach — the two pedagogy and epistemology giants (and innovative scientists in their own right) surrounding Albert Einstein in his scientific revolutionary days — once argued about. They argued about the essences, modes, limits, and expansions of science vis-a-vis Reality quite long before Einstein debated Niels Bohr on the nature of the quantum, cosmos, and Reality. And certainly long before Karl Popper outlined his epistemology and ideal criteria for "falsifiable science" against the overly-positivistic Vienna circle led by Moritz Schlick (whose position is blindly, arbitrarily taken by "throngs of scientists" in the USA and Western hemisphere as of today, whether they know it or not: few are those who are truly conversant with ontology and epistemology, and not just methodology, after all).

At the same time, in fact soon after Mach launched his epistemological program towards "purifying absolutism in science" (especially in Newtonian and celestial mechanics) in Europe, Russia, witnessed heated debates of the nature of science and philosophy vis-a-vis Reality as contested by the likes of Ouspensky (who defended the simultaneously neo-Platonic and neo-Aristotelian traditions of meta-physics), Bogdanov (who tried to generalize Machian thought into a single "empirico-monism"), and those who harshly forced the notion of "materialism over Machianism and all sorts of psychologism and idealism" on scores of Soviet scientists, gaining ultimate support from materialist philosophers and scientists such as the foremost expert on the "reflexes of the higher nervous system", Ivan Pavlov.

In the sense of critical epistemicity, Einstein, for example, criticized both certain self-assured theists and atheists, among both vocal scientists and vocal lay people concerned about often blurry, oversimplified entities such as "god" and "nature", as "rogue solipsists".

4 The Meta-Differential Logic of the Whole, the Word, and the World: Surjective Monism and the "Qualonic Unity" of Sight and Sense

What, then, is a meta-science in our case? It is none other than the great reflex of ontic-epistemic Unity — the Unity of Sight and Sense — in the sense of beholding an object (or phenomenon), while recognizing categorically (up to a point of Absolute Difference) that Existence (Nature, space-time in the most qualified phenomenological sense) is as-it-is a mirror-like apogetic Horizon and Reality is in-itself an eidetic Verizon: one "perigetically" witnesses the object in space ("sight") and "apogetically" withholds space in the object as "internal time" ("sense") whereby time here is the sensation (a priori representation) of space by way of the complete dialectical-phenomenological unity of space-time, matter, and motion (in the sense of epistemologically qualified objective events, not arbitrary "frills"). When objectivity is asymmetrically moved along social time-lines and synthetic-paradoxical thinking ("Understanding", i.e., "thinking about thinking" and "doing about doing"), it becomes "Praxis/Paradigm as it is" — Surdetermination —: a vortex of historicity, capable of creative-reflexive stellar motion at the societal stage, yet whose infinitesimal center of "insight" and "inhering" remains non-integrable and solitary. The highest (eidetic) degree of Quality concerning this, given as a Whole Object (where the Horizon is dialectically part of it, instead of arbitrarily including, eliminating, or excluding it), is none other than the furthest qualification of "noema", while it shall

be termed "surholding" in the sense of "noesis": it possesses "Surjective Verizon" as Being and "Reflexive Horizon" as Existence, and not mere inter-subjective projection and inter-objective boundary.

Mere integralism, just like non-epistemic over-simplification and over-generalization, is at best a rhapsodic trend in post-modernism and psychologism (including post-structuralism and neo-psychoanalysis); ultimately, however, it — like the psychologism of Gestalt — is no substitute for a first-principle categorical underpinning of phenomena, that is, the complete dialectical unity — the ontological-epistemological-phenomenological-axiological unicity — between the Real and the Ideal, the material and the mental, the whole and the partial, and all the asymmetric existential-predicative tension between the object and the subject in general. The same defect can be said about the uncritical use of process philosophy without original refined recourse to "noema" (objects-as-they-are) or phenomenology (at least in the sense of Husserl, who was both a mathematician and philosopher, as we need not mention how "phenomenologists" after him have easily misunderstood the fundamentals of Husserlian phenomenology and, thereafter, they have also arbitrarily misunderstood and dismissed each other in the realm of post-modernism).

Again, most post-modern authors of scientism, as well as the majority of so-called "scientists", do not seem to intuitively emphasize the need for the deconstruction of the ultimately illogical-pathological state of a world much plagued with hypersemiotics, hypernarration, oxymoronism, sycophancy, pseudo-objectivity, pseudo-science, pseudo-philosophy, pseudo-spirituality, pseudo-artistry, solipsism, and ontic-epistemic shallowness.

As easy to see, the prevalent solipsistic type of world-scientism — and, indeed the associated panhandling and psychologism of scientific affairs, coupled with superficial political and economic affairs — is ultimately unscientific and non-logical for not taking into account in the first place the important logico-phenomenological branch of dialectics, let alone of neutrosophy, namely a comprehensive science that attempts to throw light at logic, empiricism, psychologism, existentialism, essentialism, science, philosophy, and history, thereby transforming mere history into dialectical historicity.

Consensus solipsism, no matter how much it is often falsely put forth as "science" and "objectivity" before both the more naive "scientists" and the gullible public, is solely based on a desired paradigm concentrated in, and funded by, corporate and governmental hands by way of visible and invisible "control by proxy" monopoly in many aspects of life, and it attempts to primitively capsize all the rest of scientific existence under its sway by non-dialectically embedding an essentially inhomogeneous, non-simply-connected, variegated world of paradigms and ideas (which it ultimately knows not!) in its own homogenizing pseudo-parametric space, and this, with all the bias, vested political interests, and duplicity contained in it, is often neatly disguised — helplessly by way of syllogism and solipsism — as the so-called "scientific method" (thus, some have warned us that there is not a single "scientific method" — just as there is not a single quantum mechanics: there is more than one version of quantum mechanics, than the one following the "Copenhagen interpretation" — and that a scientific economy precept known as "Ockham's razor" is often misused). Clearly, a "given consensus science" hiding ulterior motives is not the same as science itself, for which new ways of thinking and genuine epistemic objectivity are the primary goals often following long processes of logico-dialectical thinking as well as solitary revolutionary thinking or ideation (alas, as Michael Crichton has pointed out, history has provided us with a set of scoundrels-in-power of mere opportunism when it comes to "consensus science").

This stuff at the heart of the matter is essentially, intellectually primitive and cumbersome, no matter how much power, psychologism, techno-scientism, and modernity it displays: a set of mere opinions made strong by way of any kind of political favoritism does not solve the age-long problem of syllogistic solipsism and solipsistic syllogism in science and philosophy. Indeed, the world of science — supposedly inherited, both arbitrarily and qualifyingly, from the "ancients" and the more recent "Aufklarung", just like the world of philosophy — still inherently suffers from mere syllogism and solipsism, albeit in a different intellectual category than other types of solipsism, thereby often resulting in advanced opaque types of dogmatism, absolutism, and relativism, and in the said types of sycophantism and sophism. Note how these are easily interchangeable in each other's garb and served with fresh inductive duplicity on the daily menu of "loud, bubbly, verbose, trendy, big-wig scientism".

That is why, a truly qualified science production is always crucial — beyond the said integralism and mere post-modern holism — in all the branches of science, including cosmology, ecological science, and the humanities: it must be based on independent, neutrosophically guided free inquiry, beyond all forms of superficial political control, especially funding systems and political interests. In this scheme, such science production is the first and foremost logical foundation of a revolutionary social-democratic culture, and not capital sums (and so not pretentious scientism — pseudo-intellectual bigotry — with all its hidden subjectivity and opportunism).

Back to the problem of ontology and epistemology as well as cosmology and cosmogony addressed herein, then wholly illuminated, by any genuine reality theory: is the Universe, our home, autonomous or is it dependent (on a supposed "demi-urge" or "creator" — while the word "creation" should in any case be epistemically qualified)? If it is autonomous, is it machine-like and ultimately random, or is it quasi-anthropomorphic and teleological, or is it absolutely autonomous? If it is dependent, what kind of dependency (or creation) is there: epiphanic (as in the neo-Platonic sense), or

theological (as in the Kalam cosmological argument and in the Thomian sense), or none of these? Before answering — or rather, epistemically addressing — such questions, a sense of mindful humility is very important, one akin to Einstein who, as known, did not believe in a personal god, but for whom — like for Spinoza — the word "God" should represent a very broad, genuine sense of Reality and Onto-Realism, namely a non-personal transcendental universal intellect whose attributes and laws are not anthropomorphic and arbitrarily projective but "summa-rational" and "meta-rational", and whose horizon in the intricate and beautiful cosmos renders "mere reflective human minds" like vanishing dots thereon.

The philosophical propositions for cosmology and cosmogony elaborated upon by such a theory must then transcend the intrinsic self-limitations and extrinsic ex-limitations of both mere dogmatic materialism (solipsistic objectivism) and psychologism (solipsistic subjectivism): a more infinitely reflexive-neutral, let alone "surjective", realism will be inherently different from mere passive, dogmatic, and biased (thus ultimately solipsistic) "randomness" and "design", especially when determining a genuine sense of cosmic semi-autonomy as well as both the weak and strong anthropic principles. Such a vein then must be seen as sincere and epistemic enough, and is meant to enrich public understanding of the matter in the very arena of "science and philosophy at a cross-roads".

Meta-physics is the science dealing not with "non-science", "non-sense", or "para-physics", as many have misinterpreted it, but with the epistemic qualification and entification of the sciences. Ockham's razor, too, is a metaphysical stance. And so is materialism. As such a "neutrosophist", in countering the currently prevalent, financially and politically more supported dogma of a self-sufficient material universe emerging by chance and populated by randomness, does not side with creationism, let alone "biblical creationism" or "intelligent design" for he has assuredly maximum epistemic distance from falling solipsistically into this or that (while, like Einstein, considering "religion" only psychologically and historically); rather, like Einstein, he aims to humbly show how the problem is not culturally settled: be it among the Greeks, among medieval thinkers, or among the contemporary minds of today. He, like Einstein, humbly sees a "superior manifestation of intelligence" in Nature and on the horizon of things and, on a psychological and historical note, is merely sympathetic with the minority in this category — and the faintest of voices —, and this is true in any case.

No matter what one's meta-physical stance is in science and philosophy, the problem presented here is a truly beautiful, profound one. In my view, Reality should be ontologically simple (yet "not that simple") in the sense of what I term the "Qualic Unity (Unicity) of Sight and Sense", while being epistemologically so complex (yet "not arbitrarily complex") at the same time: it is necessarily One-in-itself beyond concrete and abstract, even "noumenal", count. Metaphorically speaking of Reality and the Universe, onticity is the whole mountain and ontology is the peak and the verizon; epistemicity is then the quintessential gradient and epistemology is the entire slope: this makes truly qualified knowledge and understanding possible, whether universal or particular, categorical or phenomenal, philosophical or scientific; phenomenology is the mountain's appearance (verisimilitude) and "stuff" as well as the corresponding horizon and landscape; at last axiology is the rest as concerns judgment and values. This way, there is a profound, four-fold categorical, asymmetric, anholonomic difference between "Being" and "Existence" (as, again, outlined in my own "Surjective Monad Theory of Reality" as a qualified generalization of reflexive monism), just as the meta-categorical, ontic-epistemic, surjective-reflexive distance ("Qualicity") between Reality and Phenomenality is asymmetric. I will undertake to explain this a little bit, as presented below.

5 The Diffeo-Unitics of Being and Existence in Surjective Monism

Whether one is concerned about the strenuous synthesis between the mundane and the other-worldly, between the economical and the ecological, between the one and the many — that is, basically between a thesis and an anti-thesis in a rather universal sense —, phenomenologically, dialectically speaking, one is essentially referring to Existence as a "negative totality" — instead of both the arbitrary, subjective Unknown of solipsistic mysticism and the equally solipsistic, overly positivistic valence of narrow (non-dialectical) material dogmatism —; that is, Existence is an "inconsistent inner multiplicity in and of itself": it has parts that do not constitute the Whole by way of simple representation, and yet, unlike mere holism, it is livingly capable of unifying logical synthesis and determination when a portion of humanity is in touch with the said synthesis. The problem here since time immemorial, as renewed by Kantian categorical analysis, overly-symmetrically projected by Hegel, attempted by Husserlian phenomenological analysis, and brought to a further critical stand-still by Heidegger, has been the infinitesimal (essentially surdeterminate) difference between Being and Existence ("Being-as-Being" vis-a-vis "Being-here") — and also between Idealism and Realism, between noumena and phenomena, as well as between Transcendence and Immanence. Only when this is universally — that is, categorically-eidetically — solved can one truly speak of what is beyond mere essentialism and existentialism, that is, the most qualified Thing-in-itself: the Word and the World, the Whole and the While. That is, in other words, true ontic-epistemic objectivity.

This way, then, Surdetermination (universal determination) of the Whole, the Word, and the World — in the sense of Reality's Verizon and Horizon — must be aimed at the very Present, more than at the theoretical future.

A logical system is hereby categorical-synthetic-revolutionary (that is, universal) if and only if it encompasses the spiraling interaction between: 1) Existence as the eidetically negative totality and horizon of "non-A and non-non-A" for any entity "A" and the infinitesimality (surdeterminate infinite difference) of "non-A" and the infinity of "non-non-A" — the entirety of possible inter-related, compositional things — and 2) the "twice-aprioristic" (non-arbitrary objective-aprioristic) epistemic set of "A and non-A" representing things-as-they-are (categorically aprioristic-objective existents in pure phenomenological-natural space beyond mere societal conditionings). This, when fully implemented, gives a dialectical "humanity-epistemicity spiral" instead of both the concentrically closed circle of logism (such as dogmatism and monopoly) and the interconnected circles and "biosphere" of post-modernism (especially integralism). Such a fully phenomenological spiral ("connex of causation") is in the "genes" of Revolution and Praxis without any need to resort to mere idealism and integralism (of the many, especially in the post-modern sense) — other than dealing with noematic object-magnification and object-illumination: not only can an island exist after all in its essentially negative and paradoxical oceanic surroundings, it can also be of the density of a great continent with its spiraling mountain peaks and profound valleys irrespective of its phenomenal size (as perceived by the majority of people).

Having said that, I maintain that "Being-qua-Being" is the "none-of-these" part of the above meta-logic and a most direct Surdetermination ("Surholding") of Reality, in the subsequent vicinity of the most neutral "non-non-A" determination of Existence whose universal object is a "Qualon", that is [O]bject = (Surject, Prefect, Abject, Subject, Object) — again, see the work on "Surjective Monism" for the peculiar new-contented glossary of these terms.

6 Epilogue

Such a meta-categorical view on Reality, as presented above, is in eidetic and twice-aprioristic contrast to the pseudo-synthetic, inter-subjective, commutative logism of a thing "A" being arbitrarily, conditionally given as "A and non-A" at the same time by way of a homogenizing, "modernizing", "newly introduced" human interaction-type superficially (beyond just artificially!) prevalent in today's society. Consider, for example, both the case of classical Hegelian solipsistic syllogism (in the case of absolutist history and sociology) and the generic example of the one-dimensionality (one-sidedness) between technological gadgets (which can easily be substituted by any given operational post-modern notion) in the "free market" and the majority of their users: a great gap exists between the given (gadgets as conditions) and the conditioned (subjects), that is, unless the subjects are the creators or producers — not mere buyers — of the said gadgets. Here, subjects do not genuinely, aprioristically exist with respect to Existence (but only with respect to the capriciously conditioning inter-subjective society) and so are devoid of epistemicity; instead, they are conditioned by their whole range of habits determined through the given gadgets and associated contemporary urges.

The full extent of solipsism and syllogism — and the stark absence of true Eidos, Logos, and Eros (of course, not exactly in the Marcusian sense and use of the merely contrasting phrase "Logos and Eros", rather in a most unified and qualified substantiation of the "Ergo" and not a mere "ego", being somewhat akin to the very term "ergodicity") is at the very heart of the problem of contemporary neo-simplistic world at large in relation to puppetry, especially intellectual puppetry: most contemporary people do not touch the ground with their feet (to know the real contour of Existence, and not just the "societal sphere"), and they are unable and not allowed to do so; instead, they are hanging (whether high or low) by conditional proxy and post-modern threads, prodded by ultracapitalistic-ultraconsumerist-hypernarrative rods and sustained daily by superficial image-making tantamount to overall solipsistic-syllogistic defect: that of hypernarration, hyperoxymoronism, hypersemiotics, duplicity, solipsism, and utter ontic-epistemic shallowness. In other words, they are not real, as they do not inhere within Existence (let alone Being!) and its noematic mirror: they are apparitions upon Existence and that mirror. They are not "wrong": they are "not even wrong" (as a notable mathematician puts it).

The known towering figures of analytic philosophy, who have stood as stern horizons before many, have not been able to completely solve this epistemic problem, owing to the fact that their systems are largely overly-symmetrical, be they empirical, positivistic, or idealistic. Yet the fact remains that the unity referred to as Existence is indeed a negative totality with a positive nescience on the part of multiplicity of most conscious existents: it has an underlying asymmetric connection between things perceived as "parts" and is non-integrable by way of logical representation. Thus, the aim of dialectics is not to "integrate" Existence as such, but to synthesize the given ambiguities in the logical-ideal form of an eidetic-noematic category encompassing object-oriented Praxis/Paradigm, where a priori and posteriori categories are taken as not mere process (a-la Russell and Whitehead), but "surgical modalities" in the face of anti-dogmatism. This, then, would be a positive, dialectical kind of idealism capable of Progress (and real dialectical synthesis) in the real background of the said negative totality — again, akin to constituting a solid island or continent in the greatly paradoxical oceanic surroundings —, in contrast to mere syllogism and solipsism, dogmatism and sophism, absolutivism and relativism.

Except for those who are uncritically conditioned and embedded by it (unfortunately, such sorry individuals account for the majority, as in any age, which is why the superficial world of modernity remains running on misleading wheels

and false horses as it does today), Progress on all fronts of Ideation does not intrinsically belong to non-epistemic solipsism: never it has been so and never it will be. What is often taunted as "scientific progress" (not exactly the same as technological progress, let alone genuine epistemic scientific progress) in the fast linkage of contemporary dehumanization and pseudo-enlightenment (instead of a set of neutral, multifractal "micro-paradigms": a model for an epistemological scientific system incapable of being integrated arbitrarily into an embedding political bastardization of dogmatic scientism and religionism on the large scale) often entails logico-moral duplicity which in turn causes a typical inept individual and stooge to deny any existential footing, almost deliberately mistaking the superficial world (in homogeneous, conforming chains) for the real, paradoxical, non-dogmatic terrain of Existence: the weight, the feet, and the ground of Existence he never realizes and touches, for he is ineptly hoisted high by the external manipulative world upon superficial hooks, hangers, and logisms (seeming situational logical thoughts that are ultimately, on the edge of the world, "not even wrong"), and still it is somewhat guaranteed by the collective solipsism of the majority that such one is able to derive his happiness — if not his entire absurd situation and way of being — from subconscious folly and conceit often arising merely from shallow international conformity and hidden feudalism based on common image-making (indeed, instead of common good and true democracy); in other words, from internal incapacity and inconsistency as to what really transpires on the small and large scales of the cosmos and the world of human activities and considerations.

In short, solipsistic logism, including both the schemers and the blind workers, suffers from all kinds of pseudo-objectivity, especially on the horizon of things. The penultimate revolutionary-intellectual human, however, firmly touches the ground with his own feet, and is capable of the paradoxical contour of Existence — by way of encompassing the four categorical, meta-epistemic "a priori's" and "a posteriori's": ontic-eidetic-noetic, synthetic-apogetic-a priori, synthetic-peripheral-a posteriori, and subjective-psychological — leading all the way from the abyss to the summit, as Revolution in the sciences is always ardently wholly needed, not a mere reform: a new Word for the World, and a new World for the Word.

Submitted on: May 25, 2014 / Accepted on: May 30, 2014

A Closed Universe Expanding Forever

Nilton Penha Silva
Departmento de Física (Retired Professor), Universidade Federal de Minas Gerais, Belo Horizonte, MG, Brazil
Email: nilton.penha@gmail.com

In a recent paper, the expression $a(t) = e^{\frac{H_0 T_0}{\beta}\left[\left(\frac{t}{T_0}\right)^{\beta}-1\right]}$ where $\beta = 0.5804$, was proposed for the expansion factor of our Universe. According to it, gravity dominates the expansion (*matter era*) until the age of $T_\star = 3.214$ Gyr and, after that, dark energy dominates (*dark energy era*) leading to an eternal expansion, no matter if the Universe is closed, flat or open. In this paper we consider only the closed version and show that there is an upper limit for the size of the radial comoving coordinate, beyond which nothing is observed by our fundamental observer, on Earth. Our observable Universe may be only a tiny portion of a much bigger Universe most of it unobservable to us. This leads to the idea that an endless number of other fundamental observers may live on equal number of Universes similar to ours. Either we talk about many Universes — Multiverse — or about an unique Universe, only part of it observable to us.

1 Introduction

The Cosmological Principle states that the Universe is spatially homogeneous and isotropic on a sufficiently large scale [1–7]. This is expressed by the Friedmann spacetime metric:

$$ds^2 = \mathfrak{R}^2(T_0)\, a^2(t) \left(d\psi^2 + f_k^2(\psi)\left(d\theta^2 + \sin^2\theta d\phi^2\right)\right) - c^2 dt^2, \quad (1)$$

where ψ, θ and ϕ are comoving space coordinates ($0 \leqslant \psi \leqslant \pi$, for closed Universe, $0 \leqslant \psi \leqslant \infty$, for open and flat Universe, $0 \leqslant \theta \leqslant \pi$, $0 \leqslant \phi \leqslant 2\pi$), t is the proper time shown by any observer clock in the comoving system. $\mathfrak{R}(t)$ is the scale factor in units of distance; actually it is the modulus of the *radius of curvature* of the Universe. The proper time t may be identified as the cosmic time. The function $a(t)$ is the usual expansion factor

$$a(t) = \frac{\mathfrak{R}(t)}{\mathfrak{R}(T_0)}, \quad (2)$$

being T_0 the current age of the Universe. The term $f_k^2(\psi)$ assumes the following expressions:

$$f_k^2(\psi)\left\{\begin{array}{l} f_1^2(\psi) = \sin^2\psi \ \text{(closed Universe)} \\ f_0^2(\psi) = \psi^2 \ \text{(flat Universe)} \\ f_{-1}^2(\psi) = \sinh^2\psi \ \text{(open Universe)} \end{array}\right\}. \quad (3)$$

In a previous paper [8], we have succeeded in obtaining an expression for the expansion factor

$$a(t) = e^{\frac{H_0 T_0}{\beta}\left(\left(\frac{t}{T_0}\right)^{\beta}-1\right)}, \quad (4)$$

where $\beta = 0.5804$ and H_0 is the so called Hubble constant, the value of the Hubble parameter $H(t)$ at $t = T_0$, the current age of the Universe. Expression (4) is supposed to be describing the expansion of the Universe from the beginning of the so called *matter era* ($t \approx 1.3 \times 10^{-5}$ Gyr, after the Big Bang). Right before that the Universe went through the so called *radiation era*. In reference [8] we consider only the role of the matter (baryonic and non-baryonic) and the dark energy.

In Figure 1 the behaviour of the expansion acceleration, $\ddot{a}(t)$, is reproduced [8]. Before $t = T_\star = 3.214$ Gyr, acceleration is negative, and after that, acceleration is positive. To perform the numerical calculations we have used the following values: $H_0 = 69.32$ km×s^{-1}×Mpc^{-1} $= 0.0709$ Gyr^{-1}, $T_0 = 13.772$ Gyr [9].

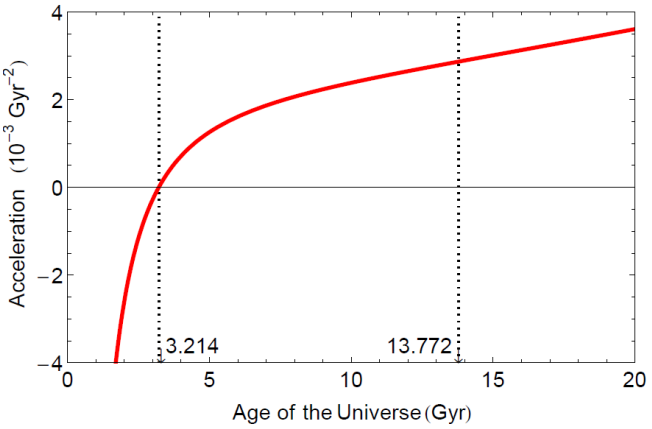

Fig. 1: $\ddot{a}(t) = a(t)\left(H_0\left(\frac{t}{T_0}\right)^{\beta} - (1-\beta)\frac{1}{t}\right) H_0\left(\frac{t}{T_0}\right)^{\beta-1}$.

2 The closed Universe

In reference [8], some properties such as Gaussian curvature $K(t)$, Ricci scalar curvature $R(t)$, matter and dark energy density parameters $(\Omega_m, \Omega_\lambda)$, matter and dark energy densities (ρ_m, ρ_λ), were calculated and plotted against the age of the Universe, for $k = 1, 0, -1$. It was found that the current curvature radius $\mathfrak{R}(T_0)$ has to be larger than 100 Gly. So, arbitrarily, we have chosen $\mathfrak{R}(T_0) = 102$ Gly. None of the results

were sufficient to decide which value of k is more appropriate for the Universe. The bigger the radius of curvature, the less we can distinguish which should be the right k.

In this paper we explore only the $k = 1$ case (closed Universe). First, we feel it is appropriate to make the following consideration. At time $t \approx 3.8\times10^{-4}$ Gyr, after the Big Bang, the temperature of the universe fell to the point where nuclei could combine with electrons to create neutral atoms and photons no longer interacted with much frequency with matter. The universe became transparent, the cosmic microwave background radiation (CMB) erupted and the structure formation took place [10]. The occurrence of such CMB and the beginning of the matter era happen at different times, but, for our purpose here, we can assume that they occured approximately at the same time $t \approx 0$, since we will be dealing with very large numbers (billion of years). We have to set that our fundamental observer (Earth) occupies the $\psi = 0$ position in the comoving reference system. To reach him(her) at cosmic time T, the CMB photons spend time T since their emission at time $t \approx 0$, at a specific value of the comoving coordinate ψ. Let us call ψ_T this specific value of ψ. We are admitting that the emission of the CMB photons occured simultaneously ($t \approx 0$) for all possible values of ψ.

Having said that, we can write, for the trajectory followed by a CMB photon ($ds^2 = 0, d\phi = d\theta = 0$), the following:

$$-\frac{cdt}{\Re(t)} = d\psi, \tag{5}$$

$$-\int_0^T \frac{c}{\Re(t)}dt = \int_{\psi_T}^0 d\psi, \tag{6}$$

$$\psi_T = \frac{c}{\Re(T_0)}\int_0^T \frac{1}{a(t)}dt. \tag{7}$$

The events ($\psi = 0$, $t = T$) and ($\psi = \psi_T$, $t = 0$) are connected by a null geodesics. ψ gets bigger out along the radial direction and has the unit of angle.

The comoving coordinate which corresponds to the current "edge" (particle horizon) of our visible (observable) Universe is

$$\begin{aligned}\psi_{T_0} &= \tfrac{c}{\Re(T_0)}\int_0^{T_0}\tfrac{1}{a(t)}dt \\ &= \tfrac{c}{\Re(T_0)}\int_0^{T_0} e^{\frac{H_0T_0}{\beta}\left(1-\left(\frac{t}{T_0}\right)^{\beta}\right)}dt \\ &= 0.275 \text{ Radians } = 15.7 \text{ Degrees.}\end{aligned} \tag{8}$$

So CMB photons emitted at ψ_{T_0} and $t = 0$ arrive at $\psi = 0$ and $t = T_0$, the current age. Along their whole trajectory, other photons emitted, at later times, by astronomical objects that lie on the way, join the troop before reaching the fundamental observer. So he(she) while looking outwards deep into the sky, may see all the information "collected" along the trajectory of primordial CMB photons. Other photons emitted at the same time $t = 0$, at a comoving position $\psi > \psi_{T_0}$ will reach $\psi = 0$ at $t > T_0$, together with the other photons provenient from astronomical objects along the way. As the Universe gets older, its "edge" becomes more distant and its size gets bigger.

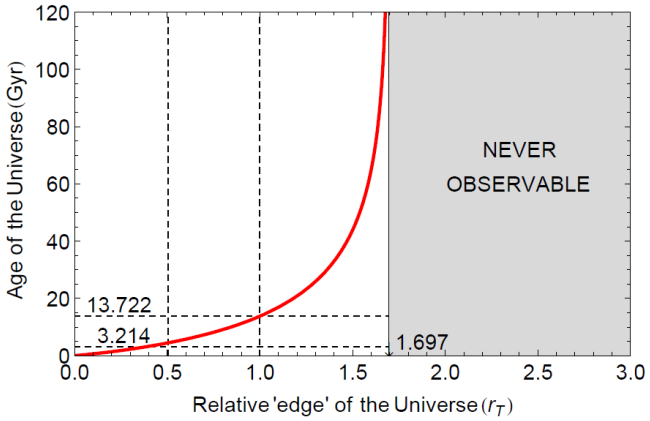

Fig. 2: $r_T = \int_0^T \frac{1}{a(t)}dt \,/\, \int_0^{T_0}\frac{1}{a(t)}dt$. The relative comoving coordinate r_T, from which CMB photons leave, at $t \approx 0$, and reach relative comoving coordinate $r = 0$ at age $t = T$ gives the relative position of the "edge" of the Universe ($r_{T\to\infty} \to 1.697$). (Axes were switched.)

The value of ψ depends on $\Re(T_0)$, the curvature radius. According to reference [8], it is important to recall that the current radius of curvature should be greater than 100 Gly and, in order to perform our numerical calculations, we choose $\Re(T_0) = 102$ Gly. The actual value for ψ_{T_0} should be, consequently, less than that above (equation (8)).

To get rid of such dependence on $\Re(T_0)$, we find convenient to work with the ratio r

$$r \equiv \frac{\psi}{\psi_{T_0}}, \tag{9}$$

which we shall call the relative comoving coordinate.

Obviously, at the age T, r_T is a relative measure of "edge" position with respect to the fundamental observer. For a plot of r_T see Figure 2.

3 Universe or Multiverse?

One question that should come out of the mind of the fundamental observer is: "Is there a maximum value for the relative comoving coordinate r?" What would be the value of r_∞?

By calculating r_∞, we get

$$r_\infty = \frac{\int_0^\infty \frac{1}{a(t)}dt}{\int_0^{T_0}\frac{1}{a(t)}dt} = \frac{47.558}{28.024} = 1.697. \tag{10}$$

To our fundamental observer (Earth), there is an upper limit for the relative comoving coordinate $r = r_\infty = 1.697$, beyond that no astronomical object can *ever* be seen. This should raise a very interesting point under consideration.

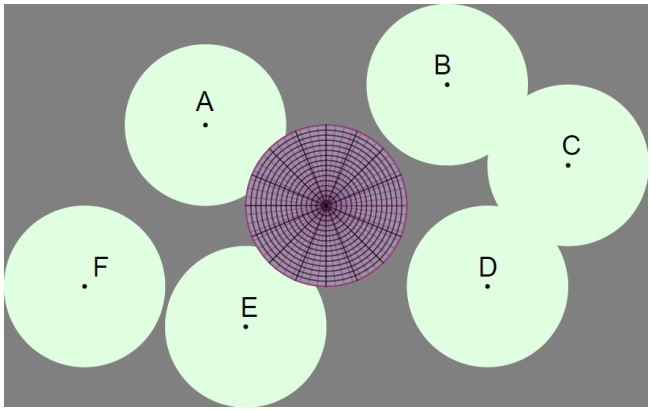

Fig. 3: This illustration tries to show schematically a hypersurface at time T with our Universe surrounded by other similar Universes, arbitrarily positioned, some of them overlapping.

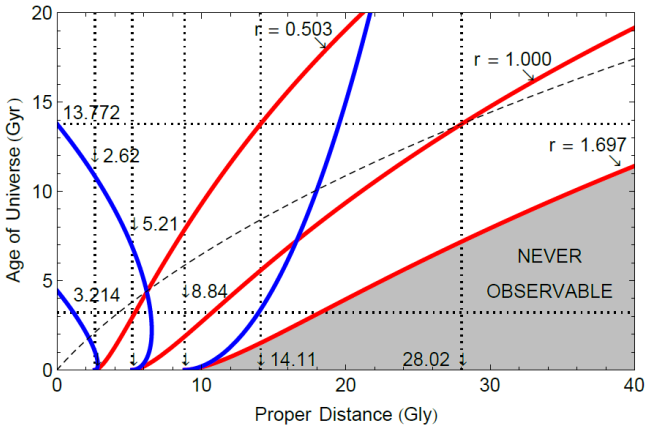

Fig. 4: Proper distances for $r = (0.503,\ 1.000,\ 1.697)$.
$d^{(r)}(T) = a(T)rd(T_0)$ (red curves),
$d(T) = a(T)r_T d(T_0)$ (dashed curve),
$d^{(r)}(T) - d(T) = a(T)(r - r_T)d(T_0)$ (blue curves).
Axes were switched for convenience.

Any other fundamental observer placed at a relative comoving coordinate $r > 2r_\infty$ $(\psi > 2\psi_\infty)$, with respect to ours, will never be able to see what is meant to be our observable Universe. He (she) will be in the middle of another visible portion of a same whole Universe; He (she) will be thinking that he (she) lives in an observable Universe, just like ours. Everything we have been debating here should equally be applicable to such an "other" Universe.

The maximum possible value of ψ is π (equation (1)), then the maximum value of r should be at least 11.43. Just recall that $r = 1$ when $\psi = \psi_{T_0}$. This ψ_{T_0} was overevaluated as being 0.275 Radians = 15.7 Degrees, in equation (8) when considering the current radius of curvature as $\Re(T_0) = 102$ Gly. As found in reference [8] $\Re(T_0)$ should be bigger than that, not smaller. Consequently the real ψ_{T_0} should be smaller than 0.275 Radians = 15.7 Degrees. One direct consequence of this is that there is room for the ocurrence of a large number of isolated similar *observable Universes* just like ours.

We may say that the Big Bang gave birth to a large Universe, of which our current observable Universe is part, perhaps a tiny part. The rest is unobservable to us and an endless number of portions just the size of our visible Universe certainly exist, each one with their fundamental observer, very much probable discussing the same Physics as us.

Of course, we have to consider also the cases of overlapping Universes.

The important thing is that we are talking about one Universe, originated from one Big Bang, and that, contains many other Universes similar to ours. Would it be a *multiverse*? See Figure 3.

4 Proper distance, volume, recession speed and redshift

When referring to the relative coordinate r_T we are not properly saying it is a function of time. Actually r_T is the value of the relative comoving coordinate r from which the CMB photons leave, at $t \approx 0$, to reach our fundamental observer at cosmic time T. Because of the expansion of the Universe, the proper distance from our observer $(r = 0)$ and a given point at $r > 0$, at the age t, is

$$d(t) = \Re(t) r\psi_{T_0} = a(t)cr \int_0^{T_0} \frac{1}{a(t')} dt'. \qquad (11)$$

The proper distance from our observer $(r = 0)$ to the farthest observable point $(r = r_T)$, at the age T, is known as horizon distance:

$$d(T) = \Re(T) \int_0^T \frac{1}{\Re(t)} dt = a(T)cr_T \int_0^{T_0} \frac{1}{a(t)} dt. \qquad (12)$$

Besides defining the "edge" of the observable Universe at age T, it is also a measure of its proper radius and does not depend on the radius of curvature. In Figure 4 it is the dashed curve. Its current value is

$$d(T_0) = c \int_0^{T_0} \frac{1}{a(t)} dt = 28.02 \text{ Gly}. \qquad (13)$$

It will become $d(T \to \infty) \to \infty$. Although there is an upper value for r (or ψ), the proper radius of the Universe is not limited because of the continuous expansion (equation 1).

The proper distance from the observer to the position of arbitrarily fixed value of r is

$$d^{(r)}(T) = a(T)rd(T_0). \qquad (14)$$

where $d(T_0)$ is given in equation (13). In Figure (4) we plot the age of the Universe as function of the proper distance, for three values of the relative comoving coordinate r (0.503, 1.000, 1.697) – red curves. Blue curves refer to null geodesics

$$d^{(r)}(T) - d(T) = a(T)(r - r_T)d(T_0) \qquad (15)$$

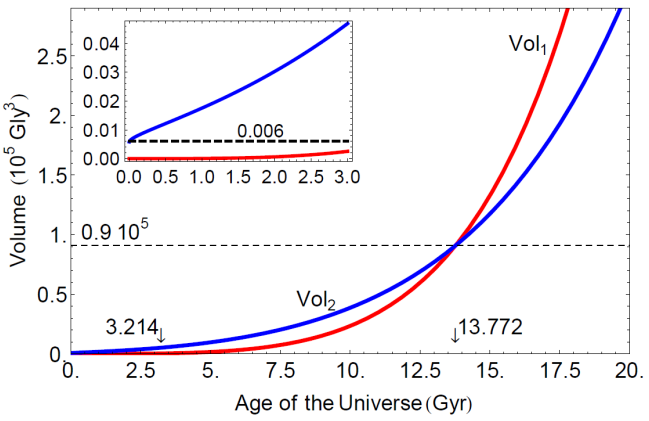

Fig. 5: Two evaluations of the volume of the Universe: $\mathrm{Vol}_1(T) = 2\pi\Re^3(T_0)a^3(T)(r_T\psi_{T_0} - \frac{1}{2}\sin 2r_T\psi_{T_0})$, $\mathrm{Vol}_2(T) = 2\pi\Re^3(T_0)a^3(T)(\psi_{T_0} - \frac{1}{2}\sin 2\psi_{T_0})$.

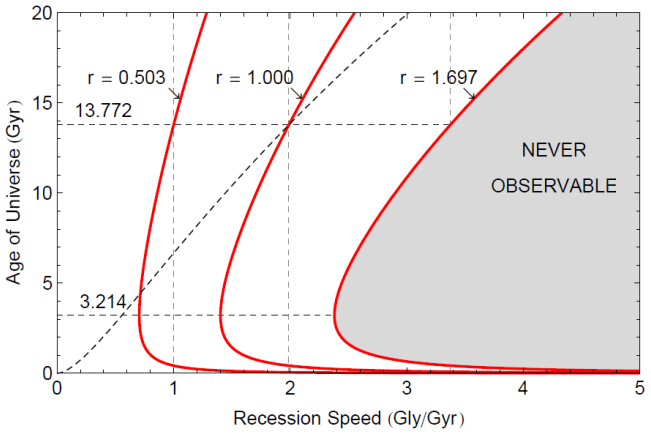

Fig. 6: $v(T) = a(T)H(T)rd(T_0)$. Recession speed is calculated for three values of the relative comoving coordinate r, as function of the age T of the Universe. For convenience the axes were switched.

for fixed values of $r \neq 0$. (The axes in Figure 4 are switched, for convenience.)

Consider the volume of our observable Universe. The general expression is

$$\begin{aligned}\mathrm{Vol}(t) &= \Re^3(T_0)a^3(t)\int_0^{\psi}\sin^2\psi d\psi\int_0^{\pi}\sin\theta d\theta\int_0^{2\pi}d\phi \\ &= 2\pi\Re^3(T_0)a^3(t)\left(\psi - \tfrac{1}{2}\sin 2\psi\right).\end{aligned} \tag{16}$$

Our fundamental observer may ask about two volumes:

First, the volume of the allways visible (observable) part since the beginning - such volume should be approximately zero for $t \approx 0$; Second, the volume of what became later the current visible part and that was not visible in its integrity in the past since $t \approx 0$. They are respectively,

$$\begin{aligned}\mathrm{Vol}_1(T) &= 2\pi\Re^3(T_0)a^3(T)(\psi - \tfrac{1}{2}\sin 2\psi) \\ &= 2\pi\Re^3(T_0)a^3(T)(r_T\psi_{T_0} - \tfrac{1}{2}\sin 2r_T\psi_{T_0}).\end{aligned} \tag{17}$$

$$\mathrm{Vol}_2(T) = 2\pi\Re^3(T_0)a^3(T)(\psi_{T_0} - \frac{1}{2}\sin 2\psi_{T_0}). \tag{18}$$

By evaluating equations (17 – 18) with $T = 0$, we get

$$\begin{aligned}\mathrm{Vol}_1(0) &= 0 \\ \mathrm{Vol}_2(0) &= 0.006\times 10^5\mathrm{Gly}^3.\end{aligned} \tag{19}$$

These results are not surprising. To our observer, located at $r = 0$, at $t \approx 0$, the visible Universe is approximately zero, just because all the *CMB* photons are "born" at the same moment ($T = 0$); He (she) sees first the closest photons and then, in the sequence, the others as time goes on.

On the other hand,

$$\mathrm{Vol}_2(T_0) = \mathrm{Vol}_1(T_0) = 0.9\times 10^5\mathrm{Gly}^3, \tag{20}$$

which is the volume of current observable Universe. See Figure 4. It is only about 150 times bigger than it was at $t = 0$.

Just one comment: If the reader wants to calculate the volume using the classical euclidean expression for the sphere ($(4\pi/3)\Re^3(T_0)a^3(t)\psi^3$), he (she) will get practically the same result. So here, as in reference [8], no distinction between $k = 0$ and $k = 1$.

The recession speed of a point of the Universe at a given relative comoving coordinate r, at cosmic time t, is

$$v(t) = a(t)H(t)rd(T_0), \tag{21}$$

where $\dot{a}(t)$ was replaced by

$$\dot{a}(t) = a(t)H(t), \tag{22}$$

and the Hubble parameter $H(t)$ is given by [8]

$$H(t) = H_0\left(\frac{t}{T_0}\right)^{\beta-1}. \tag{23}$$

The cosmological redshift is defined as

$$z = \frac{\Delta\lambda}{\lambda_e} = \frac{a(t_o)}{a(t_e)} - 1, \tag{24}$$

where λ_e and λ_o are, respectively, the photon wavelength at the source ($t = t_e$) and at the observer ($r = 0$, $t = t_o$). Due to expansion of the Universe, these two wavelengths are different. The redshift to be detected by the observer at $r = 0$, at current age should be

$$z = \frac{1}{a(t_e)} - 1 = e^{\frac{H_0T_0}{\beta}\left(1-\frac{t_e}{T_0}\right)^{\beta}} - 1. \tag{25}$$

The recession speed at coordinate r at time ($t = t_e$) is

$$v(t_e) = a(t_e)H(t_e)rd(T_0). \tag{26}$$

Fig. 7: $v(z) = \left(1 - \frac{\beta}{H_0 T_0}\mathrm{Log}(1+z)\right)^{\beta-\frac{1}{\beta}} \frac{H_0 r}{1+z} d(T_0)$. Recession speeds calculated as function of the cosmological redshift and plotted with switched axes, for convenience.

From equation (25) we obtain

$$t_e = T_0\left(1 - \frac{\beta}{H_0 T_0}\mathrm{Log}(1+z)\right)^{\frac{1}{\beta}}, \qquad (27)$$

which inserted into equation (24) gives

$$v(z) = \left(1 - \frac{\beta}{H_0 T_0}\mathrm{Log}(1+z)\right)^{\beta-\frac{1}{\beta}} \frac{H_0 r}{1+z} d(T_0). \qquad (28)$$

Because of the transition from negative to positive expansion acceleration phenomenon, we have, in many situations, two equal recession speeds separated in time leading to two different redshifts. See Figure 7.

5 Conclusion

The expansion factor $a(t) = e^{\frac{H_0 T_0}{\beta}\left(\left(\frac{t}{T_0}\right)^{\beta}-1\right)}$, where $\beta = 0.5804$ [8], is applied to our Universe, here treated as being closed ($k = 1$). We investigate properties of comoving coordinates, proper distances, volume and redshift under the mentioned expansion factor. Some very interesting conclusions were drawn. One of them is that the radial relative comoving coordinate r, measured from the fundamental observer, $r = 0$ (on Earth), to the "edge" (horizon) of our observable Universe has an upper limit. We found that $r \to 1.697$ when $T \to \infty$. Therefore all astronomical objects which lie beyond such limit would never be observed by our fundamental observer ($r = 0$). On the other hand any other fundamental observer that might exist at $r > 2\times 1.697$ would be in the middle of another Universe, just like ours; he(she) would never be able to observe our Universe. Perhaps he(she) might be thinking that his(her) Universe is the only one to exist. An endless number of other fundamental observers and an equal number of Universes similar to ours may clearly exist. Situations in which overlapping Universes should exist too. See Figure 3.

The fact is that the Big Bang originated a big Universe. A small portion of that is what we call our observable Universe. The rest is unobservable to our fundamental observer. Equal portions of the rest may be called also Universe by their fundamental observers if they exist. So we may speak about many Universes - a Multiverse - or about only one Universe, a small part of it is observable to our fundamental observer.

Acknowledgements

We wish to thank our friends Dr. Alencastro V. De Carvalho, Dr. Paulo R. Silva and Dr. Rodrigo D. Társia, for reading the manuscript and for stimulating discussions.

Submitted on June 14, 2014 / Accepted on June 17, 2014

References

1. Raine D. An Introduction to the Science Of Cosmology. Institute of Physics Publishing Ltd, 2001.
2. Peacock J.A. Cosmological Physics. Cambridge University Press, 1999.
3. Harrison E.R. Cosmology: The Science of the Universe. Cambridge University Press, 2nd ed. 2000.
4. Islam J.N. An Introduction to Mathematical Cosmology. Cambridge University Press. 2002.
5. Ellis G.F.R. et al. Relativistic Cosmology. Cambridge University Press, 2012.
6. Springel V., Frenk C. S., and White S. D. (2006). The large-scale structure of the Universe. *Nature*, 440(7088), 1137–1144.
7. Luminet J.P. Cosmic topology: twenty years after. *Gravitation and Cosmology*, 2014, v. 20, 1, 15–20
8. Silva N.P. A model for the expansion of the Universe. *Progress in Physics*, 2014, v. 10, 93–97.
9. Bennett C.L. et al. Nine-year Wilkinson Microwave Anisotropy Probe (WMAP) observations: final maps and results. arXiv: astro-ph.CO, 2013.
10. Peebles P.J.E. The Large-scale Structure of the Universe. Princeton University Press, Princeton, 1980.

New Possible Physical Evidence of the Homogeneous Electromagnetic Vector Potential for Quantum Theory.
Idea of a Test Based on a G. P. Thomson-like Arrangement

Spiridon Dumitru

(Retired) Department of Physics, "Transilvania" University, B-dul Eroilor 29, 500036 Brasov, Romania
Email: s.dumitru42@unitbv.ro

It is suggested herein a test able to reveal the physical evidence of the homogeneous electromagnetic vector potential field in relation to quantum theory. We take into consideration three reliable entities as main pieces of the test: (i) influence of a potential vector of the de Broglie wavelength (ii) a G. P. Thomson-like experimental arrangement and (iii) a special coil designed to create a homogeneous vector potential. The alluded evidence is not connected with magnetic fluxes surrounded by the vector potential field lines, rather it depends on the fluxes which are outside of the respective lines. Also the same evidence shows that the tested vector potential field is a uniquely defined physical quantity, free of any adjusting gauge. So the phenomenology of the suggested quantum test differs from that of the macroscopic theory where the vector potential is not uniquely defined and allows a gauge adjustment. Of course, we contend that this proposal has to be subsequently subjected to adequate experimental validation.

1 Introduction

The physical evidence of the vector potential $\vec{A}$ field, distinctly of electric and/or magnetic local actions, is known as Aharonov-Bohm-effect (A-B-eff). It aroused scientific discussions for more than half a century (see [1–8] and references). As a rule in the A-B-eff context, the vector potential is curl-free field, but it is non-homogeneous (**n-h**) i.e. spatially non-uniform. In the same context, the alluded evidence is connected quantitatively with magnetic fluxes surrounded by the lines of $\vec{A}$ field. In the present paper we try to suggest a test intended to reveal the possible physical evidence of a homogeneous (**h**) $\vec{A}$ field. Note that in both **n-h** and **h** cases herein, we take into consideration only fields which are constant in time.

The announced test has as constitutive pieces three reliable entities (**E**) namely:

E_1: The fact that a vector potential $\vec{A}$ field changes the values of the de Broglie wavelength λ^{dB} for electrons. ■

E_2: An experimental arrangement of the G. P. Thomson type, able to monitor the mentioned λ^{dB} values. ■

E_3: A feasible special coil designed so as to create a **h**-$\vec{A}$ field. ■

Accordingly, on the whole, the test has to put together the mentioned entities and, consequently, to synthesize a clear verdict regarding the alluded evidence of a **h**-$\vec{A}$ field.

Experimental setup of the suggested test is detailed in the next Section 2. Essential theoretical considerations concerning the action of a **h**-$\vec{A}$ field are given in Section 3. The above-noted considerations are fortified in Section 4 by a set of numerical estimations for the quantities aimed to be measured through the test. Some concluding thoughts regarding a possible positive result of the suggested test close the main body of the paper in Section 5. Constructive and computational details regarding the special coil designed to generate a **h**-$\vec{A}$ field are presented in the Appendix.

2 Setup details of the experimental arrangement

The setup of the suggested experimental test is pictured and detailed below in Fig. 1. It consists primarily of a G. P. Thomson-like arrangement partially located in an area with a **h**-$\vec{A}$ field. The alluded arrangement is inspired by some illustrative images [9, 10] about G. P. Thomson's original experiment and it disposes in a straight line of the following elements: electron source, electron beam, crystalline grating, and detecting screen. An area with a **h**-$\vec{A}$ field can be obtained through a certain special coil whose constructive and computational details are given in the above-mentioned Appendix at the end of this paper.

The following notes have to be added to the explanatory records accompanying Fig. 1.

Note 1: If in Fig. 1 the elements 7 and 8 are omitted (i.e. the sections in special coil and the lines of **h**-$\vec{A}$ field) one obtains a G. P. Thomson-like arrangement as it is illustrated in the said references [9, 10]. ■

Note 2: Surely the above mentioned G. P. Thomson-like arrangement is so designed and constructed that it can be placed inside of a vacuum glass container. The respective container is not shown in Fig. 1 and it will leave out the special coil. ■

Note 3: When incident on the crystalline foil, the electron beam must ensure a coherent and plane front of de Broglie waves. Similar ensuring is required [11] for

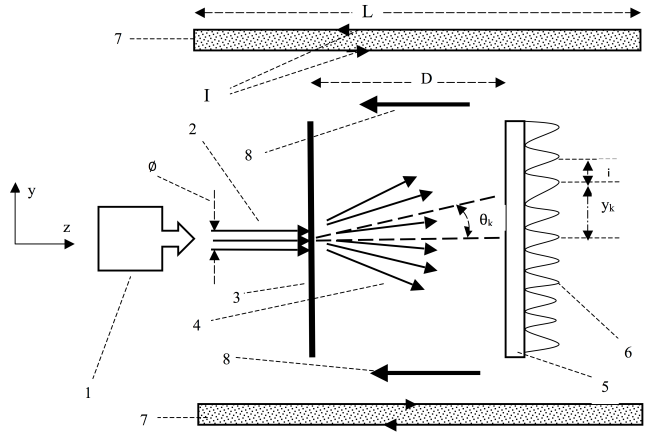

Fig. 1: Plane section in the image of suggested experimental setup, accompanied by the following explanatory records. 1 – Source for a beam of mono-energetic and parallel moving electrons; 2 –Beam of electrons in parallel movements; 3 – Thin crystalline foil as diffraction grating; 4 – Diffracted electrons; 5 – Detecting screen; 6 – Fringes in the plane section of the diffraction pattern; 7 – Sections in the special coil able to create a **h**-$\vec{A}$ field; 8 – **h**-$\vec{A}$ field ; ϕ = the width of the electron beam with $\phi \gg a$ (a = interatomic spacing in the crystal lattice of the foil -3); θ_k = diffraction angle for the k-th order fringe ($k = 0, 1, 2, 3, \ldots$); y_k = displacement from the center line of the k-th order fringe; i = interfringe width = $y_{k+1} - y_k$; D = distance between crystalline foil and screen ($D \gg \phi$); L = length of the special coil ($L \gg D$) ; I = intensity of current in wires of the coil.

optical diffracting waves at a classical diffraction grating. ■

Note 4: In Fig. 1 the detail 6 displays only the linear projections of the fringes from the diffraction pattern. On the whole, the respective pattern consists in a set of concentric circular fringes (diffraction rings). ■

3 Theoretical considerations concerning action of a h-$\vec{A}$ field

The leading idea of the above-suggested test is to search for possible changes caused by a **h**-$\vec{A}$ field in the diffraction of quantum (de Broglie) electronic waves. That is why we begin by recalling some quantitative characteristics of the diffraction phenomenon.

The most known scientific domain wherein the respective phenomenon is studied regards optical light waves [11]. In the respective domain, one uses as the main element the so-called *diffraction grating* i.e. a piece with a periodic structure having slits separated each by a distance a and which diffracts the light into beams in different directions. For a light normally incident on such an element, the grating equation (condition for intensity maximums) has the form: $a \cdot \sin\theta_k = k\lambda$, where $k = 0, 1, 2, \ldots$ In the respective equation, λ denotes the light's wavelength and θ_k is the angle at which the diffracted light has the k-th order maximum. If the diffraction pattern is received on a detecting screen, the k-th order maximum appears on the screen in the position y_k given by the relation $\tan\theta_k = (y_k/D)$, where D denotes the distance between the screen and the grating. For the distant screen assumption, when $D \gg y_k$, the following relation holds: $sin\theta_k \approx \tan\theta_k \approx (y_k/D)$. Then, with regard to the mentioned assumption, one observes that the diffraction pattern on the screen is characterized by an interfringe distance $i = y_{k+1} - y_k$ given through the relation

$$i = \lambda \frac{D}{a} . \tag{1}$$

Note the fact that the above quantitative aspects of diffraction have a generic character, i.e. they are valid for all kinds of waves including de Broglie ones. The respective fact is presumed as a main element of the experimental test suggested in the previous section. Another main element of the alluded test is the largely agreed upon idea [1–8] that the de Broglie electronic wavelength λ^{dB} is influenced by the presence of a $\vec{A}$ field. Based on the two afore-mentioned main elements the considered test can be detailed as follows.

In the experimental setup depicted in Fig. 1 the crystalline foil 3 having interatomic spacing a plays the role of a diffraction grating. In the same experiment, on the detecting screen 5 it is expected to appear a diffraction pattern of the electrons. The respective pattern would be characterized by an interfringe distance i^{dB} definable through the formula $i^{dB} = \lambda^{dB} \cdot (D/a)$. In that formula, D denotes the distance between the crystalline foil and the screen, supposed to satisfy the condition $D \gg \phi$), where ϕ represents the width of the incident electron beam. In the absence of a **h**-$\vec{A}$ field, the λ^{dB} of a non-relativistic electron is known to satisfy the following expression:

$$\lambda^{dB} = \frac{h}{p_{kin}} = \frac{h}{mv} = \frac{h}{\sqrt{2m\mathcal{E}}} . \tag{2}$$

In the above expression, h is Planck's constant while p_{kin}, m, v and $\mathcal{E}$ denote respectively the kinetic momentum, mass, velocity, and kinetic energy of the electron. If the alluded energy is obtained in the source of the electron beam (i.e. piece 1 in Fig. 1) under the influence of an accelerating voltage U, one can write $\mathcal{E} = e \cdot U$ and $p_{kin} = mv = \sqrt{2meU}$.

Now, in connection with the situation depicted in Fig. 1, let us look for the expression of the electrons' characteristic λ^{dB} and respectively of $i^{dB} = \lambda^{dB} \cdot (D/a)$ in the presence of a **h**-$\vec{A}$ field. Firstly, we note the known fact [6] that a particle with the electric charge q and the kinetic momentum $\vec{p}_{kin} = m\vec{v}$ in a potential vector $\vec{A}$ field acquires an additional (*add*) momentum, $\vec{p}_{add} = q\vec{A}$, so that its *effective* (eff) momentum is $\vec{P}_{eff} = \vec{p}_{kin} + \vec{p}_{add} = m\vec{v} + q\vec{A}$. Then for the electrons (with $q = -e$) supposed to be implied in the experiment depicted in Fig. 1, one obtains the effective (eff) quantities

$$\lambda^{dB}_{eff}(A) = \frac{h}{mv + eA} ; \quad i^{dB}_{eff}(A) = \frac{hD}{a(mv + eA)} . \tag{3}$$

Further on, we have to take into account the fact that the **h**-$\vec{A}$ field acting in the experiment presented before is generated by a special coil whose plane section is depicted by the elements 7 from Fig. 1. Then from the relation (10) established in the Appendix, we have $A = \mathcal{K} \cdot I$, where $\mathcal{K} = \frac{\mu_0 N}{2\pi} \cdot \ln\left(\frac{R_2}{R_1}\right)$. Add here the fact that in this experiment $mv = \sqrt{2meU}$. Then for the effective interfringe distance i^{dB}_{eff} of the diffracted electrons, one finds

$$i^{dB}_{eff}(A) = i^{dB}_{eff}(U, I) = \frac{hD}{a\left(\sqrt{2meU} + e\mathcal{K}I\right)}, \qquad (4)$$

respectively

$$\frac{1}{i^{dB}_{eff}(U, I)} = f(U, I) = \frac{a\sqrt{2me}}{hD}\sqrt{U} + \frac{ae\mathcal{K}}{hD} I. \qquad (5)$$

4 A set of numerical estimations

The verisimilitude of the above-suggested test can be fortified to some extent by transposing several of the previous formulas into their corresponding numerical values. For such a transposing, we firstly will appeal to numerical values known from G. P. Thomson-like experiments. So, as regarding the elements from Fig. 1, we quote the values $a = 2.55 \times 10^{-10}$ m (for a crystalline foil of copper) and $D = 0.1$ m. As regarding U, we take the often quoted value: $U = 30$ kV. Then the kinetic momentum of the electrons will be $p_{kin} = mv = \sqrt{2meU} = 9.351 \times 10^{-23}$ kg m/s. The additional (add) momentum of the electron, induced by the special coil, is of the form $p_{add} = e\mathcal{K} \times I$ where $\mathcal{K} = \frac{\mu_0 N}{2\pi} \times \ln\left(\frac{R_2}{R_1}\right)$. In order to estimate the value of $\mathcal{K}$, we propose the following practically workable values: $R_1 = 0.1$ m, $R_2 = 0.12$ m, $N = 2\pi R_1 \times n$ with $n = 2 \times 10^3$ m^{-1} = number of wires (of 1 mm in diameter) per unit length, arranged into two layers. With the well known values for e and μ_0 one obtains $p_{add} = 7.331 \times 10^{-24}$(kg m C^{-1}) $\cdot\, I$ (with C = Coulomb).

For wires of 1 mm in diameter, by changing the polarity of the voltage powering the coil, the current I can be adjusted in the range $I \in (-10\ to\ +10)A$. Then the effective momentum $\vec{P}_{eff} = \vec{p}_{kin} + \vec{p}_{add}$ of the electrons shall have the values within the interval (2.040 to 16.662) $\times 10^{-23}$ kg m/s. Consequently, due to the above mentioned values of a and D, the effective interfringe distance i^{dB}_{eff} defined in (4) changes in the range (1.558 to 12.725) mm, respectively its inverse from (5) has values within the interval (78.58 to 641.84) m^{-1}. Then it results that in this test the **h**-$\vec{A}$ field takes its magnitude within the interval $A \in (-4.5\ ,\ +4.5) \times 10^{-4}$ kg m C^{-1}, (C = Coulomb).

Now note that in the absence of the **h**-$\vec{A}$ field (i.e. when $I = 0$) the interfange distance i^{dB} specific to a simple G. P. Thomson experiment has the value $i^{dB} = \frac{hD}{a\sqrt{2meU}} = 2.776$ mm. Such a value is within the range of values of i^{dB}_{eff} characterizing the presence of the **h**-$\vec{A}$ field. This means that the quantitative evaluation of the mutual relationship of i^{dB}_{eff} versus I, and therefore the testing evidence of a **h**-$\vec{A}$ field can be done with techniques and accuracies similar to those of the G. P. Thomson experiment.

5 Some concluding remarks

The aim of the experimental test suggested above is to verify a possible physical evidence for the **h**-$\vec{A}$ field. Such a test can be done by comparative measurements of the interfringe distance i^{dB}_{eff} and of the current I. Additionally it must examine whether the results of the mentioned measurements verify the relations (4) and (5) (particularly according to (5) the quantity $(i^{dB}_{eff})^{-1}$ is expected to show a linear dependence of I). If the above outcomes are positive, one can notice the fact that a **h**-$\vec{A}$ field has its own characteristics of physical evidence. Such a fact leads in one way or another to the following remarks (**R**):

R$_1$: The physical evidence of the **h**-$\vec{A}$ field differs from the one of the **n-h**- $\vec{A}$ field which appears in the A-B-eff. This happens because, by comparison to the illustrations from [12], one can see that: *(i)* by changing the values of **n-h**- $\vec{A}$, the diffraction pattern undergoes a simple translation on the screen, without any modification of interfringe distance, while *(ii)* according to the relations (4) and (5) a change of **h**-$\vec{A}$ (by means of current I) does not translate the diffraction pattern but varies the value of associated interfringe distance i^{dB}_{eff}. The mentioned variation is similar to that induced [12] by changing (through accelerating the voltage U) the values of kinetic momentum $\vec{p}_{kin} = m\vec{v}$ for electrons. ■

R$_2$: There is a difference between the physical evidence (objectification) of the **h**-$\vec{A}$ and the **n-h**-$\vec{A}$ fields in relation with the magnetic fluxes surrounded or not by the field lines. The difference is pointed out by the following subsequent aspects:

(i) On the one hand, as it is known from the A-B-eff, in case of the **n-h**-$\vec{A}$ field, the corresponding evidence depends directly on magnetic fluxes surrounded by the $\vec{A}$ field lines.

(ii) On the other hand, the physical evidence of the **h**-$\vec{A}$ field is not connected to magnetic fluxes surrounded by the field lines. But note that due to the relations (4) and (5), the respective evidence appears to be dependent (through the current I) on magnetic fluxes not surrounded by the field lines of the **h**-$\vec{A}$. ■

R$_3$: A particular characteristic of the physical evidence forecasted above for the **h**-$\vec{A}$ regards the macroscopic versus quantum difference concerning the uniqueness (gauge freedom) of the vector potential field. As is known, in macroscopic situations [13, 14] the vector potential $\vec{A}$ field is not uniquely defined (i.e. it has a gauge freedom). In such situations, an arbitrary $\vec{A}$ field

allows a gauge fixing (adjustment), without any alteration of macroscopic relevant variables/equations (particularly of those involving the magnetic field $\vec{B}$). So two distinct vector potential fields $\vec{A}$ and $\vec{A}^1$ have the same macroscopic actions (effects) if $\vec{A}^1 = \vec{A} + \nabla f$, where f is an arbitrary gauge functions. On the other hand, in a quantum context, a **h**-$\vec{A}$ has not any gauge freedom. This is because if this test has positive results, two fields like $\mathbf{h} - \vec{A} = A \cdot \vec{k}$ and $\mathbf{h} - \vec{A}^1 = \mathbf{h} - \vec{A} + \nabla f$ are completely distinct if $f = (-z \cdot A \cdot \vec{k})$, where $\vec{k}$ denotes the unit vector of the Oz axis. So we can conclude that, with respect to the **h**-$\vec{A}$ field, the quantum aspects differ fundamentally from those aspects originating in a macroscopic consideration. Surely, such a fact (difference) and its profound implications have to be approached in subsequently more elaborated studies. ■

Postscript

As presented above, the suggested test and its positive results appear as purely hypothetical things, despite the fact that they are based on essentially reliable entities (constitutive pieces) presented in the Introduction. Of course, we hold that a true confirmation of the alluded results can be done by the action of putting in practice the whole test. Unfortunately, at the moment I do not have access to material logistics able to allow me an effective practical approach of the test in question. Thus I warmly appeal to the concerned experimentalists and researchers who have adequate logistics to put in practice the suggested test and to verify its validity.

Appendix: Constructive and computational details for a special coil able to create a h-$\vec{A}$ field

The case of an ideal coil

An experimental area of macroscopic size with the **h**-$\vec{A}$ field can be realized with the aid of a special coil whose constructive and computational details are presented below. The announced details are improvements of the ideas promoted by us in an early preprint [15].

The basic element in designing the mentioned coil is the **h**-$\vec{A}$ field generated by a rectilinear infinite conductor carrying a direct current. If the conductor is located along the axis Oz and the current has the intensity I, the Cartesian components (written in SI units) of the mentioned **h**-$\vec{A}$ field are given [16] by the following formulas:

$$A_x(1) = 0\,, \qquad A_y(1) = 0\,, \qquad A_z(1) = -\mu_0 \frac{I}{2\pi} \ln r\,. \quad (6)$$

Here r denotes the distance from the conductor of the point where the hct-$\vec{A}$ is evaluated and where μ_0 is the vacuum permeability.

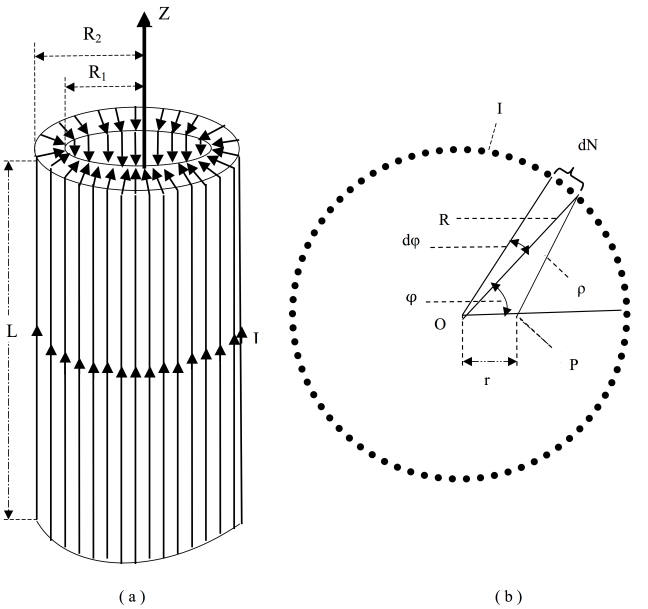

Fig. 2: Schemes for an annular special coil.

Note that formulas (6) are of ideal essence because they describe the **h**-$\vec{A}$ field generated by an infinite (ideal) rectilinear conductor. Further onwards, we firstly use the respective formulas in order to obtain the **h**-$\vec{A}$ field generated by an ideal annular coil. Later on we will specify the conditions in which the results obtained for the ideal coil can be used with fairly good approximation in the characterization of a real (non-ideal) coil of practical interest for the experimental test suggested and detailed in Sections 2,3 and 4.

The mentioned special coil has the shape depicted in Fig. 2-(a) (i.e. it is a toroidal coil with a rectangular cross section). In the respective figure the finite quantities R_1 and R_2 represent the inside and outside finite radii of the coil while $L \to \infty$ is the length of the coil. For evaluation of the **h**-$\vec{A}$ generated inside of the mentioned coil let us now consider an array of infinite rectilinear conductors carrying direct currents of the same intensity I. The conductors are mutually parallel and uniformly disposed on the circular cylindrical surface with the radius R. The conductors are also parallel with Oz as the symmetry axis. In a cross section, the considered array is disposed on a circle of radius R as can be seen in Fig. 2b. On the respective circle, the azimuthal angle φ locates the infinitesimal arc element whose length is $Rd\varphi$. On the respective arc there was placed a set of conductors whose number is $dN = \left(\frac{N}{2\pi}\right) d\varphi$, where N represents the total number of conductors in the whole considered array. Let there be an observation point P situated at distances r and ρ from the center O of the circle respectively from the infinitesimal arc (see the Fig. 2b). Then, by taking into account (6), the z-component of the **h**-$\vec{A}$ field generated in P by the dN conductors is given

by relation

$$A_z\,(dN) = A_z\,(1)\,dN = -\mu_0 \frac{NI}{4\pi^2} \ln\rho \cdot d\varphi\,, \qquad (7)$$

where $\rho = \sqrt{(R^2 + r^2 - 2Rr\cos\varphi)}$. Then all N conductors will generate in the point P a $\mathbf{h}$-$\vec{A}$ field whose value A is

$$A = A_z\,(N) = -\mu_0 \frac{NI}{8\pi^2} \int_0^{2\pi} \ln\left(R^2 + r^2 - 2Rr\cos\varphi\right) \cdot d\varphi\,. \qquad (8)$$

In calculating the above integral, the formula (4.224-14) from [17] can be used. So, one obtains

$$A = -\mu_0 \frac{NI}{2\pi} \ln R\,. \qquad (9)$$

This relation shows that the value of A does not depend on r, i.e. on the position of P inside the circle of radius R. Accordingly this means that inside the respective circle, the potential vector is homogeneous. Then starting from (9), one obtains that the inside space of an ideal annular coil depicted in Fig. 2a is characterized by the $\mathbf{h}$-$\vec{A}$ field whose value is

$$A = \mu_0 \frac{NI}{2\pi} \ln\left(\frac{R_2}{R_1}\right). \qquad (10)$$

From the ideal coil to a real one

The above-presented coil is of ideal essence because their characteristics were evaluated on the basis of an ideal formula (6). But in practical matters, such as the experimental test proposed in Sections 2 and 3, one requires a real coil which may be effectively constructed in a laboratory. That is why it is important to specify the main conditions in which the above ideal results can be used in real situations. The mentioned conditions are displayed here below.

On the geometrical sizes: In a laboratory, it is not possible to operate with objects of infinite size. Thus we must take into account the restrictive conditions so that the characteristics of the ideal coil discussed above to remain as good approximations for a real coil of similar geometric form. In the case of a finite coil having the form depicted in the Fig. 2a, the alluded restrictive conditions impose the relations $L \gg R_1$, $L \gg R_2$ and $L \gg (R_2 - R_1)$. If the respective coil is regarded as a piece in the test experiment from Fig. 1, indispensable are the relations $L \gg D$ and $L \gg \phi$.

About the marginal fragments: On the whole, the marginal fragments of coil (of width $(R_2 - R_1)$) can have disturbing effects on the Cartesian components of $\vec{A}$ inside the the space of practical interest. Note that, on the one hand, in the above-mentioned conditions $L \gg R_1$, $L \gg R_2$ and $L \gg (R_2 - R_1)$ the alluded effects can be neglected in general practical affairs. On the other hand, in the particular case of the proposed coil the alluded effects are also diminished by the symmetrical flows of currents in the respective marginal fragments.

As concerns the helicity: The discussed annular coil is supposed to be realized by winding a single piece of wire. The spirals of the respective wire are not strictly parallel to the symmetry axis of the coil (the Oz axis) but they have a certain helicity (corkscrew-like path). Of course, the alluded helicity has disturbing effects on the components of $\vec{A}$ inside the coils. Note that the mentioned helicity-effects can be diminished (and practically eliminated) by using an idea noted in another context in [18]. The respective idea proposes to arrange the spirals of the coil in an even number of layers, with the spirals from adjacent layers having equal helicity but of opposite sense.

Submitted on May 6, 2014 / Accepted on May 30, 2014

References

1. Aharonov Y., Bohm D., Significance of electromagnetic potentials in the quantum theory. *Phys. Rev.*, 1959, v. 115, 485–491.
2. Aharonov Y., Bohm D. Further considerations on electromagnetic potentials in the quantum theory. *Phys. Rev.*, 1961, v. 123 1511–1524.
3. Olariu S., Popescu I.I. The quantum effects of electromagnetic fluxes. *Rev. Mod. Phys.*, 1985, v. 57, 339–436.
4. Peshkin M., Tonomura A. The Aharonov-Bohm Effect. *Lecture Notes in Physics*, Springer, v. 340, 1989, 1–152.
5. Dennis M., Popescu S., Vaidman L., Quantum phases: 50 years of the Aharonov-Bohm effect and 25 years of the Berry phase. *J. Phys. A: Math. Theor.*, 2010, v. 43, 350301.
6. Ershkovich A. Electromagnetic potentials and Aharonov-Bohm effect. arXiv: 1209.1078
7. Leus V.A., Smith R.T., Maher S. The physical entity of vector potential in electromagnetism. *Applied Physics Research*, 2013, v. 5, 56–68.
8. Hiley B.J. The early history of the Aharonov-Bohm effect. arXiv: 1304.4736.
9. Images for G. P. Thomson experiment at http://www.google.com
10. Arias T.A. G. P. Thomson Experiment. http://muchomas.lassp.cornell.edu/8.04/1997/quiz1/node4.html
11. Born M., Wolf E. Principle of Optics, Electromagnetic Theory of Propagation, Interference and Diffraction of Light. Seventh (expanded) edition, Cambridge University Press, 2003.
12. Blinder S.M. Aharonov-Bohm Effect, from the Wolfram Demonstrations Project. http://www.youtube.com
13. Jackson J.D. Classical Electrodynamics. John Wiley, N.Y., 1962.
14. Landau L., Lifchitz E. Theorie des Champs. Ed. Mir, Moscou, 1970.
15. Dumitru S., Dumitru M. Are there observable effects of the vector potential? A suggestion for probative experiments of a new type (different from the proposed Aharonov-Bohm one). CERN Central Library PRE 24618, Barcode 38490000001, Jan 1981, 20 pages.
16. Feynman R.P., Leighton R.B., Sands M. The Feynman Lectures on Physics, vol. II. Addison-Wesley, Reading (Mass.), 1964.
17. Gradshteyn I.S., Ryzhik I.M. Table of Integrals, Series, and Products. Seventh Edition, Elsevier, 2007.
18. Costa de Beauregard O., Vigoureux J.M. Flux quantization in "autistic" magnets. *Phys. Rev. D*, 1974, v. 9, 1626–1632.

The Journal on Advanced Studies in Theoretical and Experimental Physics, including Related Themes from Mathematics

PROGRESS IN PHYSICS

A quarterly issue scientific journal, registered with the Library of Congress (DC, USA). This journal is peer reviewed and included in the abstracting and indexing coverage of: Mathematical Reviews and MathSciNet (AMS, USA), DOAJ of Lund University (Sweden), Zentralblatt MATH (Germany), Scientific Commons of the University of St. Gallen (Switzerland), Open-J-Gate (India), Referativnyi Zhurnal VINITI (Russia), etc.

Electronic version of this journal:
http://www.ptep-online.com

ISSN: 1555-5534 (print)
ISSN: 1555-5615 (online)

Standard Address Number: 297-5092
Printed in the United States of America

October 2014 **Vol. 10, Issue 4**

CONTENTS

Information for Authors and Subscribers

Progress in Physics has been created for publications on advanced studies in theoretical and experimental physics, including related themes from mathematics and astronomy. All submitted papers should be professional, in good English, containing a brief review of a problem and obtained results.

All submissions should be designed in LaTeX format using *Progress in Physics* template. This template can be downloaded from *Progress in Physics* home page http://www.ptep-online.com. Abstract and the necessary information about author(s) should be included into the papers. To submit a paper, mail the file(s) to the Editor-in-Chief.

All submitted papers should be as brief as possible. We accept brief papers, no larger than 8 typeset journal pages. Short articles are preferable. Large papers can be considered in exceptional cases to the section *Special Reports* intended for such publications in the journal. Letters related to the publications in the journal or to the events among the science community can be applied to the section *Letters to Progress in Physics*.

All that has been accepted for the online issue of *Progress in Physics* is printed in the paper version of the journal. To order printed issues, contact the Editors.

This journal is non-commercial, academic edition. It is printed from private donations. (Look for the current author fee in the online version of the journal.)

On Materiality and Dimensionality of the Space. Is There Some Unit of the Field?

Anatoly V. Belyakov

E-mail: belyakov.lih@gmail.com

The article presents arguments with a view to recognize that space is material and has possibly a fractal dimension in the range of from three to two. It is proposed that along to the unit of substance (atom) Some Unit of the field (vortex tubes) should be set. It is shown that the formation of the field structures being a kind "doubles" of atomic ones is possible. The existence of the three-zone electron structure is confirmed. It is indicated that this concept have already resulted in to the successful explanation of phenomena and to finding of their important parameters at different levels of the organization of matter.

1 Introduction

Some of the observed cosmological effects can not find a satisfactory explanation. These include, in particular, mismatch of the rotation velocity around the galactic center of the substance, located on the periphery of galaxies, to Kepler's laws.

In accordance with Kepler's laws, following the law of universal gravitation, the peripheral rotation velocity of galactic objects should, in accordance with their distancing from the galactic center to the periphery, decrease inversely proportional to the square of their distance from the center. Measurements also showed that this rotation velocity remains almost constant for many galaxies at a very significant distance from the center. The need to explain these facts has led to the conclusion that there is a dark matter filling up the galactic halo.

The other explanation was given by Israeli astrophysicist Mordechai Milgrom. His Modified Newtonian Dynamics (MOND) is an empirical correction of Newton's laws of gravity and inertia, proposed as an alternative to dark matter. The basic idea is that at accelerations below $a_0 \sim 10^{-8}$ cm/sec^2 effective gravitational attraction approaches the value $(g_N\, a_0)$, where g_N — usual Newtonian acceleration; that allows phenomenologically to reproduce the flat rotation curves of spiral galaxies [1].

It is possible that the reported anomalous acceleration detected by the Pioneer spacecrafts refers to the same type of phenomena, i.e. it is caused by not so rapid decrease in the force of attraction, as the Newton's law requires.

2 On the true dimensionality of the space and of its materiality

Is there a need to involve extra entities (dark matter) or to modify forcibly the fundamental Newton's law to explain of this and others cosmological effects? Could be more natural to accept reduction of the dimensionality of the space from three — in the region of cluster masses, to two — for the void intergalactic space?

Assume that wih distancing from the cluster masses at intergalactic distances the three-dimensional space gradually "flattens" in a two-dimensional surface. The force of gravity in the case of the three-dimensional space is inversely proportional to the square of the distance between gravitating masses. With decreasing the dimensionality of the space the natural modification of Newton's law occurs, and the force of gravitational attraction for the two-dimensional space becomes inversely proportional to the distance in the first degree, which leads to the constancy of the rotation velocity of objects at great distances from the galactic center.

Perhaps a slight dimension decreasing and therefore the modification of Newton's law manifests itself at a lower scale with the distance incresing from the Sun, which may explain the anomaly of the Pioneer spacecrafts.

Thus, a picture emerges of three-dimensional or nearly three-dimensional material galaxies islands floating in a two-dimensional or nearly two-dimensional void spatial sea. Obviously, need has ripened for recognizing of the existence of ***a unified material medium*** and for replacement by this concept of the whole variety entities like ether, physical vacuum, space, and matter.

Indeed, according to the concept of J. A. Wheeler's idea, the surface can be two-dimensional, but at the same time is fractalized, topologically non-unitary coherent and consists of linkages of "appendices" or "wormholes" of the first and subsequent orders forming as a whole the three-dimensional structure [2]. Thus matter itself can finally be organized with step-by-step complication of the initial cells and be a "woven cloth", which in its turn, is deformed into the objects (masses, substance) we observe. The objects therefore are the very fractalized (upto micro-world scales) *surfaces*, which have a fractional dimension of the value almost approaching three and presumably equal to the number e [3]. As a result, empty space is logically interpreted as a nondeformed surface and, accordingly, electromagnetic waves as surface waves thereon.

Note, it is the concept of a flat two-dimensional intergalactic space that agrees best with the point of view existing

today among the majority of cosmologists that the observable universe has zero curvature and is very close to spatially flat having local deformations at the location where there are massive objects (flat Universe).

There are also other facts pointing to the reasonableness of the foregoing. Recently in the paper [4] interesting effects have been given, namely —:

— the unusual nature of the distribution of "hot" and "cold" spots in the cosmic microwave radiation;

— the damping of a signal at large scales (there is absence of any clearly expressed "hot" or "cold" areas at the angles greater than about 60°);

— the form of small spots on the map, drawn WMAP, like an ellipse.

The authors consider that these effects can be explained by assuming that the Universe has the shape of a horn. Then its curvature explains these facts, because the whole surface of the horn is a continuous saddle. This negatively curved space acts like a distorting lens, turning spots in something like an ellipse.

It would be interesting to analyze, whether the same effects can be explained in accordance with the concept set forth above, i.e. be the result of observation out of the three-dimensional space of our galaxy of remote objects through a void two-dimensional space?

Finally, there is a known *photometric paradox* that is, in the framework of the proposed concept, explained naturally by decrease in the amount of luminous objects entering the target of the observer during the transition of a solid angle in a planar angle as far as these objects are moving away from the observer.

3 Field masses and their structurization

The idea about transitions between distant regions of space in the form of Wheeler's "appendices" or "wormholes" can be extended to the scale of macrocosm, and some contemporary astrophysical theories has already made use of it [5]. These "wormholes", obviously, should be interpreted as vortical current tubes or threads, or field lines of some kind.

It is considered that matter exists in the form of the substance and the field. A familiar element of our world is an atom, i.e. the *unit of the substance* is the structure that is, on Bohr' model, based (simplified, of course) on the balance between dynamic and electric forces. By analogy, one can imagine the *unit of the field* — the structure that is based (also simplified) on the balance between *dynamic and magnetic forces*.

In the paper [6] it is shown that the balance of dynamic and magnetic forces defines a family of unidirectional vortex threads of number n_i, of the length l_i, rotating about the longitudinal axis of the radius r_i with the rotary velocity v_{0i}; with the additional presence of the balance of *gravitational and magnetic forces* contra-directional closed vortex tubes form closed structures or contours. These structures can be attributed to some mass, but not in the ordinary sense of the word, but as having the sense of the measures of organization of the field.

It is given that the elementary unit of vortex tubes is the unit with the radius and mass close to those of a classical electron (r_e and m_e) [7, 8]. Then the linear density of the vortex tube for vacuum will be:

$$\varepsilon_0 = \frac{m_e}{r_e} = 3.231{\times}10^{-16}\ \text{kg/m}. \tag{1}$$

Accepted that for a medium other than vacuum the mass of a vortex tube or the mass of a conture, i.e. the mass per unit of the field, is proportional to the number of vortex threads in the tube. Then the total mass of the contour of the length l_i will be:

$$M_i = \varepsilon_0 n_i l_i\,. \tag{2}$$

Number of vortex threads shows how material medium differs from vacuum, and their greatest value corresponds to the ratio of electrical-to-gravitational forces, i.e. value:

$$f = \frac{c^2}{\varepsilon_0 \gamma} = 4.167{\times}10^{42}, \tag{3}$$

where c, γ are the light velocity and the gravitational constant.

The balance of *electrical and magnetic* forces gives a characteristic linear parameter that is independent of the direction of the vortex tubes and the number of charges:

$$R_c = \sqrt{2\pi}\, c \times [\text{sec}] = 7.515{\times}10^{8}\ \text{m}. \tag{4}$$

This quantity has a magnitude close to the Sun radius and the sizes of typical stars.

Further, this value corresponds to the characteristic gravitational mass, close to the *Jeans mass* during recombination:

$$M_m = R_c \frac{c^2}{\gamma} = f R_c \varepsilon_0 = 1.012{\times}10^{36}\ \text{kg}. \tag{5}$$

Let the field structure meets the above conditions and has a total mass $M_0 = z_i M_i$, i.e. consists of z_i vortex tubes which, in turn, consist of n_i of vortex threads. While atomic objects are complicated with increasing its mass, field objects are, on the contrary, complicated with decreasing its mass, forming the hierarchy of structures. These changes can be traced if some additional relations are set, for example:

$$z_i = \frac{R_c}{l_i}\,, \qquad a^j = \frac{R_c}{r_i}\,, \tag{6}$$

where a is the reciprocal fine structure constant and $j = 0, 1, 2\ldots$.

In the paper [6] the formulas are given, where all parameters of objects are expressed in the terms of a dimensionless mass $M = M_0/M_m$.

Parameters	Objects					
	Jeans mass	Typical star	Typical small planet	Biggest multicellular organism	Human individual	Most small multicellular organism
j	0	2	4	11	12	15
z_i	1	26.6	706	6.8×10^7	3.5×10^8	4.8×10^{10}
r_i, m	7.5×10^8	4.0×10^4	2.13	2.3×10^{-15}	1.7×10^{-17}	6.8×10^{-24}
l_i, m	7.5×10^8	2.8×10^7	1.1×10^6	11.0	2.13	0.016
v_{i0}, m/sec	3.0×10^8	1.1×10^7	4.2×10^5	4.4	0.85	0.0063
M_0, kg	1.0×10^{36}	2.0×10^{30}	4.1×10^{24}	4.6×10^4	65.5	1.9×10^{-7}
n_i	4.2×10^{42}	8.3×10^{36}	1.7×10^{31}	1.9×10^{11}	2.8×10^8	~1

Table that here shows the hierarchy of the parameters z_i, r_i, l_i, v_{0i}, M_0, n_i with decreasing the mass M_0 for some values of j. It is evident that the fine structure constan is the scale factor in the whole range of mass.

Calculations show that some parameters of objects are quite characteristic. For example, at $j = 2$ the mass of an object is exactly equal to the mass of the Sun, at $j = 4$ the mass of an object is equal to the mass of Earth-like planets. Apparently, the mass range for $j = 11 \ldots 15$ correspond to the masses of living multicellular organisms.

Indeed, for the minimum mass at $j = 15$ the parameter $n_i = 1$, and it limits the existence of the complex structures having masses below $1.9{\times}10^{-7}$ kg. For the maximum mass at $j > 11\, r_i < r_e$. In this case, there is a possibility of the formation within the vortex tubes of $p^+{-}e^-$ contours of general radius r_e (their parameters were previously determined from the condition of the charge constancy [7]) *of even more fine secondary structures* consisting of the vortex elements of radius r_i.

It would be reasonable to assume that the additional information filling of such structures, i.e. the ability to record and store information on a deeper level than the atomic-molecular level (DNA), just also is the condition of the formation of the most complex organisms (multicellular ones).

Provided $r_i = r_e$, the maximum mass of such organism is limited to 59 tons (with roughly at $j = 11$). The overwhelming diversity of living multicellular organisms fit into this mass range. This applies to both flora and fauna. The smallest animals endowed with a cerebrum and nervous system are rotifers (Rotatoria), and the most massive animals are whales (Cetacea), and among multicellular plants — from wolffia rootless (Wolffia arrhiza) to redwoods (Sequoia). Their mean masses are close to those specified in the table of minimum and maximum masses.

It is interesting to note that at $j = 12$ the mass of the object becomes equal to the average mass of a human individual, while the length of the vortex tube corresponds to the length of a stretched human DNA. Complexity of such a field structure containing $3.5{\times}10^8$ vortex tubes, each of which contains nearly the same amount by $2.8{\times}10^8$ vortex threads, *is comparable to the complexity of a human body*, which contains about 10^{14} cells.

Thus, the atomic structures are accompanied by their field "doubles"; this duality in general determines the total properties of objects. And possibly it is the "harmonic complexity" of the existing wave objects having masses close to that of human that defines the most highly organized biological life and the existence of mind.

One might ask why these vortex structures are not detected. But it is not quite so. There where there is a suitable material medium, plasma, for example, vortex structures manifest themselves at the different levels of organization of matter.

Undoubtedly, inside the Sun there is a gravimagnitodynamical structure that manifests itself in the form of paired dark spots in the equatorial zone of the Sun. These spots seem to be the outputs of the vortex force tubes undergoing magnetic reversal and changing their intensity and polarity. Their registered quantity (from several one to a hundred) does not contradict the calculated mean $z_i = 26.6$ [6].

On the Earth's surface the reflection of such structures are numerous geomagnetic anomalies, at least those that are not associated with the features of geological structure.

Regarding the scale of human, it can be assumed that the material essence of living in his field form is expressed through the form and structure of the corona discharge observed around living organisms (Kirlian effect).

4 About the three-zone electron structure and the divisibility of charge

In the microcosm the charge and spin of the electron are determined by momentum and angular momentum of the vortex $p^+{-}e^-$ contour, and these values are constant regardless of the size of the contour [7].

Let for some wave object, whose parameters are determined from the foregoing balances, the momentum of *one* vortex tube $M_i\, v_{0i}$ is also equal to the total momentum $p^+{-}e^-$ contour, i.e. the amount of charge (in the "coulombless" sys-

tem) corrected by the Weinberg angle cosine $e_x = e_0 \cos q_w$, where $q_w = 28.7^\circ$ [8]. Then using the formulas given in [6] *one* can find the number of vortex threads, *which one vortex tube* is composed of:

$$n_i = f\left(\frac{e_x}{c\,M_m}\right)^{2/3} = 2.973 \simeq 3. \qquad (7)$$

Thus, a unit contour or vortex tube having a momentum equivalent to the electron charge contains *three* unit vortex threads. This fact points to the three-zone electron structure and possible divisibility of the charge and confirms the conclusions reached in papers [8, 11].

5 Conclusion

The concept of the unified material medium and recognition of the existence the elementary vortex structures as material units of the field made it possible to reflect on and explain logically variety physical phenomena at the different scale levels of organization of matter using the single approach — J.Wheeler's geometrodynamic concept.

Someone might say that the author's constructions are too simplistic, mechanistic, even speculative and not supported by a properly mathematical apparatus, and some results could be occasional coincidences. However, the author has repeatedly stated that these works are not a formalized theory. These papers only have demonstrated by means of the illustrative mechanistic models the opportunities for understanding, interpretation, and, in some cases, for calculation of important physical parameters on the scale of from microcosm to cosmos.

This approach has proved successful. This proves the results, for example: the definition of the independent determination of the ultimate density of physical vacuum [3], the explanation of the nature of electron charge and finding its numerical value as well as numerical values of the constants of radiation [7, 9], the determination of the proton-electron mass ratio, the accounting of the forces of gravity in microcosm, the finding the neutron lifetime [8], the modeling the Hertzsprung-Russell diagram, the definition of model parameters of pulsars [6], the conclusion about the existence of two types of planetary systems [10], etc.

The obtained results totality, correct both qualitatively and quantitatively, is so great that this fact completely excludes the opportunity of occasional coincidences. Thus, the method of approach and proposed models can serve as a basis for the development of full physical theories based on the recognition of the existence of the unified material medium.

Submitted on June 28, 2014 / Accepted on July 02, 2014

References

1. Sanders R.H., McGaugh S.S. Modified Newtonian Dynamics as an alternative to Dark Matter. arXiv: astro-ph/0204521.
2. Dewitt B.S. Quantum gravity. *Scientific American*, v.249, December 1983, 112–129.
3. Belyakov A.V. On the independent determination of the ultimate density of physical vacuum. *Progress in Physics*, 2011, no.2, 27–29.
4. Aurich R., Lustig S., Steiner F., and Then H. Hyperbolic universes with a horned topology and the CMB anisotropy. arXiv: astro-ph/0403597.
5. Novikov I.D., Kardashev N.S., Shatskiy A.A. Multicomponent universe and astrophysic of the "wormhole". *Uspekhi-Physics*, 2007, v. 177(9), 1017–1023.
6. Belyakov A.V. Evolution of stellar objects according to J. Wheeler's geometrodynamic concept. *Progress in Physics*, 2013, v.9, no.1, 25–40.
7. Belyakov A.V. Charge of the electron, and the constants of radiation according to J. A. Wheeler's geometrodynamic model. *Progress in Physics*, 2010, v.6, no.4, 90–94.
8. Belyakov A.V. Macro-analogies and gravitation in the micro-world: further elaboration of Wheeler's model of geometrodynamics. *Progress in Physics*, 2012, v.8, no.2, 47–57.
9. Belyakov A.V. On the uniform dimension system. Is there necessity for Coulomb? *Progress in Physics*, 2013, v.9, no.3, 142–143.
10. Belyakov A.V. On some general regularities of formation of the planetary systems. *Progress in Physics*, 2014, v.10, no.1, 28–35.
11. *New Scientist*, 1998, No. 2119, 36.

LETTERS TO PROGRESS IN PHYSICS

On the Cosmophysical Origin of Random Processes

Open Letter to the Scientific Community on the Basis of Experimental Results Obtained During 1954–2014

Simon E. Shnoll

Institute of Theor. and Experim. Biophysics, Russian Academy of Sciences,
Pushino 142290, Russia. E-mail: shnoll@mail.ru

This is a summary of the presentations at the seminar headed by Yakov G. Sinai. Held in July 8, 2014, in Institute for Information Transmission Problems, Russian Academy of Sciences, in Moscow.

> "My lords! I came to you to tell most unpleasant news: random physical processes do not exist."

No one person, never, got random time series in the measurements of physical processes on the Earth. There is "non-vanishing scatter of results" which can be found in any physical measurements and observations. It remains existing in the registered data after vanishing all conceivable and inconceivable sources of errors. The "non-vanishing scatter of results" is not random. It is due to the following factors:

— the daily motion and the orbital motion of the planet Earth, where all the observers are located, through the non-isotropic and inhomogeneous cosmic space;

— the motion of the Solar System in the Galaxy;

— changes in the relative positions of the Earth, Moon, Sun and planets.

These conclusions are based on the transformation of the time series of physical measurement data into the series of "insolvent histograms" (such histograms, in which the number of bits and the number of measurements are comparable).

The evidence of non-randomness of the time series is the periodic change of shape of the insolvent histograms.

The non-randomness of shape of the insolvent histograms follows from the next experimental facts:

1. Significant similarity of the histograms obtained from the measurement any processes (from Brownian motion to the alpha-decay) that were recorded in the same moment of time, and in the same geographic location. We call this the "effect of absolute synchroneity";

2. Significant similarity of the histograms, obtained in different geographic locations, but in the same moments of local time;

3. Significantly higher probability of the similarity of the histograms created on the basis of the neighbour (near) non-overlapping segments of the time series, compared to the distant segments of the time series (the "near-zone effect");

4. The clear presence of the near-day, near 27-day, and yearly periods of the appearance of similar histograms;

5. The "space anisotropy effect". It means, in the measurement of nuclear decay fluctuations, that the histogram shape depends on the space direction of the collimators. Also, in light fluctuation measurements, the space anisotropy effect means that the histogram shape depends on the space direction of the light beam generated by LEDs or lasers;

6. The near-day periods of similar histograms were not registered when the light beam coming from a LED, or the alpha-particle beam coming through a collimator are directed to Polaris (this effect was registered in Puschino, Russia). Also, the near-day periods of similar histograms were not registered in the measurements done at the North Pole;

7. Splitting the near-day period into the "sidereal period" (1436 min) and the "solar period" (1440 min);

8. Splitting the yearly period of similar histograms into the "calendar period" (365 days), the "tropical period" (365 days, 5 hours, 48 min), and the "sidereal (stellar) period" (365 days, 6 hours, 9 min);

9. Appearance of similar histograms with the rotation periods of a source slowly rotating in a special device;

10. No near-day periods was registered on a source rotating with a speed of one revolution per day in the opposite direction than the Earth's rotation (thus compensating the daily rotation of the Earth);

11. The "palindrome effect". It is the periodic repetition of mirrored histograms in the moments of time when the daily, orbital, or artificial rotation change its sign (i.e. in the opposite locations on the rotation circle);

12. The algorithmic nature of shape of histograms. Discrete distributions of the number of cofactors. Fluctuations of the number system. Omnibus of the natural numbers.

* * *

Nature (physics) of the registered regularities that are discussed herein is as follows:

1. Because the very different scales of energies in the registered processes (Brownian motion, visible light, alpha-decay), the registered effects can not be explained by "external influences" on these processes. The effects can only be

explained due to the appearance of the observer in similar regions of space along the Earth's trajectory in the cosmos;

2. There exist an optimally small number of measurements used in the histogram creation, in which the accuracy of the similarity of histograms is maximally high. This optimally small number does not depend on the duration of the time interval of the histograms. A fractality is observed: from hours to milliseconds;

3. Similarity of "insolvent histograms" is not due to the statistical (random) regularities. Goodness criteria of hypotheses are inapplicable for histogram shape (the fine structure of insolvent histograms);

4. Beginning from some number of measurement, the fine structure of the distributions does not depend on this number. Remaining this fine structure unchanged with the increase of measurement number contradicts to the large number law. This leads to the "layered histograms phenomenon". It is unclear whether this phenomenon can be explained by the "statistical inertia" or not?

5. Could the characteristic structure of changes in the number of cofactors in the natural numbers, and the dependence of the number system on the "scale unit" to explain the regularities of insolvent histograms?

6. Is the amazing phenomenon of chirality of insolvent histograms also depending on the motion of the Earth in the anisotropic space?

7. Synchronous change of histograms in different geographic locations, with the collimators directed to some special directions in space does not depend on the distance between the locations. The measurements were done along the geographic latitude (the North Pole — Antarctic). Also, synchronous change of histograms is apparently not screened;

8. Nevertheless, when located at a fixed place on the Earth, but with the oppositely directed collimators (to the West and the East) the similarity of histograms appears with the half-day period. It was also registered in experiments with artificial rotation of the source;

9. The presence of clear daily and yearly periods of histograms means that the spatial structure (relievo) of the fractal "coastline" of the Universe remains stable (at least within the scale of our lifespan);

10. It is amazing and remains unexplained that the similarity of histogram series obtained from the measurements done in the equinox moments of time: the moments of transit of the Sun, Moon, Mars, Venus, Mercury through the "point-gap" in the plane of the celestial equator, from above or below the plane;

11. The equinox moments of time also manifested the palindrome effect — the periodic repetition of mirrored histograms.

Submitted on July 05, 2014 / Accepted on July 07, 2014

References

1. Shnoll S. E. Cosmophysical Factors in Stochastic Processes. American Research Press, Rehoboth (New Mexico, USA), 2012.
2. Shnoll S. E. Changes in the fine structure of stochastic distributions as a consequence of space-time fluctuations. *Progress in Physics*, 2006, vol. 2, issue 2, 39–45.

The Real/Virtual Exchange of Quantum Particles as a Basis for the Resolution of Wave-Particle Duality and Other Anomalies of the Quantum Phenomena

Abdul Malek

980 Rue Robert Brossard, Québec J4X 1C9, Canada. E-mail: abdulmalek@qc.aibn.com

A hypothesis based on the exchange and the inter-conversion of the "real" and the equivalent "virtual" particles of the quantum vacuum can resolve the contradiction of wave-particle duality, the "spookiness" and the other conflicting properties of the quantum particles. It can be shown using simple mathematics that the extent of the wave or the particle nature of a quantum particle depends on the rate of this "real/virtual" particle exchange, the velocity and the rest mass of the exchanging "real" particle.

The revolutionary quantum phenomena has posed both ontological and epistemological problems for natural science and philosophy; that remains unresolved even after more than a century of its discovery. The wave-particle duality, the characteristic non-locality, the prevalence of the interplay of chance and necessity among other things distinguish the quantum phenomena, from hitherto anything previous epistemology could even conceive of. The great intuition of Democritus that matter is composed of some elementary particles or atoms more or less holds true and has been vindicated even at the subatomic level; but the contrary nature of matter as a wave at quantum level has also now been well established.

This has given rise to conflicting and mutually exclusive philosophical claims of the objective reality, ranging from positivist and subjective idealism to the realist views of a deterministic, unchanging and a permanent objective reality, to a mechanistic measurement problem as expressed by the Heisenberg's uncertainty principle, But however much wildly differing interpretations of the quantum phenomena are, the rationalist notion of a certain, deterministic and inherently unchanging reality (knowable or not) as the basis of epistemology is widely accepted. At the quantum level this amounts to assuming that the stable quantum particles like protons, electrons, photons, etc., retain their unique and singular identity on a permanent basis; or at least since the creation of the universe, through a Big Bang or otherwise. The only recognized change of the stable and the everlasting fundamental particles is their fusion at the core of the stars to form higher elements.

Albert Einstein, who was a pioneer in the development of the quantum theory, rejected the "spooky" quantum phenomena for its lack of certainty and causality. He (and many others) also opposed the generally accepted but confusing and opportunistic interpretation of the Copenhagen consensus. Einstein tried to avoid the quantum conundrum by adopting a notion of physical reality based on a "continuous field" rather than material particles, particularly in his theory of general relativity (GR). In Einstein's own words, "Since the theory of general relativity (GR) implies the representation of physical reality by a continuous field, the concept of particles and material points cannot play a fundamental part and neither can the concept of motion. The particle can only appear as a limited region in space in which the field strength or energy density is particularly high" [1].

The popularity of "continuous field" based GR have been responsible for the undermining of the original particle based orientation of quantum electrodynamics (QED); as "field" based theories like quantum field theory (QFT) now dominate quantum mechanics and the related domains of cosmology. The fact that the quantum vacuum is seething with ghostly virtual particles that pop in and out of existence has been very well established after the discovery of the Lamb Shift [2], with a precision that is unmatched by any other physical measurements. The Casimir Force is also generally attributed to be due to the presence of virtual particles. These virtual particles can be made real using various well-known techniques [3]. Yet except for being a mere nuisance for creating infinities in the quantum mechanical equations, the virtual particles has so far received little attention from an ontological and epistemological point of view. A new theoretical and experimental re-evaluation of the intuitively derived uncertainty principle of Werner Heisenberg suggest that, the uncertainty does not always come from the disturbing influence of the measurement, but from the more fundamental quantum nature of the particle itself [4]. This points to a possible role of the virtual particles in the uncertainty relation.

All the experimental evidence and technological experience so far, suggest that the virtual particles of the quantum vacuum may play a significant role in determining the attributes of the quantum phenomena, namely the wave-particle duality, its non-locality, its uncertain nature and influence (based on chance and necessity) on the macroscopic biochemical and astrophysical processes etc., than hitherto appreciated.

In opposition to the view of a static objective reality, where the stable and fundamental quantum particles retain their permanent and unique identity; it is assumed in the present hypothesis that the objective reality is dynamic, where there is perpetual exchange of position and identity between the real quantum particles with their respective and reciprocal virtual counterparts; such that no permanent and unique iden-

tity of "real" quantum particles is possible. This exchange is mediated by Heisenberg's uncertainty relation:

$$\Delta E\,\Delta t \geqslant \frac{h}{4\pi}\,,$$

where ΔE is the energy gained by the virtual particle during the time interval Δt, that is equivalent to the mass/energy of the real particle that would exchange with it, and h is the Planck constant. It is clear that the time Δt required for this exchange is extremely small compared to the time of the change in position or the velocity of the real quantum particles that must be within the limit of the velocity of light (c) according to Einstein's theory of special relativity (SR).

If we consider a point source for a "real" quantum particle at the centre of a sphere, then the particle could be any where (during a specific time interval) within this sphere defined by a radius which is proportional to the velocity of the particle. The particle will then have the possibility to exchange position and identity with equivalent virtual particles within this sphere; assuming that the real/virtual exchange does not affect the velocity of the real particle under consideration. This rate (R) of exchange of "virtual" particles par "real" particle par unit time, then will be directly proportional to the volume of the sphere and inversely proportional to ΔE, the energy equivalent of the mass (m) of the real particle that is exchanged with a corresponding virtual particle, according to the following equation:

$$R = \frac{\frac{h}{4\pi}\frac{4}{3}\pi r^3}{\Delta E} = \frac{\frac{h}{3}r^3}{\Delta E} = \frac{\frac{h}{3}kv^3}{mc^2}\,,$$

where h is the Planck constant, r is the radius of the sphere that is proportional to the velocity v of the particle, and k is a proportionality constant. For a particle with the velocity of light (c), the rate is

$$R = \frac{\frac{h}{3}kc}{m}\,.$$

Now, it is obvious from the above equation that for particles with zero rest mass like photons, neutrinos, gravitons etc. the rate of exchange will be infinite, hence the particle or a group of particles will have a wave character spreading in all three dimensions and also can act as long range force carriers.

With massive and stable particles like electrons, positrons, protons, etc., this exchange rate will be finite but much smaller and hence will be restricted around the direction (from the source) of the motion of the particle as a cylindrical or a conical wave front and like an arc in two dimensions; over a tangible distance. The arc-length of the wave packet in two dimensions will depend on the mass and the velocity of the quantum particle. The heavier the mass and slower the velocity, the shorter will be the length of the arc and the wave-packet. The rapid slowing down of the quantum particle along the original direction of its motion is likely to taper down the cylindrical wave-front into a cone shape. More massive and slow moving objects will demonstrate no wave character at all and follow the laws of classical mechanics. It is because a slower velocity will cover less volume of space in specified time and the greater mass will have exorbitant energy requirement for the uncertainty principle and hence lower exchange rate with the potential virtual particles. These aspects of the wave-packet for different quantum particles can possibly be verified with adjustable two slit experiments. This approach to the problem of the propagation of quantum particles very superficially compares with the "Path Integral Formulation" of quantum mechanics by Richard Feynman, where the integration over an infinity of possible trajectories is used to compute a "quantum amplitude" [5].

This real/virtual (and vice versa) exchange of the quantum particles explains their "spookiness", the wave-particle dual character and their non-locality within the limit of the speed of light. Whether all the properties of the quantum particles aside from their charge, such as parity, spin etc. are also conserved or whether their entanglement is affected during these exchanges; needs to be worked out. This hypothesis will be contrary to the generally accepted notions of causality and formal logic, or what G. W. F. Hegel termed as "the view of understanding". But it will be in conformity with the law of "the unity of the opposites" and the other laws of dialectics.

The "view of understanding" abhors contradictions and posits a sharp distinction between the opposites, based on Aristotelian doctrine of "unity, opposition and an excluded middle in between". This view assumes the presence (at least from the time of the creation of the world) of an objective reality that is essentially permanent, certain, unchanging, deterministic and continuous etc. Any change, motion or development in this view can only come from an "impulse" from outside; following the law of cause and effect. There is little wonder that the conflicting and the uncertain nature of the quantum phenomena has given rise to confusion and to mutually exclusive philosophical claims of the objective reality, ranging from the positivist and subjective idealism to the realist views of the "guiding waves" of a continuous and permanent objective reality on the one hand and to a mechanistic and simplistic measurement problem as expressed by the Heisenberg's uncertainty principle, on the other.

An exactly opposite view of the objective reality mainly attributed to the Greek philosopher Heraclitus and later developed by G. W. F. Hegel, Karl Marx and Frederick Engels posits "eternal change due to inner strife" as the permanent feature of the objective reality and the world. Any stability or apparent permanence is only relative and conditional. The world in this view is infinite, eternal and ever changing. This view follows from Hegel's elaboration of dialectics as the "Absolute Identity of identity and non-identity" — "the unity of the opposites" i.e., a simultaneous unity and conflict of the opposites residing together at the very element of a thing or a process in a logical contradiction. Any material existence is a

contradiction of the opposites and must eternally be resolved to a new "becoming" through a dialectical "negation of the negation", in a chain of processes in triads that give rise to the phenomenology of the world. At fundamental quantum level, the objective reality is a contradiction of "being" and "nothing", giving rise to "becoming" or existence. The QED established fact that the quantum vacuum seethes with virtual particles, the notion of an eternal real/virtual exchange and a dynamic equilibrium as the basis of the objective reality is in conformity with a dialectical view of the universe.

From a dialectical point of view, "being" and "nothing" must always exist together in contradiction, as a part of the objective reality of the universe. One cannot supersede or exhaust the other, so there can be no question of a beginning or an end of the universe. For dialectics, there is also no mega-leap (like Big Bang) in nature; precisely because nature is made entirely of infinite leaps of the "negation of the negation", mediated by chance and an iron necessity that is inherent in chance! In addition to real/virtual particle exchange, inter-conversion of real and virtual particles through quantum tunnelling and through yet other still unknown processes is possible. The energetic core of the galaxies are likely to be the favourable sites for the generation of new matter and anti-matter from the virtual particles This author had previously attempted to use these ideas to explain some cosmic phenomena [6], the origin, evolution and the structure of the galaxies [7] and other aspects of modern cosmology [8].

Submitted on July 15, 2014 / Accepted on July 17, 2014

References

1. Einstein A. On the General Theory of Relativity. In: *The Scientific American Book of the Cosmos*, David Levy (Ed.), N.Y., 2000, 18–19.
2. Lamb W.E. and Retherford R.C. Fine structure of the hydrogen atom by a microwave method. *Phys. Rev.*, 1947, v.72, 241.
3. Ruffini R., Verreshchagin G., and Xue S. Electron-positron pairs in physics and astrophysics: from heavy nuclei to black holes. arXiv: 0910.0974.
4. Erhart J. et al. Experimental demonstration of a universally valid error-disturbance uncertainty relation in spin measurements. *Nature Physics Volume*, 2012, v.8, 185–189.
5. Feynman R.P., Hibbs A.R., and Styer D.F. Quantum Mechanics and Path Integrals. Dover Publications, Mineola, N.Y., pp. 29–31.
6. Malek A. The cosmic gamma-ray halo — new imperative for a dialectical perspective of the Universe. *Apeiron*, 2003, v. 10, no. 2, 165.
7. Malek A. Ambartsumian, Arp and the breeding galaxies. Apeiron, 2005, v. 12, no. 2, 256.
8. Malek A. The Dialectical Universe — Some Reflections on Cosmology. Agamee Prakashani Publishers, Dhaka, 2012.

LETTERS TO PROGRESS IN PHYSICS

The Infinite as a Hegelian Philosophical Category and Its Implication for Modern Theoretical Natural Science

Abdul Malek

980 Rue Robert Brossard, Québec J4X 1C9, Canada. E-mail: abdulmalek@qc.aibn.com

The concept of the infinite as a mathematical, a scientific and as a philosophical category is differentiated. A distinction between Hegel's dialectical concept of the infinite as opposed to his idealist-philosophical "system" of the "Absolute Idea" as the "True Infinite" is emphasized.

1 The infinite as a mathematical category

The concept of the infinite as a mathematical category arose naturally enough with the invention of the numerical system by the Sumerians around 3000 B.C. and the subsequent developments of the concepts of geometry, the measure of time, mathematical operations (arithmetic, algebraic, exponentials etc.), One could always add or subtract a unit of number, length or time to get a new one ad infinitum without an end. This infinite is undetermined, has no characterization and was termed the "spurious" or the "false" infinite (*bad infinity*) by G. W. F. Hegel (1770–1831 A.D.), as opposed to the "True Infinite" (to be discussed later).

"The spurious infinite" according to Hegel [1],

> "...seems to superficial reflection something very grand, the greatest possible. ... When time and space for example are spoken of as infinite, it is in the first place the infinite progression on which our thoughts fasten ... the infinity of which has formed the theme of barren declamation to astronomers with a talent for edification. In an attempt to contemplate such an infinite our thought, we are commonly informed, must sink exhausted. It is true indeed that we must abandon the unending contemplation, not however because the occupation is too sublime, but because it is too tedious ... the same thing is constantly recurring. We lay down a limit: then pass it: next we have a limit once more, and so for ever."

The infinite as a mathematical category took a mystical form once Pythagoras of Samoa (580?–520 B.C.), and later Plato (429–347 B.C.) idealized the numbers, their relations and geometry into their philosophical system, where the infinite along with the numbers and the forms were universals that exists in a realm beyond space and time for all eternity, a realm that sense perception cannot reach; it is only given to thought and intuition.

As Frederick Engels [2, p. 46] wrote,

> "Like all other sciences, mathematics arose out of the *need* of man; from measurement of land and of the content of vessels, from computation of time and mechanics. But, as in every department of thought, at a certain stage of development, the laws abstracted from the real world become divorced from the real world and are set over against it as something independent, as laws coming from outside to which the world has to conform. This took place in society and in the state, and in this way, and not otherwise, *pure* mathematics is subsequently *applied* to the world, although it is borrowed from this same world and only represents one section of its forms of interconnection — and it is only just precisely because of this that it can be applied at all".

The mathematical pursuit of the infinite therefore, of necessity became a spiritual endeavor. In his attempt to know the infinite and to prove his continuum hypothesis, Georg Cantor (1845–1914 A.D.) for example, was eventually compelled to make a distinction between *consistent* and *inconsistent* collections; for him only the former were *sets*. Cantor called the *inconsistent* collections the *absolute infinite* that God alone could know. His idea of an "actual infinite" attracted theological interest because of its implication for an all-encompassing God; but at the same time it inspired scorn of the contemporary mathematicians. What Cantor, other mathematicians and natural science pursued in reality is the "spurious infinite" of Hegel. An infinite series starting with a first term is also undefined, because there is no end to the other side, and one cannot come back to the first term starting from the other end. Cantor's pursuit of the infinite led him to the ridiculous idea of the *infinity* of infinities, and no other mathematicians followed his steps. If there is more than one infinite then by definition they become mere finites. Mathematicians of all ages had no clue as to the nature of the infinite; some denied its existence all together; while others maintained (following Plato) that mathematical entities can-

not be reduced to logical propositions, originating instead in the intuitions of the mind.

2 The infinite as a scientific category

Historically, natural science took a rather pragmatic and an opportunistic approach towards infinity, i.e., *reductio ad absurdum* argument which avoids the use of the infinite. It truncates infinity by putting an arbitrary limit as Georg Cantor did, and calls the rest the "absolute infinite" that is known only to infinite God. It deals with infinity with some arbitrary mathematical tricks, for example, a circle is the limit of regular polygons as the number of sides goes to infinity; an infinite series starts with a first term; in renormalization, one set of infinite is cancelled by invoking another set of infinite to get a finite result that was desired in the first place and so on.

Isaac Newton (1642–1727 A.D.) and Albert Einstein (1879–1955 A.D.) faced the same conceptual problems of the infinite universe in formulating their theories of gravity. Einstein declared, "Only the closed ness of the universe can get rid of this dilemma" [3]. He then set himself to develop a theory of gravity based on geometry, because geometry deals with closed space!

But an attempt to truncate infinity this way can only lead us back to medieval geocentric cosmology. The unpleasant fact is that, by definition a truncated infinite is also infinity and any mathematical operation on infinity leaves it unchanged as Galileo asserted in his famous 1638 pronouncement on infinity that, "Equal", "greater", and "less" cannot apply to infinite quantities [4]. The arbitrary renormalization process and *reductio ad absurdum* practiced by natural science cannot resolve the contradiction of the infinite; it only leads to more and more contradictions and a dependence on ever more mysteries and theology, as we observe in modern theoretical natural science. The reason why Albert Einstein chose a finite and closed universe as opposed to the open ones was not only to make his equations meaningful and/or because of his love for *simplicity* and *aesthetics*, as reductionist ideologues and worshipers of symmetry would have us believe, but also because of his sober realization that his Machean-philosophy based cosmology collapses in an infinite universe. If Mach's principle is followed, then an infinite universe means that the inertia and the mass of atoms etc. also become infinite. To keep the world as we see it now (inertia, mass, etc.); all Mach based cosmologies must have the universe started at a finite past and also must have a finite extension. So this way the contradiction of infinity is not solved.

The notion of the infinite in natural science became ever more clouded after Albert Einstein established the primary role of mathematics in natural science. Natural science became seduced to the idea that where experimental evidence and empirical data is difficult and/or impossible to obtain "logical consistency of mathematics" will lead the way. The stunning success of the theories of relativity in early 20th century, led Einstein to revive Pythagoras's notion of mathematics. "How can it be" he wondered, "that mathematics being a *product of human thought* which is *independent of experience*, is so admirably appropriate to the objects of reality?" [5].

The theory of general relativity is a classic example where the power of mathematics, pure thought and aesthetics devoid of any empirical content is purported to have conceived the ultimate reality of the universe. "Our experience hitherto justifies us in believing that nature is the realization of the simplest conceivable mathematical ideas. I am convinced that we can discover by means of purely mathematical constructions the concepts and the laws connecting them with each other, which furnish the key to the understanding of natural phenomena. ... In a certain sense, therefore, I hold it true that pure thought can grasp reality, as the ancients dreamed", declares Albert Einstein [6].

With his mathematical idealism Einstein erased the difference between the *pure* mathematics, whose program is the *exact* deduction of consequences from logically independent postulates, and the *applied* mathematics of *approximation* needed for science. Natural science uses approximate empirical data, which are fitted on in various ways to *analytic functions* of *pure* mathematics that helps in the systematization, generalization, and the formulation of tentative theories. But the results and the inferences are only valid in a narrow range of the data values for the argument for which approximate empirical information is available.

A convenient property of the analytic functions (such as the field equations) is that, such functions are known for all values of their argument when their values in any small range of the argument values are known and thereby allowing an unlimited extension of this procedure from the macrocosm to the microcosm. Thus, the *a priori* assumption that the laws of Nature involve *analytic functions* leads to a complete mechanistic determination of the world based on their experimentally determined value in a narrow range only. But the validity of such a procedure of unlimited extension of mathematical functions for the real world, were questioned both by mathematician/philosophers such as Bridgman [7] and scientists like Klein [8] at the advent of quantum mechanics; based as they argued (on different grounds) on the unavoidable inaccuracies of empirical knowledge. And as quantum mechanics clearly shows, there is uncertainty in the ontological nature of reality itself at micro level. So, our epistemological knowledge must always be defective, tentative and approximate, increasing in scope from one generation of humanity to the next; like an infinite mathematical series, without ever coming to a termination or without ever reaching one final and ultimate truth.

The quantum phenomena and the failure so far [9]; (in spite of over a century-long intense efforts by some of

the most brilliant mathematicians including Einstein) to unify "ALL" the particles and "ALL" the forces of Nature into a simple and reductionistic "theory of everything" demonstrate the folly of this kind of naïve and over- simplified extrapolation of idealized mathematics to the real world at the two opposite directions of infinity, i.e., macrocosm and microcosm.

3 The infinite as a philosophical category

The concept of the infinite was implicit in the early philosophical developments especially among the early Greek thinkers that centered around the basic questions of the primacy of spirit or nature, unity or multipliticity, stasis or motion. This debate divided the philosophers into two great camps. Those who asserted the primacy of spirit, unity and stasis formed the camp of idealism; the contrary camp formed the various schools of materialism.

The earliest idealist Greek philosophers (the Eleatics) denied the reality of becoming, multiplicity or motion; these characteristics they maintained, are of the sense-world or physical Nature. These they argued are not *real* but only *appearances* and hence these are illusions. For Parmenides (515–450 B.C.) for example the sole reality is Being, Being is One, only the One is; the Many not. This Being cannot be perceived by senses, it is given only to thought or mind. This line of thinking permeates the range of idealist philosophers like Plato, Aristotle, Berkeley, Hume, Hegel and all monotheistic religions. The Unity of Being in this view means that the infinite must be contained in this one Being. The Being meaning God in theological terms, the infinite, then became associated with abstract God. The idealist view of infinity was later incorporated into mathematics and theoretical natural science.

But the dialectically opposite and the materialist view of reality — i.e. the validity of the sense perception of change, multiplicity and motion in material Nature also arose simultaneously in early Greek philosophy. The founder of the dialectical view, Heraclitus (544–483 B.C.) on the contrary saw the world as a process — as changing eternally. For him Unity is not a homogenous unity, but is a "unity of the opposites or of opposite tendencies". The Unity is a complex entity that contains at least two dominant opposite fragments that are in constant conflict with each other and renders this unity susceptible to diversity, change and movement. The concept of the infinite in this view is therefore, open ended. Epicurus (341~270 B.C.) following the tradition of Heraclitus was the first to assert that the universe is infinite in its extension in all directions and that multiplicity, time and motion are endless.

Benedict Spinoza (1632–1677 A.D.) made an important advance on the concept of infinity along the dialectical tradition which helped Hegel (himself an idealist) to formulate in a comprehensive way the dialectical view of the infinite in particular and his dialectical method in general. Spinoza formulated the profound idea that to define something is to set boundaries for it; i.e., to determine is to limit. The infinite then is something that is undetermined or that has no limit or boundary. In other words the Infinite is limited only by itself and like God is "self-determined".

In popular concept, God is supposed to be infinite. Spinoza's idea of the infinite led to an insurmountable difficulty for conventional philosophy and theology which regarded the infinite and the finite as mutually exclusive opposites; absolutely cut off from each other. How then the infinite can be conceived; how infinite God can have contact with finite man, since it will limit His infiniteness. Finiteness of the world became a primary requirement for medieval theology. The inquisition did not hesitate to spill blood and torture victims to defend its doctrine. Hegel, following Spinoza called the "Absolute Idea" of his philosophy the "True Infinite" which is self-determined. For him the material world or Nature is a crude replica — an alienated form of the "Absolute Idea".

The fundamental difference between these two worldviews and hence their implication for the concept of infinity gets its concrete expression in the question of *matter* and *motion*. While Newton recognized matter as a *real entity*, for Einstein matter is a particular representation of an all pervading (space-time) reality ("Being" of Parmenides?). Einstein expressed this point of view in an unambiguous way, "Since the theory of general relativity (GR) implies the representation of physical reality by a continuous field, the concept of particles and material points cannot play a fundamental part and neither can the concept of motion. The particle can only appear as a limited region in space in which the field strength or energy density is particularly high" [10]. Motion in the view of both Newton and Einstein could only arise from an *impulse* from without — from God — the "unmoved mover". And why energy density at particular points must arbitrarily be high to form material points must also depend on intervention by Providence. For dialectics (and quantum mechanics) on the contrary, matter and motion are the fundamental elements and the primary conditions of all physical reality; *motion is the mode of existence of matter. Matter without motion is as inconceivable as motion without matter*.

The only way the conceptual problem of infinity can be resolved is through the dialectics of Hegel — the law of the unity of the opposites. The notion that the finite and the infinite reside together in a contradiction; that they are united as well as are in opposition to each other. That, the finite **is** the infinite and vice versa. That this contradiction resolves itself continuously in the never-ending development in time and extension in space of the universe, in the same way as for example intellectual advance find its resolution in the progressive evolution of humanity from one particular generation to the next. Just as Nature or the universe (ontologically) is incapable of reaching a final, ever lasting, unchanging or an ideal state so is thought (which is only a reflection of Nature in the mind of man) epistemologically is incapable of comprehending a completed, exhaustive or immutable knowledge

— the so-called absolute truth of the world. For dialectics, "eternal change" (with temporary stages of infinite number of leaps) is the only thing that is permanent and the only absolute. Hegel's dialectics therefore, is a condemnation of all claims to absolute truth by all idealism including the mathematical idealism of modern official natural science, which is but a reincarnation or rather restoration of the old idealism. In human history, as well as in the history of natural science, hitherto all claims to the "final truth" are but the partial masquerading as the complete.

The continuous resolution of the contradiction of the finite and the infinite like the other evolutionary processes are not only dialectical but they also develop historically following the three general laws i.e. i) transformation of quantity into quality and vice versa, ii) interpenetration of the opposites and iii) the negation of the negation. Engels [11] summarized these three laws from Hegel's *Logic*, where the first law comprises the *Doctrine of Being*, the second, the *Doctrine of Essence*, while the third constitutes the fundamental law for the construction of the whole system. Hegel deduced his philosophy from the history of Nature, of society and of thought. The infinite universe is not a mere abstract, quality less, boring, endless extension of uniformity (spurious or *bad infinity*), it includes a variety of qualitative contents with different forms of movements passing one into the other and developing historically. The infinite space is adorned with the drama of things "coming into being" and "passing out of existence" in each of the innumerable island universes; each island universe with innumerable galaxies and each galaxy in turn with innumerable stars and planets. Under favorable conditions, galaxies propagate [12, 13]; the stars produce the higher elements; the planets give rise to the evolution of molecules, to organic life and finally to the thinking brain through which infinite Nature (for a brief period of time) *becomes conscious of itself* ! Self-consciousness is therefore, the property of the highest developed form of matter, which like everything else comes into being and passes out of existence as temporary bubbles in the eternal and infinite universe.

The knowledge of the infinite is therefore proportional to the knowledge of the finite. This knowledge is necessarily a historical and an iterative process progressing through successive generations of mankind without ever terminating in one final or absolute truth a quest of which was the aim of all idealism — mathematical, scientific or philosophical. A progressively better understanding of the infinite universe can only come about by studying the finite around us guided by the general laws of dialectics.

There are innumerable number of water and other molecules and atoms on earth and yet we understand (in a limited sense) and live at ease with these! The properties of matter and its structure under the various conditions in terrestrial nature must be the same that exists under similar conditions billions of light years away. In fact, one sun with its planets and its life supporting earth and one Milky Way galaxy with its surrounding family group form the essential basis for an understanding of the universe. Beyond 15 billion light years there is no wonderland or lurking monsters to be seen. What we will see there is more or less the same we now see within a few million light years around us! The same applies to the micro-world. There is no limit of space, time or length in any direction; up-down, left-right; back-front, at least up to the level beyond which the terms mass, time or length lose their meaning (in the usual sense of the term) because of quantum uncertainty and due to other yet unknown effects. The limits from quasars (at the ultimate boundary of the universe?) to the quarks at the lowest end, set by Official Science must therefore be false; because this represents an arbitrary limitation of infinity, conditioned by the limitation of the empirical knowledge of our time.

4 The "Absolute Idea" of Hegel as the "True Infinite"

As Engels pointed out [14], the dialectical view of the infinite as discussed above, are necessary logical conclusions from the dialectical method of Hegel; but conclusions he himself never expressed so explicitly. Hegel was an idealist and above all he was the official philosopher of the Royal Prussian court of Frederick William III. His task was to make a system of philosophy that must specify one absolute truth or a "first cause" of the world, as tradition demanded it. Therefore, even though Hegel, especially in his *Logic* emphasized that this absolute truth is nothing but the logical. i.e., historical *process* itself, he nevertheless found it necessary to bring his dialectical process to a termination in the "Absolute Idea". For his philosophical "system" his dialectical "method" had to be untrue. Hegel also turned his philosophy upside down, where the "Absolute Idea" (like all idealism) became primary and nature only a crude reflection of the "Idea", even though (through unprecedented detail and encyclopedic work) he extracted the laws of dialectics from the history of the material and the human world.

But nevertheless, the dialectical method of Hegel helped him to overcome the impossible contradiction of the infinite and the finite faced by Spinoza, theology and all previous idealist philosophies. For Hegel, the finite and the infinite are no independent entities separated from each other by an unbridgeable gap in between, as old philosophy asserted; but these are the integral components of a single unity within which the two opposites reside together in active unity and opposition, and hence in a logical contradiction. A resolution of this contradiction to an ever new "unity of the opposites" and so on — *the negation of the negation* is what gives rise to motion, change, development, and historical evolution of the universe as a never ending process.

Idealist Hegel can terminate the infinite process of change by making his "Absolute Idea" (the self-determined, the True Infinite") as the ultimate end result of all change, motion, development or history, and making it the beginning again, i.e.

the end as the true beginning. For Hegel, the finite Nature or man IS the infinite "Absolute Idea" itself! The "Absolute Idea" alienates and disguises itself into Nature, evolves historically through all the usual twists and turns following the laws of dialectics and comes back to itself again through the consciousness of man and particularly through the philosophy of Hegel himself, who for the first time in the history of mankind perceived in thought the ultimate truth of this dialectical movement, in absolute profoundness. For Hegel the "Absolute Idea" which is the end result of all change, development, motion, history etc. — the static reality of Parmenides, the abstract God of theology, the self-determined entity of Spinoza, is the "True Infinite" and the absolute truth of the world.

But this "Absolute Idea" or the "True Infinite" of Hegel like the mathematical "Absolute Infinite" of Cantor; are only absolutes in the sense that they have absolutely nothing to say about it! Thus in spite of his prodigious intellect and in spite of the logical implication of his profound dialectical "method" to the contrary, Hegel unfortunately pursued the illusion of an absolute truth, like all the other idealist philosophers and all theological prophets of all times. The mathematical idealism and reductionism of modern official theoretical natural science inherited this illusion — i.e., the empty shell of all idealism but not the kernel — the dialectical "method" of this great idealist thinker.

5 Conclusion

During the last few centuries especially since Copernicus (1473–1543), natural science accumulated impressive empirical evidence and gained variable degrees of understanding of the terrestrial nature; that collectively vindicate Hegel's assertion that *change* is the only absolute truth and that the dialectical laws are the only eternal laws that govern the development and the transformation of matter and life. But ironically, natural science claims its own invariable truth exactly in the areas where it possesses the least empirical evidence! As intoxicated modern official natural science celebrates its achievement of a definitive knowledge of one single event i.e., the "Big Bang" origin of the universe and the triumph of its mathematical idealism; with the award of Nobel Prizes, and as the world awaits in breathless anticipation the imminent discovery of a "theory of everything" that will bring an "End of Physics" and possibly the end of all knowledge (by "knowing the mind of God", according to one of the leading physicists Stephen Hawking [15]); it would be instructive for us to remember the sober dialectical assessment of Frederick Engels [2, pp. 43–44] — one of the greatest inheritors of Hegel's philosophy:

> "The perception that all the phenomena of Nature are systematically interconnected drives science to prove this interconnection throughout, both in general and in detail. But an adequate, exhaustive scientific statement of this interconnection, the formulation in thought of an exact picture of the world system in which we live, is impossible for us, and will always remain impossible. If at any time in the evolution of mankind such a final, conclusive system of the interconnections within the world — physical as well as mental and historical — were brought to completion, this would mean that human knowledge had reached its limit, and, from the moment when society had been brought into accord with that system, further historical evolution would be cut short — which would be an absurd idea, pure nonsense. Mankind therefore finds itself faced with a contradiction; on the one hand, it has to gain an exhaustive knowledge of the world system in all in its interrelations; and on the other hand, because of the nature both of man and of the world system, this task can never be completely fulfilled. But this contradiction lies not only in the nature of the two factors — the world, and man — it is also the main lever of all intellectual advance, and finds its solution continuously, day by day, in the endless progressive evolution of humanity. . . ".

Submitted on July 15, 2014 / Accepted on July 18, 2014

References

1. Wallace W. "The Logic of Hegel". Oxford, Clarendon Press, 1892, §94. Cited from: Stace W.T. The Philosophy of Hegel. Dover, N.Y., 1955, §198.
2. Engels F. Anti-Dühring. International Publishers, N.Y., 1939.
3. Kragh H. Cosmology & Controversy. Princeton Univ. Press, 1996, p. 7.
4. Kaplan R. and Kaplan E. The Art of the Infinite. Oxford Univ. Press, Oxford, 2003, p. 228.
5. Einstein A. Sidelights on Relativity. Dover, N.Y., 1983, p. 28.
6. Einstein A. Essays in Science. Transl. by Alan Harris from: Mein Weltbild. Quedro Verlag, Amsterdam, 1933, pp. 16–17.
7. Bridgman P.W. The logic of Modern Physics. Macmillan, N.Y., 1927.
8. Klein F. Elementarmathematik von Höheren Standpunkt aus. Bd. 3, Springer, Berlin, 1924. Cited from: Condon E.U. and Morse P.M. Quantum Mechanics. McGraw-Hill, N.Y., 1929, p. 11.
9. Smolin L. The Trouble with Physics. Houghton Miffin Co., Boston–N.Y., 2006.
10. Einstein A. On the General Theory of Relativity. In: *The Scientific American Book of the Cosmos*, N.Y., 2000, p. 13.
11. Engels F. Dialectics of Nature. International Publishers, N.Y., 1940, p. 26.
12. Malek A. Ambartsumian, Arp and the breeding galaxies. *Apeiron*, 2005, v. 12, no. 2, 2005, 256–271.
13. Arp H.C. Seeing Red: Redshifts, Cosmology and Academic Science. Apeiron Publishers, Montreal, 1998.
14. Engels F. Ludwig Feuerbach and Outcome of Classical German Philosophy. International Publishers, N.Y., 1941, pp. 12–13.
15. Hawking S. A Brief History of Time. Bantam Books, N.Y., 1990, p. 175.

A Monte Carlo Simulation Framework for Testing Cosmological Models

Yuri Heymann

3 rue Chandieu, 1202 Geneva, Switzerland. E-mail: y.heymann@yahoo.com

We tested alternative cosmologies using Monte Carlo simulations based on the sampling method of the zCosmos galactic survey. The survey encompasses a collection of observable galaxies with respective redshifts that have been obtained for a given spectroscopic area of the sky. Using a cosmological model, we can convert the redshifts into light-travel times and, by slicing the survey into small redshift buckets, compute a curve of galactic density over time. Because foreground galaxies obstruct the images of more distant galaxies, we simulated the theoretical galactic density curve using an average galactic radius. By comparing the galactic density curves of the simulations with that of the survey, we could assess the cosmologies. We applied the test to the expanding-universe cosmology of de Sitter and to a dichotomous cosmology.

1 Introduction

We tested cosmological models using relatively small simulations that can be run on a home computer. Simulation is a promising and powerful tool for the field of cosmology. For example, the Millennium Simulation project at the Max Planck Institute for Astrophysics, the largest N-body simulation carried out so far, simulated the formation of large structures in the universe using a cluster of 512 processors. Our rationale was to slice a galactic survey into small redshift buckets. We then used cosmological models to compute the volume of each bucket and derived the galactic density curve versus the redshift, or light-travel time. We used the simulation to generate a uniform distribution of galaxies for each redshift bucket. We then computed the number of visible galaxies (i.e. those that were not covered by foreground galaxies) to derive a simulated galactic density curve. Our method requires only a cosmological model, a behavior for the galactic density, and the average galactic radius versus the redshift.

We are interested in a special class of cosmological models: cosmologies with a Hubble constant that does not vary over time to conform to the linear relationship between the luminosity distance and the redshift observed for Type Ia supernovae [1]. This choice was motivated by the idea that the laws of nature follow simple principles. There are two distinct cosmologies that satisfy this condition: the de Sitter flat-universe cosmology and the dichotomous cosmology introduced in [2].

The de Sitter cosmology is a solution to the Friedmann equation for an empty universe, without matter, dominated by a repulsive cosmological constant Λ corresponding to a positive vacuum energy density, which sets the expansion rate $H = \sqrt{\frac{1}{3}\Lambda}$. The dichotomous cosmology consists of a static material world and an expanding luminous world. It is not difficult to envision a mechanism whereby light expands and matter is static. For example, consider that the light wavelength is stretched via a tired-light process when photons lose energy. The number of light wave cycles is constant, resulting in an expanding luminous world and static material world. In order to maintain a constant speed of light, we would still have to introduce a time-dilation effect [2].

The same equation relates light-travel time to redshifts for both the dichotomous and the de Sitter cosmologies, making it easy to compare both models using our testing framework.

2 Method

2.1 The cosmological model

Consider an expanding luminous world, or an expanding universe, with a constant expansion rate H_0. Because of the expansion, the distance between two points is stretched. Let us introduce the Euclidean distance y, which is the equivalent distance measured if there were no expansion. The Euclidean distance is also the proper distance at the time light was emitted, which is the comoving distance times the scale factor at the time of emission. Now, consider a photon at a Euclidean distance y from the observer, moving towards the observer. Hence, y must satisfy the following differential equation:

$$\frac{dy}{dt} = -c + H_0 y\,, \tag{1}$$

where c is the speed of light.

By setting time zero at a reference T_b in the past, we get $t = T_b - T$; therefore, $dt = -dT$. Hence, (1) becomes:

$$\frac{dy}{dT} = c - H_0 y\,, \tag{2}$$

with boundary condition $y(T = 0) = 0$. Integrating (2) between 0 and T, we get:

$$y = \frac{c}{H_0}\left(1 - \exp(-H_0 T)\right)\,. \tag{3}$$

Because $dt = \frac{da}{H\,a}$, where a is the scale factor, the proper light-travel time versus redshift is:

$$T = \int_{1/(1+z)}^{1} \frac{da}{H_0\,a} = \frac{1}{H_0}\ln(1+z)\,. \tag{4}$$

By substitution of (4) into (3), we get:

$$y = \frac{c}{H_0}\frac{z}{(1+z)}\,. \tag{5}$$

As $T_0 = \frac{y}{c}$, we finally get:

$$T_0 = \frac{1}{H_0}\frac{z}{(1+z)}\,, \tag{6}$$

where T_0 is the light-travel time in the temporal reference frame of the observer, H_0 the Hubble constant, and z the redshift. Eq. (6) is our cosmological model relating light-travel time to redshifts.

2.2 The sampling method

The zCosmos-deep galactic survey [3] consists of a collection of visible galaxies with respective redshifts obtained for a given spectroscopic area in the sky. Here we used Data Release DR1, which contains galactic observations up to a redshift of 5.2. We sliced the collection of galaxies into small redshift buckets and counted the number of galaxies in each bucket. Using our cosmological model, we converted the redshifts into light-travel times. The volume of each bucket is equal to the volume of the slice for the whole sphere contained between the lower and upper radius boundaries of the bucket multiplied by the ratio of the spectroscopic area of the survey divided by the solid angle of the sphere.

For an observer at the center of a sphere, the volume of a slice of the sphere is:

$$V_i = \frac{4\pi}{3}\left(r_i^3 - r_{i-1}^3\right)\,, \tag{7}$$

where r_{i-1} and r_i are the lower and upper radius boundaries of the bucket, respectively.

The spectroscopic area of the zCosmos galactic survey was determined to be 0.075 square degrees [4]. Hence, the ratio of the survey spectroscopic area divided by the solid angle of the sphere is as follows:

$$\eta_{surv} = \frac{0.075}{4\pi(180/\pi)^2} = 1.81806\times 10^{-6}\,. \tag{8}$$

Thus, the volume of the i^{th} bucket of the survey is $\eta_{surv}V_i$. The galactic density of the bucket is the number of galaxies contained within the redshift boundaries of the bucket divided by the bucket volume. By computing the galactic density for each bucket, we get the galactic density curve of the survey versus the redshift or light-travel time.

2.3 The simulation method

To simulate the galactic density curve, we need in addition to a cosmological model, two other behaviors: the galactic density versus redshift and the relationship between the average galactic radius and redshifts. For the sake of convenience, we used the same redshift slicing that we used to compute the survey galactic-density curve, say $z \in \{0, z_1, z_2, ..., z_n\}$, where $z_{i+1} = z_i + \delta z$. By iteration from redshifts z_1 to z_n, we generated N_i galaxies with a uniform distribution in an isotropic universe and then determined whether each galaxy is visible amongst the foreground galaxies. We determined the position of each galaxy using the astronomical spherical coordinates (r, θ, φ), where r is the radial distance, $\theta \in [-\frac{\pi}{2}, \frac{\pi}{2}]$ is the declination, and $\varphi \in [0, 2\pi]$ is the right ascension. Each galaxy also has an associated radius.

First, we fixed the spectroscopic area of the simulation by taking boundaries for the declination and right ascension, say $\varphi \in [\varphi_{min}, \varphi_{max}]$ and $\theta \in [\theta_{min}, \theta_{max}]$. The spectroscopic area of the simulation is:

$$\begin{aligned}\text{specArea} = \left(\frac{180}{\pi}\right)^2 (\sin\theta_{max} - \sin\theta_{min}) \times \\ \times\, (\varphi_{max} - \varphi_{min})\end{aligned} \tag{9}$$

and the spectroscopic area of the simulation to solid angle of the sphere is:

$$\eta_{sim} = \frac{\text{specArea}}{4\pi(180/\pi)^2}\,. \tag{10}$$

To determine the number of galaxies to generate for a redshift bucket $[z_{i-1}, z_i]$, we computed the volume V_i of the spherical shell using (7) and then multiplied the galactic density by $\eta_{sim}V_i$, hence:

$$N_i = \rho_i\,\eta_{sim}V_i\,, \tag{11}$$

where N_i is the number of galaxies generated, ρ_i is the galactic density at redshift z_i, and η_{sim} and V_i are as defined previously.

To generate a galaxy, we drew two independent, uniform random variables, say X and Y, on the interval [0, 1] and computed the declination and right ascension of the galaxy as follows:

$$\begin{aligned}\theta &= \theta_{min} + X(\theta_{max} - \theta_{min}) \\ \varphi &= \varphi_{min} + Y(\varphi_{max} - \varphi_{min})\,.\end{aligned} \tag{12}$$

The newly generated galaxy was attributed the radial distance corresponding to the light-travel time at redshift z_i.

Next, we determined whether each generated galaxy was hidden by foreground galaxies. As an example, consider the calculations for galaxy B with galaxy A in the foreground. We compute the distance between the projection of galaxy A on the plan of galaxy B and galaxy B itself, which we call the "projected distance" projectedDist. If the projected distance is smaller than or equal to the critical distance, then galaxy B is determined to be not visible. The projected distance is calculated as:

$$\text{projectedDist} = \sqrt{\text{squareDist}}\,, \tag{13}$$

where the square distance is:

$$\text{squareDist} = (x_A - x_B)^2 + (y_A - y_B)^2 + (z_A - z_B)^2\,, \tag{14}$$

and (x, y, z) are the Cartesian coordinates of both galaxies projected in the plan of galaxy B, and subscripts A and B designate the coordinates of galaxies A and B, respectively.

The spherical coordinates are converted to Cartesian coordinates as follows:

$$\begin{aligned} x &= r_B \cos\theta \sin\varphi\,, \\ y &= r_B \cos\theta \cos\varphi\,, \\ z &= r_B \sin\theta\,, \end{aligned} \tag{15}$$

where r_B is the radial distance of galaxy B required to project galaxy A into the plan of galaxy B. The critical distance is calculated as:

$$\text{criticalDist} = \frac{r_B}{r_A} R_A + R_B\,, \tag{16}$$

where R_A and R_B are the respective radii of galaxies A and B. The ratio of radial distances, r_B/r_A, applied to the radius of galaxy A represents the projection of galaxy A into the plan of galaxy B according to Thales' theorem.

For the special case when the foreground galaxy A lies over galaxy B but covers it only partially (see Fig. 1), we consider galaxy B to be not visible. The zCosmos galactic survey was obtained using an automated device, and an algorithm cannot identify a galaxy that is not isolated from other sources of light. Still, galaxy B could hide more distant galaxies.

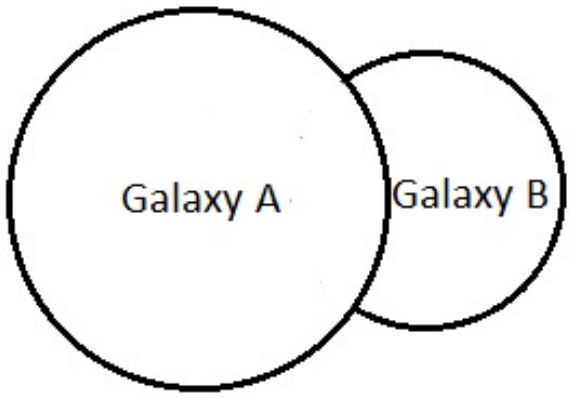

Fig. 1: A foreground galaxy partially covering a more distant galaxy.

Finally, we count the visible galaxies in each redshift bucket and multiply the counts by the ratio of the survey area to the simulated spectroscopic area in order to have numbers that are comparable between the survey and the simulation.

To generate the declination and right ascension angles of a galaxy, we used the Mersenne Twister algorithm [5], which is a pseudo-random number generator based on the Mersenne prime $2^{19937} - 1$. The algorithm has a very long period of $2^{19937} - 1$ and passes numerous tests for statistical randomness.

2.4 Galactic density and radius function of redshifts

In the dichotomous cosmology, where the material world is static and the luminous world is expanding, the galactic density is constant over time, but the image of galaxies is dilated by a factor of $(1 + z)$, because the expanding luminous world acts like a magnifying glass. Because light is stretched, the apparent size of galaxies is also stretched by the same factor, resulting in a lensing effect across the whole sky. In contrast, in the expanding universe theory, the galactic density increases by a factor $(1 + z)^3$ as we look back in time.

The radius of a galaxy in an expanding universe can be tackled in two different ways. If we consider that the whole space expands, then the galactic radius expands over time and is divided by the factor $(1 + z)$. Because the expanding universe has the same magnifying effect as the expanding luminous world, the galactic radius is also multiplied by a factor of $(1 + z)$. The net effect is that the galactic radius is constant over time, as in Expanding Cosmology A in Table 1. The other approach is to consider that galaxies do not expand in size, but because of the magnifying effect of the expansion, the image of the galaxies is dilated by a factor $(1 + z)$, as in Expanding Cosmology B in Table 1.

In Table 1, ρ_0 is the present galactic density, and R_0 is the present average galactic radius. Because of the cluster of galaxies around the Milky Way, the number of galaxies in the bucket with redshift 0.1 was generated to match the galactic density of the survey. For buckets with redshifts above 0.1, we used the functions in Table 1.

3 Results and discussion

3.1 Galactic density curves

For both the survey and simulated galactic density curves, we used redshift buckets of size $\delta z = 0.1$. We used 0.082 square degrees as the spectroscopic area for the dichotomous cosmology simulation. We used a smaller value of 0.025 square degrees for the expanding universe theory because of the large number of galaxies generated. For the Hubble constant employed in the cosmological model (6), we used a value of $H_0 = 67.3\,\text{km}\,\text{s}^{-1}\,\text{Mpc}^{-1}$, or $2.16 \times 10^{-18}\,\text{sec}^{-1}$ [1].

Figure 2 shows the simulated galactic density curve for the dichotomous cosmology versus the galactic density curve obtained from the survey. For this simulation, we used a constant galactic density of $\rho = 3 \times 10^6$ galactic counts per cubic Glyr (billion light years) and an average galactic radius of $R = 40,000\,(1 + z)$ light years. The factor $(1 + z)$ accounts for the magnifying effect of the expanding luminous world in the dichotomous cosmology (see section 2.4).

The present average galactic radius of 40,000 light years is within the range of dwarf galaxies and large galaxies. In

Table 1: Galactic density and radius functions of redshifts for the dichotomous cosmology and expanding universe theory.

	Galactic density	Galactic radius
Dichotomous Cosmology	ρ_0	$R_0(1+z)$
Expanding Cosmology A	$\rho_0(1+z)^3$	R_0
Expanding Cosmology B	$\rho_0(1+z)^3$	$R_0(1+z)$

[6], the galaxies were divided into two groups based on their respective mass: a group with $M_* \approx 10^{11} M_\odot$, corresponding to dwarf galaxies, and a group with $M_* > 10^{11.5} M_\odot$, corresponding to large galaxies. According to that study, the present average radius of dwarf galaxies is 20, 200 light years, whereas that of large galaxies is 65, 200 light years. Because dwarf galaxies are much more numerous than large galaxies, we would expect the overall average galactic radius to be smaller than 40, 000 light years. The gravitational lensing effect that creates a halo around galaxies, and some blurring effect from the luminosity of galaxies, can be accounted for by the fact that foreground galaxies obstruct the images of distant galaxies over a larger area than that of the circle defined by the intrinsic radius of the foreground galaxies. Furthermore, a minimum distance must be observed between galaxies for the selection algorithm of the telescope to be able to identify the galaxies as being distinct from one another.

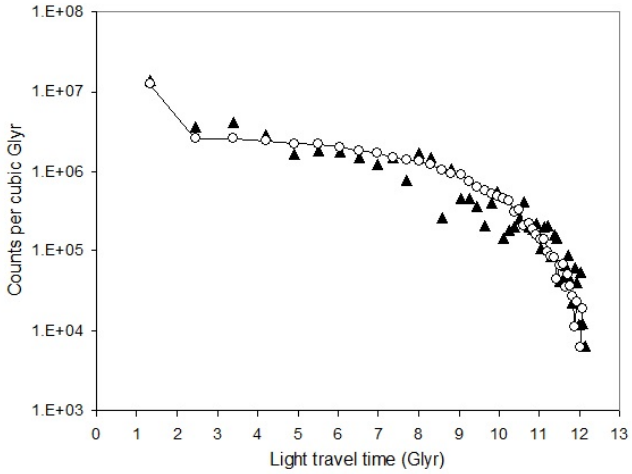

Fig. 2: Galactic density curve for the dichotomous cosmology. Glyr are billion light years. The solid triangles indicate densities based on the zCosmos survey. The open dots indicate densities obtained by Monte Carlo simulation for the dichotomous cosmology with a galactic radius of 40,000 light years.

Figure 3 shows the simulated galactic density curve for Expanding Cosmology A versus the galactic density curve obtained from the survey. The galactic density used for this simulation was $\rho = 3 \times 10^6 (1+z)^3$ counts per cubic Glyr. Two curves were simulated with an average galactic radius of 48, 000 and 78, 000 light years, respectively. The grounds for using a constant galactic radius in Expanding Cosmology A are explained in Section 2.4. In this cosmology, we can vary ρ_0 and R_0, and there is no solution such that the simulated galactic density curve matches the galactic density curve of the survey.

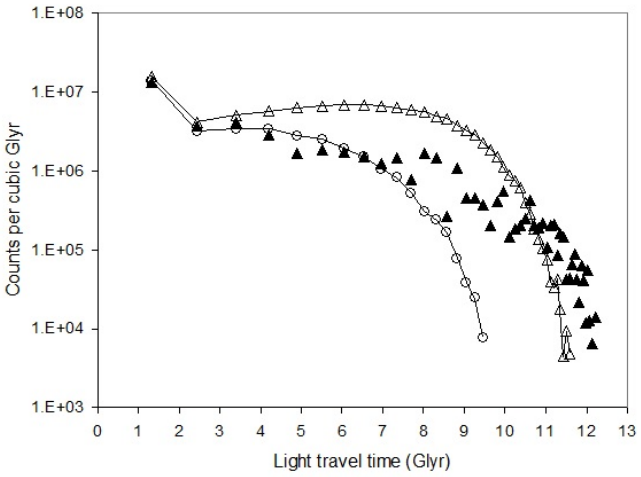

Fig. 3: Galactic density curve for Expanding Cosmology A, where Glyr are billion light years. The solid triangles indicate densities based on the zCosmos survey. The open dots indicate densities obtained by Monte Carlo simulation with a galactic radius of 78,000 light years. The open triangles are the simulated densities obtained with a galactic radius of 48,000 light years.

Figure 4 shows the simulated galactic density curve for Expanding Cosmology B versus the galactic density curve obtained from the survey. We again used a galactic density $\rho = 3 \times 10^6 (1+z)^3$ counts per cubic Glyr. The two curves simulated for this cosmology have an average galactic radius of $R = 40,000(1+z)$ light years and $R = 13,000(1+z)$ light years, respectively. There is no solution for Expanding Cosmology B such that the simulated galactic density curve matches the galactic density curve of the survey.

3.2 Size-biased selection in galactic surveys

As the redshift increases, the number of foreground galaxies increases, leaving only small areas where more distant galaxies can be observed. This effect of increasing redshifts decreases the likelihood of selecting large galaxies and smaller galaxies are preferentially selected. This size-biased selection

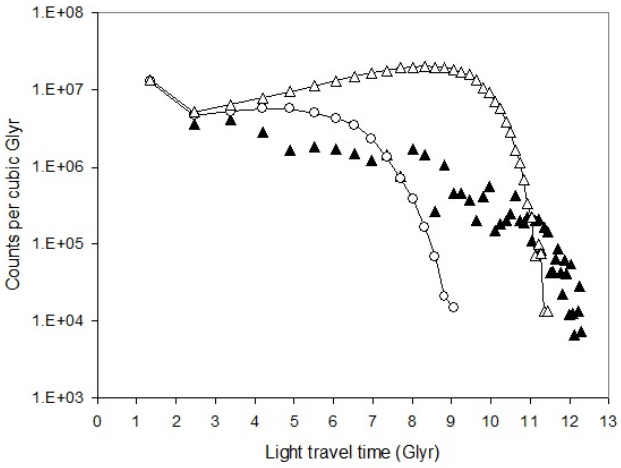

Fig. 4: Galactic density curve for Expanding Cosmology B. Glyr are billion light years. The solid triangles indicate densities based on the zCosmos survey. The open dots indicate densities obtained by Monte Carlo simulation with a galactic radius of 40,000 light years. The open triangles are the simulated densities obtained with a galactic radius of 13,000 light years.

could have a significant impact on studies of the morphological evolution of galaxies. The effect of size-biased selection can be quantified by using a Monte Carlo simulation to generate galactic radii with a size distribution obtained from galactic surveys at low redshifts.

4 Conclusion

We developed a Monte Carlo simulation framework to test cosmologies. The framework is based on the sampling method of the zCosmos galactic survey. We used simulations to generate a theoretical galactic density curve for a given cosmology. The theoretical density curve was then compared with the galactic density curve obtained from the galactic survey. We applied the test to the flat-universe de Sitter cosmology and to a dichotomous cosmology.

The simulated galactic density curve of the dichotomous cosmology matched the survey galactic density curve remarkably well. For the expanding universe classes that we considered, there was no solution such that the simulated galactic density curve matched the galactic density curve of the survey. On the basis of this test, we conclude that the dichotomous cosmology provides an accurate description of the physics underlying cosmological redshifts.

5 Acknowledgements

This work is based on zCOSMOS observations carried out using the Very Large Telescope at the ESO Paranal Observatory under Programme ID: LP175.A-0839. I would also like to thank Prof. Arto Annila for insightful comments and our inspiring discussion.

Submitted on July 20, 2014 / Accepted on July 28, 2014

References

1. Heymann Y. On the Luminosity Distance and the Hubble Constant. *Progress in Physics*, 2013, v. 3, 5–6.
2. Heymann Y. The Dichotomous Cosmology with a Static Material World and Expanding Luminous World. *Progress in Physics*, 2014, v. 10, 178–181.
3. Lilly S. J., Le Fevre O., Renzini A., Zamorani G., Scodeggio M., Contini T., Carollo C. M., Hasinger G., Kneib J.-P., Lovino A., Le Brun V., Mainieri V., Mignoli M., Silverman J., Tasca L. A. M., Bolzonella M., Bongiorno A., Bottini D., Capak P., Caputi K., Cimatti A., Cucciati O., Daddi E., Feldmann R., Franzetti P., Garilli B., Guzzo L., Ilbert O., Kampczyk P., Kovak K., Lamareille F., Leauthaud A., Le Borgne J.-F., McCracken H. J., Marinoni C., Pello R., Ricciardelli E., Scarlata C., Vergani D., Sanders D. B., Schinnerer E., Scoville N., Taniguchi Y., Arnouts S., Aussel H., Bardelli S., Brusa M., Cappi A., Ciliegi P., Finoguenov A., Foucaud S., Franceshini R., Halliday C., Impey C., Knobel C., Koekemoer A., Kurk J., Maccagni D., Maddox S., Marano B., Marconi G., Meneux B., Mobasher B., Moreau C., Peacock J. A., Porciani C., Pozzetti L., Scaramella R., Schiminovich D., Shopbell P., Smail I., Thompson D., Tresse L., Vettolani G., Zanichelli A., and Zucca E. zCosmos: A Large VLT/VIMOS Redshift Survey Covering $0 < z < 3$ in the COSMOS Field. *The Astrophysical Journal Supplement Series*, 2007, v. 172, 70–85.
4. Heymann Y. Building galactic density profiles. *Progress in Physics*, 2011, v. 4, 63–67.
5. Matsumoto M., and Nishimura T. Mersenne Twister: a 623-dimensionally equidistributed uniform pseudo-random number generator. *ACM Transactions on Modeling and Computer Simulation - Special issue on uniform random number generation*, 1998, v. 8, 3–30.
6. Stringer M. J., Shankar F., Novak G. S., Huertas-Company M., Combes F., and Moster B. P. Galaxy size trends as a consequence of cosmology. arxiv: abs/1310.3823.

Climate Change Resulting from Lunar Impact in the Year 1178 AD

David W. Chapman

Gold Mountain Technology, PO Box 1240, Palo Alto, CA 94302. E-mail: dave@goldmountain.com

In June of the year 1178, an impact was observed on the Moon. Within a few years, Europe experienced a climatic event known as the Little Ice Age. Calculations of the reduction in sunlight due to dust in high earth orbit are consistent with the historical temperature decrease. Other past temperature reductions may have resulted from similar impacts on the Moon.

1 Historical events

Shortly after sunset on June 25, 1178 AD, a large explosion occurred on the surface of the Moon. This event was observed by several people in Canterbury, England and recorded in the Chronicles of Gervase. The Julian calendar date was June 18, or June 25 Gregorian.

> In this year on the Sunday before the feast of St John the Baptist, after sunset when the Moon had first become visible, a marvellouse phenomenon was witnessed by some five or more men ...and suddenly the upper horn slit in two. From the midpoint of this division a flaming torch sprang up, spewing out over a considerable distance fire, hot coals and sparks. Meanwhile the body of the Moon which was below, writhed, as it were in anxiety... and throbbed like a wounded snake. Afterwards it resumed its proper state. This phenomenon was repeated a dozen times or more, the flames assuming various twisting shapes at random and then returning to normal. Then after these transformations the Moon from horn to horn, that is along its whole length took on a blackish appearance. [4]

2 The crater Giordano Bruno

This event was caused by the impact of a comet or asteroid onto the surface of the Moon, in the approximate area 45 degrees North latitude, 90 degrees East longitude. The crater named Giordano Bruno is believed to have been formed by this impact [6]. Giordano Bruno is a crater which is 20 kilometres in diameter, having unusually sharp rims and an extremely large system of rays. Sharp rims are indicative of recent formation, since micro-meteorites cause erosion which gradually softens land features on the surface of the Moon. Rays, which are believed to be powered material ejected during the crater's formation, do not last very long and are also regarded as evidence of very recent formation. The physical features and location of this crater are consistent with its having been formed by the event of 1178.

3 Energy of crater formation

When an object, such as a comet or asteroid, impacts the surface of the Moon, it penetrates a relatively short distance before being slowed to sub-sonic velocity. Once this has happened, vaporized material from the impact site expands up and out, forming a fireball and a crater. Factors such as the density of the impactor, the density of the target, and the angle of impact affect the size of the final crater. The most important factor is the total energy of the impacting projectile. In general, calculations involving the crater size will provide only a minimum energy of crater formation. Various formulae have been published which relate the size of a crater to the impact parameters. These formulae show a high sensitivity to the exponent used for the energy, and produce results which rarely have more than one digit of accuracy.

The first method of estimating the energy of formation of the crater is to calculate the energy using a formula which was calibrated with actual data from nuclear bomb tests and multi-ton conventional explosions.

The relationship between crater size and explosion size for an optimal crater forming explosion is the Glasstone formula [5]:

$$\text{Yield} = \left(\frac{\text{Crater Radius at Lip}}{62.5 \text{ meters}} \right)^{3.33} .$$

Yield is quoted in kilotons of TNT, which are defined in this context as 4.184×10^{12} Joules. In standard format:

$$D = 2.03 \times 10^{-2} \, E^{0.3003},$$

where D is crater diameter in meters, E is energy in Joules.

The crater Giordano Bruno has a radius of 10 km, or 10,000 meters. Using the Glasstone formula gives an explosion energy of 21,800,000 kilotons, or $9.1 \times E^{19}$ Joules. This is approximately the energy required to vaporize 21 Gigatons of rock.

A second formula has been published, based on similar data sets, the Dence formula [3]. This formula is for a crater produced by an explosion (sphere or hemisphere) on a flat surface):

$$D = 1.96 \times 10^{-2} \, E^{0.294},$$

where D is crater diameter in meters, E in energy in Joules.

Using the Dence formula gives 2.74×10^{20} Joules, or 65.5 Gigatons. This is larger than the Glasstone number by a factor of 3, which shows the difference between an optimal depth crater-forming explosion and a surface explosion.

The third method of estimating the energy of formation of the crater relies on laboratory data and computer simulations. The de Pater formula is [2]:

$$D = 1.8\rho_i^{0.11}\rho_t^{-0.33}g_t^{-0.22}\ (\sin\theta)^{0.333}\ (2r)^{0.13}\ E^{0.22}.$$

These parameters are as follows:

$D = 20,000$	crater diameter	meters,
$\rho_i = 2$	density of impactor	gram/cm^3,
$\rho_t = 3.333$	density of the Moon	gram/cm^3,
$g_t = 1.625$	gravity of the Moon	meters/sec^2,
$\theta = 45$	impact angle	degrees,
$r = 300$	radius	meters,
$v = 28,000$	velocity of impact	meters/sec,
E	energy	Joules.

This formula requires us to either make an assumption about the velocity of the incoming object, or about its mass (radius). Because of the date of the impact, the object which caused Giordano Bruno is believed to be part of the Taurid meteor complex, which would imply an impact velocity of 28000 meters/sec and a density of 2. Based on these numbers, the radius of the impactor is calculated to be 300 meters, which gives an energy of impact formula of

$$20000 = 1.8 \times 1.08 \times 0.67 \times 0.90 \times 0.89 \times 2.3 \times E^{0.22},$$

which resolves to 6.6×10^{17} Joules (158 Megatons). This is less than 1% of the Glasstone number.

The fourth method is to measure the volume of the crater in cubic meters, estimate the weight of the material which was removed, and estimate how much energy was required to remove the material. The way it works is to model the crater as a hemi-spheroid, then find the mass of the ejecta, and then to calculate the energy required to lift the ejecta to an altitude equal to the crater radius. This method produces a minimalistic number, and is intended as a sanity check on the other methods:

$$\begin{aligned}
\text{volume} &= \tfrac{2}{3}\pi \times \text{radius}^2 \times \text{depth} \\
&= \tfrac{2}{3}\pi \times 10000^2 \times 1000 \\
&= 2.09 \times 10^{11} && \text{m}^3, \\
\text{mass} &= \text{volume} \times 1000 \times \text{density} \\
&= (2.09 \times 10^{11}) \times 1000 \times 3.333 \\
&= 7.0 \times 10^{14} && \text{kg}, \\
E &= \text{mass} \times \text{g} \times \text{altitude} \\
&= (7 \times 10^{14}) \times 1.625 \times 10000 \\
&= 1.1 \times 10^{19} && \text{Joules}, \\
&= 2.7 && \text{Gigatons}.
\end{aligned}$$

In standard form, this is:

$$D = 1.9 \times 10^{-1} \times E^{0.25}.$$

Note that this formula produces a number which is proportional to the crater radius to the one-fourth power. This is consistent with the simplest formula published [2].

The four methods of estimating the energy of formation of the crater are as follows:

Glasstone	9.1×10^{19}	Joules,
Dence	2.7×10^{20}	Joules,
de Pater	6.2×10^{17}	Joules,
volume method	1.1×10^{19}	Joules.

What is interesting is how much effect the exponent in the formula has:

Glasstone	$E^{0.30}$,
Dence	$E^{0.29}$,
de Pater	$E^{0.22}$,
volume method	$E^{0.25}$.

A relatively small change in the exponent between Glasstone and Dence produced a relatively large change between those two results, and the de Pater result is far away from the others. Given that the Glasstone formula is described as calculating an explosion *at optimal cratering depth*, I suspect that the true number is somewhere between Glasstone and Dence. The best estimate for the energy of crater formation is therefore 1×10^{20} Joules.

4 Historical temperature decrease

Various historical records indicate a global temperature decrease starting in approximately the year 1190 AD [7]. The grape crop in England, which was moderately large in the year 1100, had dwindled to almost nothing by the year 1300. The records of harbour freezing in Reykjavik, Iceland, indicate that the weather became sharply colder around the year 1200. At the same time, the growing season in Greenland became so short that the Viking colonies there were abandoned. Poland and Russia experienced a major famine in the year 1215 AD, which was attributed to the cold weather causing large-scale crop failures:

> ...in AD 1215, when early frosts destroyed the harvest throughout the district around Novgorod, people ate pine bark and sold their children into slavery for bread, "many common graves were filled with corpses, but they could not bury them all. ...those who remained alive hastened to the sea".
>
> Other bad years came in 1229 and 1230, and in the latter there were many incidents of cannibalism "over the whole district of Russia with the sole exception of Kiev". [8]

Outside of Europe, tree ring data from around the world suggests that the planet became colder starting in the late 1100's [1, 7]. This temperature drop amounted to approximately 1 degree Kelvin.

5 Reduction in sunlight arriving on the planet

These recorded temperature declines are consistent with a reduction in the amount of sunlight arriving on the planet. To reduce the global temperature from 283 to 282 degrees Kelvin using a gray-body model would require that incident radiation be reduced by a factor $1-(282/283)^4$, or 1.4%. Using a more realistic model which includes positive feedback, only half of the temperature reduction needs to be caused by a decrease in sunlight. With a positive feedback model, we find that radiation needs to be reduced by a factor of $1-(282.5/283)^4$, which equals 0.7%. Such a temperature reduction would be caused by lunar dust orbiting the Earth.

The most efficient reduction in sunlight per unit mass results from dust particles approximately 1 micron in diameter. Dust particles smaller than this do not absorb light efficiently; they scatter it. Dust particles larger than 1 micron have a reduced surface area relative to their mass, and are less efficient at blocking sunlight.

Given that the required area density of dust particles is 0.7%, we find that 7×10^9 particles are needed per square meter of the Earth's surface. Assuming a dust cloud as high as the Moon, this equals an average particle density of 17.5 particles per cubic meter, or a total of 5.8×10^{26} particles:

$$\begin{aligned}\text{area shadow} &= 0.007/1\times10^{-12}\\ &= 7\times10^9 \text{ particles/m}^3,\\ \text{density of particles} &= 7\times10^9/4\times10^8\\ &= 17.5 \text{ particles/m}^3.\end{aligned}$$

An orbiting dust cloud can be modelled as a solid sphere which contains uniformly distributed particles. The cloud's radius is assumed to be at the altitude of the Moon (400,000 km). The volume is therefore:

$$\text{volume cloud} = \tfrac{4}{3}\,\pi\,(4\times10^8)^3 = 2.7\times10^{26}\text{ m}^3.$$

Assuming a mass density of 2, each particle would have a mass of 2×10^{-15} kilograms, which gives a mass for the total cloud of 9.5×10^{12} kilograms, or approximately 9.5 Gigatons:

$$\begin{aligned}\text{mass}_{\text{particle}} &= 2\times(1\times10^{-5})^3 = 2\times10^{-15}\text{ kg},\\ \text{mass}_{\text{total}} &= 2\times10^{-15}\times17.5\times2.7\times10^{26} = 9.5\times10^{12}\text{ kg}.\end{aligned}$$

The escape velocity of the Moon is 2373 m/sec, or 2.8×10^6 Joules per kilogram of mass removed from the Moon's gravity well. This gives a total energy required to lift the dust cloud of 2.6×10^{19} Joules, which is less than the calculated energy of the event:

$$E_{\text{orbital}} = 0.5\times(9.5\times10^{12})\times2373^2 = 2.6\times10^{19}\text{ Joules}.$$

Since not all of the energy went into placing matter into high earth orbit, and since not all of the orbiting matter is in the form of optimal light-blocking dust, we could expect an efficiency of perhaps 5% in converting the original explosion into an orbiting dust cloud. The indicated efficiency, given that the explosion was 1×10^{20} Joules, is 26%. This suggests that the actual energy of the crater-forming explosion was closer to the Dence number, above.

6 Orbital characteristics of a dust cloud

An orbiting dust cloud such as the one described above would not be stable. Individual particles would experience perturbations in their orbit due to the Moon's gravity, and would also be subject to orbital change due to solar wind, atmospheric drag, and collision with other particles.

In the intermediate term, particles colliding with each other would cause the cloud to assume the shape of a ring. In the long term, the particles would be removed from orbit.

The orbital velocity of the Moon is approximately 1000 meters/sec. For a dust particle moving through the dust cloud described above, the mean distance between collisions would be approximately 1.4×10^{10} meters, which is 1.4×10^7 seconds, or 6 months:

$$\begin{aligned}\text{cross section collision} &= 4\times(1\times10^{-6})^2\times17.5\\ &= 7\times10^{-11}\text{ m}^3,\\ \text{mean free path} &= 1/(7\times10^{-11})\\ &= 1.4\times10^{10}\text{ m},\\ \text{mean collision interval} &= \text{mean free path/velocity}\\ &= 1.4\times10^{10}/1000\\ &= 1.4\times10^7\text{ sec}.\end{aligned}$$

How long the cloud would remain in orbit depends on various assumptions regarding its initial orbital characteristics and the level of solar wind activity. An orbital half-life of a few decades seems reasonable.

7 Evidence of Lunar impacts in marine sediments

Much of the mass placed into earth orbit would be recaptured by the Moon, and some would escape to solar orbit, but some large fraction would be deposited on the surface of the Earth. Assuming that some large fraction of the dust eventually was deposited on the surface of the Earth, it should be possible to locate the characteristic Titanium Oxide from the Moon rock in marine sediment or polar ice core samples. If half of the total orbiting dust cloud was deposited on the Earth's surface, there would be approximately 5 grams/square meter. Of this, perhaps 10% (0.5 grams) would be Titanium.

$$\begin{aligned}\text{dust density} &= 50\%\times\text{mass}_{\text{total}}/\text{Earth surface area}\\ &= 0.5\times(9.5\times10^{12})/(4\pi\times(6.3\times10^6)^2)\\ &= 0.00475\text{ kg/m}^2,\\ \text{titanium density} &= 0.10\times\text{dust density}\\ &= 0.000475\text{ kg/m}^2.\end{aligned}$$

It must also be considered that many of the major ice ages were caused by orbiting dust from the Moon, and that they will also have left traces in the marine sediments. An examination of the sediment samples would show whether the Ice Age which began 15,000 years ago was also caused by an object impacting on the Moon.

8 Objections to this idea

It has been suggested that, after an impact on the Moon similar to the one described in this paper, a large amount of debris would impact the Earth a few days later. It has also been suggested that these impacts would create a spectacular meteor storm, and that the absence of such a meteor storm in the historical record suggests that there was no such impact in the year 1178.

Analysis shows that most of the debris would not create dramatic effects, and that the amount of light emitted by the impacts would be diffuse.

Objects falling from the altitude of the Moon will have an impact velocity approximately equal to the escape velocity of the Earth (11200 meters/sec). The energy released by a 1 micro-gram particle (the size of a grain of sand) impacting at this speed is 62.7 Joules. When this enters the Earth's atmosphere, it will look like a 60-Watt light bulb shining for one second, which is probably not going to create a big psychological impact. Dust particles will produce an even less dramatic effect. Even if 10 Megatons of lunar regolith and dust particles were to hit the Earth in the first month after the impact, it would only add up to 6×10^{14} Joules, or 240 Megawatts. More to the point, this is 4 micro-watts per square meter of the Earth's surface, which is less than 1% of the light from a full Moon.

This amount of light concentrated into a small number of fireballs might be noticed, but spread into billions of individual particles, the energy released would not be spectacular.

Submitted on August 08, 2014 / Accepted on August 12, 2014

References

1. Cook E. et al. Tree ring climate data. *Science*, Science, v. 253, 1266–1268.
2. De Pater I. and Lissauer J.J. Planetary Sciences. Cambridge University Press, 2005, page 165.
3. Dence M.C., Grieve R.A.F., and Robertson P.B. Terrestrial impact structures: Principal characteristics and energy consideration. In: *Impact and explosion cratering*, Pergamon Press, Oxford, 1977.
4. Gervase of Canterbury 1178: Chronicles Trinity College. Cambridge, UK.
5. Glasstone S. The Effects of Nuclear Weapons. US Department of Defence, 1977.
6. Hughes D.W. Giordano Bruno, the Moon's Latest Large Crater. *Nature*, 1976, v. 264, 212–213.
7. Lamb H.H. Climate: Past, Present, and Future, Volume I. Methuen, London, 1977.
8. Lamb H.H. Climate: Past, Present, and Future, Volume II. Methuen, London, 1977.

Dimension of Physical Space

Gunn Quznetsov

E-mail: gunn@mail.ru, quznets@yahoo.com

Each vector of state has its own corresponing element of the CayleyDickson algebra. Properties of a state vector require that this algebra was a normalized division algebra. By the Hurwitz and Frobenius theorems maximal dimension of such algebra is 8. Consequently, a dimension of corresponding complex state vectors is 4, and a dimension of the Clifford set elements is 4×4. Such set contains 5 matrices — among them — 3-diagonal. Hence, a dimension of the dot events space is equal to 3+1.

Further I use CayleyDickson algebras [1, 2]:

Let

$$1, \mathrm{i}, \mathrm{j}, \mathrm{k}, \mathrm{E}, \mathrm{I}, \mathrm{J}, \mathrm{K}$$

be basis elements of a 8-dimensional algebra Cayley (*the octavians algebra*) [1, 2]. A product of this algebra is defined the following way [1]:

1) For every basic element e:

$$\mathrm{ee} = -1;$$

2) If u_1, u_2, v_1, v_2 are real number then

$$(u_1 + u_2\mathrm{i})\,(v_1 + v_2\mathrm{i}) = (u_1v_1 - v_2u_2) + (v_2u_1 + u_2v_1)\,\mathrm{i}.$$

3) If u_1, u_2, v_1, v_2 are numbers of shape $w = w_1 + w_2\mathrm{i}$ (w_s, and $s \in \{1, 2\}$ are real numbers, and $\overline{w} = w_1 - w_2\mathrm{i}$) then

$$(u_1 + u_2\mathrm{j})\,(v_1 + v_2\mathrm{j}) = (u_1v_1 - \overline{v}_2u_2) + (v_2u_1 + u_2\overline{v}_1)\,\mathrm{j} \quad (1)$$

and $\mathrm{ij} = \mathrm{k}$.

4) If u_1, u_2, v_1, v_2 are number of shape $w = w_1 + w_2\mathrm{i} + w_3\mathrm{j} + w_4\mathrm{k}$ (w_s, and $s \in \{1, 2, 3, 4\}$ are real numbers, and $\overline{w} = w_1 - w_2\mathrm{i} - w_3\mathrm{j} - w_4\mathrm{k}$) then

$$(u_1 + u_2\mathrm{E})\,(v_1 + v_2\mathrm{E}) = (u_1v_1 - \overline{v}_2u_2) + (v_2u_1 + u_2\overline{v}_1)\,\mathrm{E} \quad (2)$$

and

$$\mathrm{iE} = \mathrm{I},$$
$$\mathrm{jE} = \mathrm{J},$$
$$\mathrm{kE} = \mathrm{K}.$$

Therefore, in accordance with point 2) the real numbers field (**R**) is extended to the complex numbers field (**R**), and in accordance with point 3) the complex numbers field is expanded to the quaternions field (**K**), and point 4) expands the quaternions fields to the octavians field (**O**). This method of expanding of fields is called *a Dickson doubling procedure* [1].

If

$$u = a + b\mathrm{i} + c\mathrm{j} + d\mathrm{k} + A\mathrm{E} + B\mathrm{I} + C\mathrm{J} + \mathrm{K}$$

with real a, b, c, d, A, B, C, D then a real number

$$\|u\| := \sqrt{u\overline{u}} = \left(a^2 + b^2 + c^2 + d^2 + A^2 + B^2 + C^2 + D^2\right)^{0.5}$$

is called *a norm* of octavian u [1].

For each octavians u and v:

$$\|uv\| = \|u\|\,\|v\|\,. \quad (3)$$

Algebras with this conditions are called *normalized algebras* [1, 2].

Any 3+1-vector of a probability density can be represented by the following equations in matrix form [4, 5]

$$\rho = \varphi^\dagger\varphi\,,$$
$$j_k = \varphi^\dagger\beta^{[k]}\varphi$$

with $k \in \{1, 2, 3\}$.

There $\beta^{[k]}$ are complex 2-diagonal 4×4-matrices of Clifford's set of rank 4, and φ is matrix columns with four complex components. The light and colored pentads of Clifford's set of such rank contain in threes 2-diagonal matrices, corresponding to 3 space coordinates in accordance with Dirac's equation. Hence, a space of these events is 3-dimensional.

Let $\rho(t, \mathbf{x})$ be a probability density of event $A\,(t, \mathbf{x})$, and

$$\rho_c(t, \mathbf{x}|t_0, \mathbf{x}_0)$$

be a probability density of event $A\,(t, \mathbf{x})$ on condition that event $B\,(t_0, \mathbf{x}_0)$.

In that case if function $q(t, \mathbf{x}|t_0, \mathbf{x}_0)$ is fulfilled to condition:

$$\rho_c(t, \mathbf{x}|t_0, \mathbf{x}_0) = q(t, \mathbf{x}|t_0, \mathbf{x}_0)\rho(t, \mathbf{x}), \quad (4)$$

then one is called *a disturbance function* B to A.

If $q = 1$ then B does not disturbance to A.

A conditional probability density of event $A\,(t, \mathbf{x})$ on condition that event $B\,(t_0, \mathbf{x}_0)$ is presented as:

$$\rho_c = \varphi_c^\dagger\varphi_c$$

like to a probability density of event $A\,(t, \mathbf{x})$.

Let

$$\varphi = \begin{bmatrix} \varphi_{1,1} + \mathrm{i}\varphi_{1,2} \\ \varphi_{2,1} + \mathrm{i}\varphi_{2,2} \\ \varphi_{3,1} + \mathrm{i}\varphi_{3,2} \\ \varphi_{4,1} + \mathrm{i}\varphi_{4,2} \end{bmatrix}$$

and

$$\varphi_c = \begin{bmatrix} \varphi_{c,1,1} + \mathrm{i}\varphi_{c,1,2} \\ \varphi_{c,2,1} + \mathrm{i}\varphi_{c,2,2} \\ \varphi_{c,3,1} + \mathrm{i}\varphi_{c,3,2} \\ \varphi_{c,4,1} + \mathrm{i}\varphi_{c,4,2} \end{bmatrix}$$

(all $\varphi_{r,s}$ and $\varphi_{c,r,s}$ are real numbers).

In that case octavian

$$u = \varphi_{1,1} + \varphi_{1,2}\mathrm{i} + \varphi_{2,1}\mathrm{j} + \varphi_{2,2}\mathrm{k} + \varphi_{3,1}\mathrm{E} + \\ + \varphi_{3,2}\mathrm{I} + \varphi_{4,1}\mathrm{J} + \varphi_{4,2}\mathrm{K}$$

is called *a Caylean* of φ. Therefore, octavian

$$u_c = \varphi_{c,1,1} + \varphi_{c,1,2}\mathrm{i} + \varphi_{c,2,1}\mathrm{j} + \varphi_{c,2,2}\mathrm{k} + \varphi_{c,3,1}\mathrm{E} + \\ + \varphi_{c,3,2}\mathrm{I} + \varphi_{c,4,1}\mathrm{J} + \varphi_{c,4,2}\mathrm{K}$$

is Caylean of φ_c.

In accordance with the octavian norm definition:

$$\begin{aligned} \|u_c\|^2 &= \rho_c\,, \\ \|u\|^2 &= \rho\,. \end{aligned} \tag{5}$$

Because the octavian algebra is a division algebra [1, 2] then for each octavians u and u_c there exists an octavian w such that

$$u_c = wu.$$

Because the octavians algebra is normalized then

$$\|u_c\|^2 = \|w\|^2 \|u\|^2\,.$$

Hence, from (4) and (5):

$$q = \|w\|^2\,.$$

Therefore, in a 3+1-dimensional space-time there exists an octavian-Caylean for a disturbance function of any event to any event.

In order to increase a space dimensionality the octavian algebra can be expanded by a Dickson doubling procedure:

Another 8 elements should be added to basic octavians:

$$\mathrm{z}_1,\ \mathrm{z}_2, \mathrm{z}_3,\ \mathrm{z}_4,\ \mathrm{z}_5,\ \mathrm{z}_6,\ \mathrm{z}_7,\ \mathrm{z}_8$$

such that:

$$\begin{aligned} \mathrm{z}_2 &= \mathrm{i}\mathrm{z}_1, \\ \mathrm{z}_3 &= \mathrm{j}\mathrm{z}_1, \\ \mathrm{z}_4 &= \mathrm{k}\mathrm{z}_1, \\ \mathrm{z}_5 &= \mathrm{E}\mathrm{z}_1, \\ \mathrm{z}_6 &= \mathrm{I}\mathrm{z}_1, \\ \mathrm{z}_7 &= \mathrm{J}\mathrm{z}_1, \\ \mathrm{z}_8 &= \mathrm{K}\mathrm{z}_1, \end{aligned}$$

and for every octavians u_1, u_2, v_1, v_2:

$$(u_1 + u_2\mathrm{z}_1)(v_1 + v_2\mathrm{z}_1) = (u_1v_1 - \overline{v}_2u_2) + (v_2u_1 + u_2\overline{v}_1)\,\mathrm{z}_1$$

(here: if $w = w_1 + w_2\mathrm{i} + w_3\mathrm{j} + w_4\mathrm{k} + w_5\mathrm{E} + w_6\mathrm{I} + w_7\mathrm{J} + w_8\mathrm{K}$ with real w_s then $\overline{w} = w_1 - w_2\mathrm{i} - w_3\mathrm{j} - w_4\mathrm{k} - w_5\mathrm{E} - w_6\mathrm{I} - w_7\mathrm{J} - w_8\mathrm{K}$).

It is a 16-dimensional Cayley-Dickson algebra.

In accordance with [3], for any natural number z there exists a Clifford set of rank 2^z. In considering case for $z = 3$ there is Clifford's seven:

$$\underline{\beta}^{[1]} = \begin{bmatrix} \beta^{[1]} & 0_4 \\ 0_4 & -\beta^{[1]} \end{bmatrix},\ \underline{\beta}^{[2]} = \begin{bmatrix} \beta^{[2]} & 0_4 \\ 0_4 & -\beta^{[2]} \end{bmatrix}, \tag{6}$$

$$\underline{\beta}^{[3]} = \begin{bmatrix} \beta^{[3]} & 0_4 \\ 0_4 & -\beta^{[3]} \end{bmatrix},\ \underline{\beta}^{[4]} = \begin{bmatrix} \beta^{[4]} & 0_4 \\ 0_4 & -\beta^{[4]} \end{bmatrix}, \tag{7}$$

$$\underline{\beta}^{[5]} = \begin{bmatrix} \gamma^{[0]} & 0_4 \\ 0_4 & -\gamma^{[0]} \end{bmatrix}, \tag{8}$$

$$\underline{\beta}^{[6]} = \begin{bmatrix} 0_4 & 1_4 \\ 1_4 & 0_4 \end{bmatrix},\ \underline{\beta}^{[7]} = \mathrm{i}\begin{bmatrix} 0_4 & -1_4 \\ 1_4 & 0_4 \end{bmatrix}. \tag{9}$$

Therefore, in this seven five 4-diagonal matrices (7) define a 5-dimensional space of events, and two 4-antidiagonal matrices (9) defined a 2-dimensional space for the electroweak transformations.

It is evident that such procedure of dimensions building up can be continued endlessly. But in accordance with the Hurwitz theorem* and with the generalized Frobenius theorem† a more than 8-dimensional Cayley-Dickson algebra does not a division algebra. Hence, there in a more than 3-dimensional space exist events such that a disturbance function between these events does not hold a Caylean. I call such disturbance *supernatural*.

Therefore, supernatural disturbance do not exist in a 3-dimensional space, but in a more than 3-dimensional space such supernatural disturbance act.

Submitted on August 15, 2014 / Accepted on August 17, 2014

References

1. Kantor I.L.; Solodownikow A.S. Hipercomplex Numbers, Nauka, Moscow, 1973, p. 99; Kantor I.L.; Solodownikow A.S. Hyperkomplexe Zahlen. B. G. Teubner, Leipzig, 1978.
2. Mel'nikov O.V., Remeslennikov V.N. et al. General Algebra. Nauka, Moscow, 1990, p. 396.
3. Zhelnorovich V.A. Theory of Spinors. Application to Mathematics and Physics. Nauka, Moscow, 1982, p. 21.
4. Abers E. Quantum Mechanics. Addison Wesley, 2004, p. 423.
5. Quznetsov G. Final Book on Fundamental Theoretical Physics. American Research Press, American Research Press, Rehoboth (NM), 2011, pp. 60–62.

*Every normalized algebra with unit is isomorphous to one of the following: the real numbers algebra **R**, the complex numbers algebra **C**, the quaternions algebra **K**, the octavians algebra **O** [1].

†A division algebra can be only either 1 or 2 or 4 or 8-dimensional [2].

Informational Time

Gunn Quznetsov

E-mail: gunn@mail.ru, quznets@yahoo.com

I call any subjects, connected with an information the informational objects. It is clear that information received from such informational object can be expressed by a text which is made of sentences. I call a set of sentences expressing information about some informational object recorder of this object. Some recorders systems form structures similar to clocks. The following results are obtained from the logical properties of a set of recorders: First, all such clocks have the same direction, i.e. if an event expressed by sentence A precedes an event expressed by sentence B according to one of such clocks then it is true according to the others. Secondly, time is irreversible according to these clocks, i.e. there's no recorder which can receive information about an event that has happened until this event really happens Thirdly, a set of recorders is naturally embedded into metrical space. Fourthly, if this metrical space is Euclidean, then the corresponding "space and time" of recorders obeys to transformations of the complete Poincare group. If this metric space is not Euclidean then suitable non-linear geometry may be built in this space.

Here I use numbering of definitions and theorems from book [1] which contains detailed proofs of all these theorems.

1 Recorders

Any information, received from physical devices, can be expressed by a text, made of sentences.

Let $\widehat{\mathbf{a}}$ be some object which is able to receive, save, and/or transmit an information. *A* set $\mathbf{a}$ of sentences, expressing an information of an object $\widehat{\mathbf{a}}$, is called *a recorder* of this object. Thus, statement: "Sentence $\ll A\gg$ is an element of the set $\mathbf{a}$" denotes: "$\widehat{\mathbf{a}}$ has information that the event, expressed by sentence $\ll A\gg$, took place". In short: "$\widehat{\mathbf{a}}$ knows that *A*". Or by designation: "$\mathbf{a}^\bullet \ll A\gg$".

Obviously, the following conditions are satisfied:

I. For any $\mathbf{a}$ and for every *A*: false is that $\mathbf{a}^\bullet (A\& (\neg A))$, thus, any recorder doesn't contain a logical contradiction;

II. For every $\mathbf{a}$, every *B*, and all *A*: if *B* is a logical consequence from *A*, and $\mathbf{a}^\bullet A$, then $\mathbf{a}^\bullet B$;

*III. For all $\mathbf{a}$, $\mathbf{b}$ and for every *A*: if $\mathbf{a}^\bullet \ll \mathbf{b}^\bullet A\gg$ then $\mathbf{a}^\bullet A$.

2 Time

Let's consider finite (probably empty) path of symbols of form $\mathbf{q}^\bullet$.

Def. 1.3.1: A path α is *a subpath* of a path β (design.: $\alpha \prec \beta$) if α can be got from β by deletion of some (probably all) elements.

Designation: $(\alpha)^1$ is α, and $(\alpha)^{k+1}$ is $\alpha\,(\alpha)^k$.

Therefore, if $k \leqslant l$ then $(\alpha)^k \prec (\alpha)^l$.

Def. 1.3.2: A path α is *equivalent* to a path β (design.: $\alpha \sim \beta$) if α can be got from β by substitution of a subpath of form $(\mathbf{a}^\bullet)^k$ by a path of the same form $(\mathbf{a}^\bullet)^s$.

In this case:

III. If $\beta \prec \alpha$ or $\beta \sim \alpha$ then for any *K*: if $\mathbf{a}^\bullet K$ then $\mathbf{a}^\bullet (K\& (\alpha A \Rightarrow \beta A))$.

Obviously, III is a refinement of condition *III.

Def. 1.3.3: A natural number *q* is *instant*, at which a registrates *B* according to *κ-clock* $\{\mathbf{g}_0, A, \mathbf{b}_0\}$ (design.: *q* is $[\mathbf{a}^\bullet B \uparrow \mathbf{a}, \{\mathbf{g}_0, A, \mathbf{b}_0\}]$) if:

1. for any *K*: if $\mathbf{a}^\bullet K$ then

$$\mathbf{a}^\bullet \left(K\& \left(\mathbf{a}^\bullet B \Rightarrow \mathbf{a}^\bullet \left(\mathbf{g}_0^\bullet \mathbf{b}_0^\bullet\right)^q \mathbf{g}_0^\bullet A\right)\right)$$

and

$$\mathbf{a}^\bullet \left(K\& \left(\mathbf{a}^\bullet \left(\mathbf{g}_0^\bullet \mathbf{b}_0^\bullet\right)^{q+1} \mathbf{g}_0^\bullet A \Rightarrow \mathbf{a}^\bullet B\right)\right).$$

2. $\mathbf{a}^\bullet \left(\mathbf{a}^\bullet B\& \left(\neg \mathbf{a}^\bullet \left(\mathbf{g}_0^\bullet \mathbf{b}_0^\bullet\right)^{q+1} \mathbf{g}_0^\bullet A\right)\right)$.

Def. 1.3.4: *κ*-clocks $\{\mathbf{g}_1, B, \mathbf{b}_1\}$ and $\{\mathbf{g}_2, B, \mathbf{b}_2\}$ have *the same direction* for $\mathbf{a}$ if the following condition is satisfied:

If

$$r = \left[\mathbf{a}^\bullet \left(\mathbf{g}_1^\bullet \mathbf{b}_1^\bullet\right)^q \mathbf{g}_1^\bullet B \uparrow \mathbf{a}, \{\mathbf{g}_2, B, \mathbf{b}_2\}\right],$$

$$s = \left[\mathbf{a}^\bullet \left(\mathbf{g}_1^\bullet \mathbf{b}_1^\bullet\right)^p \mathbf{g}_1^\bullet B \uparrow \mathbf{a}, \{\mathbf{g}_2, B, \mathbf{b}_2\}\right],$$

$$q < p,$$

then

$$r \leqslant s\,.$$

Th. 1.3.1: All *κ*-clocks have the same direction. Consequently, a recorder orders its sentences with respect to instants. Moreover, this order is linear and it doesn't matter according to which *κ*-clock it is established.

Def. 1.3.5: *κ*-clock $\{\mathbf{g}_2, B, \mathbf{b}_2\}$ is *k* times more precise than *κ*-clock $\{\mathbf{g}_1, B, \mathbf{b}_1\}$ for recorder $\mathbf{a}$ if for every *C* the following condition is satisfied: if

$$q_1 = [\mathbf{a}^\bullet C \uparrow \mathbf{a}, \{\mathbf{g}_1, B, \mathbf{b}_1\}],$$
$$q_2 = [\mathbf{a}^\bullet C \uparrow \mathbf{a}, \{\mathbf{g}_2, B, \mathbf{b}_2\}],$$

then

$$q_1 < \tfrac{q_2}{k} < q_1 + 1.$$

Def. 1.3.6: A sequence $\widetilde{H}$ of κ-clocks:

$$\left\langle \{\mathbf{g}_0, A, \mathbf{b}_0\},\ \{\mathbf{g}_1, A, \mathbf{b}_2\}, \ldots, \left\{\mathbf{g}_j, A, \mathbf{b}_j\right\},\ \ldots \right\rangle$$

is called *an absolutely precise* κ-clock of a recorder $\mathbf{a}$ if for every j exists a natural number k_j so that κ-clock$\left\{\mathbf{g}_j, A, \mathbf{b}_j\right\}$ is k_j times more precise than κ-clock$\left\{\mathbf{g}_{j-1}, A, \mathbf{b}_{j-1}\right\}$.

In this case if

$$q_j = \left[\mathbf{a}^\bullet C \uparrow \mathbf{a}, \left\{\mathbf{g}_j, A, \mathbf{b}_j\right\}\right]$$

and

$$t = q_0 + \sum_{j=1}^{\infty} \frac{q_j - q_{j-1} \cdot k_j}{k_1 \cdot k_2 \cdot \ldots \cdot k_j},$$

then

$$t \text{ is } \left[\mathbf{a}^\bullet C \uparrow \mathbf{a}, \widetilde{H}\right].$$

3 Space

Def. 1.4.1: A number t is called *a time, measured by a recorder* $\mathbf{a}$ *according to a* κ*-clock* $\widetilde{H}$*, during which a signal* C *did a path* $\mathbf{a}^\bullet\alpha\mathbf{a}^\bullet$, design.:

$$t := \mathfrak{m}\left(\mathbf{a}\widetilde{H}\right)(\mathbf{a}^\bullet\alpha\mathbf{a}^\bullet C),$$

if

$$t = \left[\mathbf{a}^\bullet\alpha\mathbf{a}^\bullet C \uparrow \mathbf{a}, \widetilde{H}\right] - \left[\mathbf{a}^\bullet C \uparrow \mathbf{a}, \widetilde{H}\right].$$

Th. 1.4.1:

$$\mathfrak{m}\left(\mathbf{a}\widetilde{H}\right)(\mathbf{a}^\bullet\alpha\mathbf{a}^\bullet C) \geqslant 0.$$

Def. 1.4.2:

1) for every recorder $\mathbf{a}$: $(\mathbf{a}^\bullet)^\dagger = (\mathbf{a}^\bullet)$;
2) for all paths α and β: $(\alpha\beta)^\dagger = (\beta)^\dagger(\alpha)^\dagger$.

Def. 1.4.3: A set $\mathfrak{R}$ of recorders is *an internally stationary system* for a recorder $\mathbf{a}$ with a κ-clock $\widetilde{H}$ (design.: $\mathfrak{R}$ is $ISS\left(\mathbf{a}, \widetilde{H}\right)$) if for all sentences B and C, for all elements $\mathbf{a}_1$ and $\mathbf{a}_2$ of set $\mathfrak{R}$, and for all paths α, made of elements of set $\mathfrak{R}$, the following conditions are satisfied:

1) $\left[\mathbf{a}^\bullet\mathbf{a}_2^\bullet\mathbf{a}_1^\bullet C \uparrow \mathbf{a}, \widetilde{H}\right] - \left[\mathbf{a}^\bullet\mathbf{a}_1^\bullet C \uparrow \mathbf{a}, \widetilde{H}\right] =$
$= \left[\mathbf{a}^\bullet\mathbf{a}_2^\bullet\mathbf{a}_1^\bullet B \uparrow \mathbf{a}, \widetilde{H}\right] - \left[\mathbf{a}^\bullet\mathbf{a}_1^\bullet B \uparrow \mathbf{a}, \widetilde{H}\right]$;
2) $\mathfrak{m}\left(\mathbf{a}\widetilde{H}\right)(\mathbf{a}^\bullet\alpha\mathbf{a}^\bullet C) = \mathfrak{m}\left(\mathbf{a}\widetilde{H}\right)\left(\mathbf{a}^\bullet\alpha^\dagger\mathbf{a}^\bullet C\right)$.

Th. 1.4.2:

$$\{\mathbf{a}\} - ISS\left(\mathbf{a}, \widetilde{H}\right).$$

Def. 1.4.4: A number l is called *an* $\mathbf{a}\widetilde{H}(B)$*-measure* of recorders $\mathbf{a}_1$ and $\mathbf{a}_2$, design.:

$$l = \ell\left(\mathbf{a}, \widetilde{H}, B\right)(\mathbf{a}_1, \mathbf{a}_2)$$

if

$$l = 0.5 \cdot \left(\left[\mathbf{a}^\bullet\mathbf{a}_1^\bullet\mathbf{a}_2^\bullet\mathbf{a}_1^\bullet B \uparrow \mathbf{a}, \widetilde{H}\right] - \left[\mathbf{a}^\bullet\mathbf{a}_1^\bullet B \uparrow \mathbf{a}, \widetilde{H}\right]\right).$$

Th. 1.4.3: If $\{\mathbf{a}, \mathbf{a}_1, \mathbf{a}_2, \mathbf{a}_3\}$ is $ISS\left(\mathbf{a}, \widetilde{H}\right)$ then

1) $\ell\left(\mathbf{a}, \widetilde{H}\right)(\mathbf{a}_1, \mathbf{a}_2) \geqslant 0$;
2) $\ell\left(\mathbf{a}, \widetilde{H}\right)(\mathbf{a}_1, \mathbf{a}_1) = 0$;
3) $\ell\left(\mathbf{a}, \widetilde{H}\right)(\mathbf{a}_1, \mathbf{a}_2) = \ell\left(\mathbf{a}, \widetilde{H}\right)(\mathbf{a}_2, \mathbf{a}_1)$;
4) $\ell\left(\mathbf{a}, \widetilde{H}\right)(\mathbf{a}_1, \mathbf{a}_2) + \ell\left(\mathbf{a}, \widetilde{H}\right)(\mathbf{a}_2, \mathbf{a}_3) \geqslant \ell\left(\mathbf{a}, \widetilde{H}\right)(\mathbf{a}_1, \mathbf{a}_3)$.

Thus, all four axioms of the metrical space are accomplished for $\ell\left(\mathbf{a}, \widetilde{H}\right)$ in an internally stationary systeminternally stationary system of recorders.

Consequently, $\ell\left(\mathbf{a}, \widetilde{H}\right)$ is a distance length similitude in this space.

Def. 1.4.6: B took place *in the same place as* $\mathbf{a}_1$ *for* $\mathbf{a}$ (design.: $\natural(\mathbf{a})(\mathbf{a}_1, B)$) if for every sequence α and for any sentence K the following condition is satisfied: if $\mathbf{a}^\bullet K$ then $\mathbf{a}^\bullet\left(K\&(\alpha B \Rightarrow \alpha\mathbf{a}_1^\bullet B)\right)$.

Th. 1.4.4:

$$\natural(\mathbf{a})\left(\mathbf{a}_1, \mathbf{a}_1^\bullet B\right).$$

Th. 1.4.5: If

$$\natural(\mathbf{a})(\mathbf{a}_1, B), \tag{1}$$
$$\natural(\mathbf{a})(\mathbf{a}_2, B), \tag{2}$$

then

$$\natural(\mathbf{a})(\mathbf{a}_2, \mathbf{a}_1^\bullet B).$$

Th. 1.4.6: If $\{\mathbf{a}, \mathbf{a}_1, \mathbf{a}_2\}$ is $ISS\left(\mathbf{a}, \widetilde{H}\right)$,

$$\natural(\mathbf{a})(\mathbf{a}_1, B), \tag{3}$$
$$\natural(\mathbf{a})(\mathbf{a}_2, B), \tag{4}$$

then

$$\ell\left(\mathbf{a}, \widetilde{H}\right)(\mathbf{a}_1, \mathbf{a}_2) = 0.$$

Th. 1.4.7: If $\{\mathbf{a}_1, \mathbf{a}_2, \mathbf{a}_3\}$ is $ISS\left(\mathbf{a}, \widetilde{H}\right)$ and there exists sentence B such that

$$\natural(\mathbf{a})(\mathbf{a}_1, B), \tag{5}$$
$$\natural(\mathbf{a})(\mathbf{a}_2, B), \tag{6}$$

then

$$\ell\left(\mathbf{a}, \widetilde{H}\right)(\mathbf{a}_3, \mathbf{a}_2) = \ell\left(\mathbf{a}, \widetilde{H}\right)(\mathbf{a}_3, \mathbf{a}_1).$$

Def. 1.4.7: A real number t is an instant of a sentence B in *frame of reference* $\left(\mathfrak{R}\mathbf{a}\widetilde{H}\right)$, design.:

$$t = \left[B \mid \mathfrak{R}\mathbf{a}\widetilde{H}\right],$$

if

1) $\mathfrak{R}$ is $ISS\left(\mathbf{a},\widetilde{H}\right)$,
2) there exists a recorder $\mathbf{b}$ so that $\mathbf{b}\in\mathfrak{R}$ and $\natural(\mathbf{a})(\mathbf{b},B)$,
3) $t=\left[\mathbf{a}^{\bullet}B\uparrow\mathbf{a},\widetilde{H}\right]-\ell\left(\mathbf{a},\widetilde{H}\right)(\mathbf{a},\mathbf{b})$.

Def. 1.4.8: A real number z is *a distance length* between B and C in a frame of reference $\left(\mathfrak{R}\mathbf{a}\widetilde{H}\right)$, design.:

$$z=\ell\left(\mathfrak{R}\mathbf{a}\widetilde{H}\right)(B,C),$$

if

1) $\mathfrak{R}$ is $ISS\left(\mathbf{a},\widetilde{H}\right)$,
2) there exist recorders $\mathbf{a}_1$ and $\mathbf{a}_2$ so that $\mathbf{a}_1\in\mathfrak{R}$, $\mathbf{a}_2\in\mathfrak{R}$, $\natural(\mathbf{a})(\mathbf{a}_1,B))$ and $\natural(\mathbf{a})(\mathbf{a}_2,C))$,
3) $z=\ell\left(\mathbf{a},\widetilde{H}\right)(\mathbf{a}_2,\mathbf{a}_1)$.

According to Theorem 1.4.3 such distance length satisfies conditions of all axioms of a metric space.

4 Relativity

Def. 1.5.1: Recorders $\mathbf{a}_1$ and $\mathbf{a}_2$ *equally receive a signal* about B for a recorder $\mathbf{a}$ if

$$\ll\natural(\mathbf{a})\left(\mathbf{a}_2,\mathbf{a}_1^{\bullet}B\right)\gg=\ll\natural(\mathbf{a})\left(\mathbf{a}_1,\mathbf{a}_2^{\bullet}B\right)\gg.$$

Def. 1.5.2: Set of recorders are called *a homogeneous space of recorders*, if all its elements equally receive all signals.

Def. 1.5.3: A real number c is *an information velocity about B to the recorder* $\mathbf{a}_1$ in a frame of reference $\left(\mathfrak{R}\mathbf{a}\widetilde{H}\right)$ if

$$c=\frac{\ell\left(\mathfrak{R}\mathbf{a}\widetilde{H}\right)\left(B,\mathbf{a}_1^{\bullet}B\right)}{\left[\mathbf{a}_1^{\bullet}B\mid\mathfrak{R}\mathbf{a}\widetilde{H}\right]-\left[B\mid\mathfrak{R}\mathbf{a}\widetilde{H}\right]}.$$

Th. 1.5.1: In all homogeneous spaces:

$$c=1.$$

That is in every homogenous space a propagation velocity of every information to every recorder for every frame reference equals to 1.

Th. 1.5.2: If $\mathfrak{R}$ is a homogeneous space, then

$$\left[\mathbf{a}_1^{\bullet}B\mid\mathfrak{R}\mathbf{a}\widetilde{H}\right]\geqslant\left[B\mid\mathfrak{R}\mathbf{a}\widetilde{H}\right].$$

Consequently, in any homogeneous space any recorder finds out that B "took place" not earlier than B "actually take place". "Time" is irreversible.

Th. 1.5.3: If $\mathbf{a}_1$ and $\mathbf{a}_2$ are elements of $\mathfrak{R}$,

$$\mathfrak{R}isISS\left(\mathbf{a},\widetilde{H}\right), \tag{7}$$

$$p:=\left[\mathbf{a}_1^{\bullet}B\mid\mathfrak{R}\mathbf{a}\widetilde{H}\right], \tag{8}$$

$$q:=\left[\mathbf{a}_2^{\bullet}\mathbf{a}_1^{\bullet}B\mid\mathfrak{R}\mathbf{a}\widetilde{H}\right], \tag{9}$$

$$z:=\ell\left(\mathfrak{R}\mathbf{a}\widetilde{H}\right)(\mathbf{a}_1,\mathbf{a}_2),$$

then

$$z=q-p.$$

According to Urysohn's theorem* [2]: any homogeneous space is homeomorphic to some set of points of real Hilbert space. If this homeomorphism is not Identical transformation, then $\mathfrak{R}$ will represent a non- Euclidean space. In this case in this "space-time" corresponding variant of General Relativity Theory can be constructed. Otherwise, $\mathfrak{R}$ is Euclidean space. In this case there exists *coordinates system* R^{μ} such that the following condition is satisfied: for all elements $\mathbf{a}_1$ and $\mathbf{a}_2$ of set $\mathfrak{R}$ there exist points $\mathbf{x}_1$ and $\mathbf{x}_2$ of system R^{μ} such that

$$\ell\left(\mathbf{a},\widetilde{H}\right)(\mathbf{a}_k,\mathbf{a}_s)=\left(\sum_{j=1}^{\mu}\left(x_{s,j}-x_{k,j}\right)^2\right)^{0.5}.$$

In this case R^{μ} is called *a coordinates system of frame of reference* $\left(\mathfrak{R}\mathbf{a}\widetilde{H}\right)$ and numbers $\left\langle x_{k,1},x_{k,2},\ldots,x_{k,\mu}\right\rangle$ are called *coordinates of recorder* $\mathbf{a}_k$ in R^{μ}.

A coordinates system of a frame of reference is specified accurate to transformations of shear, turn, and inversion.

Def. 1.5.4: Numbers $\left\langle x_1,x_2,\ldots,x_{\mu}\right\rangle$ are called *coordinates* of B in *a coordinate system* R^{μ} of *a frame of reference* $\left(\mathfrak{R}\mathbf{a}\widetilde{H}\right)$ if there exists a recorder $\mathbf{b}$ such that $\mathbf{b}\in\mathfrak{R}$, $\natural(\mathbf{a})(\mathbf{b},B)$ and these numbers are the coordinates in R^{μ} of this recorder.

Th. 1.5.4: In a coordinate system R^{μ} of a frame of reference $\left(\mathfrak{R}\mathbf{a}\widetilde{H}\right)$: if z is a distance length between B and C, coordinates of B are

$$(b_1,b_2,\ldots,b_n)$$

coordinates of C are

$$(c_1,c_2,\ldots,c_3)$$

then

$$z=\left(\sum_{j=1}^{\mu}\left(c_j-b_j\right)^2\right)^{0.5}.$$

Def. 1.5.5: Numbers $\left\langle x_1,x_2,\ldots,x_{\mu}\right\rangle$ are called *coordinates of the recor-der* $\mathbf{b}$ *in the coordinate system* R^{μ} *at the instant t of the frame of reference* $\left(\mathfrak{R}\mathbf{a}\widetilde{H}\right)$ if for every B the condition is satisfied: if

$$t=\left[\mathbf{b}^{\bullet}B\mid\mathfrak{R}\mathbf{a}\widetilde{H}\right]$$

then coordinates of $\ll\mathbf{b}^{\bullet}B\gg$ in coordinate system R^{μ} of frame of reference $\left(\mathfrak{R}\mathbf{a}\widetilde{H}\right)$ are the following:

$$\left\langle x_1,x_2,\ldots,x_{\mu}\right\rangle.$$

Let v be the real number such that $|v|<1$.

*Pavel Samuilovich Urysohn, a.k.a. Pavel Uryson (February 3, 1898, Odessa — August 17, 1924, Batz-sur-Mer) was a Jewish mathematician who is best known for his contributions in the theory of dimension, and for developing Urysohn's Metrization Theorem and Urysohn's Lemma, both of which are fundamental results in topology.

Th. 1.5.5: In a coordinates system R^{μ} of a frame of reference $\left(\mathfrak{R}\mathbf{a}\widetilde{H}\right)$: if in every instant t: coordinates of*:

$$\mathbf{b} : \left\langle x_{\mathbf{b},1} + v \cdot t, x_{\mathbf{b},2}, x_{\mathbf{b},3}, \ldots, x_{\mathbf{b},\mu} \right\rangle,$$
$$\mathbf{g}_0 : \left\langle x_{0,1} + v \cdot t, x_{0,2}, x_{0,3}, \ldots, x_{0,\mu} \right\rangle,$$
$$\mathbf{b}_0 : \left\langle x_{0,1} + v \cdot t, x_{0,2} + l, x_{0,3}, \ldots, x_{0,\mu} \right\rangle,$$

and

$$t_C = \left[\mathbf{b}^{\bullet} C \mid \mathfrak{R}\mathbf{a}\widetilde{H}\right],$$
$$t_D = \left[\mathbf{b}^{\bullet} D \mid \mathfrak{R}\mathbf{a}\widetilde{H}\right],$$
$$q_C = \left[\mathbf{b}^{\bullet} C \uparrow \mathbf{b}, \{\mathbf{g}_0, A, \mathbf{b}_0\}\right],$$
$$q_D = \left[\mathbf{b}^{\bullet} D \uparrow \mathbf{b}, \{\mathbf{g}_0, A, \mathbf{b}_0\}\right],$$

then

$$\lim_{l \to 0} 2 \cdot \frac{l}{\sqrt{(1 - v^2)}} \cdot \frac{q_D - q_C}{t_D - t_C} = 1.$$

Consequently, moving at speed v κ-clock are times slower than the one at rest.

Th. 1.5.6: Let: v ($|v| < 1$) and l be real numbers and k_i be natural ones.

Let in a coordinates system R^{μ} of a frame of reference $\left(\mathfrak{R}\mathbf{a}\widetilde{H}\right)$: in each instant t coordinates of

$$\mathbf{b} : \left\langle x_{b,1} + v \cdot t, x_{b,2}, x_{b,3}, \ldots, x_{b,\mu} \right\rangle,$$
$$\mathbf{g}_j : \left\langle y_{j,1} + v \cdot t, y_{j,2}, y_{j,3}, \ldots, y_{j,\mu} \right\rangle,$$
$$\mathbf{u}_j : \left\langle y_{j,1} + v \cdot t, y_{j,2} + l/\left(k_1 \cdot \ldots \cdot k_j\right), y_{j,3}, \ldots, y_{j,\mu} \right\rangle,$$

for all $\mathbf{b}_i$: if $\mathbf{b}_i \in \mathfrak{I}$, then coordinates of

$$\mathbf{b}_i : \left\langle x_{i,1} + v \cdot t, x_{i,2}, x_{i,3}, \ldots, x_{i,\mu} \right\rangle,$$
$$\widetilde{T} \text{ is } \left\langle \{\mathbf{g}_1, A, \mathbf{u}_1\}, \{\mathbf{g}_2, A, \mathbf{u}_2\}, \ldots, \left\{\mathbf{g}_j, A, \mathbf{u}_j\right\}, \ldots \right\rangle.$$

In that case: $\mathfrak{I}$ is $ISS\left(\mathbf{b}, \widetilde{T}\right)$.

Therefore, a inner stability survives on a uniform straight line motion.

Th. 1.5.7: Let:

1) in a coordinates system R^{μ} of a frame of reference $\left(\mathfrak{R}\mathbf{a}\widetilde{H}\right)$ in every instant t:

$$\mathbf{b} : \left\langle x_{\mathbf{b},1} + v \cdot t, x_{\mathbf{b},2}, x_{\mathbf{b},3}, \ldots, x_{\mathbf{b},\mu} \right\rangle,$$
$$\mathbf{g}_j : \left\langle y_{j,1} + v \cdot t, y_{j,2}, y_{j,3}, \ldots, y_{j,\mu} \right\rangle,$$
$$\mathbf{u}_j : \left\langle y_{j,1} + v \cdot t, y_{j,2} + l/\left(k_1 \cdot \ldots \cdot k_j\right), y_{j,3}, \ldots, y_{j,\mu} \right\rangle,$$

for every recorder $\mathbf{q}_i$: if $\mathbf{q}_i \in \mathfrak{I}$ then coordinates of

$$\mathbf{q}_i : \left\langle x_{i,1} + v \cdot t, x_{i,2}, x_{i,3}, \ldots, x_{i,\mu} \right\rangle,$$
$$\widetilde{T} \text{ is } \left\langle \{\mathbf{g}_1, A, \mathbf{u}_1\}, \{\mathbf{g}_2, A, \mathbf{u}_2\}, \ldots, \left\{\mathbf{g}_j, A, \mathbf{u}_j\right\}, \ldots \right\rangle,$$

$$C : \left\langle C_1, C_2, C_3, \ldots, C_{\mu} \right\rangle,$$
$$D : \left\langle D_1, D_2, D_3, \ldots, D_{\mu} \right\rangle,$$
$$t_C = \left[C \mid \mathfrak{R}\mathbf{a}\widetilde{H}\right],$$
$$t_D = \left[D \mid \mathfrak{R}\mathbf{a}\widetilde{H}\right];$$

2) in a coordinates system $R^{\mu\prime}$ of a reference frame $\left(\mathfrak{I}\mathbf{b}\widetilde{T}\right)$:

$$C : \left\langle C'_1, C'_2, C'_3, \ldots, C'_{\mu} \right\rangle,$$
$$D : \left\langle D'_1, D'_2, D'_3, \ldots, D'_{\mu} \right\rangle,$$
$$t'_C = \left[C \mid \mathfrak{I}\mathbf{b}\widetilde{T}\right],$$
$$t'_D = \left[D \mid \mathfrak{I}\mathbf{b}\widetilde{T}\right].$$

In that case:

$$t'_D - t'_C = \frac{(t_D - t_C) - v\,(D_1 - C_1)}{\sqrt{1 - v^2}},$$
$$D'_1 - C'_1 = \frac{(D_1 - C_1) - v\,(t_D - t_C)}{\sqrt{1 - v^2}}.$$

This is the Lorentz spatial-temporal transformation.

Conclusion

Thus, if you have some set of objects, dealing with information, then "time" and "space" are inevitable. And it doesn't matter whether this set is part our world or some other worlds, which don't have a space-time structure initially.

I call such "Time" the Informational Time.

Since, we get our time together with our information system all other notions of time (thermodynamical time, cosmological time, psychological time, quantum time etc.) should be defined by that Informational Time.

Submitted on August 18, 2014 / Accepted on August 20, 2014

References

1. Quznetsov G. Final Book on Fundamental Theoretical Physics. American Research Press, Rehoboth (NM), 2011, 15–48; viXra.org: 1111.0051.
2. Urysohn P. Zum Metrisationsproblem. *Math. Ann.*, 1925, v. 94, 309–315.

*Below v is a real positive number such that $|v| < 1$.

Indications for a Diurnal and Annual Variation in the Anisotropy of Diffusion Patterns — A Reanalysis of Data Presented by J. Dai (2014, Nat. Sci.)

Felix Scholkmann

Bellariarain 10, 8038 Zürich, Switzerland. E-mail: felix.scholkmann@gmail.com

Anisotropic diffusion patterns of a toluidine blue colloid solution in water were recently reported by J. Dai (*Nat. Sci.*, 2014, v. 6 (2), 54–58). According to Dai's observations the fluctuation of anisotropy showed a diurnal and annual periodicity. Since these observations were only qualitatively described in the original manuscript, the data was reassessed by performing a detailed statistical analysis. The analysis revealed that indeed (i) the diffusion patterns exhibit a non-random characteristic (i.e. the maximum diffusion trend is not uniformly distributed), and (ii) a diurnal as well as an annual oscillation could be extracted and modeled with a sinusoidal function. In conclusion, the present analysis supports Dai's findings about anisotropy in diffusion of colloids in water with a daily and annual periodicity. Possible explanations of the observed effect are discussed and suggestions for further experiments are given.

1 Introduction

Recently, J. Dai published an interesting observation [1]: the diffusion of a toluidine blue colloid solution in water measured over a 3-year time span showed anisotropic patterns, i.e. a preferred direction of diffusion (quantified by the maximum diffusion trend (MDT)) could be detected. Additionally, the MDT values showed non-random fluctuations with daily (diurnal) and yearly (annual) periods.

In the manuscript published by Dai the observed diurnal and annual variability was only qualitatively described and lacks a statistical analysis of the obtained data. This fact motivated the author of the present paper to reassess the data by performing a detailed statistical analysis. Thus, the aim of the present paper was to reanalyze the interesting experimental results reported by Dai using statistical methods.

2 Materials and methods

As reported by Dai [1] the experimental setup and the procedure was following: a circular plastic disc, covered in a container, was filled with deionized water, and 10 µl of a 0.5% Toluidine blue ($C_{15}H_{16}ClN_3S$) solution was dropped in the center of the disc filled with water. Under constant illumination and temperature, the developing diffusion pattern was then photographed at different times (t = 30 s, 630 s, 1230 s, 1830 s and 2430 s; i.e. every 10 minutes for 40 minutes after initially waiting 30 seconds). The MDT with respect to the local north-south direction of the geomagnetic field (0° = 360° = east, clockwise scaling) was determined according to the diffusion trend at t = 1830 s. According to Dai, the diffusion experiment was performed on 15 days between December 22, 2011 and March 23, 2013. On each day, the experiment was repeated each hour over the whole day (i.e. 24 experiments/day).

For the subsequent analysis, the raw data were extracted from Figure 3 of [1]. The analysis aimed to address two specific questions: (i) Do the measured MDT values follow a uniform distribution (indicating that the underlying process is purely random)? To evaluate this, the values for each day were tested using the Chi-square test to determine whether they obey a uniform distribution. The significance level was set to $\alpha = 0.05$. (ii) Is there a diurnal and annual oscillation present in the data? This was analyzed using two approaches. First, a sinusoidal function of the form $f(\mathrm{MDT}) = a_0 + a_1 \cos(\mathrm{MDT}\omega)$ (with the free parameters a_0, a_1 and ω) was fitted to the daily and the seasonally grouped data using the Trust-Region-Reflective Least Squares Algorithm. The grouping of the data according to the seasons was performed as in Dai (i.e. Table 1 of [1]). Second, it was tested whether the distributions of the MDT values differ for the four seasons. Therefore a nonparametric test (Wilcoxon rank-sum test) was employed. Due to the multiple comparison situations, a False Discovery Rate correction to the obtained p-values was applied. The data analysis was performed in Matlab (version 2008b, The MathWorks, Natick, Massachusetts).

3 Results

Figure 1(a) shows the raw (hourly) MDT data as obtained from Figure 3 of [1]. In Figure 2(b), the median values and the respective median absolute deviations of daily intervals are plotted. The data grouped according to the seasons are depicted in Figure 2(c), and Figure 2(d) shows the block average for the daily values.

The analysis about the randomness in the data revealed that neither the daily nor the seasonally grouped MDT values follow a uniform distribution ($p < 0.05$). The seasonally grouped data showed a significant trend: the MDT values in spring were higher compared to summer ($p < 0.0001$), autumn ($p < 0.0001$) and winter ($p = 0.0131$) whereas no statistically significant difference could be detected between the distribution of the MDT values for the combinations summer vs. autumn ($p = 0.7269$), summer vs. winter ($p = 0.8509$)

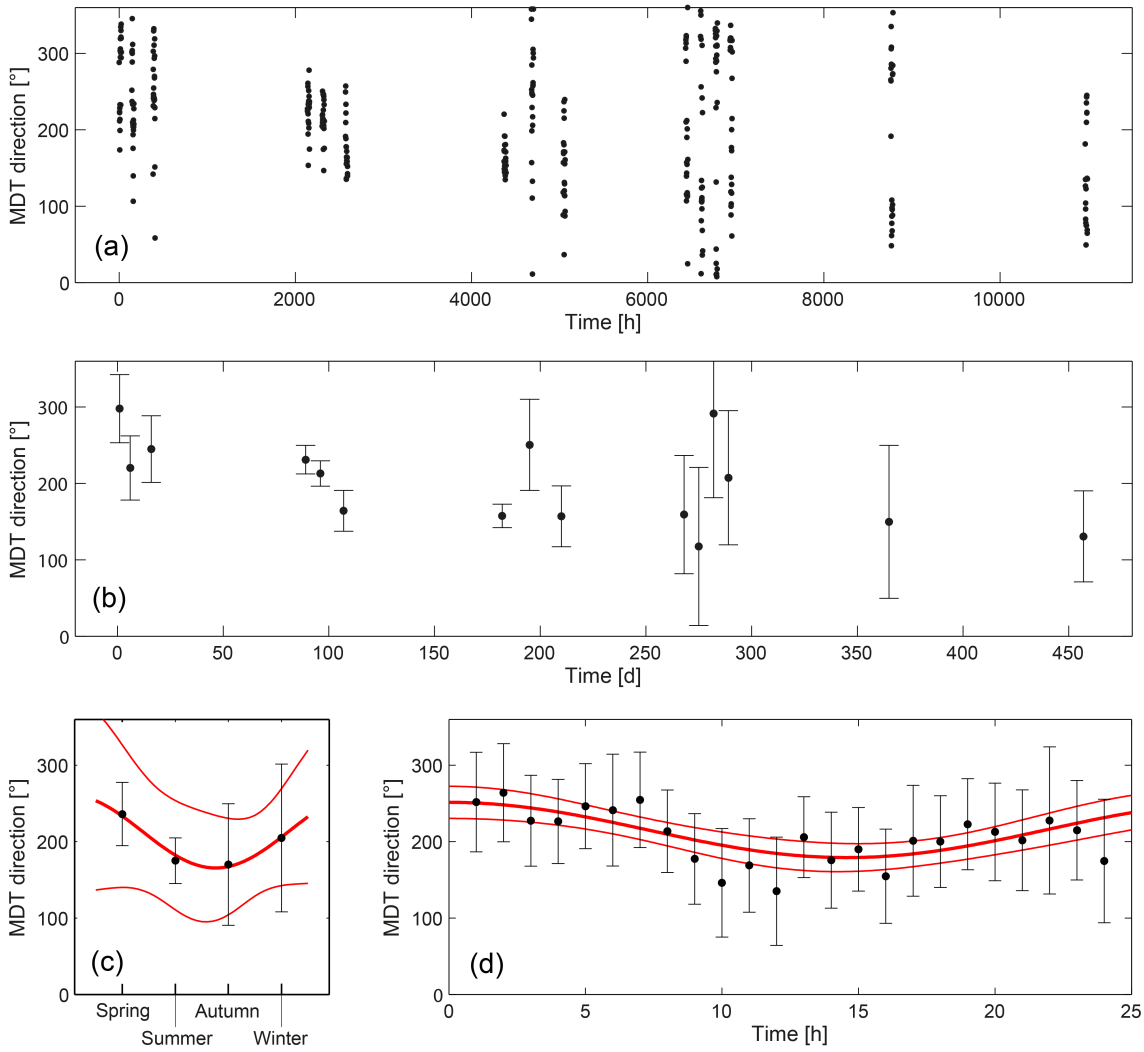

Fig. 1: (a) Raw data as given in Table 1 and Figure 1 of Dai [1]. (b) Daily averaged MDT values (median ± median absolute deviation). (c) Averages MDT values according to the seasons with fitted sinusoidal function (bold red line) and error bounds (95%, thin red lines). (d) Block average of daily MDT values with fitted sinusoidal function (bold red line) and error bounds (95%, thin red lines).

and autumn vs. winter ($p = 0.8902$). Fitting a sinusoidal function to the daily and seasonally grouped MDT data resulted in a good correlation quantified by the squared Pearson correlation coefficient (r^2) and root-mean-square error (RMSE): (i) seasonally grouped data: $r^2 = 0.9821$, RMSE = 50.25, and (ii) daily grouped data: $r^2 = 0.4885$, RMSE = 26.21. The fit with a linear function showed lower r^2 values (seasonally grouped data: $r^2 = 0.1735$, RMSE = 33.96, daily grouped data: $r^2 = 0.1579$, RMSE = 32.86).

4 Discussion

Based on the analysis performed the following two conclusion can be drawn:

(i) The measured MDT values obtained by Dai do not follow a random uniform distribution, i.e. there is a statistically significant ($p < 0.05$) trend in the direction of diffusion.

(ii) The MDT value fluctuations are not random either, i.e. a diurnal and annual oscillation explains the variability better than a linear fit.

Both conclusions are in agreement with the conclusion drawn by Dai in the original paper [1]. In order to establish the causes behind these observations, three possibilities should be considered:

Systematic errors. Changes in environmental parameters (e.g. temperature, humidity, pressure and illumination), electrostatic effects and surface irregularities of the experimental setup could have an effect on diffusion processes observed. However, even though such effects could explain the first finding (i.e. non-randomness of the MDT data) the second find-

ing (i.e. diurnal and seasonal periods in the MDT data) is hard to explain since such systemic influences must then create gradients in the diffusion process with diurnal and annual variability. In a temperature-controlled room with constant illumination and with a setup operating on a flat surface (as was the case according to Dai [1]) the formation of such periodic changes of spatial gradients is quite unlikely.

Classical geophysical and astrophysical effects. Particles of a medium in a rotating system experience a deviation of the isotropic distribution due to the centrifugal and Coriolis force [2]. Whereas the centrifugal force causes a radially outward drift of the particles, the Coriolis force induces a force perpendicular to the particle's direction of motion. Considering the earth's rotation and it's revolution around the sun, a net force can be calculated that represents a "helical force field over the earth" [3]. As discussed by He et al. [3–6] this force has a diurnal and annual variability. Another possible factor contributing to the anisotropic diffusion may be the anisotropy in arrival direction of cosmic rays. The anisotropy of cosmic rays is well documented [7–11], but it is difficult to explain how cosmic rays would cause the changes in MDT since the transported momentum of cosmic rays is very small (e.g. for a muon with a mass of $1883531475 \times 10^{-28}$ kg and travelling with light speed, a momentum in the order of 10^{-11} Ns results).

Other effects. A third option in explaining the experimental results of Dai is to consider them caused by (i) the "anisotropy of space" (as experimentally investigated over decades by Shnoll et al. [12–17]), interaction with (ii) the (quantum) vacuum (which, according to experimental findings of Graham and Lahoz, can be regarded as "something in motion" [18]), (iii) a "cosmological vector potential" [19], or (iv) a fundamental medium [20–31], also regarded as a "complex tension field" [32]. In this context, a relation of the observed anisotropic diffusion to the Saganc effect [33–36] should be considered too. Dai himself considers the observed effect caused by a global astrophysical force or entity (termed "universal field") [1, 37]. In addition, the anisotropic diffusion effect could be related to the signal (with an annual oscillation) detected by the DAMA/LIBRA/NaI experiments designed to detect dark matter [38–40], or the observation of direction-dependent temporal fluctuations in radiation from radon in air at confined conditions [41–43]. Finally, the effect could be related to the observation of an annual fluctuation in radioactive decay which was reported by several groups so far (e.g. [44–47]).

The most similar experiment to the present one was conducted by Kaminsky & Shnoll [12] who analyzed the dynamical behavior of fluctuations of the velocity of Brownian motion. Therefore, the motion fluctuations of two aqueous suspensions of 450-nm polystyrene microspheres were measured by dynamic light scattering. By analyzing the dynamical characteristics of the fluctuations with the histogram analysis method developed by the research group of Shnoll, it was discovered that the "shapes of the histograms in the independent Brownian generators vary synchronously". In a further analysis it could be shown that the direction of the experimental setup with respect to the cardinal directions has an influence on the results: the shape of the histograms were most similar when the recorded time series were not shifted to each other (in case of the alignment to the north-south direction), or shifted with $\Delta t = 11.6$ ms (in case of the alignment to the west-east direction). This clearly indicates that there is an anisotropy of the observed effect. One could speculate that the source of this anisotropy and the source of the anisotropy of diffusion as described in the present paper are similar, or even identical.

5 Conclusion

In conclusion, the re-analysis of the data obtained by Dai [1] revealed that measured MDT values (i) do not follow a random uniform distribution, and (ii) exhibit two fluctuations with a daily and annual period, respectively. For further research, the diffusion experiments need to be repeated and the experimental setup optimized. Examples of optimization include improved shielding the experimental setups against environmental influences and the simultaneous measurement of environmental parameters (e.g. temperature, humidity, pressure, illumination, acceleration of the setup in all three directions of space, fluctuations of the geomagnetic field, etc.). Performing the same experiment simultaneously at different geographical positions could also put forward new indications about the origin of the effect. Also repeating the experiments with different kinds of shielding could offer new insights.

Acknowledgement

I thank Prof. Jiapei Dai (Wuhan Institute for Neuroscience and Neuroengineering, South-Central University of Nationalities, Wuhan, China) for discussions and manuscript reviews, and Rachel Scholkmann for proofreading of the manuscript.

Submitted on August 23, 2014 / Accepted on September 1, 2014

References

1. Dai J. Macroscopic anisotropic Brownian motion is related to the directional movement of a "Universe field". *Natural Science*, 2014, v. 6 (2), 54–58.
2. Welander P. Note on the effect of rotation on diffusion processes. *Tellus*, 1965, v. 18 (1), 63–66.
3. He Y. J., Qi F. & Qi S. C. Effect of chiral helical force field on molecular helical enantiomers and possible origin of biomolecular homochirality. *Medical Hypotheses*, 1998, v. 51 (2), 125–128.
4. He Y. J., Qi F., & Qi S. C. Effect of earth's orbital chirality on elementary particles and unification of chiral asymmetries in life on different levels. *Medical Hypotheses*, 2000, v. 54 (5), 783–785.
5. He Y. J., Qi F., & Qi S. C. Periodicity of Earth's orbital chirality and possible mechanism of biological rhythms. *Medical Hypotheses*, 2000, v. 55 (3), 253–256.

6. He Y. J., Qi F., & Qi S. C. Earth's orbital chirality and driving force of biomolecular evolution. *Medical Hypotheses*, 2001, v. 56 (4), 493–496.
7. Amenomori M., Ayabe S., Bi X. J., Chen D., Cui S. W., Danzengluobu, et al. Anisotropy and corotation of galactic cosmic rays. *Science*, 2006, v. 314 (5798), 439–443.
8. Guillian G., Hosaka J., Ishihara K., Kameda J., Koshio Y., Minamino A., et al. Observation of the anisotropy of 10 TeV primary cosmic ray nuclei flux with the Super-Kamiokande-I detector. *Physical Review D*, 2007, v. 75, 062003.
9. Hayashida N., Nagano M., Nishikawa D., Ohoka H., Sakaki N., Sasaki M., et al. The anisotropy of cosmic ray arrival directions around 10^{18} eV. *Astroparticle Physics*, 1999, v. 10 (4), 303–311.
10. Monstein C., & Wesley J. P. Solar system velocity from muon flux anisotropy. *Apeiron*, 1996, v. 3 (2), 33–37.
11. Schwadron N. A., Adams F. C., Christian E. R., Desiati P., Frisch P., Funsten H. O., et al. (2014). Global anisotropies in TeV cosmic rays related to the sun's local galactic environment from IBEX. *Science*, 2014, v. 343 (6174), 988–990.
12. Kaminsky A. V., & Shnoll S. E. Cosmophysical factors in the fluctuation amplitude spectrum of brownian motion. *Progress in Physics*, 2010, v. 3, 25–30.
13. Rubinstein I. A., Kaminskiy A. V., Tolokonnikova A. A., Kolombet V. A., & Shnoll S. E. Basic phenomena of "macroscopic fluctuations" are repeated on light beams generated by lasers or light-emitting diodes. *Biophysics*, 2014, v. 59 (3), 492–502.
14. Shnoll S. E. Changes in the fine structure of stochastic distributions as a consequence of space-time fluctuations. *Progress in Physics*, 2006, v. 2 (2), 39–45.
15. Shnoll S. E. Cosmophysical factors in stochastic processes. American Research Press, Rehoboth (New Mexico, USA), 2012.
16. Shnoll S. E. Fractality, "coastline of the universe", movement of the Earth, and "macroscopic fluctuations". *Biophysics*, 2013, v. 58 (2), 265–282.
17. Shnoll S. E. On the cosmophysical origin of random processes. *Progress in Physics*, 2014, v. 10 (4), 207–208.
18. Graham G. M., & Lahoz D. G. Observation of static electromagnetic angular momentum in vacuo. *Nature*, 1980, v. 285, 154–155.
19. Baurov Yu A. Global Anisotropy of Physical Space. Nova Science Publishers, New York (USA), 2004.
20. Cahill R. T. Discovery of dynamical 3-space: Theory, experiments and observations – A review. *American Journal of Space Science*, 2013, v. 1 (2), 77–93.
21. Carvalho M. & Oliveira A. L. A new version of the Dirac's æther and its cosmological applications. *Foundations of Physics Letters*, 2003, v. 16 (3), 255–263.
22. Consoli M., Pluchino A., Rapisarda A., & Tudisco S. The vacuum as a form of turbulent fluid: Motivations, experiments, implications. *Physica A: Statistical Mechanics and its Applications*, 2014, v. 394, 61–73.
23. Davies P. Out of the ether: the changing face of the vacuum. *New Scientist*, 2011, v. 212 (2839), 50–52.
24. Davies P. C. W. Quantum vacuum friction. *Journal of Optics B: Quantum and Semiclassical Optics*, 2005, v. 7 (3), S40–S46.
25. Lee T. D. Is the physical vacuum a medium? *Transactions of the New York Academy of Sciences*, 1980, v. 40 (1), 111–123.
26. Michelson A. A. The relative motion of the earth and the luminiferous ether. *American Journal of Science*, 1881, v. 22, 120–129.
27. Michelson A. A. & Morley E. On the relative motion of the earth and the luminiferous ether. *American Journal of Science*, 1887, v. 34 (203), 333–345.
28. Miller D. C. The ether-drift experiment and the determination of the absolute motion of the earth. *Reviews of Modern Physics*, 1933, v. 5 (3), 203–242.
29. Rothall D. P., & Cahill, R. T. Dynamical 3-Space: Observing gravitational wave fluctuations and the Shnoll effect using a Zener diode quantum detector. *Progress in Physics*, 2014, v. 10 (1), 16–18.
30. Shaw D. W. Flowing aether: A concept. *Physics Essays*, 2013, v. 26 (4), 523–530.
31. Zlosnik T. G., Ferreira P. G. & Starkman G. D. Modifying gravity with the aether: An alternative to dark matter. *Physical Review D*, 2007, v. 75, 044017.
32. Roychoudhuri C. Next frontier in physics – Space as a complex tension field. *Journal of Modern Physics*, 2012, v. 3 (10), 1357–1368.
33. Bouyer P. The centenary of Sagnac effect and its applications: From electromagnetic to matter waves. *Gyroscopy and Navigation*, 2014, v. 5 (1), 20–26.
34. Gift S. J. G. Light transmission and the Sagnac effect on the rotating earth. *Applied Physics Research*, 2013, v. 5 (5), 93–106.
35. Malykin G. B. Sagnac effect and Ritz ballistic hypothesis (Review). *Optics and Spectroscopy*, 2010, v. 109v (6), 951–965.
36. Velikoseltsev A., Schreiber U., Klügel T., Voigt S., & Graham R. Sagnac interferometry for the determination of rotations in geodesy and seismology. *Gyroscopy and Navigation*, 2010, v. 1 (4), 291–296.
37. Dai J. "Universe collapse model" and its roles in the unification of four fundamental forces and the origin and the evolution of the universe. *Natural Science*, 2012, v. 4 (4), 199–203.
38. Bernabei R., Belli P., Capella F., Caracciolo V., Castellano S., Cerulli R., et al. The annual modulation signature for dark matter: DAMA/LIBRA-phase1 results and perspectives. *Advances in High Energy Physics*, 2014, 605659.
39. Bernabei R., Belli P., Capella F., Cerulli R., Dai C. J., d'Angelo A., et al. First results from DAMA/LIBRA and the combined results with DAMA/NaI. *The European Physical Journal C*, 2008, v. 56 (3), 333–355.
40. Ling F.-S., Sikivie P., & Wick S. Diurnal and annual modulation of cold dark matter signals. *Physical Review D*, 2004, v. 79, 123503.
41. Steinitz G., Kotlarsky P., & Piatibratova O. Anomalous non-isotropic temporal variation of gamma-radiation from radon (progeny) within air in confined conditions. *Geophysical Journal International*, 2013, v. 193, 1110–1118.
42. Steinitz G., Piatibratova, O., & Gazit-Yaari N. Influence of a component of solar irradiance on radon signals at 1 km depth, Gran Sasso, Italy. *Proceedings of the Royal Society A*, 2013, v. 469 (2159), 20130411.
43. Steinitz G., Piatibratova O., & Kotlarsky P. Sub-daily periodic radon signals in a confined radon system. *Journal of Environmental Radioactivity*, 2014, v. 134, 128–135.
44. Sturrock P. A., Fischbach E., Javorsek II D, Lee R. H., Nistor J. & Scargle, J.D. Comparative study of beta-decay data for eight nuclides measured at the Physikalisch-Technische Bundesanstalt. *Astroparticle Physics*, 2014, v. 59, 47–58.
45. O'Keefe D., Morreale B. L., Lee R. H., Buncher J. B., Jenkins J. H., Fischbach E., Gruenwald T, Javorsek II D & Sturrock P.A. Spectral content of 22Na/44Ti decay data: implications for a solar influence. *Astrophysics and Space Science*, 2013, v. 344 (2), 297–303.
46. Jenkins J. H., Fischbach E, Buncher J. B., Gruenwald J. T., Krause D. E., Mattes J.J. Evidence of correlations between nuclear decay rates and Earth–Sun distance. *Astrophysics and Space Science*, 2009, v. 32 (1), 42–46.
47. Parkhomov A. G. Deviations from beta radioactivity exponential drop. *Journal of Modern Physics*, 2011, v. 2 (11), 1310–1317.

Solar Flare Five-Day Predictions from Quantum Detectors of Dynamical Space Fractal Flow Turbulence: Gravitational Wave Diminution and Earth Climate Cooling

Reginald T. Cahill

School of Chemical and Physical Sciences, Flinders University, Adelaide 5001, Australia. Email: reg.cahill@flinders.edu.au

Space speed fluctuations, which have a 1/f spectrum, are shown to be the cause of solar flares. The direction and magnitude of the space flow has been detected from numerous different experimental techniques, and is close to the normal to the plane of the ecliptic. Zener diode data shows that the fluctuations in the space speed closely match the Sun Solar Cycle 23 flare count, and reveal that major solar flares follow major space speed fluctuations by some 6 days. This implies that a warning period of some 5 days in predicting major solar flares is possible using such detectors. This has significant consequences in being able to protect various spacecraft and Earth located electrical systems from the subsequent arrival of ejected plasma from a solar flare. These space speed fluctuations are the actual gravitational waves, and have a significant magnitude. This discovery is a significant application of the dynamical space phenomenon and theory. We also show that space flow turbulence impacts on the Earth's climate, as such turbulence can input energy into systems, which is the basis of the Zener Diode Quantum Detector. Large scale space fluctuations impact on both the sun and the Earth, and as well explain temperature correlations with solar activity, but that the Earth temperatures are not caused by such solar activity. This implies that the Earth climate debate has been missing a key physical process. Observed diminishing gravitational waves imply a cooling epoch for the Earth for the next 30 years.

1 Introduction

We report evidence that space flow turbulence causes solar flares, and that very simple Zener Diode Quantum Detectors, ZDQD, may be easily used to measure and characterise this turbulence. As well the major space flow turbulence precedes the solar flare eruptions by some 6 days, making it possible to have an early warning system in operation so as to limit damage to spacecraft electronics, power system networks, and other electronic infrastructure systems, when the resulting plasma reaches Earth. We demonstrate these developments by two methods: 1st by showing that the current fluctuations from ZDQD over the last Solar Cycle 23 track very accurately the Solar Flare count rate, see Fig. 1. Those correlations do not establish any causal relation. However in Fig. 6 we establish that significant space speed fluctuations cause the solar flares, as the flares are delayed by some 6 days. The solar flare data is of the Halloween Space Weather Storm of 2003, while the ZDQD data is from a GCP detector*.

*The GCP network is a worldwide collection of Zener Diode detectors that report space fluctuations every 1 sec. However it was not set up for that purpose, and was incorrectly based on the belief that quantum fluctuations are truly random and intrinsic to each quantum system, see http://noosphere.princeton.edu/. The GCP network was then being used to suggest that correlations in the network data were not caused by any physical process, but by collective human "consciousness". This has been shown to be false, as the correlated fluctuations have been shown to be caused by flowing space turbulence [1–3].

2 Dynamical space

The dynamics and detection of space is a phenomenon that physics missed from its beginning, with space modelled as a geometric entity without structure or time dependence. That has changed recently with the determination of the speed and direction of the solar system through the dynamical space, and the characterisation of the flow turbulence: gravitational waves. Detections used various techniques have all produced the same speed and direction Cahill [1–6]. The detected dynamical space was missing from all conventional theories in physics: Gravity, Electromagnetism, Atomic, Nuclear, Climate,... The detection of the dynamical space has led to a major new and extensively tested theory of reality, and goes under the general name of Process Physics [7]. Here we cite only those aspects relevant to Solar Flares and Climate Change.

The Schrödinger equation extension to include the dynamical space is [8]

$$i\hbar\frac{\partial\psi(\mathbf{r},t)}{\partial t} = -\frac{\hbar^2}{2m}\nabla^2\psi(\mathbf{r},t) + V(\mathbf{r},t)\psi(\mathbf{r},t) + -i\hbar\left(\mathbf{v}(\mathbf{r},t)\cdot\nabla + \frac{\mathbf{1}}{\mathbf{2}}\nabla\cdot\mathbf{v}(\mathbf{r},\mathbf{t})\right)\psi(\mathbf{r},t). \quad (1)$$

Here $\mathbf{v}(\mathbf{r},t)$ is the velocity field describing the dynamical space at a classical field level, and the coordinates $\mathbf{r}$ give the relative location of $\psi(\mathbf{r},t)$ and $\mathbf{v}(\mathbf{r},t)$, relative to a Euclidean embedding space, and also used by an observer to

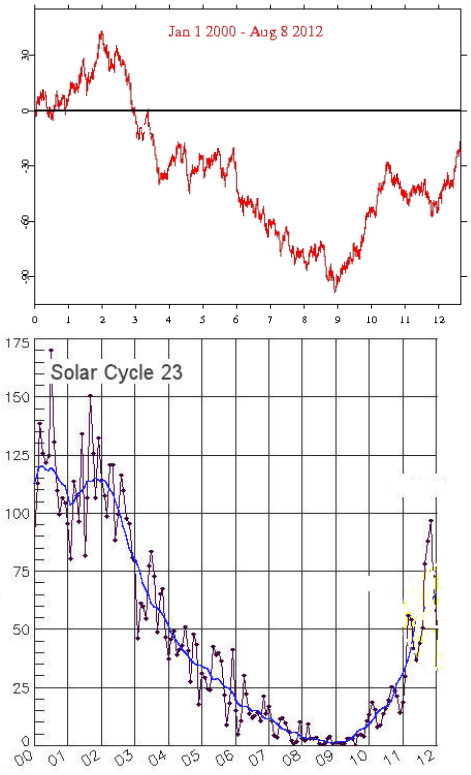

Fig. 1: Top: Measure of Zener diode GCP network current fluctuations over Solar Cycle 23, beginning with zero on January 1, 2000, adapted from R. Nelson, *Long Term Cumulative Deviation of Network Variance:* http://noosphere.princeton.edu/longterm.html. Bottom: Sunspot numbers for the same time period, adapted from T. Phillips, http://science.nasa.gov/media/medialibrary/2013/03/01/shortfall.jpg. We see the close correlation between these two phenomena. A causal relationship between space speed fluctuations and sunspots is demonstrated in Fig. 6: space flow fluctuations/turbulence precede by some 6 days the solar flares, implying that it is the space flow turbulence that causes the solar flares. This data shows the weakening of the solar cycle as being caused by weakening of the space flow turbulence. The data in Fig. 8 shows sea temperature history tracking solar flares, but not caused by the solar flares. There is a fundamental difference between correlations and cause and effect dynamics.

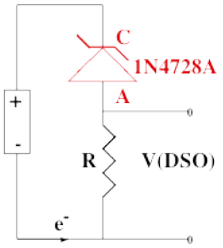

Fig. 2: Circuit of Zener Diode Gravitational Wave Detector, showing 1.5V AA battery, two 1N4728A Zener diodes operating in reverse bias mode, and having a Zener voltage of 3.3V, and resistor R= 10KΩ. Voltage V across resistor is measured and used to determine the space driven fluctuating tunnelling current through the Zener diodes. Current fluctuations from two collocated detectors are shown to be the same, but when spatially separated there is a time delay effect, so the current fluctuations are caused by space speed fluctuations [2, 3]. Using diodes in parallel increases S/N. The data used herein is from a GCP detector that has a XOR gate that partially degrades the data.

locate structures. At sufficiently small distance scales that embedding and the velocity description is conjectured to be not possible, as then the dynamical space requires an indeterminate dimension embedding space, being possibly a quantum foam [7]. This minimal generalisation of the original Schrödinger equation arises from the replacement $\partial/\partial t \rightarrow \partial/\partial t + \mathbf{v}.\nabla$, which ensures that the quantum system properties are determined by the dynamical space, and not by the embedding coordinate system. The same replacement is also to be implemented in the original Maxwell equations, yielding that the speed of light is constant only wrt the local dynamical space, as observed, and which results in lensing from stars and black holes. The extra $\nabla\cdot\mathbf{v}$ term in (1) is required to make the hamiltonian in (1) hermitian. Essentially the existence of the dynamical space in all theories has been missing. The dynamical theory of space itself is briefly reviewed below. The dynamical space velocity has been detected with numerous techniques, dating back to the 1st detection, the Michelson-Morley experiment of 1887, which was misunderstood, and which lead to physics developing flawed theories of the various phenomena noted above. A particularly good technique used the NASA Doppler shifts from spacecraft Earth-flybys, [6], to determine the anisotropy of the speed of EM waves, as indicated in Fig. 4. All successful detection techniques have observed significant fluctuations in speed and direction: these are the actually "gravitational waves", because they are associated with gravitational and other effects*

A significant effect follows from (1), namely the emergence of gravity as a quantum effect: a wave packet analysis shows that the acceleration of a wave packet, due to the space terms alone (when $V(\mathbf{r}, t) = 0$), given by $\mathbf{g} = d^2<\mathbf{r}>/dt^2$, [8], gives

$$g(\mathbf{r}, t) = \frac{\partial \mathbf{v}}{\partial t} + (\mathbf{v}\cdot\nabla)\mathbf{v}. \qquad (2)$$

That derivation showed that the acceleration is independent of the mass m: whence we have the 1st derivation of the Weak Equivalence Principle, discovered experimentally by Galileo. As noted below the dynamical theory for $\mathbf{v}(\mathbf{r}, t)$ has explained numerous gravitational phenomena.

*Note that vacuum-mode Michelson interferometers, such as LIGO, cannot detect these wave effects. Only dielectric-mode versions have detected such waves, although there is a variety of other successful techniques [1, 4]. In particular we report here the role of these waves in solar flare excitations and Earth climate science.

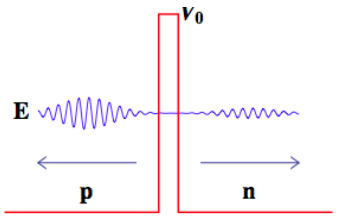

Fig. 3: Reflected (LHS) and transmitted (RHS) wave packets after interaction with barrier at a reverse-biased *pn* junction, as in Fig. 2. Energy E of wave packet is less than potential barrier height V_0. The wave function transmission varies with the speed $\mathbf{v}$ of the passing space as that varies $E \to E + \hbar\mathbf{k}\cdot\mathbf{v}$ according to (1) and so we may measure $\mathbf{v}$.

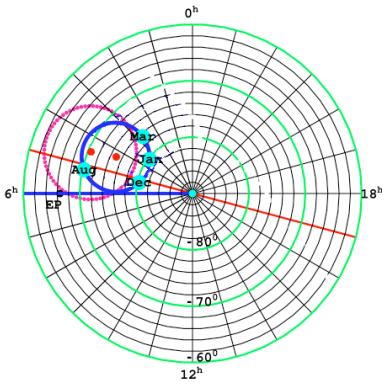

Fig. 4: South celestial pole region. The dot (red) at RA=4.3^h, Dec=75°S, and with speed 486km/s, is the direction of motion of the solar system through space determined from NASA spacecraft Earth-flyby Doppler shifts [6], as revealed by the EM radiation speed anisotropy. The thick (blue) circle centred on this direction is the observed velocity direction for different months of the year, caused by Earth orbital motion and sun 3-space inflow. The corresponding results from the 1925/26 Miller gas-mode interferometer are shown by 2nd dot (red) and its aberration circle (red dots). For December 8, 1992, the speed is 491km/s from direction RA=5.2^h, Dec=80°S, see Table 2 of [6]. EP is the pole direction of the plane of the ecliptic, and so the space flow is close to being perpendicular to the plane of the ecliptic.

3 Dynamical 3-space

The experimental data reveals the existence of a dynamical space. It is a simple matter to arrive at the dynamical theory of space, and the emergence of gravity as a quantum matter effect, as noted above. The key insight is to note that the emergent quantum-theoretic matter acceleration in (2), $\partial\mathbf{v}/\partial t + (\mathbf{v}\cdot\nabla)\mathbf{v}$, is also, and independently, the constituent Euler acceleration $\mathbf{a}(\mathbf{r}, t)$ of the space flow velocity field,

$$\mathbf{a}(\mathbf{r}, t) = \lim_{\Delta t\to 0} \frac{\mathbf{v}(\mathbf{r} + \mathbf{v}(\mathbf{r}, t)\Delta t, t + \Delta t) - \mathbf{v}(\mathbf{r}, t)}{\Delta t}$$

$$= \frac{\partial\mathbf{v}}{\partial t} + (\mathbf{v}\cdot\nabla)\mathbf{v} \qquad (3)$$

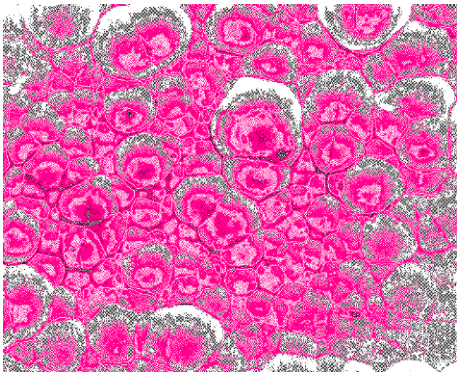

Fig. 5: Representation of the fractal wave data revealing the fractal textured structure of the 3-space, with cells of space having slightly different velocities and continually changing, and moving wrt the Earth with a speed of ~500 km/s, and in the directions indicated in Fig. 4, namely almost perpendicular to the plane of the ecliptic. This "red space" is suggestive of the 1/f spectrum of the detected fluctuations, see [5]. These space flow fluctuations inject energy into both the sun and the Earth. For solar flare effects low pass filtering of the data is necessary to isolate cells that overlap the Earth and sun, as in Fig .6.

which describes the acceleration of a constituent element of space by tracking its change in velocity. This means that space has a structure that permits its velocity to be defined and detected, which experimentally has been done. This then suggests, from (2) and (3), that the simplest dynamical equation for $\mathbf{v}(\mathbf{r}, t)$ is

$$\nabla\cdot\left(\frac{\partial\mathbf{v}}{\partial t} + (\mathbf{v}\cdot\nabla)\mathbf{v}\right) = -4\pi G\rho(\mathbf{r}, t);\quad \nabla\times\mathbf{v} = \mathbf{0} \qquad (4)$$

because it then gives $\nabla.\mathbf{g} = -4\pi G\rho(\mathbf{r}, t)$, $\nabla\times\mathbf{g} = \mathbf{0}$, which is Newton's inverse square law of gravity in differential form. Hence the fundamental insight is that Newton's gravitational acceleration field $\mathbf{g}(\mathbf{r}, t)$ for matter is really the acceleration field $\mathbf{a}(\mathbf{r}, t)$ of the structured dynamical space*, and that quantum matter acquires that acceleration because it is fundamentally a wave effect, and the wave is refracted by the accelerations of space.

While the above leads to the simplest 3-space dynamical equation this derivation is not complete yet. One can add additional terms with the same order in speed spatial derivatives, and which cannot be *a priori* neglected. There are two such terms, as in

$$\nabla\cdot\left(\frac{\partial\mathbf{v}}{\partial t} + (\mathbf{v}\cdot\nabla)\mathbf{v}\right) + \frac{5\alpha}{4}\left((trD)^2 - tr(D^2)\right) + ... = -4\pi G\rho \qquad (5)$$

where $D_{ij} = \partial v_i/\partial x_j$. However to preserve the inverse square law external to a sphere of matter the two terms must have

*With vorticity $\nabla\times\mathbf{v} \neq \mathbf{0}$ and relativistic effects, the acceleration of matter becomes different from the acceleration of space [7].

coefficients α and $-\alpha$, as shown. Here α is a dimensionless space self-interaction coupling constant, which experimental data reveals to be, approximately, the fine structure constant, $\alpha = e^2/\hbar c$, [11]. The ellipsis denotes higher order derivative terms with dimensioned coupling constants, which come into play when the flow speed changes rapidly wrt distance. The observed dynamics of stars and gas clouds near the centre of the Milky Way galaxy has revealed the need for such a term [9], and we find that the space dynamics then requires an extra term:

$$\nabla\cdot\left(\frac{\partial \mathbf{v}}{\partial t} + (\mathbf{v}\cdot\nabla)\mathbf{v}\right) + \frac{5\alpha}{4}\left((trD)^2 - tr(D^2)\right) +$$

$$+\delta^2\nabla^2\left((trD)^2 - tr(D^2)\right) + ... = -4\pi G\rho \qquad (6)$$

where δ has the dimensions of length, and appears to be a very small Planck-like length [9]. This then gives us the dynamical theory of 3-space. It can be thought of as arising via a derivative expansion from a deeper theory, such as a quantum foam theory, [7]. Note that the equation does not involve c, is non-linear and time-dependent, and involves non-local direct interactions. Its success implies that the universe is more connected than previously thought. Even in the absence of matter there can be time-dependent flows of space.

Note that the dynamical space equation, apart from the short distance effect - the δ term, there is no scale factor, and hence a scale free structure to space is to be expected, namely a fractal space. That dynamical equation has back hole and cosmic filament solutions [9, 11], which are non-singular because of the effect of the δ term. At large distance scales it appears that a homogeneous space is dynamically unstable and undergoes dynamical breakdown of symmetry to form a spatial network of black holes and filaments, [11], to which matter is attracted and coalesces into gas clouds, stars and galaxies.

The dynamical space equation (6) explains phenomena such as Earth bore-hole gravity anomalies, from which the value of α was extracted, flat rotation curves for spiral galaxies, galactic black holes and cosmic filaments, the universe growing/expanding at almost a constant rate, weak and strong gravitational lensing of light,... [4,9–11]. A significant aspect of the space dynamics is that space is not conserved: it is continually growing, giving the observed universe expansion, and is dissipated by matter. As well it has no energy density measure. Nevertheless it can generate energy into matter.

4 Detecting dynamical space speed and turbulence with diodes

The Zener diode in reverse bias mode can easily and reliably measure the space speed fluctuations, Fig. 2, and two such detectors can measure the speed and direction of the space flow and waves, Cahill [1–4]. Consider plane waves with energy $E = \hbar\omega$. Then (1) with $v = 0$ and $V = 0$ gives $\psi = e^{-\omega t + i\mathbf{k}\cdot\mathbf{r}}$. When $v \neq 0$, but locally uniform wrt to the diode, the energy becomes $E \to E + \hbar\mathbf{k}\cdot\mathbf{v}$. This energy shift can be easily detected by the diode as the electron transmission current increases with increased energy*. By using spatially separated diodes the speed and direction has been measured [1–4], and agrees with other detection techniques.

Although this Zener diode effect was only discovered in 2013, [3], Zener diode detectors have been available commercially for much longer, and are known as Random Event Generators, (REG). That terminology was based on the flawed assumption that the quantum tunnelling fluctuations were random wrt an average. However the data in [3] 1st showed that this is not the case. That experimental result contradicts the standard interpretation of "randomness" in quantum processes, which dates back to the Born interpretation in 1926. To the contrary the recent experiments show that the fluctuations are not random, but are directly determined by the fluctuations in the passing dynamical space.

5 Gravitational waves and solar flares

Fig. 1 shows the strong correlation between gravitational wave turbulence, as detected by the Earth-based ZDQD network, and the count rate of solar flares. At very low frequencies we can determine correlations based upon large "cells" of space, Fig. 5, passing almost perpendicular to the plane of the ecliptic. One key discovery herein is that the large space flow turbulences are the cause of significant solar flares, as shown in Fig. 6, top plot. That shows that the pattern of solar flares during the Halloween Space Weather Storms of 2003 closely match the pattern of 6-day-delayed space turbulence. Hence by using low-pass filtered data from Earth based ZDQD it is possible to predict with some 5 day warning the occurrence of major solar flares. This effect reveals the the space turbulence generates energetic activity in the sun, which eventually reaches the surface. However Fig. 6, bottom plot, suggests that the same mechanism is not relevant to Coronal Mass Ejections, although the data reported herein is limited to only one case.

6 Space flow turbulence and earth weather

There have been many studies noting correlations between solar cycles and changes in the Earth Weather, see [13] for review and references. The most notable being the Maunder minimum 1645-1715, during which there was no sunspot activity, and which coincided with the "little ice age". However correlations do not provide causal relations. The assumption has always been that increased sunspot activity results in increased solar irradiance which subsequently causes increased Earth temperatures, although no convincing mechanism has

*The Zener diode currents reported in [1–4] were incorrectly determined. The Digital Storage Oscilloscope (DSO)was operated with 50Ω input impedance, which meant the voltage was developed across that resistance and not the 10kΩ cited, and shown in Fig. 2. This means that the actual tunnelling currents were 200 times larger. This had no effect on the conclusions.

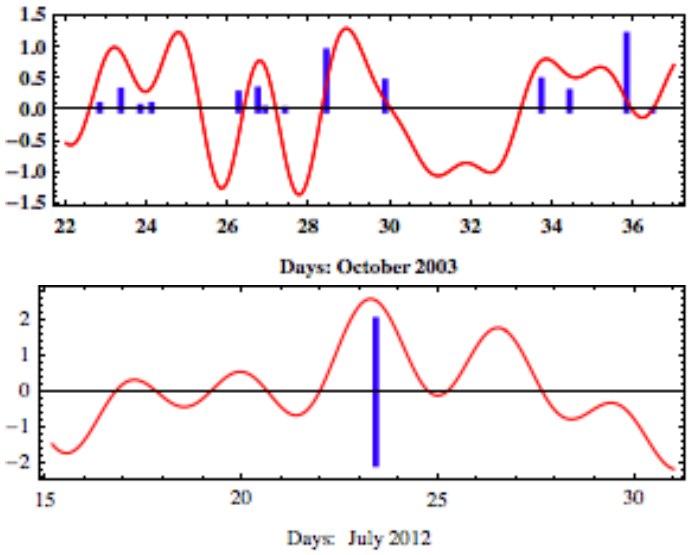

Fig. 6: Top: Vertical blue lines indicate start times of major solar flares beginning October 22, 2003. The height of the lines is indicative of the magnitude of the solar flare, and is on a logarithmic scale. These solar flares are known as the Halloween Space Weather Storms of 2003, [12]. The curve is data from a single ZDQD, located in Switzerland, low-pass filtered to include only periods longer than 2 days, and advanced in time by 6 days, and plotted relative to the average. For a space speed of 500 km/s this corresponds to a cell size ~0.5 of the Sun-Earth distance. This advance followed from matching the two data sets. The low-pass filter ensures that we see space fluctuations corresponding to cell sizes that can overlap the Earth and the sun, as the space flow is close to being perpendicular to the plane of the ecliptic, as shown by the analysis of the NASA Earth-flyby spacecraft Doppler shifts in Fig. 4, [6]. The strong correlation between the two data sets show that solar flares follow increases in the space velocity, by some 6 days: the solar flares are caused by the space fluctuations: these fluctuations are a galactic phenomenon. Bottom: Vertical blue line indicates start of massive Coronal Mass Ejection (CME) on July 23, 2012, and plotted with ZDQD low-pass data, but without time shift. The main speed fluctuation peak coincides with the CME, on July 23. This suggests that CME may not be caused by space fluctuations, and that the coincident peak may be gravitational waves produced by the extremely large mass ejection, although there is a smaller peak in the ZDQD data some 6 days earlier.

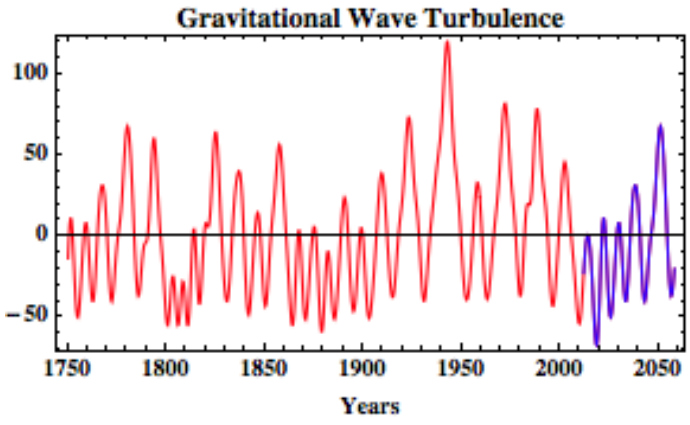

Fig. 7: Plot of Gravitational Wave Turbulence vs years 1749 to present (red plot), based upon Solar Flare counts as a proxy, as shown in Fig. 1. Data adapted from from D. Archibald, Solar Update March 2012 (http://www.warwickhughes.com/blog/?p=2753), [15]. The Solar Flare data has been low-pass filtered using Fast Fourier Transfoms. It is argued herein that the 11 year cycle and longer cycles are caused by galactic space flow turbulence, which can now be easily measured using ZDQD. Beyond 2014 we have used the Fourier amplitudes to extrapolate to 2050 (blue plot), which assumes an ongoing 1/f spectrum. This extrapolation suggests we are facing an epoch of low space flow turbulence, and hence reduced Earth temperatures. The modern warm period extended from 1900s to end of solar cycle 23 (the last cycle in red).

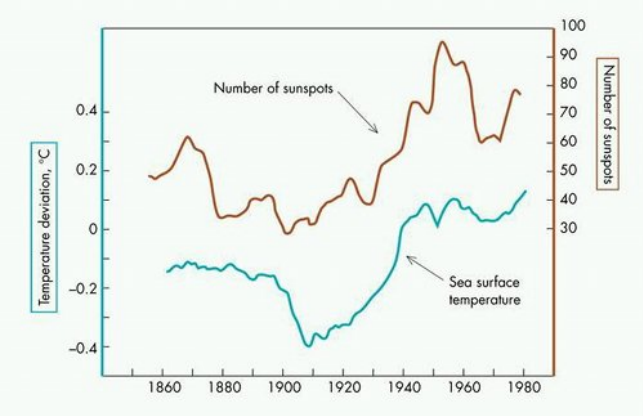

Fig. 8: Shows strong correlations between solar sunspot numbers and Earth sea surface temperature deviations. This, however, does not imply a causal relation between these two phenomena, as was also noted in Fig. 1. It is conjectured herein that the cause is the galactic space flow turbulence, which pumps energy into both the sun and the Earth.

been accepted. However the variation in irradiation is too small to cause the observed Earth temperature fluctuations. See Fig. 8 for correlations between sea temperature and solar flare counts. However the data herein offers a different mechanism, namely that the Earth's climate is affected by changes in the space flow turbulence, which is very evident in Fig. 1, with the causal relation established in Fig. 6. Such space flow fluctuations change the energy of matter, according to $\hbar\mathbf{v}\cdot\mathbf{k}$, as discussed above. These energy changes are the basis of the detection of the space flow turbulence by the ZDQD technique. So this suggests another possible factor affecting the Earth's climate, namely an energy generation that arises from space flow turbulence directly interacting with the Earth. The heating mechanism is that atoms/molecules having a momentary wave vector $\mathbf{k}$ have their energy raised if $\mathbf{k}\cdot\mathbf{v} > 0$. These then scatter with lower energy atoms/molecules and so dissipate the temporary energy lift to the gas in general. The GCP ZDQD data, going back some 18 years, thus provides an incredible data set that could be used to test this conjecture. Another indication of heat production internal to the Earth is that the geoneutrino flux from the decay of uranium-238 and thorium-232 can explain only about 50% of the heat production of the Earth of some 44.2±1.0 TW [14]. So there would appear to be another source of ongoing energy production within the Earth, and this could arise from space-flow turbulence effects.

Beginning Solar Cycle 24 is the weakest in more than 50 years. Fig. 7 shows the low frequency gravitational wave turbulence measure using the solar flare count as a proxy, which follows from the data in Fig. 1, and so permitting an analysis of such turbulence back to 1750. However by using Fourier transforms to extract the frequency spectrum and phases we may use that data to extrapolate into the future, which is shown in blue in Fig. 7, from mid 2014 to 2050. The prediction is that there will be a reduced energy generation in the Earth system over the next 30 years, as the galactic space turbulence will enter an epoch of reduced turbulence, as in 1860-1910, and resulting in the cooling of the Earth's atmosphere.

7 Conclusions

The discovery of the Zener Diode quantum detector effect has rendered the detection of 3-space flow turbulence, gravitational waves*, to be trivial and robust. The speed and direction of the flow from such detectors has confirmed the results from earlier experiments, beginning with Michelson and Morley in 1887 using a gas-mode interferometer. Other experimental techniques have used RF speeds in coaxial cables, dual RF coaxial cables and optical fibers, RF speeds in dual coaxial cables, to mention only some: see [1, 4] for recent reviews. The major implication is that space exists, because it is detectable, has significant fractal flow turbulence, and is a complex dynamical system, contrary to the claims since 1905 that space does not exist. The turbulence effects are significant, typically some 20% of the average flow velocity at present. The dynamical theory has become well established by testing against various experimental and observational phenomena [6, 9–11]. Here we have reported evidence that solar flares are caused by major gravitational wave fluctuations. Using Zener Diode gravitational wave detectors and low pass filtering the data now offers the opportunity to predict with some 5 days warning of a major solar flare. As these detectors are so simple they could be included on all future space probes, as a larger scanning region would considerably increase reliability of the new warning system. The data used here comes from the GCP project, which has had Zener diode detectors operating for some 18 years, but was based upon an incorrect assumption that the current fluctuations in the reverse-biased pn junction were random quantum fluctuation, as asserted in the usual interpretation of the quantum theory. However recent experiments [2, 3], and without the XOR gate used in GCP detectors, it was shown that the diode current fluctuations are completely determined by fluctuations in the passing space. Nevertheless the GCP data base represents an enormously significant record of 3-space turbulence, which will permit various studies to be undertaken. A second major discovery is that the long established correlations between Earth temperature fluctuations and solar flare counts is explained by both phenomena being a result of gravitational waves, and not by the very small changes in sun irradiance that accompanies solar flares. This has led to the prediction that there is a diminution epoch of gravitational waves that is already detectable in Figs. 1 and 6, that will

*The detected gravitational waves are not those of GR. Such waves have never been detected.

result in a cooling of the Earth's atmosphere, as was experienced in earlier Earth epochs when the gravitational waves underwent a period of diminished activity. Dropping temperatures would normally decrease cereal food production, but that may be compensated for by extra growth following form the increased CO_2 levels. We note that the statistical arguments in [16] are invalidated by the discovery of the space flow turbulence effect reported herein: Climate Science has been missing a key physical process until now.

Acknowledgements

This report is from the Flinders University Gravitational Wave Detector Project. Thanks to GCP and its director Dr Roger Nelson for the public availability of extensive and valuable data from the GCP ZenerDiode international network: http://noosphere.princeton.edu/extract.html

Submitted on September 6, 2014 / Accepted on September 11, 2014

References

1. Cahill R.T. Review of Gravitational Wave Detections: Dynamical Space, *Physics International*, 2014, v. 5(1), 49–86.
2. Cahill R.T. Gravitational Wave Experiments with Zener Diode Quantum Detectors: Fractal Dynamical Space and Universe Expansion with Inflation Epoch. *Progress in Physics*, 2014, v. 10(3), 131–138.
3. Cahill R.T. Nanotechnology Quantum Detectors for Gravitational Waves: Adelaide to London Correlations Observed. *Progress in Physics*, 2013, v. 4, 57–62.
4. Cahill R.T. Discovery of Dynamical 3-Space: Theory, Experiments and Observations - A Review. *American Journal of Space Science*, 2013, v. 1(2), 77–93.
5. Cahill R.T. Characterisation of Low Frequency Gravitational Waves from Dual RF Coaxial-Cable Detector: Fractal Textured Dynamical 3-Space. *Progress in Physics*, 2012, v. 3, 3–10.
6. Cahill R.T. Combining NASA/JPL One-Way Optical-Fiber Light-Speed Data with Spacecraft Earth-Flyby Doppler-Shift Data to Characterise 3-Space Flow. *Progress in Physics*, 2009, v. 4, 50–64.
7. Cahill R.T. Process Physics: From Information Theory to Quantum Space and Matter. *Nova Science Pub., New York*, 2005.
8. Cahill R.T. Dynamical Fractal 3-Space and the Generalised Schrödinger Equation: Equivalence Principle and Vorticity Effects, *Progress in Physics*, 2006, v. 1, 27–34.
9. Cahill R.T. and Kerrigan D. Dynamical Space: Supermassive Black Holes and Cosmic Filaments. *Progress in Physics*, 2011, v. 4, 79–82.
10. Cahill R.T. and Rothall D. Discovery of Uniformly Expanding Universe. *Progress in Physics*, 2012, v. 1, 63–68.
11. Rothall D.P. and Cahill R.T. Dynamical 3-Space: Black Holes in an Expanding Universe, *Progress in Physics*, 2013, v. 4, 25–31.
12. Weaver M. (ed) *et al.* Halloween Space Weather Storms of 2003, NOAA Technical Memorandum OAR SEC-88, 2004.
13. Phillips T. Solar Variability and Terrestrial Climate, http://science.nasa.gov/science-news/science-at-nasa/2013/08jan_sunclimate/
14. KamLAND Collaboration, Partial Radiogenic Heat Model for Earth Revealed by Geoneutrino Measurements. *Nature Geoscience*, 2011, v. 4, 647–651.
15. Archibald D. The Past and Future of Climate, 2010, http://www.davidarchibald.info/papers/Past-and-Future-of-Climate.pdf
16. Kokic P., Crimp S., Howden M. A Probabilistic Analysis of Human Influence on Recent Record Global Mean Temperature Changes, *Climate Risk Management*, 2014, v. 3, 1–12.

Proton-Neutron Bonding in the Deuteron Atom and its Relation to the Strong Force as Viewed from the Planck Vacuum Theory

William C. Daywitt

National Institute for Standards and Technology (retired), Boulder, Colorado. Email: wcdaywitt@me.com

This paper argues that the two-particle proton-neutron bond results from the proton-proton/Planck-vacuum coupling force associated with the two particles. The neutron is assumed to be a proton with a weakly attached electron whose sole function is to eliminate the Coulomb repulsion between the two protons. Results lead to a simple model of the deuteron atom and a definition for the strong force.

1 Introduction

The proton core (e_*, m_p) located at the radius $r = 0$ exerts the two-term coupling force [1]

$$F(r) = -\left(\frac{e_*^2}{r^2} - \frac{m_p c^2}{r}\right) = -\frac{e_*^2}{r^2}\left(1 - \frac{r}{r_p}\right) \qquad (1)$$

on the omnipresent Planck vacuum (PV) state, where r_p $(= e_*^2/m_p c^2)$ is the Compton radius at which the force vanishes. The radius r extends from the core to any point within the PV continuum. The massless bare charge is e_* and m_p is the proton rest mass. Since the Planck particles within the PV suffer a primordial zero-point agitation that is the source of the zero-point electromagnetic fields, the radius r in (1) is an average over the small instantaneous random motion $(r(t) - r$ at $r \approx 0)$ of the proton's bare charge (e_*) [2, 3]. In part, the response of the PV to the force (1) is to create the proton mass m_p from the zero-point-field driven proton charge (e_*).

Figure 1 is a plot of the normalized coupling force

$$\frac{F(r)}{e_*^2/r_p^2} = \frac{F(r)}{m_p c^2/r_p} = -\frac{r_p^2}{r^2} + \frac{r_p}{r} \qquad (2)$$

where the abscissa is in units of r_p (equation (5) is used in the calculation). The two fiducial points, $r = r_p$ and $r = 2r_p$, are the radii at which the force vanishes and attains its maximum respectively. The Compton radius r_p has been discussed in a number of earlier papers (see `www.planckvacuum.com`). It is seen in what follows that the separation between the proton and neutron cores in the deuteron is related to the maximum at $2r_p$.

The coupling potential from (1) is

$$V(r) = -\int F(r)dr + V_0 \qquad (3)$$

where $V(r_p) = 0$ yields the normalized potential

$$\frac{V(r)}{m_p c^2} = -\frac{r_p}{r} + 1 + \ln\frac{r_p}{r}\,. \qquad (4)$$

The corresponding mass and Compton radius of the proton are tied to the PV state via the Compton relations

$$r_p m_p c^2 = r_* m_* c^2 = e_*^2 \qquad (= c\hbar) \qquad (5)$$

which are a manifestation of the fact that the proton possesses a Compton radius r_p, where r_* and m_* are the Compton radius and mass of the Planck particles making up the negative energy PV.

For $r \ll r_p$, (1) reduces to

$$F(r) = -\frac{e_*^2}{r^2} = \frac{(e_*)(-e_*)}{r^2} \qquad (6)$$

where (e_*) belongs to the proton and $(-e_*)$ belongs to the separate Planck particles of the PV.

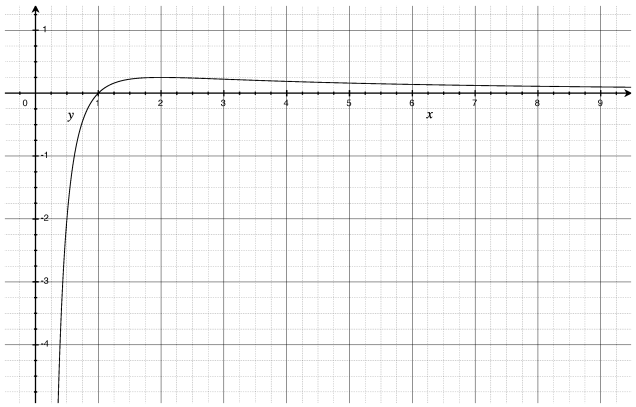

Fig. 1: The graph plots $F(r)/(e_*^2/r_p^2)$, with $r_p = 1$. The maximum of the curve is at $2r_p = 2$.

The neutron is assumed to be a proton with a negative charge weakly attached to make the neutron charge-neutral. Theoretically, it is tempting to assume that this added negative charge is the massless bare charge $(-e_*)$. However, the zero-point fields permeate both free space and any particle in that space [3]; and if that particle is the bare charge, that bare charge rapidly becomes an electron or a proton, depending upon whether the charge is negative or positive respectively. Thus the added negative charge in the neutron is assumed in the PV theory to be an electron.

2 Proton-proton bond

The PV is a degenerate state [5], which implies that the force in (1) does not distort the vacuum structure, except possibly

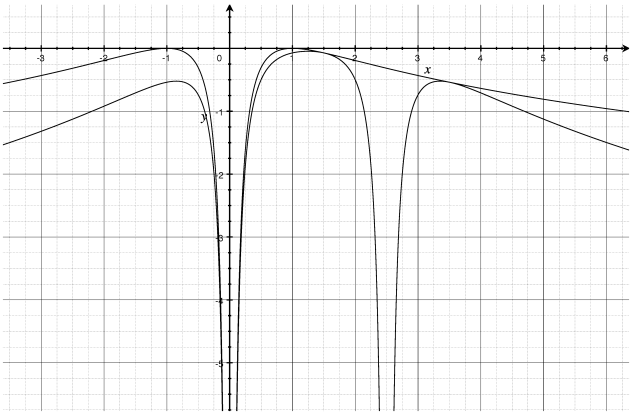

Fig. 2: The graph plots $V(t)/m_pc^2$ (the upper curve) and $V_t(r)/m_pc^2$ (the three-humped curve) with $x_0 = 2.5r_p$ and $r_p = 1$. The two intersect points are at $r = x_0 \pm r_p = 2.5 \pm 1$.

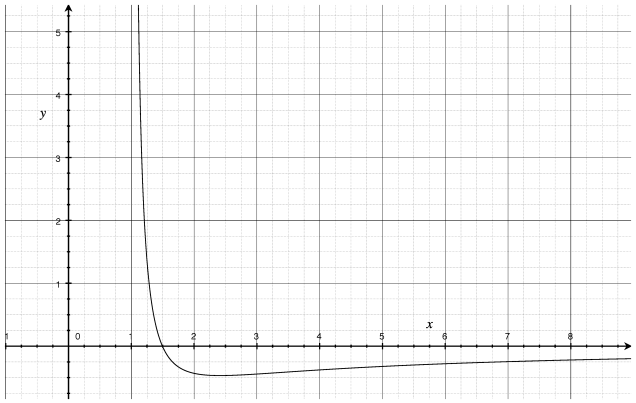

Fig. 3: The graph plots $W(x_0)$ with $r_p = 1$. The minimum of the curve is at $x_0 \approx 2.4r_p = 2.4$.

deep within the proton core. Thus the total coupling force felt by the PV due to two protons (the free proton and the proton in the neutron) is the sum of two forces similar to (1). If the two protons are separated by distance equal to x_0, with one of the protons at the origin, the total normalized proton-proton/PV coupling potential is simply (with $\mathbf{r} = (x, 0, 0)$)

$$\frac{V_t(r)}{m_pc^2} = -\frac{r_p}{r} + 1 + \ln\frac{r_p}{r} - \frac{r_p}{|r-x_0|} + 1 + \ln\frac{r_p}{|r-x_0|}$$

$$= -r_p\left(\frac{r+|r-x_0|}{r|r-x_0|}\right) + 2 + \ln\left(\frac{r_p^2}{r|r-x_0|}\right) \qquad (7)$$

which is plotted in Figure 2 with x_0 set to $2.5r_p$, where the abscissa is in units of the proton Compton radius r_p. The upper curve is the potential for a single proton at the coordinate origin. The three-hump two-proton curve intersects the single-proton curve at the two points (8) where the second potential in the first equation of (7) vanishes. The potential difference between the intersect points provides a means for determining the equilibrium separation $\overline{x_0}$ (the assumed separation between the proton and neutron cores in the deuterium atom). The two intersect radii in Figure 2 follow easily from

$$V_t(r) = V(r) \qquad \Longrightarrow \qquad r = x_0 \pm r_p \qquad (8)$$

and appear on either side of x_0.

To determine the equilibrium $\overline{x}_0$, it is convenient to define

$$W(x_0) \equiv \frac{V_t(x_0+r_p) - V_t(x_0-r_p)}{m_pc^2} \qquad (9)$$

$$= \frac{V(x_0+r_p) - V(x_0-r_p)}{m_pc^2} \qquad (10)$$

in terms of the separation distance x_0, which is plotted in Figure 3 with r_p set to one. The equilibrium $\overline{x_0}$ is then obtained from

$$\frac{dW(x_0)}{dx_0} = \frac{2r_p(x_0^2 - r_p^2) - 4r_p^2x_0}{(x_0^2 - r_p^2)^2} = 0 \qquad (11)$$

whose solution is

$$x_0 = (1 \pm 2^{1/2})r_p \qquad (12)$$

yielding

$$\overline{x_0} = (1 + 2^{1/2})r_p \approx 2.4r_p \qquad (13)$$

for the deuteron proton-neutron core separation. A very rough experimental estimate (Appendix A) for the separation is $3.0r_p$.

3 Strong force

The vanishingly small magnitude ($< r_p/39000$) of the proton-core radius [4] suggests that it may be related to the so called strong force F_s. So identifying the Coulomb force from (6) as the strong force leads to the ratio

$$\frac{F_s(r)}{F_g(r)} = \frac{(e_*)(-e_*)/r^2}{-m_p^2G/r^2} = \frac{m_*^2}{m_p^2} = \frac{r_p^2}{r_*^2} \sim 10^{38} \qquad (14)$$

of that force to the gravitational force F_g between two proton masses separated by a distance r ($G = e_*^2/m_*^2$ from [1, 5], and (5) are used in the calculation).

To reiterate, the positive charge in (14) is the bare charge of the proton and the negative charge corresponds to the bare charges of the separate Planck particles in the PV. So (14) is a composite ratio involving the proton-PV coupling force for $r \ll r_p$ and the free-space gravitational force.

4 Summary and comments

The PV theory assumes that the proton-neutron bond results from the proton-proton/PV coupling force associated with the proton and the proton-part of the neutron. It explains the proton-neutron bond as a minimum in the proton/PV coupling

potentials as characterized by equations (8)–(13) and Figure 3, with a minimum at $2.4r_p$ that is directly related to the maximum force at $2r_p$ in Figure 1. This characterization assumes that the bonding takes place suddenly when $x_0 = \overline{x_0}$ as the proton and neutron approach each other. That is, the two nucleons do not possess some type of strong *mutual* attraction for $x_0 \neq \overline{x_0}$. In summary, then, the proton-neutron bond in the PV theory is a new type of bonding that intimately involves the invisible, negative-energy vacuum state and its interaction with the proton core (e_*, m_p).

The strong force, $(e_*)(-e_*)/r^2$, is seen to be a force existing between the positive proton charge and the separate negative charges of the PV. It is not a force acting between two free space particles.

Appendix A: deuteron size

This is a rough heuristic estimate of the separation distance between the proton and neutron cores within the deuteron. It starts with the standard formula for the radius of the stable nucleus with a mass number A [6, p.551]

$$R(A) = 1.2\,A^{1/3}\,[\text{fm}] = 5.71 r_p A^{1/3} \qquad \text{(A1)}$$

in units of femtometers or the proton Compton radius r_p (= 0.21 fm). The radii of the proton and neutron are defined by $A = 1$, and the deuteron by $A = 2$. Inserting these parameters into (A1) leads to the radii $R_1 = 5.71r_p$ and $R_2 = 7.19r_p$ for the nucleons and deuteron respectively.

Taking the cores at the origin of the two spheres defined by R_1 and R_2, it is easy to see that the separation between the nucleon cores in the deuteron is

$$2(R_2 - R_1) = 2(7.19r_p - 5.71r_p) \approx 3.0r_p\,. \qquad \text{(A2)}$$

Submitted on September 7, 2014 / Accepted on September 13, 2014

References

1. Daywitt W.C. The Electron and Proton Planck-Vacuum Forces and the Dirac Equation. *Progress in Physics*, 2014, v. 2, 114–115.
2. Daywitt W.C. Why the Proton is Smaller and Heavier than the Electron. *Progress in Physics*, 2014, v. 10, 175–177.
3. Daywitt W.C. The Source of the Quantum Vacuum. *Progress in Physics*, 2009, v. 1, 27–32. In the first line of the last paragraph in Appendix A of this paper "$p = \hbar/r_L$" should read "$m\gamma c = \hbar/r_L$".
4. Daywitt W.C. The Dirac Proton and its Structure. To be published in the International Journal of Advanced Research in Physical Science (IJARPS). See also `www.planckvacuum.com`.
5. Daywitt W.C. The Planck Vacuum. *Progress in Physics*, 2009, v. 1, 20–26.
6. Leighton R.B. *Principles of Modern Physics*. McGraw-Hill Book Co., New York, Toranto, London, 1959.

Properties of Nuclear Superdeformed Rotational Bands in A ∼ 190 Mass Region

A. M. Khalaf[1] and M. D. Okasha[2]

[1]Physics Department, Faculty of Science, Al-Azhar University, Cairo, Egypt. E-mail: ali_khalaf43@hotmail.com
[2]Physics Department, Faculty of Science (Girls College), Al-Azhar University, Cairo, Egypt. E-mail: mady200315@yahoo.com

Two-parameters formula based on the conventional collective rotational model is applied to describe superdeformed rotational bands (SDRB's) in nuclei in the $A \sim 190$ mass region, namely the five SDRB's ^{192}Hg(SD1), ^{194}Hg(SD1), ^{194}Hg(SD2), ^{194}Pb(SD1) and ^{194}Pb(SD2). The bandhead spins of the observed levels have been extracted by first and second-hand estimation corresponding to pure rotator and our proposed formula respectively by plotting the E-Gamma Over Spin (EGOS) versus spin. A computer simulated search program is used to extract the model parameters in order to obtain a minimum root mean square (rms) deviation between the calculated and the experimental transition energies The values of spins resulting from second estimation method are excellent consistent with spin assignment of other models. The calculated transition energies, level spins, rotational frequencies, kinematic and dynamic moments of inertia are systematically examined. The difference in γ- ray transition energies ΔE_γ between transitions in the two isotones ^{192}Hg(SD1) and ^{194}Pb(SD1) were small and constant up to rotational frequency $\hbar\omega \sim 0.25$ MeV. Therefore, these two bands have been considered as identical bands. The $\Delta I = 2$ energy staggering observed in ^{194}Hg(SD1) and ^{194}Hg(SD2) of our selected SDRB's are also described from a smooth reference representing the finite difference approximation to the fourth order derivative of the transition energies at a given spin.

1 Introduction

Superdeformed (SD) nuclei were observed in a wide range of nuclear chart, and a wealth of experimental data on the resulting superdeformed rotational bands (SDRR's) was accumulated in recent years [1, 2]. These bands consists of long cascades of regularly spaced quadruple γ-ray transitions, which reveal a high degree of collectivity in a strongly deformed prolate nucleus. Lifetime measurements lead to very large values for the quadrupole moments of $Q_0 \sim 15 - 20$ eb which indeed correspond to an elongated ellipsoid with an axis ratio close to 2:1.

The superdeformation at high angular momentum remains one of the most interesting and challenging topics of nuclear structure. At present, although a general understanding of the properties of such SD nuclei has been achieved, there are still many open un expected problems. One of the outstanding experimental problems in the study of SD nuclei concerns their decay to the ground state. After a rapid decay out occurs over 2-4 states, and transitions linking the SD band to known levels in the first well are unobserved. As a result, the excitation energy, spin and parity of the levels in the first well are unobserved. As a result several theoretical approaches to predict the spins of SD bands were suggested [3–14].

To date, SD spectroscopy has given us much information concerning the behavior of moment of inertia in SD nuclei. For example it was shown [15] that for SD nuclei near $A \sim 150$, the variation in the dynamical moment of inertia $J^{(2)}$ with rotational frequency $\hbar\omega$ is dependant on the proton and neutron occupation of high-N intruder orbitals. For most SD bands in even-even and odd-A nuclei in the $A \sim 190$, $J^{(2)}$ exhibits a smooth gradual increase with increasing $\hbar\omega$ [16], which is due to the gradual alignment of quasinucleons occupying high -N intruder orbitals (originating from the $i_{13/2}$ proton and $j_{15/2}$ neutron subshells)in the presence of the pair correlations, while in the odd-odd nuclei, quite a good part of the moments of inertia for SD bands keep constant.

An unexpected discovery was the existence of identical bands (IB's) [17–21]. IB's are two bands in different nuclei, which have essentially identical transition energies within 2 keV, and thus essentially identical dynamical moment of inertia.

It was found that some SDRB's in different mass regions show an unexpected $\Delta I = 2$ staggering effects in the γ-ray energies [22–25]. The effect is best seen in long rotational sequences, where the expected regular behavior of the energy levels with respect to spin or to rotational frequency, is perturbed. The result is that the rotational sequences is split into two parts with states separated by $\Delta I = 4$ (bifurcation) shifting up in energy and the intermediate states shifting down in energy. The curve found by smoothly interpolating the band energy of the spin sequence $I, I + 4, I + 8, ...$, is some what displaced from the corresponding curve of the sequence $I+2, I+6, I+10, ...$ The magnitude of the displacement in the gamma transition energy is found to be in the range of some hundred eV to a few keV. The $\Delta I = 2$ staggering effect has attracted considerable interest in the nuclear structure community. A few theoretical proposal for the possible explanation of this $\Delta I = 2$ staggering have already been made [26–31].

Calculations using the cranked Nilsson-Strutinsky

method [32], and the Hartee-Fock method [33] suggest that nuclei with $N = 112$ and $Z = 80$ or 82 should be particularly stable, due to the existence of SD gaps in the single particle spectrum. As a result ^{192}Hg and ^{194}Pb are considered as doubly magic SD nuclei. Excited SD bands in these two nuclei are therefore expected to exist a somewhat higher excitation energies, and consequently to be populated with lower intensity than excited SD bands in other nuclei in this region.

In this paper, we shall present a theoretical study for Hg and Pb nuclei, our results are in framework of collective rotational formula including two parameters, obtained by adopted best fit method. We need first and second estimation to predict the spins for the studied SDRB's, and the best fitted parameters have been used to evaluate the E2 transition γ-ray energies, rotational frequencies, kinematic and dynamic moments of inertia. The appearance of identical bands (IB's) and the occurrance of a $\Delta I = 2$ staggering effect have been examined.

2 Parametrization of SDRB's by Two-Parameter Collective Rotational Formula

For the description of normally deformed (ND) bands, some useful expressions were presented. Bohr and Mottelson [34] pointed out that, under the adiabatic approximation, the rotational energy of an axially symmetric even-even nucleus may be expanded as (for $k = 0$, where k is the projection of the angular momentum I onto the symmetric axis) a power series in terms of of I^2=I(I+1):

$$E(I) = A[I(I+1)] + B[I(I+1)]^2 \tag{1}$$

with common constants A and B. We will adopt the energy of the SD state with spin I by equation (1).

For SD bands, gamma-ray transition energies are unfortunately, the only spectroscopic information universally available. The gamma-ray transition energy between levels differing by two units of angular momentum $\Delta I = 2$ are:

$$\begin{aligned} E_\gamma(I) &= E(I) - E(I-2) \\ &= (I-1/2)\left[4A + 8B(I^2 - I + 1)\right]. \end{aligned} \tag{2}$$

3 Spin Assignment of SDRB's in A ∼ 190 Mass Region

In the method used, the energies of the SD nuclear rotational bands are firstly expressed by pure rotator as a first estimation of bandhead spin

$$E(I) = AI(I+1). \tag{3}$$

Thus

$$E_\gamma(I) = 4A(I - 1/2). \tag{4}$$

If I_0 represent the bandhead spin, then

$$\frac{E_\gamma(I_0+4)}{E_\gamma(I_0+2)} = \frac{4I_0+14}{4I_0+6}. \tag{5}$$

Therefore,

$$I_0 = \frac{1}{4}\left[\frac{8E_\gamma(I_0+2)}{E_\gamma(I_0+4) - E_\gamma(I_0+2)} - 6\right]. \tag{6}$$

The ratio $E_\gamma(I)$ over spin I (E-Gamma Over Spin(EGOS)) is given by

$$EGOS = \frac{E_\gamma(I)}{I - 1/2} = 4A \tag{7}$$

when EGOS plotted against spin, it gives horizontal line.

For second estimation of bandhead spin, our proposed formula equation (1) is used, thus EGOS becomes

$$EGOS = 4A + 8B(I^2 - I + 1) \tag{8}$$

which decrease hyperbolically.

4 Rotational Frequency and Moments of Inertia

In the framework of nuclear collective rotational model with $k = 0$, the rotational frequency $\hbar\omega$ for the expression (1) is given by

$$\begin{aligned} \hbar\omega(I) &= \frac{dE(I)}{d\sqrt{I(I+1)}} \\ &= 2A\left[I(I+1)\right]^{\frac{1}{2}} + 4B\left[I(I+1)\right]^{\frac{3}{2}}. \end{aligned} \tag{9}$$

The kinematic $J^{(1)}$ and dynamic $J^{(2)}$ moments of inertia for the expression(1) are:

$$\begin{aligned} \frac{J^{(1)}}{\hbar^2} &= \frac{1}{\sqrt{I(I+1)}}\left[\frac{dE(I)}{d\sqrt{I(I+1)}}\right]^{-1} \\ &= J_0 - \frac{B}{A^2}[I(I+1)] \\ &+ \frac{2B^2}{A^3}[I(I+1)]^2 - 4\frac{B^3}{A^4}[I(I+1)]^3 \end{aligned} \tag{10}$$

$$\begin{aligned} \frac{J^{(2)}}{\hbar^2} &= \left[\frac{d^2E(I)}{d[I(I+1)]^2}\right]^{-1} \\ &= J_0 - 3\frac{B}{A^2}[I(I+1)] \\ &+ 18\frac{B^2}{A^3}[I(I+1)^2] - 108\frac{B^3}{A^4}[I(I+1)]^3 \end{aligned} \tag{11}$$

where J_0 is refereed to as the bandhead moment of inertia

$$J_0 = \frac{1}{2A}. \tag{12}$$

The two moments of inertia are obviously dependent.

One has

$$J^{(2)} = J^{(1)} + \omega\frac{dJ^{(1)}}{d\omega}. \tag{13}$$

Table 1: Bandhead spin for ^{194}Hg(SD1) derived from EGOS for first estimation A=5.2902 keV, $I_0 = 10.5$

I	E_γ	EGOS^{cal}(keV/$\hbar$)			EGOS^{exp}(keV/$\hbar$)		
$\hbar$	(keV)	I_0-2	I_0	I_0+2	I_0-2	I_0	I_0+2
12.5	253.929	25.392	21.16	18.137	25.393	21.160	18.137
14.5	296.2512	24.687	21.16	18.515	24.665	21.142	18.499
16.5	338.572	24.183	21.16	18.809	24.084	21.073	18.732
18.5	380.894	23.805	21.16	19.044	23.586	20.966	18.869
20.5	423.216	23.512	21.16	19.237	23.144	20.830	18.936
22.5	465.537	23.376	21.16	19.397	22.738	20.670	18.948
24.5	507.859	23.084	21.16	19.533	22.357	20.494	18.917
26.5	550.180	22.924	21.16	19.649	21.995	20.303	18.852
28.5	592.502	22.788	21.16	19.750	21.650	20.104	18.764
30.5	634.824	22.672	21.16	19.838	21.316	19.895	18.652
32.5	677.145	22.571	21.16	19.916	20.997	19.685	18.527
34.5	719.467	22.483	21.16	19.985	20.689	19.472	18.390
36.5	761.788	22.405	21.16	20.047	20.394	19.261	18.247
38.5	804.110	22.336	21.16	20.102	20.108	19.050	18.097
40.5	846.432	22.274	21.16	20.153	19.840	18.848	17.950
42.5	888.753	22.218	21.16	20.198	19.591	18.658	17.810
44.5	931.075	22.168	21.16	20.240	19.360	18.480	17.676
46.5	973.396	22.122	21.16	20.279	19.148	18.316	17.553

The dynamical moment of inertia varies often in a very sensitive way with rotational frequency $\hbar\omega$. In particular for rigid rotor, we shall obtain:

$$J^{(2)} = J^{(1)} = J_{rigid}. \tag{14}$$

Experimentally, for SDRB's, the gamma-ray transition energies are the only spectroscopic information universally available. Therefore, to compare the structure of the SD bands, information about their gamma-ray transition energies are commonly translated into values of rotational frequency $\hbar\omega$ and moments of inertia:

$$\hbar\omega = \frac{1}{4}[E_\gamma(I) + E_\gamma(I+2)] \qquad \text{(MeV)} \tag{15}$$

$$J^{(1)}(I-1) = \frac{2I-1}{E_\gamma(I)} \qquad (\hbar^2\text{MeV}^{-1}) \tag{16}$$

$$J^{(2)}(I) = \frac{4}{\Delta E_\gamma(I)} \qquad (\hbar^2\text{MeV}^{-1}) \tag{17}$$

where $\Delta E_\gamma(I)$=$E_\gamma(I+2)$-$E_\gamma(I)$ is the difference between two consecutive transition energies. Therefore, the dynamical moment of inertia $J^{(2)}$ which is linked to the second derivatives of energy, does not depend on the knowledge of the spin I but only on the measured transition energies. Theoretically, the $J^{(2)}$ moment of inertia reflects the curvature of the single-particle orbitals, while experimentally it is simply extracted from the measured γ-ray energies. In terms of A and B, yield directly:

$$J^{(1)} = \frac{1}{2[A + 2B(I^2 - 2I + 1)]}, \tag{18}$$

$$J^{(2)} = \frac{1}{2[A + B(6I^2 + 6I + 5)]}. \tag{19}$$

5 Identical Bands in SDRB's

Since the experimental discovery of SD bands in rapidly rotating nuclei, many unexpected features of these highly excited configurations were observed. One of the most striking feature is the existence of identical bands (IB's) or twin bands, that is identical transition energies E_γ in bands belonging to neighboring nuclei with different mass numbers. To determine whether a pair of bands is identical or not, one must calculate the difference between their gamma-transition energies of the two bands 1 and 2, ΔE_γ=$E_\gamma(1)$-$E_\gamma(2)$.

6 ΔI = 2 Staggering Effect in Transition Energies

To explore more clearly the $\Delta I = 2$ staggering, for each band the deviation of transition energies from a smooth reference is determined by calculating the finite difference approximation to the fourth derivative of the γ-ray energies at a given spin d^4E_γ/dI^4. This smooth reference is given by

$$\begin{aligned}\Delta^4 E_\gamma(I) &= \tfrac{1}{16}[E_\gamma(I-4) \\ &\quad -4E_\gamma(I-2) + 6E_\gamma(I) \\ &\quad -4E_\gamma(I+2) + E_\gamma(I+4)].\end{aligned} \tag{20}$$

This formula includes five consecutive transition energies and is denoted by five-point formula. For equation (1), we can easily notice that in this case $\Delta^4 E_\gamma(I)$ vanishes.

Table 2: The same as in Table (1) but for second estimation $A = 5.5904$ keV and B= -3.395×10^{-4} keV, $I_0 = 10$

I	E_γ	EGOS^{cal}(keV/$\hbar$)			EGOS^{exp}(keV/$\hbar$)		
$\hbar$	(keV)	I_0-2	I_0	I_0+2	I_0-2	I_0	I_0+2
12	253.102	26.642	22.008	18.748	26.729	22.080	18.809
14	295.399	25.686	21.881	19.058	25.738	21.925	19.096
16	336.884	24.954	21.734	19.250	24.976	21.753	19.267
18	377.513	24.355	21.572	19.359	24.347	21.565	19.353
20	417.181	23.838	21.393	19.403	23.805	21.364	19.376
22	455.830	23.375	21.201	19.397	23.321	21.151	19.351
24	493.408	22.949	20.996	19.349	22.877	20.930	19.288
26	529.873	22.547	20.779	19.268	22.462	20.701	19.195
28	565.185	22.164	20.552	19.158	22.075	20.469	19.082
30	599.324	21.793	20.316	19.026	21.704	20.232	18.948
32	632.266	21.432	20.071	18.873	21.353	19.997	18.803
34	664.012	21.079	19.821	18.704	21.018	19.763	18.649
36	694.573	20.733	19.565	18.521	20.698	19.532	18.490
38	723.943	20.392	19.305	18.327	20.391	19.304	18.326
40	752.145	20.057	19.041	18.123	20.104	19.086	18.166
42	779.183	19.726	18.775	17.912	19.839	18.883	18.015
44	805.102	19.400	18.508	17.694	19.593	18.692	17.870
46	829.924	19.078	18.240	17.472	19.368	18.517	17.737

7 Results and Discussion

The SDRB's ^{192}Hg(SD1), ^{194}Hg(SD1), ^{194}Hg(SD2), ^{194}Pb(SD1) and ^{196}Pb(SD1) in $A \sim 190$ mass region are considered. For each nucleus the optimized two parameters A,B of the model in question are fitted to reproduce the observed experimental γ-ray transition energies $E_\gamma^{exp}(I)$. The procedure is repeated for several trial values A,B by using a computer simulation search programm. The best parameters lead to minimize the root mean square (rms) deviation

$$\chi = \left[\frac{1}{N}\sum_{i=1}^{N}\left[\frac{E_\gamma^{exp}(I_i) - E_\gamma^{cal}(I_i)}{E_\gamma^{exp}(I_i)}\right]^2\right]^{\frac{1}{2}} \qquad (21)$$

where N is the total number of experimental points considered in fitting procedure. The experimental data are taken from reference [1,2]. The bandhead spins of the observed levels have been extracted by applying the first and second-hand estimations corresponding to pure rotator and our proposed formula respectively by plotting EGOS versus spin.

The EGOS is a horizontal line for the exact I_0 and will shift to parabola when $I_0 \pm 2$ is assigned to I_0 for pure rotator (first estimation) and three parabola curves for our proposed model (second estimation). As an example, this procedure illustrated in Figure (1) for ^{194}Hg(SD1) for bandheads $I_0 + 2$, I_0, $I_0 - 2$. The closed circles represents the experimental values while the solid curves the calculated ones. The numerical values are presented in Tables (1,2).

The resulting best parameters A,B of the model and the values of the lowest bandhead spins I_0 and the bandhead moment of inertia J_0 for our selected SDRB's are listed in Table (3).

In framework of the applied theoretical model, the dynamic $J^{(2)}$ and kinematic $J^{(1)}$ moments of inertia corresponding to the calculated spins have been extracted. The comparison between the experimental γ-ray transition energies and our calculations using the values of the model parameters given in Table(1) for the SD bands of our selected nuclei is illustrated in Figure(2).

Figure (3) illustrates the calculated kinematic $J^{(1)}$ (open circle) and dynamic $J^{(2)}$ (closed circle) moments of inertia as a function of rotational frequency $\hbar\omega$. Both the moments of inertia $J^{(1)}$ and $J^{(2)}$ exhibits a smooth increase with increasing rotational frequency, the $J^{(2)}$ is significantly larger than $J^{(1)}$ over a large rotational frequency range.

Investigating the tables and figures, we know that the γ-ray transition energies, the kinematic $J^{(1)}$ and dynamic $J^{(2)}$ moments of inertia of the SD states can be quantitatively described excellently with our two-parameters collective rotational formula. The $J^{(2)}$ values for both ^{192}Hg(SD1) and ^{194}Pb(SD1) are very close over the entire frequency range $\hbar\omega < 0.25$ MeV. However, at higher frequencies the differences in transition energies are no longer constant.

Moreover, the SD band of ^{194}Pb(SD1) is populated at lower spin values $I_0 = 6\hbar$ than that of ^{192}Hg(SD1), $I_0 = 10\hbar$. The difference in γ-ray energies ΔE_γ between transitions in ^{192}Hg(SD1) and ^{194}Pb(SD1) are plotted in Figure (4). Up to $\hbar\omega \sim 0.25$ MeV, the ΔE_γ values are small and constant. Therefore, these two bands have been considered as identical bands (IB), however at higher frequency the difference in transition energies are no longer constant. also the difference

Table 3: The adapted model parameters A,B obtained by fitting procedure, the suggested bandhead spins I_0 and the bandhead moments of inertia J_0. The SDRB's are identified by the lowest observed E_γ.

SDRB	A(keV)	$B(10^{-4}\text{keV})$	$I_0(\hbar)$	$J_0(\hbar^2\text{MeV}^{-1})$	E_γ(keV)
^{192}Hg(SD1)	5.6470	-3.5087	8	88.5425	214.4
^{194}Hg(SD1)	5.5904	-3.3951	10	89.4390	253.93
^{194}Hg(SD2)	5.3154	-2.2537	8	94.0662	200.79
^{194}Pb(SD1)	5.6637	-1.5590	4	88.2815	124.9
^{196}Pb(SD1)	5.7282	-3.1319	6	87.2874	171.5

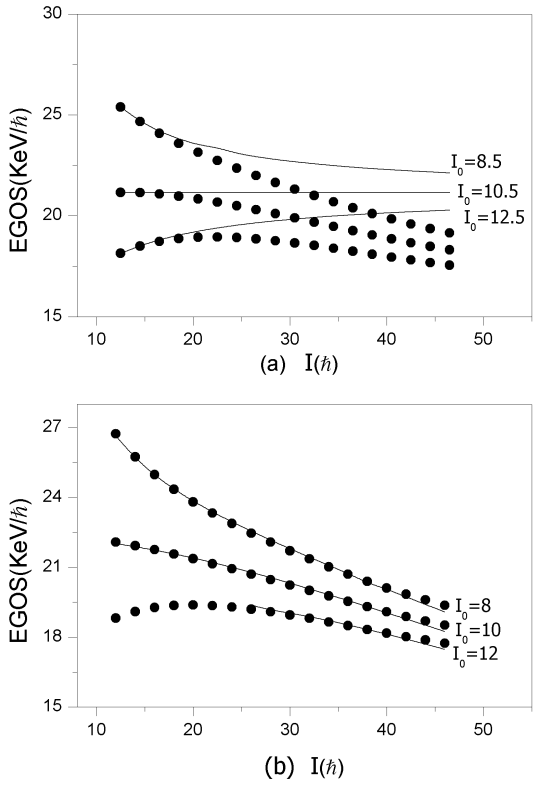

Fig. 1: EGOS versus spin to determine the band head spin for ^{194}Hg(SD-1) (a) for first estimation (b) for second estimation.

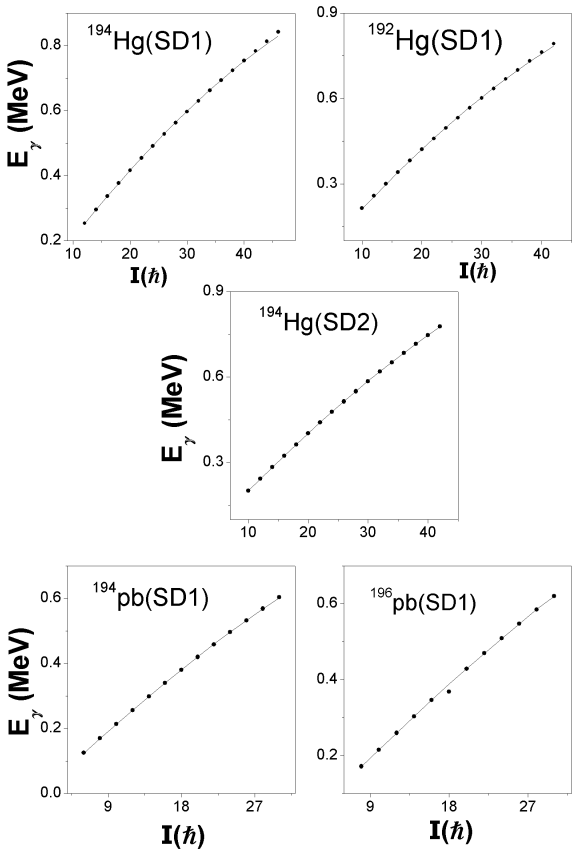

Fig. 2: Theoretical (solid curve) and experimental (closed circles) gamma-ray transition energies E_γ of the SD bands observed in even-even Hg and Pb nuclei. The theoretical values are calculated with the corresponding parameters taken from Table (3).

ΔE_γ between ^{194}Hg(SD1) and ^{192}Hg(SD1) is approximately 4 keV at low frequency (see Figure (4)) are too longer to consider these two bands as identical ones.

Another result of the present work is the observation of a $\Delta I = 2$ staggering effects in the transition energies for ^{194}Hg(SD1) and ^{194}Hg(SD2). For each band, the deviation of the γ-ray transition energies from a smooth reference representing the finite difference approximation to the fourth derivative of the γ-ray transition energies in a $\Delta I = 2$ band is calculated. Figure (5) show the resulting values of $\Delta^4 E_\gamma(I)$ against rotational frequency $\hbar\omega$ for the two SD bands. A significant staggering has been observed for ^{194}Hg(SD2) in frequency range $\hbar\omega \sim 0.3$ MeV.

8 Conclusion

We studied in a simple version of two parameters collective model the five SDRB's ^{192}Hg(SD1), ^{194}Hg(SD1,SD2), ^{194}Pb(SD1) and ^{196}Pb(SD1) in the mass region 190. Transition energies, rotational frequencies, dynamic and kinematic

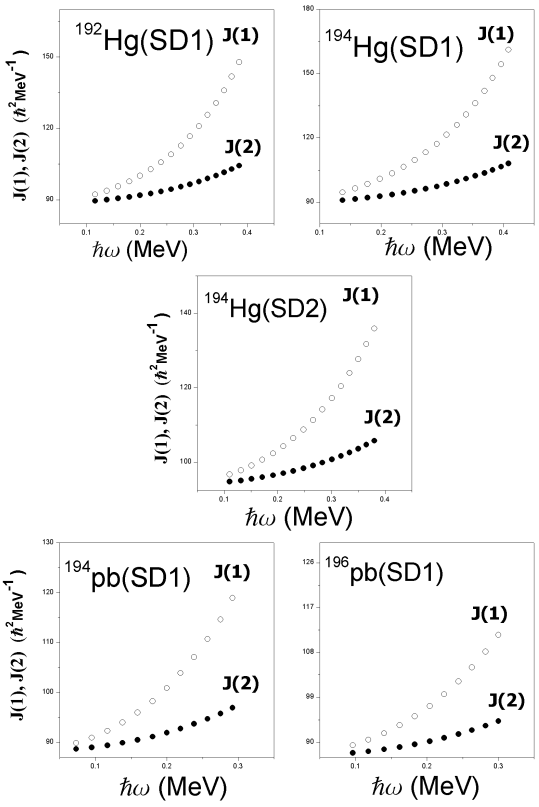

Fig. 3: The calculated results of kinematic $J^{(1)}$ (open circles) and dynematic $J^{(2)}$ (closed circles) moments of inertia plotted as a function of the rotational frequency $\hbar\omega$ for the studied SDRB's.

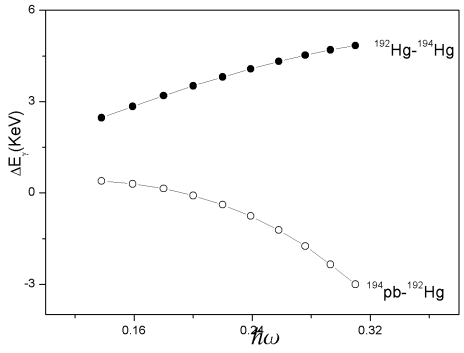

Fig. 4: Differences in the calculated γ-ray transition energies between ^{192}Hg(SD-1)-^{194}Pb(SD-1) and between ^{192}Hg(SD-1)-^{194}Hg(SD-1).

moments of inertia have been calculated. An excellent agreement with the experimental data justifies the application of

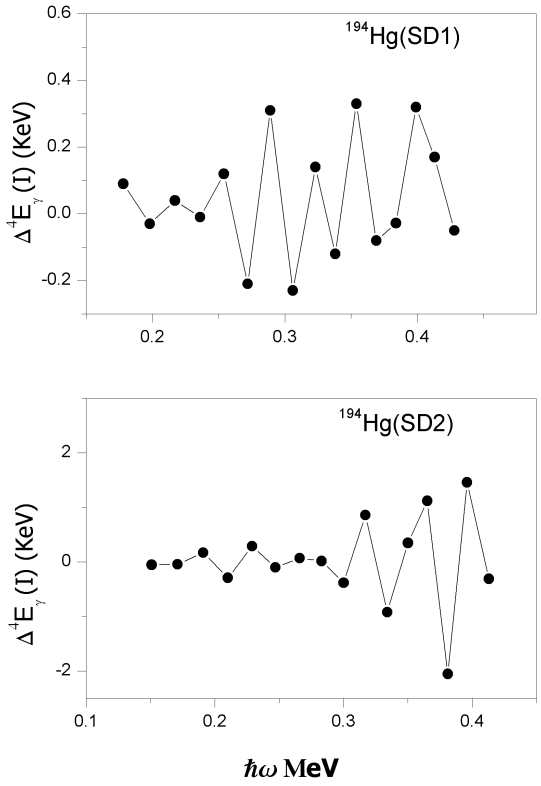

Fig. 5: The $\Delta = 2$ staggering obtained by the five points formula $\Delta^4 E_\gamma(I)$ as a function of rotational frequency $\hbar\omega$ for ^{194}Hg(SD-1, SD-2).

this version of the model. For the first-hand estimation of the bandhead spin I_0 of each SD band we have used the simple rigid rotator to extrapolated the experimentally transition energies, and from the ratio between two consecutive transition energies $\frac{E_\gamma(I_0+4)}{E_\gamma(I_0+2)}$, the spin value of the bandhead has been calculated. For second hand estimation of I_0, the EGOS versus spin for our model are plotted, the plot gives three parabola curves for I_0 and $I_0 \pm 2$. The existence of identical bands in the isotones ^{192}Hg(SD1) and ^{194}Pb(SD1) are investigated. The $\Delta I = 2$ staggering has been examined in the notation of Cedercwall [23]. The staggering plot has been extracted and investigated.

Submitted on August 21, 2014 / Accepted on August 29, 2014

References

1. Singh B., Zymwina R. and Firestone R.B. Table of Superdeformed Nuclear Bands and Fission Isomers: Third Edition. *Nuclear Data Sheets*, 2002, v. 97, 41–295.
2. National Nuclear Data Center NNDC, Brookhaven National Laboratory [Cited on July 2012] http://www.nndc.bnl.gov/chart/
3. Becker J.A. et al. Level spin and moments of inertia in superdeformed nuclei near A = 194. *Nuclear Physics*, 1990, v. A520, C187–C194.

4. Draper J.E. et al. Spins in superdeformed bands in the mass 190 region. *Physical Review*, 1990, v. C42, R1791.
5. Zeng J.Y. et al. Criteria of the Spin Assignment of Rotational Band. *Communications in Theoretical Physics*, 1995, v. 24, 425.
6. Hegazi A.M., Ghoniem M.H. and Khalaf A.M. Theoretical Spin Assignment for Superdeformed Rotational Bands in Mercury and Lead Nuclei. *Egyptian Journal of Physics*, 1999, v. 30, 293–303.
7. Khalaf A.M. et al. Bandhead Spin Determination and Moment of Inertia of Superdeformed Nuclei in Mass Region 60-90 Using Variable Moment of Inertia Model. *Egyptian Journal of Physics*, 2002, v. 41, 151–165.
8. Saber E. Spin Propostion of Rotational Bands in Superdeformed Nuclei by Using Experimental Gamma-Transition Energies. M.Sc. Thesis, Al-Azhar University, Egypt, 2005.
9. Gaballah N. Properties of Dynamical Moments of Inertia in Superdeformed Nuclei. M.Sc. Thesis, Al-Azhar University, Egypt, 2008.
10. Taha M.M. Behavior of Interacting Boson Model In Framework of Group Theory. Ph.D. Thesis, Al-Azhar University, Egypt, 2010.
11. Sayed M.S. Properties of Superdeformed Nuclei and High Spin States. M.Sc. Thesis, Cairo University, Egypt, 2004.
12. Inakurr T. et al. Static and Dynamic Non-Axial Octupole Deformations Suggested by SKYRME-HF and Selfconsistent RPA Calculations. *International Journal of Modern Physics*, 2004, v. E13, 157–167.
13. Muntain I. and Sabiczcwski A. Superdeformed ground state of superheavy nuclei. *Physics Letters*, 2004, v. B586, 254–257.
14. He X.T. et al. The intruder orbitals in superdeformed bands and alignment additivity of odd-odd nuclei in the A∼190 region. *Nuclear Physics*, 2005, v. A760, 263–273.
15. W. Nazarewicz W., Wgss R. and Jhonson A. Structure of superdeformed bands in the A ∼ 150 mass region. *Nuclear Physics*, 2005, v. A503, 285–330.
16. Janssens R.V.F. and Khoo T.L. Superdeformed Nuclei. *Annual Review of Nuclear and Particle Science*, 1991, v. 41, 321–355.
17. Byrski T. et al. Observation of identical superdeformed bands in N=86 nuclei. *Physical Review Letters*, 1990, v. 64, 1650–1657.
18. Girod M. et al. Microscopic descriptions of collective SD bands in the A=190 mass region with the Gogny force. *Zeitschrift für Physik A, Hadrons and Nuclei*, 1997, v. A358, 177–178.
19. He X.T. et al. The $i_{13/2}$ proton intruder orbital and the identical superdeformed bands in 193, 194, 195Tl. *European Physical Journal*, 2005, v. A23, 217–222.
20. Chen Y.J. et al. Theoretical simulation for identical bands. *European Physical Journal*, 2005, v. A24, 185–191.
21. Khalaf A.M., Taha M.M. and Kotb M. Identical Bands and $\Delta I = 2$ Staggering in superdeformed Nuclei in A ∼ 150 Mass Region using Three Parameters Rotational Model. *Progress in Physics*, 2012, v. 4, 39–43.
22. Flibotte S. et al. $\Delta I = 4$ bifurcation in a superdeformed band: Evidence for a C4 symmetry. *Physical Review Letters*, 1993, v. 71, 4299–4305.
23. Cederwall B. et al. New features of superdeformed bands in Hg194. *Physical Review Letters*, 1994, v. 72, 3150–3155.
24. Flibotte S. et al. Multiparticle excitations and identical bands in the superdeformed Gd-149 nucleus. *Nuclear Physics* , 1995, v. A584, 373–396.
25. Haslip D.S. et al. $\Delta I = 4$ Bifurcation in Identical Superdeformed Bands. *Physical Review Letters*, 1997, v. 78, 3447–3461.
26. Hamamoto I. and Mottelson B. Superdeformed rotational bands in the presence of Y44 deformation. *Physics Letters*, 1994, v. B333, 294–298.
27. Pavlichenkov L.M. and Flibotte S. C4 symmetry and bifurcation in superdeformed bands. *Physical Review*, 1995, v. C51, R460.
28. Macchiovelli A.O. et al. C4 symmetry effects in nuclear rotational motion. *Physical Review*, 1995, v. C51, R1.
29. Lian-Ao Wu and Hiroshi Toki. Evidence on delta I = 4 bifurcation in ground bands of even-even nuclei and the theoretical explanation with the interacting boson model. *Physical Review Letters* ,1997, v. 79, 2006–2009.
30. Khalaf A.M. and Sirag M.M. Analysis of $\Delta I = 2$ Staggering in Nuclear Superdeformed Rotational Bands. *Egyptian Journal of Physics*, 2006, v. 35, 359–375.
31. Saber E. Theoretical Study of Staggering Phenomena in Energies of High Spin Nuclear Rotational Bands. Ph. D. Thesis, Al-Azhar University, Egypt, 2009.
32. Satula W. et al. Structure of superdeformed states in Au and Ra nuclei. *Nuclear Physics*, 1991, v. A529, 289–314.
33. Krieger S.J. et al. Super-deformation and shape isomerism: Mapping the isthmus. *Nuclear Physics*, 1992, v. A542, 43–52.
34. Bohr A. and Mettelson B.R. Nuclear Structure, vol. 2, W.A. Benjamin, 1975.

First and Second Least Action Principles: de Broglie Frequency and Neutron Decay

Paulo Roberto Silva

Departmento de Física (Retired Associate Professor), ICEx, Universidade Federal de Minas Gerais, Belo Horizonte, MG, Brazil.
E-mail: prsilvafis@gmail.com

We propose two kinds of least action principles. The first one is defined in a periodic time, and when applied to creation and annihilation of particle pairs, leads to the formula for the de Broglie frequency. The second one is defined in a double-time's metric, namely the longitudinal and transverse (related to the discreteness of the space) times. If applied to a problem dealing with the fluctuations of the metric, this second principle permit us to infer a coherence time. We interpret this as the neutron decay time, where we take the fluctuation in the kinetic energy as being the difference between the mass-energy of the neutron minus the sum of the mass-energies of the proton and electron. The neutron decay time evaluated in this way, does not make any explicit reference to the weak interactions.

1 Introduction

The least action (or Hamilton's) principle [1, 2] states that the variation of the action A gives null result, namely

$$\delta A = \delta \int L dt = 0. \tag{1}$$

In equation (1) L is the Lagrangian function, which depends on the coordinates and velocities and sometimes also on the time. Performing the variation of the action A we consider the various paths, all of them starting in the initial time t_1 and ending in the final time t_2.

2 The de Broglie Frequency

In this section we are giving somewhat more general character to the Lagrangian L, as being associated to some kind of field which is able to create or to destroy virtual particles pairs from the vacuum. Let us take the difference between the initial and final times, as being a time interval of period T,

$$t_2 - t_1 = T. \tag{2}$$

Now we write

$$\delta A = \delta \oint L dt = \oint \delta L \, dt = 0. \tag{3}$$

In equation (3) we used the closed-line-integral symbol, but here it means that the difference in time is a periodic time interval. Pursuing further we get

$$\oint \delta L \, dt = \int_0^{T/2} \delta L \, dt + \int_{T/2}^{T} \delta L \, dt = 0. \tag{4}$$

Indeed the creation and annihilation of particles pairs is a stochastic process, but we are going to consider a "regularized" form of it and we write

$$\int_0^{T/2} \delta L \, dt = -h, \text{ and } \int_{T/2}^{T} \delta \mathrm{L} \, \mathrm{dt} = +\mathrm{h}. \tag{5}$$

According to equation (5), in the first half period a quantum of action is destroyed, and in the second half one a quantum of action is created. The sum of the two contributions gives null result, recovering the classical case of the least action principle.

Now we take the first integral of (5) as being the process of creation of a virtual particle-antiparticle pair. We have

$$\int_0^{T/2} \delta L \, dt = < \delta L > \int_0^{T/2} dt \tag{6}$$

In equation (6) $< \delta L >$ corresponds to a time average of the quantity δL. Next we interpret it as the energy decreasing of the vacuum as a means to create a particle-antiparticle pair. Therefore we have

$$< \delta L >_{|\text{first half period}} = -2mc^2. \tag{7}$$

From equations (6) and (7), we get

$$2mc^2 \frac{T}{2} = h, \tag{8}$$

leading to

$$mc^2 = h\nu. \tag{9}$$

Observe that equation (9) is the relation for the de Broglie's frequency, where $\nu \equiv 1/T$.

3 The second action and the time of coherence

Inspired in the spirit of the string theory [3], we define a second action $A^{(2)}$, where the integration of the Lagrangian function will be also done along a "transverse time" t', besides the integration which is usually performed along the "longitudinal time" t. We write

$$A^{(2)} = \int \int L \, dt dt'. \tag{10}$$

Now let us consider, as in reference [4], a fluctuating contribution for the Lagrangian such that

$$\delta L = \frac{1}{2m} p_i \chi_{ij} p_j, \tag{11}$$

where χ_{ij} is a tensor connecting the fluctuating momenta of a particle of mass m. By taking the variation of the second action, equation (10), we have

$$\delta A^{(2)} =< \delta L > \int\int dt dt' = 0. \tag{12}$$

We observe that in this case, the average quantity $< \delta L >$ is equal to zero, due to the fluctuating nature of δL, namely

$$< \delta L >= \frac{1}{2m} < p_i \chi_{ij} p_j >= 0. \tag{13}$$

In equation (12) we have extracted from the double integral, the "first momentum" or the time-average of the function δL.

By analogy with the previous section where we have obtained the frequency of de Broglie, let us evaluate the second momentum (the variance) of δL. We write

$$\int\int (\delta L)^2 dt dt' =< (\delta L)^2 > \int_0^{\tau/2} dt \int_0^{\lambda/c} dt' = h^2, \tag{14}$$

where τ is the coherence time and λ is the Planck length. Meanwhile we have

$$< (\delta L)^2 >= \frac{p^4}{4m^2}. \tag{15}$$

From equation (14) and (15) we have

$$\frac{p^4}{4m^2} \frac{\tau\lambda}{2c} = h^2, \tag{16}$$

and solving equation (16)for the coherence time we get

$$\tau = \frac{8m^2 ch^2}{p^4 \lambda}. \tag{17}$$

4 Neutron decay and the discreteness of the space-time

In the previous section, the quantum fluctuations on the metric [4] were related to the discreteness of the space-time. Then a transverse time λ/c was considered, by taking a string of width equal to the Planck length λ. On the other hand, in the neutron-decay's reaction, we have the available maximum kinetic energy K given by

$$K = (m_n - M_p - m_e)c^2 = \frac{p^2}{2m}. \tag{18}$$

From equations (17) and (18) we get

$$\tau = \frac{2ch^2}{K^2 \lambda}. \tag{19}$$

Numerical evaluation of equation (19) gives for the coherence time τ, the magnitude

$$\tau = 1.04 \times 10^3 s. \tag{20}$$

This value for the coherence time must be compared with the calculated and measured times of the neutron decay, both of approximately 900 s (please see references [5] and [6]). This result suggests that the neutron decay, besides being a process governed by the weak interactions, can also be related to the fluctuations of the metric and to the discreteness of the space-time.

5 Concluding remarks

Besides to be essentially a quantum object, due to its size and its mass-energy content, neutron also is a composed particle with its three constituent quarks of two down and one upper flavor. Proton also is a composed particle, but some conservation laws seem to forbid its decay. We can imagine that in the decay process of the neutron, there is an intermediate step where we have a fluctuation between the wave function describing the integer neutron and the total wave function describing the reaction's products. It seems that the fluctuating kinetic energy introduced in section 4, nicely accounts for this feature of the neutron decay. Jointly with the here introduced concept of second action, which also considers the discreteness of the space-time, we were able to estimate the neutron decay time without explicit reference to the weak interactions [5–7]. Finally a paper entitled "Improved Determination of the Neutron Lifetime", was recently published in the Physical Review Letters [8] (please see the discussions and the references cited therein.)

Submitted on September 26, 2014 / Accepted on September 29, 2014

References

1. Tolman R.C. The Principles of Statistical Mechanics, Oxford University Press, 1967, p. 16.
2. Landau L. and Lifchitz E. Mécanique, Editions Mir, Moscow, 1966.
3. McMahon, String Theory Demystified, McGrawHill, 2009.
4. Chaves A.S. et al, Annals of Physics (NY), 1994, v. 231, 174.
5. Silva P.R. Weak Interactions Made Simple, viXra: 1210.0014v1.
6. Particle Data Group, *Physics Letters*, 1008, v. 204B, 1.
7. Griffiths D.J. Introduction to Elementary Particles, Wiley, New York, 1987.
8. A.T. Yue et al. *Physical Review Letters*, 2013, v. 111, 222501.

Wave-Particle Duality in the Elastodynamics of the Spacetime Continuum (STCED)

Pierre A. Millette

E-mail: PierreAMillette@alumni.uottawa.ca, Ottawa, Canada

We examine the nature of the wave-particle duality in the Elastodynamics of the Spacetime Continuum (STCED), due to the propagation of deformations in the STC by longitudinal dilatation and transverse distortion wave displacements. We first consider the special case of Electromagnetism which consists of transverse waves only, and use the photon wavefunction to demonstrate that $|\Psi|^2$ represents a physical energy density, not a probability density. However, normalization by the system energy allows use of the probabilistic formulation of quantum theory. In the STCED longitudinal and transverse wave equations, the transverse wave is the source of the interference pattern in double slit experiments, influencing the location of the longitudinal wave, as observed experimentally. We note the similarity of STCED wave-particle duality and Louis de Broglie's "double solution".

1 Introduction

As shown previously, in the Elastodynamics of the Spacetime Continuum (*STCED*) [1–6], energy propagates in the STC (spacetime continuum) as wave-like deformations which can be decomposed into *dilatations* and *distortions*.

Dilatations include an invariant change in volume of the spacetime continuum which is the source of the associated rest-mass energy density of the deformation. The rest-mass energy density of this longitudinal mode is given by [1, see Eq.(32)]

$$\rho c^2 = 4\bar{\kappa}_0 \varepsilon \tag{1}$$

where ρ is the dilatation rest-mass density, c is the speed of light, $\bar{\kappa}_0$ is the bulk modulus of the *STC* (the resistance of the spacetime continuum to *dilatations*), and ε is the volume dilatation. On the other hand, *distortions* correspond to a change of shape (shearing stress) of the spacetime continuum without a change in volume and are thus massless.

Thus deformations propagate in the spacetime continuum by longitudinal (*dilatation*) and transverse (*distortion*) wave displacements. This provides a natural explanation for wave-particle duality, with the transverse mode corresponding to the wave aspects of the deformations and the longitudinal mode corresponding to the particle aspects of the deformations.

2 Wave-particle duality in Electromagnetism

In Electromagnetism, as shown in [1, see (121)], the volume dilatation is $\varepsilon = 0$. Hence, the photon is massless and there is no longitudinal mode of propagation. Electromagnetic waves are massless transverse distortion waves.

The photons correspond to an energy flow along the direction of propagation in 3-space resulting from the Poynting vector. This longitudinal electromagnetic energy flux is massless as it is due to distortion, not dilatation, of the spacetime continuum. However, because this energy flux is along the direction of propagation, it gives rise to the particle aspect of the electromagnetic field, the photon. We should note however that the modern understanding of photons is that they are massless excitations of the quantized electromagnetic field, not particles *per se*. Thus in this case, the kinetic energy in the longitudinal direction is carried by the distortion part of the deformation, while the dilatation part, which carries the rest-mass energy, is not present as the mass is 0.

This situation provides us with an opportunity to investigate the transverse mode of propagation, independently of the longitudinal mode. In general, the transverse propagation of electromagnetic waves is given by sinusoidal waves ψ and the intensity of the waves, corresponding to the energy density, is given by $|\psi|^2$. This is equivalent to the modulus squared of the wavefunction used in Quantum Mechanics as a probability density. A full analysis requires that we investigate further the Quantum Mechanics of the photon, and in particular, the photon wavefunction.

2.1 Photon wavefunction

The photon wavefunction is a first quantization description of the electromagnetic field [7,8]. Historically, this development was not done, as second quantization of the electromagnetic field was first developed. As a result, photon wave mechanics is not fully accepted in the scientific community, mainly because of the differences between particle and photon dynamics. As opposed to a particle, the photon has zero rest-mass and propagates at the speed of light. In addition, the position operator cannot be defined for a photon, only the momentum operator (photon localization problem).

Bialynicki-Birula [8–12], Sipe [13], and more recently Mohr [14], Raymer and Smith [15–17] and others have derived and promoted the use of the photon wavefunction. Bialynicki-Birula defines the photon wavefunction as "a complex vector-function of space coordinates r and time t that adequately describes the quantum state of a single photon" [8].

He sees three advantages to introducing a photon wavefunction [11]: it provides 1) a unified description of both massive and massless particles both in first quantization and second quantization; 2) an easier description of photon dynamics without having to resort to second quantization; 3) new methods of describing photons.

As pointed out in [7] and references therein, the photon wave equation is now used to study the propagation of photons in media, the quantum properties of electromagnetic waves in structured media, and the scattering of electromagnetic waves in both isotropic and anisotropic inhomogeneous media. Raymer and Smith [16, 17] have extended the use of the photon wavefunction to the analysis of multi-photon states and coherence theory. To the above list, in this paper, we add an additional benefit of the photon wavefunction: the clarification of the physical interpretation of the quantum mechanical wavefunction.

The photon wavefunction is derived from the description of the electromagnetic field based on the complex form of the Maxwell equations first used by Riemann, Silberstein and Bateman [8] (the Riemann–Silberstein vector). As summarized by Bialynicki-Birula [12], "[t]he Riemann–Silberstein vector on the one hand contains full information about the state of the classical electromagnetic field and on the other hand it may serve as the photon wave function in the quantum theory". The Maxwell equations are then written as [8]

$$\begin{aligned} i\,\partial_t \mathbf{F}(\mathbf{r},t) &= c\,\nabla\times\mathbf{F}(\mathbf{r},t) \\ \nabla\cdot\mathbf{F}(\mathbf{r},t) &= 0 \end{aligned} \tag{2}$$

where

$$\mathbf{F}(\mathbf{r},t) = \left(\frac{\mathbf{D}(\mathbf{r},t)}{\sqrt{2\epsilon_0}} + i\,\frac{\mathbf{B}(\mathbf{r},t)}{\sqrt{2\mu_0}}\right) \tag{3}$$

and where $\mathbf{D}(\mathbf{r},t)$ and $\mathbf{B}(\mathbf{r},t)$ have their usual significance.

Then the dynamical quantities like the energy density and the Poynting vector are given by [8]

$$\begin{aligned} E &= \int \mathbf{F}^*\cdot\mathbf{F}\;\mathrm{d}^3r \\ \mathbf{S} &= \frac{1}{2ic}\int \mathbf{F}^*\times\mathbf{F}\;\mathrm{d}^3r \end{aligned} \tag{4}$$

where $\mathbf{F}^*$ denotes the complex conjugate. The sign selected in (3) reflects positive helicity (projection of the spin on the direction of momentum) corresponding to left-handed circular polarization. Photons of negative helicity corresponding to right-handed circular polarization are represented by changing the sign from i to $-i$ in (3). Hence (3) can be written as

$$\mathbf{F}_{\pm}(\mathbf{r},t) = \left(\frac{\mathbf{D}(\mathbf{r},t)}{\sqrt{2\epsilon_0}} \pm i\,\frac{\mathbf{B}(\mathbf{r},t)}{\sqrt{2\mu_0}}\right) \tag{5}$$

to represent both photon polarization states.

A photon of arbitrary polarization is thus represented by a combination of left- and right-handed circular polarization states. The photon wavefunction is then given by the six-component vector

$$\Psi(\mathbf{r},t) = \begin{pmatrix} \mathbf{F}_+(\mathbf{r},t) \\ \mathbf{F}_-(\mathbf{r},t) \end{pmatrix}. \tag{6}$$

The corresponding photon wave equation is discussed in [11].

2.2 Physical interpretation of the photon wavefunction

From (6) and (5), we calculate the modulus squared of the photon wavefunction to obtain [7]

$$|\Psi(\mathbf{r},t)|^2 = \left(\frac{\epsilon_0|\mathbf{E}|^2}{2} + \frac{|\mathbf{B}|^2}{2\mu_0}\right). \tag{7}$$

The modulus squared of the photon wavefunction $\Psi(\mathbf{r},t)$ gives the electromagnetic energy density at a given position and time. This is the physical interpretation of the quantum mechanical $|\Psi(\mathbf{r},t)|^2$ for electromagnetic transverse waves in the absence of longitudinal waves.

Bialynicki-Birula proposes to convert $|\Psi(\mathbf{r},t)|^2$ to a probability density as required by the accepted quantum mechanical probabilistic interpretation [11]. This he achieves by dividing the modulus squared of the photon wavefunction by the expectation value of the energy $<E>$ [11, see his equation (44)]. In this way, it is made to describe in probabilistic terms the energy distribution in space associated with a photon.

Thus the probabilistic formulation of quantum theory is preserved, while the physical interpretation of $|\Psi|^2$ is shown to correspond to an energy density. Raymer and Smith [17] state that "[a] strong argument in favour of the energy-density wave function form of PWM [Photon Wave Mechanics] is that it bears strong connections to other, well-established theories—both quantum and classical—such as photodetection theory, classical and quantum optical coherence theory, and the biphoton amplitude, which is used in most discussions of spontaneous parametric down conversion".

Hence, we have to conclude that the appropriate physical interpretation of $|\Psi|^2$ is that it represents a physical energy density, not a probability density. However, the energy density can be converted to a probability density once it is normalized with the system energy (as done by Bialynicki-Birula for the photon wavefunction). In this way, *STCED* does not replace the probabilistic formulation of quantum theory, it just helps to understand the physics of quantum theory. The two formulations are equivalent, which explains the success of the probabilistic formulation of quantum theory. In actual practice, the quantum mechanical probability formulation can be used as is, as it gives the same results as the physical energy density formulation of *STCED*. However, the physical intensity waves of *STCED* help us understand the physics of the quantum mechanical wavefunction and the physics of wave-particle duality.

It is important to note that the energy density physical interpretation of $|\Psi|^2$ applies just as much to systems as to single particles, as for the probability density interpretation.

3 Wave-particle duality in STCED

In *STCED*, the displacement u^ν of a deformation from its undeformed state can be decomposed into a longitudinal (dilatation) component $u^\nu_\parallel$ and a transverse (distortion) component $u^\nu_\perp$. The volume dilatation ε is given by the relation [1, see (44)]

$$\varepsilon = {u_\parallel}^\mu{}_{;\mu}. \tag{8}$$

The longitudinal displacement wave equation and the transverse displacement wave equation of a deformation are given respectively by [1, see (196)]

$$\begin{aligned} \nabla^2 u^\nu_\parallel &= -\frac{\bar\mu_0 + \bar\lambda_0}{\bar\mu_0}\varepsilon^{;\nu} \\ \nabla^2 u^\nu_\perp &+ \frac{\bar k_0}{\bar\mu_0}\,\varepsilon(x^\mu)\; u^\nu_\perp = 0 \end{aligned} \tag{9}$$

where ∇^2 is the 4-D operator, $\bar\lambda_0$ and $\bar\mu_0$ are the Lamé elastic constants of the spacetime continuum and $\bar k_0$ is the elastic force constant of the spacetime continuum. The constant $\bar\mu_0$ is the shear modulus (the resistance of the continuum to *distortions*) and $\bar\lambda_0$ is expressed in terms of $\bar\kappa_0$, the bulk modulus (as in (1) in Section 1) according to

$$\bar\lambda_0 = \bar\kappa_0 - \bar\mu_0/2 \tag{10}$$

in a four-dimensional continuum. The wave equation for $u^\nu_\parallel$ describes the propagation of longitudinal displacements, while the wave equation for $u^\nu_\perp$ describes the propagation of transverse displacements in the spacetime continuum. The *STCED* deformation wave displacements solution is similar to Louis de Broglie's "double solution" [18, 19].

3.1 Wave propagation in STCED

The electromagnetic case, as seen in Section 2, provides a physical interpretation of the wavefunction for transverse wave displacements. This interpretation should apply in general to any wavefunction Ψ. In *STCED*, in the general case, every deformation can be decomposed into a combination of a transverse mode corresponding to the wave aspect of the deformation, and a longitudinal mode corresponding to the particle aspect of the deformation [2]. Thus the physical interpretation of Section 2.2 applies to the general *STCED* transverse wave displacements, not only to the electromagnetic ones.

Hence, $|\Psi|^2$ represents the physical intensity (energy density) of the transverse (*distortion*) wave, rather than the probability density of quantum theory. It corresponds to the transverse field energy of the deformation. It is not the same as the particle, which corresponds to the longitudinal (*dilatation*) wave displacement and is localized within the deformation via the massive volume dilatation, as discussed in the next Section 3.2. However, $|\Psi|^2$ can be normalized with the system energy and converted into a probability density, thus allowing the use of the existing probabilistic formulation of quantum theory. Additionally, the physical intensity waves of *STCED* help us understand the physics of wave-particle duality and resolve the paradoxes of quantum theory.

3.2 Particle propagation in STCED

Particles propagate in the spacetime continuum as longitudinal wave displacements. Mass is proportional to the volume dilatation ε of the longitudinal mode of the deformation as per (1). This longitudinal mode displacement satisfies a wave equation for ε, different from the transverse mode displacement wave equation for Ψ. This longitudinal dilatation wave equation for ε is given by [1, see (204)]

$$\nabla^2\varepsilon = -\frac{\bar k_0}{2\bar\mu_0 + \bar\lambda_0}\, u^\nu_\perp \varepsilon_{;\nu}\,. \tag{11}$$

It is important to note that the inhomogeneous term on the R.H.S. includes a dot product coupling between the transverse displacement $u^\nu_\perp$ and the gradient of the volume dilatation $\varepsilon_{;\nu}$ for the solution of the longitudinal dilatation wave equation for ε. This explains the behavior of electrons in the double slit interference experiment.

The transverse distortion wave equation for $\omega^{\mu\nu}$ [1, see (210)]

$$\nabla^2\omega^{\mu\nu} + \frac{\bar k_0}{\bar\mu_0}\,\varepsilon(x^\mu)\;\omega^{\mu\nu} = \frac{1}{2}\frac{\bar k_0}{\bar\mu_0}\left(\varepsilon^{;\mu}u^\nu_\perp - \varepsilon^{;\nu}u^\mu_\perp\right) \tag{12}$$

shows a R.H.S. cross product coupling between the transverse displacement $u^\nu_\perp$ and the gradient of the volume dilatation $\varepsilon^{;\mu}$ for the solution of the transverse distortion wave equation for $\omega^{\mu\nu}$. The transverse distortion wave $\omega^{\mu\nu}$ corresponds to a multi-component wavefunction Ψ.

A deformation propagating in the spacetime continuum consists of a combination of a transverse and a longitudinal wave. The transverse wave is the source of the interference pattern in double slit experiments, which impacts the location of the associated longitudinal wave of the individual particle in generating the interference pattern. The longitudinal dilatation wave behaves as a particle and goes through one of the slits, even as it follows the interference pattern dictated by the transverse distortion wave, as observed experimentally [20, see in particular Figure 4] and as seen in the coupling between $\varepsilon_{;\nu}$ and $u^\nu_\perp$ in (11) and (12) above.

These results are in agreement with the results of the Jánossy-Naray, Clauser, and Dagenais and Mandel experiments on the self-interference of photons and the neutron interferometry experiments performed by Bonse and Rauch [21, see pp. 73-81]. The transverse distortion wave generates the interference pattern, while the longitudinal wave's dilatation (particle) follows a specific action, with its final location guided by the transverse wave's interference pattern.

The longitudinal wave is similar to the de Broglie "singularity-wave function" [18]. However, in *STCED* the particle is not a singularity of the wave, but is instead characterized by its mass which arises from the volume dilatation propagating as part of the longitudinal wave. There is no need for the collapse of the wavefunction Ψ, as the particle resides in the longitudinal wave, not the transverse one. A measurement of a particle's position is a measurement of the longitudinal wave, not the transverse wave.

4 Discussion and conclusion

In this paper, we have examined the nature of the wave-particle duality that comes out of the Elastodynamics of the Spacetime Continuum (*STCED*). We have noted that deformations propagate in the spacetime continuum by longitudinal (*dilatation*) and transverse (*distortion*) wave displacements, which provides a natural explanation for wave-particle duality, with the transverse mode corresponding to the wave aspects of the deformations and the longitudinal mode corresponding to the particle aspects of the deformations.

We have considered the special case of Electromagnetism, which is characterized by a transverse mode (the electromagnetic radiation), but no longitudinal mode (as the photon is massless), to help in the clarification of the physical interpretation of the quantum mechanical wavefunction. To that purpose, we have considered the photon wavefunction, and have demonstrated that the physical interpretation of $|\Psi|^2$ represents an energy density, not a probability density. However, it can be normalized with the system energy to be converted to a probability density and allow the use of the probabilistic formulation of quantum theory. We have also noted that the energy density physical interpretation of $|\Psi|^2$ applies just as much to systems as to single particles.

We have then looked at the general *STCED* case, where every deformation can be decomposed into a combination of a transverse mode corresponding to the wave aspect of the deformation, and a longitudinal mode corresponding to the particle aspect of the deformation, and concluded that the physical interpretation of the photon wavefunction applies to the general *STCED* transverse wave displacements, not only to the electromagnetic ones.

We have reviewed the *STCED* longitudinal dilatation wave equation for ε corresponding to the mass component (particle) and the transverse distortion wave equation for $\omega^{\mu\nu}$ corresponding to a multi-component wavefunction Ψ. We have noted the coupling on the R.H.S. of both equations between $\varepsilon^{,\mu}$ and $u^{\nu}_{\perp}$, showing that even though the transverse wave is the source of the interference pattern in double slit experiments as for the photon wavefunction, and the longitudinal dilatation wave behaves as a particle, the latter follows the interference pattern dictated by the transverse distortion wave as observed experimentally.

We have also noted the similarity of *STCED* wave-particle duality to Louis de Broglie's "double solution" and "singularity-wave function", even though in *STCED* the particle is not a singularity of the wave, but is instead characterized by its mass which arises from the volume dilatation propagating as part of the longitudinal wave.

Submitted on September 15, 2014 / Accepted on October 6, 2014

References

1. Millette P. A. Elastodynamics of the Spacetime Continuum. *The Abraham Zelmanov Journal*, 2012, v. 5, 221–277.
2. Millette P. A. On the Decomposition of the Spacetime Metric Tensor and of Tensor Fields in Strained Spacetime. *Progress in Physics*, 2012, v. 4, 5–8.
3. Millette P. A. The Elastodynamics of the Spacetime Continuum as a Framework for Strained Spacetime. *Progress in Physics*, 2013, v. 1, 55–59.
4. Millette P. A. Derivation of Electromagnetism from the Elastodynamics of the Spacetime Continuum. *Progress in Physics*, 2013, v. 2, 12–15.
5. Millette P. A. Strain Energy Density in the Elastodynamics of the Spacetime Continuum and the Electromagnetic Field. *Progress in Physics*, 2013, v. 2, 82–86.
6. Millette P. A. Dilatation–Distortion Decomposition of the Ricci Tensor. *Progress in Physics*, 2013, v. 4, 32–33.
7. Chandrasekar N. Quantum Mechanics of Photons. *Adv. Studies Theor. Phys.*, 2012, v. 6 (8), 391–397.
8. Byalinicki-Birula I. Photon Wave Function. In Wolf E., ed. Progress in Optics XXXVI. Elsevier, Amsterdam, 1996, 245–294. arXiv: quant-ph/0508202v1.
9. Byalinicki-Birula I. On the Wave Function of the Photon. *Acta Physica Polonica A*, 1994, v. 86, 97–116.
10. Byalinicki-Birula I. *Acta Physica Polonica A*, 1995, v. 34, 885.
11. Byalinicki-Birula I. The Photon Wave Function. In Eberly J. H., Mandel L., Wolf E., eds. Coherence and Quantum Optics VII. Plenum, New York, 1996, 313–294.
12. Byalinicki-Birula I. Photon as a Quantum Particle. *Acta Physica Polonica B*, 2006, v. 37 (3), 935–946.
13. Sipe J. E. Photon Wave Functions. *Phys. Rev. A*, 1995, v. 52, 1875–1883.
14. Mohr P. J. Solutions of the Maxwell Equations and Photon Wave Functions. *Annals of Physics*, 2010, v. 325, 607–663.
15. Raymer M. G., Smith B. J. The Maxwell Wave Function of the Photon. *Proc. SPIE*, 2005, v. 5866, 293. arXiv: quant-ph/0604169.
16. Smith B. J., Raymer M. G. Two-Photon Wave Mechanics. *Phys. Rev. A* 2006, v. 74 062104. arXiv: quant-ph/0605149v3.
17. Smith B. J., Raymer M. G. Photon Wave Functions, Wave-Packet Quantization of Light, and Coherence Theory. *New Journal of Physics*, 2007, v. 9, 414. arXiv: 0708.0831.
18. de Broglie L. Non-Linear Wave Mechanics. Elsevier Publishing, Amsterdam, 1960.
19. de Broglie L. Les incertitudes d'Heisenberg et l'interprétation probabiliste de la Mécanique Ondulatoire. Gauthier-Villars, Paris, 1982. Available in English: Heisenberg's Uncertainties and the Probabilistic Interpretation of Wave Mechanics. Kluwer Academic Publishers, Dordrecht, 1990.
20. Hasselbach F. Recent Contributions of Electron Interferometry to Wave-Particle Duality. In Selleri F., ed. Wave-Particle Duality. Plenum, New York, 1992, 109–125.
21. Selleri F. Quantum Paradoxes and Physical Reality. Kluwer Academic Publishers, Dordrecht, 1990.

Gödel's Universe Revisited

Patrick Marquet

11 rue des Chapelles, 94350 Villiers/Marne, Paris, France
E-mail: patrick.marquet6@wanadoo.fr

This paper investigates the Gödel's exact solution of the Einstein equations which describes a stationary homogeneous cosmological Universe inducing closed timelike curves CTCs). This model is generally dismissed because it exhibits a rotational symmetry and it requires a non zero cosmological constant in contradiction with the current astronomical observations. If the cosmological term is assumed to be slightly variable, we show that this metric can be compatible with the Hubble expansion, which makes the Gödel model a viable representation of our Universe.

Introduction

In his original paper [1], Kurt Gödel has derived an exact solution to Einstein's field equations in which the matter takes the form of a pressure-free perfect fluid (dust solution). This $\mathfrak{R}^4$ manifold is homogeneous but non-isotropic and it exhibits a specific rotational symmetry which allows for the existence of *closed time like curves* since the light cone opens up and tips over as the Gödel radial coordinate increases. In addition, it implies a *non zero cosmological term* and a constant scalar curvature, therefore it doesnot admit a *Hubble* expansion *in the whole*, which tends to contradict all current observations.

We suggest here to stick to the Gödel model which we consider as the *true* Universe, and we state that the Hubble expansion can yet be maintained in a particular location with specific coordinates transformations, where the Gödel rotation is *unobservable*.

In this distinguished location, our derivations lead to an *open Universe* without cosmological term and as a result, no future singularity will ever appear in this *local* World.

Our model however, is bound to a main restriction: for physical reasons, it provides a solution which holds only for the existence of the cosmic scale factor, *within* the Gödel metric.

This improved Gödel Universe which we present here, has nevertheless the advantage of agreeably coping with the observational facts.

Some notations

Space-time indices: 0, 1, 2, 3.
Newton's gravitation constant: G.
The velocity of light is $c = 1$.
Space-time signature: -2.

1 Homogeneous space-times

1.1 Roberston-Walker space

Our actual observed Universe is spatially *homogeneous*: if we can see these observations identically in different directions, the model is said *isotropic*. The Robertson-Walker metric is an exact spherically symmetric solution. This property would imply that the Universe admits a six-parameter group of isometries whose surfaces of transitivity are space-like three-surfaces of constant curvatures. (An action of a group is transitive on the manifold $\mathfrak{M}$, if it can map any point of $\mathfrak{M}$ into any other point of $\mathfrak{M}$.) The spatial metric is expressed by

$$dl^2 = \frac{dr^2}{1 + r^2/F^2} + r^2\left(\sin^2\theta\, d\varphi^2 + d\theta^2\right). \qquad (1.1)$$

In the full RW model $F(t)$ is called the *cosmic scale factor* which varies with the (cosmic) proper time t of the whole space.

For an *open* (*infinite*) Universe, with *negative* curvature

$$K(t) = \frac{k}{F^2}, \qquad \text{where } k = -1. \qquad (1.2)$$

and the three-spaces are *diffeomorphic* to $\mathfrak{R}_3$.

The standard formulation is given by

$$(ds^2)_{\mathrm{RW}} = F^2\left(d\eta^2 - d\chi^2 - \sinh^2\chi\left(\sin^2\theta\, d\varphi^2 + d\theta^2\right)\right) \qquad (1.3)$$

with the usual parametrizations

$$dt = F\, d\eta \quad \text{and} \quad r = F\sinh\chi\,. \qquad (1.4)$$

In the RW Universe, the matter with mean density ρ is non interacting (dust) and the energy-momentum tensor is that of a *pressure free perfect fluid*:

$$T_{ab} = \rho\, u_a\, u_b\,. \qquad (1.5)$$

From the corresponding field equations we arrive at the temporal coordinate [2]

$$\eta = \pm\int \frac{dF}{F\sqrt{\left[\frac{8\pi G}{3}\rho F^2 + 1\right]}}, \qquad (1.6)$$

$$F = F_0\left(\cosh\eta - 1\right), \qquad (1.7)$$

with

$$F_0 = \frac{4\pi G\rho F^3}{3}, \qquad (1.8)$$

Where the $\pm$ sign depends on the light emitted either from the coordinates origin or reaching this origin.

1.2 The Gödel metric

The Gödel line element is generically given by

$$(ds^2)_{\mathrm{G}} = B^2\left[\, dx_0^2 - dx_1^2 + \frac{e^{2x_1}}{2}\, dx_2^2 - dx_3^2 + \right. \\ \left. + 2\, e^{2x_1}\,(dx_0 + dx_2)\right], \qquad (1.9)$$

where $B > 0$ is a constant in the original formulation.

This space-time has a five dimensional group of isometries which is transitive. It admits a five dimensional *Lie algebra of Killing vector fields* generated by a time translation ∂_{x_0}, two spatial translations ∂_{x_1}, ∂_{x_2} plus two further Killing vector fields:

$$\partial_{x_3} - x_2\partial_{x_3} \quad \text{and} \quad 2\, e^{x_1}\partial_{x_0} + x_2\,\partial_{x_3} + \left[\, e^{2x_1} - \frac{x_2^2}{2}\,\partial_{x_2}\right].$$

In all current papers, the Gödel metric is always described as the direct sum of the metric

$$(ds^2)_{\mathrm{G}_1} = B^2\left[\, dx_0^2 - dx_1^2 + dx_2^2\,\frac{e^{2x_1}}{2} + \right. \\ \left. + 2\, e^{x_1}\,(dx_0 + dx_2)\right] \qquad (1.10)$$

on the manifold $\mathfrak{M}_1 = \mathfrak{R}_3$ and

$$(ds^2)_{\mathrm{G}_2} = B^2(-dx_3^2) \qquad (1.11)$$

on the manifold $\mathfrak{M}_2 = \mathfrak{R}_1$.

This means that in the usual treatments, in order to analyze the properties of the Gödel solution it is always sufficient to consider only $\mathfrak{M}_1$. The coordinate dx_3 is deemed irrelevant and is thus simply suppressed in the classical representation, which in our opinion reveals a certain lack of completeness. In what follows, we consider the complete solution, where we assign a specific meaning to dx_3.

Let us remark that the Gödel space is homogeneous but not isotropic.

1.3 Classical features of Gödel's metric

Computing the connection coefficients $\Gamma_{ab}^{\ c}$ from the g_{ab} given in (1.9) eventually yield

$$R_{00} = 1, \quad R_{22} = e^{2x_1}, \quad R_{02} = R_{20} = e^{x_1}. \qquad (1.12)$$

All other R_{ab} vanish.

Hence:

$$R = \frac{1}{B^2}\,. \qquad (1.13)$$

The unit vector (world velocity) following the x_0-lines is shown to have the following contravariant components

$$\frac{1}{B},\ 0,\ 0,\ 0$$

and the covariant components

$$B,\ 0,\ B\,e^{x_1},\ 0$$

so we obtain

$$R_{ab} = \frac{1}{B^2}\, u_a\, u_b\,. \qquad (1.14)$$

Since the curvature scalar is a constant, the Gödel field equations read

$$(G_{ab})_{\mathrm{G}} = R_{ab} - \frac{1}{2}\, g_{ab} R = 8\pi G\rho\, u_a\, u_b + \Lambda\, g_{ab}\,, \qquad (1.15)$$

where Λ is the cosmological term which is here inferred as $-4\pi G\rho$, i.e.:

$$\frac{1}{B^2} = 8\pi G\rho\,, \qquad (1.16)$$

$$\Lambda = -\frac{R}{2} = -\frac{1}{2B^2}\,. \qquad (1.17)$$

We next define new coordinates (t, w, ϕ) on $\mathfrak{M}_1$ by

$$E^{x_1} = \cosh 2w + \cos\phi\, \sinh 2w\,, \qquad (1.18)$$

$$x_2\, e^{x_1} = \sqrt{2}\, \sin\phi\, \sinh 2w\,, \qquad (1.19)$$

$$\tan\frac{1}{2}\left(\phi + \frac{x_0 - 2t}{\sqrt{2}}\right) = e^{-2w} \tan\frac{\phi}{2}\,. \qquad (1.20)$$

This leads to the new line element

$$(ds^2)_{\mathrm{G}} = 4B^2\left(\left(dt^2 - dw^2 - dy^2 + \sinh^4 w - \sinh^2 w\right) d\phi^2 + \right. \\ \left. + 2\,\sqrt{2}\, \sinh^2 w\, d\phi\, dt\right) \qquad (1.21)$$

which exhibits the rotational symmetry of the solution about the axis $w = 0$, since we clearly see that the g_{ab} do not depend on θ. Gödel inferred that matter everywhere rotates with the angular velocity $2\sqrt{4\pi G\rho}$.

Let us consider the *reduced* Gödel metric

$$(ds^2)_{\mathrm{G}_1} = 4B^2\Big(\left(dt^2 - dw^2 + \sinh^4 w - \sinh^2 w\right) d\phi^2 + \\ + 2\,\sqrt{2}\, \sinh^2 w\, d\phi\, dt\Big).$$

All light rays emitted from an event on the symmetry axis reconverge at a later event on this axis, with the null geodesics forming a circular *cusp* [3].

If a curve c is defined by $\sinh^4 w = 1$, that is

$$c = \ln(1 + \sqrt{2}), \qquad (1.22)$$

hence, any circle $w > \ln(1+\sqrt{2})$ in the plane $t = 0$, is a *closed timelike curve*.

2 The modified Gödel metric

2.1 Conformal transformation

Now we will assume that the Λ-term is slightly varying with the time t, so B is also variable through the dust density. See (1.16) for detail.

By setting

$$y = r\cosh w, \tag{2.1}$$

where r is another radial parameter, we choose:

$$B = \frac{1}{2}\left(1 - \frac{L_0}{2\sqrt{t^2-y^2}}\right)^2 \tag{2.2}$$

where L_0 is a constant whose meaning will become apparent in the next sub-section. B is now identified with a conformal factor.

Note: one of the *Kretschmann scalar* is no longer an invariant

$$R_{abcd}R^{abcd} = \frac{6}{B^4} \tag{2.3}$$

which reflects the fact that the Gödel space-time may be not fully homogeneous.

Anticipating on our postulate, we will state that the variation of B is only localized in a certain region of the Gödel model. The Λ-term remains constant throughout the complete metric as initially derived, thus preserving its homogeneity.

2.2 The postulate

Our fundamental assumption will now consist of considering our *observed* Universe as being *local*. By local we mean that the rotation ϕ is *unobservable* since we assume that our world is situated at

$$w = 0.$$

Our (local) Universe is now becoming isotropic.

In this case, the Gödel metric reduces to a standard *conformal solution* where the light cone is centered about the t-axis:

$$(ds^2)_{\mathrm{G}} = \left[1 - \frac{L_0}{2\sqrt{t^2-r^2}}\right]^4 \left(dt^2 - dr^2\right). \tag{2.4}$$

We now make the following transformations

$$L_0 = F_0 \tag{2.5}$$

with F_0 defined in (1.8)

$$r = \frac{F_0}{2}e^{\eta}\sinh\chi\,, \qquad t = \frac{F_0}{2}e^{\eta}\cosh\chi\,, \tag{2.6}$$

$$\frac{F_0}{2}e^{\eta} = \sqrt{t^2-r^2}\,, \tag{2.7}$$

$$\tanh\chi = \frac{r}{t}\,, \tag{2.8}$$

and we retrieve the *Roberston-Walker* metric for an *open* Universe with the sole radial coordinate r:

$$(ds^2)_{\mathrm{RW}} = F^2(\eta)\left[d\eta^2 - d\chi^2\right]. \tag{2.9}$$

Remark: The Weyl tensor of the Gödel solution

$$C^{ab}{}_{cd} = R^{ab}{}_{cd} + \frac{R}{3}\delta^a{}_{[c}\delta_{d]}{}^b + 2\delta^{[a}{}_{[c}R_{d]}{}^{b]} \tag{2.10}$$

which has Petrov type D, vanishes for (2.9). Indeed, the equivalent metric (2.4) implies that $C^{ab}{}_{cd} = 0$ for this conformally flat space-time.

Our observed Universe would then be devoid of the Weyl curvature which explains why it is purely described in terms of the Ricci tensor alone. In this view, Einstein was perhaps an even more exceptional visionary mind than is yet currently admitted.

2.3 Hubble expansion

In our local world, the null geodesics are obviously given by $(ds^2)_{\mathrm{RW}} = 0$, that is

$$d\eta = \pm\, d\chi \tag{2.11}$$

and integrating

$$\chi = \pm\eta + const. \tag{2.12}$$

Let us place ourselves at $t(\eta)$, where we observe a light ray emitted at χ where its frequency is ν_0. In virtue of (2.12), the emission time will be $t(\eta-\chi)$, and we observe an apparent frequency given by:

$$\nu = \frac{\nu_0 F(\eta-\chi)}{F(\eta)}\,. \tag{2.13}$$

As $F(\eta)$ increases monotonically, we have $\nu < \nu_0$ which is the expression of a red shifted light. Most observed red shifts are rather small, so that $F(\eta-\chi)$ can be expanded as a Taylor series about $t(\eta-\chi) = t(\eta)$ and we finally get, limiting to the first two terms

$$F(\eta-\chi) = F(\eta) + \left[t(\eta-\chi) - t(\eta)\right]F'(\eta) \tag{2.14}$$

$$= F(\eta)\left\{1 + H_0\left[t(\eta-\chi) - t(\eta)\right]\right\} \tag{2.15}$$

where F' denotes differentiation with respect to η

$$H_0 = \frac{F'(\eta)}{F(\eta)} \tag{2.16}$$

is the present numerical value of *Hubble constant*.

The Gödel solution has a non-zero cosmological term, but **not** the local RW metric.

This agrees with the fact that our open local Universe has a singularity in the past and no singularity in the future [4], in accordance with astronomical observations.

Concluding remarks

Closed timelike curves turn out to exist in many other exact solutions to Einstein's field equations.

It would seem that the first model exhibiting this property was pioneered by C. Lanczos in 1924 [5], and later rediscovered under another form by W. J. Van Stockum in 1937 [6].

However, unlike the Gödel solution, the dust particles of these Universes are rotating about a geometrically distinguished axis.

Even worse, the matter density is shown to increase with radius w, a feature which seriously contradicts all current observations.

In this sense, the Gödel metric appears as a more plausible model characterizing a broaden Universe which is compatible with our astronomical data, provided one is prepared to accept the fact that our observed world is purely local.

Submitted on September 7, 2014 / Accepted on October 1, 2014

References

1. Gödel K. An example of a new type of cosmological solutions of Einstein's field equations of gravitation. *Reviews of Modern Physics*, 1949, v. 21, no. 3, 447–450.
2. Landau L. and Lifshitz E. The Classical Theory of Fields. Addison-Wesley, Reading (Massachusetts), 1962, p. 402 (French translation).
3. Hawking S. W. The Large Scale Structure of Space-Time. Cambridge University Press, Cambridge, 1987.
4. Fang Li Zhi and Ruffini R. Basic Concepts in Relativistic Astrophysics. World Scientific (Singapore), 1983.
5. Lanczos C. Über eine Stationäre Kosmologie im Sinne der Einsteinischer Gravitationstheorie. *Zeitschrift für Physik*, 1924, Bd. 21, 73.
6. Van Stockum W. J. The gravitational field of a distribution of particles rotating around an axis of symmetry. *Proc. Roy. Soc. Edinburgh*, 1937, v. A57, 135.

Progress in Physics is an American scientific journal on advanced studies in physics, registered with the Library of Congress (DC, USA): ISSN 1555-5534 (print version) and ISSN 1555-5615 (online version). The journal is peer reviewed and listed in the abstracting and indexing coverage of: Mathematical Reviews of the AMS (USA), DOAJ of Lund University (Sweden), Zentralblatt MATH (Germany), Scientific Commons of the University of St.Gallen (Switzerland), Open-J-Gate (India), Referential Journal of VINITI (Russia), etc. Progress in Physics is an open-access journal published and distributed in accordance with the Budapest Open Initiative: this means that the electronic copies of both full-size version of the journal and the individual papers published therein will always be acessed for reading, download, and copying for any user free of charge. The journal is issued quarterly (four volumes per year).

Electronic version of this journal: http://www.ptep-online.com

Postal address:
Department of Mathematics and Science,
University of New Mexico, 705 Gurley Avenue, Gallup, NM 87301, USA

Printed in the United States of America